



ISSN 2518-718X (Print)  
ISSN 2663-4872 (Online)

# BULLETIN

## OF THE KARAGANDA UNIVERSITY

# CHEMISTRY

## Series

**№ 4(108)/2022**

ISSN 2663-4872 (Online)  
ISSN-L 2518-718X (Print)  
Индексі 74617  
Индекс 74617

ҚАРАҒАНДЫ  
УНИВЕРСИТЕТІНІҢ  
ХАБАРШЫСЫ

**ВЕСТНИК**  
КАРАГАНДИНСКОГО  
УНИВЕРСИТЕТА

**BULLETIN**  
OF THE KARAGANDA  
UNIVERSITY

**ХИМИЯ** сериясы

Серия **ХИМИЯ**

**CHEMISTRY Series**

**№ 4(108)/2022**

Қазан–қараша–желтоқсан  
30 желтоқсан 2022 ж.

Октябрь–ноябрь–декабрь  
30 декабря 2022 г.

October–November–December  
December, 30<sup>th</sup>, 2022

1996 жылдан бастап шығады  
Издается с 1996 года  
Founded in 1996

Жылына 4 рет шығады  
Выходит 4 раза в год  
Published 4 times a year

Қарағанды, 2022  
Караганда, 2022  
Karaganda, 2022

*Editor-in-Chief*

Doctor of Chemical sciences

**Ye.M. Tazhbayev**

*Executive Editor*

Candidate of Chemical sciences

**I.A. Pustolaikina**

*Editorial board*

- Z.M. Muldakhmetov**, Academician of NAS RK, Doctor of chem. sciences, Institute of Organic Synthesis and Coal Chemistry of the Republic of Kazakhstan, Karaganda (Kazakhstan);
- S.M. Adekenov**, Academician of NAS RK, Doctor of chem. sciences, International Research and Production Holding “Phytochemistry”, Karaganda (Kazakhstan);
- S.E. Kudaibergenov**, Doctor of chem. sciences, Institute of Polymer Materials and Technologies, Almaty (Kazakhstan);
- V. Khutoryanskiy**, Professor, University of Reading, Reading (United Kingdom);
- Fengyun Ma**, Professor, Xinjiang University, Urumqi (PRC);
- Xintai Su**, Professor, South China University of Technology, Guangzhou (PRC);
- R.R. Rakhimov**, Doctor of chem. sciences, Norfolk State University, Norfolk (USA);
- M.B. Batkibekova**, Academician of the Engineering Academy of the Kyrgyz Republic, Doctor of chem. sciences, Kyrgyz State Technical University named after I. Razzakov, Bishkek (Kyrgyzstan);
- S.A. Beznosyuk**, Doctor of phys.-math. sciences, Altai State University, Barnaul (Russia);
- B.F. Minaev**, Doctor of chem. sciences, Bohdan Khmelnytsky National University of Cherkasy, Cherkasy (Ukraine);
- I.V. Kulakov**, Doctor of chem. sciences, University of Tyumen (Russia);
- R.P. Bhole**, PhD, Associate Professor, Dr. D.Y. Patil Institute of Pharmaceutical Sciences and Research, Sant Tukaram Nagar, Pimpri, Pune (India);
- A.M. Makasheva**, Doctor of techn. sciences, Zh. Abishev Chemical-Metallurgical Institute, Karaganda (Kazakhstan);
- M.I. Baikenov**, Doctor of chem. sciences, Karagandy University of the name of acad. E.A. Buketov (Kazakhstan);
- L.K. Salkeeva**, Doctor of chem. sciences, Karagandy University of the name of acad. E.A. Buketov (Kazakhstan);
- Ye.M. Tazhbaev**, Doctor of chem. sciences, Karagandy University of the name of acad. E.A. Buketov (Kazakhstan);
- O.G. Yaroshenko**, Doctor of Pedagogical Sciences, Academician of the National Academy of Pedagogical Sciences of Ukraine, Institute of Higher Education of the National Academy of Educational Sciences of Ukraine, Kyiv (Ukraine);
- V.N. Fomin**, Cand. of chemical science, Head of the laboratory of engineering profile “Physical and chemical research methods”, Karagandy University of the name of acad. E.A. Buketov (Kazakhstan)

*Postal address:* 28, University Str., Karaganda, 100024, Kazakhstan

Tel./fax: (7212) 34-19-40.

E-mail: [chemistry.vestnik@ksu.kz](mailto:chemistry.vestnik@ksu.kz); [irina.pustolaikina@ksu.kz](mailto:irina.pustolaikina@ksu.kz)

Web-site: <http://chemistry-vestnik.ksu.kz>

*Editors* Zh.T. Nurmukhanova, S.S. Balkeyeva, I.N. Murtazina

*Computer layout* V.V. Butyaikin

**Bulletin of the Karaganda University. Chemistry series.**

**ISSN 2663-4872 (Online). ISSN-L 2518-718X (Print).**

Proprietary: NLC “Karagandy University of the name of academician E.A. Buketov”.

Registered by the Ministry of Information and Social Development of the Republic of Kazakhstan.

Rediscount certificate No. KZ27VPY00027382 dated 30.09.2020.

Signed in print 29.12.2022. Format 60×84 1/8. Offset paper. Volume 24,13 p.sh. Circulation 200 copies.

Price upon request. Order № 145.

Printed in the Publishing house of NLC “Karagandy University of the name of acad. E.A. Buketov”.

28, University Str., Karaganda, 100024, Kazakhstan. Tel.: (7212) 35-63-16. E-mail: [izd\\_kargu@mail.ru](mailto:izd_kargu@mail.ru)

---

# CONTENTS

## ORGANIC CHEMISTRY

- Panshina S.Yu., Bakibaev A.A., Guslyakov A.N., Malkov V.S.* Synthesis of Cucurbit[6]uril Using 1-Hydroxyethylidene-1,1-Diphosphonic Acid as a “Green Catalyst” ..... 5
- Ayazbayeva A.Ye., Shakhvorostov A.V., Kudaibergenov S.E.* Temperature and Salt Responsivity of Anionic, Cationic and Amphoteric Nanogels Based on N-Isopropylacrylamide, 2-Acrylamido-2-Methyl-1-Propanesulfonic Acid Sodium Salt and (3-Acrylamidopropyl) Trimethylammonium Chloride ..... 14
- Turgunaliyeva D.M., Dilbaryan D.S., Vasilchenko A.S., Nurkenov O.A., Fazylov S.D., Karipova G.Zh., Seilkhanov T.M., Kulakov I.V.* Synthesis and Antibacterial Activity of Hydrazones of Isonicotinic and Salicylic Acids Based on Acetyl Derivatives of Coumarin and Benzo[g][1,3,5]Oxadiazocine..... 25
- Normurodov N.F., Berdinazarov Q.N., Abdurazakov M., Ashurov N.R.* Mechanical and Thermal Properties of Biodegradable Composites Based on graft copolymer LLDPE-g-MA/Gelatin ..... 35
- Bhole R.P., Karche P.M., Shinde Y., Kute P.R., Gurav S.S., Wavhale R.D.* Design and Synthesis of Vitamin Drug Conjugate for its Probable Potential Against SARS-COV-2 Infections ..... 46

## PHYSICAL AND ANALYTICAL CHEMISTRY

- Gandhi S.P., Gawhane A.R., Kapse S.D., Nagore D., Chitlange S.S.* Validated High Performance Thin Layer Chromatography Method for Simultaneous Estimation for Gallic Acid and Quercetin in Polyherbal Blend and Their Quantitative Estimation..... 54
- Makasheva A.M., Malyshev V.P., Bekbayeva L.A.* Direct Correlation between Fluid Cluster Structure and Its Viscosity ..... 65
- Bhimanwar R., Thomas A., Kothapalli L., Godase A., Gandhi S., Chandani S., More G., Jadhav G., Choudhary S.* Prospective Hybrid Molecules with Dual Anti-Viral and Anti-Thrombotic Activity Against the SARS-CoV-2 Infection and Its Associated Complications Employing *in Silico* Studies ..... 76
- Tyanakh S., Baikenov M.I., Gulmaliev A.M., Ma Feng-Yun, Musina G., Khamitova T.O., Bolatbay A.N.* Kinetics of Thermolysis of a Low-Temperature Tar in the Presence of a Catalyzer Agent with Deposited Metals..... 89
- Shelkovnikov V.V., Altyev A.M., Fryanova M.S.* Study of the Methionine Electrooxidation at an Electrode Modified with Vitamin B<sub>12</sub> and Multi-Walled Carbon Nanotubes ..... 99
- Fomin V.N., Usmanova E.R., Gyul E.F., Kelesbek N.K., Turovets M.A., Zemskiy O.I., Saulebekov D.M., Aldabergenova S.K.* Method for Qualitative and Quantitative Analysis of Ancient Lead Enamel Using Laser Inducted Breakdown Spectroscopy..... 107

## INORGANIC CHEMISTRY

- Zulfugarova S.M., Azimova G.R., Aleskerova Z.F., Litvishkov Yu.N., Tagiyev D.B.* Synthesis of Transition Metal Ferrites (Co, Cu, Ni, Mn) by the Sol-Gel Method with Combustion and the Use of Microwave Processing..... 118
- Kasenov B.K., Kasenova Sh.B., Sagintaeva Zh.I., Baisanov S.O., Lu N.Yu., Kuanyshbekov E.E., Turtubaeva M.O., Isabaeva M.A.* Novel Titanium-Manganites of Lanthanum and Alkali Metals ..... 136
- Houbi A., Zharmenov A.A., Atassi Y., Bagasharova Z.T., Mirzaliyeva S., Karibayev B.A.* Synthesis and Microwave Absorption Properties of (Ni<sub>0.5</sub>Zn<sub>0.5</sub>Fe<sub>2</sub>O<sub>4</sub>/Cl/CB) Ternary Composites..... 142
- Bayeshov A., Kadirbayeva A.S., Bayeshova A.K., Zharmenov A.A.* Electrochemical Method for Producing a TiO<sub>2</sub> Film with Photocatalytic Properties..... 152

## CHEMICAL TECHNOLOGY

- Guseinova E.A.* Adsorption Purification of Used Industrial Oil Using Natural Aluminosilicates ..... 162

---

<i>Chekanova L.G., Vaulina V.N., Elchischeva Yu.B., Bardina E.S., Pavlov P.T.</i> The Selection of Reagents for Ionic Flotation of Non-Ferrous Metals in the Series of N-Acyl-N'-Mezylhydrazines.....	171
<i>Muldakhmetov Z.M., Gazaliev A.M., Zhakina A.Kh., Vassilets Ye.P., Arnt O.V.</i> Synthesis of a Composite Based on Humic Acid Tuned to Sorbed Copper Ion.....	182
Index of articles published in “Bulletin of the Karaganda University. Chemistry Series” in 2022.....	190

## ORGANIC CHEMISTRY

Article Received: 31 May 2022 | Revised: 26 August 2022 | Accepted: 30 September 2022 | Published online: 8 November 2022

UDC 544.42+519.242.7

<https://doi.org/10.31489/2022Ch4/4-22-3>

S.Yu. Panshina<sup>1\*</sup>, A.A. Bakibaev<sup>2</sup>, A.N. Guslyakov<sup>2</sup>, V.S. Malkov<sup>2</sup>

<sup>1</sup>Karagandy University of the name of academician E.A. Buketov, Karaganda, Kazakhstan;

<sup>2</sup>National Research Tomsk State University, Tomsk, Russian Federation

(\*Corresponding author's e-mail: [janim\\_svetatusik@mail.ru](mailto:janim_svetatusik@mail.ru))

### Synthesis of Cucurbit[6]uril Using 1-Hydroxyethylidene-1,1-Diphosphonic Acid as a “Green Catalyst”

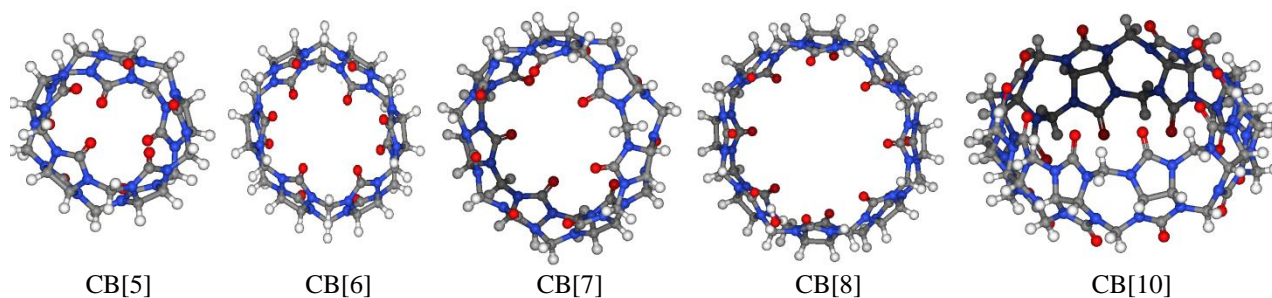
Glycoluril (2,4,6,8-tetraazabicyclo[3.3.0]octane-3,7-dione) and its derivatives have a special place in chemistry of heterocyclic compounds. The macrocyclic derivatives of glycoluril, namely cucurbit[n]urils have recently attracted the greatest interest due to their unique properties. Cucurbit[n]urils are usually synthesized by the condensation reaction of glycoluril with paraformaldehyde using strong mineral acids as a catalyst. In this work, 1-hydroxyethylidene-1,1-diphosphonic acid (HEDP) was used for the first time as a catalyst for “Green chemistry” in the synthesis of cucurbit[6]uril in an aqueous medium. The reaction of glycoluril and paraformaldehyde in a ratio of 1: 2 with two equivalents of 1-hydroxyethylidene-1,1-diphosphonic acid as a catalyst was carried out, in which the hexamer of cucurbituril ( $n = 6$ ) was obtained in 25 % yield. The clathrate of cucurbit[6]uril with acetone was obtained by treating the cucurbituril hexamer with acetone. The reaction of glycoluril with paraformaldehyde in the presence of HEDP can be used as a competitive method for the synthesis of cucurbit[6]uril. The structures of the obtained compounds were proven by NMR and IR spectroscopy methods. The phase composition of isolated crystals of cucurbit[6]uril hydrate was analyzed by the powder X-ray diffraction (XRD).

**Keywords:** cucurbit[6]uril, 1-hydroxyethylidene-1,1-diphosphonic acid, glycoluril, paraformaldehyde, NMR, “Green” catalyst, oligomer, “guest-host” interactions.

#### Introduction

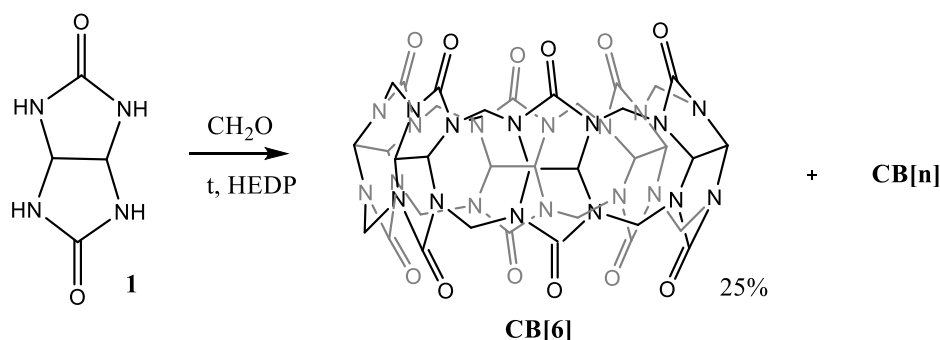
2,4,6,8-Tetraazabicyclo[3.3.0]octane-3,7-dione (glycoluril) **1** (Scheme 1) and its derivatives are the most interesting objects among bicyclic bisureas, which have a special place in the chemistry of heterocyclic compounds [1]. It has been reflected in the creation of valuable substances in various fields of human activity such as disinfectants [2, 3], medicines [4, 5], polymer stabilizers [6], and other important substances and materials based on these compounds. Geometrical features of glycoluril **1** determined the possibility of synthesis and investigation of macromolecular and supramolecular compounds on its basis [7–21]. Cucurbit[n]urils (**CB[n]**) are the main representatives of this type of compounds [9–21]. Macrocycles **CB[n]** have a narrowed hydrophobic cavity, which is outlined by two identical polar portals of carbonyl groups (Fig. 1 [16]). Hexamer cucurbit[6]uril **CB[6]** is the major reaction product due to the favorable deformation and abundance of hydrogen bonds [17–21].

In recent years, cucurbit[n]urils have attracted the significant interest due to their unique properties [11]. It is known [11, 16–21], that cucurbit[n]urils **CB[n]** are usually synthesized by the condensation reaction of glycoluril **1** with formaldehyde or paraformaldehyde in solutions of strong mineral acids at temperatures above 50 °C for a day or more. The use of organic acids in the synthesis of cucurbit[n]urils **CB[n]** is limited only by the use of methanesulfonic acid [21].

Figure 1. Cucurbit[*n*]urils, CB[*n*], *n* = 5, 6, 7, 8, 10.

More recently, in a number of works [22–25] it was shown that 1-hydroxyethylidene-1,1-diphosphonic acid (HEDP) proved to be a convenient “green” catalyst in heterocyclization reactions. 1-Hydroxyethylidene diphosphonic acid (HEDP) is known for its anti-corrosion properties. It is used as a retardant in concrete, scale and corrosion inhibition in circulating cool water system, oil field and low-pressure boilers in fields such as electric power, chemical industry, metallurgy, fertilizer, etc [26]. The HEDP substance decomposes at a temperature of about 250 °C, and decomposes in aqueous solutions at 140 °C [26]. In natural water bodies, HEDP rapidly decomposes under the action of ultraviolet light, and the decomposition products are used as fertilizers [27].

In this work, we first carried out the synthesis of cucurbit[6]uril **CB[6]** in the presence of HEDP as a “green” catalyst (Scheme 1).

Scheme 1. The synthesis of cucurbit[6]uril **CB[6]** in the presence of HEDP

### Experimental

**NMR spectra** were recorded on a Bruker AVANCE III HD spectrometer (Bruker Corporation, Germany) with an operating frequency of 400 and 100 MHz for  $^1\text{H}$  and  $^{13}\text{C}$  nuclei respectively, in solutions of  $\text{DMSO-d}_6$  and  $\text{F}_3\text{CSO}_3\text{H}$ . The internal standard was tetramethylsilane (TMS).

**IR spectra** were recorded on a Nicolet 6700 IR spectrometer, Thermo Fisher Scientific. The samples were studied by the method of disturbed total internal reflection in the spectral range from 400 to 4000  $\text{cm}^{-1}$ .

**Powder X-ray diffraction** for substance **CB[6]** was recorded on a Shimadzu XRD 7000 diffractometer using  $\text{Cu K}\alpha$  radiation at  $\lambda = 1.54053 \text{ \AA}$ . Reflections were collected from 5 to 50 in  $2\theta$  with a step of 0.014, a rate of 20 deg / min and a step time of 21.49 s at 17 °C.

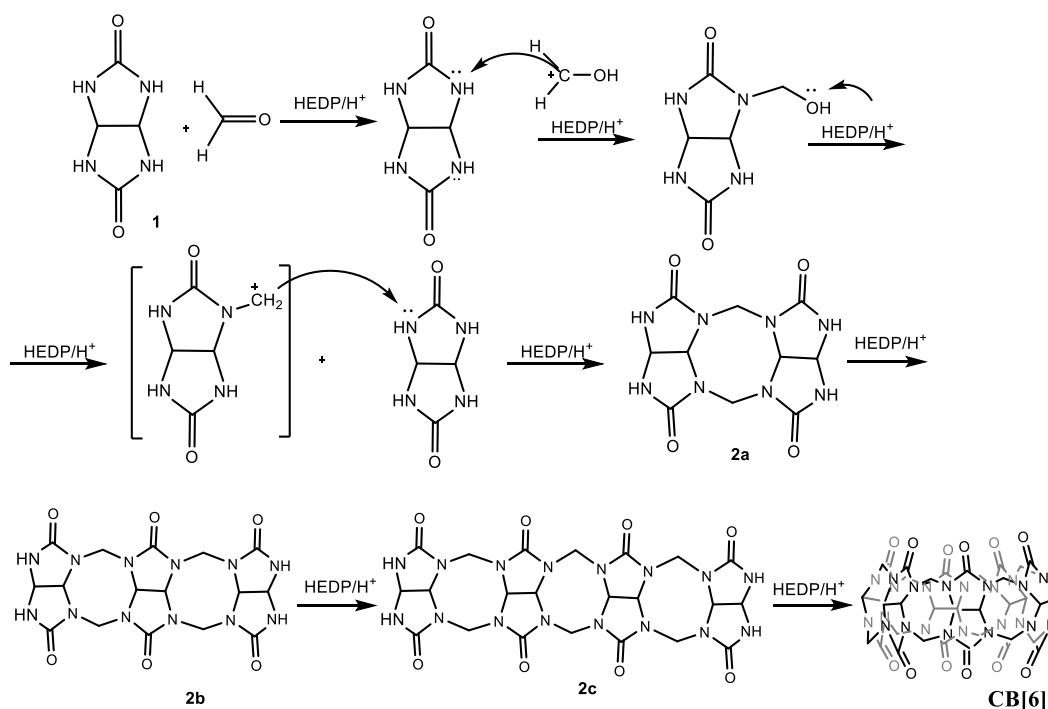
**Synthesis of cucurbit[6]uril hydrate **CB[6]** using HEDP.** Glycoluril **1** (21.4 g, 0.15 mol), HEDP (61.8 g, 0.30 mol) and 120 ml of water were added to a 250 mL round-bottomed flask equipped with a magnetic stir bar. The mixture was heated to 50 °C and then paraformaldehyde (9 g, 0.30 mol) was slowly added, allowing the solution to stir well. The viscous solution was allowed to stir for 30 min more until the solution set as a gel, which then was heated to 100 °C resulting in a rapid dissolution of the gel. The reaction mass was refluxed for 20 h at 100 °C. Then it was allowed to cool down to room temperature. The resulting precipitate was filtered off and washed with boiling water, after which it was dissolved in boiling 37 % HCl acid. The resulting solution was cooled and left at 0 °C for a week for crystallization. The colorless hexagonal crystals of cucurbit[6]uril hydrate **CB[6]** with high purity were formed on the vessel walls. Substance **CB[6]** is white powder with a yield of **CB[6]** 6.3 g (25 %). T. of decomp. is more than 400 °C. IR spectrum,  $\nu$ ,  $\text{cm}^{-1}$ : 3441 ( $\text{H}_2\text{O}$ ), 2927 (CH), 1712 (C = O).  $^1\text{H}$  NMR (400 MHz,  $\text{F}_3\text{CSO}_3\text{H}/\text{D}_2\text{O}$ ):  $\delta = 5.82$  (s, 12H, CH),

5.58 (d,  $J = 16.4$ , 12H, CH<sub>2</sub>), 4.63 (d,  $J = 16.6$ , 12H, CH<sub>2</sub>). <sup>13</sup>C NMR (101 MHz, F<sub>3</sub>CSO<sub>3</sub>H/D<sub>2</sub>O):  $\delta = 160.21$  (C=O), 72.71 (CH), 52.04 (CH<sub>2</sub>).

The obtained **CB[6]** powder was treated with hot acetone, where the clathrate of hydrate of the cucurbit[6]uril with acetone **CB[6]A** [19] was obtained in a yield of 6.1 g (23 %). The substance **CB[6]A** is practically insoluble in concentrated boiling acids HCl, H<sub>2</sub>SO<sub>4</sub> and hardly soluble in F<sub>3</sub>CSO<sub>3</sub>H. T. of decomp. is more than 400 °C. IR spectrum,  $\nu$ , cm<sup>-1</sup>: 3503 (H<sub>2</sub>O), 2998 (CH<sub>3</sub>), 2933 (CH), 1730 (C=O). <sup>1</sup>H NMR (400 MHz, F<sub>3</sub>CSO<sub>3</sub>H/D<sub>2</sub>O):  $\delta = 5.81$  (d,  $J = 5.6$ , 12H, CH), 5.56 (d,  $J = 13.9$ , 12H, CH<sub>2</sub>), 4.61 (d,  $J = 14.5$ , 12H, CH<sub>2</sub>), 2.67 (s, 3H, CH<sub>3</sub>). <sup>13</sup>C NMR (101 MHz, F<sub>3</sub>CSO<sub>3</sub>H/D<sub>2</sub>O):  $\delta = 198.49$  (C=O<sub>acetone</sub>), 160.11 (C=O), 72.68 (CH), 51.87 (CH<sub>2</sub>), 29.97 (CH<sub>3 acetone</sub>).

### Results and Discussion

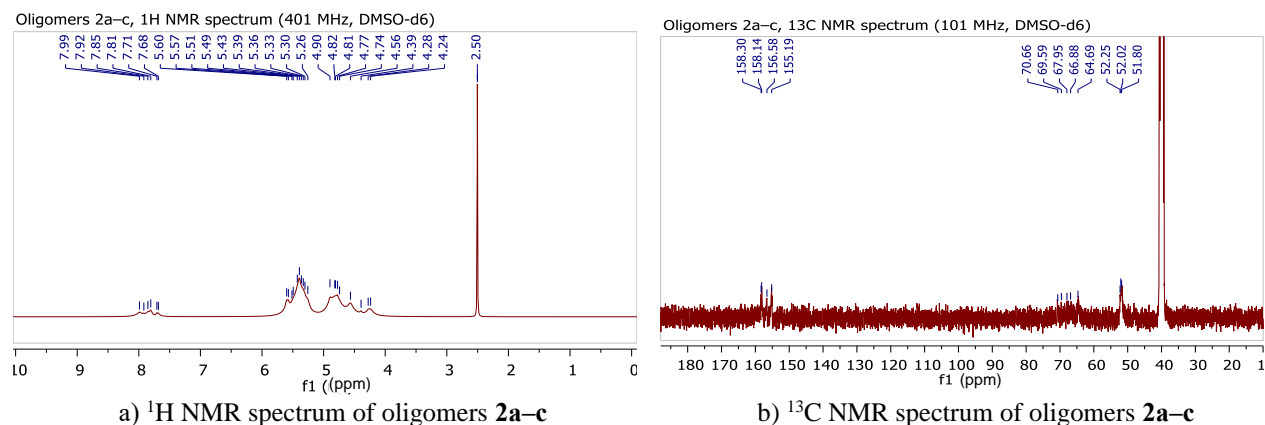
The reaction (Scheme 1) of glycoluril **1** and paraformaldehyde in a ratio of 1:2 was carried out with the traditional procedure [19], but HEDP was used as a catalyst in two equivalents relative to substrate **1**. It was suggested [28] that HEDP promoted more efficient transfer of glycoluril **1** into solution, which significantly accelerated the condensation reaction. In the process of carrying out the synthesis of **CB[6]** upon heating, the reaction mass was homogenized after 5 minutes. Then, after 20 minutes of reaction, a precipitate formed. These are intermediate oligomers **2a–c** of the cucurbit[6]uril **CB[6]** synthesis [18], the proposed structures of which are shown in Scheme 2.



Scheme 2. Formation of cucurbit[6]uril **CB[n]** by stepwise oligomerization

The reaction mixture was heated for 20 hours and then left to stand in a cold place overnight to crystallize the precipitate, which was isolated and washed with hot water. When the washing solution was cooled, precipitates of intermediate oligomers **2a–c** precipitated. According to the NMR results of the reaction mixture, glycoluril **1** reacted completely.

In the <sup>1</sup>H NMR spectrum (DMSO-d<sub>6</sub>) of oligomers **2a–c**, there are multiplets of the main signals of the structure, namely chemical shifts of NH-groups are found at  $\delta$  7.68–7.99 ppm, signals of protons of the methine group CH–CH are resonated at  $\delta$  5.26–5.60 ppm, and the chemical shifts of the protons of the methylene N–CH<sub>2</sub>–N groups are at  $\delta$  4.24–4.90 ppm (Fig. 2, a).

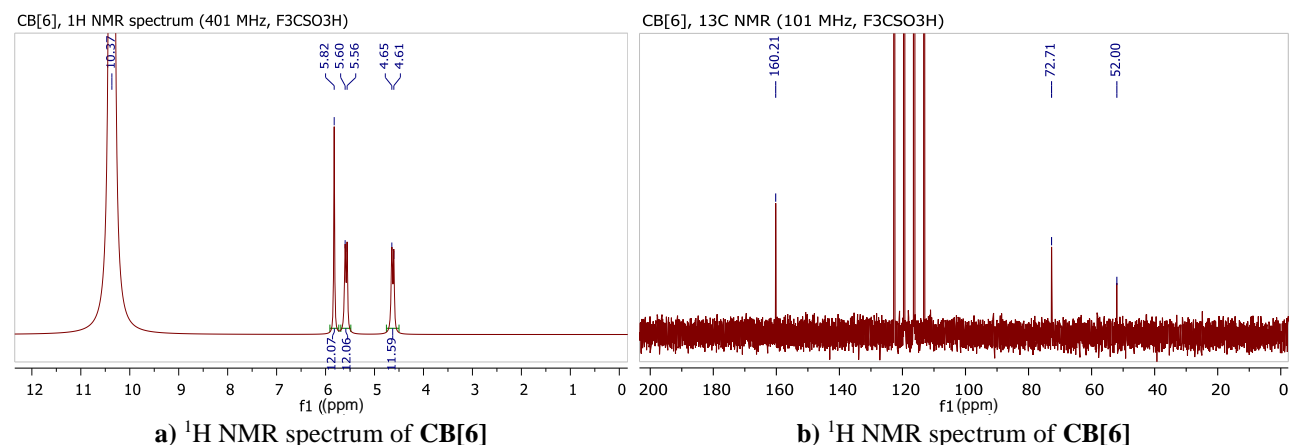
Figure 2. The NMR spectra of oligomers 2a-c in DMSO- $d_6$ 

In the  $^{13}\text{C}$  NMR spectrum (DMSO- $d_6$ ) of oligomers 2a-c, chemical shifts are observed at  $\delta$  51.8–52.3 ppm,  $\delta$  64.7–70.6 ppm and  $\delta$  155.2–158.3 ppm, which refer to carbon atoms of N-CH<sub>2</sub>-N, CH-CH and C=O, respectively (Fig. 2, b). In the IR spectrum of oligomers 2a-c there are characteristic absorption bands indicating the linearity of the structure of the obtained substances, namely the band at 3231  $\text{cm}^{-1}$  corresponds to NH-groups and the band at 1673  $\text{cm}^{-1}$  corresponds to amide C=O-groups.

The formation of acyclic structures 2a-c shows that HEDP acts as a trigger for the formation of a linear platform for further thermodynamically cyclization to cucurbit[*n*]urils **CB**[*n*] in an aqueous medium. The obtained cucurbit[6]uril **CB**[6] and non-cyclized oligomers with a high molecular weight are equally insoluble in water, which makes it difficult to isolate **CB**[6] from the aqueous medium. In the IR spectrum of the final precipitate, characteristic absorption bands of C=O-groups of non-cyclized oligomers (1675  $\text{cm}^{-1}$ ) and C=O-groups of cucurbit[6]uril **CB**[6] (1714  $\text{cm}^{-1}$ ) are observed. The characteristic absorption band of C=O-groups of cucurbit[6]uril **CB**[6] is shifted to short-wavelength region due to the resonance of the negative charge of the carbamide group of the cavity of cucurbit[6]uril **CB**[6].

Isolation and purification of cucurbit[6]uril **CB**[6] was carried out in accordance with the procedure [19]. The separated precipitate was dissolved in boiling 37 % acid HCl and left in the cold place. After a week, colorless hexagonal crystals of cucurbit[6]uril **CB**[6] hydrate were obtained.

Due to the low solubility of cucurbit[6]uril **CB**[6], NMR spectra were recorded in a trifluoromethanesulfonic acid solution (Fig. 3a, b).

Figure 3. The NMR spectra of **CB**[6] in F<sub>3</sub>CSO<sub>3</sub>H

The recorded NMR spectra of the substance **CB**[6] (Fig. 3a, b), in general, are identical to those previously recorded in the solvent DCI [18, 19].

We additionally analyzed the phase composition of the isolated crystals of cucurbit[6]uril hydrate **CB**[6] by the powder X-ray diffraction (XRD) (Fig. 4). XRD analysis showed that the type of crystal lattice and phase composition of crystals of cucurbit[6]uril hydrate **CB**[6] obtained in the presence of HEDP was

identical to crystals of cucurbit[6]uril hydrate  $\text{CB}[6] \cdot 4.66 \text{H}_2\text{O}$  [19], which were synthesized in the presence of HCl acid as a catalyst.

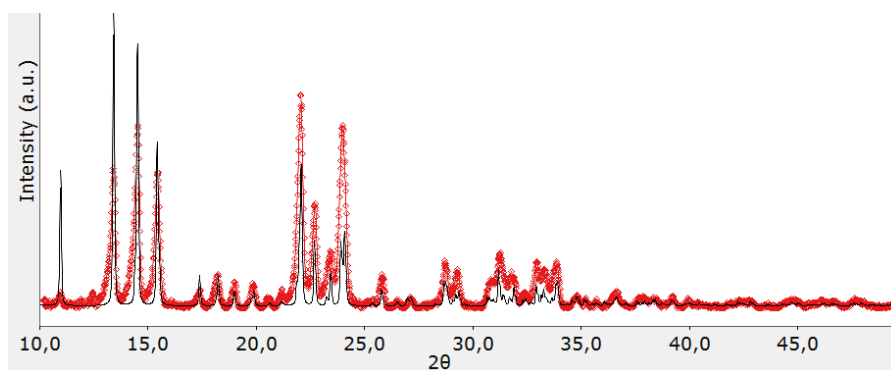
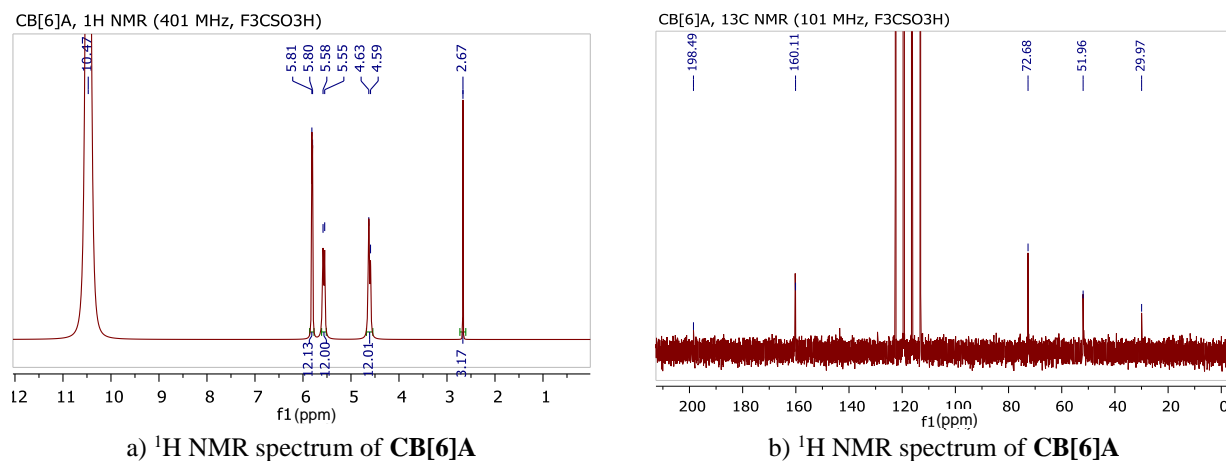


Figure 4. XRD of powder crystals of the isolated hydrate cucurbit[6]uril  $\text{CB}[6]$  structure (red line) and the corresponding theoretical picture of hydrate cucurbit[6]uril, (black line)

The clathrate of cucurbit[6]uril with acetone  $\text{CB}[6]\text{A}$  was obtained by treating the substance  $\text{CB}[6]$  with hot acetone. Substance  $\text{CB}[6]\text{A}$  is insoluble in concentrated acids HCl,  $\text{H}_2\text{SO}_4$  and slightly soluble in  $\text{F}_3\text{CSO}_3\text{H}$  acid. The structure of  $\text{CB}[6]\text{A}$  was investigated by IR- and NMR spectroscopy (Fig. 5a, b).



a)  $^1\text{H}$  NMR spectrum of  $\text{CB}[6]\text{A}$

b)  $^{13}\text{C}$  NMR spectrum of  $\text{CB}[6]\text{A}$

Figure 5. The NMR spectra of  $\text{CB}[6]\text{A}$  in  $\text{F}_3\text{CSO}_3\text{H}$

Previously, a similar clathrate [19], was described using X-ray diffraction analysis, the structure of which was a composition of one  $\text{CB}[6]$  per one acetone and eight water molecules. In our case, according to NMR data, the ratio of  $\text{CB}[6]$  and acetone molecules was also 1:1 in the clathrate. In the NMR spectra (Fig. 5a, b) of the clathrate  $\text{CB}[6]\text{A}$ , in addition to the main chemical shifts of cucurbit[6]uril  $\text{CB}[6]$ , there are chemical shifts of acetone.

“Guest-host” interactions in cucurbit[ $n$ ]uril chemistry have been studied in detail [11], and ion-dipole and dipole-dipole interactions are considered as the main driving forces for binding various guests (acetone) with  $\text{CB}[6]$ . Dipole-dipole interactions are shown in NMR spectra, where in the  $^{13}\text{C}$  NMR spectrum the peak of the  $\text{C}=\text{O}$  group of acetone is shielding by an average of 8 ppm (Fig. 5b), and in the  $^1\text{H}$  NMR spectrum the chemical shift of the  $\text{CH}_3$ -groups of acetone is deshielding by an average of 0.3 ppm (Fig. 5a), relative to chemical shifts of a free acetone molecule.

### Conclusions

Thus, HEDP has been first used in the synthesis of cucurbit[6]uril as a catalyst for “green chemistry” in an aqueous medium. It has been shown that HEDP not only forms linear structures, but also cyclizes oligomers into cucurbit[ $n$ ]urils, where the most probable and stable hexamer of cucurbituril ( $n = 6$ ) is obtained in 25 % yield.

The reaction of glycoluril with paraformaldehyde in the presence of HEDP can be used as a competitive method for the synthesis of cucurbit[6]uril. The advantages of using HEDP are in the “green” synthesis conditions and in the rapidity of the formation of the crystal structure of cucurbit[6]uril **CB[6]** hydrate, however, at the purification stage it is necessary to use mineral acids to separate linear products with similar solubility in water.

### Acknowledgments

We thank Tomsk State University for financial support to our research groups.

### References

- 1 Bakibaev A. Synthesis of glycolurils and hydantoins by reaction of urea and 1, 2-dicarbonyl compounds using etidronic acid as a “green catalyst” / A. Bakibaev, A. Uhov, V. Malkov, S. Panshina // *J. Heterocyclic Chem.* — 2020. — Vol. 57. — P. 4262–4270. <https://doi.org/10.1002/jhet.4132>
- 2 Patent 102004059041 Germany. Verwendung von Formaldehyd und Formaldehyd freisetzenden Verbindungen in einer Zusammensetzung zur Bekämpfung von Mykobakterien / Beilfuss W., Gradtke R., Krull I., Steinhauer, K. Publication date 08.06.2006.
- 3 Patent 2354771 Great Britain. Bactericide combinations in detergents / Denk A., Emter A., Moddick C. Publication date 04.04.2001.
- 4 Bakibaev A.A. 1D and 2D NMR spectroscopy for identification of carbamide-containing biologically active compounds / A.A. Bakibaev, S.Yu. Panshina, O.V. Ponomarenko, V.S. Malkov, O.A. Kotelnikov, A.K. Tashenov // *Bulletin of the university of Karaganda—Chemistry.* — 2021. — Vol. 101, No 1. — P. 71–81. <https://doi.org/10.31489/2021Ch1/71-81>
- 5 Машковский М.Д. Лекарственные средства: пособие для врачей: справочник / М.Д. Машковский. — 15-е изд. — М.: Новая волна, 2005. — 1164 с.
- 6 Bakibaev A.A. Methods of synthesis of nitrogen-containing heterocycles using ureas and related compounds / A.A. Bakibaev, A.Yu. Yagovkin, S.N. Vostretsov // *Russ. Chem. Rev.* — 1988. — Vol. 67, No. 4. — P. 295–314. <https://doi.org/10.1070/RC1998v067n04ABEH000295>
- 7 Havel V. Modulation of Bambusuril Anion Affinity in Water / V. Havel, M. Babiak, V. Sindelar // *Chemistry-A European Journal.* — 2017. — Vol. 23, No. 37. — P. 8963–8968. <https://doi.org/10.1002/chem.201701316>
- 8 Svec J. Bambus[6]uril / J. Svec, M. Necas, V. Sindelar // *Angewandte Chemie International Edition.* — 2010. — Vol. 122. — P. 2428–2431. <https://doi.org/10.1002/anie.201000420>
- 9 Nandi S. Cucurbit[6]uril-Stabilized Palladium Nanoparticles as a Highly Active Catalyst for Chemoselective Hydrogenation of Various Reducible Groups in Aqueous Media / S. Nandi, P. Patel, A. Jakhar, N.H. Khan, A.V. Biradar, R.I. Kureshy, H.C. Bajaj // *ChemistrySelect.* — 2017. — Vol. 171, No. 2. — P. 9911–9919. <https://doi.org/10.1002/slct.201702196>.
- 10 Kornmuller A. Cucurbituril for water treatment. Part II: Ozonation and oxidative regeneration of cucurbituril / A. Kornmuller, S. Karcher, M. Jekel // *Water Res.* — 2001. — Vol. 35, No. 14. — P. 3317–3324. [https://doi.org/10.1016/S0043-1354\(01\)00039-2](https://doi.org/10.1016/S0043-1354(01)00039-2)
- 11 Assaf K.I. Cucurbiturils: from synthesis to high-affinity binding and catalysis / K.I. Assaf, W.M. Nau // *Chem. Soc. Rev.* — 2015. — Vol. 44. — P. 394–418. <https://doi.org/10.1039/C4CS00273C>
- 12 Barrow S.J. Cucurbituril-based molecular recognition / S.J. Barrow, S. Kasera, M.J. Rowland, J.del Barrio, O.A. Scherman // *Chem. Rev.* — 2015. — Vol. 115. — P. 12320–12406. <https://doi.org/10.1021/acs.chemrev.5b00341>
- 13 Isobe H. Ternary Complexes Between DNA, Polyamine, and Cucurbituril: A Modular Approach to DNA-Binding Molecules / H. Isobe, N. Tomita, J.W. Lee, H.-J. Kim, K. Kim, E. Nakamura, // *Angew. Chem. Int. Ed.* — 2000. — Vol. 39, No. 23. — P. 4257–4260. [https://doi.org/10.1002/1521-3773\(20001201\)39:23%3C4257::AID-ANIE4257%3E3.0.CO;2-6](https://doi.org/10.1002/1521-3773(20001201)39:23%3C4257::AID-ANIE4257%3E3.0.CO;2-6)
- 14 Chen C. Fabrication, characterization and adsorption properties of cucurbit[7]uril-functionalized polycaprolactone electrospun nanofibrous membranes / C. Chen, F. Liu, X. Zhang, Z. Zhao, S. Liu // *Beilstein J. Org. Chem.* — 2019. — Vol. 15. — P. 992–999. <https://doi.org/10.3762/bjoc.15.97>
- 15 Tuncel D. Cucurbituril-based Functional Materials / Eds.: D. Tuncel. — Royal Society of Chemistry. — London, 2019. — 303 p. <https://pubs.rsc.org/en/content/ebook/978-1-78801-488-5>.
- 16 Cong H. Synthesis and separation of cucurbit[n]urils and their derivatives / H. Cong, X. Ni, X. Xiao, Y. Huang, Q. Zhu, S. Xue, Z. Tao, L.F. Lindoy, G. Wei // *Org. Biomol. Chem.* — 2016. — Vol. 14. — P. 4335–4364. <https://doi.org/10.1039/C6OB00268D>.
- 17 Kim J. New Cucurbituril Homologues: Syntheses, Isolation, Characterization, and X-ray Crystal Structures of Cucurbit[n]uril (n = 5, 7, and 8) / J. Kim, I.S. Jung, S.Y. Kim, E. Lee, J.K. Kang, S. Sakamoto, K. Yamaguchi, K. Kim. // *J. Am. Chem. Soc.* — 2000. — Vol. 122. — P. 540–541. <https://doi.org/10.1021/ja993376p>
- 18 Day A. Controlling Factors in the Synthesis of Cucurbituril and Its Homologues / A. Day, A.P. Arnold, R.J. Blanch, B. Snushall // *The Journal of Organic Chemistry.* — 2001. — Vol. 66, No. 24. — P. 8094–8100. <https://doi.org/10.1021/jo015897c>.

- 19 Bardelang D. Cucurbit[n]urils (n = 5-8): A Comprehensive Solid State Study / D. Bardelang, K.A. Udachin, D.M. Leek, J.C. Margeson, G. Chan, C.I. Ratcliffe, J.A. Ripmeester // Cryst. Growth. Des. — 2011. — Vol. 11. — P. 5598–5614. <https://doi.org/10.1021/cg201173j>
- 20 Huang W.H. Cucurbit[n]uril Formation Proceeds by Step-Growth Cyclo-oligomerization / W.H. Huang, P.Y. Zavalij, L. Isaacs // Journal of the American Chemical Society. — 2008. — Vol. 130, No. 26. — P. 8446–8454. <https://doi.org/10.1021/ja8013693>
- 21 Patent WO2000068232A1 Australia. Cucurbiturils and method for synthesis / Day A.I., Arnold A.P., Blanch R.J. Publication date 16.11.2000. <https://patents.google.com/patent/WO2000068232A1/en>
- 22 Pansuriya A.M. One-pot synthesis of 5-carboxanilide-dihydropyrimidinones using etidronic Acid / A.M. Pansuriya, M.M. Savant, C.V. Bhuvu, J. Singh, Y.T. Naliapara // Arkivoc. — 2009. — No. 7. — P. 79–85. <https://doi.org/10.3998/ark.5550190.0010.707>
- 23 Vilapara K.V. Etidronic Acid Promoted Sequential One-Pot Strategy for the Synthesis of 1H-Imidazo[1,2-b]pyrazoles: A Green Catalyst for Groebke-Blackburn-Bienaymé Reaction / K.V. Vilapara, S.P. Gami, Sh.A. Gadara, Y.T. Naliapara // ChemistrySelect. — 2019. — Vol. 4. — P. 11235–11238. <https://doi.org/10.1002/slct.201902997>
- 24 Savant M.M. Etidronic Acid: a New and Efficient Catalyst for the Synthesis of Novel 5-Nitro-3,4-Dihydropyrimidin-2(1H)-Ones / M.M. Savant, A.M. Pansuriya, C.V. Bhuvu, N.P. Kapuriya, Y.T. Naliapara // Catal. Lett. — 2009. — Vol. 132, No. 1. — P. 281–284. <https://doi.org/10.1007/s10562-009-0112-y>
- 25 Panshina S. New Synthesis of 2,4,6,8-Tetramethyl-2,4,6,8-tetraazabicyclo[3.3.0]octane-3,7-dione Using Etidronic Acid as a “Green” Catalyst / S. Panshina, O.V. Ponomarenko, A. Bakibaev, V. Malkov // Russian Journal of Organic Chemistry. — 2020. — Vol. 56, No. 12. — P. 2067–2073. <https://doi.org/10.1134/S1070428020120039>
- 26 Кабачник М.И. Оксипропилендифосфоновая кислота и ее применение / М.И. Кабачник, Н.М. Дятлова, Т.Я. Медведь, Б.И. Бихман и др. // Химическая промышленность. — 1975. — № 4. — С. 254–258.
- 27 Дятлова Н.М. Комплексоны и комплексонаты металлов / Н.М. Дятлова, В.Я. Темкина, К.И. Попов. — М.: Химия, 1988. — 544 с.
- 28 Bakibaev A.A. Efficient Synthesis of Tetraacetylglucuril in the Presence of Phosphorus-Containing Catalysts / A.A. Bakibaev, S.Y. Panshina, N.F. Hoang, D.A. Kurgachev, A.E. Ukhov, V.S. Malkov, K.B. Zhumanov // Russian Journal of Organic Chemistry. — 2021. — Vol. 57, No 1. — P. 58–63. <https://doi.org/10.1134/S1070428021010085>

С.Ю. Паншина, А.А. Бакибаев, А.Н. Гусяков, В.С. Малков

## Кукурбит[6]урилдің синтезі 1-гидроксиэтан-1,1-дифосфон қышқылын «жасыл катализатор» ретінде пайдалану

Гетероциклді қосылыстар химиясында гликолурил (2,4,6,8-тетраазабицикло[3.3.0]октан-3,7-дион) және оның туындылары ерекше орын алады. Атап айтқанда, гликолурилдің макроциклді туындылары, кукурбит[n]урилдер, өзінің бірегей қасиеттеріне байланысты соңғы уақытта үлкен қызығушылық тудырды. Кукурбит[n]урилдер әдетте катализатор ретінде күшті минералды қышқылдарды пайдалана отырып, гликолурилдің параформальдегидпен конденсациялану реакциясы арқылы синтезделеді. Жакында бірқатар зерттеулер 1-гидроксиэтан-1,1-дифосфон қышқылының (ОЭДФ) гетероциклизация реакцияларында ыңғайлы «жасыл» катализатор екенін дәлелдеді. Бұл жұмыста сулы ортадағы «жасыл химия» катализаторы ретінде кукурбит[6]урил синтезінде 1-гидроксиэтан-1,1-дифосфон қышқылы алғаш рет қолданылған. Гликолурил мен параформальдегидтің катализатор ретінде екі эквивалентті 1-гидроксиэтан-1,1-дифосфон қышқылымен 1:2 қатынасында реакциясы жүргізілді, мұнда 25 % шығымда кукурбитурил гексамер ( $n = 6$ ) алынды. ОЭДФ қатысуымен гликолурилдің параформальдегидпен реакциясы кукурбит[6]урил синтезі үшін бәсекегеқабілетті әдіс ретінде пайдаланылуы мүмкін. Оқшауланған кукурбит[6]урил гексамеры ацетонмен өңделіп, «Қонақ-қожайын» әрекеттесуі арқылы қосылыс алынды. Алынған қосылыстардың құрылымы ЯМР және ИҚ спектроскопиясы арқылы дәлелденді. Кукурбит[6]урил гидратының оқшауланған кристалдарының фазалық құрамы ұнтақ рентгендік дифракциямен (РФТ) сипатталды. РФТ талдауы кристалдық тордың түрі мен 1-гидроксиэтан-1,1-дифосфон қышқы қатысуымен алынған кукурбит[6]урил гидрат кристалдарының фазалық құрамы классикалық әдістермен синтезделген кукурбит[6]урил гидратының кристалдарымен бірдей екенін көрсетті.

*Кілт сөздер:* кукурбит[6]урил, 1-гидроксиэтан-1,1-дифосфон қышқылы, гликолурил, параформальдегид, ЯМР, «жасыл» катализатор, олигомер, «Қонақ-қожайын» әрекеттесуі.

С.Ю. Паншина, А.А. Бакибаев, А.Н. Гусяков, В.С. Мальков

## Синтез кукурбит[6]урилы с использованием 1-гидроксиэтан-1,1-дифосфоновой кислоты в качестве «зеленого» катализатора

В химии гетероциклических соединений особое место занимают гликолурил (2,4,6,8-тетраазабицикло[3.3.0]октан-3,7-дион) и его производные. Особенно в последнее время наибольший интерес вызывают макроциклические производные гликолурилы — кукурбит[*n*]урилы, что связано с их уникальными свойствами. Кукурбит[*n*]урилы обычно синтезируют реакцией конденсации гликолурилы с параформальдегидом с использованием сильных минеральных кислот в качестве катализатора. Совсем недавно в ряде работ было показано, что 1-гидроксиэтан-1,1-дифосфоновая кислота (ОЭДФ) оказалась удобным «зеленым» катализатором в реакциях гетероциклизации. В настоящей работе нами впервые была использована 1-гидроксиэтан-1,1-дифосфоновая кислота в синтезе кукурбит[6]урилы в качестве катализатора «зеленой» химии в водной среде. Проведена реакция гликолурилы и параформальдегида в соотношении 1:2 с двумя эквивалентами 1-гидроксиэтан-1,1-дифосфоновой кислоты в качестве катализатора, где гексамер кукурбитурилы ( $n = 6$ ) получен с выходом 25 %. Реакцию гликолурилы с параформальдегидом в присутствии ОЭДФ можно использовать как конкурентный метод синтеза кукурбит[6]урилы. Выделенный гексамер кукурбит[6]урилы обрабатывали ацетоном, с получением соединения по типу взаимодействия «гость–хозяин». Строение полученных соединений доказано методами ЯМР и ИК-спектроскопии. Фазовый состав выделенных кристаллов кукурбит[6]урилы гидрата охарактеризован методом порошковой рентгенографии (РФА). РФА анализ показал, что тип кристаллической решетки и фазовый состав кристаллов гидрата кукурбит[6]урилы, полученных в присутствии ОЭДФ, идентичны кристаллам гидрата кукурбит[6]урилы, синтезируемым классическими методами.

**Ключевые слова:** кукурбит[6]урил; 1-гидроксиэтан-1,1-дифосфоновая кислота; гликолурил; параформальдегид; ЯМР; «зеленый» катализатор, олигомер, взаимодействия «гость–хозяин».

### References

- 1 Bakibaev, A. Uhov, A. Malkov, V. & Panshina, S. (2020). Synthesis of glycolurils and hydantoin by reaction of urea and 1,2-dicarbonyl compounds using etidronic acid as a “green catalyst”. *J. Heterocyclic Chem.*, 57, 4262–4270. <https://doi.org/10.1002/jhet.4132>
- 2 Beilfuss, W., Gradtko R., Krull I. & Steinhauer, K. (2006). Verwendung von Formaldehyd und Formaldehyd freisetzenden Verbindungen in einer Zusammensetzung zur Bekämpfung von Mykobakterien. Patent DE No 102004059041(A1). Munich, Germany: DE Deutsches Patent- und Markenamt.
- 3 Denk, A., Emter, A. & Moddick, C. (2001). Patent UK No. GB2354771(A). London, Great Britain: The Patent Office.
- 4 Bakibaev, A.A., Panshina, S.Yu., Ponomarenko, O.V., Malkov, V.S., Kotelnikov, O.A. & Tashenov, A.K. (2021). 1D and 2D NMR spectroscopy for identification of carbamide-containing biologically active compounds. *Bulletin of the university of Karaganda-Chemistry*, 101(1), 71–81. <https://doi.org/10.31489/2021Ch1/71-81>
- 5 Mashkovskii, M.D. (2005). *Lekarstvennye sredstva: posobie dlia vrachei [Medicines: a manual for doctors]*. — 15th ed. — Moscow: Novaia volna [in Russian].
- 6 Bakibaev, A.A., Yagovkin, A. Yu. & Vostretsov, S. N. (1998). Methods of synthesis of nitrogen-containing heterocycles using ureas and related compounds. *Russian Chemical Reviews*, 67 (4), 295–314. <https://doi.org/10.1070/rc1998v067n04abeh000295>
- 7 Havel, V., Babiak, M. & Sindelar, V. (2017). Modulation of Bambusuril Anion Affinity in Water. *Chemistry-A European Journal*, 23(37), 8963–8968. <https://doi.org/10.1002/chem.201701316>
- 8 Svec, J., Necas, M. & Sindelar, V. (2010). Bambus[6]uril. *Angewandte Chemie International Edition*, 122, 2428–2431. <https://doi.org/10.1002/anie.201000420>
- 9 Nandi, S. Patel, P. Jakhar, A. Khan, N.H. Biradar, A.V. Kureshy, R.I. & Bajaj, H. C. (2017). Cucurbit[6]uril-Stabilized Palladium Nanoparticles as a Highly Active Catalyst for Chemoselective Hydrogenation of Various Reducible Groups in Aqueous Media. *ChemistrySelect*, 171 (2), 9911–9919. <https://doi.org/10.1002/slct.201702196>.
- 10 Kornmuller, A. Karcher, S. & Jekel M. (2001) Cucurbituril for water treatment. Part II: Ozonation and oxidative regeneration of cucurbituril, *Water Res.*, 35(14), 3317–3324. [https://doi.org/10.1016/S0043-1354\(01\)00039-2](https://doi.org/10.1016/S0043-1354(01)00039-2)
- 11 Assaf, K.I., & Nau, W.M. (2015). Cucurbiturils: from synthesis to high-affinity binding and catalysis, *Chemical Society Reviews*, 44, 394–418. <https://doi.org/10.1039/C4CS00273C>
- 12 Barrow, S.J., Kasera, S., Rowland, M.J., del Barrio, J. & Scherman, O.A. (2015). Cucurbituril-Based Molecular Recognition. *Chemical Reviews*, 115(22), 12320–12406. <https://doi.org/10.1021/acs.chemrev.5b00341>
- 13 Isobe, H. Tomita, N., Lee, J.W., Kim, H. -J. Kim, K. & Nakamura, E. (2000) Ternary Complexes Between DNA, Polyamine, and Cucurbituril: A Modular Approach to DNA-Binding Molecules, *Angew. Chem. Int. Ed.*, 39(23), 4257–4260. [https://doi.org/10.1002/1521-3773\(20001201\)39:23<4257::aid-anie4257>3.0.co;2-6](https://doi.org/10.1002/1521-3773(20001201)39:23<4257::aid-anie4257>3.0.co;2-6)

- 14 Chen, C., Liu, F., Zhang, X., Zhao, Z. & Liu S. (2019). Fabrication, characterization and adsorption properties of cucurbit[7]uril-functionalized polycaprolactone electrospun nanofibrous membranes, *Beilstein J. Org. Chem.*, *15*, 992–999. <https://doi.org/10.3762/bjoc.15.97>
- 15 Tuncel, D. (2019) Cucurbituril-based Functional Materials. London: Royal Society of Chemistry. <https://pubs.rsc.org/en/content/ebook/978-1-78801-488-5>.
- 16 Cong, H., Ni, X., Xiao, X., Huang, Y., Zhu, Q., Xue, S., Tao, Z., Lindoy, L. F. Wei, G. (2016). Synthesis and separation of cucurbit[n]urils and their derivatives, *Org. Biomol. Chem.*, *14*, 4335–4364. <https://doi.org/10.1039/C6OB00268D>.
- 17 Kim, J., Jung, I.S., Kim, S.Y., Lee, E., Kang, J.K., Sakamoto, S., Yamaguchi, K. & Kim, K. J. (2000). New Cucurbituril Homologues: Syntheses, Isolation, Characterization, and X-ray Crystal Structures of Cucurbit[n]uril (n = 5, 7, and 8), *J. Kim, Am. Chem. Soc.*, *122*, 540–541. <https://doi.org/10.1021/ja993376p>
- 18 Day, A., Arnold, A.P., Blanch, R.J. & Snushall, B. (2001). Controlling Factors in the Synthesis of Cucurbituril and Its Homologues. *The Journal of Organic Chemistry*, *66*(24), 8094–8100. <https://doi.org/10.1021/jo015897c>
- 19 Bardelang, D., Udachin, K.A., Leek, D.M., Margeson, J.C., Chan, G., Ratcliffe, C.I. & Ripmeester, J.A. (2011) Cucurbit[n]urils (n = 5–8): A Comprehensive Solid State Study, *Cryst. Growth. Des.*, *11*, 5598–5614. <https://doi.org/10.1021/cg201173j>
- 20 Huang, W.H., Zavalij, P.Y. & Isaacs, L. (2008). Cucurbit[n]uril Formation Proceeds by Step-Growth Cyclo-oligomerization, *Journal of the American Chemical Society*, *130*(26), 8446–8454. <https://doi.org/10.1021/ja8013693>
- 21 Day, A.I., Arnold, A.P., Blanch, R.J. (2002). Patent AU No WO2000068232(A1). Sydney, Australia: Freehills Carter Smith & Beadle. <https://patents.google.com/patent/WO2000068232A1/en>
- 22 Pansuriya, A.M. Savant, M.M., Bhuva, C.V., Singh, J. & Naliapara Y.T. (2009). One-pot synthesis of 5-carboxanilide-dihydropyrimidinones using etidronic Acid, *Arkivoc*, *7*, 79–85. <https://doi.org/10.3998/ark.5550190.0010.707>
- 23 Vilapara, K.V., Gami, S.P., Gadara, Sh.A., & Naliapara, Y.T. (2019). Etidronic Acid Promoted Sequential One-Pot Strategy for the Synthesis of 1H-Imidazo[1,2-b]pyrazoles: A Green Catalyst for Groebke-Blackburn-Bienaymé Reaction, *ChemistrySelect*, *4*, 11235–11238. <https://doi.org/10.1002/slct.201902997>
- 24 Savant, M.M., Pansuriya, A.M., Bhuva, C.V., Kapuriya, N.P. & Naliapara, Y.T. (2009). Etidronic Acid: a New and Efficient Catalyst for the Synthesis of Novel 5-Nitro-3,4-Dihydropyrimidin-2(1H)-Ones, *Catal. Lett.*, *132*(1), 281–284. <https://doi.org/10.1007/s10562-009-0112-y>
- 25 Panshina, S., Ponomarenko, O., Bakibaev, A., Malkov, V. (2020) New Synthesis of 2,4,6,8-Tetramethyl-2,4,6,8-tetraazabicyclo[3.3.0]octane-3,7-dione Using Etidronic Acid as a “Green” Catalyst. *Russian Journal of Organic Chemistry*, *56*(12), 2067–2073. <https://doi.org/10.1134/S1070428020120039>
- 26 Kabachnik, M.I., Dyatlova, N.M., Medved, T.Ya., & Bikhman, B.I. et al. (1975). Oksietilendifosfonovaya kislota i ee primeneniye [Oxyethylenediphosphonic acid and its application]. *Khimicheskaya promyshlennost — Chemical industry*, *4*, 254–258 [in Russian].
- 27 Dyatlova, N.M., Temkina, V.Ya., & Popov, K.I. (1988). *Kompleksy i kompleksonaty metallov [Complexones and complexonates of metals]*. Moscow: Khimiia [in Russian].
- 28 Bakibaev, A.A., Ukhov, A.E., Malkov, V.S., Zhumanov, K.B. (2021) Efficient Synthesis of Tetraacetylglucosyluril in the Presence of Phosphorus-Containing Catalysts. *Russian Journal of Organic Chemistry*, *57*(1), 58–63. <https://doi.org/10.1134/S1070428021010085>

#### Information about authors\*

**Panshina, Svetlana Yur’evna** — (*corresponding author*) Postgraduate of chemistry specialty, Department of Organic Chemistry and Polymers, Karagandy University of the name of academician E.A. Buketov, Universitetskaya street, 28, 100024, Karaganda, Kazakhstan; e-mail: [janim\\_svetatusik@mail.ru](mailto:janim_svetatusik@mail.ru); <https://orcid.org/0000-0001-6824-2645>

**Bakibaev, Abdigali Abdimanapvich** — Doctor of Chemical Sciences, Professor, Leading Researcher of the Laboratory of Organic Synthesis, National Research Tomsk State University, Lenin str., 36, 634050, Tomsk, Russia; e-mail: [bakibaev@mail.ru](mailto:bakibaev@mail.ru); <https://orcid.org/0000-0002-3335-3166>

**Guslyakov, Alexey Nikolaevich** — 1<sup>st</sup> year PhD student, Laboratory of Organic Synthesis, National Research Tomsk State University, Lenin str., 36, 634050, Tomsk, Russia; e-mail: [guslyakov.aleksej@bk.ru](mailto:guslyakov.aleksej@bk.ru); <https://orcid.org/0000-0001-8807-8766>

**Malkov, Victor Sergeevich** — Candidate of Chemical Sciences, Head of the Laboratory of Organic Synthesis, National Research Tomsk State University, Lenin str., 36, 634050, Tomsk, Russia; e-mail: [malkov.vics@gmail.com](mailto:malkov.vics@gmail.com); <https://orcid.org/0000-0003-4532-2882>

\*The author's name is presented in the order: *Last Name, First and Middle Names*

Article

Received: 22 August 2022 | Revised: 7 November 2022 | Accepted: 15 November 2022 | Published online: 25 November 2022

UDC 541.64+678.744

<https://doi.org/10.31489/2022Ch4/4-22-15>

A.Ye. Ayazbayeva<sup>1,2\*</sup>, A.V. Shakhvorostov<sup>1</sup>, S.E. Kudaibergenov<sup>1</sup>

<sup>1</sup>*Institute of Polymer Materials and Technology, Almaty, Kazakhstan;*

<sup>2</sup>*Satbayev University, Almaty, Kazakhstan*

(\*Corresponding author's e-mail: [ayazbayeva.aigerim@gmail.com](mailto:ayazbayeva.aigerim@gmail.com))

## Temperature and Salt Responsivity of Anionic, Cationic and Amphoteric Nanogels Based on N-Isopropylacrylamide, 2-Acrylamido-2-Methyl-1-Propanesulfonic Acid Sodium Salt and (3-Acrylamidopropyl) Trimethylammonium Chloride

Three different nanogels possessing anionic, cationic and amphoteric character were synthesized via conventional redox initiated free radical copolymerization of N-isopropylacrylamide (NIPAM), 2-acrylamido-2-methyl-1-propanesulfonic acid sodium salt (AMPS) and (3-acrylamidopropyl) trimethylammonium chloride (APTAC). The negatively charged [NIPAM]:[AMPS] = 90:10 mol.%, positively charged [NIPAM]:[APTAC] = 90:10 mol.%, and charge-balanced amphoteric nanogels [NIPAM]:[APTAC]:[AMPS] = 90:5:5 mol.% abbreviated as NIPAM<sub>90</sub>-AMPS<sub>10</sub>, NIPAM<sub>90</sub>-APTAC<sub>10</sub>, and NIPAM<sub>90</sub>-APTAC<sub>5</sub>-AMPS<sub>5</sub>, respectively, were characterized by FTIR spectroscopy, TGA, UV-Vis spectroscopy and DLS measurements. The temperature and salt responsive properties of nanogels in aqueous and aqueous-salt solutions were studied in the temperature range of 25–60 °C and ionic strength ( $\mu$ ) of 0.001–1.0 M NaCl. Anionic NIPAM<sub>90</sub>-AMPS<sub>10</sub> and cationic NIPAM<sub>90</sub>-APTAC<sub>10</sub> nanogels, exhibit a pronounced polyelectrolyte effect in aqueous-salt solution due to screening of the negative or positive charges by low-molecular-weight salt. Whereas the charge-balanced amphoteric nanogel NIPAM<sub>90</sub>-APTAC<sub>5</sub>-AMPS<sub>5</sub> exhibits an antipolyelectrolyte effect due to the screening of electrostatic attraction between opposite charges by low-molecular-weight salt. The difference between the temperature-dependent behaviors of anionic, cationic and amphoteric nanogels is explained by shrinking (polyelectrolyte effect) and expanding (antipolyelectrolyte effect) of macromolecular chains in aqueous-salt solutions.

**Keywords:** polyampholyte nanogels, poly-N-isopropylacrylamide, ionic monomers, volume phase transition temperature, amphoteric nanogel, anionic nanogel, cationic nanogel.

### Introduction

Nanogels are three-dimensional structures that have the properties of both nanomaterials and hydrogels [1]. The main advantages of nanogels are their small size (from 1 to 100 nm), high degree of swelling in water, high stability, biodegradability, adjustable toxicity, stimuli-sensitivity etc. [2–6].

Thermoresponsive nanogels respond to changes in ambient temperature. The temperature at which the nanogel acquires the largest and sharpest change in hydrodynamic diameter due to swelling/deswelling is called the volume phase transition temperature (VPTT). Nanogel swells in water at temperatures below VPTT, and shrinks at temperatures above VPTT [7, 8]. Hydrophobic fragments attached as side chains in the main chain impart thermoresponsive properties to the nanogel [1]. For example, Judah et. al. synthesized nanogels based on NIPAM, N-hydroxyethylacrylamide and N-acryloyl-L-proline by high dilution radical polymerization using DMSO as a solvent. The temperature-responsive properties have been studied in various buffer media and their dependence on the chemical structure of the polymer network has been proven. A slight change in the chemical structure of the side chains of monomers from branched isopropyl groups to linear propyl groups leads to a decrease in the VPTT value by about 10°C [9].

The most common thermoresponsive polymer is poly-N-isopropylacrylamide (PNIPAM), which contains in structure hydrophilic amide and hydrophobic isopropyl groups [10]. NIPAM-based nanogels can be modified by incorporating various comonomers and cross-linking agents, which can reduce or increase VPTT [11]. Copolymerization of NIPAM and various ionic monomers makes it possible to obtain thermoresponsive nanogels with increased VPTT [12, 13]. It is possible to control the VPTT and use the resulting nanogels for controlled drug release by modifying a PNIPAM-based nanogel with different amounts of

acrylic acid (AAc) [14]. The PNIPAM-co-AAc nanogels showed two volume phase transitions and the VPTT increased with AAc content.

The authors [15] describe the synthesis of thermoresponsive nanogels based on NIPAM and allylacetic acid (AAA) by radical polymerization. The DLS data at various pH values demonstrate that the phase transition temperature of the microgel shifts towards higher temperatures with an increase in the amount of comonomer AAA.

Zhou et. al. synthesized nanogels based on NIPAM and strongly ionic 2-acrylamido-2-methyl-1-propanesulfonic acid sodium salt (AMPS) by precipitation polymerization in the presence of Fe<sub>3</sub>O<sub>4</sub>. The resulting nanogels have thermoresponsive and paramagnetic properties, which allows them to be used as draw agents in forward osmosis [16].

In general, despite the progress in the field of synthesis and study of stimuli-responsive polymers, information on comparative study of thermo- and salt responsive polyelectrolyte and polyampholyte nanogels is limited. This article describes the synthesis and characterization of anionic, cationic and amphoteric nanogels based on N-isopropylacrylamide (NIPAM), (3-acrylamidopropyl) trimethylammonium chloride (APTAC) and 2-acrylamido-2-methyl-1-propanesulfonic acid sodium salt (AMPS). The volume phase transition behavior of nanogels was studied in aqueous and aqueous-salt solutions depending on the charge of ionic monomers.

## Experimental

### Materials

The following chemicals were used: N-isopropylacrylamide (NIPAM, 97 % purity), 2-acrylamido-2-methylpropanesulfonic acid sodium salt (AMPS, 50 wt.%) and (3-acrylamidopropyl) trimethylammonium chloride (APTAC, 75 wt.%) as monomers; ammonium persulfate (APS, 98 % purity) and sodium metabisulfite (SMBS, 97 % purity) as redox initiator; sodium dodecyl sulfate (SDS, 99 % purity) as surfactant; N,N-methylenebis(acrylamide) (MBAA, 99 % purity) as crosslinking agent; sodium chloride (NaCl) and dialysis tubing cellulose membrane (12–14 kDa) as further materials. All chemicals were purchased from Sigma-Aldrich Chemical Co. and used as received.

### Methods

#### Synthesis of nanogels based on NIPAM, APTAC and AMPS

Nanogels NIPAM<sub>90</sub>-APTAC<sub>10</sub>, NIPAM<sub>90</sub>-AMPS<sub>10</sub> and NIPAM<sub>90</sub>-APTAC<sub>5</sub>-AMPS<sub>5</sub> were synthesized via conventional redox initiated free radical copolymerization.

The required amounts of monomers (NIPAM, APTAC and (or) AMPS), MBAA and SDS, listed in Table 1 were dissolved in deionized water with constant stirring. Further, the required amount of APS/SMBS redox system was added to the solution and stirred until complete dissolution. The solution with dissolved monomers, crosslinking agent, surfactant and redox system was transferred to a round bottom flask and heated on a water bath. Free radical copolymerization was carried out at 80 °C for 4 h in an inert atmosphere with constant stirring of the solution. The resulting solutions of nanogels of the indicated compositions were dialyzed against deionized water for 14 days to remove unreacted residues.

Table 1

Ratios of NIPAM, APTAC and AMPS for nanogels synthesis

Nanogel sample	NIPAM, g	APTAC, g	AMPS, g	APS, mg	MBAA, g	SMBS, mg	SDS, g	H <sub>2</sub> O, mL	Yield, wt.%
NIPAM <sub>90</sub> -APTAC <sub>10</sub>	0.83	0.225	–	50	0.125	10	0.35	97	90
NIPAM <sub>90</sub> -AMPS <sub>10</sub>	0.815	–	0.367	30	0.123		0.23	97.5	72
NIPAM <sub>90</sub> -APTAC <sub>5</sub> -AMPS <sub>5</sub>	0.735	0.099	0.165	30	0.11		0.23	98.5	70

**FTIR spectroscopy.** Chemical structure of nanogels was characterized using Cary 660 FTIR spectroscopy (Agilent, USA). Before measurements, nanogels were freeze-dried for 24 h until moisture was removed. The FTIR spectra were measured at room temperature within the 700–4000 cm<sup>-1</sup> wavenumber range.

**TGA analysis.** Thermogravimetric analysis of nanogels was carried out using LabSys Evo device (Setaram, France) in the temperature range 25–500 °C (heating rate is 10 °C·min<sup>-1</sup>) in an inert atmosphere. The maximum decomposition temperature of the nanogels was determined from the differential thermal analysis (DTA) curve.

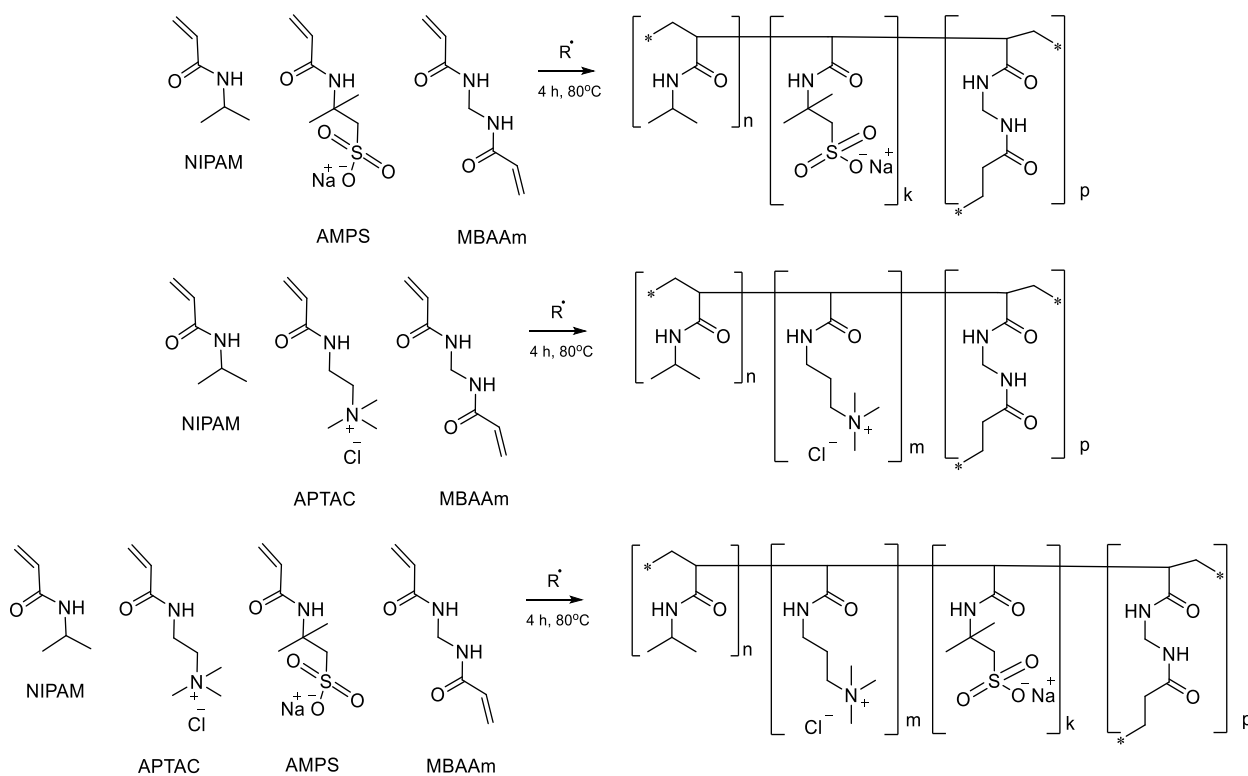
*VPTT determination for NIPAM<sub>90</sub>-APTAC<sub>10</sub>, NIPAM<sub>90</sub>-AMPS<sub>10</sub> and NIPAM<sub>90</sub>-APTAC<sub>5</sub>-AMPS<sub>5</sub> nanogels in aqueous and aqueous-salt solutions.* The method for determining the volume phase transition temperature was described in our previous studies [17, 18]. Experiments were carried out at  $\lambda = 700$  nm at a nanogel concentration of 0.1 wt.%, in the temperature range of 25–60 °C (0.5 °C·min<sup>-1</sup> heating rate). The VPTT of NIPAM<sub>90</sub>-AMPS<sub>10</sub>, NIPAM<sub>90</sub>-APTAC<sub>10</sub> and NIPAM<sub>90</sub>-APTAC<sub>5</sub>-AMPS<sub>5</sub> nanogels in NaCl solutions with  $\mu = 0.001$ ; 0.01; 0.1; 0.5 and 1 M corresponds to the minimum points on the DTA curves.

*DLS measurements.* Dynamic Light Scattering (DLS) data were obtained using Zetasizer Nano ZS 90 (Malvern, UK) with a 633 nm laser beam. The mean hydrodynamic radius ( $R_h$ ) was measured in a 0.1 wt.% solution of nanogels in the temperature range from 25 to 60 °C with an interval of 5 °C and at  $\mu = 0.001$ ; 0.1 and 1 M NaCl.

### Results and Discussion

*Synthesis and characterization of NIPAM<sub>90</sub>-AMPS<sub>10</sub>, NIPAM<sub>90</sub>-APTAC<sub>10</sub> and NIPAM<sub>90</sub>-APTAC<sub>5</sub>-AMPS<sub>5</sub> nanogels*

The NIPAM<sub>90</sub>-AMPS<sub>10</sub>, NIPAM<sub>90</sub>-APTAC<sub>10</sub> and NIPAM<sub>90</sub>-APTAC<sub>5</sub>-AMPS<sub>5</sub> nanogels were synthesized *via* conventional redox initiated free radical copolymerization (Scheme 1).



Scheme 1. Nanogels synthesized by free radical copolymerization of NIPAM, APTAC and AMPS monomers in the presence of MBAA

The NIPAM<sub>90</sub>-AMPS<sub>10</sub> and NIPAM<sub>90</sub>-APTAC<sub>10</sub> nanogels contain either anionic or cationic monomers; NIPAM<sub>90</sub>-AMPS<sub>10</sub> is negatively charged, while NIPAM<sub>90</sub>-APTAC<sub>10</sub> is positively charged. The NIPAM<sub>90</sub>-APTAC<sub>5</sub>-AMPS<sub>5</sub> nanogel has an equal molar ratio of cationic (APTAC) and anionic (AMPS) monomers, therefore, it belongs to charge-balanced nanogel.

*FTIR analysis of the NIPAM<sub>90</sub>-AMPS<sub>10</sub>, NIPAM<sub>90</sub>-APTAC<sub>10</sub> and NIPAM<sub>90</sub>-APTAC<sub>5</sub>-AMPS<sub>5</sub> nanogels*

Figure 1 shows the FTIR spectra of the NIPAM<sub>90</sub>-APTAC<sub>10</sub>, NIPAM<sub>90</sub>-AMPS<sub>10</sub> and NIPAM<sub>90</sub>-APTAC<sub>5</sub>-AMPS<sub>5</sub> nanogels. The broad absorption band in the region of 3290–3500 cm<sup>-1</sup> corresponds to the secondary and tertiary amine groups, and the absorption bands in the region of 2800–3000 cm<sup>-1</sup> correspond to the asymmetric and symmetric vibrations of CH groups. Intensive peaks at  $\nu = 1640$  and 1540 cm<sup>-1</sup> belong to N-substituted groups (amide I and amide II). The S=O groups containing in AMPS fragments are detected at  $\nu = 1040$  cm<sup>-1</sup>.

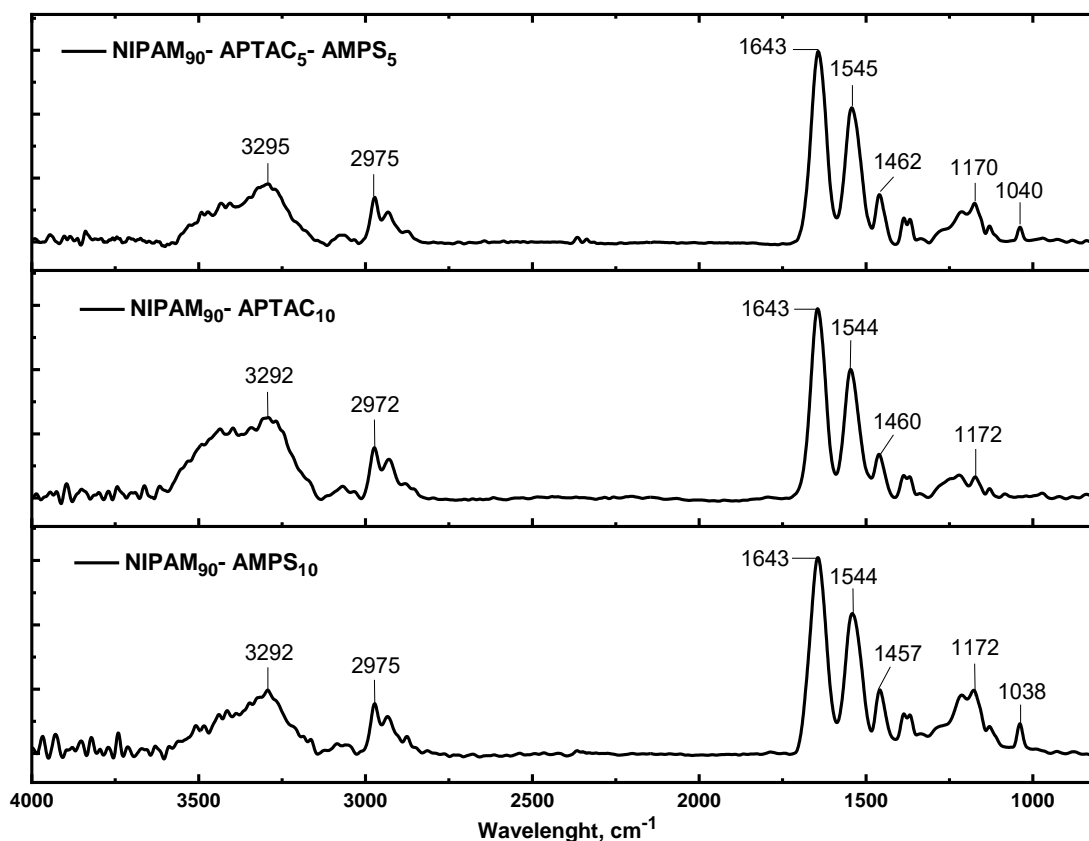


Figure 1. FTIR spectra of the NIPAM<sub>90</sub>-APTAC<sub>10</sub>, NIPAM<sub>90</sub>-AMPS<sub>10</sub> and NIPAM<sub>90</sub>-APTAC<sub>5</sub>-AMPS<sub>5</sub> nanogels

*TGA and DTA data of the NIPAM<sub>90</sub>-AMPS<sub>10</sub>, NIPAM<sub>90</sub>-APTAC<sub>10</sub> and NIPAM<sub>90</sub>-APTAC<sub>5</sub>-AMPS<sub>5</sub> nanogels*

Figure 2 shows the thermogravimetric and differential thermal analysis data for nanogels from which 3 regions can be defined.

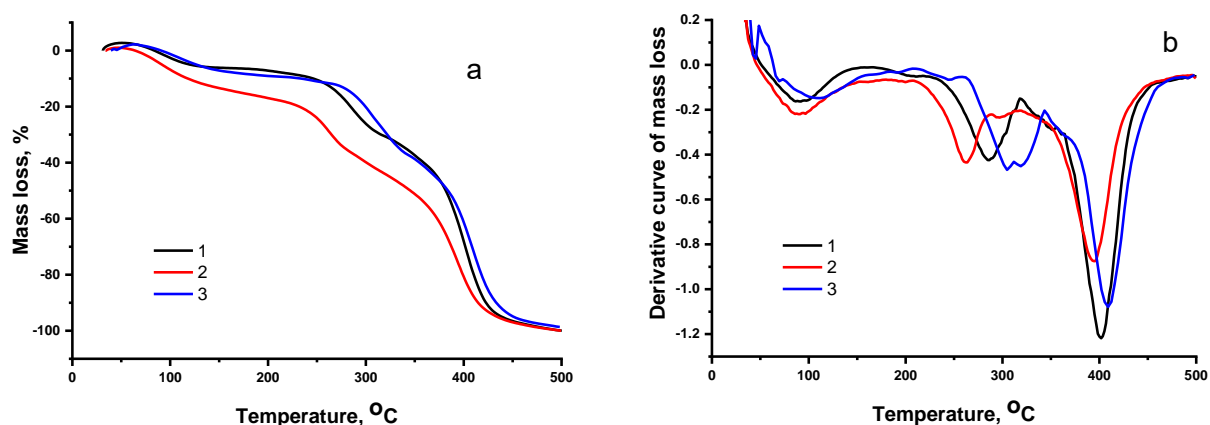


Figure 2. (a) TGA and (b) DTA curves of (1) NIPAM<sub>90</sub>-AMPS<sub>10</sub>; (2) NIPAM<sub>90</sub>-APTAC<sub>10</sub>; (3) NIPAM<sub>90</sub>-APTAC<sub>5</sub>-AMPS<sub>5</sub> nanogels

The sample mass is lost at >100 °C, probably due to the evaporation of physically adsorbed moisture. The weight loss between 250–300 °C is probably due to the decomposition of NIPAM fragments. Complete thermal decomposition of nanogels occurs in the temperature range of 410–420 °C. The thermal stability of nanogels changes in the following order: NIPAM<sub>90</sub>-APTAC<sub>5</sub>-AMPS<sub>5</sub> > NIPAM<sub>90</sub>-AMPS<sub>10</sub> > NIPAM<sub>90</sub>-APTAC<sub>10</sub>. This demonstrates that the charge-balanced nanogel is more stable than the anionic and cationic ones.

*Volume Phase Transition Behavior (VPTB) of NIPAM<sub>90</sub>-AMPS<sub>10</sub> and NIPAM<sub>90</sub>-APTAC<sub>10</sub> nanogels in aqueous and aqueous-salt solutions*

Figures 3, 4 show the effect of temperature and salt additive on the phase behavior of the anionic NIPAM<sub>90</sub>-AMPS<sub>10</sub> and cationic NIPAM<sub>90</sub>-APTAC<sub>10</sub> nanogels. Since the NIPAM<sub>90</sub>-AMPS<sub>10</sub> and NIPAM<sub>90</sub>-APTAC<sub>10</sub> nanogels are anionic and cationic polyelectrolytes, the addition of a salt leads to the screening of electrostatic repulsion between uniformly charged groups respectively. As a result, the macromolecular chains tend to shrink. However, there are no changes in the phase behavior of the NIPAM<sub>90</sub>-AMPS<sub>10</sub> nanogel and the transmittance remain constant at ionic strengths  $\mu = 0.001-0.01$  M. Only starting from  $\mu = 0.1$  M NaCl the polyelectrolyte effect is suppressed and the value of VPTT is equal to 42.1 °C (Fig. 3, Table 2). As a further increase in the ionic strength to  $\mu = 0.5$  and 1 M NaCl, the VPTT values of NIPAM<sub>90</sub>-AMPS<sub>10</sub> decrease and amount to 36.2 and 31.3 °C, respectively. The VPTT value at  $\mu = 1$  M is less than the LCST of pure PNIPAM, which is ~33 °C. It is likely that, at high NaCl concentrations, the screening of electrostatic repulsion between negatively charged AMPS groups is so effective that the phase behavior and solubility of NIPAM<sub>90</sub>-AMPS<sub>10</sub> nanogel is determined by NIPAM<sub>90</sub> fragments. In case of NIPAM<sub>90</sub>-APTAC<sub>10</sub> nanogel the ionic strength in the range of  $\mu = 0.001-0.1$  M NaCl does not significantly change the phase behavior of the NIPAM<sub>90</sub>-APTAC<sub>10</sub> nanogel and the values of VPTT are equal to 46.4, 47.7, and 45.2 °C, respectively (Fig. 4, Table 2). Even further increase of the ionic strength up to  $\mu = 0.5$  and 1 M slightly changes the solubility and phase behavior of the NIPAM<sub>90</sub>-APTAC<sub>10</sub> nanogel. This is probably due to the stronger polyelectrolyte character of NIPAM<sub>90</sub>-APTAC<sub>10</sub> nanogel compared to NIPAM<sub>90</sub>-AMPS<sub>10</sub> and its less salt-sensitivity. An increase in temperature enhances inter- and intramolecular hydrophobic interactions between NIPAM<sub>90</sub> fragments, thereby causing a shift in the VPTT towards lower temperatures, that are equal to 41.8 and 35.9 °C, respectively.

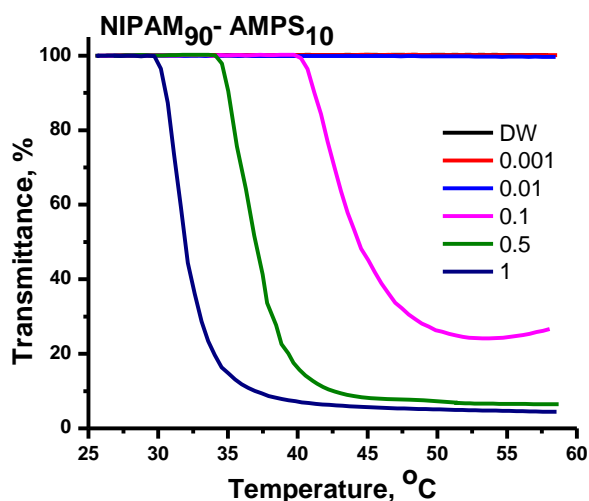


Figure 3. Effect of temperature and ionic strength ( $\mu$ ) on transmittance of NIPAM<sub>90</sub>-AMPS<sub>10</sub> nanogel

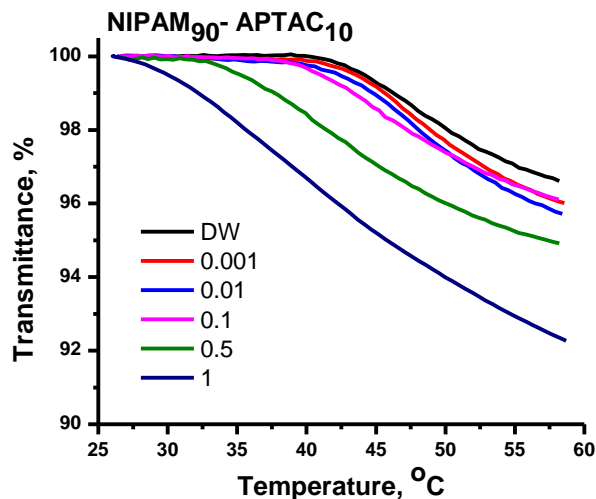


Figure 4. Effect of temperature and ionic strength ( $\mu$ ) on transmittance of NIPAM<sub>90</sub>-APTAC<sub>10</sub> nanogel

Table 2

**The effect of the ionic strength on the volume phase transition temperature of NIPAM<sub>90</sub>-AMPS<sub>10</sub>, NIPAM<sub>90</sub>-APTAC<sub>10</sub> and NIPAM<sub>90</sub>-APTAC<sub>5</sub>-AMPS<sub>5</sub> nanogels**

Nanogel	Ionic strength, $\mu$ , mol·L <sup>-1</sup> (NaCl)					
	0	0.001	0.01	0.1	1.0	
Volume phase transition temperature, VPTT, °C						
NIPAM <sub>90</sub> -AMPS <sub>10</sub>	–	–	–	42.1	36.2	31.3
NIPAM <sub>90</sub> -APTAC <sub>10</sub>	48	46.4	47.7	45.2	41.8	35.9
NIPAM <sub>90</sub> -APTAC <sub>5</sub> -AMPS <sub>5</sub>	40.4	39.2	40.4	47.8	45.1	38.3

Thus, NIPAM<sub>90</sub>-AMPS<sub>10</sub> and NIPAM<sub>90</sub>-APTAC<sub>10</sub> nanogels exhibit a strong polyelectrolyte effect and only at higher ionic strength  $\mu > 0.1$  M NaCl the polyelectrolyte effect is suppressed due to screening of the electrostatic repulsion between uniformly charged groups by low-molecular-weight electrolytes.

*Volume Phase Transition Behavior (VPTT) of charge-balanced NIPAM<sub>90</sub>-APTAC<sub>5</sub>-AMPS<sub>5</sub> nanogel in aqueous-salt solutions*

Figure 5 shows the effect of temperature and ionic strength on the phase behavior of the charge-balanced NIPAM<sub>90</sub>-APTAC<sub>5</sub>-AMPS<sub>5</sub> nanogel. At ionic strengths equal to  $\mu = 0.001$  and  $0.01$ , the phase transition temperatures are equal to  $39.2$  °C and  $40.4$  °C and shift towards higher temperatures, respectively. The reason for this phenomenon is the demonstration of the antipolyelectrolyte effect, in which there is a gradual destruction of ionic contacts between the APTAC and AMPS monomers due to the screening of the electrostatic attraction between oppositely charged fragments by low-molecular-weight salts. The antipolyelectrolyte effect is characterized by the unfolding (swelling) of macromolecules of charge-balanced polyampholytes in a quasi-neutral state in a low-molecular-weight salt solution due to screening of the electrostatic attraction of oppositely charged fragments.

A further increase in ionic strength shifts the VPTT to maximal value  $47.8$  °C at  $\mu = 0.1$  M. The VPTT values decrease to  $45.1$  and  $38.3$  °C at  $\mu = 0.5$  and  $1$  M respectively. At extremely high ionic strengths ( $\mu = 0.5$  and  $1$  M), the charged macromolecules approach neutrality due to a sufficient number of counterions, therefore, complete screening of opposite charges. In addition, probably there is a “salting out” effect of ionic groups, which leads to a decrease of VPTT. Under these conditions, NIPAM<sub>90</sub> fragments determine the solubility and phase behavior of the charge-balanced NIPAM<sub>90</sub>-APTAC<sub>5</sub>-AMPS<sub>5</sub> nanogel.

It should be noted that at  $\mu > 0.1$  M, a smaller change in the turbidity of the NIPAM<sub>90</sub>-APTAC<sub>5</sub>-AMPS<sub>5</sub> solution observed than when the nanogel is in solutions with a lower concentration of salt. This is due to the dependence of light scattering on the size, density of individual particles and the increase in temperature at which particles stick together, hence the change in transmittance.

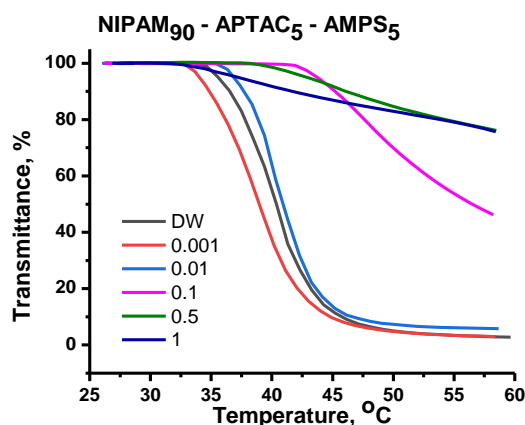


Figure 5. Effect of temperature and ionic strength ( $\mu$ ) on transmittance of the nanogel NIPAM<sub>90</sub>-APTAC<sub>5</sub>-AMPS<sub>5</sub>

Thus, the addition of a low-molecular-weight salt promotes an increase in the hydrophilicity of ionic groups of the charge-balanced NIPAM<sub>90</sub>-APTAC<sub>5</sub>-AMPS<sub>5</sub> nanogel due to the antipolyelectrolyte effect, as well as an increase in the hydrophobicity of NIPAM due to enhancement of inter- and intramolecular hydrophobic interactions. An increase in temperature reduces the quality of water in relation to NIPAM<sub>90</sub> fragments, causing phase separation.

*The mean hydrodynamic radius ( $R_h$ ) of NIPAM<sub>90</sub>-AMPS<sub>10</sub> and NIPAM<sub>90</sub>-APTAC<sub>10</sub> nanogels in aqueous-salt solutions*

The mean hydrodynamic radius was measured in a  $0.1$  wt.% solution of NIPAM<sub>90</sub>-AMPS<sub>10</sub> and NIPAM<sub>90</sub>-APTAC<sub>10</sub> nanogels in the temperature range from  $25$  to  $50$  °C with an interval of  $5$  °C in *deionized* water and in NaCl solutions with  $\mu = 0.001$ ;  $0.1$  and  $1$  M.

The dependence of the average hydrodynamic particle size of the NIPAM<sub>90</sub>-AMPS<sub>10</sub> nanogel on temperature and ionic strength is shown in Figure 6. It was previously described that the ionic strength equal to  $\mu = 0.001$  M does not affect the phase behavior of the nanogel, the transmittance remains constant (Fig. 3). Therefore, an increase of temperature does not affect the nanogel particle size, in the temperature range of

25–50 °C in 0.001 M NaCl solution  $R_h$  is  $\sim 10\text{--}20(\pm 1)$  nm (Fig. 6a). At  $\mu = 0.1$  M and temperatures of 25–35 °C, there are particles with sizes of  $\sim 12(\pm 0.5)$ ,  $60(\pm 1)$  and  $100(\pm 5)$  nm (Fig. 6b). The VPTT of the nanogel in a 0.1 M NaCl solution is 42.1 °C (Table 2); upon reaching 40 °C, in addition to particles with a size of  $\sim 12(\pm 0.5)$  nm, the aggregation of nanogel particles is observed and  $R_h$  increases up to  $300(\pm 5)$  nm. At 45 and 50 °C, the  $R_h$  particle size is  $\sim 250(\pm 2)$  and  $300(\pm 5)$  nm, respectively.

At 25 °C and ionic strength  $\mu = 1$  M, the particle size is  $\sim 15(\pm 1)$  nm (Fig. 6c). Raising the temperature to 30 °C causes the aggregation of nanoparticles and their size  $R_h$  is  $240(\pm 5)$  nm. The VPTT of the NIPAM<sub>90</sub>-AMPS<sub>10</sub> nanogel in 1 M NaCl is 31.3 °C (Table 2), therefore, an increase in size up to  $\sim 550(\pm 10)$  nm at 35–40 °C is observed. A further increase in temperature to 45–50 °C leads to a decrease in the particle size to  $310\text{--}420(\pm 5)$  nm; probably, the formed nanogel aggregates begin to shrink.

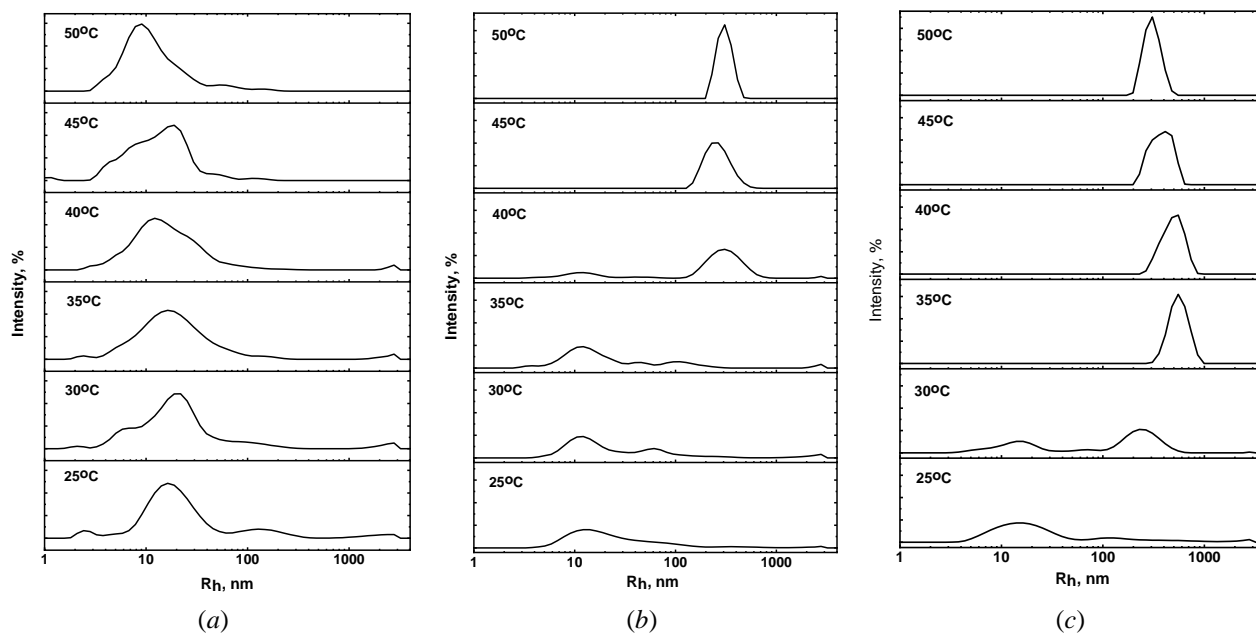


Figure 6. Effect of temperature and ionic strength ( $\mu$ ) on the mean hydrodynamic radius ( $R_h$ ) of NIPAM<sub>90</sub>-AMPS<sub>10</sub> at  $\mu =$  (a) 0.001, (b) 0.1 and (c) 1.0

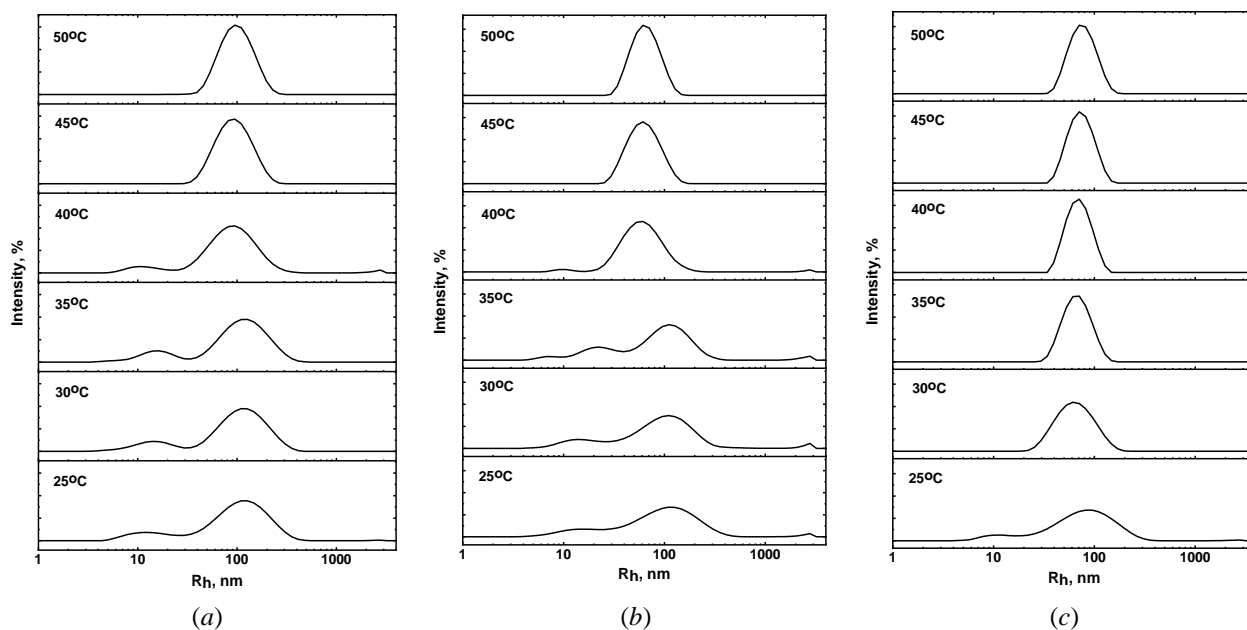


Figure 7. Effect of temperature and ionic strength ( $\mu$ ) on the mean hydrodynamic radius ( $R_h$ ) of NIPAM<sub>90</sub>-APTAC<sub>10</sub> at  $\mu =$  (a) 0.001, (b) 0.1 and (c) 1.0

The effect of temperature and salt additive on the average hydrodynamic particle size of the NIPAM<sub>90</sub>-APTAC<sub>10</sub> nanogel is shown in Figure 7. At ionic strength  $\mu = 0.001$  and  $0.1$  M and in the temperature range of  $25$ – $35$  °C, the particle size  $R_h$  is  $\sim 15(\pm 2)$ ,  $115(\pm 5)$  nm (Fig. 7a, 7b). An increase of temperature to  $40$  °C leads to a decrease in the size of  $R_h$  particles to  $\sim 10(\pm 0.5)$  and  $60(\pm 5)$  nm. At  $45$  and  $50$  °C, temperatures close to VPTT (Table 2), the particle size distribution becomes monomodal and have values  $\sim 95(\pm 1)$  nm in  $0.001$  M NaCl solution and  $\sim 60(\pm 1)$  nm in  $0.01$  M. In solutions with ionic strength  $\mu = 1$  M at room temperature, the  $R_h$  is  $\sim 10(\pm 0.5)$  and  $90(\pm 0.5)$  nm (Fig. 7c). With a further increase in temperature from  $30$  to  $50$  °C, the average  $R_h$  values are in the range of  $60$ – $70$  ( $\pm 5$ ) nm; therefore, at temperatures close to the VPTT, no significant changes in size occur.

*The mean hydrodynamic radius ( $R_h$ ) of NIPAM<sub>90</sub>-APTAC<sub>5</sub>-AMPS<sub>5</sub> nanogel in aqueous and aqueous-salt solutions*

The mean hydrodynamic size of NIPAM<sub>90</sub>-APTAC<sub>5</sub>-AMPS<sub>5</sub> was measured in a  $0.1$  wt.% solution of nanogel in the temperature range from  $25$  to  $50$  °C with an interval of  $5$  °C in *deionized* water and in NaCl solutions with  $\mu = 0.001$ ;  $0.1$  and  $1$  M (Fig. 8).

A particle size of  $\sim 18(\pm 1)$  nm is observed in solution with an ionic strength of  $\mu = 0.001$  M at  $25$  °C (Fig. 8a). An increase in the ionic strength to  $\mu = 0.1$  and  $1$  M leads to the appearance of particles with sizes of  $\sim 10$ ,  $45$  and  $90$  ( $\pm 1$ ) nm. Most likely, the appearance of large particles leads to the determination of the antipolyelectrolyte effect, due to unfolding of macromolecules and the aggregation of nanogel particles occurs.

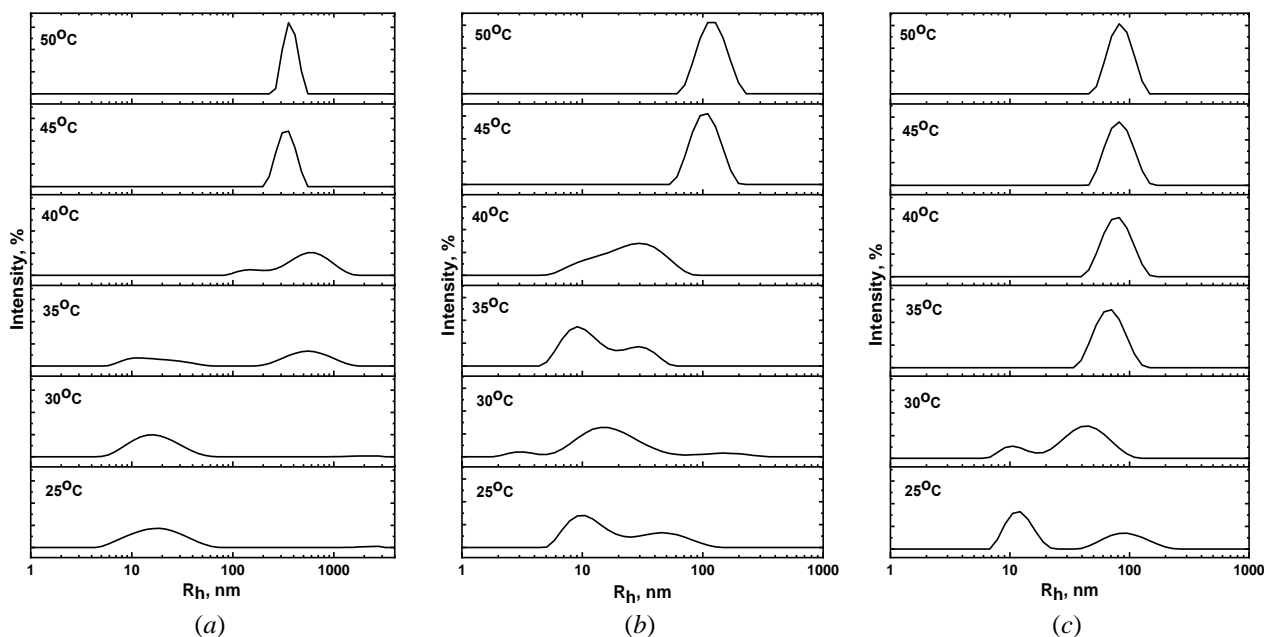


Figure 8. Effect of temperature and ionic strength ( $\mu$ ) on the mean hydrodynamic radius ( $R_h$ ) of NIPAM<sub>90</sub>-APTAC<sub>5</sub>-AMPS<sub>5</sub>:  $\mu =$  (a)  $0.001$ , (b)  $0.1$  and (c)  $1.0$

An increase in temperature promotes the aggregation of nanogels. Aggregates with  $R_h \sim 560$ – $600$  ( $\pm 10$ ) nm formed in  $0.001$  M NaCl solution at  $35$  and  $40$  °C. Under these conditions, the hydrophobicity of the NIPAM regions prevails over the antipolyelectrolyte effect. In a  $0.1$  M salt solution at  $47.8$  °C, a bulk phase transition observed (Fig. 8b). An increase of temperature directly proportionally affects the aggregation of nanogel particles, reaching a maximum at  $45.1$  °C. A further increase in temperature does not affect the size and structure of nanogel particles. As the ionic strength increases, the opposing AMPS and APTAC blocks electrostatically screened. A bulk phase transition observed by NIPAM fragments at  $\mu = 1$  M, since the antipolyelectrolyte effect is suppressed (Fig. 8c). The increase in nanogel particles size remained colloidal stable above the VPTT.

### Conclusions

Polyelectrolyte NIPAM<sub>90</sub>-AMPS<sub>10</sub>, NIPAM<sub>90</sub>-APTAC<sub>10</sub> and polyampholyte NIPAM<sub>90</sub>-APTAC<sub>5</sub>-AMPS<sub>5</sub> nanogels were obtained *via* conventional redox initiated free radical copolymerization with N,N-methylenebis(acrylamide) (MBAA) as a crosslinking agent.

The effect of ionic monomers on the volume phase transition behavior of nanogels based on the results of UV-Vis and DLS measurements was studied. Negatively and positively charged nanogels NIPAM<sub>90</sub>-AMPS<sub>10</sub> and NIPAM<sub>90</sub>-APTAC<sub>10</sub> demonstrate a volume phase transition at ionic strengths equal to or higher than 0.1 M NaCl due to the presence of polyelectrolyte effect. The volume phase transition temperature (VPTT) of the amphoteric nanogel NIPAM<sub>90</sub>-APTAC<sub>5</sub>-AMPS<sub>5</sub> increases with the addition of salt, which can be explained by the antipolyelectrolyte effect. With an increase in ionic strength, the general hydrophobization of macromolecular chains occurs and, as a result, the VPTT of NIPAM<sub>90</sub>-APTAC<sub>5</sub>-AMPS<sub>5</sub> decreases.

### Acknowledgments

This research has been funded by the Science Committee of the Ministry of Education and Science of the Republic of Kazakhstan (Grant No. AP08855552). Kudaibergenov S.E. thanks the Horizon 2020 research and innovation program of the European Union Maria Skłodowska-Curie (grant agreement 823883-NanoPol-MSCA-RISE-2018) for financial support.

### References

- 1 Ghaeini-Hesaroeiye, S., Razmi Bagtash, H., Boddohi, S., Vasheghani-Farahani, E., & Jabbari, E. (2020). Thermoresponsive Nanogels Based on Different Polymeric Moieties for Biomedical Applications. *Gels*, 6(3), 20. <https://doi.org/10.3390/gels6030020>
- 2 Vinogradov, S.V. (2010). Nanogels in the race for drug delivery. *Nanomedicine*, 5(2), 165–168. <https://doi.org/10.2217/nnm.09.103>
- 3 Kohli, E., Han, H.-Y., Zeman, A. D., & Vinogradov, S.V. (2007). Formulations of biodegradable Nanogel carriers with 5'-triphosphates of nucleoside analogs that display a reduced cytotoxicity and enhanced drug activity. *Journal of Controlled Release*, 121(1-2), 19–27. <https://doi.org/10.1016/j.jconrel.2007.04.007>
- 4 Bhuchar, N., Sunasee, R., Ishihara, K., Thundat, T., & Narain, R. (2011). Degradable Thermoresponsive Nanogels for Protein Encapsulation and Controlled Release. *Bioconjugate Chemistry*, 23(1), 75–83. <https://doi.org/10.1021/bc2003814>
- 5 Iyer, S., & Das, A. (2021). Responsive nanogels for anti-cancer therapy. *Materials Today: Proceedings*, 44, 2330–2333. <https://doi.org/10.1016/j.matpr.2020.12.415>
- 6 Chen, S., Bian, Q., Wang, P., Zheng, X., Lv, L., Dang, Z., & Wang, G. (2017). Photo, pH and redox multi-responsive nanogels for drug delivery and fluorescence cell imaging. *Polymer Chemistry*, 8(39), 6150–6157. <https://doi.org/10.1039/c7py01424d>
- 7 Wang, Y., Xu, H., & Ma, L. (2015). Recent advances of thermally responsive nanogels for cancer therapy. *Therapeutic Delivery*, 6(10), 1157–1169. <https://doi.org/10.4155/tde.15.63>
- 8 McDaniel, J.R., Dewhirst, M.W., & Chilkoti, A. (2013). Actively targeting solid tumours with thermoresponsive drug delivery systems that respond to mild hyperthermia. *International Journal of Hyperthermia*, 29(6), 501–510. <https://doi.org/10.3109/02656736.2013.819999>
- 9 Judah, H.L., Liu, P., Zarbakhsh, A., & Resmini, M. (2020). Influence of Buffers, Ionic Strength, and pH on the Volume Phase Transition Behavior of Acrylamide-Based Nanogels. *Polymers*, 12(11), 2590. <https://doi.org/10.3390/polym12112590>
- 10 Yu, T., Geng, S., Li, H., Wan, J., Peng, X., Liu, W., Zhao, Y., Yang, X., & Xu, H. (2015). The stimuli-responsive multiphase behavior of core-shell nanogels with opposite charges and their potential application in situ gelling system. *Colloids and Surfaces B: Biointerfaces*, 136, 99–104. <https://doi.org/10.1016/j.colsurfb.2015.08.049>
- 11 Zhang, Q., Zha, L., Ma, J., & Liang, B. (2009). A novel route to prepare pH- and temperature-sensitive nanogels via a semi-batch process. *Journal of Colloid and Interface Science*, 330(2), 330–336. <https://doi.org/10.1016/j.jcis.2008.09.077>
- 12 Koc, K., & Alveroglu, E. (2015). Tuning the gel size and LCST of N-isopropylacrylamide nanogels by anionic fluoroprobe. *Colloid and Polymer Science*, 294(2), 285–290. <https://doi.org/10.1007/s00396-015-3779-1>
- 13 Jain, K., Vedarajan, R., Watanabe, M., Ishikiriya, M., & Matsumi, N. (2015). Tunable LCST behavior of poly(N-isopropylacrylamide/ionic liquid) copolymers. *Polymer Chemistry*, 6(38), 6819–6825. doi:10.1039/c5py00998g.
- 14 Kim, Y.K., Kim, E.-J., Lim, J. H., Cho, H. K., Hong, W. J., Jeon, H. H., & Chung, B. G. (2019). Dual Stimuli-Triggered Nanogels in Response to Temperature and pH Changes for Controlled Drug Release. *Nanoscale Research Letters*, 14(1). <https://doi.org/10.1186/s11671-019-2909-y>
- 15 Karg, M., Pastoriza-Santos, I., Rodriguez-González, B., von Klitzing, R., Wellert, S., & Hellweg, T. (2008). Temperature, pH, and Ionic Strength Induced Changes of the Swelling Behavior of PNIPAM-Poly(allylacetic acid) Copolymer Microgels. *Langmuir*, 24(12), 6300–6306. <https://doi.org/10.1021/la702996p>
- 16 Zhou, A., Luo, H., Wang, Q., Chen, L., Zhang, T. C., & Tao, T. (2015). Magnetic thermoresponsive ionic nanogels as novel draw agents in forward osmosis. *RSC Advances*, 5(20), 15359–15365. <https://doi.org/10.1039/c4ra12102c>

17 Ayazbayeva, A.Ye., Shakhvorostov, A.V., Seikhanov, T.M., Aseyev, V.O., & Kudaibergenov, S.E. (2021). Synthesis and characterization of novel thermo- and salt-sensitive amphoteric terpolymers based on acrylamide derivatives. *Bulletin of the University of Karaganda Chemistry*, 104(4), 9–20. <https://doi.org/10.31489/2021Ch4/9-20>.

18 Ayazbayeva, A.Ye., Nauryzova, S.Z., Aseyev, V.O., & Shakhvorostov, A.V. (2022) Immobilization of Methyl Orange and Methylene Blue Within the Matrix of Charge-Imbalanced Amphoteric Nanogels and Study of Dye Release Kinetics as a Function of Temperature and Ionic Strength. *Bulletin of the University of Karaganda Chemistry*. <https://doi.org/10.31489/2022Ch3/3-22-4>

А.Е. Аязбаева, А.В. Шахворостов, С.Е. Құдайбергенов

## **Н-изопропилакриламид, 2-акриламидо-2-метил-1-пропансульфон қышқылы натрий тұзы және (3-акриламидопропил)триметиламмоний хлориді негізіндегі анионды, катионды және амфотерлі наногельдердің температураға және тұзға сезімталдығы**

Н-изопропилакриламид (НИПАМ), 2-акриламидо-2-метилпропансульфонат натрий тұзы (АМПС) және 3-акриламидопропилтриметиламмоний хлориді (АПТАХ) негізінде бос радикалды сополимерлеу арқылы аниондық, катиондық және амфотерлік сипаттағы үш түрлі наногельдер синтезделді. Төріс зарядталған [НИПАМ]:[АМПС] = 90:10 моль.%, оң зарядталған [НИПАМ]:[АПТАХ] = 90:10 моль.% және амфотерлік заряд теңестірілген [НИПАМ]:[АПТАХ]:[АМПС] = 90:5:5 моль.%, тиісінше NIPAM<sub>90</sub>-AMPS<sub>10</sub>, NIPAM<sub>90</sub>-APTAC<sub>10</sub> және NIPAM<sub>90</sub>-APTAC<sub>5</sub>-AMPS<sub>5</sub> деп қысқартылған наногельдері ИК спектроскопиясы, ТГА, УФ-көрінісін спектроскопиясы және ДЛС өлшемдерімен сипатталды. Наногельдердің су және тұз ерітінділеріндегі температура мен тұзға сезімталдық қасиеттері 25–60 °С температура диапазонында және иондық күші (μ) 0.001–1.0 М NaCl аралығында зерттелді. Аниондық NIPAM<sub>90</sub>-AMPS<sub>10</sub> және катиондық NIPAM<sub>90</sub>-APTAC<sub>10</sub> наногельдері төмен молекулалық салмақ тұзымен төріс немесе оң зарядты скринингке байланысты тұз ерітіндісінде айқын полиэлектролиттік әсер көрсетеді. Зарядпен теңестірілген амфотерлік наногель NIPAM<sub>90</sub>-APTAC<sub>5</sub>-AMPS<sub>5</sub> төмен молекулалық салмақты тұзбен қарама-қарсы зарядтар арасындағы электростатикалық тартылысты қорғауға байланысты антиполиэлектролит әсерін көрсетеді. Аниондық, катиондық және амфотерлік наногельдердің температураға тәуелді әрекетінің айырмашылығы тұз ерітінділеріндегі макромолекулалық тізбектердің қысылуымен (полиэлектролиттік әсер) және кеңеюімен (антиполиэлектролиттік әсер) түсіндіріледі.

*Кілт сөздер:* полиамфолит наногельдер, поли-Н-изопропилакриламид, иондық мономерлер, көлемдік фазалық ауысу температурасы, амфотерлік наногель, анионды наногель, катионды наногель.

А.Е. Аязбаева, А.В. Шахворостов, С.Е. Кудайбергенов

## **Температурная и солевая чувствительность анионного, катионного и амфотерного наногелей на основе N-изопропилакриламида, натриевой соли 2-акриламидо-2-метил-1-пропансульфоновой кислоты и (3-акриламидопропил)триметиламмоний хлорида**

Три различных наногеля, обладающих анионным, катионным и амфотерным характером, были синтезированы с помощью обычной свободнорадикальной сополимеризации N-изопропилакриламида (НИПАМ), натриевой соли 2-акриламидо-2-метил-1-пропансульфоновой кислоты (АМПС) и (3-акриламидопропила) триметиламмоний хлорида (АПТАХ). Отрицательно заряженный [НИПАМ]:[АМПС] = 90:10 мол.%, положительно заряженный [НИПАМ]:[АПТАХ] = 90:10 мол.% и амфотерный со сбалансированным зарядом [НИПАМ]:[АПТАХ]:[АМПС] = 90:5:5 мол.% наногели, сокращенно NIPAM<sub>90</sub>-AMPS<sub>10</sub>, NIPAM<sub>90</sub>-APTAC<sub>10</sub> и NIPAM<sub>90</sub>-APTAC<sub>5</sub>-AMPS<sub>5</sub>, соответственно, были охарактеризованы с помощью ИК-спектроскопии, ТГА, УФ-видимой спектроскопии и измерений ДЛС. Температурные и солевые чувствительные свойства наногелей в водных и водно-солевых растворах изучали в интервале температур 25–60 °С и ионной силы (μ) 0.001–1.0 М NaCl. Анионный NIPAM<sub>90</sub>-AMPS<sub>10</sub> и катионный NIPAM<sub>90</sub>-APTAC<sub>10</sub> наногели проявляют выраженный полиэлектролитный эффект в водно-солевом растворе за счет экранирования отрицательного или положительного заряда низкомолекулярной солью. В то время как заряд-сбалансированный амфотерный наногель NIPAM<sub>90</sub>-APTAC<sub>5</sub>-AMPS<sub>5</sub> проявляет антиполиэлектролитный эффект за счет экранирования электростатического притяжения между противоположными зарядами низкомолекулярной солью. Различие в температурно-зависимом поведении анионного, катионного и амфотерного наногелей объясняется сжатием (поли-

электролитный эффект) и расширением (антиполиэлектролитный эффект) макромолекулярных цепей в водно-солевых растворах.

*Ключевые слова:* полиамфолитные наногели, поли-N-изопропилакриламид, ионные мономеры, температура объемно-фазового перехода, амфотерный наногель, анионный наногель, катионный наногель.

#### Information about authors\*

**Ayazbayeva, Aigerim Yerlanovna** (*corresponding author*) — PhD student, Satbayev University, Satpayev str., 22, 050013, Almaty, Kazakhstan; e-mail: [ayazbayeva.aigerim@gmail.com](mailto:ayazbayeva.aigerim@gmail.com); <https://orcid.org/0000-0003-1313-895X>

**Shakhvorostov, Alexey Valerievich** — PhD, Institute of Polymer Materials and Technology, Atyrau-1, 3/1, 050019, Almaty, Kazakhstan; e-mail: [alex.hv91@gmail.com](mailto:alex.hv91@gmail.com); <https://orcid.org/0000-0003-3502-6123>

**Kudaibergenov, Sarkyt Elekenovich** — Doctor of Chemical Sciences, Full Professor, Director of Institute of Polymer Materials and Technology, Atyrau-1, 3/1, 050019, Almaty, Kazakhstan; e-mail: [skudai@mail.ru](mailto:skudai@mail.ru); <https://orcid.org/0000-0002-1166-7826>

---

\*The author's name is presented in the order: *Last Name, First and Middle Names*

D.M. Turgunaliyeva<sup>1</sup>, D.S. Dilbaryan<sup>2</sup>, A.S. Vasilchenko<sup>2</sup>, O.A. Nurkenov<sup>3</sup>,  
S.D. Fazylov<sup>3</sup>, G.Zh. Karipova<sup>3</sup>, T.M. Seilkhanov<sup>4</sup>, I.V. Kulakov<sup>1\*</sup>

<sup>1</sup>*Institute of Chemistry, University of Tyumen, Tyumen, Russia;*

<sup>2</sup>*Institute of Environmental and Agricultural Biology (X-Bio), University of Tyumen, Tyumen, Russia;*

<sup>3</sup>*LLP "Institute of Organic Synthesis and Coal Chemistry of the Republic of Kazakhstan", Karaganda, Kazakhstan;*

<sup>4</sup>*Sh. Ualikhanov Kokshetau University, Kokshetau, Kazakhstan*

(\*Corresponding author's e-mail: [i.v.kulakov@utmn.ru](mailto:i.v.kulakov@utmn.ru))

## Synthesis and Antibacterial Activity of Hydrazones of Isonicotinic and Salicylic Acids Based on Acetyl Derivatives of Coumarin and Benzo[g][1,3,5]Oxadiazocine

In recent decades, the efforts of many researchers in the sphere of organic chemistry, physics and pharmacology have been focused on the search for new agents with pronounced antibacterial and especially antifungal activity. This is due to the widespread increase in the resistance of many bacterial strains and fungi to antibiotics and antifungal drugs available in medical practice. In this regard, the number of works related to the synthesis of new potential antibiotics from the most diverse class of organic derivatives, which either include known pharmacophore groups or represent a new structural class of compounds with unknown and unexplored activity, is increasing in the scientific literature. In this work, new previously undescribed hydrazones derivatives were obtained on the basis of physiologically active isonicotinic and salicylic acid hydroxides and laboratory-available acetyl-substituted heterocycles, namely 3-acetyl-2H-chromen-2-one 3,2-acetyl-3H-benzo[f]chromen-3-one 4 and 2,6-methanobenzo[g][1,3,5]oxadiazocine 5. The obtained hydrazones structure is explicitly proved by IR and <sup>1</sup>H, <sup>13</sup>C NMR spectroscopy data. The synthesized six new hydrazones underwent biological screening for antibacterial and antifungal activity on strains of microorganisms, namely gram-positive bacterium *Staphylococcus aureus* 209P, gram-negative bacterium *Pectobacterium carotovorum* VKM-B1247, and yeast-like fungus *Candida albicans* ATCC 10231. Screening revealed three compounds with antimicrobial activity and one promising compound — (E)-2-hydroxy-N'-(1-(2-oxochroman-3-yl)ethylidene)benzohydrazide 9, which also exhibits antifungal activity along with antimicrobial activity.

**Keywords:** hydrazides, isoniazid, salicylic acid hydrazide, coumarins, 3-acetyl-2H-chromen-2-one, 2-acetyl-3H-benzo[f]chromen-3-one, 2,6-methanobenzo[g][1,3,5]oxadiazocine, hydrazones, antimicrobial activity.

### Introduction

Over the years the attention of many researchers in the field of medicinal chemistry has been focused on the search and development of new antibacterial drugs. Due to the widespread uncontrolled use of various antibiotics in recent decades, there has been a significant increase in antimicrobial resistance against many viruses, bacteria and fungi [1–3].

According to the World Health Organization (WHO) antimicrobial resistance is among the ten major public health problems that are progressing worldwide [4, 5]. Antibiotics, antiviral, antifungal and antiparasitic agents are combined into one class of compounds called antimicrobials. The devastating consequences related to resistance are much more global than it seems. Threats to human health caused by both gram-negative and gram-positive resistant strains of bacteria force scientists to investigate new classes of compounds exhibiting antibacterial biological effects and new approaches to solving the antimicrobial resistance problem [6, 7].

It is known that hydrazides and their various derivatives, including hydrazones, have a wide range of biological activity [8–12]. Anti-tuberculosis drugs such as isoniazid (isonicotinic acid hydrazide) and ftivazid (vanillin isonicotinoyl hydrazone) are well known among this class of compounds [13]. Moreover hydrazones are worth noticing due to the presence of antibacterial and analgesic properties [14–16].

Isonicotinic acid hydrazide (tubazid, isoniazid) is especially noteworthy among them, which despite the presence of a huge number of new drugs used in the tuberculosis treatment practice [17], currently holds a leading place in the treatment of various forms of tuberculosis as a new dosage form (“Isonicotinoyl Hydrazine iron sulfate” or the trade name “*Fenazid*”), i.e. its complex with iron (II) sulfate [18]. Modification of

isoniazid in particular its hydrazone with vanillin ("Ftivazid") (Fig. 1) led not only to a decrease in toxicity, but also to a better individual tolerance of the drug [19].

Salicylic acid hydrazone should also be noted among other hydrazides. Its derivatives such as *Diflunisal* [20] and *Salsalate* [21, 22] are used as antipyretic and anti-inflammatory agents [23]. In the case of *Salsalate* scientists investigated the possibility of its application in the treatment of diabetes [24, 25].

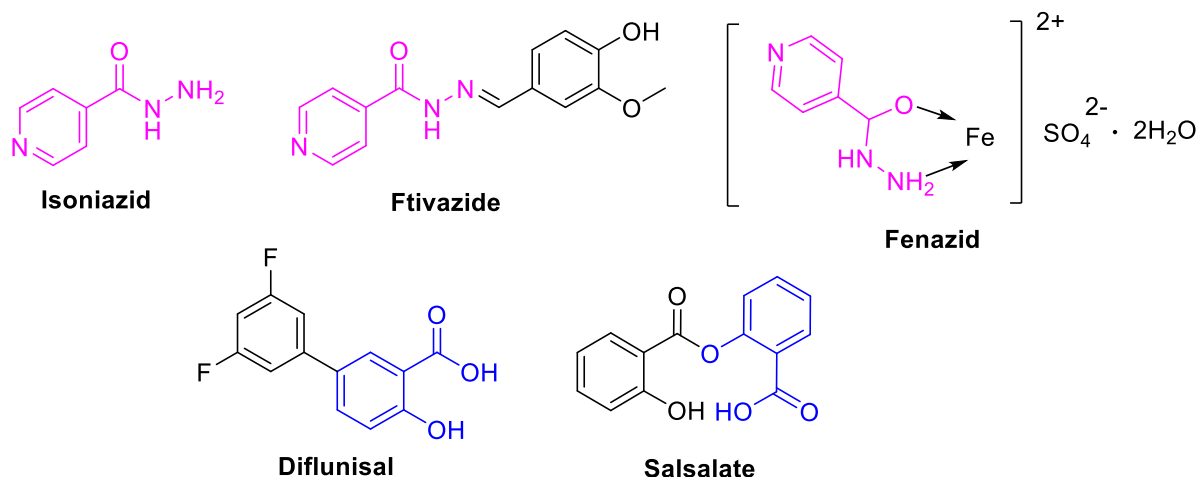


Figure 1. Derivatives of isonicotinic and salicylic acid used as pharmaceuticals

Thus, we took well-known pharmacophores, namely hydrazides of isonicotinic and salicylic acids as the chemical modification basis in order to obtain new hydrazones with potential antimicrobial activity.

### Experimental

#### Materials and Methods

FTIR spectra were obtained with an Agilent Cary 630 spectrophotometer in a thin sample layer on a crystal attachment.  $^1\text{H}$  and  $^{13}\text{C}$  NMR spectra were recorded on a JNN-ECA Jeol 400 (400 and 100 MHz, respectively) and Magritek spinsolve 80 carbon ultra (81 and 20 MHz, respectively) instruments using  $\text{DMSO-}d_6$ , the internal standard was residual solvent signals (2.49 and 39.9 ppm for  $^1\text{H}$  and  $^{13}\text{C}$  nuclei in  $\text{DMSO-}d_6$ ).

The reactions progress and the products purity were monitored by TLC on Sorbfil plates and visualized using iodine vapor or UV light.

#### Synthetic procedures

**(E)-N'-(1-(2-oxo-2H-chromen-3-yl)ethylidene)isonicotinohydrazide (8).** The solution of **3** (1.88 g, 10 mmol) and hydrazide **6** (1.37 g, 10 mmol) in 2-PrOH was heated at reflux for 10 h. The resulting yellow precipitate was filtered off. The yield was 60 %. Recrystallization from 2-PrOH gave yellow crystals, mp 237–240 °C.

$^1\text{H}$  NMR (400 MHz,  $\text{DMSO-}d_6$ ),  $\delta$ , ppm: 2.33 s (3 H,  $\text{CH}_3$ ), 7.35–7.44 m (3 H, H-6, H-7, H-8), 7.63 d (1H,  $J = 7.1$ , H-5), 7.75 d (2H,  $J = 2.2$ , H-3', H-5', Py), 7.82 s (1H, H-4), 8.73 d (2H,  $J = 2.7$ , H-2', H-6', Py), 11.02 br. s (1H, NH).

**(E)-2-hydroxy-N'-(1-(2-oxo-2H-chromen-3-yl)ethylidene)benzohydrazide (9).** The solution of **3** (1.50 g, 8.0 mmol) and hydrazide **7** (1.22 g, 8.0 mmol) in 2-PrOH was heated at reflux for 10 h. The resulting orange precipitate was filtered off. The yield was 78 %. Recrystallization from 2-PrOH gave orange crystals, mp 230–233 °C.

$^1\text{H}$  NMR (400 MHz,  $\text{DMSO-}d_6$ ),  $\delta$ , ppm: 2.28 s (3 H,  $\text{CH}_3$ ), 6.98 t (1 H,  $J = 7.3$  Hz, H-5'), 7.03 d (1 H,  $J = 7.8$  Hz, H-3'), 7.38–7.46 m (3H, H6, H-8, H-4'), 7.66 t (1H,  $J = 8.0$  Hz, H-7), 7.89 d (1H,  $J = 7.8$  Hz, H-5), 7.98 d (1H,  $J = 7.3$  Hz, H-6'), 8.27 s (1H, H-4), 11.38 br. s (1H, NH), 11.74 br. s (1H, OH).

**(E)-2-hydroxy-N'-(1-(2-oxo-3,4-dihydro-2H-benzo[h]chromen-3-yl)ethylidene)isonicotinohydrazide (10).** The solution of **4** (0.48 g, 2 mmol) and hydrazide **6** (0.27 g, 2 mmol) in 2-PrOH was heated at reflux for 10 h. The resulting dark orange precipitate was filtered off. The yield was 65 %. Recrystallization from 2-PrOH gave orange crystals, mp 224–225 °C.

$^1\text{H}$  NMR (80 MHz, DMSO- $d_6$ ),  $\delta$ , ppm: 2.40 s (3H,  $\text{CH}_3$ ), 7.47 br. s (1H, H-5), 7.58 br. s (1H, H-6), 7.67 br. s (1H, H-9), 7.75 br. t (1H,  $J = 7.5$ , H-8), 7.82 br. s (2H, H-3', H-5', Py), 8.21 d (1H,  $J = 8.7$  Hz, H-7), 8.56 d (1H,  $J = 8.2$ , H-10), 8.72 br. s (2H, H-2', H-6', Py), 8.93 s (1 H, H-1), 11.11 br. s (1H, NH).

**(E)-2-hydroxy-N'-(1-(2-oxo-3,4-dihydro-2H-benzo[h]chromen-3-yl)ethylidene)benzohydrazide (11).** The solution of **4** (0.48 g, 2 mmol) and hydrazide **7** (0.30 g, 2 mmol) in 2-PrOH was heated at reflux for 10 h. The resulting orange precipitate was filtered off. The yield was 80 %. Recrystallization from 2-PrOH gave orange crystals, mp 266–267 °C.

$^1\text{H}$  NMR (400 MHz, DMSO- $d_6$ ),  $\delta$ , ppm: 2.34 s (3H,  $\text{CH}_3$ ), 6.99 t (1H,  $J = 7.1$  Hz, H-5'), 7.04 d (1 H,  $J = 8.2$  Hz, H-3'), 7.43 t (1H,  $J = 7.1$  Hz, H-4'), 7.57 d (1H,  $J = 7.8$ , H-5), 7.64 d (1H,  $J = 7.8$ , H-6), 7.73 t (1H,  $J = 7.8$ , H-9), 7.75 t (1H,  $J = 7.8$ , H-8), 8.01 d (1H,  $J = 7.3$  Hz, H-6'), 8.21 d (1H,  $J = 8.7$  Hz, H-7), 8.57 d (1H,  $J = 8.2$  Hz, H-10), 8.91 s (1 H, H-1), 11.44 br. s (1H, NH), 11.76 br. s (1H, OH).

**(E)-N'-(1-(1-(2-methyl-4-thioxo-3,4,5,6-tetrahydro-2H-2,6-methanobenzo[g][1,3,5]oxadiazocin-11-yl)ethylidene]isonicotinohydrazide (12).** The solution of **5** (0.48 g, 2 mmol) and hydrazide **6** (0.30 g, 2 mmol) in 2-PrOH was heated at reflux for 24 h. The resulting white precipitate was filtered off and washed with water. The yield was 82 %. Recrystallization from 2-PrOH with 1,4-dioxane gave white crystals, mp 248–250 °C.

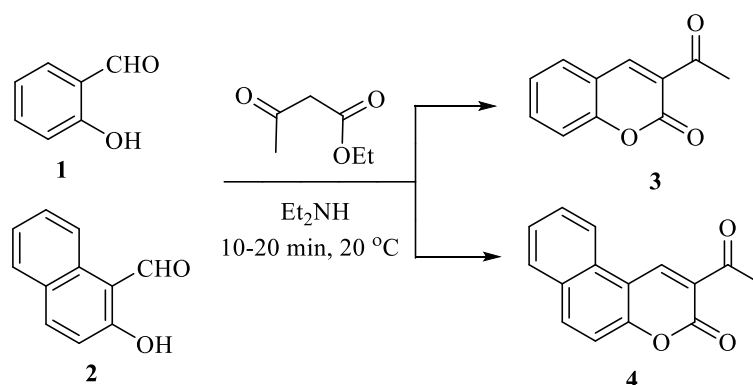
$^1\text{H}$  NMR (400 MHz, DMSO- $d_6$ ),  $\delta$ , ppm: 1.83 s (3H,  $\text{CH}_3$ ), 2.05 s (3H,  $\text{N}=\text{C}-\text{CH}_3$ ), 3.17 br. s (1H, H-11), 4.49 br. s (1 H, H-6), 6.83 d (1H,  $J = 8.2$ , H-10), 6.93 t (1H,  $J = 7.3$ , H-9), 7.17–7.24 m (2H, H-7, H-8), 7.72 d (2H,  $J = 2.2$ , H-3', H-5', Py), 8.73 br. s (2H, H-2', H-6', Py), 9.03 br. s (1H, 3-NH), 9.10 br. d (1H,  $J = 10.5$  Hz, 5-NH), 10.97 br. s (1H, NH).

**(E)-2-hydroxy-N'-(1-(1-(2-methyl-4-thioxo-3,4,5,6-tetrahydro-2H-2,6-methanobenzo[g][1,3,5]oxadiazocin-11-yl)ethylidene]benzohydrazide (13).** The solution of **5** (0.26 g, 1 mmol) and hydrazide **7** (0.20 g, 1 mmol) in 2-PrOH was heated at reflux for 24 h. The resulting white precipitate was filtered off and washed with water. The yield was 73 %. Recrystallization from 2-PrOH gave white crystals, mp 230–232 °C.

$^1\text{H}$  NMR (400 MHz, DMSO- $d_6$ ),  $\delta$ , ppm: 1.80 s (3H,  $\text{CH}_3$ ), 2.02 s (3H,  $\text{N}=\text{C}-\text{CH}_3$ ), 3.16 br. s (1H, H-11), 4.48 d (1 H,  $J = 3.2$  Hz, H-6), 6.84 d (1H,  $J = 8.2$ , H-10), 6.91–6.97 m (2H, H-9, H-5'), 7.00 d (1 H,  $J = 8.2$  Hz, H-3'), 7.18–7.23 m (2H, H-7, H-8), 7.40 t (1H,  $J = 7.3$  Hz, H-4'), 7.94 d (1H,  $J = 7.3$  Hz, H-6'), 9.08 br. d (1H,  $J = 4.6$  Hz, 5-NH), 9.14 br. s (1H, 3-NH), 11.14 br. s (1H, NH), 11.76 br. s (1H, OH).

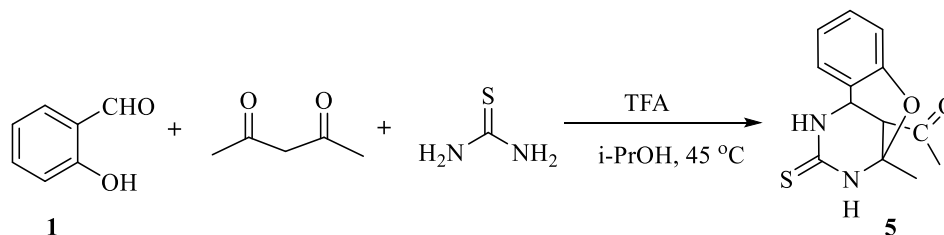
### Results and Discussion

Based on the initial aim and the literature review data, it was of great interest to combine several pharmacophore groups in one molecule, namely isonicotinic and salicylic acid hydrazide and laboratory available acetyl-substituted heterocycles such as acetyl derivatives of coumarin **3**, **4** (Scheme 1) and 2,6-methanobenzo[g][1,3,5]oxadiazocine **5** (Scheme 2). The choice was also based on the absence of such derivatives in chemical databases. The Perkin reaction is the main method of synthesis of coumarins and their derivatives, in which 2-hydroxyaromatic aldehydes are used as initial compounds. 3-Acetyl-2H-chromen-2-one **3** and 2-acetyl-3H-benzo[f]chromen-3-one **4** [26] were obtained with high yields by the reaction of acetoacetic ester with the corresponding salicylic and 2-hydroxynaphthaldehyde and diethylamine as a catalyst (Scheme 1).



Scheme 1

The obtained acetylcoumarins **3**, **4** were identified by comparing their literature data on melting points and the  $^1\text{H}$  NMR spectra. The Biginelli reaction product, namely 2,6-methanobenzo[*g*][1,3,5]oxadiazocine **5** was synthesized according to the method specified in the article [27] (Scheme 2).



The structure of compound **5** was also identified by a comparative analysis of the melting point and  $^1\text{H}$  NMR spectrum [27].

Listed acetyl-substituted heterocycles were chosen because many natural coumarins are biologically active compounds (Fig. 2) with different effects on the organism, namely hepatoprotective, diuretic, analgesic, anti-microbial (*Scoparone*) [28]; antitumor, cardioprotective, neuroprotective (*Isofraxidin*) [29, 30], antidepressant [31], hepatoprotective [32] and antioxidant [33] (*Scopoletin*) ones; and also show photosensitizing and antitumor activity [34–37].

Many researchers refer derivatives of 2,6-methanobenzo[*g*][1,3,5]oxadiazocine to the analogues of the anti-cancer drug *monastrol*, which has the structure of pyrimidinethione [38] (Fig. 2), but with an oxygen linkage. *Monastrol* has revealed a completely new mechanism of anticancer effects due to its specific effect on mitosis, which makes it a unique precursor in the synthesis of a wide range of biologically active compounds, in particular, pharmaceuticals.

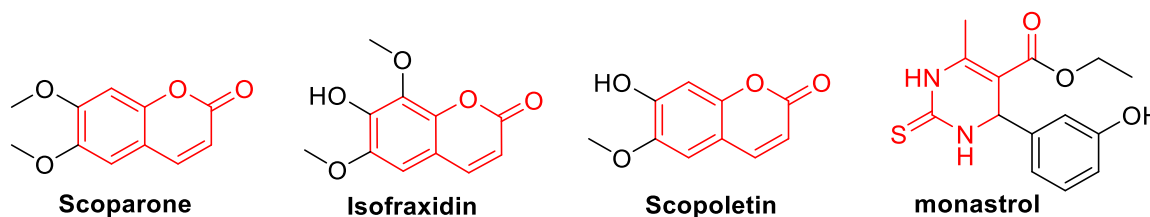


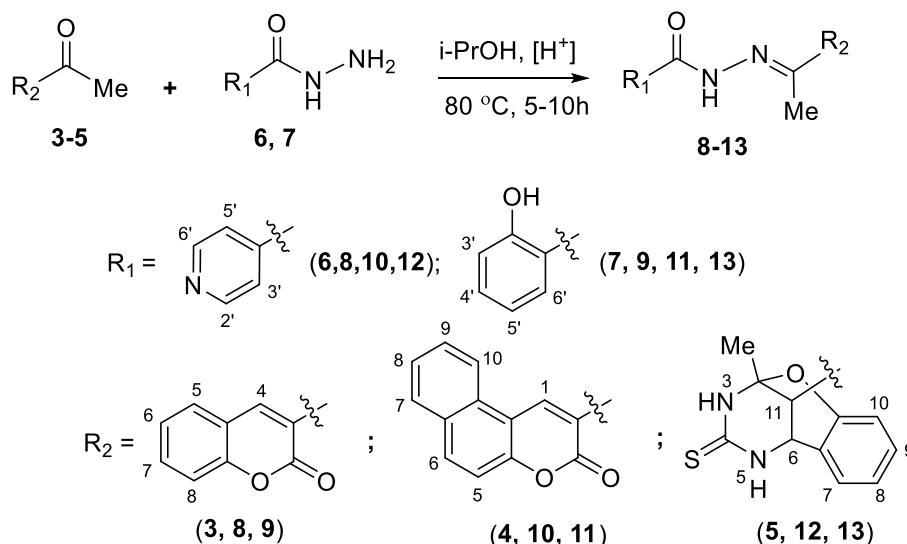
Figure 2. Chemical structure of biologically active derivatives of coumarin and monastrol

The incorporation of another active pharmacophore group into the structure of a physiologically active substance is a widely used method for obtaining new biologically active compounds in medicinal chemistry. The combination of two or more pharmacophore groups in one molecule increases the likelihood of the synthesized substance showing not only high biological activity, but also the presence of a new therapeutic potential.

Therefore, the introduction of pharmacophore groups into the structure of biologically active hydrazones can result in potentially increased biological activity. And in turn, the synthesis of coumarin derivatives is also an urgent task for the researchers in terms of finding new compounds with a diverse effect on the human organism.

The synthesis of hydrazones was carried out by boiling the initial hydrazides **6**, **7** with acetyl derivatives **3-5** in 2-PrOH in the presence of catalytic amounts of formic acid (Scheme 3).

The obtained hydrazones **8-13** are yellowish crystals that are difficult to dissolve in common organic solvents. The structure of compounds **8-13** was confirmed by IR and NMR spectroscopy data. Thus, in the  $^1\text{H}$  NMR spectrum of compound **9**, methyl group protons were registered by a singlet at 2.28 ppm. There were also singlets of the OH-group proton at 11.74 ppm and NH-group proton at 11.38 ppm.



Scheme 3

### Biological studies

All the biological tests were carried out in the Laboratory of Antimicrobial Resistance, Institute of Environmental and Agricultural Biology (X-BIO) of University of Tyumen.

Taking into account the enlisted data in the literature review on the potential antibacterial activity of hydrazone derivatives, we carried out some biological studies of the compounds **8–13**. The antimicrobial activity of the synthesized samples was evaluated by diffusion into agar using the following strains of microorganisms: gram-positive bacterium — *Staphylococcus aureus* 209P, gram-negative bacterium — *Pectobacterium carotovorum* VKM-B1247 — (antibacterial activity) and yeast-like fungus — *Candida albicans* ATCC 10231 — (antifungal activity).

Microorganisms *Staphylococcus aureus* 209 P and *Pectobacterium carotovorum* VKM-B 1247 were cultivated on a liquid nutrient solution Luria–Bertani (LB) containing: trypton — 10 g/l (“Diaem”, Russia), yeast extract ultrafiltered powder — 5 g/l (“Diaem”, Russia), sodium chloride (“Diaem”, Russia) — 5 g/l. *Staphylococcus aureus* 209 P and *Pectobacterium carotovorum* VKM-B 1247 were grown at 37 °C (pressure index: 150 rpm) and 28 °C (pressure index: 150 rpm), respectively. Yeast-like fungus *Candida albicans* ATCC 10231 was cultivated on a liquid nutrient solution YPD: peptone — 20 g/l (“Diaem”, Russia), yeast extract — 10 g/l (“Diaem”, Russia), glucose — 20 g/l (“Diaem”, Russia). *Candida albicans* ATCC 10231 was grown at 37 °C (pressure index: 150 rpm).

Samples with a volume of 10 mql (at a concentration of 10 mg/ml, 5 mg/ml, 1 mg/ml) were applied to the surface of a nutrient solution (0.75 % LB) inoculated with the corresponding test strain. Petri dishes were incubated for 24 h, namely *Staphylococcus aureus* 209P and *Candida albicans* ATCC 10231 at 37 °C, *Pectobacterium carotovorum* VKM-B1247 at 28 °C. On the next day, the diameter of the microbial growth suppression zones was measured. Screening results of the compounds **8–13** for antimicrobial activity are shown in Table 1.

Table 1

### Zones diameter of microorganisms' growth suppression by compounds 8-13

Compound	<i>Staphylococcus aureus</i>			<i>Pectobacterium carotovorum</i>			<i>Candida albicans</i>		
	10 mg/ml	5 mg/ml	1 mg/ml	10 mg/ml	5 mg/ml	1 mg/ml	10 mg/ml	5 mg/ml	1 mg/ml
8	5 mm / +/-	—	—	—	—	—	—	—	—
9	11 mm / ++	9 mm / ++	—	5 mm / +/-	—	—	4 mm / +/-	—	—
10	—	—	—	—	—	—	—	—	—
11	—	—	—	—	—	—	—	—	—
12	5 mm / +/-	4 mm / +/-	—	—	—	—	—	—	—
13	—	—	—	—	—	—	—	—	—

Antimicrobial effect: ++ pronounced antimicrobial activity; +/- very weak antimicrobial activity; — no activity

Compound **9** exhibits the highest antimicrobial activity against a gram-positive microorganism — *Staphylococcus aureus* 209P at a concentration of 10 mg/ml. Compounds **8** and **12** showed a weak bacteriostatic effect at a concentration of 10 mg/ml. A low bacteriostatic effect against a gram-negative microorganism — *Pectobacterium carotovorum* VKM-B1247 and a yeast-free fungus — *Candida albicans* ATCC 10231 was demonstrated by the compound **9** at a concentration of 10 mg/ml.

### Conclusions

Thus, new derivatives of hydrazones, which had not been described in the literature before, were obtained based on physiologically active hydrazides of isonicotinic and salicylic acids and acetyl-substituted heterocycles, namely 3-acetyl-2*H*-chromen-2-one **3**, 2-acetyl-3*H*-benzo[*f*]chromen-3-one **4** and 2,6-methanobenzo[*g*][1,3,5]oxadiazocine **5**. Obtained hydrazones structure was explicitly proved by IR and <sup>1</sup>H, <sup>13</sup>C NMR spectroscopy data. As a result of the carried out biological antibacterial and antifungal studies on strains of microorganisms, namely gram-positive bacterium — *Staphylococcus aureus* 209P, gram-negative bacterium — *Pectobacterium carotovorum* VKM-B1247, yeast-like fungus — *Candida albicans* ATCC 10231, three compounds demonstrated antimicrobial activity and compound **9** was also a promising agent since it exhibited anti-fungal effect along with antimicrobial activity.

### Acknowledgments

The work was carried out within the framework of the project No. AP14869941 for grant financing of the Science Committee of the Ministry of Education and Science of the Republic of Kazakhstan.

### References

- 1 Kennedy D.A. Why the evolution of vaccine resistance is less of a concern than the evolution of drug resistance / A.F. Read // PNAS. — 2018. — Vol. 115. — P. 12878–12886. <https://doi.org/10.1073/pnas.1717159115>
- 2 Prestinaci F. Antimicrobial Resistance: A Global Multifaceted Phenomenon. / P. Pezzotti, A. Pantosti // Pathog. Glob. Health. — 2015. — Vol. 109, No. 7. — P. 309–318. <https://doi.org/10.1179/2047773215Y.0000000030>
- 3 Johansson M.H.K. Detection of Mobile Genetic Elements Associated with Antibiotic Resistance in Salmonella Enterica Using a Newly Developed. / V. Bortolaia, S. Tansirichaiya, F.M. Aarestrup, A.P. Roberts, T.N. Petersen // J. Antimicrob. Chemother. — 2020. — Vol. 76. — P. 101–109. <https://doi.org/10.1093/jac/dkaa390>
- 4 [Электронный ресурс]. — Режим доступа: <https://www.who.int/news-room/fact-sheets/detail/antimicrobial-resistance> (accessed on 15.09.2022).
- 5 [Электронный ресурс]. — Режим доступа: <https://www.who.int/campaigns/world-antibiotic-awareness-week> (accessed on 15.09.2022).
- 6 Saha M. Review on Multiple Facets of Drug Resistance: A Rising Challenge in the 21st Century. / A. Sarkar // J. Xenobiot. — 2021. — Vol. 11, No. 4. — P. 197–214. <https://doi.org/10.3390/jox11040013>
- 7 Rajpara N. Role of integrons, plasmids and SXT elements in multidrug resistance of Vibrio cholerae and Providencia vermicola obtained from a clinical isolate of diarrhea. / B.M. Kutar, R. Sinha, D. Nag, H. Koley, T. Ramamurthy, A.K. Bhardwaj // Front Microbiol. — 2015. — Vol. 6. — P. 57. <https://doi.org/10.3389/fmicb.2015.00057>
- 8 Khan M.S. A systematic review on the synthesis and biological activity of hydrazide derivatives. / S.P. Siddiqui, N. Tarannum // Hygeia. J.D. Med. — 2017. — Vol. 9, No. 1. — P. 61–79. <https://doi.org/10.15254/H.J.D. Med.9.2017.165>
- 9 Narang R. A review on biological activities and chemical synthesis of hydrazide derivatives. / B. Narasimhan, S. Sharma // Curr Med Chem. — 2012. — Vol. 19. — P. 569–612. <https://doi.org/10.2174/092986712798918789>
- 10 Mali S.N. Mini-Review of the Importance of Hydrazides and Their Derivatives — Synthesis and Biological Activity. / B.R. Thorat, D.R. Gupta, A. Pandey // Eng. Proc. — 2021. — Vol. 11. — P. 21. <https://doi.org/10.3390/ASEC2021-11157>
- 11 Verma G. A review exploring biological activities of hydrazones. / A. Marella, M. Shaquiquzzaman, M. Akhtar, M.R. Ali, M.M. Alam // J. Pharm. Bioallied. Sci. — 2014. — Vol. 6, No. 2. — P. 69–80. <https://doi.org/10.4103/0975-7406.129170>
- 12 Кулаков И.В. Синтез и туберкулостатическая активность гидразидов и ацилгидразидов аминокислот на основе эфедриновых алкалоидов / И.В. Кулаков, О.А. Нуркенов, М.А. Газалиева, С.К. Жаугашева, Ж.О. Исакова // Хим.-фарм. журн. — 2007. — Т. 41. № 11. — С. 52. <https://doi.org/10.30906/0023-1134-2007-41-11-52-56>
- 13 Машковский М.Д. Лекарственные средства / М.Д. Машковский. — М.: Новая волна, 2012. — 856 с.
- 14 Rollas S. Biological Activities of Hydrazone Derivatives. / S.G. Küçükgülzel // Molecules. — 2007. — Vol. 12, No. 8. — P. 1910. <https://doi.org/10.3390/12081910>
- 15 Manikandan V. Synthesis and antimicrobial activities of some (E)-N'-1-(substituted benzylidene)benzohydrazides / S. Balaji, R. Senbagam, R. Vijayakumar, M. Rajarajan, G. Vanangamudi, G. Thirunarayanan // IJAC. — 2017. — Vol. 5, No. 1. — P. 17. <https://doi.org/10.14419/ijac.v5i1.7155>

- 16 Popiołek Ł. Synthesis and investigation of antimicrobial activities of nitrofurazone analogues containing hydrazide-hydrazone moiety. / A. Biernasiuk // Saudi Pharm. J. — 2017. — Vol. 25, No. 7. — P. 1097. <https://doi.org/10.1016/j.jsps.2017.05.006>
- 17 Raja A.S. Antibacterial and antitubercular activities of some diphenyl hydrazones and semicarbazones. / A.K. Agarwal, N. Mahajan, S.N. Pandeya, S. Ananthan // Indian J. Chem. Sect. B. — 2010. — Vol. 49. — P. 1384–1388.
- 18 Государственный реестр лекарственных средств: [В 2 т.]. — Офиц. изд. — М.: Медицинский совет, 2009. — Т. 2, Ч. 1. — 568 с.; Ч. 2. — 560 с.
- 19 Глушков Г. Современные тенденции развития поиска и создания новых лекарственных средств / Г. Глушков, М.Д. Машковский // Хим.-фарм. журн. — 1990. — № 7. — 4 с.
- 20 Brogden R.N. Diflunisal: a review of its pharmacological properties and therapeutic use in pain and musculoskeletal strains and sprains and pain in osteoarthritis. / R.C. Heel, G.E. Pakes, T.M. Speight, G.S. Avery. // Drugs. — 1980. — Vol. 19, No. 2. — P. 84–106. <https://doi.org/10.2165/00003495-198019020-00002>
- 21 Shoelson S.E. Inflammation and insulin resistance / J. Lee, A.B. Goldfine // J Clin Invest. — 2006. — Vol. 116, No. 7. — P. 1793–801. <https://doi.org/10.1172/JCI29069>
- 22 Fleischman A. Salsalate improves glycemia and inflammatory parameters in obese young adults / S.E. Shoelson, R. Bernier, A.B. Goldfine // Diabetes Care. — 2008. — Vol. 31. — P. 289–294. <https://doi.org/10.2337/dc07-1338>
- 23 Иванский И.В. Химия органических препаратов / И.В. Иванский. — М.: Высш. шк., Нет данных. — 178 с.
- 24 Goldfine A.B. Targeting Inflammation Using Salsalate in Type 2 Diabetes Study Team. Salicylate (salsalate) in patients with type 2 diabetes: a randomized trial / V. Fonseca, K.A. Jablonski, Y.D. Chen, L. Tipton, M.A. Staten, S.E. Shoelson // Ann Intern Med. — 2013. — Vol. 159, No. 1. — P. 1–12.
- 25 Anderson K. Salsalate, an old, inexpensive drug with potential new indications: a review of the evidence from 3 recent studies. / L. Wherle, M. Park, K. Nelson, L. Nguyen // Am Health Drug Benefits. — 2014. — Vol. 7, No. 4. — P. 231–235.
- 26 Kumar N. Synthesis of 3-(4,5-dihydro-1-phenyl-5-substituted phenyl-1H-pyrazol-3-yl)-2H-chromen -2-one derivatives and evaluation of their anticancer activity. / A. Bhatnagar, R. Dudhe // Arabian Journal of Chemistry. — 2017. — Vol. 10, No. 2. — P. 2443–2452.
- 27 Kulakov I.V. Synthesis, structure and antiradical activity of new derivatives of methano[1,3]thiazolo-[2,3-D][1,3,5]-benzoxadiazocin / S.A. Talipov, Z.T. Shulgau., T.M. Seilkhanov // Chem. Heterocycl. Compd. — 2014. — Vol. 50. — P. 1477.
- 28 Hui Y. Scoparone as a therapeutic drug in liver diseases: pharmacology, pharmacokinetics and molecular mechanisms of action / X. Wang, Z. Yu, X. Fan, B. Cui, T. Zhao, L. Mao, H. Feng, L. Lin, Q. Yu, J. Zhang, B. Wang, X. Chen, X. Zhao, C. Sun // Pharmacol. Res. — 2020. — Vol. 160. — P. 105170. <https://doi.org/10.1016/j.phrs.2020.105170>
- 29 Lin J. Isofraxidin inhibits interleukin-1 $\beta$  induced inflammatory response in human osteoarthritis chondrocytes. / X. Li, W. Qi, Y. Yan, K. Chen, X. Xue., X. Xu, Z. Feng, X. Pan // Int. Immunopharm. — 2018. — Vol. 64. — P. 238–245. <https://doi.org/10.1016/j.intimp.2018.09.003>
- 30 Majnooni M.B. Isofraxidin: Synthesis, Biosynthesis, Isolation, Pharmacokinetic and Pharmacological Properties. / S. Fakhri, Y. Shokoohinia, M. Mojarrah, S. Kazemi-Afrakoti, M.H. Farzaei // Molecules. — 2020. — Vol. 25, No. 9. — P. 2040. <https://doi.org/10.3390/molecules25092040>
- 31 Capra J.C. Antidepressant-like effect of scopoletin, a coumarin isolated from Polygala sabulosa (Polygaceae) in mice: evidence for the involvement of monoaminergic systems / M.P. Cunha, D.G. Machado, A.D.E. Zomkowski, B.G. Mendes, A.R.S. Santos, M.G. Pizzolatti, A.L.S. Rodrigues // Eur. J. Pharmacol. — 2010. — Vol. 643. — P. 232–238. <https://doi.org/10.1016/j.ejphar.2010.06.043>
- 32 Kang S.Y. Hepatoprotective activity of scopoletin, a constituent of Solanum lyratum / S.H. Sung, J.H. Park, Y.C. Kim // Arch Pharm. Res. (Seoul). — 1998. — Vol. 21. — P. 718. <https://doi.org/10.1007/BF02976764>
- 33 Mogana R. Anti-inflammatory, anticholinesterase, and antioxidant potential of scopoletin isolated from canarium patentinerivium Miq. (Burseraceae Kunth) / K. Teng-Jin, C. Wiart // Evid.-Based Complement. Altern. Med. ECAM. — 2013. — P. 734824. <https://doi.org/10.1155/2013/734824>
- 34 Kirsch G. Natural and Synthetic Coumarins with Effects on Inflammation / A.B. Abdelwahab, P. Chaimbault // Molecules. — 2016. — Vol. 21. — P. 1322. <https://doi.org/10.3390/molecules21101322>
- 35 Fylaktakidou K.C. Natural and synthetic coumarin derivatives with anti-inflammatory and antioxidant activities / D.J. Hadjipavlou-Litina, K.E. Litinas, D.N. Nicolaides // Curr Pharm. — 2004. — Vol. 10, No. 30. — P. 3813–3833. <https://doi.org/10.2174/1381612043382710>
- 36 Gouda M. A Review: Synthesis and Medicinal Importance of Coumarins and their Analogues (Part II) / B. Hussein, A. El-Demerdash, M. Elsayed., M. Salem, M. Helal, W. Hamama // Current Bioactive Compounds. — 2019. — P. 15. <https://doi.org/10.2174/1573407215666191111120604>
- 37 Kubrak T. Natural and Synthetic Coumarins and their Pharmacological Activity. / Podgórski, R., Stompor-Gorący, M. // European Journal of Clinical and Experimental Medicine. — 2017. — Vol. 15. — P. 169–175. <https://doi.org/10.2174/1381612043382710>
- 38 Mayer T.U. Small Molecule Inhibitor of Mitotic Spindle Bipolarity Identified in a Phenotype-Based Screen. / T.M. Kapoor, S.J. Haggarty, R.W. King, S.L. Schreiber, T.J. Mitchison // Science. — 1999. — Vol. 286. — P. 971. <https://doi.org/10.1126/science.286.5441.971>

Д.М. Тургуналиева, Д.С. Дилбарян, А.С. Васильченко, О.А. Нуркенов,  
С.Д. Фазылов, Г.Ж. Кәріпова, Т.М. Сейлханов, И.В. Кулаков

### **Кумарин мен бензо[g][1,3,5]оксадиазоцин ацетил туындылары негізінде изоникотин және салицил қышқылдары гидразондарының синтезі және бактерияғақарсы белсенділігі**

Соңғы онжылдықтарда көптеген органик-химиктер, дәрігерлер мен фармакологтардың көптеген зерттеушілерінің назары айқын бактерияғақарсы және әсіресе зеңгеқарсы белсенділігі бар жаңа заттарды табуға бағытталған. Бұл көптеген бактериялық штамдар мен саңырауқұлақтардың медициналық тәжірибеде бар антибиотиктер мен зеңгеқарсы препараттарға төзімділігінің кең таралуына байланысты. Осыған байланысты ғылыми әдебиеттерде белгілі фармакофорлық топтарды қамтитын немесе белгісіз және зерттелмеген белсенділігі бар қосылыстардың жаңа құрылымдық тобы болып табылатын органикалық туындылардың әр түрлі тобынан жаңа потенциалды антибиотиктерді синтездеуге байланысты жұмыстар саны артып келеді. Осы жұмыста изоникотин мен салицил қышқылдарының физиологиялық белсенді гидразидтері және зертханалық қолжетімді ацетилмен орынбасылған гетероциклдар негізінде әдебиетте сипатталмаған гидразондардың жаңа туындылары — 3-ацетил-2*H*-хромен-2-он 3, 2-ацетил-3*H*-бензо[f]хромен-3-он 4 және 2,6-метанобензо[g][1,3,5]-оксадиазоцин 5 алынды. Алынған гидразондардың құрылымы ИҚ- және ЯМР <sup>1</sup>H, <sup>13</sup>C-спектроскопия деректерімен дәлелденді. Синтезделген жаңа 6 гидразон грамоң бактериялар *Staphylococcus aureus* 209P, грамтеріс бактериялар *Pectobacterium carotovorum* VKM-B1247, ашытқы тәрізді саңырауқұлақтар *Candida albicans* ATCC 10231 микроорганизмдер штамдарында бактерияғақарсы және зеңгеқарсы белсенділікке биологиялық скринингтен өтті. Скрининг нәтижесінде микробқақарсы белсенділігі бар 3 қосылыс және бір перспективалы қосылыс — (E)-2-гидрокси-N<sup>1</sup>-(1-(2-оксохроман-3-ил)этилиден)бензогидразид 9 анықталды, ол микробқақарсы белсенділікпен қатар, зеңге қарсы белсенділікті де көрсетті.

*Кілт сөздер:* гидразидтер, изониазид, салицил қышқылы гидразиді, кумариндер, 3-ацетил-2*H*-хромен-2-он, 2-ацетил-3*H*-бензо[f]хромен-3-он, 2,6-метанобензо[g][1,3,5]оксадиазоцин, гидразондар, микробқақарсы белсенділік.

Д.М. Тургуналиева, Д.С. Дилбарян, А.С. Васильченко, О.А. Нуркенов,  
С.Д. Фазылов, Г.Ж. Карипова, Т.М. Сейлханов, И.В. Кулаков

### **Синтез и антибактериальная активность гидразонов изоникотиновой и салициловой кислот на основе ацетилпроизводных кумарина и бензо[g][1,3,5]оксадиазоцина**

В последние десятилетия усилия многих исследователей химиков-органиков, медиков и фармакологов сосредоточены на поиске новых средств с выраженной антибактериальной и, особенно, противогрибковой активностью. Это связано с повсеместным ростом резистентности многих бактериальных штаммов и грибов к имеющимся в медицинской практике антибиотикам и противогрибковым препаратам. В связи с этим в научной литературе увеличивается число работ, связанных с синтезом новых потенциальных антибиотиков из самого разнообразного класса органических производных, которые либо включают известные фармакофорные группы, либо представляют собой новый структурный класс соединений с неизвестной и неизученной активностью. В настоящей работе нами показано, что на основе физиологически активных гидразидов изоникотиновой и салициловой кислот и лабораторно доступных ацетилзамещенных гетероциклов — 3-ацетил-2*H*-хромен-2-он 3, 2-ацетил-3*H*-бензо[f]хромен-3-он 4 и 2,6-метанобензо[g][1,3,5]оксадиазоцин 5 были получены новые неописанные в литературе производные гидразонов. Структура полученных гидразонов однозначно доказана данными ИК- и ЯМР <sup>1</sup>H, <sup>13</sup>C- спектроскопией. Синтезированные новые шесть гидразонов прошли биологический скрининг на антибактериальную и противогрибковую активность на штаммах микроорганизмов: грамположительной бактерии *Staphylococcus aureus* 209P, грамотрицательной бактерии *Pectobacterium carotovorum* VKM-B1247, дрожжеподобного гриба *Candida albicans* ATCC 10231. В результате скрининга было выявлено три соединения, обладающих антимикробной активностью, и одно перспективное соединение — (E)-2-гидрокси-N<sup>1</sup>-(1-(2-оксохроман-3-ил)этилиден)бензогидразид 9, которое, наряду с антимикробной активностью, также проявляет и противогрибковую.

*Ключевые слова:* гидразиды, изониазид, гидразид салициловой кислоты, кумарины, 3-ацетил-2*H*-хромен-2-он, 2-ацетил-3*H*-бензо[f]хромен-3-он, 2,6-метанобензо[g][1,3,5]оксадиазоцин, гидразоны, антимикробная активность.

## References

- 1 Kennedy, D.A., Read, A.F. (2018). Why the evolution of vaccine resistance is less of a concern than the evolution of drug resistance *PNAS*, 115, 12878–12886. <https://doi.org/10.1073/pnas.1717159115>
- 2 Prestinaci, F., Pezzotti, P., Pantosti, A. (2015). Antimicrobial Resistance: A Global Multifaceted Phenomenon. *Pathog. Glob. Health*, 109(7), 309–318. <https://doi.org/10.1179/2047773215Y.0000000030>
- 3 Johansson, M.H.K., Bortolaia, V., Tansirichaiya, S., Aarestrup, F.M., Roberts, A.P., Petersen, T.N. (2020). Detection of Mobile Genetic Elements Associated with Antibiotic Resistance in Salmonella Enterica Using a Newly Developed. *J. Antimicrob. Chemother.*, 76, 101–109. <https://doi.org/10.1093/jac/dkaa390>
- 4 Retrieved from: <https://www.who.int/news-room/fact-sheets/detail/antimicrobial-resistance>.
- 5 Retrieved from: <https://www.who.int/campaigns/world-antibiotic-awareness-week>.
- 6 Saha M., Sarkar A. (2021). Review on Multiple Facets of Drug Resistance: A Rising Challenge in the 21st Century. *J. Xenobiot.* 11(4), 197–214. <https://doi.org/10.3390/jox11040013>
- 7 Rajpara N., Kutar B. M., Sinha R., Nag D., Koley H., Ramamurthy T., Bhardwaj A. K. (2015). Role of integrons, plasmids and SXT elements in multidrug resistance of *Vibrio cholerae* and *Providencia vermicola* obtained from a clinical isolate of diarrhea. *Front Microbiol.*, 6, 57. <https://doi.org/10.3389/fmicb.2015.00057>
- 8 Khan M.S., Siddiqui S.P., Tarannum N. (2017). A systematic review on the synthesis and biological activity of hydrazide derivatives. *Hygeia. J.D. Med.*, 9(1), 61–79. <https://doi.org/10.15254/H.J.D. Med.9.2017.165>
- 9 Narang R., Narasimhan B., Sharma S. (2012). A review on biological activities and chemical synthesis of hydrazide derivatives. *Curr Med Chem.*, 19, 569–612. <https://doi.org/10.2174/092986712798918789>
- 10 Mali, S.N., Thorat, B.R., Gupta, D.R., Pandey, A. (2021). Mini-Review of the Importance of Hydrazides and Their Derivatives — Synthesis and Biological Activity. *Eng. Proc.*, 11, 21. <https://doi.org/10.3390/ASEC2021-11157>
- 11 Verma, G., Marella, A., Shaquiquzzaman, M., Akhtar, M., Ali, M.R., Alam, M.M. (2014). A review exploring biological activities of hydrazones. *J. Pharm. Bioallied. Sci.*, 6(2), 69–80. <https://doi.org/10.4103/0975-7406.129170>
- 12 Kulakov, I.V., Nurkenov, O.A., Gazalieva, M.A., Zhaugasheva, C.K., & Isakova, Zh.O. (2007). Sintez i tuberkulostaticheskaia aktivnost gidrazidov i atsilgidrazidov aminouksusnykh kislot na osnove efedrinovykh alkaloidov [Synthesis and tuberculostatic activity of hydrazides and acylhydrazides of aminoacetic acids based on ephedrine alkaloids]. *Khimiko-farmatsevticheskii zhurnal — Pharmaceutical Chemistry Journal*, 41(11), 52 [in Russian].
- 13 Mashkovskii, M.D. (2012). *Lekarstvennye sredstva [Medicines]*. Moscow: Novaia volna [in Russian].
- 14 Rollas, S., Küçükgülzel, S.G. (2007). Biological Activities of Hydrazone Derivatives. *Molecules*, 12(8), 1910. <https://doi.org/10.3390/12081910>
- 15 Manikandan, V., Balaji, S., Senbagam, R., Vijayakumar, R., Rajarajan, M., Vanangamudi, G., Thirunarayanan, G. (2017). Synthesis and antimicrobial activities of some (E)-N<sup>1</sup>-(substituted benzylidene)benzohydrazides. *IJAC*, 5(1), 17. <https://doi.org/10.14419/ijac.v5i1.7155>
- 16 Popiolek, Ł., Biernasiuk, A. (2017). Synthesis and investigation of antimicrobial activities of nitrofurazone analogues containing hydrazide-hydrazone moiety. *Saudi Pharm. J.*, 25(7), 1097. <https://doi.org/10.1016/j.jsps.2017.05.006>
- 17 Raja, A.S., Agarwal, A.K., Mahajan, N., Pandeya, S.N., Ananthan, S. (2010). Antibacterial and antitubercular activities of some diphenyl hydrazones and semicarbazones. *Indian J. Chem. Sect. B.*, 49, 1384–1388.
- 18 *Gosudarstvennyi reestr lekarstvennykh sredstv [State register of medicines]*. (2009). (In 2 vols.) Moscow: Meditsinskii sovet [in Russian].
- 19 Glushkov, G., & Mashkovskiy, M.D. (1990). Sovremennye tendentsii razvitiia poiska i sodaniia novykh lekarstvennykh sredstv [Modern trends in the development of the search for and creation of new drugs]. *Khimiko-farmatsevticheskii zhurnal — Pharmaceutical Chemistry Journal*, 7, 4 [in Russian].
- 20 Brogden, R.N., Heel, R.C., Pakes, G.E., Speight, T.M., Avery, G.S. (1980). Diflunisal: a review of its pharmacological properties and therapeutic use in pain and musculoskeletal strains and sprains and pain in osteoarthritis. *Drugs*, 19(2), 84–106. <https://doi.org/10.2165/00003495-198019020-00002>
- 21 Shoelson S.E., Lee J., Goldfine A.B. (2006). Inflammation and insulin resistance. *J. Clin. Invest.*, 116(7), 1793–801. <https://doi.org/10.1172/JCI29069>
- 22 Fleischman, A., Shoelson, S.E., Bernier, R., Goldfine, A.B. (2008). Salsalate improves glycemia and inflammatory parameters in obese young adults. *Diabetes Care*, 31, 289–294. <https://doi.org/10.2337/dc07-1338>
- 23 Ivanskii, I.V. (n.d.). *Khimiiia organicheskikh preparatov [Chemistry of organic pharmaceutical]*. Moscow: Vysshiaia shkola [in Russian].
- 24 Goldfine A.B., Fonseca V., Jablonski K.A., Chen Y.D., Tipton L., Staten M.A., Shoelson S.E. (2013). Targeting Inflammation Using Salsalate in Type 2 Diabetes Study Team. Salicylate (salsalate) in patients with type 2 diabetes: a randomized trial. *Ann Intern Med.*, 159(1), 1–12.
- 25 Anderson, K., Wherle, L., Park, M., Nelson, K., Nguyen, L. (2014). Salsalate, an old, inexpensive drug with potential new indications: a review of the evidence from 3 recent studies. *Am Health Drug Benefits*, 7(4), 231-5.
- 26 Kumar, N., Bhatnagar, A., Dudhe, R. (2017). Synthesis of 3-(4,5-dihydro-1-phenyl-5-substituted phenyl-1H-pyrazol-3-yl)-2H-chromen-2-one derivatives and evaluation of their anticancer activity. *Arabian Journal of Chemistry*, 10(2), 2443-2452.
- 27 Kulakov, I.V., Talipov, S.A., Shulgau, Z.T., Seilkhanov, T.M. (2014). Synthesis, structure and antiradical activity of new derivatives of methano[1,3]thiazolo- [2,3-D] [1,3,5] benzoxadiazocin. *Chem. Heterocycl. Compd.*, 50, 1477.

- 28 Hui, Y., Wang, X., Yu, Z., Fan, X., Cui, B., Zhao, T., Mao, L., Feng, H., Lin, L., Yu, Q., Zhang, J., Wang, B., Chen, X., Zhao, X., Sun, C. (2020). Scoparone as a therapeutic drug in liver diseases: pharmacology, pharmacokinetics and molecular mechanisms of action. *Pharmacol. Res.*, 160, 105170. <https://doi.org/10.1016/j.phrs.2020.105170>
- 29 Lin, J., Li, X., Qi, W., Yan, Y., Chen, K., Xue, X., Xu, X., Feng, Z., Pan, X. (2018). Isofraxidin inhibits interleukin-1 $\beta$  induced inflammatory response in human osteoarthritis chondrocytes. *Int. Immunopharm.*, 64, 238–245. <https://doi.org/10.1016/j.in-timp.2018.09.003>
- 30 Majnooni, M.B., Fakhri, S., Shokoohinia, Y., Mojarrab, M., Kazemi-Afrakoti, S., Farzaei, M.H. (2020). Isofraxidin: Synthesis, Biosynthesis, Isolation, Pharmacokinetic and Pharmacological Properties. *Molecules*, 25(9), 2040. <https://doi.org/10.3390/molecules25092040>
- 31 Capra, J.C., Cunha, M.P., Machado, D.G., Zomkowski, A.D.E., Mendes, B.G., Santos, A.R. S., Pizzolatti, M.G., Rodrigues, A.L.S. (2010). Antidepressant-like effect of scopoletin, a coumarin isolated from *Polygala sabulosa* (Polygala-laceae) in mice: evidence for the involvement of monoaminergic systems. *Eur. J. Pharmacol.*, 643, 232–238. <https://doi.org/10.1016/j.ejphar.2010.06.043>
- 32 Kang, S.Y., Sung, S.H., Park, J.H., Kim, Y.C. (1998). Hepatoprotective activity of scopoletin, a constituent of *Sola-num lyratum*. *Arch Pharm. Res. (Seoul)*, 21, 718. <https://doi.org/10.1007/BF02976764>
- 33 Mogana, R., Teng-Jin, K., Wiart, C. (2013). Anti-inflammatory, anticholinesterase, and antioxidant potential of scopoletin isolated from canarium patentinervium Miq. (Burseraceae Kunth). *Evid.-Based Complement. Altern. Med. ECAM*, 734824. <https://doi.org/10.1155/2013/734824>
- 34 Kirsch, G., Abdelwahab, A.B., Chaimbault, P. (2016). Natural and Synthetic Coumarins with Effects on Inflammation. *Molecules*, 21, 1322. <https://doi.org/10.3390/molecules21101322>
- 35 Fylaktakidou K.C., Hadjipavlou-Litina D.J., Litinas K.E., Nicolaidis D.N. (2004). Natural and synthetic coumarin derivatives with anti-inflammatory and antioxidant activities. *Curr Pharm.*, 10(30), 3813-33. <https://doi.org/10.2174/1381612043382710>
- 36 Gouda, M., Hussein, B., El-Demerdash, A., Elsayed, M., Salem, M., Helal, M., Hamama, W. (2019). A Review: Synthesis and Medicinal Importance of Coumarins and their Analogues (Part II). *Current Bioactive Compounds*, 15. <https://doi.org/10.2174/157340721566619111120604>
- 37 Kubrak, T., Podgórski, R., Stompor — Gorący, M. (2017). Natural and Synthetic Coumarins and their Pharmacological Activity. *European Journal of Clinical and Experimental Medicine*, 15, 169-175. <https://doi.org/10.2174/1381612043382710>
- 38 Mayer, T.U., Kapoor, T.M., Haggarty, S.J., King, R.W., Schreiber, S.L., Mitchison, T.J. (1999). Small Molecule Inhibitor of Mitotic Spindle Bipolarity Identified in a Phenotype-Based Screen. *Science*, 286, 971. <https://doi.org/10.1126/science.286.5441.971>

#### Information about authors\*

**Turgunalieva, Daria Maratovna** — postgraduate student, Institute of Chemistry, University of Tyumen, Perekopskaya St., 15a, 625003, Tyumen, Russia; e-mail: [d.m.turgunalieva@utmn.ru](mailto:d.m.turgunalieva@utmn.ru);

**Dilbaryan, Diana Saghatelovna** — Research laboratory assistant, Laboratory of Antimicrobial Resistance, Institute of Environmental and Agricultural Biology (X-BIO), University of Tyumen, Lenina St., 23, Tyumen, 625003, Russia; e-mail: [d.s.dilbaryan@utmn.ru](mailto:d.s.dilbaryan@utmn.ru);

**Vasilchenko, Alexey Sergeevich** — Candidate of biological sciences, Laboratory of Antimicrobial Resistance, Institute of Environmental and Agricultural Biology (X-BIO), University of Tyumen, Lenina St., 23, 625003, Tyumen, Russia, [a.s.vasilchenko@utmn.ru](mailto:a.s.vasilchenko@utmn.ru); <https://orcid.org/0000-0001-9970-4881>;

**Kulakov, Ivan Vyacheslavovich** (*corresponding author*) — Doctor of chemical sciences, Associated Professor, Institute of Chemistry, University of Tyumen, Perekopskaya St., 15a, 625003, Tyumen, Russia; e-mail: [i.v.kulakov@utmn.ru](mailto:i.v.kulakov@utmn.ru); <https://orcid.org/0000-0001-5772-2096>;

**Nurkenov, Oralgazy Aktayevich** — Doctor of chemical sciences, Professor, LLP "Institute of Organic Synthesis and Coal Chemistry of the Republic of Kazakhstan", Alikhanov str., 1, 100000, Karaganda, Kazakhstan; e-mail: [nurkenov\\_oral@mail.ru](mailto:nurkenov_oral@mail.ru); <https://orcid.org/0000-0003-1878-2787>;

**Fazylov, Serik Drakhmetovich** — Academician of the National Academy of Sciences of the Republic of Kazakhstan, Doctor of chemical sciences, Professor, LLP "Institute of Organic Synthesis and Coal Chemistry of the Republic of Kazakhstan", Alikhanov str., 1, 100000, Karaganda, Kazakhstan; e-mail: [iosu8990@mail.ru](mailto:iosu8990@mail.ru); <https://orcid.org/0000-0002-4240-6450>;

**Karipova, Gulzhanat Zhumazhanovna** — Master, researcher, LLP "Institute of Organic Synthesis and Coal Chemistry of the Republic of Kazakhstan", Alikhanov str., 1, 100000, Karaganda, Kazakhstan; e-mail: [gulja\\_1708@mail.ru](mailto:gulja_1708@mail.ru); <https://orcid.org/0000-0002-3896-6156>

**Seilkhanov, Tolegen Muratovich** — Candidate of Chemical Sciences, Head of the laboratory of engineering profile NMR spectroscopy, Sh. Ualikhanov Kokshetau State University, Abay str., 76, 020000, Kokshetau, Kazakhstan. e-mail: [tseilkhanov@mail.ru](mailto:tseilkhanov@mail.ru), <https://orcid.org/0000-0003-0079-4755>.

\*The author's name is presented in the order: *Last Name, First and Middle Names*

N.F. Normurodov\*, Q.N. Berdinazarov, M. Abdurazakov, N.R. Ashurov

*Uzbekistan Academy of Sciences, Institute of Polymer Chemistry and Physics, Tashkent, Uzbekistan*

(\*Corresponding author's e-mail: [nmf7mf7@gmail.com](mailto:nmf7mf7@gmail.com))

## **Mechanical and Thermal Properties of Biodegradable Composites Based on graft copolymer LLDPE-g-MA/Gelatin**

The uncontrolled development of morphology at the stage of formation of biodegradable compositions based on synthetic and natural polymers limits the possibility of achieving satisfactory physical and mechanical and operational characteristics. In the present work, to achieve finely dispersed mixture morphology, an approach was proposed for reactive mixing of functionalized polyethylene with gelatin to form a linear low density polyethylene-grafted-maleic anhydride and gelatin (LLDPE-g-MA/GEL) graft copolymer. Using the selective extraction of the mixture components, we determined amount of graft copolymer LLDPE-g-MA/GEL, free gelatin, mechanical and thermal properties, as well as biodegradability data. It was found that as the amount of maleic groups in the polyethylene macromolecule increased, the amount of graft copolymer increased, and an increase in the content of gelatin in the blend led to a noticeable increase in the elastic modulus, tensile strength, and a decrease in elongation at break. Due to the degradation of gelatin, the thermal stability of the composite (initial temperature) decreased with increasing gelatin content. The maximum rate of destruction of the graft copolymer in the temperature range of 400–500 °C increased markedly with an increase in the content of gelatin. It was found that the rate of biodegradability would increase with an increase in the content of gelatin in the blend; the maximum level of degradation was observed during the first 10 days and was more than 50 %. It was found that the maximum degree of grafting LLDPE-g-MA and gelatin to each other depended on the amount of maleic anhydride in the graft copolymer. The maximum degree of grafting was observed to be higher with increasing amount of maleic anhydride in the composites.

*Keywords:* Biodegradation, gelatin, glycerin, polyethylene, maleic anhydride, polymer composite.

### *Introduction*

The packaging industry needs biodegradable materials. Traditional synthetic polymers, in particular polyolefins, despite a good combination of production technology, the possibility of varying physical and mechanical characteristics and prices, pose significant problems for ecology and the environment.

An analysis of the scientific literature indicates that the solution to this problem is seen in the use of biopolymers, or their combination with synthetic polymers. These approaches, of course, have their limitations, such as optimization of physical and mechanical characteristics (with accelerated natural biodegradability) and limited degradability, depending on the biopolymer/synthetic polymer ratio, respectively. The list of promising biopolymers includes proteins (soy and milk proteins, gelatin, etc.) and polysaccharides (chitosan, carboxymethylcellulose, starch, etc.). Gelatin and starch occupy leading positions in the creation of packaging materials based on them due to their low cost [1–4]. The special structure of these biopolymers, that is, the presence of a dense network of hydrogen bonds between macromolecules, requires plasticization to transfer to a thermoplastic state. Many studies carried out in this direction [5–11] have shown the fundamental possibility of forming biodegradable high-quality films with satisfactory physical and mechanical properties. Generally accepted, gelatin is defined as the product obtained by the partial hydrolysis of collagen present in the skin, connective tissues and bones of animals [12, 13]. The structure of gelatin includes a certain sequence of hydrophilic amino acids (glycine, proline, hydroxyproline), when an aqueous solution of gelatin is cooled, a gel is formed with the restoration of the collagen triple helix. The most effective plasticizers for gelatin are glycerol, sorbitol, polyethylene glycols, the variation of the content of which makes it possible to obtain films with a tensile strength in the range of one hundred MPa and more, an elastic modulus of hundreds of MPa with very low relative deformation. At the same time, the high sensitivity of gelatin to water, that is low barrier properties to water vapor (swelling, dissolution) hinder the scale of production and use [14–16].

From this point of view, interest in the creation of blends of gelatin with synthetic polymers continues unabated [17]. At the same time, it was noted that the usual mixing of gelatin with polyolefin in various rati-

os gave very low biodegradability rates (up to 10 %). Optimization of the blend morphology by transferring gelatin to a thermoplastic state slightly increased this indicator, and record biodegradability rates were achieved when creating conditions for the formation of graft copolymers of polyethylene with gelatin (more than 80 %) [18].

In this work, the formation of such a structure was carried out by means of an additional stage; blends of gelatin with polyethylene were obtained on pre-irradiated polyethylene ( $^{60}\text{Co}$  source, dose 3.4 kGy/h). Unfortunately, these studies lack the structural data of the polyethylene matrix and their inherent physico-mechanical and thermal characteristics. Previously, we showed [19] the realization of such a possibility on maleated polyethylene.

This approach was implemented via the formation of a graft copolymer throughout the entire volume of the sample, which ultimately resulted in the desired finely dispersed mixture morphology. In mixtures, depending on the content of gelatin and the level of maleated polyethylene, along with the graft copolymer, the presence of free gelatin was detected. The latter, as a rule, aggregated with the gelatin fragment of the graft copolymer. It was of interest to reveal the relationship of structural elements with the physical, mechanical and temperature characteristics of the compositions. The results obtained indicated that mixtures with a finely dispersed morphology increased elastic-strength properties with satisfactory deformability.

### *Materials and research methods*

#### *Materials*

Linear low-density polyethylene (LLDPE, Shurtan Gas Chemical Complex of the Republic of Uzbekistan) grade F-0320,  $d = 0.920 \text{ g/cm}^3$ , MFI = 2.5 g/10 min (at a load of 2.16 kg,) and edible gelatin (GEL) grade P-200 (State Standard 11293–2019, JSC “MOGELIT”, Belarus) were used without any purification. Maleic anhydride (MA,  $\text{C}_4\text{H}_2\text{O}_3$ , analytical grade, colorless rhombic crystals,  $M_r = 98.06 \text{ g/mol}$ ) was distilled at  $T_{\text{bp}} = 84.0 \text{ }^\circ\text{C}/14 \text{ mm Hg}$ ,  $T_m = 60 \text{ }^\circ\text{C}$ ,  $\rho^{60} = 1.3140 \text{ g/cm}^3$ .

#### *Preparation of thermoplastic gelatin*

To dissolve gelatin granules and make them thermoplastic, glycerin was added to distilled water and stirred until the same mixture was obtained. Gelatin was added to the resulting mixture and mixed again, then heated in an oven at  $80 \text{ }^\circ\text{C}$  for two hours.

#### *Functionalization*

Functionalization of LLDPE with maleic anhydride (LLDPE-g-MA) was carried out on a Brabender plastograph (Plasticorder Brabender OHGDUISBURG Germany), with a cam velocity of 98 rpm and at a temperature of  $180 \pm 5 \text{ }^\circ\text{C}$  [19]. The concentration of grafted maleic anhydride was varied in the range of 0.5–5.0 wt%.

Polymer blends based on LLDPE-g-MA and gelatin were obtained on a Brabender plastograph, for 30 min, at 50 rpm and  $180 \pm 5 \text{ }^\circ\text{C}$  by adding plasticized gelatin to the LLDPE-g-MA melt.

The maximum grafting percentage of LLDPE-g-MA and gelatin was 114 %; the grafting percentage was calculated by extracting unreacted PE and gelatin with water and xylene.

Grafting rate was calculated using the following formula:

$$\text{Grafting \%} = (W_g - W_o) / W_o \times 100, \quad (1)$$

where  $W_o$  and  $W_g$  are the masses of the initial composite and after the complete removal of polyethylene and gelatin that did not participate in the reaction, respectively [18].

#### *Bio-degradability test (Soil Degradation)*

The polymer compositions were tested for biodegradation in the form of films in a specially prepared soil (with a moisture content of at least 25 %). During the testing period, the soil moisture was maintained at 30 %, and the samples were immersed to a depth of 15 cm. Soil samples were removed every 10 days for biodegradation testing, washed in ethanol, wiped and equilibrated in a desiccator for at least one day before weight was recorded. Sample weight loss ( $W$ ) in % was determined depending on the number of days as follows:

$$W = (W_0 - W_i) / W_0 \times 100. \quad (2)$$

Weight loss in % after every 10 days ( $W_{\text{di}}$ ):

$$W_{\text{di}} = (W_i - W_{i-1}) / W_i \times 100, \quad (3)$$

where  $W_0$  is the initial mass, g;  $W_i$  is the final weight every 10 days;  $W_{i-1}$  is the initial weight every 10 days [18, 20].

*Physico-mechanical tests*

The tensile diagrams of the samples were determined on a SHIMADZU AG-X plus universal testing machine (JAPAN) in the uniaxial tensile mode with a set strain rate in accordance with the requirements established by ASTM D 638-99 "Standard Test Method for the Strength Properties of Plastics".

For analysis, at least five samples of the studied material were used, made in the form of double-sided blades with a thickness of 2 mm. For measuring tensile module (E), 1 mm/min crosshead velocity was chosen until 0.3 % deformation, after that crosshead velocity was increased immediately to 20 mm/min for further exploring yield stress ( $\sigma$ ) and deformation ( $\epsilon$ ).

*DSC and TGA measurements*

Thermal analyses DSC and TGA of polymer blends was carried out in a dynamic mode on a LINSEIS THERMAL ANALYSIS PT1600 [thermogravimetric analysis (TGA)] instrument (in air atmosphere) in the range from room temperature to 1000 °C, guided by the requirements established by the ASTM E 1131 standard. The heating rate was 10 °C/min; the sample weight for analysis was from 2 to 100 mg.

*Results and Discussion*

The uniform distribution of the gelatin phase in the polyethylene matrix and their accessibility to microorganisms determine the biodegradation efficiency of such compositions [20]. The desired uniform distribution is achievable by grafting gelatin onto the polyethylene macromolecules. The possibility of implementing this reaction was shown by us [21] using a maleated linear copolymer of ethylene with butene-1 (MA content was 0.5–5 wt %) and in [18] on pre-irradiated polyethylene [22]. It should be noted that before obtaining blends of polyethylene with gelatin, the latter must be transferred to a thermoplastic state by plasticizing the optimal ratio of glycerol with water [23–25].

To determine the blends compositions at the selected polyethylene/gelatin ratios, the extraction experiments were carried out using xylene and water to selectively dissolve the components, respectively. Due to the gelatin degradation under conditions of LLDPE dissolution in xylene at a temperature of 120 °C, we analyzed only the extraction data in an aqueous medium. Taking into account that unreacted gelatin was extracted under these conditions, we calculated the amount of polyethylene-gelatin graft copolymer (Table 1).

Table 1

**Amount of grafted LLDPE-g-MA/gelatin and unreacted gelatin**

Samples	70/30	60/40	50/50	40/60
Extraction Products	%	%	%	%
LLDPE-g-MA(0.5 %)/GEL				
Pure gelatin %	7.6	10.8	20.5	39.5
LLDPE-g-MA-g-GEL %	39.6	59.5	79.6	90.8
LLDPE-g-MA(5 %)/GEL				
Pure gelatin %	1.8	8.5	13.7	24
LLDPE-g-MA-g-GEL %	42	61	86.3	114

As can be seen from the table, the amount of free gelatin varied between 1.8–24 % by weight when its content in the composition of the initial blend was 30–60 % wt., respectively, in relation to the content of PE. Based on these data, the grafting degree of gelatin to polyethylene was determined. Naturally, as the gelatin increased, the degree of grafting increased in the range of 42–114 % by weight. Blends formed in the presence of thermoplastic gelatin with the formation of a graft copolymer were homogeneous formations with a uniform distribution of components [19]. Increasing the gelatin concentration above equimolar with respect to the concentration of maleic groups in polyethylene resulted in the formation of an additional gelatin phase, which agglomerated with the gelatin end of the graft copolymer in the form of a dispersed phase.

As expected, blends of gelatin with polyethylene containing 0.5 % wt. of maleic anhydride contained a markedly higher amount of unreacted gelatin, 7.6–39.5 % wt. On that case, the grafting degree for the same initial formulations was 39.6–90.8 % by weight.

TGA and DSC measurements

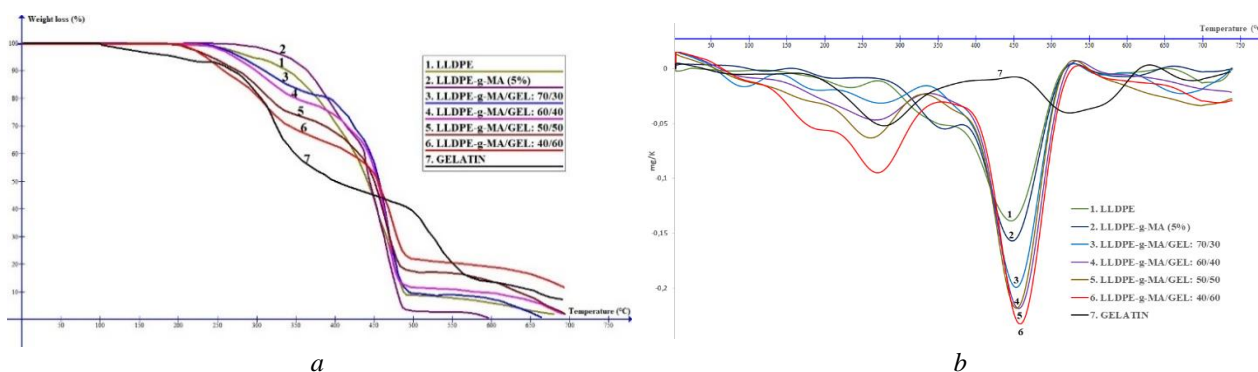


Figure 1. Thermogravimetric curves (a) and the first derivative of the TGA curves (b) of the film sample

In mixtures, depending on the content of gelatin and the level of polyethylene maleization, along with the graft copolymer, the presence of free gelatin was detected. The latter, as a rule, aggregated with the gelatin fragment of the graft copolymer.

The presence of these reaction products was noticeably manifested in the thermogravimetric characteristics (Fig. 1). The initial degradation temperature ( $T_i$ ) and the temperature of the maximum degradation rate ( $T_{max}$ ) for various compositions of mixtures and initial components are given in Table 2.

Table 2

Thermal characteristics of LLDPE-g-MA/gelatin blends

No.	Sample name and component ratio (wt%)	The temperature corresponding to the loss of mass is °C			Degree of crystallinity, %	
		Initial degradation temperature $T_i$ , °C	Maximum thermal decomposition rates ( $T_{max}$ ), °C			
			first stage	second stage	third stage	
1	LLDPE	186	100–200 °C $m(mg) \leq 10\%$	275–400 °C $10 \leq m(mg) \leq 50\%$	400–500 °C $m(mg) \geq 50\%$	19.85
2	LLDPE-g-MA (5 %)	242				18.15
3	LLDPE-g-MA/GEL 70/30	233				14.85
4	LLDPE-g-MA/GEL 60/40	223				13.32
5	LLDPE-g-MA/GEL 50/50	190				12.02
6	LLDPE-g-MA/GEL 40/60	201				10.4
7	GELATIN	97				-

The thermal decomposition of the LLDPE-g-MA/gelatin mixture on TGA curves consisted of three sequential stages. The first stage in the temperature range of 100–200 °C was due to the loss of absorbed and bound water molecules (weight loss less than 10 % weight). The second stage, observed in the region of 275–400 °C (weight loss in the range of 10–50 wt%), corresponded to the breaking of peptide bonds in the gelatin macrochain [26]. Temperatures, depending on the expected rate of thermal decomposition of the gelatin phase, were found in the range of 250–280 °C. A partial contribution to the consumption of the composition in this area included the beginning of LLDPE-g-MA dehydration, an increased rate of thermal decomposition (third stage), which felt at a temperature of 450 °C. The position of this peak was practically independent of the content of gelatin in the composition; as the content of gelatin increased, it increased significantly at high temperatures (up to 7 °C). Summarizing the above TGA data, it can be noted that the formation of a graft copolymer LLDPE-g-MA/gelatin led to the decrease in thermal stability in terms of  $T_i$  by 10–40 °C, depending on the content of gelatin 30–60 wt%, respectively. While the maximum rate of thermal decomposition of the graft copolymer (third stage) increase in the biopolymer content increased significantly (from –0.14 to –0.23 mg/K) due to degradation of the grafted gelatin.

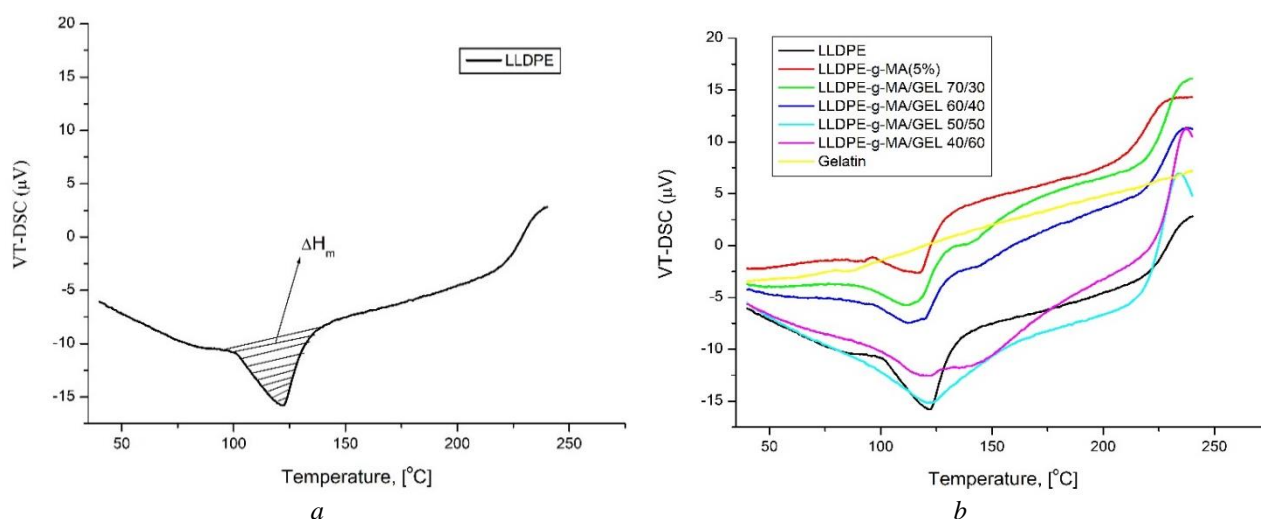


Figure 2. A fragment of the DSC curve of PE (a) Fragments of the DSC curves of the studied compositions (b)

Figure 2 a) shows a fragment of the DSC curve for a PE sample in the melting region. The endothermic peak is highlighted here (shaded part). The melting enthalpy  $\Delta H_m$  PE was determined, with the help of which it was possible to calculate the crystallinity degree of PE  $\chi_c$  (%) as a percentage according to equation (4):

$$\chi_c (\%) = \Delta H_m / \Delta H_{m0} \times 100 \%, \quad (4)$$

where  $\Delta H_{m0}$  is the value of the melting enthalpy of a hypothetical fully crystalline PE, which is equal to 293 J/g [27].

The values of  $\chi_c$  (%) for the rest of the studied samples were calculated in a similar way. For this, fragments of DSC curves were used, shown in Figure 2 b). This figure shows that the gelatin sample does not have an endothermic peak corresponding to the melting process, i.e. it does not crystallize. The calculations results of the crystallinity degree of all samples are presented in Table 2.

#### Mechanical properties

Interfacial adhesion is the determining parameter of the deformation process for the systems under consideration with an elastic matrix and rigid inclusions (gelatinous phase). It should be noted that the studied LLDPE-g-MA/gelatin blends differ from classical two-phase blends [28–34] in the form of clearly separated continuous and dispersed phases. In our case, the dispersed phase consists of segregated domains of grafted gelatin macrochains with free unreacted gelatin.

The general picture of the deformation process for blends proposed in [35] includes three stages, elastic (stage I — up to 1 % deformation), then slight delamination of the matrix from the surface of a rigid inclusion until the appearance of dumbbell-shaped microvoids (stage II — reaching the yield point) and the last stage (III stage) can manifest itself in two forms, as the destruction of the sample due to the coalescence of microvoids, or the ordering of macromolecules in the direction of the applied stress (called orientational crystallization, recrystallization, cold — drawing). Exactly on that part, interfacial adhesion is determined, the strengthening of which is accompanied by an increase in the stress at the yield point and the level of deformation.

Let's consider the features of the curves  $\sigma$ - $\varepsilon$  of the compositions studied (Fig. 3).

The introduction of maleic groups into the polyethylene macromolecule did not introduce significant changes in the shape of the  $\sigma$ - $\varepsilon$  curves; they contained all three stages of the deformation process. At the same time, the strengthening of intermolecular interactions, due to the presence of maleic functional groups (0.5–5 wt%), resulted in a noticeable increase in the yield stress (from 8.5 MPa to 13.5 MPa), tensile strength at break (from 11 MPa to 14.5 MPa), modulus of elasticity (from 130 MPa to 220 MPa).

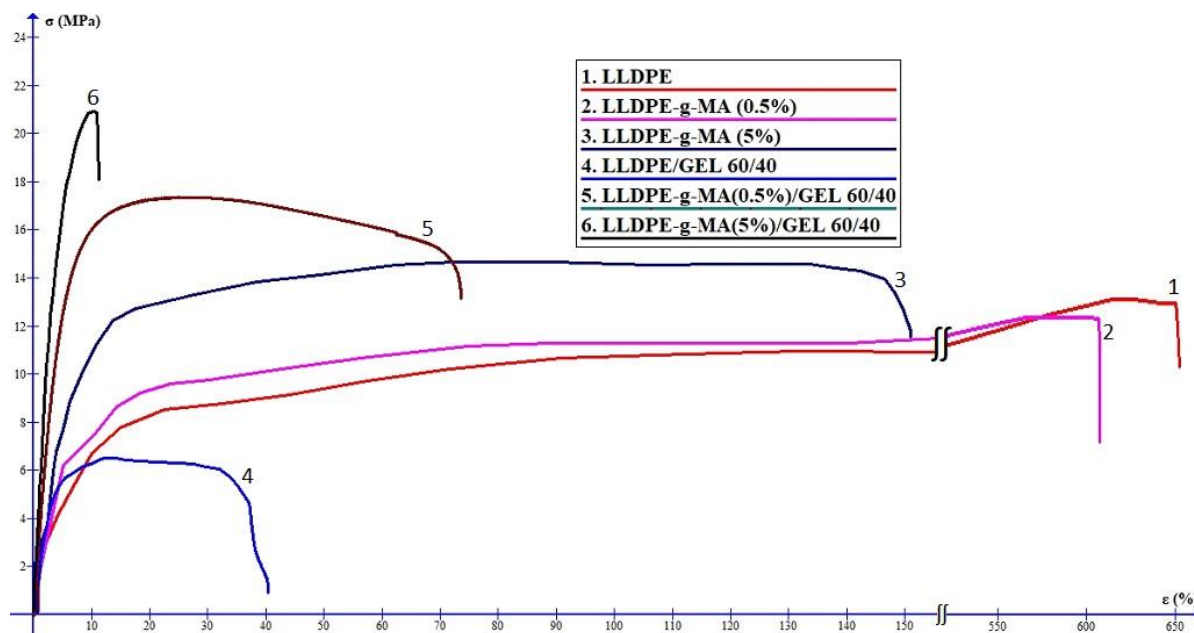


Figure 3. Mechanical properties of samples of different composition

There are curves of deformation of the composition of polyethylene with gelatin (ratio 60/40 % wt.) based on polyethylene with a content of 0 %, 0.5 %, 5 % wt. MA groups were undergone significant changes. On the  $\sigma$ - $\epsilon$  curves, the length of the orientational ordering stage noticeably decreased, that was, after reaching the yield stress, the coalescence of microvoids around inhomogeneities led to a sequence of fibrillation and rapid destruction processes. This was most pronounced for conventional blends of polyethylene with gelatin and polyethylene with a content of 5 % by weight, maleic groups, the relative elongation at break of which was 48 % and 11.5 %, respectively. Accounting for 80 % deformability, maleinization of polyethylene at the level of 0.5 % wt. was also significantly inferior to the original polyethylene (600 %). Let's consider the mechanical properties of the PE/gelatin composition by varying the content of gelatin based on polyethylene with different content of maleic groups (Table 3).

Table 3

**Physical and mechanical properties of composites**

No.	Content of composites	Tensile strength, MPa	Elongation at break, %	Young modulus, MPa
LLDPE/GEL				
1	LLDPE	11±0.22	655±0.5	129.9±3.6
2	70/30	7.03±0.31	125.6±11.3	237.79±10.12
3	60/40	6.52±0.28	48±10.4	253.19±31.96
4	50/50	3.8±0.26	26.8±6.6	179.8±31.12
5	40/60	4.4±0.21	15.6±5.3	293.62±44.78
LLDPE-g-MA(0.5 %)/GEL				
6	LLDPE-g-MA(0.5 %)	10.92±0.5	610.1±18.03	119.25±10.34
7	70/30	16.20±0.33	122.71±10.58	286.46±3.64
8	60/40	17.48±0.15	78.65±5.24	338.31±10.07
9	50/50	17.68±0.91	54.88±2.96	278.41±12.33
10	40/60	19.84±1.02	26.21±2.15	335.99±34.66
LLDPE-g-MA(5 %)/GEL				
11	LLDPE-g-MA(5 %)	14.65±0.28	146.8±7,32	218.1±5.8
12	70/30	17.41±1.9	12.40±1.84	481±10.98
13	60/40	20.63±1.74	11.43±1.41	550±27.77
14	50/50	24.02±3.24	10.21±1.29	676±8.07
15	40/60	27.56±2.42	6.73±1.06	736.53±49.84

In conventional compositions (the absence of graft copolymers), due to the lack of interfacial adhesion, and hence the weak stress transfer at the PE/gelatin interface, as the gelatin content increased, a noticeable drop in  $\sigma_y$ ,  $\sigma_{break}$ , and  $\varepsilon_{break}$  by more than 40 % was observed.

On the contrary, the presence of graft copolymers segregated with free gelatin enhanced  $\sigma_y$  and  $\sigma_{break}$  by 20-80 % (0.5 % wt. MA) and more than 100 % in polyethylene compositions with gelatin at content of 5 % wt. MA on a polyethylene macromolecule.

At the same time, the relative elongation at break for the composition based on graft copolymers, due to the presence of inhomogeneities at the phase boundary, as well as for conventional PE/gelatin compositions, was significantly reduced. As can be seen from Table 3, for all three groups of the composition, as the gelatin content increased, despite the insignificant degree of crystallinity of the polyethylene phase (Table 2), it increased in comparison with the original polyethylene and maleated polyethylenes in the range of 130 %, 180 %, and 240 %, respectively. This effect was due to the fact that the presence of hydrogen bonds in the structure of double helices of crystalline sections of gelatin provided a high elastic modulus, more than 1000 MPa [36, 37] compared to PE. Therefore, it can be observed that as the content of grafted gelatin increased, the elastic modulus increased for formulations with gelatin content of 60 % by weight from 300 MPa to more than 700 MPa.

Based on the totality of all mechanical characteristics, compositions of polyethylene with gelatin with a content of 0.5 wt % MA in the polyethylene chain are of the greatest interest for applications.

#### *Biodegradation of polymer composites*

The biodegradability of LLDPE-g-MA/gelatin compositions is shown in Figure 3 as a function of residence time in soil. As is known, attacking agents of the biodegradation process are microorganisms such as actinomycetes, fungi and bacteria [18, 38]. Almost all compositions reached the level of maximum degradation on the 40th-50th day of testing. The level of degradation as the content of gelatin in the composition increased (30 %, 40 %, 50 %, and 60 % by weight) was on the order of 20 %, 35 %, 48 %, 58 %, respectively. The highest degradation rate was observed for a mixture containing 60 wt% gelatin, less than 10 days degradation rate was 55 %.

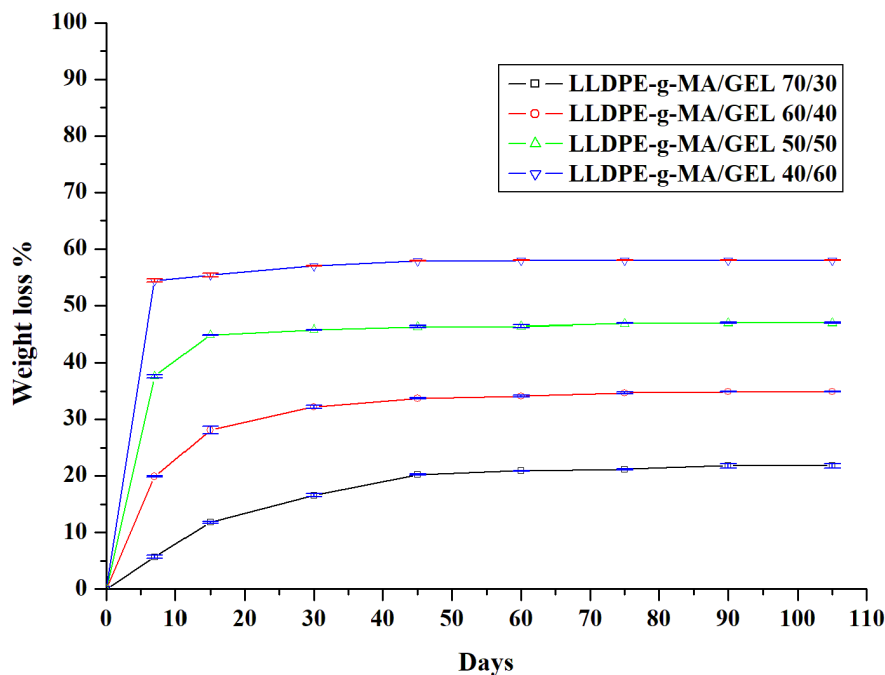


Figure 3. Weight loss of composites in the soil

Thus, the carried out studies showed the fundamental possibility of creating highly efficient biodegradable systems with a wide range of possible elastic and elastic properties. The achieved performance was due to the optimal morphology of the mixture and satisfactory interfacial adhesion of the components because of the formation of grafted LLDPE-g-MA/gelatin copolymers and segregated domains of grafted fragments and free gelatin.

### Conclusions

The grafting of thermoplastic gelatin to maleated polyethylene promoted the formation of homogeneous compositions with a finer dispersion of the gelatin phase in the polyethylene matrix. Depending on the content of maleic groups in polyethylene and the content of gelatin in the blend, the grafting degree varied between 40–150 %. Three stages of thermal decomposition of the LLDPE-g-MA/gelatin composition associated with the presence of water molecules, degradation of the gelatin and polyethylene phases were identified. The presence of gelatin significantly shifted the onset temperature of decomposition towards low temperatures (from 242 °C to 201 °C), while the temperature range of degradation of the polyethylene matrix did not undergo significant changes. The maximum rate of degradation of the graft copolymer in the temperature range of 400–500 °C with an increase in the content of gelatin noticeably increased from –0.14 to –0.23 mg/K.

The presence of gelatin in the composition in the form of grafted chains, compared to conventional blends of polyethylene with gelatin, led to an increase in yield stress, stress at breaking and elastic modulus by 80 % and 240 %, respectively. This trend was the most pronounced for the composition of PE with the content of MA groups of 5 wt%.

In terms of applications, polyethylene compositions with 0.5 wt. MA-groups exhibited good strength properties and modulus of elasticity in combination with satisfactory deformability. The resulting compositions exhibited high biodegradability of up to 58 %, the level of maximum degradation was observed on the 40-50th day. The weight loss rate was observed for the composition with a gelatin content of 60 wt%.

### References

- 1 Jayasekara, R., Harding, I., Bowater, I., & Lonergan, G. (2005). Biodegradability of a selected range of polymers and polymer blends and standard methods for assessment of biodegradation. *Journal of Polymers and the Environment*, 13(3), 231–251. <https://doi.org/10.1007/s10924-005-4758-2>
- 2 Rahman, M.M., & Khan, M.A. (2007). Surface treatment of coir (Cocos nucifera) fibers and its influence on the fibers' physico-mechanical properties. *Composites science and technology*, 67 (11–12), 2369–2376. <https://doi.org/10.1016/j.compscitech.2007.01.009>.
- 3 Willett, J.L., & Shogren, R.L. (2002). Processing and properties of extruded starch/polymer foams. *Polymer*, 43 (22), 5935–5947. [https://doi.org/10.1016/S0032-3861\(02\)00497-4](https://doi.org/10.1016/S0032-3861(02)00497-4)
- 4 Rahmani, B., Hosseini, H., Khani, M., Farhoodi, M., Honarvar, Z., Feizollahi, E., & Shojaee-Aliabadi, S. (2017). Development and characterisation of chitosan or alginate-coated low density polyethylene films containing *Satureja hortensis* extract. *International journal of biological macromolecules*, 105, 121–130. <https://doi.org/10.1016/j.ijbiomac.2017.07.002>
- 5 Khan, R.A., Khan, M.A., Sarker, B., Saha, S., Das, A.K., Noor, N., & Saha, M. (2010). Fabrication and Characterization of Gelatin Fiber-based Linear Low-density Polyethylene Foamed Composite. *Journal of reinforced plastics and composites*, 29(16), 2438–2449. <https://doi.org/10.1177/0731684409351168>
- 6 Hanani, Z.N., Roos, Y.H., & Kerry, J.P. (2014). Use and application of gelatin as potential biodegradable packaging materials for food products. *International journal of biological macromolecules*, 71, 94–102. <https://doi.org/10.1016/j.ijbiomac.2014.04.027>
- 7 Wang, L.Z., Liu, L., Holmes, J., Kerry, J.F., & Kerry, J.P. (2007). Assessment of film-forming potential and properties of protein and polysaccharide-based biopolymer films. *International journal of food science & technology*, 42(9), 1128–1138. <https://doi.org/10.1111/j.1365-2621.2006.01440.x>
- 8 Suderman, N., Isa, M.I.N., & Sarbon, N.M. (2018). The effect of plasticizers on the functional properties of biodegradable gelatin-based film: A review. *Food bioscience*, 24, 111–119. <https://doi.org/10.1016/j.fbio.2018.06.006>
- 9 Podshivalov, A., Zakharova, M., Glazacheva, E., & Uspenskaya, M. (2017). Gelatin/potato starch edible biocomposite films: Correlation between morphology and physical properties. *Carbohydrate Polymers*, 157, 1162–1172. <https://doi.org/10.1016/j.carbpol.2016.10.079>
- 10 Cho, S. Y., Park, J. W., & Rhee, C. (2002). Properties of laminated films from whey powder and sodium caseinate mixtures and zein layers. *LWT-Food Science and Technology*, 35(2), 135–139. <https://doi.org/10.1006/food.2001.0826>
- 11 Wangtueai, S., Chaiyaso, T., Rachtanapun, P., Jantrawut, P., Ruksiriwanich, W., Seesuriyachan, P., & Jantanasakulwong, K. (2022). Thermoplastic cassava starch blend with polyethylene-grafted-maleic anhydride and gelatin core-shell structure compatibilizer. *International Journal of Biological Macromolecules*, 197, 49–54. <https://doi.org/10.1016/j.ijbiomac.2021.12.003>
- 12 Ghorbani, K., Kouchaki, S., Sadeghi, N., Eslamifarsani, E., Rabbani, F., & Beyramysoltan, S. (2020). Distinguishing tissue origin of bovine gelatin in processed products using LC/MS technique in combination with chemometrics tools. *Food chemistry*, 319, 126302. <https://doi.org/10.1016/j.foodchem.2020.126302>

- 13 Wangtueai, S., Noomhorm, A., & Regenstein, J. M. (2010). Effect of microbial transglutaminase on gel properties and film characteristics of gelatin from lizardfish (*Saurida* spp.) scales. *Journal of food science*, 75(9), C731–C739. <https://doi.org/10.1111/j.1750-3841.2010.01835.x>
- 14 Wangtueai, S., Siebenhandl-Ehn, S., & Haltrich, D. (2016). Optimization of the preparation of gelatin hydrolysates with anti-oxidative activity from lizardfish (*Saurida* spp.) scales gelatin. *Chiang Mai J. Sci*, 43(1), 1122–1133. <https://epg.science.cmu.ac.th/ejournal/>
- 15 Yap, B.K., & Gam, L.H. (2019). Differentiation of bovine from porcine gelatin capsules using gel electrophoresis method. *Food chemistry*, 274, 16–19. <https://doi.org/10.1016/j.foodchem.2018.08.111>
- 16 Hanani, Z.N., Roos, Y.H., & Kerry, J.P. (2014). Use and application of gelatin as potential biodegradable packaging materials for food products. *International journal of biological macromolecules*, 71, 94–102. <https://doi.org/10.1016/j.ijbiomac.2014.04.027>
- 17 Sarker, B., Dey, K., & Khan, R.A. (2011). Effect of incorporation of polypropylene on the physico-mechanical and thermo-mechanical properties of gelatin fiber based linear low density polyethylene bio-foamed composite. *Journal of Thermoplastic Composite Materials*, 24(5), 679–694. <https://doi.org/10.1177/0892705711403525>
- 18 Kaur, I., Bhalla, T.C., Deepika, N., & Gautam, N. (2008). Biodegradation and swelling studies of gelatin-grafted polyethylene. *Journal of applied polymer science*, 107(6), 3878–3884. <https://doi.org/10.1002/app.27245>
- 19 Ashurov N.R., Sadikov Sh. G., Khakberdiev E.O., Berdinazarov K.N., Normurodov N.F. (2020). Preparation and properties of compositions based on polyethylene and gelatin. *Uzbek chemical journal*, 6(3), 53–60. <https://slib.uz/uz/edition/file-view?id=1154>
- 20 Mizanur Rahman, M., Karim, R., Mustafa, A.I., & Khan, M.A. (2012). Preparation and characterization of bioblends from gelatin and linear low density polyethylene (LLDPE) by extrusion method. *Journal of Adhesion Science and Technology*, 26(8–9), 1281–1294. <https://doi.org/10.1163/156856111x593603>
- 21 Ashurov, N.R., Sadikov, S.G., Normurodov, N.F., Berdinazarov, Q.N., & Khakberdiev, E.O. (2020). Degradation Features Of Polyethylene And Gelatin Compositions. *The American Journal of Applied Sciences*, 11(2), 131–138. <https://doi.org/10.37547/tajas/volume02issue11-24>
- 22 Kaur, I., Bhalla, T.C., Deepika, N., & Gautam, N. (2009). Study of the biodegradation behavior of soy protein-grafted polyethylene by the soil burial method. *Journal of Applied Polymer Science*, 111(5), 2460–2467. <https://doi.org/10.1002/app.29206>
- 23 Park, J.W., Whiteside, W.S., & Cho, S.Y. (2008). Mechanical and water vapor barrier properties of extruded and heat-pressed gelatin films. *LWT-Food Science and Technology*, 41(4), 692–700. <https://doi.org/10.1016/j.lwt.2007.04.015>
- 24 Ramos, M., Valdés, A., Beltran, A., & Garrigós, M.C. (2016). Gelatin-based films and coatings for food packaging applications. *Coatings*, 6(4), 41. <https://doi.org/10.3390/coatings6040041>
- 25 Biscarat, J., Charmette, C., Sanchez, J., & Pochat-Bohatier, C. (2015). Development of a new family of food packaging bioplastics from cross-linked gelatin based films. *The Canadian Journal of Chemical Engineering*, 93(2), 176–182. <https://doi.org/10.1002/cjce.22077>
- 26 Moreno, O., Díaz, R., Atarés, L., & Chiralt, A. (2016). Influence of the processing method and antimicrobial agents on properties of starch-gelatin biodegradable films. *Polymer International*, 65(8), 905–914. <https://doi.org/10.1002/pi.5115>
- 27 Sitnikova, V.E. (2021). *Methods of Thermal Analysis*; Sitnikova, V.E., Ponomareva, A.A., Uspenskaya, M.V., Eds.; ITMO University: St. Petersburg, Russia, p. 152, 47–51 [in Russian]
- 28 Harrats, C., Benabdallah, T., Groeninckx, G., & Jérôme, R. (2005). Stress-strain behavior of low-density polyethylene/poly (methyl methacrylate) blends with modulated interfaces with a hydrogenated polybutadiene-block-poly (methyl methacrylate) diblock copolymer. *Journal of Polymer Science Part B: Polymer Physics*, 43(1), 22–34. <https://doi.org/10.1002/polb.20300>
- 29 Kambour, R.P. (1973). A review of crazing and fracture in thermoplastics. *Journal of Polymer Science: Macromolecular Reviews*, 7(1), 1–154. <https://doi.org/10.1002/pol.1973.230070101>
- 30 Araki, T., Shibayama, M., & Tran-Cong, Q. (Eds.). (1998). *Structure and properties of multiphase polymeric materials* (Vol. 46). CRC Press. <https://doi.org/10.1021/ja985648e>
- 31 Bucknall, C.B. (1977). *Toughened plastics* (p. 188). London: Applied Science Publishers. <https://doi.org/10.1002/pol.1978.130160714>
- 32 Buckley Jr, D.J. (1993). *Toughening mechanisms in the high strain rate deformation of rubber-modified polymer glasses*. Cornell University. <https://doi.org/10.1002/app.1993.070480117>
- 33 Painter, P.C., Coleman, M.M., & Paul, D.R. (2000). *Polymer Blends*. John Wiley & Sons, New York, 1. <https://doi.org/10.1086/ahr/105.4.1321>
- 34 Araki, T., Shibayama, M., & Tran-Cong, Q. (Eds.). (1998). *Structure and properties of multiphase polymeric materials* (Vol. 46). CRC Press. <https://doi.org/10.1021/ja985648e>
- 35 Friedrich, K., & Karsch, U.A. (1981). Failure processes in particulate filled polypropylene. *Journal of materials science*, 16(8), 2167–2175. <https://doi.org/10.1007/bf00542377>
- 36 French, D. (1984). *Organization of Starch Granules in Starch: Chemistry and Technology*; Whistler, RL; BeMiller, JN; Paschall, EF, Eds. <https://doi.org/10.1016/b978-0-12-746270-7.50005-7>
- 37 Pal, J., Ghosh, A.K., & Singh, H. (2008). Environmentally degradable LLDPE/esterified styrene-maleic anhydride (ESMA) blends. *European polymer journal*, 44(4), 1261–1274. <https://doi.org/10.1016/j.eurpolymj.2007.11.013>

38 Gautam, N., & Kaur, I. (2013). Soil burial biodegradation studies of starch grafted polyethylene and identification of *Rhizobium meliloti* therefrom. *Journal of Environmental Chemistry and Ecotoxicology*, 5(6), 147–158. <https://doi.org/10.5897/JECE09.022>

Н.Ф. Нормуродов, Қ.Н. Бердиназаров, М. Абдуразақов, Н.Р. Ашуrow

### **Полиэтилен және желатин негізіндегі биологиялық ыдырайтын композиттердің механикалық және термиялық қасиеттері**

Синтетикалық және табиғи полимерлер негізіндегі биологиялық ыдырайтын композициялардың қалыптасу сатысындағы морфологияның бақылаусыз дамуы қанағаттанарлық физикалық, механикалық және эксплуатациялық сипаттамаларға қол жеткізу мүмкіндігін шектейді. Жұмыста қоспаның ұсақдисперсті морфологиясына қол жеткізу үшін функционалды полиэтиленді желатинмен реакциялық араластырып, егілген малеин ангидридi мен желатинмен (LLDPE-g-MA/GEL) егілген төмен тығыздықтағы сызықтық полиэтилен сополимерiн қалыптастыру тәсілі ұсынылған. Қоспаның құрамдас бөліктерiн селективті алу әдісімен егілген LLDPE-mma/GEL сополимерiнiң мөлшері, бос желатин, механикалық және термиялық қасиеттері, сондай-ақ биологиялық ыдырау деректері анықталды. Полиэтиленнiң макромолекуласындағы малеиндік топтардың мөлшері артқан сайын егілген сополимер мөлшері көбейетiнi, ал қоспадағы желатин мөлшерiнiң артуы серпiмдiлiк модулінің айтарлықтай жоғарылауына, кернеудiң бұзылуына және бұзылған кезде салыстырмалы ұзаруға әкелетiнi анықталды. Желатиннiң ыдырауына байланысты композиттің термиялық тұрақтылығы (бастапқы температура) желатин мөлшерiнiң жоғарылауымен төмендейдi. 400–500 °С температура диапазонында трансплантат сополимерiнiң максималды бұзылу жылдамдығы желатин мөлшерiнiң жоғарылауымен айтарлықтай артады. Қоспадағы желатиннiң жоғарылауымен биоыдыраудың жылдамдығы өседi, деградацияның максималды деңгейі алғашқы 10 күнде байқалады және 50%- дан асады. ПОЭМА мен желатиндi бiр-бiрiне егудiң максималды дәрежесi егілген сополимердегі малеин ангидридiнiң мөлшерiне байланысты екендiгi айқындалды. Композиттердегі малеин ангидридiнiң мөлшерiнiң жоғарылауымен егудiң максималды дәрежесi жоғары болғаны байқалды.

*Кілт сөздер:* биоыдырау, желатин, глицерин, полиэтилен, малеин ангидридi, полимерлі композит.

Н.Ф. Нормуродов, Қ.Н. Бердиназаров, М. Абдуразақов, Н.Р. Ашуrow

### **Механические и термические свойства биоразлагаемых композитов на основе полиэтилена и желатина**

Неконтролируемое развитие морфологии на стадии формирования биоразлагаемых композиций на основе синтетических и природных полимеров ограничивает возможность достижения удовлетворительных физико-механических и эксплуатационных характеристик. В настоящей работе для достижения мелкодисперсной морфологии смеси был предложен подход к реакционному смешению функционализованного полиэтилена с желатином с образованием привитого сополимера линейного полиэтилена низкой плотности с привитым малеиновым ангидридом и желатином (LLDPE-g-MA/GEL). Методом селективного извлечения компонентов смеси определяли количество привитого сополимера LLDPE-g-MA/GEL, свободного желатина, механические и термические свойства, а также данные по биоразлагаемости. Выявлено, что, по мере увеличения малеиновых групп в макромолекуле полиэтилена, количество привитого сополимера возрастает, увеличение содержания желатина в смеси приводит к заметному увеличению модуля упругости, разрушающего напряжения и падению относительно удлинения при разрушении. Ввиду деградации желатина термостабильность композита (начальная температура) при увеличении содержания желатина снижается. Максимальная скорость деструкции привитого сополимера в области температур 400–500 °С, по мере увеличения содержания желатина, заметно увеличивается. Обнаружено, что скорость биodeградируемости возрастает при увеличении содержания желатина в смеси, максимальный уровень деградации наблюдается в течение первых 10 дней и составляет более 50 %. Установлено, что максимальная степень прививки ПЭМА и желатина друг к другу зависит от количества малеинового ангидрида в привитом сополимере. Замечено, что максимальная степень прививки была выше с увеличением количества малеинового ангидрида в композитах.

*Ключевые слова:* биodeградация, желатин, глицерин, полиэтилен, малеиновый ангидрид, полимерный композит.

## Information about authors\*

**Normurodov, Nurbek Fayzullo ugli** (*corresponding author*) — PhD student, Uzbekistan Academy of Sciences, Institute of Polymer Chemistry and Physics, 7“b”, str. A. Kadyri, 100128, Tashkent, Uzbekistan; e-mail: [nnf7nnf7@gmail.com](mailto:nnf7nnf7@gmail.com); <https://orcid.org/0000-0002-9817-9066>

**Berdinazarov, Qodirbek Nuridin ugli** — PhD student, Uzbekistan Academy of Sciences, Institute of Polymer Chemistry and Physics, 7“b”, str. A. Kadyri, 100128, Tashkent, Uzbekistan; e-mail: [qodirberdinazarov@mail.ru](mailto:qodirberdinazarov@mail.ru); <https://orcid.org/0000-0001-8888-2359>

**Abdurazakov, Mukhitdin** — Candidate of technical sciences, Uzbekistan Academy of Sciences, Institute of Polymer Chemistry and Physics, 7“b”, str. A. Kadyri, 100128, Tashkent, Uzbekistan; e-mail: [mukhitdin49@mail.ru](mailto:mukhitdin49@mail.ru)

**Ashurov, Nigmat Rustamovich** — Doctor of Science (Technical), Professor, Uzbekistan Academy of Sciences, Institute of Polymer Chemistry and Physics, 7“b”, str. A. Kadyri, 100128, Tashkent, Uzbekistan; e-mail: [nigmat.ashurov@gmail.com](mailto:nigmat.ashurov@gmail.com); <https://orcid.org/0000-0003-0765-5942>

---

\*The author's name is presented in the order: *Last Name, First and Middle Names*

Article

Received: 31 August 2022 | Revised: 27 October 2022 | Accepted: 04 November 2022 | Published online: 02 December 2022

UDC 544.42+519.242.7

<https://doi.org/10.31489/2022Ch4/4-22-18>

R.P. Bhole<sup>1\*</sup>, P.M. Karche<sup>1</sup>, Y. Shinde<sup>1</sup>,  
P.R. Kute<sup>1</sup>, S.S. Gurav<sup>2</sup>, R.D. Wavhale<sup>1</sup>

<sup>1</sup>Department of Pharmaceutical Chemistry, Dr. D.Y. Patil Institute of Pharmaceutical Sciences and Research, Pimpri, Pune, India;

<sup>2</sup>Goa College of Pharmacy, Panjim, Goa

(\*Corresponding author's e-mail: [ritesh.bhole@dypvp.edu.in](mailto:ritesh.bhole@dypvp.edu.in))

## Design and Synthesis of Vitamin Drug Conjugate for its Probable Potential Against SARS-COV-2 Infections

The novel corona virus infection had become a global epidemic due to its rapid spread. So, there is an urgent need to treat COVID-19 patients. The aim of this research was to hypothesize and examine vitamin drug conjugate as targeted moiety. The present scaffold may have potential role to fight against COVID-19 infection due to its antimicrobial, antioxidants and immunomodulatory activities. Here, we've highlighted the term Vitamin Drug Conjugate as possible therapy approach for SARS-COV-2 infection. As a result, we synthesize, characterized, and evaluated a Hydroxychloroquine — Folic Acid conjugate (HCQ-FA) by esterification mechanism to provide effective treatment against SARS-CoV-2 infection by enhancing therapeutic effect through synergistic mechanism, masking undesired side effects, and improving cellular internalization. By using prodrug, the efficacy and bioavailability of existing antiviral drugs could be improved. The structure of the conjugate was determined by spectroscopic data like IR, NMR, and mass spectra, which indicates that HCQ-FA conjugate formed by esteric conjugation. Molecular docking studies revealed that HCQ-FA conjugate shows good level of docking as well as binding interaction with main protease moiety. Molecular dynamic stimulation revealed that this conjugate shows good stability at the binding site of SARS main protease moiety and exhibits inhibitory activity against COVID-19 infection.

**Keywords:** Vitamin drug conjugate, SARS-COV-2, Hydroxychloroquine, Folic acid, Molecular modelling, Molecular Dynamic stimulation.

### Introduction

Coronavirus infection (COVID-19) has received a lot of attention around the world due to its quick transmission within humans and extremely high mortality [1]. The coronavirus outbreak that began in Wuhan, China in December 2019 has become now a global disaster [2, 3]. The novel corona virus is also known as SARS-COV-2 and causes a contagious disease called COVID-19 [4, 5].

But there are currently no therapies for COVID-19 that have been approved by the FDA [6]. During the COVID-19 pandemic, significant efforts have been made to develop therapeutic methods for the treatment and prevention of SARS-CoV-2 infection, but still no drug therapy has proven effective against SARS-COV-2 infection. But there is hope on the drugs such as hydroxychloroquine, remdesivir, favipiravir, lopinavir and ritonavir, which are used in the treatment guidelines in many hospitals around the world, and these drugs play a vital role in prevention a novel coronavirus infection [2, 7–8]. However, it was found that each antiviral drug alone is ineffective in the therapy of COVID-19 individuals, particularly in severe instances. Combination drug therapy is used to increase their effectiveness, which invariably result in adverse effects. As a result, there is an urgent need for treatment alternatives necessary to manage the COVID-19 epidemic with minimizing adverse effects [1, 9]. Another way to prevent this disease is by enhancing immunity, as it plays a critical role in fighting against SARS-COV-2 infection [6–7]. Apart from this many studies have explored that vitamins play a critical role against SARS-COV-2 infection through antioxidant, immunomodulatory and antimicrobial effects. According to new research, significantly higher dosages of nutrients including vitamins D, B, C, E, Zinc, and Omega-3 fatty acids may have a positive impact, potentially reducing SARS-CoV-2 viral infection and duration of hospitalization. It has recently been found that deficiency of these vitamins is associated with COVID-19 progression and an increase in patient mortality [6–10]. So here we highlighted the emerging concept “Vitamin-Drug Conjugate” which could be potential therapeutic option to treat SARS-COV-2 infection. Although coronavirus illness is being continuously increasing, there is current-

ly no particular antiviral drug effective on COVID-19. So it is required to develop targeted drug delivery with minimal side effects. This requirement can be met by the development of a “Vitamin-Drug Conjugate” (targeted) [10–12].

To create a pharmacologically active novel chemical entity, a drug is coupled to the targeted moiety through a spacer during the synthesis of a vitamin-drug conjugate. Vitamin drug conjugates will be non-toxic, specifically internalize into infected cells and release the medications without loss of activity, reduce toxic effects by remaining stable in blood circulation, and provide a target-specific delivery without harming normal cells, will help to minimize side effects [13, 14]. A vitamin-drug conjugate is one of the most promising methods for treating illnesses including cancer, tuberculosis, and a range of viral infections while also enhancing the therapeutic result. It selectively delivers medicine to the intended target [15–18].

Hydroxychloroquine and folic acid were used as raw materials to synthesize vitamin drug conjugates in this work. In addition, high-yield synthetic procedures for conjugate synthesis are presented in this paper, as well as detailed characterization information. Molecular modeling studies were also performed to compare the binding affinity of the supplied synthetic conjugate to the significant protease of SARS-COV-2. Molecular docking study was conducted to comprehend how Hydroxychloroquine Folic Acid Conjugate (HCQFA) binds to the main protease of SAR-CoV-2. We ran the molecular dynamic (MD) simulation to better understand the complex's stability. According to docking experiments, the HCQ-FA compound effectively inhibits the primary protease of the SARS-COV-2 virus. The current prodrug strategy may also improve drug potency and bioavailability and offer efficient treatment for new coronaviruses [19].

### Experimental

*Materials:* All of the reactants used in this experiment were of analytical grade. Hydroxychloroquine sulphate was purchased from BLD Pharmatech Pvt. Ltd. Folic acid was purchased from Loba Chemie Pvt. Ltd. N-Hydroxy Succinimide (NHS) and 1-(3-Dimethylaminopropyl)ethyl carbodiimide HCl (EDC·HCl) were purchased from Sisco research laboratories Pvt. Ltd. and 4-Dimethylaminopyridine (DMAP) was purchased from Research lab fine chem industries.

*Instruments used:* Melting point was determined by using melting-boiling point apparatus (Veego). TLC was performed by using Silica Gel plates F254 on Aluminium sheets to monitor the reaction process and assess the purity of the product. Spectroscopic data were recorded using following instruments. The Shimadzu FT-IR 8400S FTIR spectrophotometer was used to record FTIR spectra. Tetramethylsilane served as an internal standard, and DMSO was used as the solvent to acquire nuclear magnetic resonance spectra. Mass spectra were captured using a Shimadzu LC-MS 8040 mass spectrometer. Schrodinger software was used to conduct docking studies. A 100 ns molecular dynamic (MD) simulation was run using the AMBER18 programme.

#### Methodology:

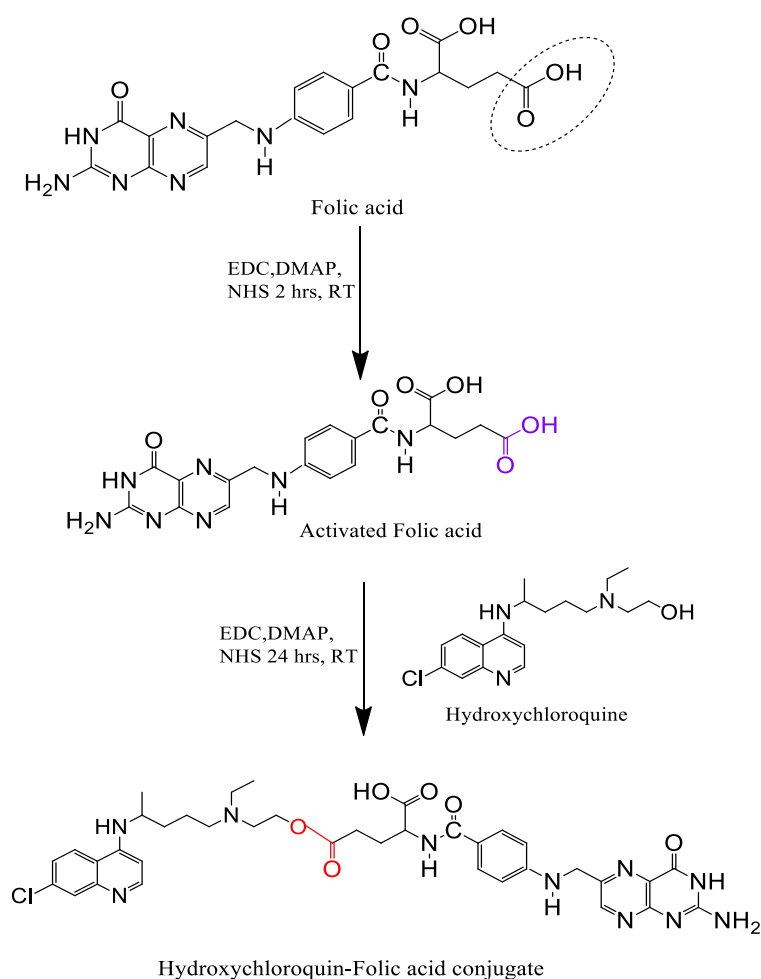
##### *Hydroxychloroquine-Folic Acid Conjugate (HCQ-FA Conjugate)*

HCQ-FA Conjugate were synthesized as per the synthetic route shown in Scheme 1. An esterification method was used to synthesize HCQ-FA conjugate where HCQ hydroxyl group reacts with carboxyl group of folic acid result into formation of esteric derivative. Briefly, FA and EDC, DMAP, NHS were utilized to make activated folic acid and after that HCQ was added to generate HCQ-FA derivative.

The mixture containing Folic acid (440mg) were dissolved in 5 ml of distilled water and EDC, DMAP and NHS were added in the FA:EDC:DMAP:NHS in molar ratio of 1:2:3:1 to generate activated folic acid. The carboxyl group of FA were activated by stirred the reaction mixture using magnetic stirrer for 2 hrs. at room temperature by keeping the dark environment. After that, in the solution of activated folic acid, 400 mg of HCQ was added and left the reaction mixture to react for next 24 hrs. at room temperature by keeping dark environment. The reaction mixture was continuously monitored by TLC. The reaction was terminated once folic acid and HCQ were no longer present in the reaction mixture, and the product was then isolated using column chromatography. The given separated solution was then filtered and evaporated at 40°C in a rotary evaporator. The synthesized product's yield and Rf values were recorded.

##### *Physical and Spectral data values of HCQ-FA Conjugate:*

M.P. — 186–188 °C; IR (KBr, 4000–400 cm<sup>-1</sup>) 1737.92 C=O (ester), 1693 (C=O carboxylic), 3093 (C-H stretch), 3338.89 (N-H stretch), 1417.73 (C-C stretch), 1291 (C-N), 2555 (O-H), 1635 (N-H); <sup>1</sup>H NMR (DMSO, 500 MHz): δ (ppm) = <sup>1</sup>H NMR δ = 6.5 to 8.5 (10H, Ar-H), 1.15 (t, 3H), 1.17 (t, 3H), 1.37 (p, 2H), 1.44 (q, 2H), 2.35 (t, 2H), 2.43 (t, 2H), 4.35 (t, 2H), 4.39 (d, 2H), 4.55 (q, 1H), 11.5 (s, 1H), 6.63 (s, 2H), Ms: m/z(%) =759.04 (M+).



Scheme 1. Synthetic route of Hydroxychloroquine-Folic Acid conjugate

### Molecular docking studies

The Schrodinger suite's Glide module was used to perform extra-precision (XP) molecular docking on the compounds. A grid generating approach was used to determine the binding location prior to the docking studies. The already-bound ligand was used as a reference site for the grid generation using the Glide grid module. The experiment involving docking also made use of the created grid. To lessen the potential of non-polar components on drug molecules, the van der Waals radii and scaling factor for the docking approach were set to 0.80 and 0.15, respectively. Throughout the entire docking protocol, the ligands were unrestricted. A maximum of five optimal postures for each ligand could be provided by post-docking minimization, which could then be included in the docking output file as reduced docked structures. The docking approach enables the drug molecules to be flexible. Each molecule's RMSD, docking score, glide score, and binding energy were noted.

### Molecular Dynamics (MD) Simulations

In order to investigate the structural, energetic, and steric refinement of the docked complex, an all-atom MD simulation lasting 100 ns was carried out using the AMBER18 software. A total of 24,515 water molecules were present in the system when the docked complexes were submerged in truncated TIP3P water octahedrons. To neutralize the system and reach an ionic strength of 0.1M (which mimics the physiological pH), enough  $\text{Na}^+$  and  $\text{Cl}^-$  counterions were added. Using the PMEMD, the complete MD simulation experiment was run on the Nvidia V100-SXM2-16GB Graphic Processing Unit. The Computational Shared Facility (CSF3) at the University of Manchester in the UK has a CUDA module installed. Simulations were carried out utilizing the Langevin thermostat at 300 K, a Monte Carlo barostat at 1 atm, and volume exchange attempts every 100 fs. The integration step used was 2 fs. Using the SHAKE algorithm, covalent bonds, including hydrogen, are restricted. An 8-cutoff was used for short-range nonbonded interactions, while the particle mesh Ewald approach was used to handle long-range electrostatics. For a total of 10 ns, equilibration involved cycles of NVT and NPT equilibration. A 100 ns production MD run was completed. CPPTRAJ was

used to assess the root-mean-square deviation (RMSD), root-mean-square fluctuation (RMSF), and other interactions along the entire trajectory, obtaining configuration measurements every 4 ps.

### Results and Discussion

Scheme 1 shows the synthesis process for the HCQ-FA conjugate. Melting point and TLC tests were performed on the synthesized conjugate to ensure that it was pure and homogeneous. The structures of HCQ-FA Conjugate were ascertained through the use of IR, NMR, and mass spectrometry. Results from IR, NMR, and mass spectrometry were listed in the experiment section. In order to determine the conjugate's binding affinity to the SARS-COV-2 Main protease, molecular docking and MD stimulation studies were conducted. The results of MD stimulation of the HCQ-FA Conjugate and molecular docking investigations have also been presented in the experimental section.

#### FTIR

In the IR spectra of HCQ-FA, the primary peaks observed for C=O carboxylic acid  $1693\text{ cm}^{-1}$ ,  $3093\text{ cm}^{-1}$  for C-H aromatic stretching,  $3338.89\text{ cm}^{-1}$  for N-H stretching. The C-N and O-H stretching were observed at  $1291$  and  $2555\text{ cm}^{-1}$ . Peaks at  $17237.92\text{ cm}^{-1}$  for C=O of ester which indicate the formation of HCQ-FA conjugate through the formation of esteric bond. The development of an esteric linkage is only seen in the IR spectra of HCQ-FA conjugate but not observed in other molecules.

#### NMR

HCQ-FA Conjugate shows  $^1\text{H}$  NMR at  $\delta$  values, 4.35 (t, 2H), 4.39 (d, 2H), 4.55 (q, 1H) respectively. The HCQ-FA Conjugates NMR spectra indicate peaks at the above-mentioned  $\delta$  values, confirming the structure of the HCQ-FA Conjugate. Peaks in the 3-5 ppm range suggest the development of an esteric bonding in the conjugate.

#### Mass Spectroscopy:

The structural conformation of HCQ-FA conjugate was determined using mass spectra. The molecular ion peak at  $759.04\text{ m/z}$  in the mass spectra of HCQ-FA conjugate confirms the conjugation of HCQ with Vitamin Folic acid through the development of an esteric linkage and confirms the synthesis of the final product, i.e., HCQ-FA conjugate.

#### Molecular modeling:

Molecular docking study was performed to comprehend how Hydroxychloroquine Folic Acid Conjugate (HCQFA) binds to the main protease of SAR-CoV2. The inhibitor N3 was complexed with the main protease of SAR-CoV-2 in the crystal structure (PDB:6LU7). Water molecules and other crystallographic solvents were removed from the target receptor during processing, and the protein was reduced according to the Glide protein preparation methodology. The HCQFA was docked using the extra precision (XP) technique, and the Grid generation was carried out using N3 as the reference ligand. In comparison to hydroxychloroquine ( $-6.3\text{ Kcal/mol}$ ), the best docked pose had a dock score of  $-7.4\text{ Kcal/mol}$  (Fig. 1). Thus, it was established that the target protein binds more strongly when the HCQ-FA conjugate is formed.

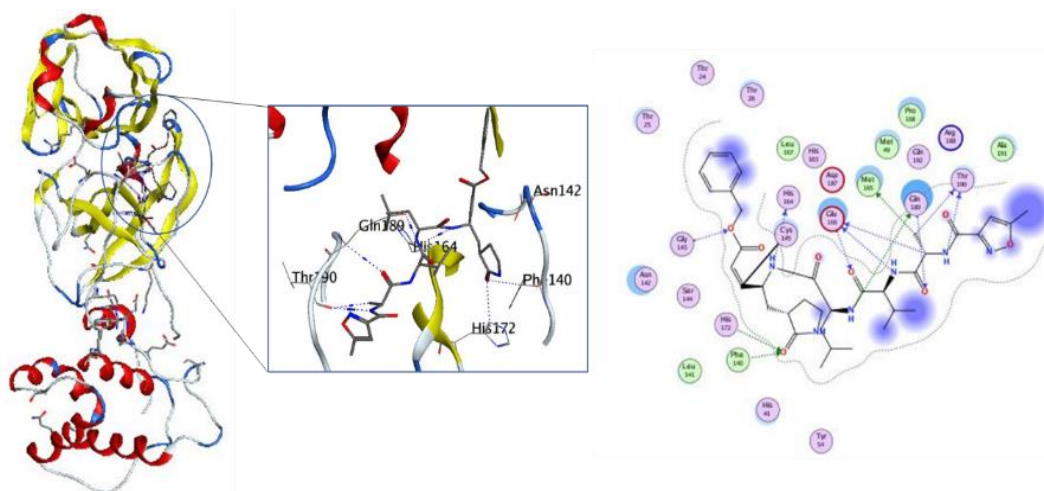


Figure 1. Docked complex of HCQFA with the SAR-CoV-2 main protease, the highlighted region shows the 3D image of protein ligand interactions and the 2D image shows the formation of various interaction between the ligand and receptor

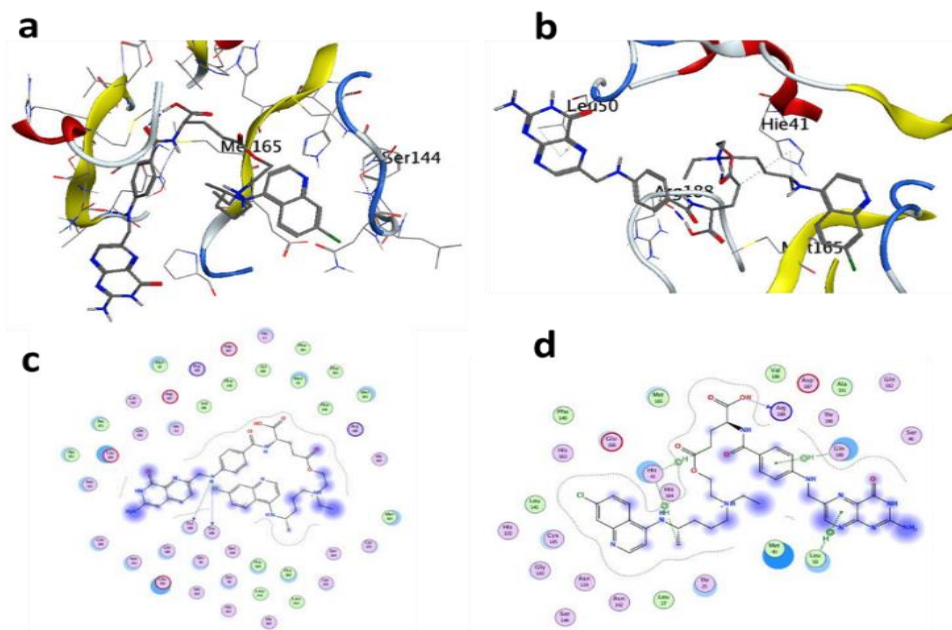
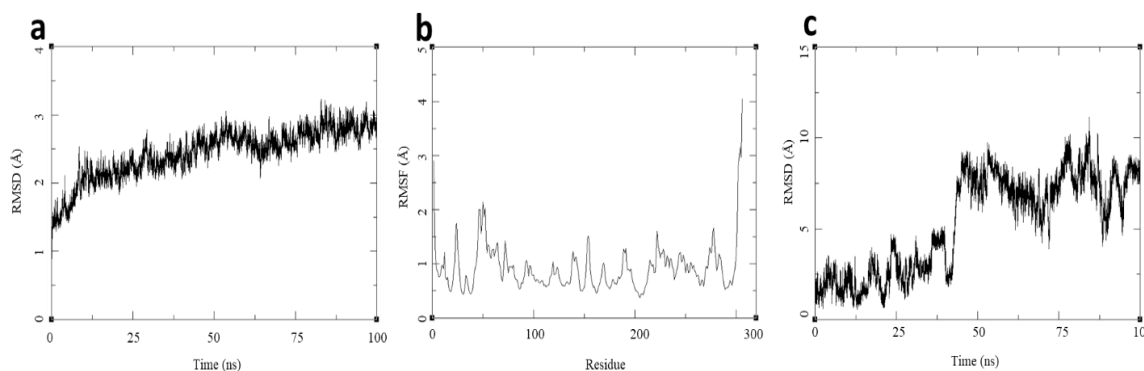


Figure 2. The figure 2a, c and 2b, d shows the initial and final conformations from the simulation of the protein-ligand complex for 100 ns

The ligand was seen to create multiple hydrogen bonds with the receptor's active site residues. The most significant ones are displayed in the three-dimensional (3D) schematic of the ligand-receptor interaction, where hydrogen bonds are formed by the amino acids Thr190, Gln189, His164, His172, Phe140, and Asn142.

We ran the MD simulation to better understand the stability of the complex. Figures 2a, 2b, and 2d show the simulation's initial and final conformations, respectively, while Figure 3 displays the findings from an examination of the complex's MD trajectory data.



a — Protein RMSD; b — Protein RMSF; c — Ligand RMSD

Figure 3. The trajectory analysis of the Protein-ligand complex

According to the MD simulation, the receptor residues engage in a number of novel interactions with HCQFA throughout the simulation, including the creation of hydrogen bonds with Met165 and Ser144 (Fig. 2a, c). The last frame of the MD simulation underwent examination, and it revealed the creation of hydrogen bonds with Arg188, His41, and His164. The conjugate's phenyl ring and the residue Gln180 interact through an arene (Fig. 2). With the use of CPPTRAJ and XMGRACE software, the MD trajectory was analyzed and graphs were created. The protein's RMSD points to a seamless transition and convergence between 1.5 and 3.0 Å. The conjugate's phenyl ring and the residue Gln180 interact through an arene. Throughout the simulation, the RMSF for the majority of the residues was below 2.0 Å additionally, it was discovered that the ligand experiences a conformational change that is reflected in its RMSD (Fig. 3c). At this time, the ligand's

RMSD varies between 1 and 5 and then rises sharply from 5 to 10 before stabilizing for the remainder of the simulation. All of these results point to good docking and even better stability over the majority of the MD simulation duration.

### Conclusions

Hydroxychloroquine-Folic acid (HCQ-FA) conjugate was synthesized, characterized and evaluated. HCQ-FA conjugate may act as a novel approach against COVID-19 infection. HCQ-FA conjugate may exhibit synergistic antiviral activity against COVID-19 infection, indicating that this combination therapy could be used to combat the COVID-19 outbreak. This HCQ-FA conjugate was developed and investigated as a novel prodrug method to address HCQ's non-specificity and toxicology problems. The efficacy and bioavailability of the present antiviral drugs could be improved by using this prodrug method. Molecular docking studies demonstrated that HCQ-FA conjugate shows good docking score as well as greater binding towards target protein as compare to HCQ. MD stimulation revealed that this conjugate shows good stability at the binding site of SARS main protease moiety and exhibits inhibitory activity against COVID-19 infection. We concluded that this study could be useful for developing an effective therapeutic agent for SARS-COV-2 infection due to the additive effect of HCQ-FA conjugate. It can exhibit excellent antiviral activity and also helps to modulate immune system by synergistic mechanism.

### References

- Basiri, A., Pazhouhnia, Z., Beheshtizadeh, N. *et al.* (2021). Regenerative Medicine in COVID-19 Treatment: Real Opportunities and Range of Promises. *Stem Cell Rev and Rep*, 17, 163–175 <https://doi.org/10.1007/s12015-020-09994-5>
- Khuroo, M.S. (2020). Chloroquine and hydroxychloroquine in coronavirus disease 2019 (COVID-19). Facts, fiction and the hype: a critical appraisal. *International Journal of Antimicrobial Agents*, 56(3), 106101. <https://doi.org/10.1016/j.ijantimicag.2020.106101>
- Bhole, R.P., Swamy, M.R., Wavhale, R., Bonde, C.G., & Chikhale, R. (2022). Design of potential vitamin-drug conjugate for enhanced anticancer activity. *Bulletin of university of Karaganda Chemistry*, 105(1), 6–14. <https://doi.org/10.31489/2022Ch1/6-14>.
- Gates, B. (2020). Responding to COVID-19 — a once-in-a-century pandemic? *New England Journal of Medicine*, 382(18), 1677–1679. <https://doi.org/10.1056/NEJMp2003762>.
- Bhole, R.P., Bonde, C.G., Bonde, S.C., Chikhale, R.V., & Wavhale, R.D. (2021). Pharmacophore model and atom-based 3D quantitative structure activity relationship (QSAR) of human immunodeficiency virus-1 (HIV-1) capsid assembly inhibitors. *Journal of Biomolecular Structure and Dynamics*, 39(2), 718–727. <https://doi.org/10.1080/07391102.2020.1715258>.
- Carella, A.M., Benvenuto, A., Lagattolla, V., Marinelli, T., De Luca, P., Ciavarrella, G., Modola, G., Di Pumpo, M., Ponziano, E., & Benvenuto, M. (2020). Vitamin supplements in the Era of SARS-Cov2 pandemic. *GSC Biological and Pharmaceutical Sciences*, 11(2), 007–019. <https://doi.org/10.30574/gscbps.2020.11.2.0114>.
- Wang, C., Horby, P.W., Hayden, F.G., & Gao, G.F. (2020). A novel coronavirus outbreak of global health concern. *The Lancet*, 395(10223), 470–473. [https://doi.org/10.1016/S0140-6736\(20\)30185-9](https://doi.org/10.1016/S0140-6736(20)30185-9).
- Bhole, R.P., Jadhav, S., Zambare, Y.B., Chikhale, R.V., & Bonde, C.G. (2020). Vitamin-anticancer drug conjugates: a new era for cancer therapy. *Journal of the Faculty of Pharmacy of Istanbul University*, 50(3), 312.
- Shakoor, H., Feehan, J., Al Dhaheri, A. S., Ali, H. I., Platat, C., Ismail, L. C., Apostolopoulos, V., & Stojanovska, L. (2021). Immune-boosting role of vitamins D, C, E, zinc, selenium and omega-3 fatty acids: Could they help against COVID-19? *Maturitas*, 143, 1–9. <https://doi.org/10.1016/j.maturitas.2020.08.003>.
- Alam, P., Alajmi, M., Siddiqui, N. A., & Basudan, O. (2014). Determination of bioactive marker glycyrrhizin in Glycyrrhiza glabra root and commercial formulation by validated HPTLC-densitometric method. *Journal of Coastal Life Medicine*. <https://doi.org/10.3389/fphar.2021.659577>.
- Lai, C.C., Shih, T.P., Ko, W. C., Tang, H. J., & Hsueh, P. R. (2020). Severe acute respiratory syndrome coronavirus 2 (SARS-CoV-2) and coronavirus disease-2019 (COVID-19): The epidemic and the challenges. *International journal of antimicrobial agents*, 55(3), 105924. <https://doi.org/10.1016/j.ijantimicag.2020.105924>.
- Bhole, R., Bonde, C., Kadam, P., & Wavhale, R. (2021). A comprehensive review on photodynamic therapy (PDT) and photothermal therapy (PTT) for cancer treatment. *Turk Onkoloji Dergisi*, 36(1), 125–132. <https://doi.org/10.5505/tjo.2020.2400>.
- Wang, Y., Fan, G., Salam, A., Horby, P., Hayden, F. G., Chen, C., Pan, J., Zheng, J., Lu, B., Guo, L., Wang, C., & Cao, B. (2020). Comparative Effectiveness of Combined Favipiravir and Oseltamivir Therapy Versus Oseltamivir Monotherapy in Critically Ill Patients with Influenza Virus Infection. *Journal of Infectious Diseases*, 221(10), 1688–1698 <https://doi.org/10.1093/infdis/jiz656>.
- Bhole, R.P., & Bhusari, K.P. (2011). Synthesis and antitumor activity of (4-hydroxyphenyl)[5-substituted alkyl(aryl)-2-thioxo-1,3-thiadiazol-3-yl] methanone and [(3,4-disubstituted)-1,3-thiazol-2ylidene]-4-hydroxybenzohydrazide. *Medicinal Chemistry Research*, 20(6), 695–704. <https://doi.org/10.1007/s00044-010-9371-9>
- Gombart, A.F., Pierre, A., & Maggini, S. (2020). A review of micronutrients and the immune system—working in harmony to reduce the risk of infection. *Nutrients*, 12(1), 236. <https://doi.org/10.3390/nu12010236>.

16 Calder, P.C. (2020). Nutrition, immunity and COVID-19. *BMJ Nutrition, Prevention & Health*, 3(1), 74–92. <https://doi.org/10.1136/bmjnph-2020-000085>.

17 Andersen, K.G., Rambaut, A., Lipkin, W.I., Holmes, E.C., & Garry, R.F. (2020). The proximal origin of SARS-CoV-2. *Nature Medicine*, 26(4), 450–452. <https://doi.org/10.1038/s41591-020-0820-9>.

18 Bao, L., Deng, W., Huang, B., Gao, H., Liu, J., Ren, L., Wei, Q., Yu, P., Xu, Y., Qi, F., Qu, Y., Li, F., Lv, Q., Wang, W., Xue, J., Gong, S., Liu, M., Wang, G., Wang, S., & Qin, C. (2020). The pathogenicity of SARS-CoV-2 in hACE2 transgenic mice. *Nature*, 583(7818), 830–833. <https://doi.org/10.1038/s41586-020-2312-y>.

19 Bourgonje, A.R., Abdulle, A. E., Timens, W., Hillebrands, J. L., Navis, G. J., Gordijn, S. J., Bolling, M. C., Dijkstra, G., Voors, A. A., Osterhaus, A. D. M. E., van der Voort, P. H. J., Mulder, D. J., & van Goor, H. (2020). Angiotensin-converting enzyme 2 (ACE2), SARS-CoV-2 and the pathophysiology of coronavirus disease 2019 (COVID-19). *Journal of Pathology*, 251(3), 228–248. <https://doi.org/10.1002/path.5471>.

Р.П. Бhole, П.М. Карче, Ю. Шинде, П.Р. Куте, С.С. Гурав, Р.Д. Вавхейл

### **SARS-COV-2 инфекцияларына қарсы ықтимал әлеуеті бар витамин-дәрілік конъюгаттың дамуы және синтезі**

Жаңа коронавирустық инфекция тез таралуына байланысты жаһандық эпидемия мәртебесін алды. Осыған байланысты бүгінде COVID-19-мен ауыратын науқастарды тиімді емдеудің өзекті қажеттілігі туындап отыр. Зерттеудің мақсаты — мақсатты дәрі ретінде витаминді-дәрілік конъюгаттарды болжау және зерттеу. Мұндай конъюгаттың микробқақарсы, антиоксиданттық және иммуномодуляциялық белсенділігіне байланысты COVID-19 инфекциясымен күресуде айтарлықтай әлеуеті болуы мүмкін. Жұмыста SARS-CoV-2 инфекциясын емдеуге ықтимал тәсіл ретінде «дәрумен-дәрілік конъюгат» термині көрсетілген. Гидроксихлорохин-фолий қышқылы (ГХХ-ФК) конъюгаты этерификация механизмі арқылы синтезделді, синергетикалық механизм арқылы терапевтік әсерді күшейту, қажетсіз жанама әсерлерді жасыру және жасушалық интернализацияны жақсарту арқылы SARS-CoV-2 инфекциясын тиімді емдеуді қамтамасыз ету үшін сипатталды және бағаланды. Қолданыстағы вирусқақарсы препараттардың тиімділігі мен биотиімділігін осындай алдын ала препаратпен жақсартуға болады. Конъюгат құрылымы ИК, ЯМР және массалық спектрлер сияқты спектроскопиялық деректермен анықталды. Алынған спектрлік деректер ГХХ-ФК конъюгаты қосылыстың күрделі эфир реакциясы нәтижесінде пайда болғанын растайды. Молекулалық докинг арқылы ГХХ-ФК конъюгаты жақсы тоғысу деңгейін, сондай-ақ протеазаның негізгі бөлігімен байланыстыратын өзара әрекеттесуін көрсетті. Молекулалық динамикалық модельдеуді қолдана отырып, SARS протеазасының негізгі бөлігінің байланысу орнында ГХХ-ФК конъюгатының жақсы тұрақтылығы және COVID-19 инфекциясына қарсы тежегіш белсенділігі атап өтілген.

*Кілт сөздер:* витамин-дәрілік конъюгат, SARS-CoV-2, гидроксихлорохин, фолий қышқылы, молекулалық модельдеу, молекулалық динамикалық модельдеу.

Р.П. Бhole, П.М. Карче, Ю. Шинде, П.Р. Куте, С.С. Гурав, Р.Д. Вавхейл

### **Разработка и синтез витаминно-лекарственного конъюгата с вероятным потенциалом против инфекций SARS-COV-2**

Из-за быстрого распространения новая коронавирусная инфекция получила статус глобальной эпидемии. В связи с этим сегодня существует острая необходимость в поиске эффективного лечения пациентов с COVID-19. Цель настоящего исследования состояла в том, чтобы выдвинуть гипотезу и изучить конъюгаты витаминов и лекарственных средств в качестве целевого препарата. Такой конъюгат может иметь значительный потенциал в борьбе с инфекцией COVID-19 благодаря своей антимикробной, антиоксидантной и иммуномодулирующей активности. В работе показан термин «витаминно-лекарственный конъюгат» как возможный подход к терапии инфекции SARS-CoV-2. Конъюгат гидроксихлорохин-фолиевая кислота (ГХХ-ФК) был синтезирован по механизму этерификации, охарактеризован и оценен с целью обеспечения эффективного лечения инфекции SARS-CoV-2 через усиление терапевтического эффекта за счет синергетического механизма, маскирования нежелательных побочных эффектов и улучшения клеточной интернализации. Эффективность и биодоступность существующих противовирусных препаратов могут быть улучшены с помощью такого пролекарства. Структуру конъюгата определяли по спектроскопическим данным, таким как ИК, ЯМР и масс-спектры. Полученные спектральные данные указывают на то, что ГХХ-ФК конъюгат образовался в результате сложноэфирной реакции соединения. Методом молекулярного докинга показано, что ГХХ-ФК конъюгат демонстрирует хороший уровень стыковки, а также связывающее взаимодействие с основной частью протеазы. С помощью молекулярно-динамического моделирования отмечена хорошая

стабильность ГХХ-ФК конъюгата в месте связывания основной части протеазы SARS и ингибирующая активность в отношении инфекции COVID-19.

*Ключевые слова:* витаминно-лекарственный конъюгат, SARS-COV-2, гидроксихлорохин, фолиевая кислота, молекулярное моделирование, молекулярно-динамическое моделирование.

#### Information about authors\*

**Bhole, Ritesh Prakash** (*corresponding author*) — PhD, Associate Professor, Dr. D.Y. Patil Institute of Pharmaceutical Sciences and Research, Sant Tukaram Nagar, Pimpri, Pune-411018, India; e-mail: [ritesh.bhole@dypvp.edu.in](mailto:ritesh.bhole@dypvp.edu.in); <https://orcid.org/0000-0003-4088-7470>

**Shinde, Yogita** — M. Pharm, Research Scholar, Dr. D.Y. Patil Institute of Pharmaceutical Sciences and Research, Sant Tukaram Nagar, Pimpri, Pune-411018, India; e-mail: [shindeyogita48@gmail.com](mailto:shindeyogita48@gmail.com);

**Karche, Payal Manik** — M. Pharm, Research Scholar, Dr. D.Y. Patil Institute of Pharmaceutical Sciences and Research, Sant Tukaram Nagar, Pimpri, Pune-411018, India; e-mail: [karchepayal@gmail.com](mailto:karchepayal@gmail.com); <https://orcid.org/0000-0003-3725-1121>

**Kute, Payal Ramesh** — M. Pharm, Research Scholar, Dr. D.Y. Patil Institute of Pharmaceutical Sciences and Research, Sant Tukaram Nagar, Pimpri, Pune-411018, India; e-mail: [kutepayal99@gmail.com](mailto:kutepayal99@gmail.com); <https://orcid.org/0000-0003-4779-6408>

**Gurav, Shaliendra Shivaji** — Professor, Goa College of Pharmacy, Goa; e-mail: [shailugurav@gmail.com](mailto:shailugurav@gmail.com), <https://orcid.org/0000-0001-5564-2121>

**Wavhale, Ravindra** — PhD, Assistant Professor, Dr. D.Y. Patil Institute of Pharmaceutical Sciences and Research, Sant Tukaram Nagar, Pimpri, Pune-411018, India; e-mail: [ravindra.wavhale@dypvp.edu.in](mailto:ravindra.wavhale@dypvp.edu.in), <https://orcid.org/0000-0003-1614-9742>

---

\*The author's name is presented in the order: *Last Name, First and Middle Names*

## PHYSICAL AND ANALYTICAL CHEMISTRY

Article Received: 29 April 2022 | Revised: 13 October 2022 | Accepted: 31 October 2022 | Published online: 16 November 2022

UDC 543.06

<https://doi.org/10.31489/2022Ch4/4-22-4>

S.P. Gandhi\*, A.R. Gawhane, S.D. Kapse, D. Nagore, S.S. Chitlange

Dr. D.Y. Patil Institute of Pharmaceutical Sciences and Research, Sant Tukaram Nagar, Pimpri, Pune, Maharashtra, India  
(\*Corresponding author's e-mail: [sejal.gandhi@dypvp.edu.in](mailto:sejal.gandhi@dypvp.edu.in))

### Validated High Performance Thin Layer Chromatography Method for Simultaneous Estimation for Gallic Acid and Quercetin in Polyherbal Blend and Their Quantitative Estimation

Simple, sensitive high performance thin layer chromatography method for the estimation of gallic acid and quercetin in in-house polyherbal blend has been developed and validated. Methanolic solution of herbal blend comprising of *Embllica officinalis*, *Camellia sinensis* and *Garcinia cambogia* was used for analysis. The separation was performed on TLC aluminum plates precoated with silica gel G60 F<sub>254</sub> and toluene: ethyl acetate: formic acid (5:1.5:1 v/v/v) at 254 nm scanning wavelength. The system gave well resolved peaks for gallic acid and quercetin at R<sub>f</sub> 0.14 and R<sub>f</sub> 0.29 respectively. The method validated as per ICH Q2R1 guidelines which shows regression co-efficient 0.9939 for gallic acid and 0.9988 for quercetin in range of 2–6 µg/ml. Recovery of gallic acid and quercetin was found in range of 98–102 % which confirms the accuracy of method. Precision study (interday & intraday) showed that the relative standard deviation is less than 2 %, showing method is well precise. Proposed validated HPTLC method is simple, precise, specific, robust and accurate, and could find application in routine quality-control analysis. The method was used for quantitative estimation of gallic acid and quercetin in the polyherbal blend and was found as 1.648 % w/w and 3.165 % w/w respectively.

**Keywords:** gallic acid, quercetin, simultaneous estimation, high performance thin layer chromatography, validation, quantification, polyherbal, herbal, extracts.

#### Introduction

During past decades, public interest in herbal has increased exponentially. According to WHO, mass population (about 80 %) in developing countries depends essentially on herbal plants for primary health care needs owing to efficacy and lower side effect. Also now researchers are exploring plants as source for new lead structure against different diseases [1–2]. Many herbal formulations as single and polyherbal have been proved to be active and are widely available in market. The major cause of concern with herbal plants is biodiversity and quality of the plants which ultimately affects the efficacy of the formulation. High performance thin layer chromatography (HPTLC) has become a widely acceptable analytical tool for the quality control of herbal drugs. It serves as a low operation- cost and quick analysis tool in herbal analysis.

The polyherbal mixture prepared for the study comprised of three plants viz. *Embllica officinalis*, *Camellia sinensis* and *Garcinia cambogia*, each of which are known to have therapeutic value [3–5]. The polyherbal blend was prepared with the aim to enhance the overall potential of the herbal extracts as these are used as antioxidant, anti-inflammatory and anti-obesity agent. These herbal plants consist of various phytoconstituents as alkaloids, flavanoids, tannins and polyphenols which contribute to their pharmacological activity. To be specific quercetin, gallic acid, ellagic acid and ascorbic acid are present in polyherbal blend and known for its effect.

Some methods are reported which includes HPTLC method for simultaneous estimation of quercetin and gallic acid in *Leea indica* [6], in *Eclipta alba* and *Guiera senegalensis* simultaneous HPTLC method is developed for estimation of quercetin and gallic acid [7], HPTLC simultaneous estimation of gallic acid and quercetin is also reported in single plant extract of *Abutilon indicus* [8] and HPTLC method is also reported in literature for estimation of gallic acid, rutin and quercetin in aqueous extract of *Terminalia chebula* [9] But simultaneous estimation of gallic acid and quercetin is not reported in polyherbal blend viz. three herbal plant mixture. Hence the present study aims to determine gallic acid and quercetin simultaneously in polyherbal blend. Same developed and validated method can be used for quantification of the biomarker in herbal mixture consisting of gallic acid and quercetin.

Gallic acid is phenyl propanoid, chemically it is 3,4,5-Trihydroxybenzoic acid, and possesses anti-oxidant, anti-inflammatory and astringent activity [10–11]. Quercetin is 3,3,4,5,7-pentahydroxyflavone and possesses anti-inflammatory, antihypertensive, vasodilator effects, antiobesity, antihypercholesterolemic and antiatherosclerotic activities [12–13].

### Experimental

#### Chemicals and solvents

Reference standard quercetin was purchased from Cayman Chemical Company, USA and gallic acid from Natural Remedies, India. All chemicals and solvents used were of analytical grade.

#### Plant material

Herbal plant powder extracts of *Embllica officinalis*, *Camellia sinensis* and *Garcinia cambogia* were procured from Kisalaya Herbals Ltd., Indore, Madhya Pradesh.

#### Polyherbal blend composition

A polyherbal blend was prepared by mixing equal amount of fruit of *Embllica officinalis*, leaves of *Camellia sinensis* and fruit of *Garcinia cambogia* extracts.

#### HPTLC analysis

##### a) Preparation of standard solution of gallic acid and quercetin

Standard stock solution of Gallic acid and Quercetin was prepared separately by dissolving 10 mg of Gallic acid and Quercetin up to 10 ml of methanol, to get stock solution containing 1000 µg/ml of Gallic acid and Quercetin. 5 µl of the above solution was applied on plate to obtain standard densitogram of Gallic acid and quercetin.

##### b) Preparation of sample solution of Herbal blend

Sample stock solution was prepared by dissolving 50 mg of mixture in 1ml methanol sonicated for 10 min any insoluble fraction was removed by filtration. 30 µl of the above solution was applied on plate to obtain standard densitogram of blend. Presence of Gallic acid and Quercetin in blend was confirmed by overlay spectra.

##### c) Chromatographic condition

Based on sample solubility, stability and suitability various mobile phase compositions were tried to get a good resolution and sharp peaks. The standard and sample solution was run in various mobile phases, showed that Toluene, Ethyl acetate and Formic acid in proportion of 5:1.5:1 (v/v/v) was best suitable for Herbal mixture. Chromatography was performed using commercially-prepared, pre-activated (110 °C) silica gel 60 F<sub>254</sub> TLC plates (10×10 cm). A Linomat IV (Camag, Muttenz, Switzerland) semi-automatic TLC applicator was used to apply samples and standards onto the TLC plate under a flow of nitrogen gas. After the application of sample, the chromatogram was developed in twin trough glass chamber 10×10 cm saturated with previously equilibrated mobile phase for 15 min. The chromatographic conditions were optimized to obtain the best peak shape. The plates were fixed in the scanner stage (CAMAG TLC SCANNER) and scanning was done at UV 254 nm. The peak table, peak display, spectrum mode were recorded. The retention factor (R<sub>f</sub>) was calculated by WINCAT'S software version 1.4.3.6336

##### d) Validation

ICH Q2 (R1) guidelines were followed for the validation of the analytical method developed. Calibration curve for gallic acid and quercetin was obtained from the system as graph of concentration versus absorbance. The precision of the method was determined by interday and intraday precision by analyzing sample solutions at different time intervals on the same day and on three different days, respectively. System precision was evaluated from six replicate application of standard as 6µl of gallic acid and quercetin at 3 tracks and method precision was carried out from six replicate applications (30 µl application at 3 tracks) and was expressed as % relative standard deviation. Recovery studies were performed using standard addition

method and at three different levels viz. at 80, 100 and 120 % of the test concentration as per ICH guidelines. Limit of Detection (LOD) and Limit of Quantification (LOQ) were determined using the formula based on the standard deviation of the response and the slope. To evaluate the robustness of the proposed method, small but deliberate variations in the optimized method parameters such as composition of the mobile phase and chamber saturation time in the range of  $\pm 0.2$  ml and  $\pm 5$  min, respectively was carried out. The effect of these changes on  $R_f$  values and peak area were studied.

*e) Quantification of Standard Gallic acid and Quercetin in Herbal blend*

Concentration of Gallic acid and Quercetin in Herbal blend was calculated using linearity equation of gallic acid and Quercetin.

*Result and Discussion*

Figure 1 shows developed HPTLC plate. Optimized chromatographic conditions are shown in Table 1.



Tracks — Blank, Gallic acid, quercetin and herbal blend at different concentrations

Figure 1. Developed HPTLC plate under UV light at 254 nm

Table 1

**Optimized Chromatographic Condition**

Sr. No.	Parameters	Details
1	Stationary phase	Silica gel 60 F <sub>254</sub> plates
2	Mobile Phase	Toluene: Ethyl Acetate: Formic Acid
3	Sample Applicator	Camag linomat V applicator
4	Development chamber	Twin-through glass chamber, 10×10 cm with stainless steel lid
5	Saturation time	15 min
6	Scanning wavelength	254 nm
7	Syringe	Camag 100 ul syringe
8	TLC Scanner	Camag TLC scanner III
9	Software	WinCATs software version 1.4.3.6336

Optimized mobile phase gave sharp peak for gallic acid at  $R_f$  0.14 (Figure 2) and Quercetin at  $R_f$  0.29 (Figure 3). Herbal blend showed the presence of both actives at  $R_f$  0.14 for gallic acid and  $R_f$  0.29 for Quercetin (Figure 4). Presence of gallic acid and Quercetin in herbal blend was confirmed by overlay spectra as shown in Figure 5 and 6.

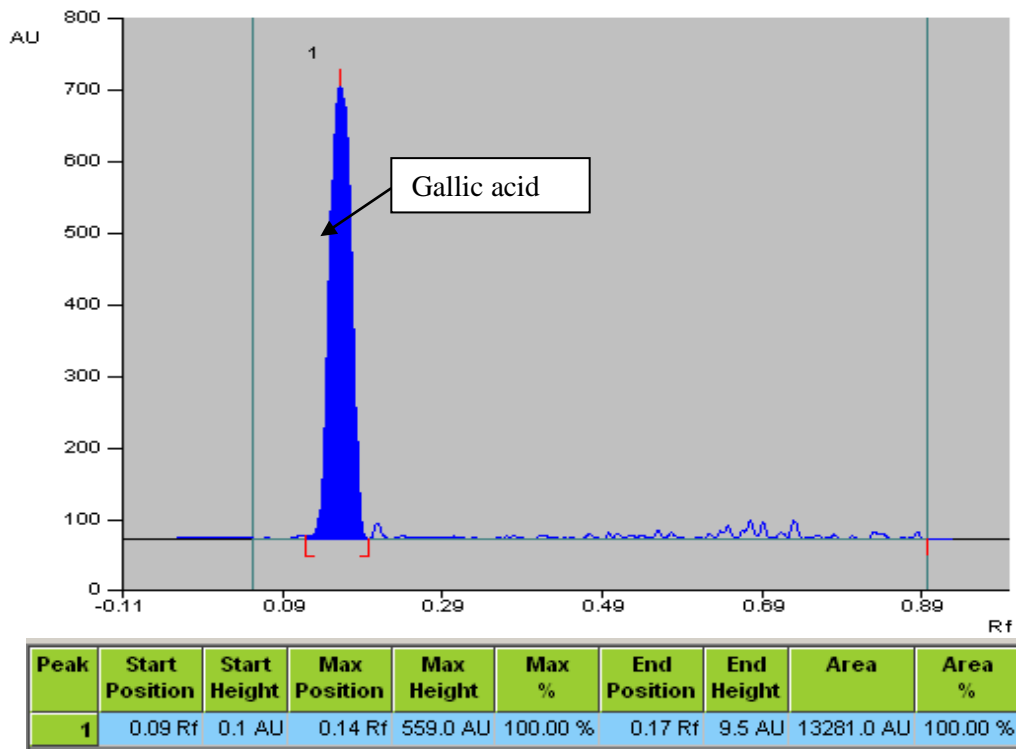


Figure 2. Densitogram of Standard Gallic Acid (5 µg/ml)

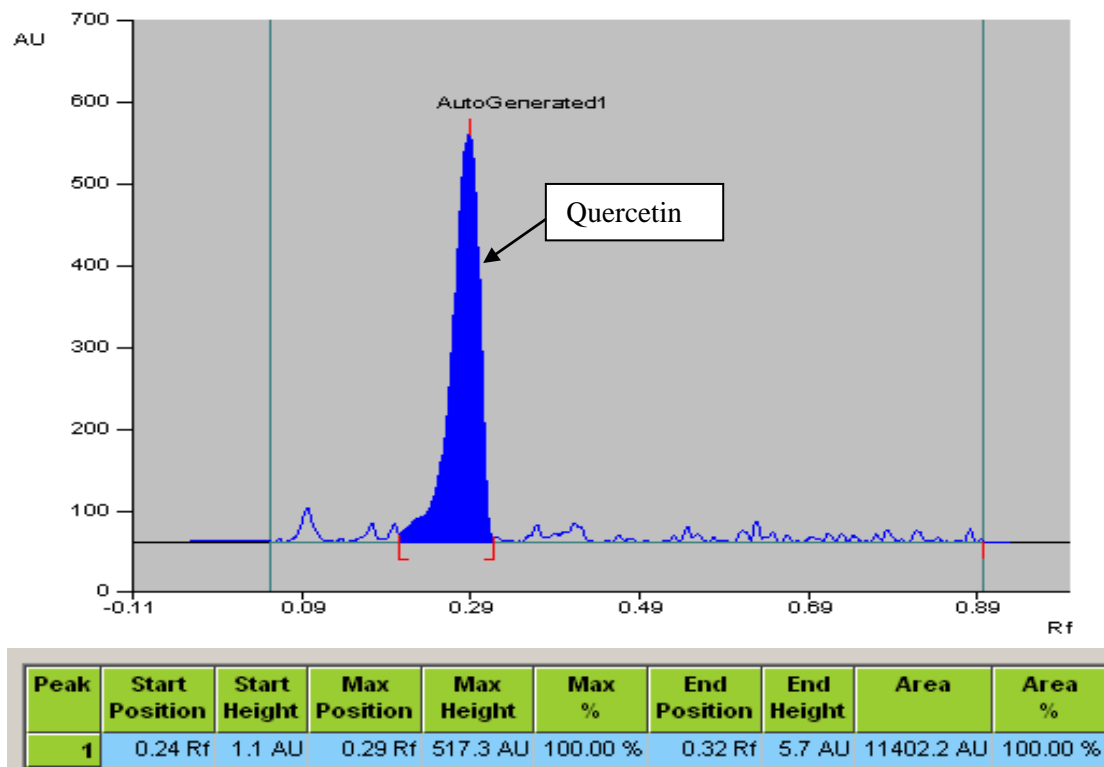


Figure 3. Densitogram of Standard Quercetin (5 µg/ml)

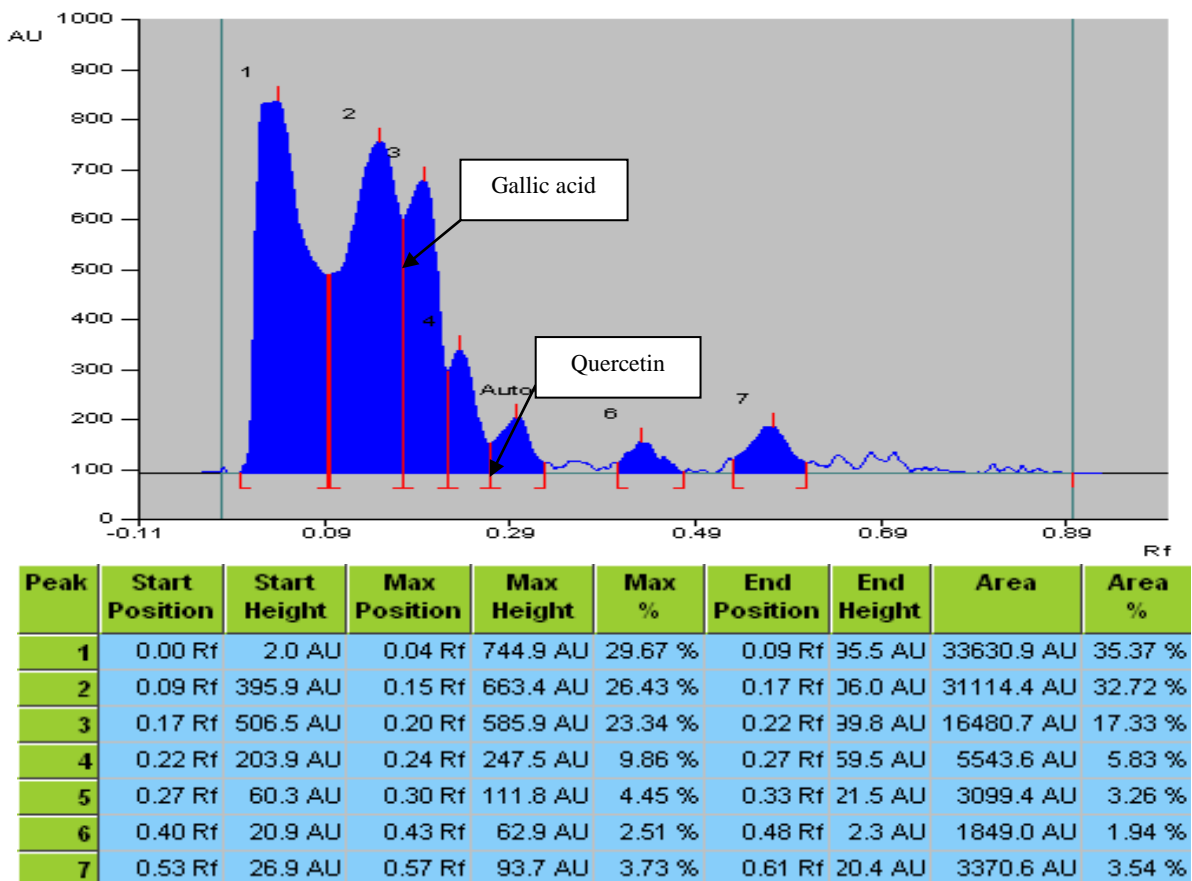


Figure 4. Densitogram of Herbal blend (1500 µg)

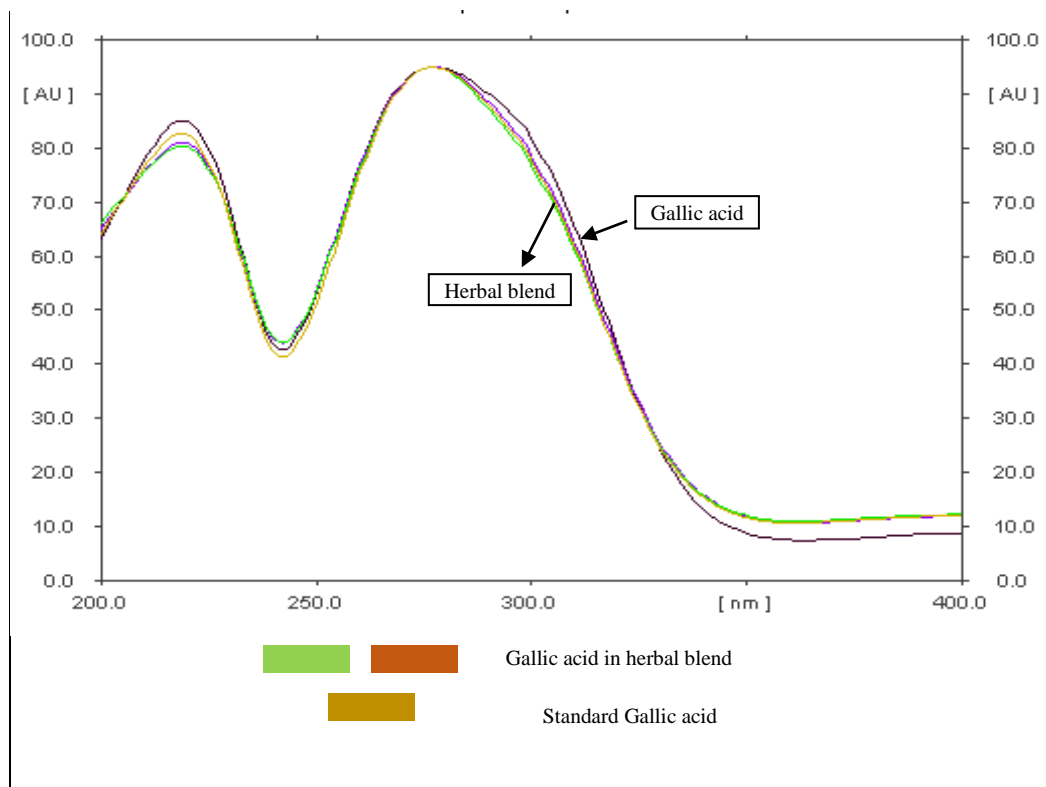


Figure 5. Overlay Spectra of Gallic acid standard and Gallic acid in Herbal blend

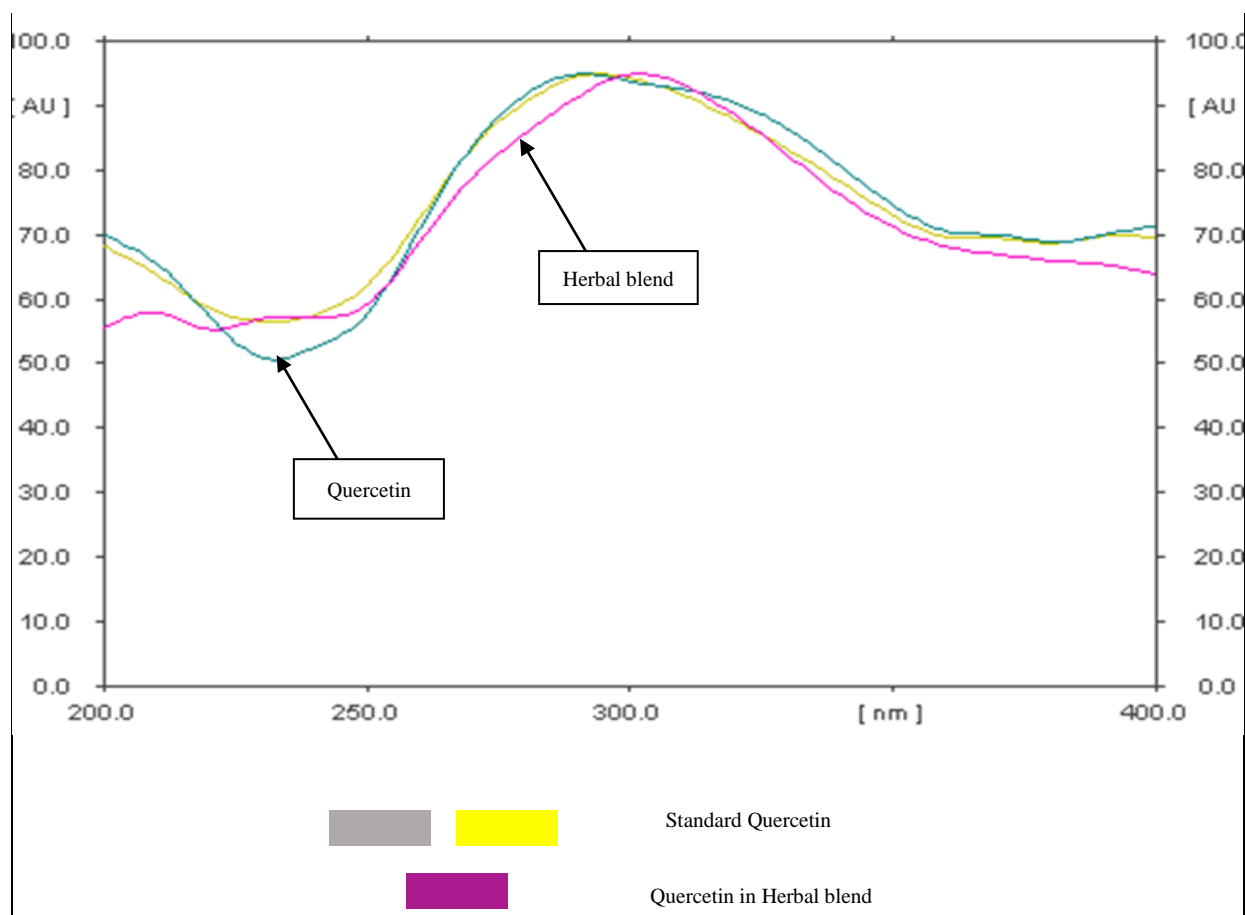


Figure 6. Overlay Spectra of Quercetin standard and Quercetin in Herbal blend

The linearity of calibration curve in pure solution, over the concentration range of 2-6  $\mu\text{l}$  (1 mg/ml) through proposed HPTLC method was carried out and regression co-efficient was obtained 0.9939 (Figure 7) & 0.9988 (Figure 8) for Gallic acid and Quercetin respectively.

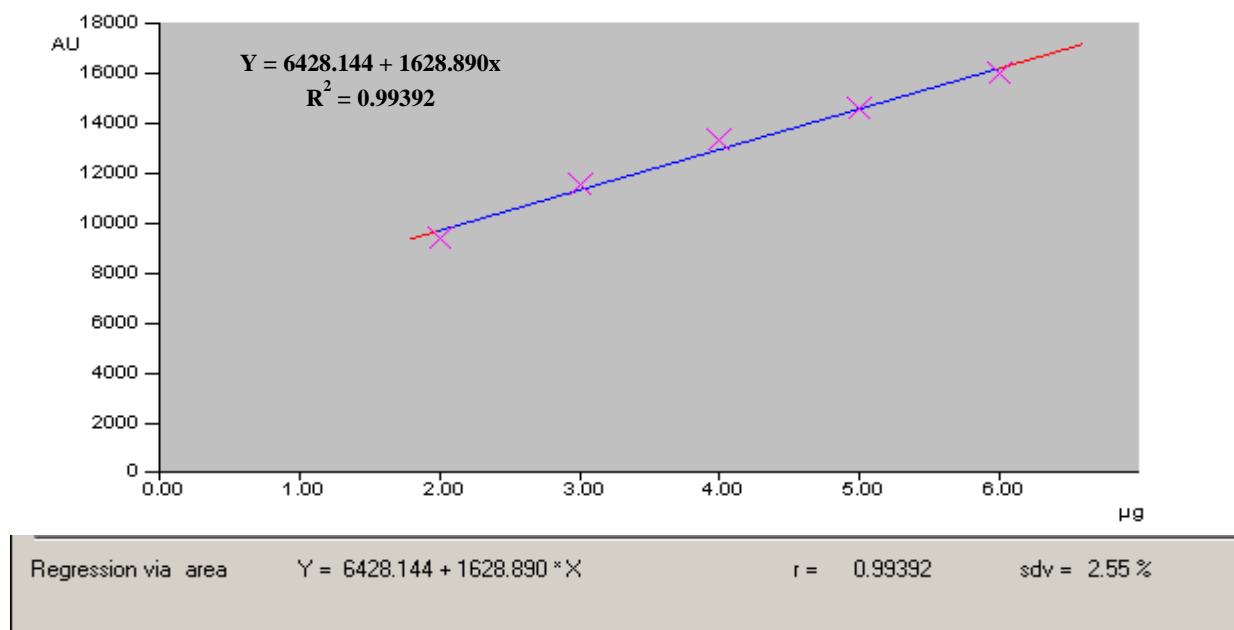


Figure 7. Calibration Curve of Gallic acid ( $R^2 = 0.9939$ )

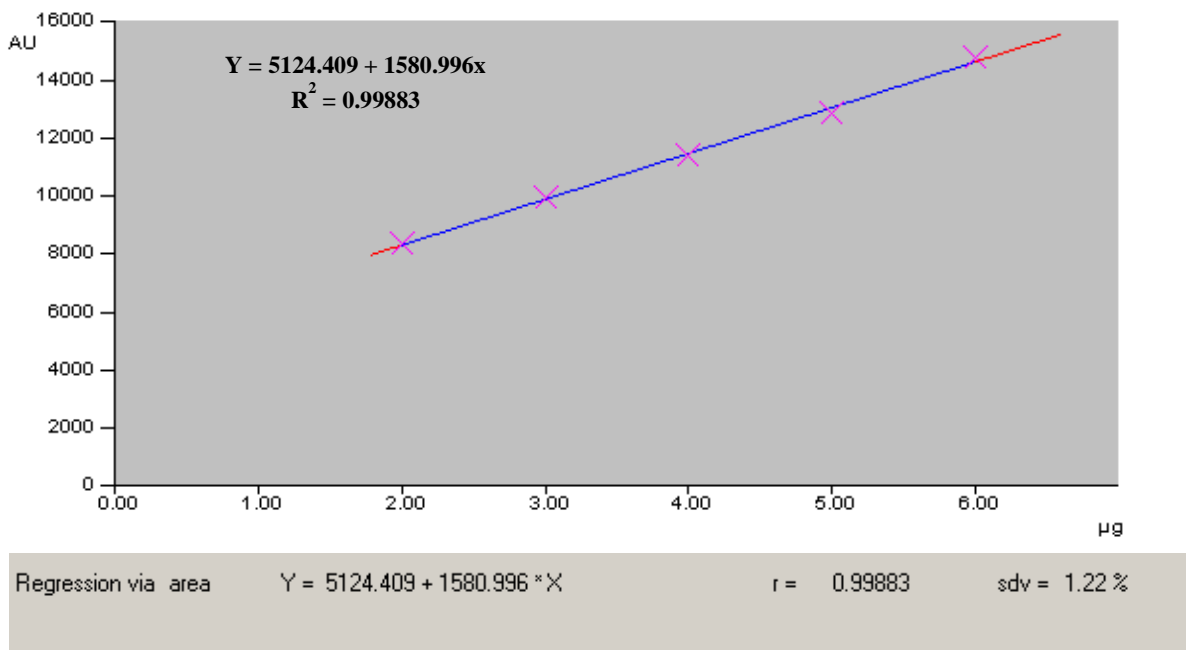


Figure 8. Calibration Curve of Quercetin (0.9988)

3D densitogram of linearity of standard gallic acid and quercetin is shown in Figure 9.

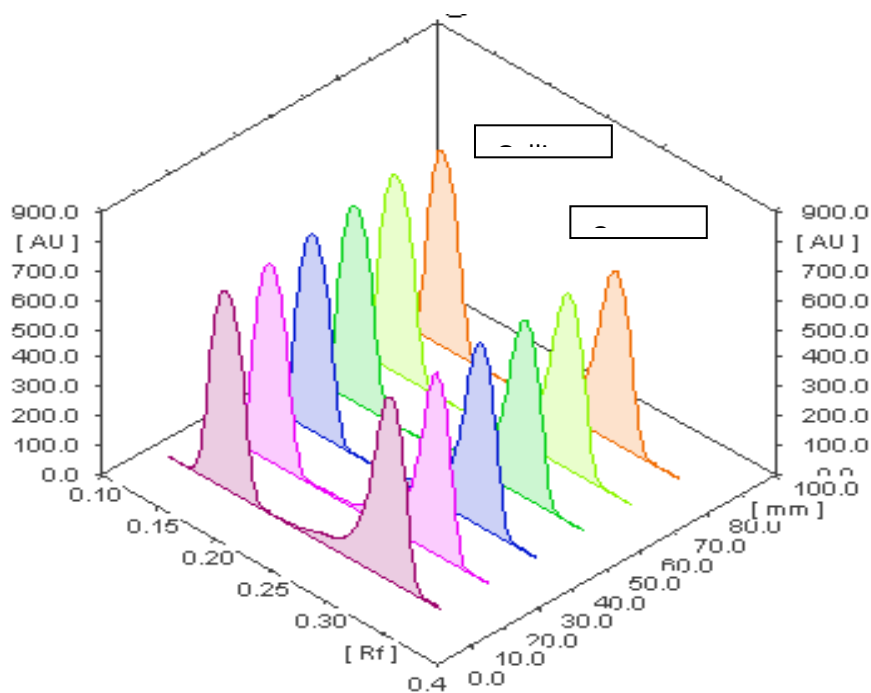


Figure 9. 3D densitogram of linearity of gallic acid and quercetin

System precision and method precision was carried out using standard Gallic acid, Quercetin and Herbal blend and % relative standard deviation was calculated. The repeatability of sample application and measurement of the peak area was expressed in terms of % RSD. The % RSD found was in the acceptable limit that is less than 2.0 which indicates that the method has an acceptable level of precision. Data is shown in Table 2 and 3 for system precision and method precision.

Table 2

## System precision

Sr. no.	Peak area (AU)	
	Gallic acid	Quercetin
1	15740.21	16010.02
2	15589.45	15680.20
3	15837.19	15848.01
4	15674.14	15828.97
5	15904.31	15986.17
6	15447.08	15749.17
SD	166.8	129.3
% RSD	1.06	0.82

Table 3

## Method precision

Sr. no.	Peak Area of Herbal blend (30 µl)	
	Gallic acid	Quercetin
1	9009.75	14126.60
2	9021.30	14128.14
3	9029.00	14120.39
4	9015.10	14126.02
5	9020.12	14122.22
6	9014.62	14122.90
SD	6.69	2.98
% RSD	0.074	0.02

The accuracy levels were checked at three levels of 80 %, 100 % and 120 % using standard addition method by over spotting herbal extract with standard. The amount of the standard recovered were within acceptable limits as per ICH guidelines. The percent recovery was found to be 98.52–101.04 % for gallic acid and 98.92–101.04 % for quercetin. Data represented in Table 4 and 5 is of recovery obtained for gallic acid and quercetin respectively by standard addition method.

Table 4

## Accuracy studies for Gallic acid

Sr. no	Level of recovery	Amount of Herbal blend taken	Amount of Std. Gallic acid Added	Amount of Gallic acid Recovered	% Recovery
		(µg/band)	(µg/band)	(µg/band)	
1	80 %	1500	3.2	3.153	98.53
		1500	3.2	3.171	99.09
		1500	3.2	3.222	100.68
2	100 %	1500	4.0	3.981	99.52
		1500	4.0	4.038	100.95
		1500	4.0	3.961	99.03
3	120 %	1500	4.8	4.834	100.70
		1500	4.8	4.821	100.44
		1500	4.8	4.85	101.04

Table 5

## Accuracy studies for Quercetin

Sr. no	Level of recovery	Amount of Herbal blend taken	Amount of Std Quercetin Added	Amount of Quercetin Recovered	% Recovery
		(µg/band)	(µg/band)	(µg/band)	
1	80 %	1500	3.2	3.194	99.81
		1500	3.2	3.165	98.92
		1500	3.2	3.182	99.43
2	100 %	1500	4.0	4.031	100.78
		1500	4.0	4.026	100.65
		1500	4.0	4.001	100.25
3	120 %	1500	4.8	4.819	100.39
		1500	4.8	4.826	100.54
		1500	4.8	4.84	101.04

The limits of detection (LOD) were obtained 0.35 & 0.027 µg/ml and limit of quantification (LOQ) 0.106 & 0.082 µg/ml for Gallic acid and Quercetin respectively.

The method was found to be robust and specific.

All the validation parameter results are shown in Table 6

Quantitative estimation have found out that in 1500 $\mu$ g of Herbal blend (Figure 10) 0.065  $\mu$ g of Gallic acid i.e. 1.648 % and 0.13  $\mu$ g of Quercetin i.e. 3.165 % was present. Table 7

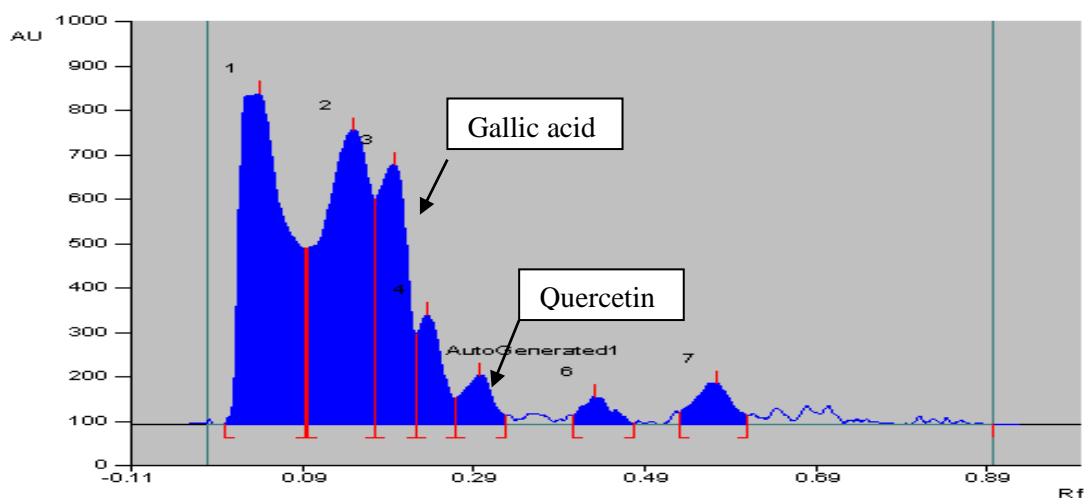


Figure 10. Densitogram of Herbal blend (1500  $\mu$ g/ml)

Table 6

#### Validation parameters of gallic acid and quercetin

Parameters	Result	
	Gallic acid	Quercetin
Correlation coefficient	0.993	0.998
Linearity range (ng/band)	2000–6000 ng/band	2000–6000 ng/band
Precision (C.V)		
System Precision	1.06	0.82
Method precision	0.074	0.02
Intra day	0.21	0.14
Inter day	0.45	0.09
Limit of Detection (ng/band)	35	27
Limit of Quantification	106	82
Accuracy (%)	98.52–101.04	98.92–101.04
Specificity	Specific	Specific

Table 7

#### Quantification of gallic acid and quercetin in Herbal blend

Phytochemical	Stock solution of extract	Concentration of extract spotted on TLC plate	Area	Calculated concentration in extract	% in extract
Gallic acid	(50 mg/ml)	30 $\mu$ l (1500 $\mu$ g/band)	13281.05	0.065 $\mu$ g	1.648 %
Quercetin	(50 mg/ml)	30 $\mu$ l (1500 $\mu$ g/band)	11402.21	0.13 $\mu$ g	3.165 %

#### Conclusions

Thus, a rapid, simple, accurate and specific HPTLC method for quantitative estimation of Gallic acid and Quercetin in polyherbal blend comprising of *Emblica officinalis*, *Camellia sinensis* and *Garcinia cambogia* has been developed and validated as per ICH guidelines. The method used in this work resulted in good peak shape with good resolution of Gallic acid and Quercetin from other constituents of the plant mate-

rial. Also it didn't show any interference of any other constituents with Gallic acid and Quercetin proving method specificity. The data could be used as a quality standard method for simultaneous estimation of these phytochemicals in single and polyherbal blend in in-house or marketed formulations. Also the developed method can be used for quantification of gallic acid and quercetin in the herbal mixture. Gallic acid and quercetin are the biomarkers available in most of the herbal plants and have been proved to be an important phytoconstituents responsible for the activity.

#### Acknowledgement

Authors are thankful to Kisalaya Herbals Ltd., Indore, Madhya Pradesh for providing extracts as gift samples.

#### References

- 1 De Smet, P. (1997). The Role of Plant-Derived Drugs and Herbal Medicines in Healthcare. *Drugs*, 54(6): 801–840. <https://doi.org/10.2165/00003495-199754060-00003>
- 2 Calixto, J. (2000). Efficacy, safety, quality control, marketing and regulatory guidelines for herbal medicines (phytotherapeutic agents). *Brazilian Journal of Medical and Biological Research*, 33(2), 179–189. <https://doi.org/10.1590/s0100-879x2000000200004>
- 3 Jain, R., Pandey, R., Mahant, R.N., and Rathore, D.S. (2015). A review on medicinal importance of *Embllica Officinalis*. *International Journal of Pharmaceutical Sciences and Research*, 6(1), 72–84. [https://doi.org/10.13040/IJPSR.0975-8232.6\(1\).72-84](https://doi.org/10.13040/IJPSR.0975-8232.6(1).72-84)
- 4 Bhatt, P., Pandya, K. and Sheth, N. (2010). *Camellia Sinensis* (L): The medicinal beverage: A review. *International Journal of Pharmaceutical Sciences and Research*, 3(2), Article 002, 6–9.
- 5 Semwal, R., Semwal, D., Vermaak, I. and Viljoen, A. (2015). A comprehensive scientific overview of *Garcinia cambogia*. *Fitoterapia*, 102, 134–148. <https://doi.org/10.1016/j.fitote.2015.02.012>
- 6 Patel, A., Amin, A., Patwari, A. and Shah, M. (2017). Validated high performance thin layer chromatography method for simultaneous determination of quercetin and gallic acid in *Leea indica*. *Brazilian Journal of Pharmacognosy*, 27, 50–53. <https://doi.org/10.1016/j.bjp.2016.05.017>
- 7 Khalid, M., Alqarni, M.H. and Foudah, A.I. (2021). A high performance thin-layer chromatography method for the simultaneous determination of quercetin and gallic acid in *Eclipta alba* and *Guiera senegalensis*. *Journal of Planer Chromatography*, 34, 71–77. <https://doi.org/10.1007/s00764-021-00084-x>
- 8 Hussain, S., Fareed, S., Ali, M. and Rahman, A. (2012). Validation of the method for the simultaneous estimation of bioactive marker gallic acid and quercetin in *Abutilon indicum* by HPTLC. *Asian Pacific Journal of Tropical Disease*, 2 (1), S76-S83. [https://doi.org/10.1016/S2222-1808\(12\)60127-3](https://doi.org/10.1016/S2222-1808(12)60127-3)
- 9 Kumar, A., Lakshman, K., Jayaveera, K.N. and Tripathi, S.N. (2010). Estimation of Gallic acid, Rutin and Quercetin in *Terminalia chebula* by HPTLC. *Jordan Journal of Pharmaceutical Sciences*, 3(1), 63–68.
- 10 Nikolic, K. (2007). Theoretical study of phenolic antioxidants properties in reaction with oxygen-centered radicals. *Journal of Molecular Structure: Theochem*, 774(1–3), 95–105. <https://doi.org/10.1016/j.theochem.2006.07.017>
- 11 Hertog, M.G. and Hollman, P.C. (1997). Potential health effects of the dietary flavonol Quercetin. *European Journal of Clinical Nutrition*, 50(2), 63–71.
- 12 Carrasco-Pozo, C., Cires, M. and Gotteland, M. (2019). Quercetin and epigallocatechin gallate in the prevention and treatment of obesity: From molecular to clinical studies. *Journal of Medicinal Food*, 22(8), 753–770. <https://doi.org/10.1089/jmf.2018.0193>
- 13 Lesjak, M., Beara, I., Simin, N., Pintac, D., Majkic, T., Bekvalac, K., Orcic, D. and Dukic, N. (2018). Antioxidant and anti-inflammatory activities of quercetin and its derivatives. *Journal of Functional Foods*, 40, 68–75. <https://doi.org/10.3390/molecules24061123>

С.П. Ганди, А.Р. Гавейн, С.Д. Капсе, Д. Нагоре, С.С. Читланге

### Көпшөпті қоспадағы галл қышқылы мен кверцетинді бір уақытта бағалау және сандық анықтау үшін расталған жоғарыөнімді жұқа валидацияланған хроматография әдісі

Қарапайым, сезімтал, жоғарыөнімді жұқа қабатты хроматография әдісі үйде өндірілген көпшөпті қоспадағы галл қышқылы мен кверцетиннің құрамын бағалау үшін әзірленді және расталды. Талдау үшін *Embllica officinalis*, *Camellia sinensis* және *Garcinia cambogia* қоса, шөп қоспасының метанолды ерітіндісі пайдаланылды. Бөлу 254 нм сканерлеу толқын ұзындығында G60 F<sub>254</sub> силикагельмен және

толуол : этилацетат : құмырсқа қышқылымен (5:1,5:1 көлем/көлем/көлем) алдын ала қапталған алюминий TLC пластиналарында орындалды. Жүйе сәйкесінше  $R_f$  0,14 және  $R_f$  0,29 шамасында галл қышқылы мен кверцетин үшін жақсы шешілген шындарды берді. Әдіс 2–6 мкг/мл диапазонында галл қышқылы үшін 0,9939 және кверцетин үшін 0,9988 регрессия коэффициентін беретін ICH Q2R1 нұсқауларына сәйкес расталды. Галл қышқылы мен кверцетинді алу 98–102 % аралығында, бұл әдістің дәлдігін нақтылайды. Дәлдікті зерттеу (күн аралық және күндізгі) салыстырмалы стандартты ауытқу 2 %-дан аз екенін көрсетті, бұл әдістің жоғары дәлдігін айқындайды. Ұсынылған валидацияланған HPTLC әдісі қарапайым, дәл, нақты және сенімді және күнделікті сапаны бақылау талдауында пайдаланылуы мүмкін. Бұл әдіс көпшөпті қоспадағы галл қышқылы мен кверцетиннің мөлшерін анықтау үшін қолданылды, ол тиісінше 1,648 % масса/масса және 3,165 % масса/масса құрады.

*Кілт сөздер:* галл қышқылы, кверцетин, синхронды бағалау, жоғарыөнімді жұқа қабат хроматографиясы, валидация, сандық анықтау, көпшөптер қоспасы, шөптер, сығындылар.

С.П. Ганди, А.Р. Гавейн, С.Д. Капсе, Д. Нагоре, С.С. Читланге

## Валидированный метод высокоэффективной тонкослойной хроматографии для одновременной оценки содержания галловой кислоты и кверцетина в политравной смеси и их количественная оценка

Был разработан и валидирован простой, чувствительный высокоэффективный метод тонкослойной хроматографии для оценки содержания галловой кислоты и кверцетина в политравной смеси собственного производства. Для анализа использовали метанольный раствор травяной смеси, включающей *Emblia officinalis*, *Camellia sinensis* и *Garcinia cambogia*. Разделение проводили на алюминиевых пластинах для ТСХ, предварительно покрытых силикагелем G60 F<sub>254</sub> и смесью толуол : этилацетат: муравьиная кислота (5:1,5:1 об./об./об.) при длине волны сканирования 254 нм. Система дала хорошо разрешенные пики для галловой кислоты и кверцетина при  $R_f$  0,14 и  $R_f$  0,29 соответственно. Метод валидирован в соответствии с рекомендациями ICH Q2R1, что дает коэффициент регрессии 0,9939 для галловой кислоты и 0,9988 для кверцетина в диапазоне 2–6 мкг/мл. Извлечение галловой кислоты и кверцетина находится в пределах 98–102 %, что подтверждает точность метода. Исследование точности (междневной и внутривневной) показало, что относительное стандартное отклонение составляет менее 2 %, что свидетельствует о высокой точности метода. Предлагаемый валидированный метод ВЭТСХ прост, точен, специфичен и надежен, может найти применение в рутинном анализе контроля качества. Данный метод был использован для количественной оценки содержания галловой кислоты и кверцетина в политравной смеси, которое составило 1,648 % масс./масс. и 3,165 % масс./масс. соответственно.

*Ключевые слова:* галловая кислота, кверцетин, одновременная оценка, высокоэффективная тонкослойная хроматография, валидация, количественная оценка, политравная смесь, травы, экстракты.

### Information about authors\*

**Gandhi, Sejal Prakash** — Assistant Professor, Department of Pharmaceutical Chemistry, Dr. D.Y. Patil Institute of Pharmaceutical Sciences and Research, Pimpri, Pune, 411018, Maharashtra, India; e-mail: [sejal.gandhi@dypvp.edu.in](mailto:sejal.gandhi@dypvp.edu.in); <https://orcid.org/0000-0002-7079-1886>

**Gawhane, Ashwini Ramachandra** — Department of Pharmaceutical Quality Assurance, Dr. D.Y. Patil Institute of Pharmaceutical Sciences and Research, Pimpri, Pune, 411018, Maharashtra, India; e-mail: [ar-gawhane@gmail.com](mailto:ar-gawhane@gmail.com)

**Kapse, Snehal Dnyandev** — Department of Pharmaceutical Quality Assurance, Dr. D.Y. Patil Institute of Pharmaceutical Sciences and Research, Pimpri, Pune, 411018, Maharashtra, India; e-mail: [kapsesnehal1553@gmail.com](mailto:kapsesnehal1553@gmail.com); <https://orcid.org/0000-0001-6803-2031>

**Nagore, Dheeraj** — Assistant Professor, Department of Pharmacognosy, Dr. D.Y. Patil Institute of Pharmaceutical Sciences and Research, Pimpri, Pune, Maharashtra, 411018, India; e-mail: [nagoredheeraj@gmail.com](mailto:nagoredheeraj@gmail.com); <https://orcid.org/0000-0002-6804-6262>

**Chitlange, Sohan Satyanarayan** — Principal, Department of Pharmaceutical Chemistry, Dr. D.Y. Patil Institute of Pharmaceutical Sciences and Research, Pimpri, Pune, 411018, Maharashtra, India; e-mail: [sohanchitlange@rediffmail.com](mailto:sohanchitlange@rediffmail.com); <https://orcid.org/0000-0002-9355-3303>

\*The author's name is presented in the order: *Last Name, First and Middle Names*

A.M. Makasheva<sup>1, 2\*</sup>, V.P. Malyshev<sup>1</sup>, L.A. Bekbayeva<sup>2</sup>

<sup>1</sup>*Abishev Chemical-Metallurgical Institute, Karaganda, Kazakhstan;*

<sup>2</sup>*Karaganda Technical University, Karaganda, Kazakhstan*

(\*Corresponding author's e-mail: [astra\\_mun@mail.ru](mailto:astra_mun@mail.ru))

## Direct Correlation between Fluid Cluster Structure and Its Viscosity

The research purpose is to prove the probability of a direct quantitative correlation between proportion of these clusters and liquid viscosity. A quasi-polycrystalline clustering model of the liquid (in particular, melts) should be used. The Boltzmann distribution, the concepts of the chaotic particles and the virtual cluster size distribution should be applied to achieve this purpose. This study analyzed the complete reference data on the temperature dependences of the dynamic viscosity for the alkali metals. As a result, a directly proportional correlation between viscosity and cluster content in liquid has been determined. It has provided the probability for the quantitative concept of the quasi-polycrystalline clustering model on the liquid state of matter due to its properties. The concept of the chaotic particles in direct correlation to the Boltzmann distribution has been used as a basis. The Boltzmann energy spectrum has been used for the kinetic energy of the chaotic thermal particle motion in the solid, liquid and gaseous states of matter. As a result, their three energy classes have been distinguished with their presence in all aggregate states and in the sum constantly equal to one. Formulas to calculate the proportion of the virtually ordered clustering and complete chaotic fluid components were deduced. These formulas have been derived with using the particle distributions by the energy class and cluster sizes.

**Keywords:** Boltzmann distribution, randomized particles, probability, virtuality, cluster, melt, viscosity, alkali metals.

### Introduction

The most adequate physical model of a liquid and, in particular, of melts, is the quasi-polycrystalline model [1–4]. The most relevant physical model for liquids (namely, melts) is a quasi-polycrystalline model [1–4]. This model examined the melt as a combination of two structural components such as clusters and the separating clusters. Thus, clusters were microvolumes with an ordered particle arrangement, close as in a crystal. By contrast, the separating clusters had a disordered zone with the chaotic and loose particle arrangement. The disordered zone has formed a continuous three-dimensional cellular network in the melt, which filled the gaps between the clusters. The gaps were disorderly oriented in relation to each other.

The clusters and a disordered zone were thermodynamically unstable. After the energy fluctuations, they continuously regenerated each other. The volume ratio filled with clusters and a disordered zone was established by a temperature of the melt. Thus, the temperature rise led to a decrease in the proportion of clusters due to an increasing of their disordered zone. It was assumed that the cluster zone disappeared at some temperature. It probably corresponded to a “contrary flexure” on the “physical property-temperature” curve and transition of the curvilinear section to a straight-line one.

This idea of the cluster disappearance was questionable. Thus, any contrary flexures, i.e. breaks were not actually observed on such curves. The straight-line proportions were an asymptotic approximation in the decreasing curvature region with the single temperature dependence of the physical property. In any case, there was no prohibition to form clusters based on fundamental laws relating to the liquid nature. In addition, the quasi-polycrystalline model had no analytical expression or the mathematical semi empirical interpretation.

As a result, the physical model was insufficiently developed. Since, some paradoxes of the temperature correlation of viscosity were not explained by the quasi-polycrystalline model [5]. Also works were being studied to determine the shape and structure of clusters with using their formation based on the solid phase nanoparticles during the melting of matter [6]. To date, the analysis of the unstable clustering phase in the liquid demonstrated that the structural approach dominated despite the advantage of such phase in a state without structure [7–10].

Thus, the obvious virtuality of the cluster existence and the disordered zone in the liquid has showed that a probability interpretation of its nature and all aggregate states of matter was relevant. Academician M.A. Leontovich's point was fundamental to use the Boltzmann distribution (an energy spectrum) on the kinetic energy of the chaotic (thermal) particle motion to the gaseous and liquid, solid states of matter [11].

The research purpose is to substantiate the probability of a direct quantitative correlation between proportion of these clusters and liquid viscosity. A quasi-polycrystalline clustering model of the liquid (in particular, melts) should be applied. The Boltzmann distribution, the concepts of the chaotic particles and the virtual cluster size distribution should be used to realize this purpose.

### Experimental

The Boltzmann distribution and the concept of chaotic particles as a virtual basis

$$P_i = N_i / N = \exp[-\varepsilon_i / kT] / \sum_{i=1}^n \exp[-\varepsilon_i / kT], \quad (1)$$

where  $P_i$  and  $N_i$  are share and number of particles with average  $\varepsilon_i$  kinetic energy;  $N$  is the total amount of particles in the system;  $k$  is the Boltzmann constant;  $n$  is the number of energy levels taken into account.

A significant advantage of the shared distribution was able to interpret  $P_i$  as the particle content with a certain energy level and probability to form and detect them. Therefore, the laws of the accidental events based on combining of the probability of the elementary events were used for them. The different fundamental property for this distribution was a universal expression of the thermal energy reserve at any temperature in an aggregate state as  $kT$  (per mol  $RT$ ). And it did not depend on the continuous or discrete nature of this distribution [12–15].

The ability was additionally created to determine the proportion of the super-barrier, sub-barrier and inter-barrier particles, i.e. any energy classes. Thus, the total proportion of such particles was equal to one. As a result, a faithful scientific basis was to develop the chaotic particles concepts and to apply their crossing or not crossing the thermal barriers of  $RT_m$  melting and  $RT_b$  boiling [16, 17].

This concept has demonstrated three particle energy classes at all temperatures and in all aggregate states:

the *crystal-mobile* particles with energy no more than the thermal barrier  $RT_m$  and proportions:

$$P_{crm} = 1 - \exp[-RT_m / (RT)] = 1 - \exp(-T_m / T), \quad (2)$$

the *liquid-mobile* particles with energy above  $RT_m$ , but no more than  $RT_b$  and proportions:

$$P_{lqm} = \exp(-T_m / T) - \exp(-T_b / T), \quad (3)$$

the *vapor-mobile* particles with energy above  $RT_b$  and proportions:

$$P_{vm} = \exp(-T_b / T) \quad (4)$$

upon condition

$$P_{crm} + P_{lqm} + P_{vm} = 1. \quad (5)$$

In this instance, this nature has been displayed with the melting and boiling points relevant to energy levels of  $kT_m$  and  $kT_b$ .

The temperature range showed that the regions of the crystalline, liquid, vapor states and *crm*, *lqm*- and *vm*-particles in each of them should be well defined. The real properties of these states corresponded to it.

The feature of the liquid-mobile particles was compared to the crystal-mobile and vapor-mobile particles. The proportion of the first above in the full temperature range (from zero to infinity) varied from 1 to 0. The proportion of the second above varied from 0 to 1. As a result, the feature was defined by difference between unity and sum of the oppositely varying fractions of *crm*- and *vm*-particles, as per (3). Thus, the fraction of *lqm*-particles varied from zero to zero passing through some maximum. Its position is analytically calculated by (3) and corresponds to a temperature:

$$T_{lqm,max} = (T_b - T_m) / \ln(T_b / T_m). \quad (6)$$

The obvious dominance of the crystalline particles was observed up to the boiling point. This predominance was characteristic for the Boltzmann energy spectrum. As a result, the lower levels were more filled than the upper ones. The crystal-mobile particles were low-energy and realized their dominance. They reduced their proportion in a liquid state from the predominant one at a melting point to others at the boiling point. Thus, it was requested to determine their form in the liquid. If it was abstract from a specific structure of clusters, it can be argued that *crm*-particles should be associated or virtually condensed. If the particles

constantly hit with each other and with all other particles, they should correspond to some virtual distribution by the number of particles included in cluster, i.e. to be one-, two-, three- and  $n$ -particle clusters. Herewith, abstraction from a specific cluster structures did not mean its ignoring. By contrast, it should be examined as separation of the chaotic basis to make the certain structures under influence of the potential energy for attraction or repulse of particles. The last mentioned above were explicitly analyzed in some papers, namely, in a review of [18].

In order to determine such distribution, it should be stated that a quantitative expression for the total matter proportion was first received by a quasi-polycrystalline clustering model of the liquid state based on the chaotic particles concept. It was as a reservoir to form the clusters. Thereat, this proportion was compliant with the universal criteria for the structural stability of the complex systems [19–21], specifically, by the proportion of the golden section.

Further development of the chaotic particles concept proved the virtuality of their existence in the form of cluster distribution by the number of the included particles. The equality conditions of probabilities for the mutual conversion of clusters were applied, thus, it led to the maximum uncertainty of their system [17].

$$P_{cm,n} = (1 - P_{cm}) P_{cm}^n, \quad (7)$$

where  $P_{cm}^n$  is the proportion of  $n$ -partial clusters.

As applied to the quasi-polycrystalline model of a liquid [1–4], it has been required to use the found particle distributions by the energy classes and cluster sizes to distinguish the virtually ordered cluster and fully chaotic components of the liquid. The last above mentioned was represented by single particles. It included all liquid-mobile, vapor-mobile and single crystal-mobile particles. They were the most energy-intensive in their class and as a transition to liquid-mobile ones. The total proportion of such particles calling as free, as described in (2)–(5) and (7) should be [17]

$$P_{fr} = P_{cm,1} + (P_{lqm} + P_{vm}) = P_{cm} (1 - P_{cm}) + (1 - P_{cm}) = 1 - P_{cm}^2. \quad (8)$$

Thereafter, the cluster zone should take a proportion of

$$P_{cl} = 1 - P_{fr} = P_{cm}^2. \quad (9)$$

Integrally, the chaotic component of matter was studied. It was a primary basis to examine the ordered component through the characteristics of dependence. Besides, the probabilistic distribution of clusters according to the number of the included particles created a reservoir to form the supracluster compounds — associates. The associates were detected in the liquid crystallization area [22]. The recording this loss of simplicity required the special study in relation to the liquid properties as described in our paper [20] with regard to viscosity. In all cases, the Boltzmann distribution was an inexhaustible source to develop the theory of a matter [23–25].

It should be previously to assure oneself of the most direct quantitative correlation of any physicochemical liquid property with the found cluster proportions. This could be exemplified by a dynamic viscosity for the most typical liquid metals of the basic subgroup of the first group of the periodic element system.

### Results and Discussion

The correlation of the dynamic viscosity of the liquid alkali metals to their cluster content should be present below.

The chaotic particles concept and the quasi-polycrystalline clustering model of a liquid demonstrated that its viscosity should not be defined by all proportion of the crystal-mobile  $P_{cm}$  particles. It should be determined by its part belonging to non-single virtual formations. Thus, it should be equal to  $P_{cm}^2$ . It might be illustrated with the most complete reference data on the temperature dependences of the dynamic viscosity of alkali metals [26, 27].

Data correlation of  $\eta$ , mPa·c, with  $P_{cm} = 1 - \exp(-T_m/T)$  and  $P_{cm}^2 = [1 - \exp(-T_m/T)]^2$  in the range from  $T_m$  to  $T_b$  are resulted in Tables 1–5 and Figures 1–5.

Table 1

The dependence of the dynamic lithium viscosity on the temperature [26, 27] and proportion of the crystal-mobile  $P_{crm}$  particles and  $P_{crm}^2$  clusters

$T, K$	$\eta, mPa \cdot c$	$P_{crm}$	$P_{crm}^2$	$T, K$	$\eta, mPa \cdot c$	$P_{crm}$	$P_{crm}^2$
$T_m = 453.7$	–	0.632	0.400	1073	0.238	0.345	0.119
473	0.566	0.617	0.380	1173	0.219	0.321	0.103
573	0.453	0.547	0.299	1273	0.204	0.300	0.089
673	0.379	0.490	0.240	1373	0.191	0.281	0.079
773	0.328	0.444	0.197	1473	0.180	0.265	0.070
873	0.290	0.405	0.164	1573	0.170	0.251	0.063
973	0.261	0.373	0.139	$T_b = 1615$	–	0.245	0.060

Table 2

The dependence of the dynamic sodium viscosity on the temperature [26, 27] and proportion of the crystal-mobile  $P_{crm}$  particles and  $P_{crm}^2$  clusters

$T, K$	$\eta, mPa \cdot c$	$P_{crm}$	$P_{crm}^2$	$T, K$	$\eta, mPa \cdot c$	$P_{crm}$	$P_{crm}^2$
$T_m = 371$	–	0.632	0.400	773	0.237	0.381	0.145
373	0.687	0.630	0.397	873	0.208	0.346	0.120
473	0.451	0.544	0.296	973	0.186	0.317	0.100
573	0.341	0.477	0.227	1073	0.170	0.282	0.085
673	0.278	0.424	0.180	$T_b = 1156$	–	0.274	0.075

Table 3

The dependence of the dynamic potassium viscosity on the temperature [26, 27] and proportion of the crystal-mobile  $P_{crm}$  particles and  $P_{crm}^2$  clusters

$T, K$	$\eta, mPa \cdot c$	$P_{crm}$	$P_{crm}^2$	$T, K$	$\eta, mPa \cdot c$	$P_{crm}$	$P_{crm}^2$
$T_m = 337$	–	0.632	0.400	773	0.166	0.353	0.125
373	0.441	0.585	0.354	873	0.146	0.320	0.103
473	0.303	0.510	0.260	973	0.132	0.293	0.086
573	0.234	0.444	0.198	$T_b = 1032$	–	0.279	0.078
673	0.193	0.394	0.155				

Table 4

The dependence of the dynamic rubidium viscosity on the temperature [26, 27] and proportion of the crystal-mobile  $P_{crm}$  particles and  $P_{crm}^2$  clusters

$T, K$	$\eta, mPa \cdot c$	$P_{crm}$	$P_{crm}^2$	$T, K$	$\eta, mPa \cdot c$	$P_{crm}$	$P_{crm}^2$
$T_m = 312.5$	–	0.632	0.400	673	0.212	0.371	0.138
373	0.435	0.567	0.322	773	0.185	0.332	0.111
473	0.316	0.484	0.234	873	0.165	0.301	0.090
573	0.252	0.420	0.177	$T_b = 961$	–	0.278	0.077

Table 5

The dependence of the dynamic cesium viscosity on the temperature [26, 27] and proportion of the crystal-mobile  $P_{crm}$  particles and  $P_{crm}^2$  clusters

$T, K$	$\eta, mPa \cdot c$	$P_{crm}$	$P_{crm}^2$	$T, K$	$\eta, mPa \cdot c$	$P_{crm}$	$P_{crm}^2$
$T_m = 301.7$	–	0.632	0.400	673	0.221	0.365	0.130
373	0.469	0.555	0.308	773	0.192	0.323	0.104
473	0.334	0.472	0.222	873	0.171	0.292	0.085
573	0.264	0.409	0.168	$T_b = 944$	–	0.274	0.075

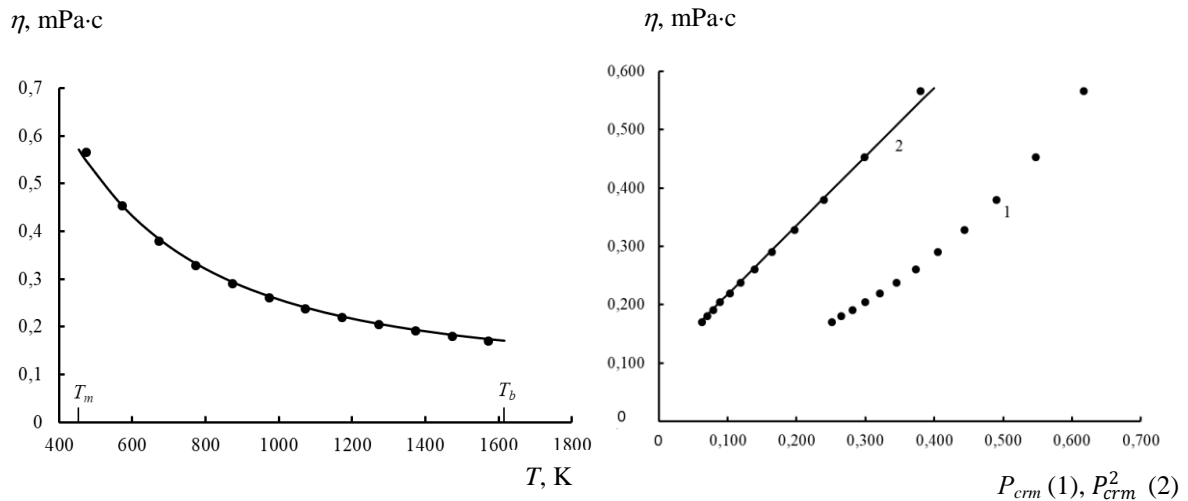


Figure 1. The dependence of the dynamic lithium viscosity on temperature [26, 27] and proportion of the crystal-mobile  $P_{crm}$  particles and  $P_{crm}^2$  clusters (lines by (10))

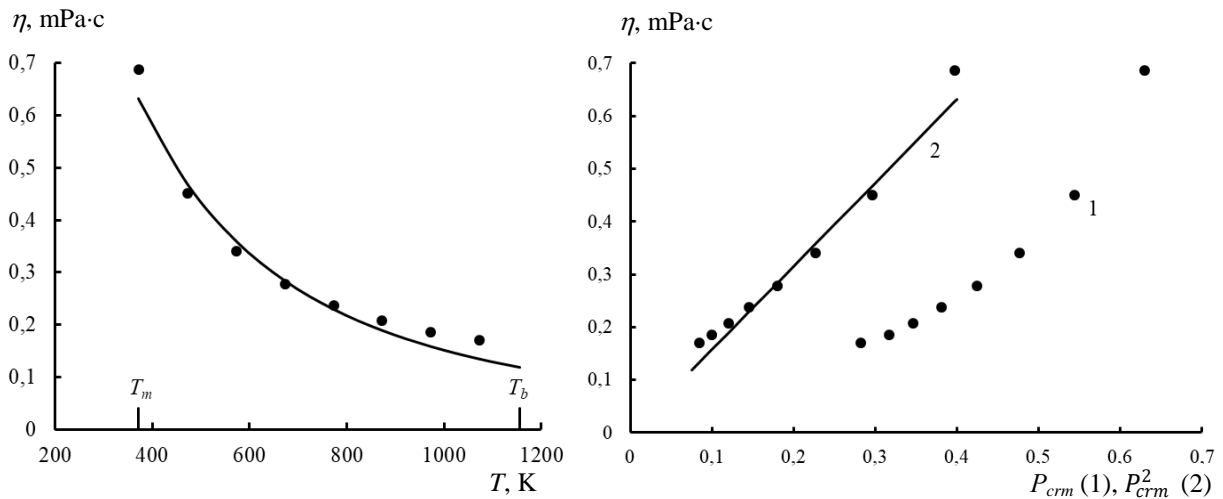


Figure 2. The dependence of the dynamic sodium viscosity on temperature [26, 27] and proportion of the crystal-mobile  $P_{crm}$  particles and  $P_{crm}^2$  clusters (lines by (10))

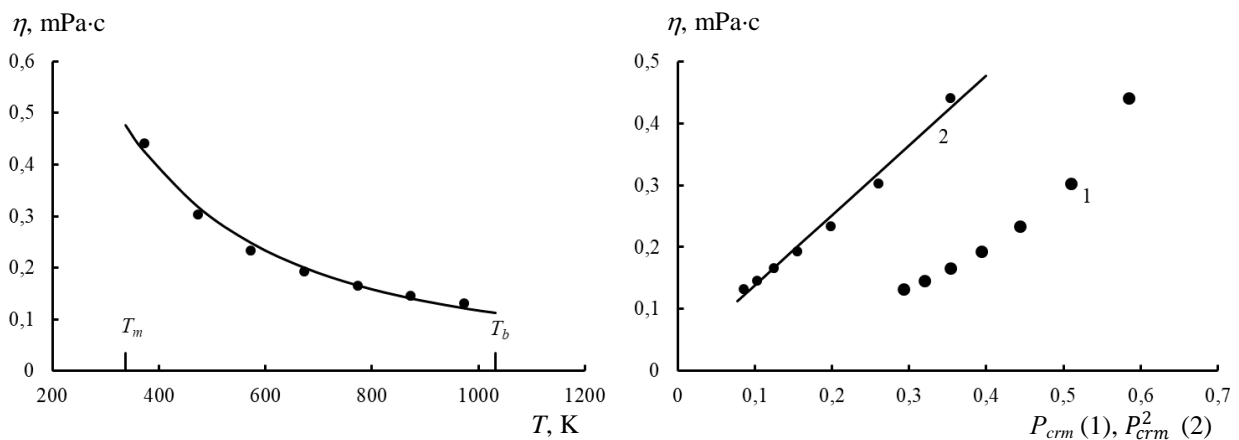


Figure 3. The dependence of the dynamic potassium viscosity on temperature [26, 27] and proportion of the crystal-mobile  $P_{crm}$  particles and  $P_{crm}^2$  clusters (lines by (10))

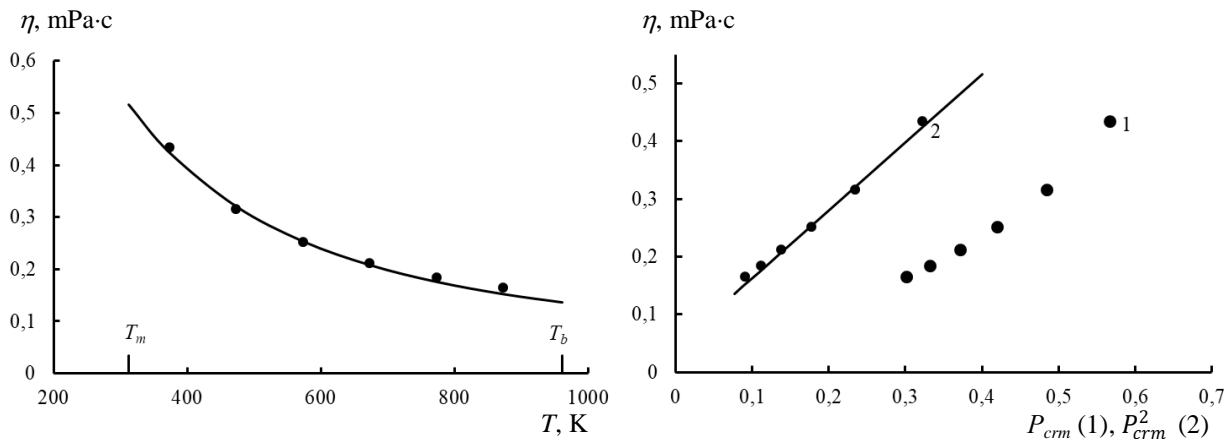


Figure 4. The dependence of the dynamic rubidium viscosity on temperature [26, 27] and proportion of the crystal-mobile  $P_{crm}$  particles and  $P_{crm}^2$  clusters (lines by (10))

All figures illustrated a uniform variation in the forms of the dynamic viscosity correlations: from obvious nonlinear by temperature to smoothed proportion of the crystal-mobile particles and clear enough straight-line by cluster proportions. Thus, the directly proportional correlation of the viscosity directly with the cluster content in the liquid was proved.

The probability was discovered for the quantitative concept of the quasi-polycrystalline clustering model of the liquid matter state through its properties. Therefore, the chaotic particles concept and the Boltzmann distribution were applied.

In a first approximation, such dependence might be represented as a straight line equation. After calculation of the  $P_{crm}^2$  variable, the viscosity was showed as

$$\eta = a + bP_{crm}^2 = a + b[1 - \exp(-T_m / T)]^2, \tag{10}$$

where  $a$  and  $b$  are free term and proportionality coefficient, respectively. They could be found by the least squares method. Then they should be used to determine the physical meaning.

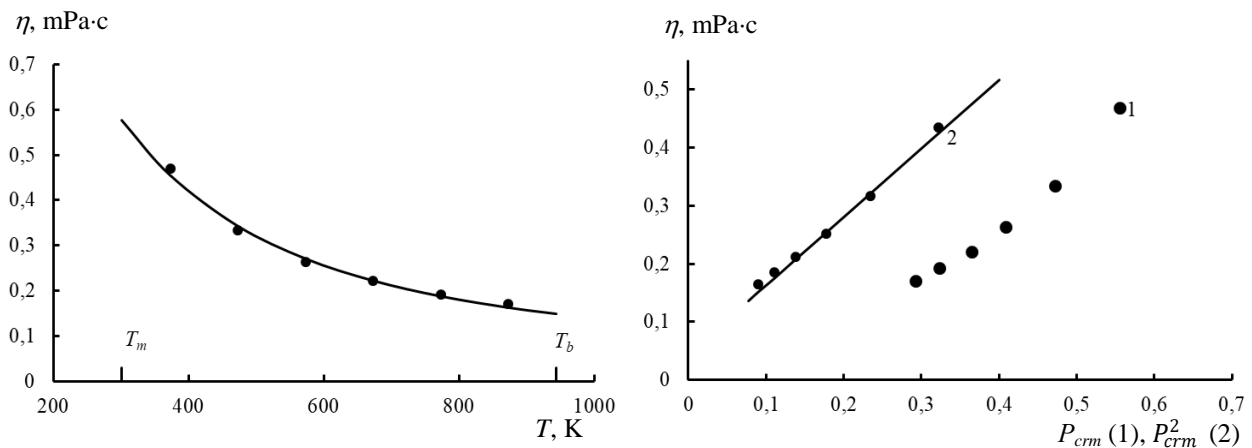


Figure 5. The dependence of the dynamic cesium viscosity on temperature [26, 27] and proportion of the crystal-mobile  $P_{crm}$  particles and  $P_{crm}^2$  clusters (lines by (10))

For instance, at a melting point, the equation (10) had a single formula for all substances

$$\eta = a + 0.400b. \tag{11}$$

The different substances were compared by this viscosity value. Since it referred to the liquid phase at a melting point, where the liquid and solid states were in equilibrium. Thus, the direct experimental definition of viscosity was difficult due to the simultaneous presence and uncertain ratio of the solid and liquid phases.

It was required to ascertain that the straight-line dependence of the discussed data for alkali metals was adequate. With this view, they were processed by the least squares method to obtain the numerical values of parameters of  $a$  and  $b$ , the  $R$  correlation coefficient and its significance for the 95 % confidence level ( $t_R > 2$ ), the determination degree of the received dependencies ( $D = R^2$ ) [28] and the  $\eta_m$  melting viscosity. Results are presented in Table 6 and Figures of 1–5.

Table 6

Parameters of equation (12) for alkali metals

Element	$T_m$ , K	$a$	$b$	$R$	$t_R$	$D$	$\eta_m$ , mPa·c
Lithium	453.7	0.100	1.18	0.9986	813 > 2	0.9971	0.572
Sodium	371	0.000	1.58	0.9815	60 > 2	0.9634	0.632
Potassium	337	0.025	1.13	0.9907	118 > 2	0.9815	0.478
Rubidium	312.5	0.045	1.18	0.9948	189 > 2	0.9896	0.517
Cesium	301.7	0.050	1.32	0.9960	249 > 2	0.9920	0.578

The Table 6 demonstrated that a high adequacy of the straight-line correlation of viscosity with the cluster proportions and directly with temperature was established for all alkali metals. Since, they were displayed by a single equation (10). A high degree to determine these dependencies indicated their proximity to the fundamental pattern based on the physical nature of the liquid state.

Somewhat worse correlation of the data for sodium had a physical explanation. Thus, the experimental values of viscosity were markedly higher than the calculated values at 373 K by two degrees above a melting point. It might be due to the probability of a partial presence of the solid phase within the accuracy of melt temperature maintenance.

For all other alkali metals, the first experimental point was established at a temperature no less than twenty degrees above a melting point.

Herewith, the  $\eta_m$  melting viscosity for sodium was abnormally high. A comparative analysis of the data on this value became difficult because it was a characteristic for the contribution of the chaotic virtual component of the melting viscosity.

The graphical data for sodium showed some residual curvature of the correlation on the cluster proportion. It was less visible on similar dependences for other metals. It indicated a more complex nature of the cluster influence on the melt viscosity. It might be caused by formation of more complex super-cluster virtual structures of less strong cluster associates. This aspect was examined in the monograph [17]. It ended with construction of a more accurate semi-empirical cluster-associated viscosity model. Thus, the cluster association degree was applied, and the correlation with activation energy of fluidity was discovered by the Frenkel-Andrade viscosity model [29–31].

It was important to state that determination of the activation energy was possible due to linearization of this model. It was widespread procedure to analyze and process data for the complex physicochemical patterns in order to define their adequacy and apply them to the real processes.

### Conclusions

The probabilistic nature of formation and the virtual existence of the solid phase clusters in liquid were applied to develop the existing quasi-polycrystalline clustering model of the liquid state of matter.

It was studied by Boltzmann distribution of an energy spectrum and the chaotic particles concept with using an additional cluster distribution per the number of the crystal-mobile particles included in them.

The form of this distribution was defined by the equal probability of the mutual cluster conversions and expressed by the virtuality essence of the liquid state.

The proportional correlation of viscosity directly with the cluster content in the liquid was established by the analysis of the most complete reference data on temperature dependences of dynamic viscosity for alkali metals. Probability was provided to quantitative concept of the quasi-polycrystalline clustering model of the liquid state of matter based on its properties with using the chaotic particles concept and the Boltzmann distribution.

It was clear that each straight-line correlation was not functional. In this case, the argument (the cluster proportions of  $P_{cm}^2$ ) and function (viscosity) were related as cause and effect. The cluster proportions were determined by the fundamental Boltzmann distribution. It was found the proportion of low-energy (the crys-

tal-mobile) particles in it. It was as a reservoir to form (virtual crystallization) clusters. They created more chaotic particles and a thicker consistency of the liquid state. This consistency might be equated with the liquid viscosity. It was quite possible that a similar straight-line correlation of cluster proportions could be discovered with other properties of the liquid, e.g., by density and electrical conductivity.

In reference to correlation between the cluster proportions and viscosity, it might be physically compared with the state of a mechanical mixture of water and sand. The sand played the role as a cluster phase, and created the emulsion viscosity. It was important to state that the rectilinearity of correlation between the cluster proportions and viscosity did not apply to all crystal-mobile particles ( $P_{cm}$ ). It was applied for two or more partial formations ( $P_{cm}^2$ ). It was clearly illustrated by the graphical data for alkali metals. In this case, it was of no concern a structure of the formed clusters. Since, the chaotic component of the substance was used. Thus, its contribution to the liquid state was examined. The influence of the potential energy of attraction and repulse of particles might add the general picture of such state as certain cluster structure formation. However, the chaotic component of matter by the kinetic energy of the thermal particle motion was basic to display the formation and properties of matter as a whole.

## References

- 1 Архаров В.И. О квазиполикристаллической модели расплавов / В.И. Архаров, И.А. Новохатский / Строение и свойства металлических и шлаковых расплавов: науч. сообщ. Всесоюз. конф. по строению и свойствам металлических и шлаковых расплавов. — Свердловск, 1974. — С. 52, 53.
- 2 Еланский Г.Н. Свойства и строение расплавов на основе железа / Г.Н. Еланский, В.А. Кудрин // Вестн. ЮУрГУ. Сер. Metallurgy. — 2015. — Т. 15. № 3. — С. 11–19.
- 3 Баум Б.А. Фундаментальные исследования физикохимии металлических расплавов / Б.А. Баум, Г.В. Тягунов, Е.Е. Барышев, Е.С. Цепелев. — М.: ИКЦ «Академкнига», 2002. — 469 с.
- 4 Еланский Г.Н. Строение и свойства металлических расплавов: учеб. пос. для вузов / Г.Н. Еланский, Д.Г. Еланский. — М.: Юрайт, 2020. — 212 с.
- 5 Новохатский И.А. О вязком течении металлических расплавов при больших перегревах / И.А. Новохатский, В.И. Архаров, В.И. Ладьянов // Докл. АН СССР. — 1979. — Т. 247. № 4. — С. 849–851.
- 6 Meyer N. The role of chemical order in the temperature and composition dependence of the viscosity of liquid alloys / N. Meyer, H. Xu, J.-F. Wax. // J. Chem. Phys. — 2019. — Vol. 150. — P. 17. <https://doi.org/10.1063/1.5092694>
- 7 Zhang Fan. Modeling the viscosity of liquid alloys with associates / Fan Zhang, Shiyi Wen, Yuling Liu // J. Mol. Liq. — 2019. — Vol. 291. — P. 111345. <https://doi.org/10.1016/j.molliq.2019.111345>
- 8 Asnani M. Crystallization of organically templated phosphomolybdate cluster-based solids from aqueous solution / M. Asnani, D. Kumar, T. Duraisamy, A. Ramanan // J. Chem. Sci. — 2012. — Vol. 124, No 6. — P. 1275–1286. <https://doi.org/10.1007/s12039-012-0328-z>
- 9 Thomas J. Phosphomolybdate cluster based solids mediated by transition metal complexes / J. Thomas, A. Ramanan // Inorg. Chim. Acta. — 2011. — Vol. 372. — P. 243–249. <https://doi.org/10.1016/j.ica.2011.02.028>
- 10 Jisha J. Role of supramolecular interactions in crystal packing of Strandberg-type cluster-based hybrid solids / J. Jisha, W. Cinu, S. Bharti, J. Jemini, T. Jency // J. Chem. Sci. — 2020. — Vol. 132. — P. 137. <https://doi.org/10.1007/s12039-020-01826-w>
- 11 Леонтович М.А. Введение в термодинамику. Статистическая физика / М.А. Леонтович. — М.: Высш. шк., 1983. — 416 с.
- 12 Малышев В.П. О взаимосвязи и соразмерности дискретных и непрерывных зависимостей / В.П. Малышев, А.М. Макашева, Ю.С. Зубрина (Красикова) // Докл. НАН РК. — 2016. — № 1. — С. 49–56.
- 13 Малышев В.П. Распределение Больцмана как бесконечная последовательность и сходящийся ряд / В.П. Малышев, Ю.С. Зубрина, А.М. Макашева // Вестн. НАН РК. — 2017. — № 1. — С. 49–58.
- 14 Malyshev V.P. Quantization of particle energy in the analysis of the Boltzmann distribution and entropy / V.P. Malyshev, Yu.S. Zubrina, A.M. Makasheva // J. Math. and Sys. Sci. — 2017. — № 10. — P. 278–288.
- 15 Малышев В.П. Распределение и энтропия Больцмана как бесконечные сходящиеся последовательности / В.П. Малышев, А.М. Макашева, Ю.С. Красикова // Вестн. Караганд. ун-та. Сер. Физика. — 2018. — № 3. — С. 42–58.
- 16 Малышев В.П. Концепция хаотизированных частиц как основа единого отображения твердого, жидкого и газообразного состояний вещества / В.П. Малышев, А.М. Нурмагамбетова (Макашева) // Вестн. Казах. нац. ун-та. Сер. хим. — 2004. — № 3(35). — С. 53–67.
- 17 Malyshev V.P. Viscosity, fluidity and density of substances. Aspect of Chaotization / V.P. Malyshev, A.M. Makasheva, N.S. Bekturganov. — Lambert: Academic Publishing (Germany), 2013. — 340 p.
- 18 Daeneke T. Liquid metals: fundamentals and applications in chemistry / T. Daeneke, K. Khoshmanesh, N. Mahmood, I.A. de Castro, D. Esrafilzadeh, S.J. Barrow, M.D. Dickey, K. Kalantarzadeh // Chem. Soc. Rev. — 2018. — Vol. 47. — P. 4073–4111. DOI: 10.1039/c7cs00043j

- 19 Сороко Э.М. Золотые сечения, процессы самоорганизации и эволюции систем. Введение в общую теорию гармонии систем / Э.М. Сороко. — М.: URSS, 2019. — 264 с.
- 20 Седов Е.А. Взаимосвязь энергии, информации и энтропии в процессах управления и самоорганизации. Информация и управление / Е.А. Седов. — М.: Наука, 1985. — С. 31–45.
- 21 Малышев В.П. Вероятностно-детерминированное отображение / В.П. Малышев. — Алматы: Ғылым, 1994. — 376 с.
- 22 Мелихов И.В. Физико-химическая эволюция твердого вещества / И.В. Мелихов. — М.: БИНОМ; Лаборатория знаний, 2006. — 309 с.
- 23 Больцман Л. Избранные труды. Молекулярно-кинетическая теория газов. Термодинамика. Статистическая механика. Теория излучения. Общие вопросы физики / Л. Больцман. — М.: Наука, 1984. — 590 с.
- 24 Galkin V.A. Analysis of mathematical models: systems of conservation laws, Boltzmann and Smoluchowski equations / V.A. Galkin. — Moscow: Laboratoriia Znaniia, 2009. — 408 p.
- 25 Малышев В.П. Вязкость и текучесть расплавов в аспекте их хаотизации (неорганические соединения и сплавы) / В.П. Малышев, А.М. Макашева. — Lambert: Academic Publishing (Germany), 2020. — 153 с.
- 26 Волков А.И. Большой химический справочник / А.И. Волков, И.М. Жарский. — Минск: Современная школа, 2005. — 608 с.
- 27 Shpil'rain E.E. In Handbook of Thermodynamic and Transport Properties of the Alkali Metals / E.E. Shpil'rain, K.A. Yakimovich, Y.A. Fomin, S.N. Skovorodjko, A.G. Mozgovoi. — Oxford: Bledewell Scientific Publ., 1985. — 325 p.
- 28 Shannon R. The art and science of optical design / Shannon R. — Cambridge: Cambridge University Press, 1997. — P. 630.
- 29 Malyshev V.P. Relationship between the cluster theory of liquids and the Frenkel-Andrade viscosity model / V.P. Malyshev, A.M. Makasheva // Russ. Chem. Bull. — 2020. — Vol. 69. — P. 1296–1305. <https://doi.org/10.1007/s11172-020-2901-9>
- 30 Makasheva A.M. Cluster-Associate Model for the Viscosity of Sodium Fluoride in Comparison with the Frenkel Model / A.M. Makasheva, V.P. Malyshev // Russ. Metall. (Metally). — 2021. — Vol. 2. — P. 176–180. <https://doi.org/10.1134/S0036029521020154>
- 31 Malyshev V.P. Invariants of ratio of crystal-mobile, liquid-mobile, and vaporized chaotized particles in solid, liquid, and gas states of substance / V.P. Malyshev, A.M. Makasheva, L.A. Bekbaeva // Bulletin of the Karaganda University, Chemistry Series. — 2021. — № 4(104). — С. 69–78. <https://doi.org/10.31489/2021Ch4/69-78>

А.М. Макашева, В.П. Малышев, Л.А. Бекбаева

## Сұйықтықтың кластерлік құрылымының тікелей байланысы және оның тұтқырлығы туралы

Жұмыстың мақсаты — Больцман үлестірімін, ретсіз бөлшектер тұжырымдамасын және кластерлердің виртуалды үлестірілуін қолдана отырып, олардың өлшемдері бойынша сұйықтықтың (атап айтқанда, балқымалар) квазиполикристалды кластерлік моделі аясында осы кластерлердің үлесін сұйықтықтың тұтқырлығымен тікелей сандық байланыс мүмкіндігін негіздеу. Мақалада сілтілік металдардың динамикалық тұтқырлығының температуралық тәуелділігі бойынша ең толық анықтамалық мәліметтерді талдау мысалында тұтқырлықтың сұйықтықтағы кластерлердің құрамымен тікелей пропорционалды байланысы анықталған. Бұл Больцманның таралуына тікелей байланысты хаотикалық бөлшектер тұжырымдамасына негізделген заттың сұйық күйінің квазиполикристалды (кластерлік) моделін оның қасиеттері арқылы сандық түрде білдіру мүмкіндігін қамтамасыз етеді. Заттың қатты, сұйық және газ тәрізді күйлеріндегі бөлшектердің ретсіз жылулық қозғалысының кинетикалық энергиясына қолданылатын Больцмонның энергетикалық спектрі олардың барлық агрегаттық күйлерінде болуымен олардың үш энергетикалық класын ажыратуға мүмкіндік берді, ал қосынды әрқашан біреуге тең. Кластерлердің энергетикалық кластары мен өлшемдері бойынша бөлшектердің таралуы арқылы табылған виртуалды реттелген кластерлік және толығымен хаотикалық сұйықтық компоненттерінің үлесін есептеу бойынша формулалары келтірілген.

*Кілт сөздер:* Больцманның таралуы, ретсіз бөлшектер, ықтималдылық, виртуалдылық, кластер, балқыма, тұтқырлық, сілтілік металдар.

А.М. Макашева, В.П. Малышев, Л.А. Бекбаева

## О прямой связи кластерного строения жидкости и ее вязкости

Цель работы — в рамках квазиполикристаллической кластерной модели жидкости (в частности, расплавов) с помощью распределения Больцмана, концепции хаотизированных частиц и виртуального распределения кластеров по их размерам обосновать возможность прямой количественной связи доли этих кластеров с вязкостью жидкости. В статье на примере анализа наиболее полных справочных дан-

ных по температурным зависимостям динамической вязкости щелочных металлов установлена прямо пропорциональная связь вязкости непосредственно с содержанием кластеров в жидкости. Этим обеспечивается возможность количественного выражения квазиполикристаллической (кластерной) модели жидкого состояния вещества через ее свойства на основе концепции хаотизированных частиц в прямой связи с распределением Больцмана. Энергетический спектр Больцмана применительно к кинетической энергии хаотического теплового движения частиц в твердом, жидком и газообразном состояниях вещества позволил выделить три энергетических класса с присутствием их во всех агрегатных состояниях и в сумме, всегда равной единице. Приведены формулы по расчету доли виртуально упорядоченной кластерной и полностью хаотизированной составляющих жидкости, найденных с помощью распределений частиц по энергетическим классам и размерам кластеров.

*Ключевые слова:* распределение Больцмана, хаотизированные частицы, вероятность, виртуальность, кластер, расплав, вязкость, щелочные металлы.

## References

- 1 Arkharov, V.I., & Novokhatskii, I.A. (1974). O kvazipolikristallicheskoj modeli rasplavov [On the quasi-polycrystalline model of melts]. *Stroenie i svoystva metallicheskih i shlakovykh rasplavov: nauchnye soobshcheniia Vsesoyuznoi konferentsii po stroeniiu i svoystvam metallicheskih i shlakovykh rasplavov — Structure and properties of metal and slag melts: scientific report of the All-Union Conference on the structure and properties of metal and slag melts, Russia*. Sverdlovsk, 52 [in Russian].
- 2 Elansky, G.N., & Kudrin, V.A. (2015). Svoystva i stroenie rasplavov na osnove zheleza [The properties and structure of iron-based melts]. *Vestnik Yuzhno-Uralskogo gosudarstvennogo universiteta. Seriya Metallurgiya — Bull. of the South Ural State University, Ser. Metallurgy*, 15, 3 [in Russian].
- 3 Baum, B.A., Tyagunov, G.V., Baryshev, E.E., & Tsepelev, E.S. (2002). Fundamentalnyye issledovaniia fizikokhimii metallicheskih rasplavov [Basic Research of the Physical Chemistry of Metal Melts]. Moscow: Akademkniga [in Russian].
- 4 Elansky, G.N., & Elansky, D.G. (2020). *Stroenie i svoystva metallicheskih rasplavov [The Structure and Properties of Metal Melts]*. Moscow: Yurait [in Russian].
- 5 Novokhatskii, I.A., Arkharov, V.I., & Lad'yanov, V.I. (1979) O viazkom techenii metallicheckikh rasplavov pri bolshikh peregrevah [On viscous flow of metal melts at high superheats]. *Rep. of the USSR Acad. of Sci.*, 247, 4 [in Russian].
- 6 Meyer N., Xu H., & Wax J.-F. (2019). The role of chemical order in the temperature and composition dependence of the viscosity of liquid alloys. *J. of Chem. Phys.*, 150, 17. <https://doi.org/10.1063/1.5092694>
- 7 Zhang Fan, Wen Shiyi, & Liu Yuling. (2019) Modelling the viscosity of liquid alloys with associates. *J. of Molec. Liq.*, 291, 111345. <https://doi.org/10.1016/j.molliq.2019.111345>
- 8 Asnani M., Kumar D., Duraisamy T., & Ramanan A. (2012) Crystallization of organically templated phosphomolybdate cluster-based solids from aqueous solution. *J. Chem. Sci.*, 124, 1275–1286. <https://doi.org/10.1007/s12039-012-0328-z>
- 9 Thomas J., & Ramanan A. (2011) Phosphomolybdate cluster based solids mediated by transition metal complexes. *Inorg. Chim. Acta*, 372, 243–249. <https://doi.org/10.1016/j.ica.2011.02.028>
- 10 Jisha J., Cinu W., Bharti S., Jemini J., & Jency T. (2020) Role of supramolecular interactions in crystal packing of Strandberg-type cluster-based hybrid solids. *J. Chem. Sci.*, 132, 137. <https://doi.org/10.1007/s12039-020-01826-w>
- 11 Leontovich, M.A. (1983). Vvedenie v termodinamiku. Statisticheskaja fizika [Introduction to Thermodynamics. Statistical Physics: textbook for universities]. Moscow: Vysshaja shkola [in Russian].
- 12 Malyshev V.P., Makasheva A.M., & Zubrina (Krasikova) Yu.S. (2016) O vzaimosvazi i sorazmernosti diskretnykh i nepre-ryvnykh zavisimostei [On the relationship and proportionality of discrete and continuous dependencies]. *Doklady Natsionalnoi akademii nauk Respubliki Kazakhstan — Reports of the National Academy of Sciences of Kazakhstan*, 1, 49–56 [in Russian].
- 13 Malyshev, V.P., Zubrina, Yu.S., & Makasheva A.M. (2017). Raspredelenie Boltsmana kak beskonechnaja posledovatel'nost' i skhodiashchiesia riad [Boltzmann distribution as an infinite sequence and a converging series]. *Vestnik Natsionalnoi akademii nauk Respubliki Kazakhstan — Bull. of the National Academy of Sciences of the Republic of Kazakhstan*, 1, 49–58 [in Russian].
- 14 Malyshev V.P., Zubrina Yu.S., & Makasheva A.M. (2017) Quantization of particle energy in the analysis of the Boltzmann distribution and entropy. *J. of Math. and Syst. Sci.*, 10, 278–288.
- 15 Malyshev, V.P., Makasheva, A.M., & Krasikova, Yu.S. (2018). Raspredelenie i entropiia Boltsmana kak beskonechnye skhodiashchiesia posledovatel'nosti [Boltzmann distribution and entropy as infinite converging sequences]. *Vestnik Karagandinskogo universiteta. Seriya Fizika — Bull. of the Karaganda University, Physics Ser.*, 3, 42–58 [in Russian].
- 16 Malyshev, V.P., & Nurmagambetova (Makasheva), A.M. (2004). Kontseptsiiia khaotizirovannykh chastits kak osnova edinogo otobrazheniia tverdogo, zhidkogo i gazoobraznogo sostoianii veshchestva [The concept of chaotic particles as the basis for a unified display of solid, liquid and gaseous states of matter]. *Vestnik Kazakhskogo natsionalnogo universiteta — Bull. of the KazNU, Ser. Chemistry*, 3, 53–67 [in Russian].
- 17 Malyshev V.P., Makasheva A.M., & Bekturganov N.S. (2013) Viscosity, fluidity and density of substances. *Aspect of Chaotization*. Lambert: Academic Publishing.

- 18 Daeneke T., Khoshmanesh K., Mahmood N., de Castro I.A., Esrafilzadeh D., Barrow S.J., Dickey M.D., & Kalantarzadeh K. (2018) Liquid metals: fundamentals and applications in chemistry. *Chem. Soc. Rev.*, 47, 4073-4111. <https://doi.org/10.1039/c7cs00043j>
- 19 Soroko, E.M. (2019). Zolotye secheniia, protsessy samoorganizatsii i evoliutsii sistem. Vvedenie v obshchuiu teoriuu garmonii sistem [Golden sections, processes of self-organization and evolution of systems. Introduction to the general theory of harmony of systems]. Moscow: URSS [in Russian].
- 20 Sedov, E.A. (1985). Vzaimosviaz energii, informatsii i entropii v protsessakh upravleniia i samoorganizatsii. Informatsiia i upravlenie [The relationship of energy, information and entropy in the processes of management and self-organization]. Moscow: Nauka [in Russian].
- 21 Malyshev, V.P. (1994). Veroiatnostno-determinirovannoe otobrazhenie [Probabilistic-deterministic mapping]. Almaty: Gylym [in Russian].
- 22 Melikhov, I.V. (2006). Fiziko-khimicheskaia evoliutsiia tverdogo veshchestva [Physicochemical Evolution of the Solid]. Moscow: Laboratoriia znanii [in Russian].
- 23 Boltzmann, L. (1984). Izbrannye trudy. Molekuliarno-kineticheskaia teoriia gazov. Termodinamika. Statisticheskaiia mekhanika. Teoriia izlucheniia. Obshchie voprosy fiziki [Selected works. Molecular-kinetic theory of gases. Thermodynamics. Statistical mechanics. Theory of radiation. General questions of physics]. Moscow: Nauka [in Russian].
- 24 Galkin V.A. (2009) Analysis of mathematical models: systems of conservation laws, Boltzmann and Smoluchowski equations. Moscow: Laboratoriya Znanii.
- 25 Malyshev, V.P., & Makasheva, A.M. (2020). *Viazkost i tekuchest rasplavov v aspekte ikh khaotizatsii (neorganicheskie soedineniia i splavy)* [Viscosity and fluidity of melts in the aspect of their randomization (inorganic compounds and alloys)]. Lambert: Academic Publishing [in Russian].
- 26 Volkov, A.I., & Zharsky, I.M. (2005). *Bolshoi khimicheskii spravochnik* [Big chemical reference book]. Minsk: Sovremeniia shkola [in Russian].
- 27 Shpil'rain E.E., Yakimovich K.A., Fomin Y.A., Skovorodjko S.N., & Mozgovoii A.G. (1985) Handbook of Thermodynamic and Transport Properties of the Alkali Metals, IUPAC Chemical Data Series. Oxford: Blackwell Scientific Publications, The Alden Press.
- 28 Shannon R. (1997) The art and science of optical design. Cambridge: Cambridge University Press.
- 29 Malyshev V.P., & Makasheva A.M. (2020) Relationship between the cluster theory of liquids and the Frenkel-Andrade viscosity model. *Russ. Chem. Bull.*, 69, 1296–1305. <https://doi.org/10.1007/s11172-020-2901-9>
- 30 Makasheva A.M., & Malyshev V.P. (2021) Cluster-Associate Model for the Viscosity of Sodium Fluoride in Comparison with the Frenkel Model. *Russ. Metall. (Metally)*, 2, 176-180. <https://doi.org/10.1134/S0036029521020154>
- 31 Malyshev V.P., Makasheva A.M., & L.A. Bekbaeva (2021) Invariants of ratio of crystal-mobile, liquid-mobile, and vaporized chaotized particles in solid, liquid, and gas states of substance. *Bulletin of the University of Karaganda Chemistry*, 4(104), 69–78. <https://doi.org/10.31489/2021Ch4/69-78>

#### Information about authors\*

**Makasheva, Astra Mundukovna** (*corresponding author*) — Doctor of Technical Sciences, Professor, Karaganda Technical University, Nazarbaev av., 56, 100027, Karaganda, Kazakhstan; e-mail: [astra\\_mun@mail.ru](mailto:astra_mun@mail.ru); <https://orcid.org/0000-0003-2249-3435>

**Malyshev, Vitalyi Pavlovich** — Doctor of Technical Sciences, Professor, Chief Researcher, Abishev Chemical-Metallurgical Institute, Ermekov street, 63, 100009, Karaganda, Kazakhstan; e-mail: [eia\\_hmi@mail.ru](mailto:eia_hmi@mail.ru); <https://orcid.org/0000-0002-3996-1533>

**Bekbayeva, Lazzat Akyibaikyzy** — Doctoral student, Karaganda Technical University, Nazarbaev av., 56, 100027, Karaganda, Kazakhstan; e-mail: [lyazzat.bekbaeva@mail.ru](mailto:lyazzat.bekbaeva@mail.ru); <https://orcid.org/0000-0003-2543-6380>

---

\*The author's name is presented in the order: *Last Name, First and Middle Names*

R. Bhimanwar<sup>1</sup>, A. Thomas<sup>1\*</sup>, L. Kothapalli<sup>1</sup>, A. Godase<sup>1</sup>, S. Gandhi<sup>1</sup>,  
S. Chandani<sup>1</sup>, G. More<sup>1</sup>, G. Jadhav<sup>2</sup>, S. Choudhary<sup>3</sup>

<sup>1</sup>Department of Pharmaceutical Chemistry, Dr. D.Y. Patil Institute of Pharmaceutical Sciences and Research, Pune, Maharashtra, India (Affiliated to Savitribai Phule Pune University, Pune);

<sup>2</sup>School of Medicine, Omaha Campus, Creighton University, NE, USA;

<sup>3</sup>RASA Life Science Informatics, Pune, Maharashtra, India

(\*Corresponding author's e-mail: [asha.thomas@dypvp.edu.in](mailto:asha.thomas@dypvp.edu.in))

## Prospective Hybrid Molecules with Dual Anti-Viral and Anti-Thrombotic Activity Against the SARS-CoV-2 Infection and Its Associated Complications Employing *in Silico* Studies

Covid-19, a SARS-CoV virus-based disease, was identified in Wuhan, China, in December 2019. Initially, it was considered just an infection of the respiratory system, but due to its transmittable nature, it was declared a pandemic. A variety of treatment options were implemented, including antivirals like remdesvir, favipiravir along with vitamins and antioxidants. Further investigations revealed that the Covid-19 infection results in thrombotic cardiovascular complications, which are the major concern for the increased mortality associated with this disease. This study investigates the *in Silico* design of hybrid molecules with antiviral and anti-thrombotic properties. A docking study was performed using Autodock Vina software, and binding energies of the designed compounds were determined for papain-like protease (PDB: 3E9S) and 3-chymotrypsin-like cysteine protease (PDB: 6LU7). The docked poses and amino acids interactions were verified using Biovia Discovery studio 4.5. The binding energies of all designed compounds were compared with the standards, Compound RL1 (2-(5-(3-carbamoyl-1H-1,2,4-triazol-1-yl)-3,4-dihydroxytetrahydrofuran-2-yl)methoxy)-carbonyl)amino)(hydroxy)methyl)carbamoyl)phenyl acetate) and Compound FL2 (8-hydroxy-2-(3-hydroxy-4-methoxyphenyl)-4-oxochroman-6-yl)(2-(6-flouro-3-oxo-3,4-dihydropyrazine-2-carboxamido)-1-hydroxy-3-phenylpropyl)carbamate) proved to be promising agents with strong binding interactions. Hybrid molecules that inhibit viral replication, possibly as transition state inhibitors, can be investigated further for use in the treatment of SARS-Co-V infection and its associated complications.

**Keywords:** COVID-19; CL-pro, PL-pro, antiviral, antithrombotic, molecular docking, *in Silico*, hybrid molecule.

### Introduction

The Covid-19 pandemic caused by Severe acute respiratory syndrome coronavirus (SARS-CoV-2) virus has affected majority of population around the globe and has resulted in significant mortality and morbidity. It has been initially identified as a respiratory illness, but has now demonstrated extreme individual variability in its symptoms, and severity of infection [1, 2]. This highly infectious virus has undergone rapid mutations with “the double mutant” strain leading to the second wave in almost all countries worldwide. This double mutant Covid strain has been found to be more infectious and lethal and has increased the health risk in patients with high mortality rate [3]. The SARS-CoV-2 belongs to  $\beta$ -coronavirus family and is SS RNA enveloped protein with 9860 amino acids. SARS-CoV-2 gene fragment consists of structural and nonstructural proteins encoded from S, E, M and N gene and ORF region, respectively [4, 5]. Spike glycoprotein (S protein) present on the virus surface is the key component for viral entry into the host cell through recognition and binding with ACE2 (angiotensin-converting enzyme 2) receptor. S1 subunit of S protein recognizes the binding site and binds to the host receptor and S2 subunit forms six-helical bundle with the help of heptad repeat (HR1 and HR2) and mediates fusion cell membrane. Fusion of host and viral membrane is achieved by host protease, which cleaves site at the border of S1 and S2. Sixteen nonstructural proteins perform different function and carry out processing and replication of RNA [6, 7].

Angiotensin-converting enzyme 2 (ACE2) protein, target for coronavirus is found in alveolar epithelial cells of lungs and in small intestines enterocytes. Breakdown of ACE2 finally causes systemic inflammation in the host cell leading to critical illness and multiorgan dysfunction. Covid-19 patients with cardiovascular

disease have been severely affected and an increase in mortality rate has been observed. Adverse outcomes have been observed due to systemic inflammation, which destabilizes vascular plaques finally demanding increased cardiac activity. Increased levels of IL6, D-dimer and troponins (cardiac specific) direct the patient towards increased risk of pulmonary embolism and thrombosis [8–12].

Currently the treatment line of SARS-CoV-2 infection involves use of anti-virals like remdesivir, favipiravir, ritonavir to address the pulmonary infection phase; while for suppressing the inflammatory/coagulopathy phase, drugs like Tocilizumab, Anakinra, Baricitinib, Eculizumab, Emapalumab and Heparin, including low molecular weight heparins (e.g enoxaprin) are utilized [13, 14]. Several vaccine candidates have received approval for emergency use across the globe [15] and mass immunization drives are under progress [16]. However until a considerable mass of population is vaccinated and herd immunity is achieved, therapeutic interventions will be required to combat the situation.

Latest developments show that SARS-CoV-2 infection precipitates variety of haematological complications associated with increase in D-Dimer and blood thickening. Mortality occurs either due to respiratory failure or thrombotic cardiovascular complications, which requires the management of multiple associated pathways [17–20].

Development of hybrid molecules is an attractive strategy of drug design to achieve multiple targeting, enhance biological activity and improve kinetics [21, 22]. In the past decades, several researchers have utilized this concept to develop agents with antimicrobial [23–25], anti-malarial [26–28] and anti-cancer activity [29, 30]. Researchers have developed multifunctional drugs comprising of two or more pharmacophores with benefits in treatment of multi-factorial diseases [31–35].

So an attempt was made to design hybrids with dual action, namely antiviral and anti-coagulant activity, which would prove advantageous in treatment of the multiple complications occurring during SARS-CoV-2 infection. The strategy involved designing of hybrids of reported anti-viral agents with anti-coagulant molecules through suitable linkers converting them into potentially active molecules, which were studied against suitable anti-viral targets. The hybrids were generated by linking antiviral molecules [36–38], namely ribavirin, favipiravir, oseltimivir and acyclovir with established anti-platelet drugs [39–43] viz. hesperitin, resveratrol and aspirin as test compounds. The selected anti-coagulants are reported to possess dual anti-thrombotic and antiviral action. The criteria for selection of these agents are summarized in Table 1. The linkers selected for the design of molecules included hydrolysable and cleavable linkers like 2-amino 2-hydroxy ethyl amide, malonic acid and succinic acid.

Table 1

#### Selection of anti-viral and anti-platelet molecules for design of hybrid molecules

Selected Anti-viral molecules	
Ribavirin	Broad activity toward conventional and novel viruses of DNA and RNA types; Multiple mechanisms of direct antiviral action; Random mutagenesis of viruses to promote T cell response; Tolerable and well-characterized side effect profile; Mature clinical experience & comprehensive demographic characterization; Accessibility & affordability
Favipiravir	Employed for clinical intervention of COVID-19 treatment; Exhibits faster viral clearance and better chest CT changes; Adverse events are rare and tolerable
Oseltimivir	Clinical study suggests that Remdesivir treatment among all of antivirals such as Ribavirin, Favipiravir and Oseltamivir proved promising therapeutics in COVID treatment
Acyclovir	Similar clinical target as approved drug Remdesivir
Selected Anti-platelet agents	
Hesperitin	Anti-platelet, anticoagulant, antioxidant, radical scavenging activity and anti-inflammatory activities; Demonstrated antiviral activity by altering the immune system mainly via regulating interferons in the influenza A virus
Resveratrol	Inhibits platelet aggregation and platelet membrane-bound fibrinogen (Pfig) induced by adenosine diphosphate (ADP through decreased activity of PLC beta of platelets; Antioxidant-promote nitric oxide production, Cardioprotective agent, Antiinflammatory, Neuroprotective, Antiviral properties
Aspirin	Proven anticoagulant action, considerable dose-dependent antiviral activity (CA9, HRV1A, HRV2 and substantial activity against FluA H1N1, HRV14 and HRV39); Possible MOA-involvement of the NF-κB-pathway, Differential regulation of influenza virus RNA synthesis by NF-κB, iNOS expression by down regulating the promoter activity, mRNA and protein expression levels involvement of p38

## Experimental

### Selection of Protein

COVID-19 papain-like protease (PL-pro) (PDB ID- 3E9S) and 3-chymotrypsin-like cysteine protease (CL-pro) (PDB ID- 6LU7) were selected as the protein targets for the present study. The crystal structure of desired proteins was downloaded from RCSB Protein data bank in.pdb format. The native ligand present in protein 6LU7 is n-[(5-methylisoxazol-3-yl)carbonyl]alanyl-l-valyl-n~1~((1r,2z)-4-(benzyloxy)-4-oxo-1-[(3r)-2-oxopyrrolidin-3-yl]methyl}but-2-enyl)-l-leucinamide and in 3E9S is 5-amino-2-methyl-N-[(1R)-1-naphthalen-1-ylethyl]benzamide.

### Selection of Ligands

Hybrid ligands that can exhibit dual action, anti-viral activity against the SARS-CoV-2 along with anti-thrombotic activity with improved affinity and efficacy in combination were designed. Promising anti-viral agents that are currently recommended in treatment of the SARS-CoV-2 infection like oseltamavir, ribavirin, fevipiravir and acyclovir (Figure 1A) with molecules like salicylic acid, resveratrol and hesperitin with potent anti-viral and well-established anti-thrombosis profile (Figure 1B) were selected to design the hybrid molecules using appropriate linkers (Figure 1C).

The 3D structures of hybrid type ligands were drawn using Chem Draw in.mol file with all possible combinations and Open Babel ([http://openbabel.org/wiki/Main\\_Page](http://openbabel.org/wiki/Main_Page)) was used to convert. mol to. pdbqt files. Drug-like properties of the ligands were computed using ADME Schrodinger software QikProp (<https://www.schrodinger.com/QikProp>).

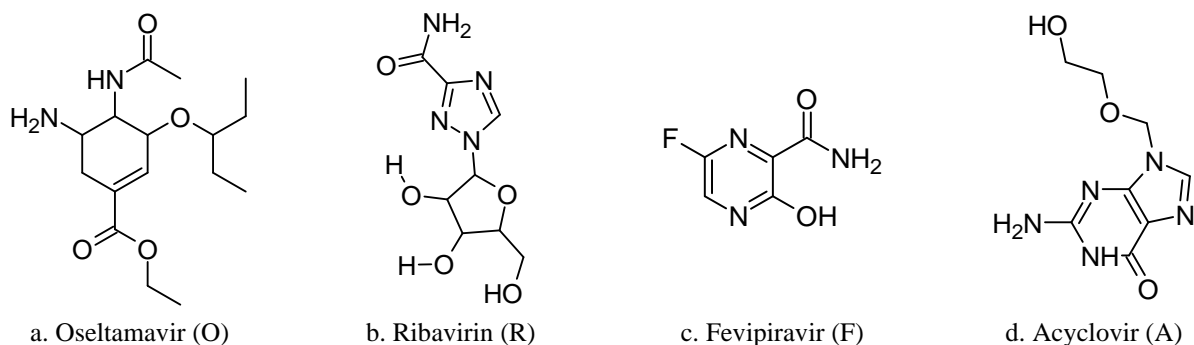


Figure 1A. Selected Anti-viral agents

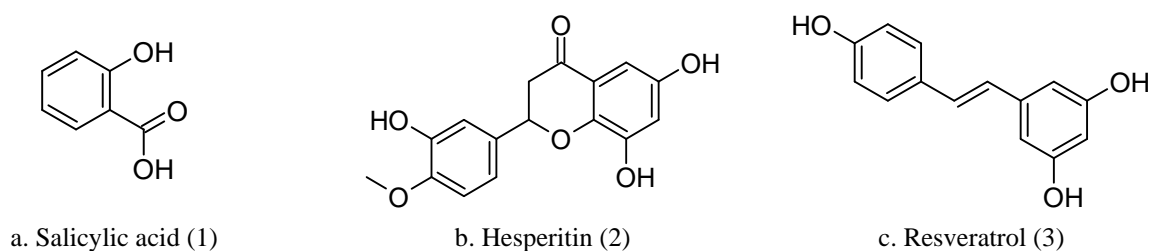


Figure 1B. Selected anti-thrombotic agents

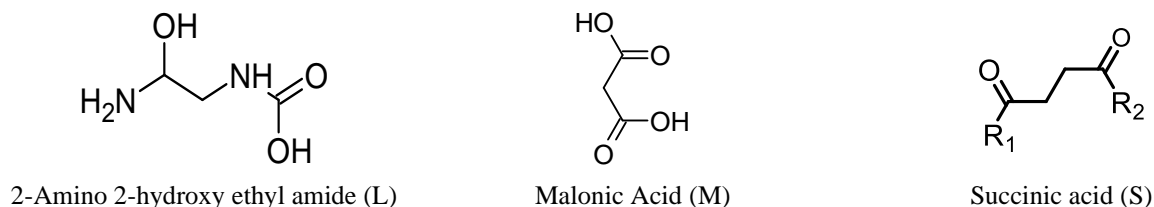


Figure 1C. 2-D Structure of the selected linkers

### Molecular Docking studies

Molecular docking studies were carried out using Autodock Vina software. Optimisation of the ligands and proteins and grid box creation were carried out using Graphical User Interface program Autodock Tools. Target proteins were optimised using Autodock Tools by adding polar hydrogen groups, removing water

molecules, adding kollman and Gasteiger charges and prepared file was saved as.pdbqt file. Ligands were optimised and converted into.pdbqt file using Open Babel software.

The amino acids making up the active site of the target proteins were established by visualization of the binding of native ligands using Biovia Discovery Studio 2016. Grid box was generated by arranging the grid coordinates (X, Y and Z) about the proteins active site. The grid size was set to 40×40×40 xyz points for both targets with grid centre designated at dimensions (x, y and z): –10.891, 16.159 and 66.647 for CL-pro and –30.52, 22.402, 30.288 for PL-pro. During the docking procedure, both the proteins and ligands were considered as rigid structures. The root-mean-square deviation (RMSD) was observed, the pose with the most favourable free binding energy was considered (RMSD value less than 0.1Å). Then with the help of Biovia discovery studio, the pose with lowest energy of binding was aligned with receptor structure for further analysis.

#### *Validation of Target Proteins*

Target validation was performed to understand the accuracy and reproducibility of the docking process and targets selected for the study. The native ligands n-[(5-methylisoxazol-3-yl)carbonyl]alanyl-l-valyl-n~1~--((1r,2z)-4-(benzyloxy)-4-oxo-1-{[(3r)-2-oxopyrrolidin-3-yl]methyl}but-2-enyl)-l-leucinamide and 5-amino-2-methyl-N-[(1R)-1-naphthalen-1-ylethyl]benzamide present in target proteins 6LU7 and 3E9S, respectively, were removed from the protein structures and were re-docked into the active sites using Auto-dock Vina software. The procedure was performed on both the target proteins in Biovia Discovery software; the native ligands were removed from the co-crystallized complexes and saved in PDB file format. Grids were generated about the active sites of the target proteins and the docked complexes were superimposed on their respective reference co-crystallized complexes and the root mean square deviation (RMSD) was computed.

#### *Prediction of ADME properties*

Along with the biological activity, the pharmacokinetic properties of compounds are critical for selection of good drug candidates. In our study we used ADME Schrodinger online software to predict ADME properties i.e. Absorption, Distribution, Metabolism, and Excretion/Elimination using Lipinski Rule of drug-likeness.

### *Results and Discussion*

#### *Target validation*

Target validation studies using the selected targets and native co-crystallized ligands indicated low RMSD values within runs confirming the accuracy and repeatability of the docking procedure. The docking results of native ligands with targets are shown in Figure 2.

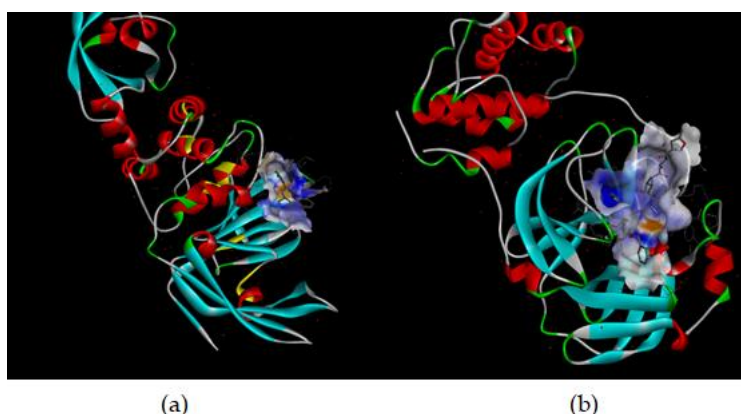


Figure 2. *a* — Papain-like protease with native ligand;  
*b* — 3-chymotrypsin-like cysteine protease with native ligand

#### *Molecular Docking studies*

For the docking studies, 24 hybrid ligands were designed using suitable combinations of the anti-viral and anti-thrombosis agents with selected linkers. Among these hybrids, six ligands demonstrated favourable affinity for the selected target proteins (PL-pro and CL-pro) with low binding energy comparable to the selected standards (Remdesivir, Acyclovir, Ribavirin, Oseltamavir and Fevipiravir). The results of the docking

studies of standards and with interacting amino acid residues and type of interactions are summarized in Table 2.

Table 2

**Docking analysis of Standards with target proteins**

Compound Name	Binding Energy (kcal/mol)	Interacting Amino acids	Bond type
Target: Papain-like protease (PDB ID- 3E9S)			
Remdesivir	-6.0	Tyr 269, Tyr 265 Ala 250, Tyr 269 Tyr 274	H- bond $\pi$ - $\pi$ stacking $\pi$ - $\pi$ stacking
Acyclovir	-6.3	Gln 270, Gly164 Tyr269 Tyr274 Asp165	$\pi$ - $\pi$ stacking H-bond H-bond H-bond
Ribavirin	-6.8	Tyr 265 Asp 165 Tyr274 Gly164, Gly267	$\pi$ - $\pi$ stacking $\pi$ - $\pi$ stacking H-bond H-bond
Oseltamavir	-5.8	Tyr 269 Asp165 Tyr 265 Tyr274	H-bond H-bond $\pi$ -alkyl stacking $\pi$ -alkyl stacking
Fevipiravir	-5.7	Tyr 265 Asp 165 Tyr274 Thr 302, Arg 167 Tyr 274	$\pi$ - $\pi$ stacking $\pi$ - $\pi$ stacking H-bond H-bond H-bond
Target: 3-chymotrypsin-like cysteine protease (PDB ID- 6LU7)			
Remdesivir	-8.2	His 163, Phe 140 Gly 143 His 41, Met49,165	H-bond H-bond $\pi$ - $\pi$ stacking $\pi$ - $\pi$ stacking
Acyclovir	-5.8	Leu 141 Ser 144 Cys 145, Glu 166 His 163	H-bond H-bond H-bond $\pi$ - $\pi$ stacking
Ribavirin	-6.3	Cys 145 His 163 Thr 26 Gly 143	H-bond, $\pi$ - $\pi$ stacking H-bond H-bond H-bond
Oseltamavir	-6.0	Glu 166 Met 49, Met165 His 41	H-bond $\pi$ -alkyl stacking $\pi$ -alkyl stacking
Fevipiravir	-6.3	Asp 187, Tyr 54 His 41 Met 165 Arg 188	H-bond H-bond $\pi$ - $\pi$ stacking Halogen interaction

The best six hybrid ligands with low binding energies were selected for further docking interaction analysis. Figure 3 displays the 2-D structure of these hybrid ligands. The best-docked complexes of these ligands with their interacting amino acid residues are shown in Figures 4 and 5, respectively.

Based on the docking results, among the six hybrid ligands, compound RL1 exhibited high binding affinity with both the target proteins (PDB:3E9S and PDB: 6LU7) with dock score of -8.1 and -8.0, respectively. In the interaction study with PL-pro, the hydrogen bonds were observed with Tyr 269, Gln 270, Tyr 274 and Asp 165,  $\pi$ - $\pi$  interactions with Gly 164, Leu 163 (Figure 4A). With 3CL-pro, compound RL1 formed hydrogen bonds with Thr 24, 25, 26, Thr 45, Ser 46, Ser 144, Gly 143 and  $\pi$ - $\pi$  interactions with Met 165, 49, His 41(Figure 5A).

Compound FL2 exhibited the highest binding affinity with both the target proteins (PDB:3E9S and PDB: 6LU7) with dock score of  $-9.1$  and  $-9.0$ , respectively. With PL-pro, compound FL2 formed hydrogen bonds with Arg 167, Asp 165 and  $\pi$ - $\pi$  interactions with Tyr 264 and Lys 158 (Figure 4B). In interaction with 3CL-pro, the hydrogen bonds were observed with Thr 24,25,45, Asn 14 and His 164,  $\pi$ - $\pi$  interactions with His 41, Met 49, Thr 24 (Figure 5B).

Also, ligand FL3 (Figure 4C) showed greater binding affinity (dock score  $-8.1$ ) to PL-pro compared to the standards, which exhibited dock score between  $-5.7$  to  $-6.3$ . However, it exhibited lower affinity (Dock score  $-7.9$ ) with 3-CLpro protease compared to the other docked ligands, but with greater affinity when compared to the standards (Dock score  $-5.7$  to  $-6.3$ ) with the exception of Remdisivir, which showed improved affinity with dock score of  $-8.2$ . With PL-pro (PDB:3E9S), ligand FL3 formed hydrogen bond interaction with Thr 266 and  $\pi$ - $\pi$  interactions of phenyl rings with Tyr 265, Thr 302, Tyr 269, Arg 167 and Pro 249. In interaction with 3-CLpro, the hydrogen bonds were observed with Gly 143, Ser 144, Thr 26, Cys 145, Thr 190 and  $\pi$ - $\pi$  interactions with Met 165, Met 49 (Figure 5C).

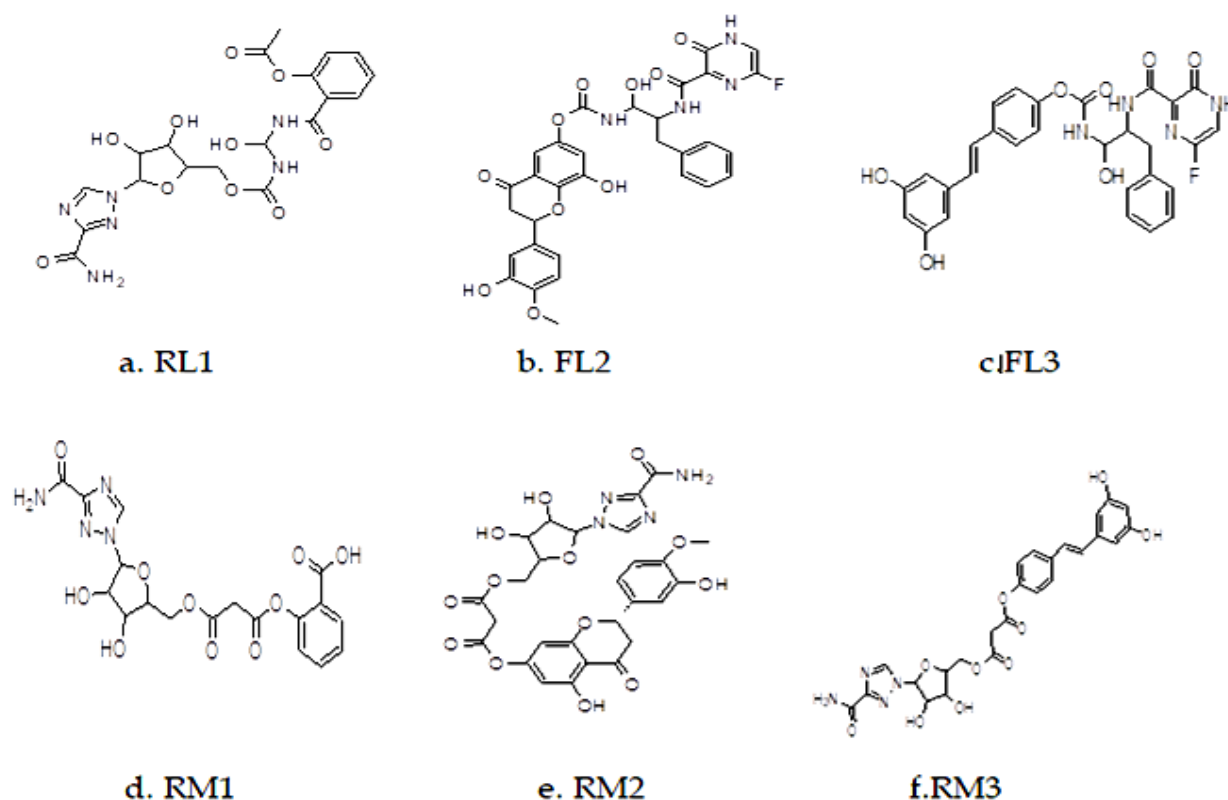


Figure 3. 2-D structures of selected hybrid ligands

Compound RM1 showed the interaction with PL-pro (PDB:3E9S) and formed hydrogen bond interaction with Tyr 269, Asn 268, Gly 267, Tyr 274 and  $\pi$ - $\pi$  interactions of triazole rings with Asp 165, Tyr 265 (Figure 4D). Figure 5D shows interaction of RM1 with 3-CLpro, the hydrogen bonds were observed with Gly 189, Glu 166, Met 49, Asp 187, Ser 144, Cys 145 and  $\pi$ - $\pi$  interactions with His 41, Met 49 and Glu 166.

Figure 4E shows the interaction of RM2 with PL-pro (PDB:3E9S) and hydrogen bond interaction with Tyr 274, Gly 164, Tyr 269, Asn 268, Gly 267 and  $\pi$ - $\pi$  interactions with Asp 165, Tyr 265. In interaction with 3-CLpro, the hydrogen bonds were observed with Gln 189, Met 49, Gly 143, Ser 144, Cys 145 and  $\pi$ - $\pi$  interactions with Met 49, His 41, Glu 166 (Figure 5E). Among the docked ligands, RM2 showed good affinity to CL-Pro with dock score of  $-8.6$  when compared to the standard and other ligands.

In Figure 4F, compound RM3 showed the interaction with PL-pro (PDB:3E9S) and formed hydrogen bond interaction with Tyr 274, Glu 251 and  $\pi$ - $\pi$  interactions with Asp 165, Lys 158, Pro 249. Figure 5F shows interaction of RM3 with 3-CLpro, the hydrogen bonds were observed with Thr 24,25,45, Ser 46, Cys 145 and  $\pi$ - $\pi$  interactions of triazole ring with Met 49 and phenyl ring with Pro 168 AND Met 165.

Some of the common interacting amino acid residues involved in hydrogen bond formation, which play a vital role in binding to the target, identified through our docking studies include residues Tyr 265, 269,

274, Thr 266, Asn 268 with the papain-like protease and residues Thr 24,25,26, Cys 145, Ser 144 with the 3-chymotrypsin-like cysteine protease receptor.

The ADME prediction study of the best six molecules evaluated on QikProp ADME Schrodinger online software, demonstrated relatively satisfactory drug like properties.

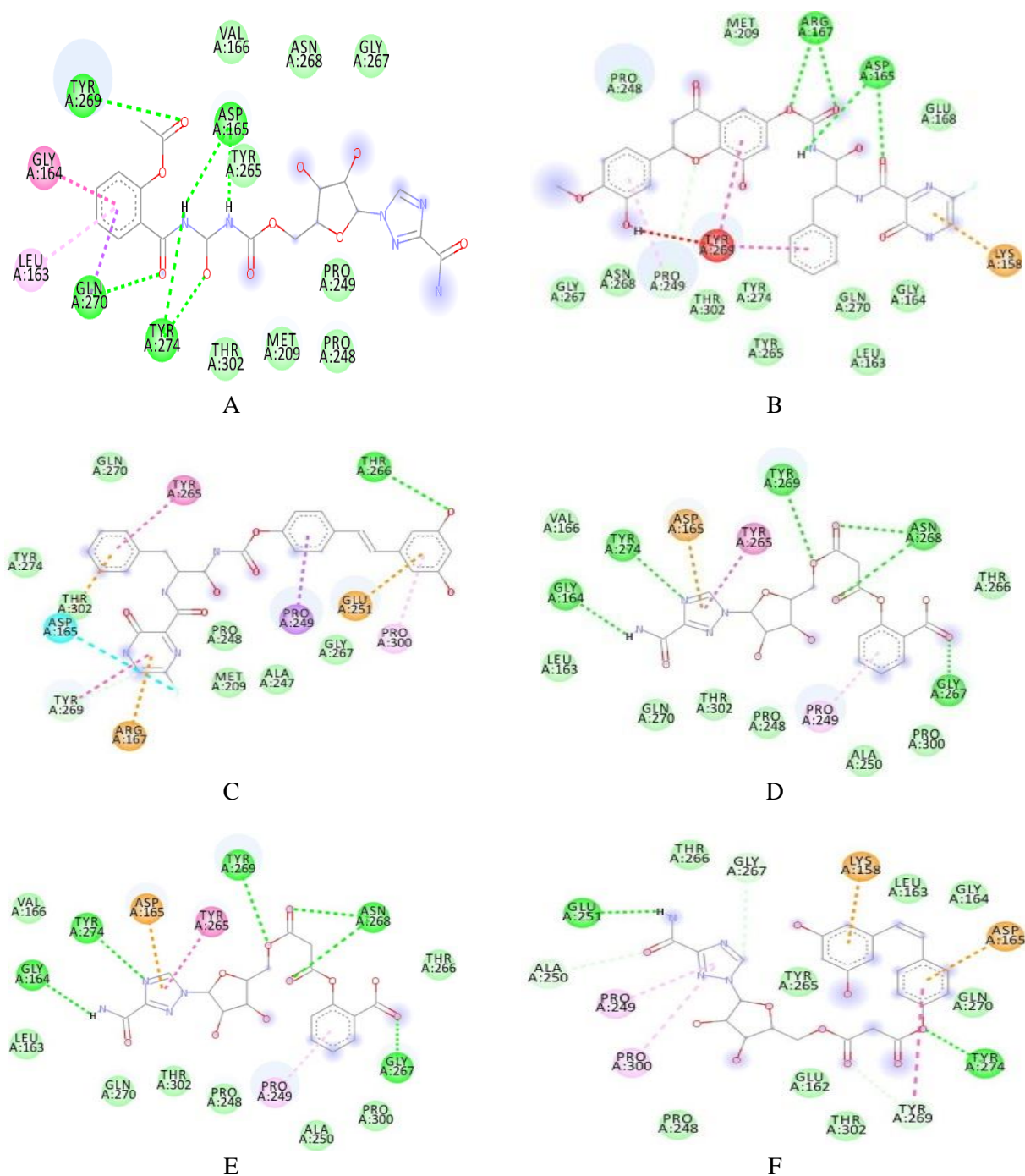


Figure 4. Docked poses in 3E9S receptor binding pocket A) Compound RL1 B) Compound FL2 C) Compound FL3 D) Compound RM1 E) Compound RM2 F) Compound RM3

(The figure shows the ligands docking within the active site. The hydrogen bonds are represented by green dotted lines,  $\pi$ - $\pi$  interactions with yellow/pink dotted lines

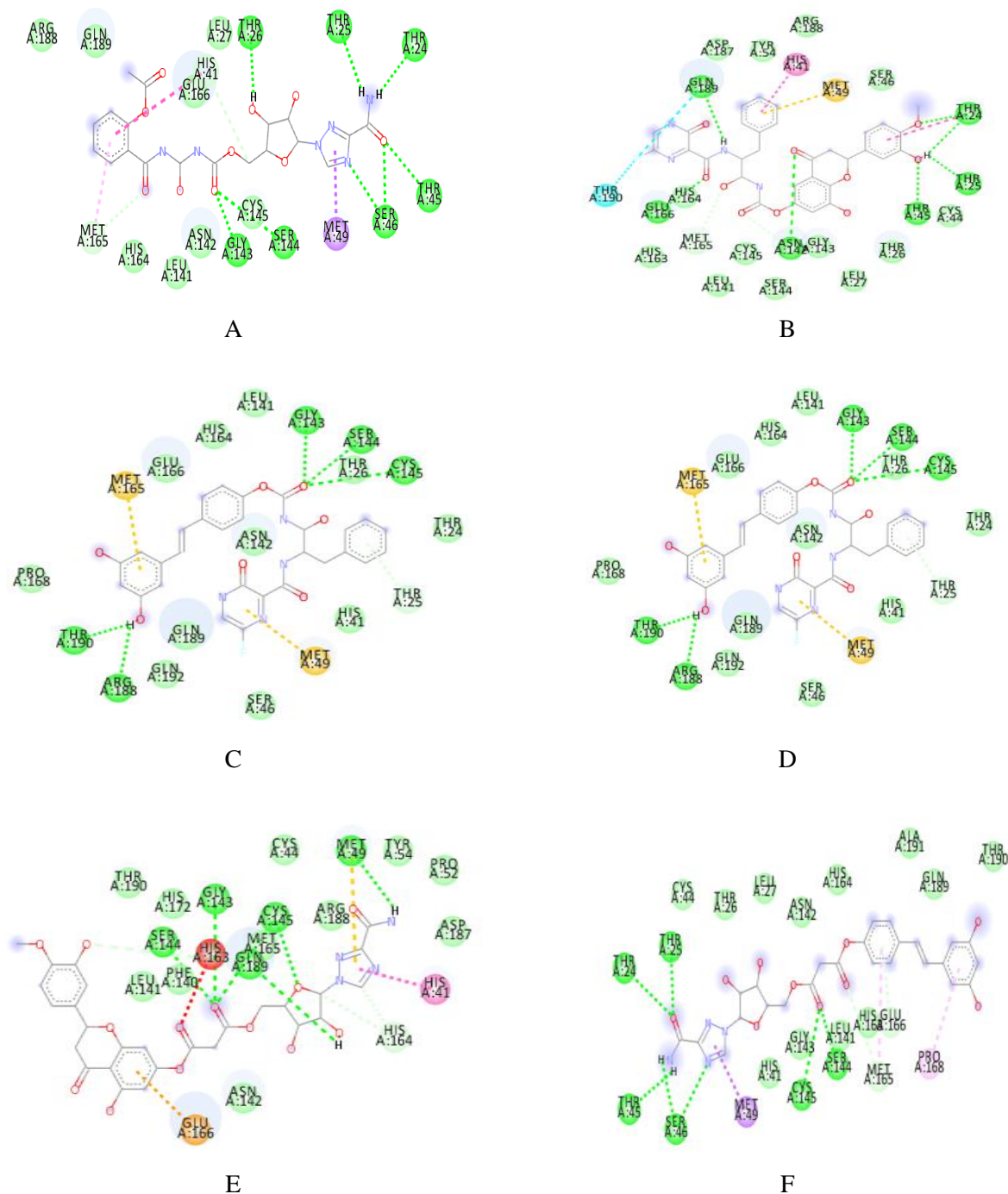


Figure 5. Docked poses in 6LU7 receptor binding pocket A) Compound RL1 B) Compound FL2 C) Compound FL3 D) Compound RM1 E) Compound RM2. F) Compound RM3.

(The figure shows the ligands docking within the active site. The hydrogen bonds are represented by green dotted lines,  $\pi$ - $\pi$  interactions with yellow/pink dotted lines

Based on the docking and ADME prediction studies on papain-like protease (PL-pro) (PDB ID- 3E9S) and 3-chymotrypsin-like cysteine protease (CL-pro), two cysteine proteases of the SARS-CoV-2 virus that are vital for the replication and transcription of the viral genome, there was observed that FL2, which was a hybrid of favipiravir and hesperitin through 2-amino 2-hydroxy ethyl amide linker seemed to be the most promising hybrid designed to act with almost similar affinity to both the targets.

Also, RL1, a hybrid of ribavarin and salicylic acid linked with the 2-amino 2-hydroxy ethyl amide chain showed comparable efficacy against both the protease targets. Figure 6 represents the docking poses of the most promising hybrids obtained through this in silico study. Both the identified hybrids contain the

hydroxyethylamine linker that is an important structural component of currently clinically employed HIV protease inhibitors like Nelfinavir, Indinavir and other protease inhibitors used in the treatment of HIV infection. The incorporation of this hydroxyethylamine linker may help to mimic the transition state of the reactions catalysed by the PL-pro and CL-pro enzymes in the viral replication cycle. These designed inhibitors may serve as transition state inhibitors that may bind with greater affinity to the active site and may be less prone to hydrolysis. Hence these hybrid molecules may represent a new class of anti-viral agents with improved affinity than the individual substrates.

However it is anticipated that the likely hydrolysis of these hybrids may release the individual substrates that may also separately bind to the anti-viral targets and provide synergistic activity. Also as herperitin and salicyclic acid are well established anti-thrombotic agents, they may also elucidate this response, thereby proving to be of great potential in treatment of the rising associated complications of the viral infection.

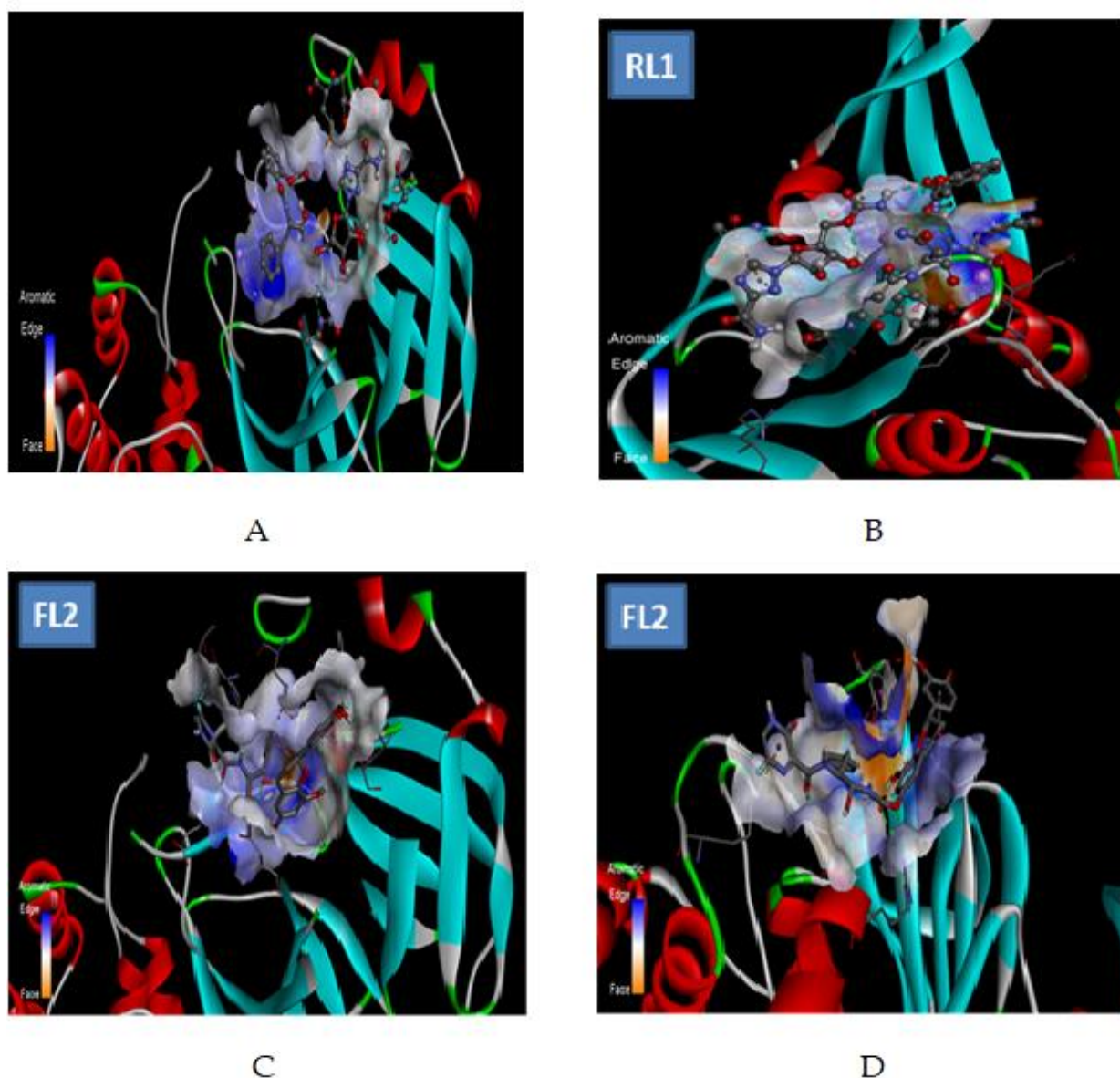


Figure 6. Docking Poses of RL1 in A) CL-pro and B) PL-pro; Docking Poses of FL2 in C) CL-pro and D) PL-pro

### Conclusions

The present study focuses on the design of novel hybrids of antiviral and antithrombotic agents for synergistic use in the treatment of infections caused by the SARS-CoV-2 virus. Among the 24 compounds

screened using Autodock vina software, Compound FL2 i.e., 8-hydroxy-2-(3-hydroxy-4-methoxyphenyl)-4-oxochroman-6-yl(2-(6-flouro-3-oxo-3,4-dihydropyrazine-2 carboxamido)-1-hydroxy-3-phenylpropyl)carbamate and Compound RL1 i.e., 2-((((5-(3-carbamoyl-1H-1,2,4-triazol-1-yl)-3,4-dihydroxytetrahydrofuran-2-yl)methoxy)carbonyl)amino)(hydroxy)methyl)carbamoyl)phenyl acetate prove to be promising agents with good affinity and strong binding interactions with both target proteins, papain-like protease (PDB:3E9S) and 3-chymotrypsin-like cysteine protease (PDB: 6LU7). The results of this study can prove to be useful to medicinal chemists involved in design of newer agents to fight the COVID pandemic. This novel class of hybrid agents may help to address the coronavirus infection and its associated complications and may be further explored for design of novel molecules in this field.

## References

- 1 World health organization official website <https://www.who.int/emergencies/diseases/novel-coronavirus-2019> (accessed on 10th May 2021)
- 2 Retrived from <https://www.medscape.com/answers/2500114-197401/what-is-covid-19> (accessed on 10th May 2021)
- 3 Retrived from <https://www.republicworld.com/world-news/uk-news/uk-strain-spreads-to-30-countries-as-world-enters-2021-with-new-covid-variant.html> (accessed on 10th May 2021)
- 4 Chan Y., Xin-feng X., Wei X., & Shu-wen L. (2020). Structural and functional properties of SARS-CoV-2 spike protein: potential antiviral drug development for COVID-19. *Acta Pharmacologica Sinica*, 41, 1141–1149. <https://doi.org/10.1038/s41401-020-0485-4>
- 5 Leila M., & Sorayya G. (2021). Genotype and phenotype of COVID-19: Their roles in pathogenesis. *Journal of Microbiology, Immunology and Infection*, 57, 159–163. <https://doi.org/10.1016/j.jmii.2020.03.022>
- 6 Mittal A., Manjunath K., Ranjan R., Kaushik S., Kumar S., & Verma V. (2020). COVID-19 pandemic: Insights into structure, function, and hACE2 receptor recognition by SARS-CoV-2. *PLoS Pathog.*, 16(8), e1008762. <https://doi.org/10.1371/journal.ppat.1008762>
- 7 Wang M., Rong Z., Li-Juan G., Xue-fei G. De-Ping W., & Ji-Min Cao. (2020). SARS-CoV-2: Structure, Biology, and Structure-Based Therapeutics Development. *Front. Cell. Infect. Microbiol.*, 10, 587269. <https://doi.org/10.3389/fcimb.2020.587269>
- 8 Brit L., William J. B., Alex K. & Michael G. (2020). Cardiovascular complications in COVID-19. *Am J Emerg Med.*, 38(7), 1504–1507. <https://doi.org/10.1016/j.ajem.2020.04.048>
- 9 Samidurai A., & Das A. (2020). Cardiovascular Complications Associated with COVID-19 and Potential Therapeutic Strategies. *Int J Mol Sci.*, 21(18), 6790. <https://doi.org/10.3390/ijms21186790>
- 10 Petrovic V., Radenkovic D., Radenkovic G., Djordjevic V., Banach M. (2020). Pathophysiology of Cardiovascular Complications in COVID-19. *Front. Physiol.*, 11, 575600. <https://doi.org/10.3389/fphys.2020.575600>
- 11 Page E., & Ariens R. (2021). Mechanisms of thrombosis and cardiovascular complications in COVID-19. *Thromb Res*, 200, 1–8. <https://doi.org/10.1016/j.thromres.2021.01.005>
- 12 Al-Mohammad A., & Partridge D. (2020). The cardiac complications of Covid-19 many publications, multiple uncertainties. *Vas. Biology*, 2 (1), R105–R114. <https://doi.org/10.1530/VB-20-0009>
- 13 Magro G. (2020). COVID-19: Review on latest available drugs and therapies against SARS-CoV-2. Coagulation and inflammation cross-talking. *Virus Res*, 286, 198070. <https://doi.org/10.1016/j.virusres.2020.198070>
- 14 Asselah T., Durantel D., Pasmant E., Lau G., & Schinazi R. (2020). COVID-19: discovery, diagnostics and drug development. *J Hepatol*, 74(1), 168–184. <https://doi.org/10.1016/j.jhep.2020.09.031>
- 15 RAPS, Regulatory Affairs Professionals Society. Retrived from <https://www.raps.org/news-and-articles/news-articles/2020/3/covid-19-vaccine-tracker> (accessed May 12, 2021)
- 16 Our world in Data. Retrived from <https://ourworldindata.org/covid-vaccinations> (accessed May 12,2021)
- 17 McGovern R., Conway P., Pekrul I., & Tujjar O. (2020). The Role of Therapeutic Anticoagulation in COVID-19. *Case Rep Crit Care*, 1–7. <https://doi.org/10.1155/2020/8835627>
- 18 Liao S., Shao S., Chen Y., Chen Y., & Hung M. (2020). Incidence and mortality of pulmonary embolism in COVID-19: a systematic review and meta-analysis. *Crit Care*, 24(1), 1-5. <https://doi.org/10.1186/s13054-020-03175-z>
- 19 Costanzo, L., Palumbo, F., Ardita, G., Antignani, P., Arosio, E., & Failla, G. (2020). Coagulopathy, thromboembolic complications, and the use of heparin in COVID-19 pneumonia. *J Vasc Surg Venous Lymphat Disord*, 8(5), 711–716. <https://doi.org/10.1016/j.jvsv.2020.05.018>
- 20 Abdolmaleki A., & Ghasemi J. (2017). Dual-acting of Hybrid Compounds — A New Dawn in the Discovery of Multi-target Drugs: Lead Generation Approaches. *Curr Top Med Chem*, 17(9), 1096-1114. <https://doi.org/10.2174/1568026616666160927151144>
- 21 Pawelczyk A., Sowa-Kasprzak K., Olender D., & Zaprutko L. (2018). Molecular Consortia-Variou Structural and Synthetic Concepts for More Effective Therapeutics Synthesis. *Int J Mol Sci.*, 19(4), 1104. <https://doi.org/10.3390/ijms19041104>
- 22 Gupta V., & Datta P. (2019). Next-generation strategy for treating drug resistant bacteria: Antibiotic hybrids. *Indian J Med Res.*, 149 (2), 97–106. [https://doi.org/10.4103/ijmr.IJMR\\_755\\_18](https://doi.org/10.4103/ijmr.IJMR_755_18)

- 23 Pokrovskaya V., & Baasov T. (2010). Dual-acting hybrid antibiotics: a promising strategy to combat bacterial resistance. *Expert Opin Drug Discov.*, 5(9), 883–902. <https://doi.org/10.1517/17460441.2010.508069>
- 24 Brötz-Oesterhelt H., & Brenner N. (2008). How many modes of action should an antibiotic have? *Curr Opin Pharmacol.*, 8, 564–573. <https://doi.org/10.1016/j.coph.2008.06.008>
- 25 Meunier B. (2008). Hybrid molecules with a dual mode of action: dream or reality? *Acc Chem Res.*, 41(1), 69–77. <https://pubs.acs.org/doi/10.1021/ar7000843>
- 26 Dana S., Valissery P., Kumar S., Gurung S., Mondal N., Dhar S., & Mukhopadhyay P. (2020). Synthesis of Novel Ciprofloxacin-Based Hybrid Molecules toward Potent Antimalarial Activity. *ACS Med Chem Lett.*, 11(7), 1450–1456. <https://doi.org/10.1021/acsmchemlett.0c00196>
- 27 Pepe D., Toumpa D., André-Barrès C., Menendez C., Mouray E., Baltas M., Grellier P., Papaioannou D., & Athanassopoulos C. (2020). Synthesis of Novel G Factor or Chloroquine-Artemisinin Hybrids and Conjugates with Potent Antiplasmodial Activity. *ACS Med Chem Lett.*, 11(5), 921–927. <https://doi.org/10.1021/acsmchemlett.9b00669>
- 28 Contreras J., & Sippl W. (2008). Homo and heterodimer ligands: The twin drug approach. In: Wermuth CG. (Eds) *The practice of medicinal chemistry*. 3rd edition. Academic Press Elsevier; New York, NY, USA, 380–414. <https://dx.doi.org/10.1016%2Fj.bmc.2015.06.034>
- 29 Hasan M., Leak R., Stratford R., Zlotos D., & Witt-Enderby P. (2018). Drug conjugates—an emerging approach to treat breast cancer. *Pharmacol Res Perspect.*, 6(4), e00417. <https://doi.org/10.1002/prp2.417>
- 30 Rodríguez-Franco M., Fernández-Bachiller M., Pérez C., Hernández-Ledesma B., & Bartolomé B. (2006). Novel tacrine-melatonin hybrids as dual-acting drugs for Alzheimer disease, with improved acetylcholinesterase inhibitory and antioxidant properties. *J Med Chem.*, 49(2), 459–462. <https://doi.org/10.1021/jm050746d>
- 31 Decker M. (2017). *Design of hybrid molecules for drug development*. New York, NY, USA: Elsevier.
- 32 Bansal Y., & Silakari O. (2014). Multifunctional compounds: smart molecules for multifactorial diseases. *Eur J Med Chem.*, 76, 31–42. <https://doi.org/10.1016/j.ejmech.2014.01.060>
- 33 Przybyłowska M., Dzierzbicka K., Kowalski S., Chmielewska K., & Inkielewicz-Stepniak I. (2020). Therapeutic Potential Of Multifunctional Derivatives Of Cholinesterase Inhibitors. *Curr Neuropharmacol.*, 19(8), 1323–1344. <https://doi.org/10.2174/1570159X19666201218103434>
- 34 Starnowska-Sokół J., & Przewłocka B. (2020). Multifunctional Opioid-Derived Hybrids in Neuropathic Pain: Preclinical Evidence, Ideas and Challenges. *Molecules*, 25(23), 5520. <https://doi.org/10.3390/molecules25235520>
- 35 Khalili J., Zhu H., Mak N., Yan Y., & Zhu Y. (2020). Novel coronavirus treatment with ribavirin: Groundwork for an evaluation concerning COVID-19. *J Med Virol.*, 92(7), 740–746. <https://doi.org/10.1002/jmv.25798>
- 36 Cai Q., Yang M., Liu D., Chen J., Shu D., Xia J., Liao X., Gu Y., Cai Q., Yang Y., & Shen C. (2020). Experimental treatment with favipiravir for COVID-19: an open-label control study. *Engineering*. 6(10), 1192–1198. <https://doi.org/10.1016/j.eng.2020.03.007>
- 37 Vafaei S., Razmi M., Mansoori M., Asadi-Lari M., & Madjd Z. (2020). Spotlight of Remdesivir in comparison with ribavirin, Favipiravir, Oseltamivir and Umifenovir in coronavirus disease 2019 (COVID-19) pandemic. <http://dx.doi.org/10.2139/ssrn.3569866>
- 38 Carvallo H., Hirsch R., & Farinella M. (2020). Safety and Efficacy of the combined use of ivermectin, dexamethasone, enoxaparin and aspirin against COVID-19. medRxiv. <https://doi.org/10.1101/2020.09.10.20191619>
- 39 Glatthaar Saalmüller B., Mair K., & Saalmüller A. (2017). Antiviral activity of aspirin against RNA viruses of the respiratory tract — an in vitro study. *Influenza Other Respir Viruses.*, 11(1), 85–92. <https://doi.org/10.1111/irv.12421>
- 40 Yang Y., Wang X., Wang S., Wang H., & Chen J. (2008). Suppressive effect in vitro of resveratrol on ADP induced human platelet aggregation and its active mechanism. *Yao Xue Xue Bao.*, 43(4), 356–360. <https://doi.org/10.1111/irv.12421>
- 41 Bhat K., Kosmeder J., & Pezzuto J. (2001). Biological effects of resveratrol. *Antioxid Redox Signal.*, 3(6), 1041–1064. <https://doi.org/10.1089/152308601317203567>
- 42 Randall R., & Goodbourn S. (2008). Interferons and viruses: an interplay between induction, signalling, antiviral responses and virus countermeasures. *J Gen Virol.*, 89(1), 1–47. <https://doi.org/10.1099/vir.0.83391-0>
- 43 Roohbakhsh A., Parhiz H., Soltani F., Rezaee R., & Iranshahi M. (2015). Molecular mechanisms behind the biological effects of hesperidin and hesperetin for the prevention of cancer and cardiovascular diseases. *Life Sci.*, 124, 64–74. <https://doi.org/10.1016/j.lfs.2014.12.030>

Р. Бхиманвар, А. Томас, Л. Котхапаллы, А. Годасе,  
С. Ганди, С. Чанданы, Г. Мор, Г. Джадхав, С. Чоудхари

## **SARS-CoV-2 инфекцияларына және онымен байланысты асқынуларға қарсы қос антивирустық және антитромботикалық потенциалы бар әлеуетті гибриді молекулалар *in silico* зерттеулерін қолдану**

COVID, SARS-CoV вирусына негізделген ауру 2019 жылдың желтоқсан айында Қытайдың Ухань қаласында анықталды. Бастапқыда бұл жай ғана тыныс алу жүйесінің инфекциясы болып саналды, бірақ кейін оның таралу сипатына байланысты пандемия жарияланды. Емдеудің әртүрлі нұсқалары жүзеге асырылды, соның ішінде ремдесвир, фавипиравир сияқты вирусқа қарсы препараттар, сонымен қатар витаминдер мен антиоксиданттар да бар. Кейінгі зерттеулер COVID-19 инфекциясының тромбоздық жүрек-қантамырлық асқынуларға әкелетінін анықтады, бұл осы инфекциямен байланысты өлім-жітімнің артуына басты алаңдаушылық тудырады. Осы зерттеуде вирусқа қарсы және антитромботикалық қасиеттері бар гибриді молекулалардың *in silico* конструкциясы зерттелді. Autodock Vina бағдарламалық құралын пайдалану арқылы докингті зерттеу жүргізілді және жобаланған қосылыстардың байланысу энергиясы папаинтәрізді протеаза (PDB: 3E9S) және 3-химотрипсинтәрізді цистеин протеазасы (PDB: 6LU7) үшін анықталды. Түйіскен позалар мен аминқышқылдарының өзара әрекеттесуі Biovia Discovery studio 4.5 көмегімен тексерілді. Барлық жобаланған қосылыстардың байланысу энергиялары стандарттармен салыстырылды, қосылыс RL1 (2-(5-(3-карбамоил-1Н-1,2,4-триазол-1-ил)-3,4-дигидрокситетрагидрофуран-2-ил)метокси)карбонил амин)-(гидрокси)метилкарбамоил)фенилацетат және қосылыс FL2 (8-гидрокси-2-(3-гидрокси-4-метоксифенил)-4-оксохроман-6-ил-(2-(6-фтор)3-оксо-3,4-дигидропиразин-2-карбоксамидо)-1-гидрокси-3-фенилпропил)карбамат күшті байланысуы бар перспективалы агенттер болып шықты. Вирустық репликацияны тежейтін гибриді молекулалар, мүмкін өтпелі күй ингибиторлары ретінде, SARA-Co-V инфекциясын және онымен байланысты асқынуларды емдеуде пайдалану үшін әрі қарай зерттелуі мүмкін.

*Кілт сөздер:* COVID-19, CL-рго, PL-рго, вирусқа қарсы, антитромботикалық, молекулалық докинг, гибриді молекула.

Р. Бхиманвар, А. Томас, Л. Котхапаллы, А. Годасе,  
С. Ганди, С. Чанданы, Г. Мор, Г. Джадхав, С. Чоудхари

## **Потенциальные гибридные молекулы с двойным противовирусным и антитромботическим действием против инфекции SARS-CoV-2 и связанных с ней осложнений с использованием исследования *in silico***

COVID-19, заболевание, вызванное вирусом SARS-CoV, было выявлено в Ухане (Китай) в декабре 2019 г. Первоначально оно считалось просто инфекцией дыхательной системы, но из-за его трансмиссивного характера оно было объявлено пандемией. Были реализованы различные варианты лечения, включая противовирусные препараты, такие как ремдесвир, фавипиравир, а также витамины и антиоксиданты. Дальнейшие исследования показали, что инфекция Covid-19 приводит к тромботическим сердечно-сосудистым осложнениям, что является основной причиной повышенной смертности, связанной с этой инфекцией. В этом исследовании изучена конструкция *in silico* гибридных молекул с противовирусными и антитромботическими свойствами. Исследование докинга проводили с использованием программного обеспечения Autodock Vina, а энергии связывания разработанных соединений определяли для папаиноподобной протеазы (PDB: 3E9S) и 3-химотрипсинаподобной цистеиновой протеазы (PDB: 6LU7). Состыкованные позы и взаимодействия аминокислот были проверены с использованием Biovia Discovery studio 4.5. Энергии связи всех разработанных соединений сравнивали со стандартами, соединение RL1 (2-(5-(3-карбамоил-1Н-1,2,4-триазол-1-ил)-3,4-дигидрокситетрагидрофуран-2-ил)метокси)карбонил)амино(гидрокси)метилкарбамоил)фенилацетат) и соединение FL2 (8-гидрокси-2-(3-гидрокси-4-метоксифенил)-4-оксохроман-6-ил-(2-(6-фтор-3-оксо-3,4-дигидропиразин-2-карбоксамидо)-1-гидрокси-3-фенилпропил)карбамат) оказались многообещающими агентами с сильным связывающим взаимодействием. Гибридные молекулы, которые ингибируют репликацию вируса, возможно, в качестве ингибиторов переходного состояния, могут быть дополнительно исследованы для использования в лечении инфекции SARS-CoV и связанных с ней осложнений.

*Ключевые слова:* COVID-19, CL-рго, PL-рго, противовирусный, антитромботический, молекулярный докинг, гибридная молекула.

### Information about authors\*

**Bhimanwar, Rachana** — Assistant Professor, Department of Pharmaceutical Chemistry, Dr. D.Y. Patil Institute of Pharmaceutical Sciences and Research, Pune- 411018, Maharashtra, India; e-mail: [rachana.bhimanwar@dypvp.edu.in](mailto:rachana.bhimanwar@dypvp.edu.in); <https://orcid.org/0000-0001-6392-1526>

**Thomas, Asha** (*corresponding author*) — HOD and Professor, Department of Pharmaceutical Chemistry, Dr. D.Y. Patil Institute of Pharmaceutical Sciences and Research, Pune- 411018, Maharashtra, India; e-mail: [asha.thomas@dypvp.edu.in](mailto:asha.thomas@dypvp.edu.in); <https://orcid.org/0000-0003-1058-8779>

**Kothapalli, Lata** — Associate Professor, Department of Pharmaceutical Chemistry, Dr. D.Y. Patil Institute of Pharmaceutical Sciences and Research, Pune- 411018, Maharashtra, India; e-mail: [lata.kothapalli@dypvp.edu.in](mailto:lata.kothapalli@dypvp.edu.in); <https://orcid.org/0000-0002-7412-5805>

**Godase, Anagha** — Assistant Professor, Department of Pharmaceutical Chemistry, Dr. D.Y. Patil Institute of Pharmaceutical Sciences and Research, Pune- 411018, Maharashtra, India; e-mail: [angha.godse@dypvp.edu.in](mailto:angha.godse@dypvp.edu.in); <https://orcid.org/0000-0001-9145-2990>

**Gandhi, Sejal** — Assistant Professor, Department of Pharmaceutical Chemistry, Dr. D.Y. Patil Institute of Pharmaceutical Sciences and Research, Pune- 411018, Maharashtra, India; e-mail: [sejal.gandhi@dypvp.edu.in](mailto:sejal.gandhi@dypvp.edu.in); <https://orcid.org/0000-0002-7079-1886>

**Chandani, Sneha** — Assistant Professor, Department of Pharmaceutical Chemistry, Dr. D.Y. Patil Institute of Pharmaceutical Sciences and Research, Pune- 411018, Maharashtra, India; e-mail: [sneha.chandani@dypvp.edu.in](mailto:sneha.chandani@dypvp.edu.in); <https://orcid.org/0000-0003-3891-2841>

**More, Ghansham** — Department of Pharmaceutical Chemistry, Dr. D.Y. Patil Institute of Pharmaceutical Sciences and Research, Pune- 411018, Maharashtra, India; e-mail: [gsmniper@gmail.com](mailto:gsmniper@gmail.com); <https://orcid.org/0000-0002-9010-2275>

**Jadhav, Gopal** — School of Medicine, Omaha Campus, Creighton University, NE; e-mail: [gopaljadhav@creighton.edu](mailto:gopaljadhav@creighton.edu); <https://orcid.org/0000-0002-2883-5574>

**Choudhary, Sameer** — RASA Life Science Informatics, Pune, Maharashtra, India; e-mail: [aftab@rasalsi.com](mailto:aftab@rasalsi.com); <https://orcid.org/0000-0001-8056-1374>

---

\*The author's name is presented in the order: *Last Name, First and Middle Names*

S. Tyanakh<sup>1\*</sup>, M.I. Baikenov<sup>1</sup>, A.M. Gulmaliev<sup>2</sup>, Feng-Yun Ma<sup>3</sup>,  
G. Musina<sup>4</sup>, T.O. Khamitova<sup>5</sup>, A.N. Bolatbay<sup>1</sup>

<sup>1</sup>Karagandy University of the name of academician E.A. Buketov, Karaganda, Kazakhstan;

<sup>2</sup>Federal State-Funded Institution of Science, Topchiev University of Petrochemical Synthesis RAS, Moscow, Russia;

<sup>3</sup>Xinjiang University, Xinjiang, China;

<sup>4</sup>Karaganda Polytechnic University, Karaganda, Kazakhstan;

<sup>5</sup>Kazakh Agrotechnical University named after Saken Seifullin, Astana, Kazakhstan

(\*Corresponding author's e-mail: [saika\\_8989@mail.ru](mailto:saika_8989@mail.ru))

## Kinetics of Thermolysis of a Low-Temperature Tar in the Presence of a Catalyzer Agent with Deposited Metals

The thermal decomposition of low-temperature coal tar (LTCT) obtained from the coals of Shubarkol Komir JSC of the Republic of Qazaqstan in the presence of nanocatalysts with metal oxides (iron, cobalt and nickel) supported on microsiliate was studied for the first time. Microsilicate acts as a carrier and catalyst. Microsilicate is a product of the Karaganda silicon plant of “Tau-Ken.temir” LLP. The main chemical component of the original microsilicate is silicon oxide. The individual and chemical phase composition of the microsilicate was determined using X-ray spectral analysis. The particle size of the initial microsilicate and the mixture of microsilicate with metal oxide catalysts (nickel, cobalt, and iron) was determined using a nanosizer. Stages of thermal decomposition of LTCT and a mixture of LTCT with catalysts under conditions of programmed heating up to 640 °C in a nitrogen atmosphere have been established. On the basis of thermogravimetric analysis, the kinetic parameters (activation energy, mass loss rate, and pre-exponential factor) of LTCT pyrolysis and mixture with added catalysts were determined. The modelless integral isoconversion Ozawa–Flynn–Wall method was used to determine the kinetic parameters. The values of the activation energy for the thermal destruction of the LTCT in the absence and presence of the nanocatalyst ranged from 54.04 to 297.5 kJ/mol. A kinetic compensation effect was revealed, probably due to the multicomponent composition of the LTCT and the influence of added catalysts to the LTCT. The thermogravimetry method showed a high effect of the supported catalysts on the thermal degradation of LTCT. This method was used to determine the values of the activation energy and the pre-exponential degradation factor for the LTCT and the mixture with catalysts at different heating rates, which allows a detailed interpretation of the thermal analysis data. The obtained results of the kinetics of decomposition of LTCT can be used to create a database for mathematical modeling of the process of processing this type of raw material.

**Keywords:** kinetics, accelerant, microsilica, low-temperature coal tar, thermogravimetric analysis, iron, nickel, cobalt.

### Introduction

At present, thermogravimetric analysis is widely used to study the kinetics of thermal decomposition of organic materials, such as LTCT, coal, and polymeric materials [1–5]. Due to the complex composition of LTCT, it is very important to obtain information about the kinetics of LTCT decomposition in the presence of various catalysts containing metal oxides of Group VIII of the Mendeleev Periodic Table. To determine the kinetic parameters of the thermal decomposition of LTCT in the presence of catalysts containing metal oxides (iron, nickel, cobalt), the integral method presented in [1] and the method for determining the thermokinetic parameters from the inflection point on the thermogravimetric curve [2] were used. Sources [6, 7] evidence that the mathematical models, which are used to determine the kinetic performance of polymer degradation, cause certain difficulties when applied to the thermal breakdown of low-temperature coal resin (LTCR) due to their complex structure, the variety of chemical bonds, and simultaneously occurring reactions. In this regard, one of the most important tasks facing the researchers is the designing of recommendations for the selection and development of an adequate kinetic model of LTCR thermal breakdown in the presence of a catalyst and the formation of a database of kinetic performance.

The organic mass of LTCT contains various aromatic, heterocyclic compounds. Due to the complex composition of the LTCT, it is difficult to select an efficient and selective catalyst for LTCT processing based on the kinetics of decomposition of the LTCT organic matter. When studying the kinetics of pyrolysis of organic substances, the thermogravimetric method of analysis (TGA) is widely used [6]. In the literature [8–10], various methods are known for determining the kinetic parameters of nonisothermal pyrolysis, which can be divided into model (model-fitting) and model-free (model-free) or isoconversion. One of them is the Ozawa-Flylin-Wall model-free method for calculating the kinetic parameters [11, 12], which requires the construction of kinetic curves at different heating rates.

The purpose of this work is to study the kinetics of thermal degradation of LTCT in the presence of catalysts with oxides of nickel, cobalt, and iron supported on microsilicate using thermogravimetric analysis methods.

### Experimental

For the study of thermokinetic decomposition of low-temperature coal tar the raw material obtained during coal coking at the coking plant of JSC “Shubarkol komir” was used.

Physical and chemical characteristics of low-temperature coal tar JSC “Shubarkol Komir”» presented in the paper [13].

The used microsilica performs the role of carrier and catalyst — the product of Karaganda silicon plant LLP “Tau-Ken.temir”.

The component chemical composition of the initial microsilica was determined by using X-ray and spectral analysis (Table. 1).

Table 1

Composition of initial microsilicate after leaching

Content of components, %									
SiO <sub>2</sub>	TiO <sub>2</sub>	Al <sub>2</sub> O <sub>3</sub>	Fe <sub>2</sub> O <sub>3</sub>	CaO	MgO	MnO	P <sub>2</sub> O <sub>5</sub>	K <sub>2</sub> O	Na <sub>2</sub> O
95.5	0.02	<0.95	<1.0	-0.5	0.4	0.04	0.06	<0.1	0.3

The initial microsilicate was preliminarily grinded, then samples with a particle size of 0.1 mm were taken by screen analysis. The initial microsilicate was leached using a 20 % hydrochloric acid solution to remove alkali and alkali earth metals.

The size of the particles of the original microsilica and the catalyst samples were determined by using the laser particle size detector Nano-S90 (Fig. 1).

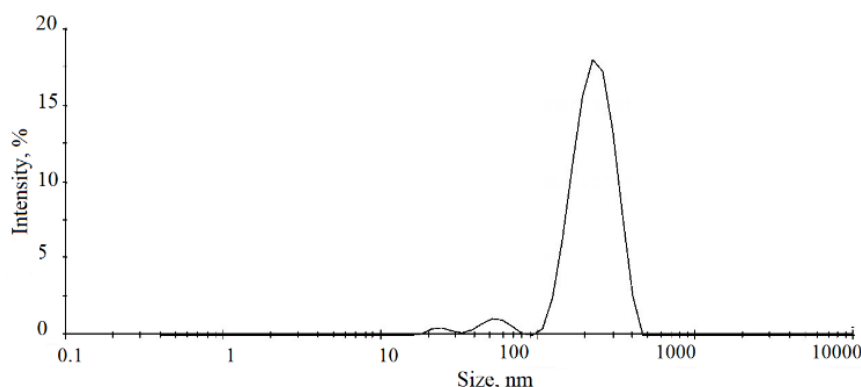


Figure 1. Particle size (sample 1) of the source microsilica

Figure 1 shows the particle size of the original microsilica — 232 nanometers. Size of metal-coated catalyst particles: sample 2 (microsilica+Ni) — 324.2 nanometers, sample 3 (microsilica + Co) — 139.4 nanometers, sample 4 (microsilica + Fe) — 196.3 nanometers.

The catalyst was obtained by wet impregnation of leached microsilica with a 1.5 % solution of CoCl<sub>2</sub>·6H<sub>2</sub>O, NiCl<sub>2</sub>·6H<sub>2</sub>O, FeSO<sub>4</sub>·7H<sub>2</sub>O salts. The salt-soaked microsilica was kept in the dryer for 2 hours, at 80–90 °C, and then dried at 105 °C also for 2 hours. Further, the catalyst samples obtained were calcified

in the muffle oven at 550 °C for 2 hours (applied catalyst). The component chemical composition of the microsilicate after leaching was established using the X-ray spectral and gravimetric method and was presented in the (Table 2).

Table 2

Composition of initial microsilicate after leaching

Content of components, %									
SiO <sub>2</sub>	TiO <sub>2</sub>	Al <sub>2</sub> O <sub>3</sub>	Fe <sub>2</sub> O <sub>3</sub>	CaO	MgO	MnO	P <sub>2</sub> O <sub>5</sub>	K <sub>2</sub> O	Na <sub>2</sub> O
97.439	0.023	<0.95	<1.0	0.414	0.304	0.033	0.057	<0.1	0.276

As it can be seen from the data in Tables 1 and 2, the chemical composition of the initial microsilicate before and after leaching changed insignificantly.

Thermogravimetric study was performed using a *Labsys Evo TG-DTA/DSC* 1600 derivatograph (*Setaram*, France) in corundum crucibles in the temperature range from 30 to 600 °C in a nitrogen flow (flow rate of protective and purge gases was 20 and 50 ml/min<sup>-1</sup> respectively). The sample weight for DTA analysis was 0.01 g. Kinetic parameters of thermal decomposition (rate constant, activation energy, and pre-exponential factor) of low-temperature coal tar (LTCT) with catalysts and microsilicate were calculated by the methods presented in works [11, 12]. Kinetic characteristics were determined on the basis of TGA — data at three different heating rates of 10, 20, and 30 deg/min<sup>-1</sup>. Calculation and report of measurement results was performed using the software package “*OriginLab*” and the Python distribution “*Anaconda3*”.

The model-free Ozawa-Flynn-Wall (OFW) method was used [11, 12] when calculating the kinetic parameters of low-temperature coal resin (LTCR) thermal breakdown in the presence of a catalyst.

### Results and Discussion

We previously used the integral method to determine the thermogravimetric parameters [1] and the method by the inflection point on the thermogravimetric curve [2].

The curves dependence of samples mass loss on temperature are shown in Figure 1 at heating rates  $\beta$  — 10 °C/min,  $\beta$  — 20 °C/min,  $\beta$  — 30 °C/min at intervals of 140–480 °C using the Ozawa-Flynn-Wells (OFW) method. The reactivity of a substance can be described by the activation energy value.

The determination of the activation energy values was based on the generalized value expression (1) for the rate of the solid-phase reaction under nonisothermal conditions:

$$d\alpha / dT = A / \beta e^{(-Ea/RT)} f(\alpha), \quad (1)$$

where  $\alpha$  is fractional conversion of raw material;  $\beta$  is the linear heating rate of samples, °C/min;  $A$  is the pre-exponential factor,  $c^{-1}$ ;  $T$  is the absolute temperature, K;  $E$  is the activation energy, kJ/mol;  $R$  is the gas constant, kJ/mol K;  $f(\alpha)$  is a mathematical model of the dimensionless kinetic function depending on the type and mechanism of the reaction.

The value  $\alpha$  in equation (1) is the relative degree of oil sludge transformation, defined as  $\alpha = m_s - m / m_s - m_f$  where  $m_s$  and  $m_f$  are the initial and final mass of the substance,  $m$  is the mass of the substance at the measurement point [14].

*Ozawa-Flynn-Walls Method* According to the Ozawa-Flynn-Walls method of non-isothermal kinetics, when integrating and then taking logarithm equation (1), we obtain expressions (2)

$$\ln G(\alpha) = \ln(AE / R) - \ln \beta + \ln p(z). \quad (2)$$

$G(\alpha)$  for a first-order reaction is equal to

$$\int_0^a d\alpha / f\alpha = \int_0^a da / 1 - a = -\ln(1 - a);$$

$$p(z) = e^{-z} / z - \int_{-\infty}^z e^{-z} / z dz; z = E / RT.$$

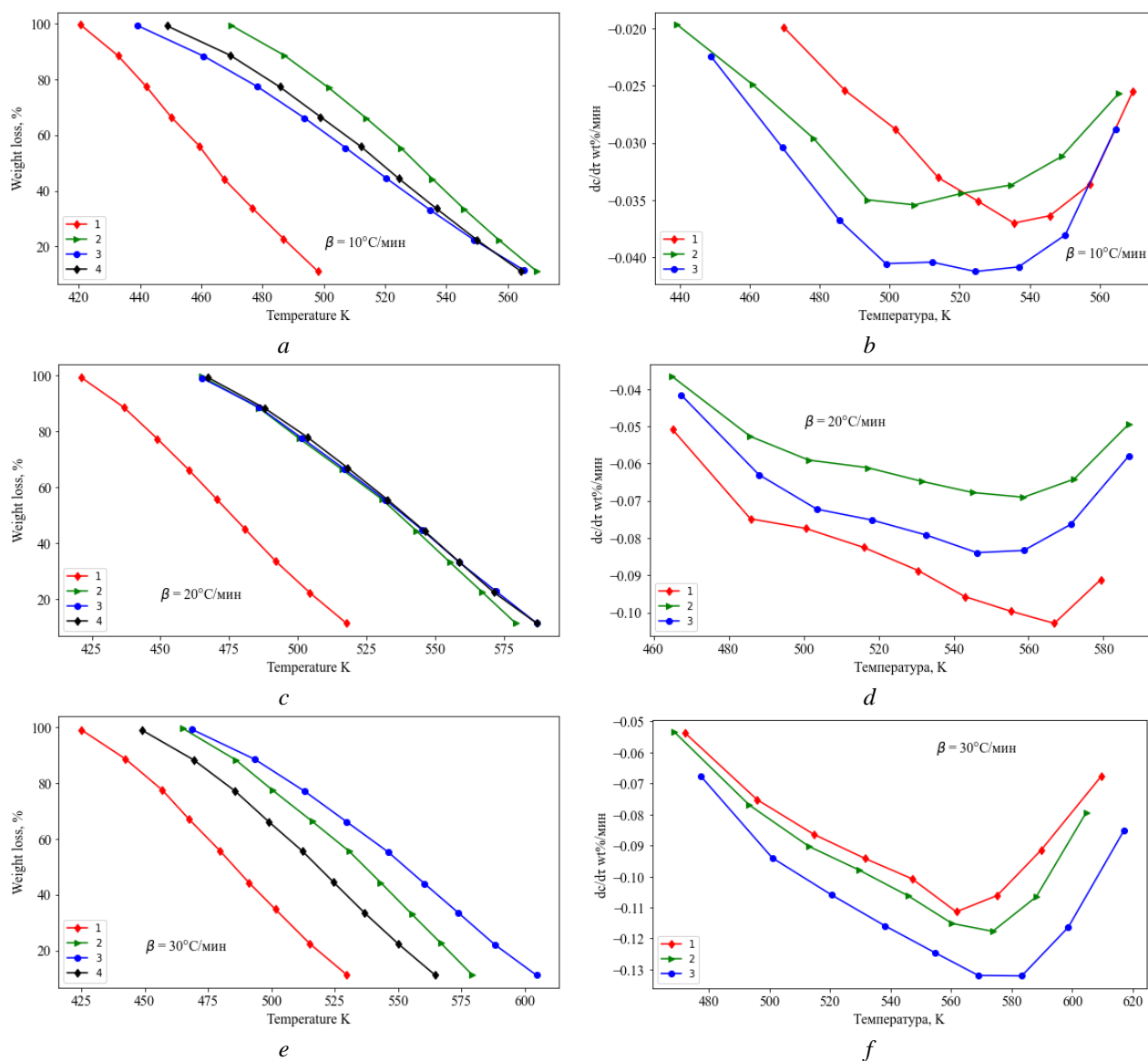
Using the Doyle approximation [15] we obtain equation (3) for substitution into expression (2):

$$\ln p(z) = -5.3305 - 1.052z. \quad (3)$$

The OFW method is based on the assumption that the reaction rate at a constant value of  $\alpha$  depends only on temperature. When analyzing non-isothermal kinetics, the following equation is used:

$$\ln \beta_i = \ln [A_\alpha E_\alpha / Rg(\alpha)] - 5.331 - 1.052E_\alpha / RT_{\alpha,i}. \quad (4)$$

Substitutions (2) and (3) provide the OFW equation (4) to calculate how thermal breakdown rate of catalyst mixtures with LTCR depends on inverse temperature calculated the activation energy and the pre-exponential multiplier [15]. Thermogravimetric (TG) curves (Fig. 2) were constructed by low-temperature coal tar to assess the influence of metal-coated microsiliate catalysts (iron, nickel, cobalt) on the thermal degradation rate. Thermogravimetric (TG) curves (Fig. 2) were constructed by low-temperature coal tar to assess the impact of metal-based microsilia catalysts (iron, nickel, cobalt) on thermal degradation rates. For this purpose, based on the thermogravimetry data of the low-temperature coal resin and the catalyst for their mixtures of a known composition, TG curves and mass loss rates were calculated at three heating speeds  $\beta$  — 10 °C/min,  $\beta$  — 20 °C/min,  $\beta$  — 30 °C/min, which described the thermolysis process of the low-temperature coal resin mixture and with the catalyst (Fig. 2 *a-f*).



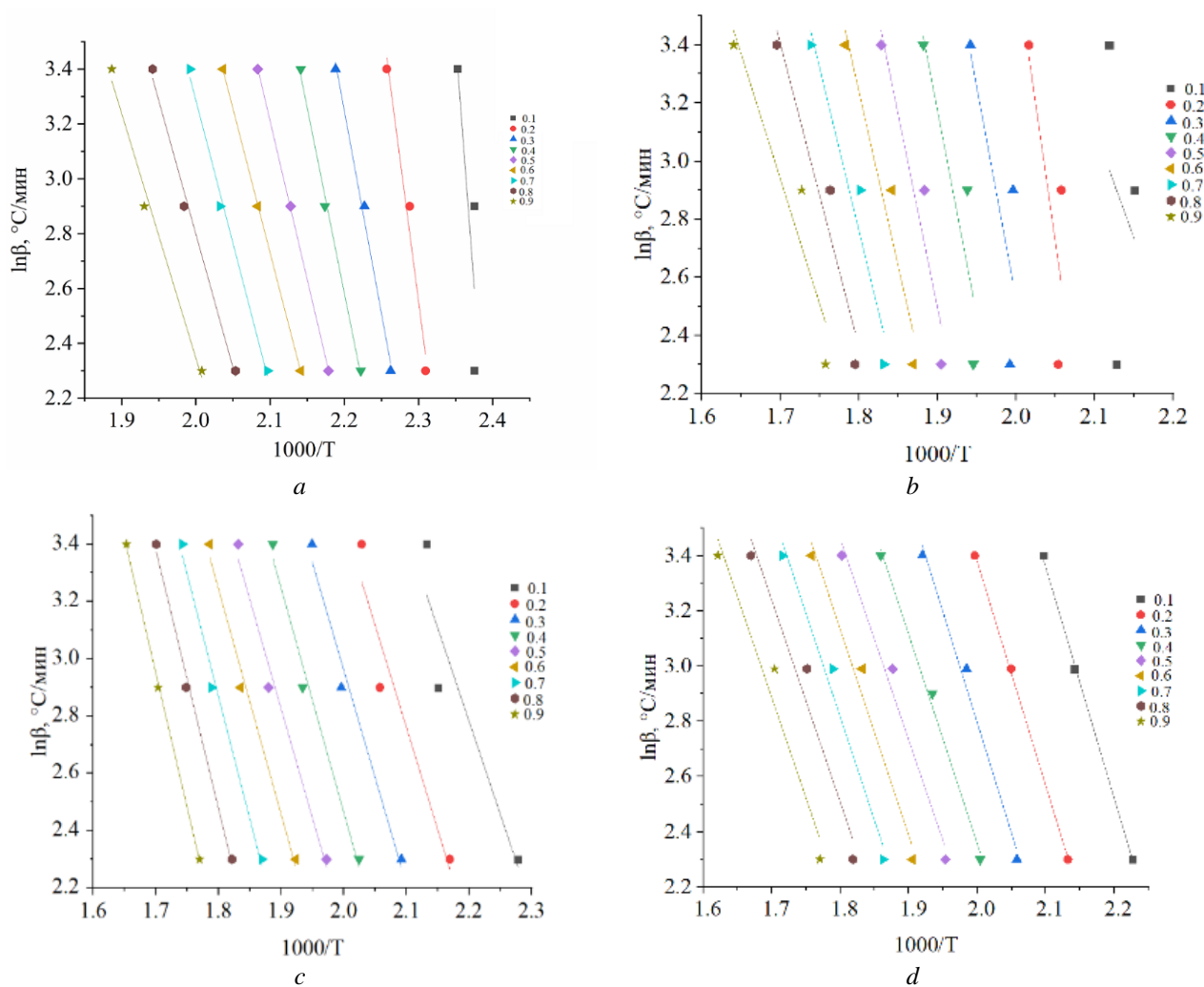
1 — low-temperature coal tar; 2 — low-temperature coal tar with applied nickel;  
3 — low-temperature coal tar with cobalt applied; 4 — low-temperature coal tar with iron applied

Figure 2. Thermogravimetric mass loss curves (*a*), (*c*), (*e*) and mass loss rate (*b*), (*d*), (*f*) of tested NCC samples in the presence of microsilia with applied catalyst

On the curves, the mass loss rate at three heating speeds  $\beta$  is one maximum (Fig. 2 *b, d, f*), due to the decomposition of the organic mass of low-temperature coal tar in the presence of nickel, cobalt and iron to the formation of volatile substances. It has been established that, when iron is applied to microsilia (Fig. 2 *b*), the maximum decomposition of the organic mass of low-temperature coal tar is achieved at a temperature

of 525 K. When the nickel applied to microsilica, the maximum decomposition rate of the organic mass of low-temperature coal tar is reached at a temperature of 537 K (Fig. 2 *d*) and when iron is added, there is a maximum decomposition of the organic mass of low-temperature coal tar at 579 K (Fig. 2 *f*).

Equation (4) implies that for a series of temperature measurements of thermal degradation of low-temperature coal tar catalyst mixtures obtained at different  $\beta$  heating speeds of samples and fixed values of their transformation degree  $\alpha$ , the graph of the function  $\ln\beta = f(1/T)$  gives straight lines (isoconversion lines) the tangent of the inclination of which  $-1.052E/R$  is directly proportional to the activation energy [15] (Fig. 3 *a-d*).



*a* — low-temperature coal tar; *b* — low-temperature coal tar with nickel applied to microsilica,  
*c* — low-temperature coal tar with cobalt applied to microsilica;  
*d* — low-temperature coal tar with iron applied to microsilica

Figure 3. Heating rate logarithm dependence  $\beta$  — 10  $^{\circ}\text{C}/\text{min}$ ,  $\beta$  — 20  $^{\circ}\text{C}/\text{min}$ ,  $\beta$  — 30  $^{\circ}\text{C}/\text{min}$   
 low-temperature coal tar mixture samples

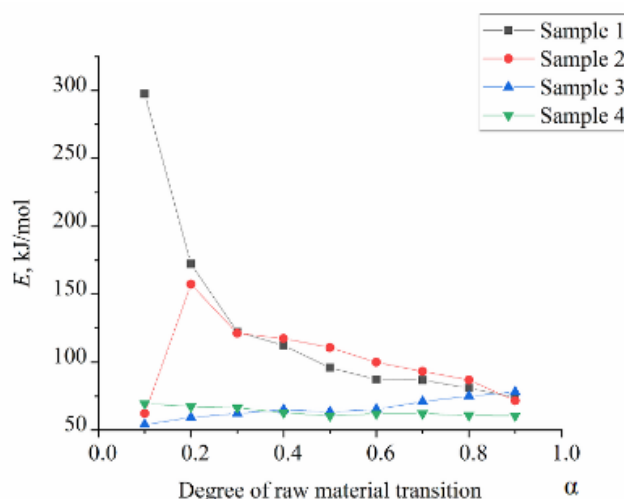
The experimental points lie adequately on straight lines in the entire range of conversion degrees, indicating the correct Doyle approximation used in the mathematical treatment of thermogravimetric data. The calculated activation energy values and preexponential multiplier shows a high correlation coefficient ( $R^2 \geq 0.997$ ) of Table 3.

Energy Activation of Thermal Destruction of Low-temperature Coal Tar Blend and Microsilica with Applied Catalysts (Table 3).

**Energy Activation of Thermal Destruction of Low-temperature Coal Tar Blend and Microsilica with Applied Catalysts**

Relative degree of conversion, $\alpha$	Sample 1 (low-temperature coal tar without catalyst)		Sample 2 (microsilica + Ni 1.5 % + low-temperature coal tar, particle size 0.1 mm)		Sample 3 (microsilica + Co 1.5 % + low-temperature coal tar, particle size 0.1 mm)		Sample 4 (microsilica + Fe 1.5 % + low-temperature coal tar, particle size 0.1 mm)	
	$E_a$ , KJ/mol	$\ln A c^{-1}$	$E_a$ , KJ/mol	$\ln A c^{-1}$	$E_a$ , KJ/mol	$\ln A c^{-1}$	$E_a$ , KJ/mol	$\ln A c^{-1}$
0.1	297.5	87.6	62.18	18.8	54.04	17.09	69.53	20.92
0.2	172.3	50.2	157.3	41.5	59.27	17.74	67.32	19.57
0.3	122.3	35.7	121.2	31.6	62.18	17.93	66.42	18.77
0.4	112.3	32.3	117.4	30.01	65.01	18.11	62.84	17.47
0.5	95.9	27.4	110.7	27.79	63.35	17.31	60.51	16.55
0.6	87.3	24.7	99.9	24.88	65.34	17.40	62.06	16.56
0.7	86.7	24.1	93.2	22.94	70.91	18.22	62.22	16.28
0.8	80.9	22.2	86.8	21.15	74.99	18.72	60.75	15.65
0.9	74.1	20.1	71.6	17.59	77.98	18.89	60.48	15.25

On the Figure 4 activation energy dependence on conversion rate ( $\alpha$ ) of low-temperature coal tar without catalyst and sample mixture of low-temperature coal tar with catalyst. Ozawa – Flynn – Wells Curve —  $E = f(\alpha)$  (Fig. 4) shows the complex process of thermal destruction of the low-temperature coal tar mixture with the catalyst.



- 1 — low-temperature coal tar; 2 — low-temperature coal tar with nickel applied to microsilica;  
 3 — low-temperature coal tar with cobalt applied to microsilica;  
 4 — low-temperature coal tar with iron applied to microsilica

Figure 4. Dependence of activation energy  $E$  on the level of conversion of  $\alpha$  samples (Ozawa – Flynn – Wells analysis)

Figure 4 shows the calculated activation energy values represented by the thermal breakdown degree  $\alpha$  of low-temperature coal resin and the sample mixture of the low-temperature coal resin with catalyst. It is shown that for Sample 1 activation energy with increased conversion decreases from 297.5 to 74.1 kJ/mol. Sample 2 with the conversion degree from 0.1 to 0.2 the activation energy increases from 62.18 to 157.3 kJ/mol, and further conversion increase rate leads to a reduction in activation energy from 121.2 to 71.6 kJ/mol. For Sample 3 with increased conversion rate, there is a significant change in activation energy from 54.04 to 77.98 kJ/mol. Slight activation energy change with conversion degree obsession is observed for sample 4 from 69.53 to 60.48 kJ/mol.

Figure 4 shows that for the sample, the first stage of thermal decomposition is flowing with a high amount of activation energy, which may be due to a low degradation of high molecular weight asphaltene and tar compounds. Thermal decomposition of the low-temperature coal tar mixture with nickel, cobalt and

iron applied to microsilica is described by more complex kinetic curves. The initial stages of the activation energy of sample 2, sample 3 and sample 4 proceed with a lower activation energy than for sample 1. It seems to be due to the fact that an organo structure with added metals is formed, the latter act as a catalyst, that is, they accelerate the reaction of the destruction of the organic mass of the low-temperature coal tar and thus lead to a decrease in the activation energy (Table 3 and Fig. 4.). Among the number of metals added to the microsilica, cobalt and iron were the most influential, and the addition of nickel with an increased conversion rate of 0.1–0.2 leads to an increase in activation energy and a pre exponential factor, and further increasing the conversion rate from 0.3 to 0.9 significantly reducing the activation energy. Low activation energy appears to be associated with the splitting of the weakest oxygen-containing, nitrogen-containing bonds and the influence of catalytic additives on the thermal degradation of low-temperature coal tar. High activation energy values are associated with low volatility of condensed aromatic hydrocarbons contained in the original low-temperature coal tar. Solid semi-coke is formed by condensation of solids that do not degrade.

### Conclusions

The information above about the influence of catalysts on the destruction of low-temperature coal resin shows that the method of thermogravimetry makes it possible to determine sufficiently the influence of the applied catalysts on the thermal breakdown of low-temperature coal resin. On the basis of TG-analysis, the kinetic parameters (activation energy and pre-exponential factor) were determined using the model-free OFW method. The obtained experimental data on the kinetics of LTCT destruction were verified by correlation coefficients ( $R^2 \geq 0.997$ ).

By changing the organometallic structure of low-temperature coal tar with applied catalyst due to metabolic reaction with metal, it is possible to control the process of thermal destruction, changing its speed and kinetic parameters, and to test selected catalysts for thermal destruction of low-temperature coal tar.

### References

- 1 Букварева О.Ф. Кинетика и термодеструкция процессов термодеструкции углеродсодержащих веществ / О.Ф. Букварева, Т.В. Бухаркина. — М.: РХТУ им. Д.И. Менделеева, 2001. — 28 с.
- 2 Гюльмалиев А.М. Теоретические основы химии угля / А.М. Гюльмалиев, Г.С. Головин, Т.Г. Гладун. — М.: Изд-во Моск. гос. гор. ун-та, 2003. — 556 с.
- 3 Тянах С. Кинетическое изучение термического разложения первичной каменноугольной смолы в присутствии катализаторов с нанесенными на микросиликат оксидами никеля, кобальта и железа / С. Тянах, А. Тусипхан, А.М. Гюльмалиев, Ма Фэн-Юнь, Г.Г. Байкенов, Д.А. Кайкенов, А.И. Халитова, М.И. Байкенов // Химия твердого топлива. — 2022. — № 1. — С. 19–27. <https://doi.org/10.31857/S002311772201008X>
- 4 Burkeev M. Kinetic parameters of thermal destruction of the copolymer of polyethylene glycol fumarate with acrylic acid in inert medium / M. Burkeev, A. Bolatbay, D. Havlicek, Y. Tazhbayev, S. Davrenbekov, L. Zhaparova // Chemical Bulletin of Kazakh National University. — 2022 — Vol. 105, No. 2. — P. 26–33. <https://doi.org/10.15328/cb1260>
- 5 Фетисова Ю.О. Кинетическое изучение стадийности термического разложения различных углей Монголии / Ю.О. Фетисова, П.Н. Кузнецов, Б. Пуревсурен, Б. Авид // Химия твердого топлива. — 2021. — № 1. — С. 3. <https://doi.org/10.31857/S0023117721010035>
- 6 Du Z. Activation energy in temperature-programmed desorption: Modeling and application to the soot-oxygen system / Z. Du, A.F. Sarofim, J.P. Longwell // Energy and Fuels. — 1990. — Vol. 4. — P. 296.
- 7 Бодыков Д.У. Переработка нефтешлама с использованием электрогидравлического эффекта / Д.У. Бодыков, М.С. Абдикаримов, М.А. Сейтжанова, Ж.К. Елемесова // Горение и плазмохимия. — 2017. — Т. 15, № 2. — С. 140–147.
- 8 Li Y. Effects of different ionizable groups on the thermal properties of waterborne polyurethanes used in bulletproof composites / Y. Li, J. Zheng, Y. Luo, H. Zhou, and Q. Wang // J. Appl. Polym. Sci. — 2015. — Vol. 132. — P. 42374. <https://doi.org/10.1002/app.42374>
- 9 Hui K. Status and prospect of oil recovery from oily sludge: A review / K. Hui, Ju. Tang, H. Lu, B. Xi, Ch. Qu, J. Li // Arab. J. Chem. — 2020. — Vol. 13, No. 8. — P. 6523. <https://doi.org/10.1016/j.arabjc.2020.06.009>
- 10 Flynn J.A Quick, Direct Method for the Determination of Activation Energy from Thermogravimetric Data / J. Flynn, L. Wall // J. Polym. Sci. Part B: Polym. Phys. — 1966. — Vol. 4. — P. 296.
- 11 Ozawa T.A New Method of Analyzing Thermogravimetric Data / T. Ozawa // Bulletin of the Chemical Society of Japan. — 1965. — Vol. 38. — P. 1881–1886.
- 12 Aitbekova D.E. Hydrogen distribution in primary coke oven tar and its fractions / D.E. Aitbekova, D.K. Makenov, E.I. Andreikov, A.G. Tsaur, Ma Feng Yung, G.G. Baikenova, A. Tusipkhan, A.A. Muratbekova, M.I. Baikenov // Bull. University Karaganda. Chemistry. — 2021. — Vol. 101, No. 1. — P. 82. <https://doi.org/10.31489/2021Ch1/82-90>

13 Doyle C.D. Kinetic Analysis of Thermogravimetric Data / C.D. Doyle // Appl. Polymer Science. — 1961. — Vol. 15, № 5. — P. 285.

14 Стрижаков Д.А. Кинетика термолитиза смеси гудрона и сосновых опилок / Д.А. Стрижаков, А.И. Юсевич, В.В. Юрчак, Х.М. Кадиев, В.Е. Агабеков, С.Н. Хаджиев // Нефтехимия. — 2016 — Т. 56, № 5. — С. 475–482 <https://doi.org/10.1134/S0965544116080168>

15 Balpanova N.Zh. Thermokinetic parameters of the primary coal tars destruction in the presence of catalysts and polymeric materials / N.Zh. Balpanova, M.I. Baikenov, A.M. Gyulmaliev, Z.B. Absat, Zh. Batkhan, F. Ma, K. Su, S.V. Kim, G.G. Baikenova, D.E. Aitbekova, A. Tusipkhan // Bulletin of University of Karaganda. Series «Chemistry». — 2021. — № 2 (102). — P. 86–95. <https://doi.org/10.31489/2021Ch2/86-95>

С. Тянах, М.И. Байкенов, А.М. Гюльмалиев, Ма Фэн-Юн,  
Г. Мусина, Т.О. Хамитова, А.Н. Болатбай

### **Металдармен байытылған катализдік қоспа қатысындағы төментемпературалы шайыр термолитизінің кинетикасы**

Алғаш рет металл оксидтері (темір, кобальт және никель) бар микросиликатқа енгізілген нанокатализаторлардың қатысуымен Қазақстан Республикасы «Шұбаркөл Көмір» АҚ көмірлерінен алынған төментемпературалы таскөмір шайырының (ТТТШ) термиялықдырауы зерттелді. Микросиликат тасымалдаушы және катализатор қызметін атқарады. Микросиликат — «Тау-Кен.темір» ЖШС Қарағанды кремний зауытының өнімі. Бастапқы микросиликаттың негізгі компоненті кремний оксиді. Микросиликаттың жеке және химиялық фазалық құрамы рентгендік спектрлік талдау арқылы анықталды. Бастапқы микросиликаттың бөлшектерінің өлшемі және микросиликаттың металл оксиді катализаторларымен қоспасы (никель, кобальт және темір) наносайзердің көмегімен табылды. Азот атмосферасында 640 °С дейін бағдарламаланған қыздыру жағдайында ТТТШ термиялықдырау сатысы және катализаторлармен ТТТШ қоспасы дәлелденген. Термогравиметриялық талдау негізінде ТТТШ пиролизі және катализаторлар қосылған ТТТШ қоспасының кинетикалық параметрлері (активтендіру энергиясы, массаның жоғалу жылдамдығы және алдындағы экспоненциалды көбейткіш) анықталды. Кинетикалық параметрлерді анықтау үшін Озава – Флинн – Уоллдың модельсіз интегралды изоконверсиялық әдісі қолданылды. Нанокатализатор бар болған және болмаған кезде төментемпературалы таскөмір шайырының термиялықдырау активтендіру энергиясының мәндері 54,04-тен 297,5 кДж/мольге дейін ауытқиды. Кинетикалық компенсация әсері анықталды, бұл төментемпературалы таскөмір шайырының көпкомпонентті құрамына және төментемпературалы таскөмір шайырына қосылған катализаторлардың әсеріне байланысты болуы мүмкін. Төментемпературалы таскөмір шайырының ыдырау кинетикасынан алынған нәтижелерді көрсетілген шикізаттың түрін қайта өңдеу процесінде математикалық модельдеуді жүргізу үшін деректер базасын құру кезінде пайдалануға болады.

*Кілт сөздер:* кинетика, катализатор, микросиликат, төментемпературалы таскөмір шайыры, темір, никель, кобальт.

С. Тянах, М.И. Байкенов, А.М. Гюльмалиев, Ма Фэн-Юн,  
Г. Мусина, Т.О. Хамитова, А.Н. Болатбай

### **Кинетика термолитиза низкотемпературной смолы в присутствии каталитической добавки с нанесенными металлами**

Впервые изучено термическое разложение низкотемпературной каменноугольной смолы (НКС), полученной из углей АО «Шубарколь комир» Республики Казахстан, в присутствии нанокатализаторов с нанесенными на микросиликат оксиды металлов (железо, кобальт и никель). Микросиликат выполняет роль носителя и катализатора. Микросиликат — продукт Карагандинского кремниевого завода ТОО «Тау-Кен.темір». Основным химическим компонентом исходного микросиликата является оксид кремния. Индивидуальный и химический фазовый состав микросиликата определяли с помощью рентгеноспектрального анализа. Размер частиц исходного микросиликата и смеси микросиликата с катализаторами оксида металлов (никель, кобальт и железо) определяли с помощью наносайзера. Установлены стадийность терморазложения НКС и смесь НКС с катализаторами в условиях программируемого нагрева до 640 °С в атмосфере азота. На основе термогравиметрического анализа определены кинетические параметры (энергия активации, скорость потери массы и предэкспоненциальный множитель) пиролиза НКС и смеси НКС с добавленными катализаторами. Для определения кинетических параметров использован безмодельный интегральный изоконверсионный метод Озава–

Флинн–Уолла. Значения энергии активации термодеструкции НКС в отсутствие и в присутствии нанокатализатора находились в диапазоне 54,04–297,5 кДж/моль. Выявлен кинетический компенсационный эффект, вероятно, обусловленный многокомпонентным составом НКС и влиянием добавленных катализаторов к НКС. Метод термогравиметрии показал высокое влияние нанесенных катализаторов на термодеструкцию НКС. С помощью данного метода определены значения энергии активации и предэкспоненциальный множитель деструкции НКС и смеси НКС с катализаторами при различных скоростях нагрева, что позволяет подробно интерпретировать данные термического анализа. Полученные результаты кинетики разложения НКС могут быть использованы при создании базы данных для проведения математического моделирования процесса переработки указанного вида сырья.

*Ключевые слова:* кинетика, катализатор, микросиликат, низкотемпературная каменноугольная смола, железо, никель, кобальт.

## References

- 1 Bukhareva, O.F., & Bukharkina, T.V. (2001). *Kinetika i termokhimiia protsessov termodestruktsii uglerodsoderzhashchikh veshchestv* [Kinetics and Thermochemistry of the Thermal Destruction of Carbon-Containing Substances]. Moscow: RKHTU imeni D.I. Mendeleeva [in Russian].
- 2 Gyulmaliev, A.M., Golovin, G.S., & Gladun, T.G. (2003). *Teoreticheskie osnovy khimii uglia* [Theoretical foundations of coal chemistry]. Moscow: Izdatelstvo Moskovskogo gosudarstvennogo univrsiteta [in Russian].
- 3 Tyanakh, S., Tusipkhan, A., Gyulmaliev, A.M., Ma, Feng Yung, Baikenova, G.G., Kaikenov, D.A., Khalitova, A.I., & Baikenov, M.I. (2022). Kineticheskoe izuchenie termicheskogo razlozheniia pervichnoi kamennougolnoi smoly v prisutstvii katalizatorov s nanesennymi na miksosilikat oksidami nikelia, kobolta i zheleza [A Kinetic Study of the Thermal Decomposition of Primary Coal Tar in the Presence of Catalysts with Nickel, Cobalt, and Iron Oxides Supported onto Microsilicate]. *Khimiia tverdogo topliva — Solid fuel chemistry*, 56, 1, 29–36 [in Russian]. <https://doi.org/10.3103/S0361521922010086>.
- 4 Burkeev, M., Bolatbay, A., Havlicek, D., Tazhbayev, Y., Davrenbekov, S., & Zhaparova, L. (2022). Kinetic parameters of thermal destruction of the copolymer of polyethylene glycol fumarate with acrylic acid in inert medium. *Chemical Bulletin of Kazakh National University*, 105(2), 26–33. <https://doi.org/10.15328/cb1260>
- 5 Fetisova, Yu.O., Kuznetsov, P.N., Purevsuren, B., & Avid, B. (2021). Kineticheskoe izuchenie stadiinosti termicheskogo razlozheniia razlichnykh uglei Mongolii [A Kinetic Study of the Stepwise Thermal Decomposition of Various Coals from Mongolia] *Khimiia tverdogo topliva — Solid fuel chemistry*, 55, 1, 1. <https://doi.org/10.31857/S0023117721010035> [in Russian].
- 6 Du, Z., Sarofim, A.F., & Longwell, J.P. (1990). Activation energy distribution in temperature-programmed desorption: modeling and application to the soot oxygen system. *Energy & Fuels*, 4(3), 296–302. <https://doi.org/10.1021/ef00021a014>
- 7 Bodykov, D.U., Abdikarimov, M.S., Seitzhanova, M.A., Yelemesova, Zh.K. (2017) Pererabotka nefteshlama s ispolzovaniem elektrogidravlicheskogo effecta [Processing of oil sludge using electro-hydraulic effect]. *Combustion and plasma chemistry*, 15, 2, 140–147 [in Russian].
- 8 Li, Y., Zheng, J., Luo, Y., Zhou, H., & Wang, Q. (2015). Effects of different ionizable groups on the thermal properties of waterborne polyurethanes used in bulletproof composites. *J. Appl. Polym. Sci.*, 132, 42374. <https://doi.org/10.1002/app.42374>
- 9 Hui K., Tang Ju., Lu H., Xi B., Qu Ch., Li J. (2020). Status and prospect of oil recovery from oily sludge: A review. *Arab. J. Chem.*, 13, 8, 6523. <https://doi.org/10.1016/j.arabjc.2020.06.009>
- 10 Flynn, J. Wall, L. (1966). A Quick, Direct Method for the Determination of Activation Energy from Thermogravimetric Data. *Polym. Sci. Part B: Polym. Phys.* 4, 296.
- 11 Ozawa T. (1965) A New Method of Analyzing Thermogravimetric Data. *Bulletin of the Chemical Society of Japan*. 38, 1881–1886.
- 12 Aitbekova, D.E., Makenov, D.K., Andreikov, E.I., Tsaur, A.G., Ma Feng Yung, Baikenova, G.G., Tusipkhan, A., Muratbekova, A.A., & Baikenov, M.I. (2021). Hydrogen distribution in primary coke oven tar and its fractions. *Bulletin of the University of Karaganda — Chemistry*, 1(101), 82–90. <https://doi.org/10.31489/2021Ch1/82-90>
- 13 Doyle, C.D. (1961). Kinetic Analysis of Thermogravimetric Data. *Appl. Polymer Science*, 15, 5, 285.
- 14 Strizhakov, D.A., Yusevich, A.I., & Yurachka, V.V. et al. (2016). Kinetika termoliza smesi gudrona i sosnovykh opilok [Kinetics of thermolysis of vacuum tower bottoms mixed with pine sawdust]. *Pet. Chem.*, 56, 703–710 [in Russian]. <https://doi.org/10.1134/S0965544116080168>
- 15 Balpanova, N.Zh., Baikenov, M.I., Gyulmaliev, A.M., Absat, Z.B., Batkhan, Zh., Ma F., Su K., Kim, S.V., Baikenova, G.G., Aitbekova, D.E., Tusipkhan, A. (2021). Thermokinetic parameters of the primary coal tars destruction in the presence of catalysts and polymeric materials. *Bulletin of the University of Karaganda Chemistry*, 2(102), 86–95. <https://doi.org/10.31489/2021Ch2/86-95>

### Information about authors\*

**Tyanakh, Sairagul** (*corresponding author*) — master, doctoral student Karagandy University of the name of academician E.A. Buketov, Universitetskaya street, 28, 100024, Karaganda, Kazakhstan; e-mail: [saika\\_8989@mail.ru](mailto:saika_8989@mail.ru); <https://orcid.org/0000-0001-5343-4695>

**Baikenov, Murzabek Ispolovich** — professor, Karagandy University of the name of academician E.A. Buketov, Universitetskaya street, 28, 100024, Karaganda, Kazakhstan; e-mail: [murzabek\\_b@mail.ru](mailto:murzabek_b@mail.ru); <https://orcid.org/0000-0002-8703-0397>

**Gyulmaliyev, Agadzhan Mirzoevich** — chief researcher, A.V. Topchiev Institute of Petrochemical Synthesis, RAS, Leninsky prospect, 29, 119991, Moscow, Russia; e-mail: [gyulmaliev@ips.ac.ru](mailto:gyulmaliev@ips.ac.ru); <https://orcid.org/0000-0003-2458-6686>

**Ma, Feng-Yun** — PhD, Professor, Xinjiang University, Urumqi, Nan Min Lu street, 666, Xinjiang Uygur Autonomous Region (XUAR) People's Republic of China (PCR); e-mail: [ma\\_fy@126.com](mailto:ma_fy@126.com);

**Musina, Gulnaz Nurgaliyevna** — candidate of chemical Sciences, Karaganda technical University, Ave. Nursultan Nazarbayev, 56, 100027, Karaganda, Kazakhstan; e-mail: [kargtu@kstu.kz](mailto:kargtu@kstu.kz); <https://orcid.org/0000-0003-4683-2868>

**Khamitova, Tolkyn Ondirisovna** — PhD, Agronomic Faculty, S. Seifullin Kazakh Agro Technical University, Zhenis avenue, 62, 010011, Astana, Kazakhstan; e-mail: [khamitova.t@inbox.ru](mailto:khamitova.t@inbox.ru); <https://orcid.org/0000-0002-4691-3732>

**Bolatbay, Abylaikhan Nurlanuly** — master, doctoral student, Karagandy University of the name of academician E.A. Buketov, Universitetskaya street, 28, 100024, Karaganda, Kazakhstan; e-mail: [abylai\\_bolatabai@mail.ru](mailto:abylai_bolatabai@mail.ru); <https://orcid.org/0000-0001-5047-3066>

---

\*The author's name is presented in the order: *Last Name, First and Middle Names*

V.V. Shelkovnikov\*, A.M. Altyev, M.S. Fryanova

<sup>1</sup>National Research Tomsk State University, Tomsk, Russian Federation

(\*Corresponding author's e-mail: [shvv@chem.tsu.ru](mailto:shvv@chem.tsu.ru))

## Study of the Methionine Electrooxidation at an Electrode Modified with Vitamin B<sub>12</sub> and Multi-Walled Carbon Nanotubes

The electrochemical behavior of methionine at an electrode modified with vitamin B<sub>12</sub> and multi-walled carbon nanotubes has been studied in this work. A possible mechanism of redox processes occurring on the modified electrode is proposed. When the electrode is formed, vitamin B<sub>12</sub> is fixed on the surface of a carbon-containing electrode modified with multi-walled carbon nanotubes due to adsorption. In the process of cathodic polarization, cobalt(III) in cobalamin is reduced to cobalt(II) to which a partially negatively-charged sulfur atom in the methionine molecule is attached due to electrostatic interactions. During anodic polarization, cobalt(II) in the complex is oxidized up to Co<sup>3+</sup>, the methyl group from methionine is transferred to cobalamin, and homocysteine passes into the solution, which is proved by Raman spectra. Based on the study of the dependence of current and potential on the sweep speed, it was found that the oxidation process is not reversible, the limiting stage is adsorption, and one proton and one electron participate in the electrochemical stage. The following optimal conditions for recording an analytical signal were selected: the background electrolyte is a tartrate buffer solution with pH = 4.01; the electrolysis potential is 1.6 V; the accumulation time is up to 180 s. The metrological characteristics of the procedure for determining methionine were estimated. The accuracy index did not exceed 29 %, the repeatability and intermediate precision indices did not exceed 14 % and 16 %, respectively. The range of detectable contents was (1–50)×10<sup>-7</sup>; the detection limit was 5.0×10<sup>-8</sup> M. It was shown that a 10-fold excess of ascorbic acid, tryptophan, glycine, cysteine and tyrosine does not have a noticeable distorting effect on the procedure for determining methionine.

**Keywords:** methionine, modified electrode, vitamin B<sub>12</sub>, electrooxidation, cobalamin, electron, proton, stripping voltammetry, multi-walled carbon nanotubes.

### Introduction

Methionine is an essential amino acid that plays an important role as a precursor for all other sulfur-bearing amino acids and their derivatives in living organisms. It involves in the regulation of metabolic processes of the immune system and has antioxidant activity. The methionine concentration in the range of 5–15 μmol/l is considered normal for men and women. The increased content of methionine is associated with damage caused to nucleic acids, with various types of cancer and cardiovascular diseases. The reduced methionine concentration leads to neurodegenerative diseases [1–6]. In this regard, the determination of the methionine content in foodstuff and biological fluids is a relevant task. Electrochemical methods of analysis are promising for this purpose.

The mechanism of methionine electrooxidation remains ambiguous. In 1960, dehydro-methionine was proposed in [7] as an intermediate of the product of anodic oxidation of methionine at a platinum wire electrode with pH = 7.0. Dehydro-methionine was also identified as a by-product of methionine oxidation using various analytical methods [8–10]. A few years later, voltammetric determination of methionine at platinum electrodes was reported in [11]. The authors observed a voltammetric wave between +0.7 and +1.0 V (calomel electrode), which manifested itself only in acidic media and only in the presence of hydrogen and chloride ions [11]. Later, owing to the development of new electrode materials, more detailed studies were carried out. In [12] the authors demonstrated methionine oxidation at a graphite electrode, which is an irreversible process controlled by diffusion. In [13], the authors reported that the oxidation potential of methionine at a glassy-carbon electrode remains constant in the pH range from 3 to 7. The authors also noted that the voltammetric wave of methionine oxidation strongly resembles cystine obtained in similar experimental conditions [12] at the glassy-carbon electrode. In 1994, the authors [14] showed that the neighboring carboxylate and amino groups of thioester, which modifies the electrode, play an important role in the methionine elec-

trooxidation at the carbon electrode, even if these groups are not rigidly held in a fixed position relatively the function of thioester in the molecular skeleton. Later, in 2011, glassy-carbon and diamond electrodes doped with boron were used to study the electrochemical oxidation of methionine in a wide pH range using cyclic and differential pulse voltammetry [15]. The results conform fully to the conclusions of the work [13]. In [15] the oxidation reaction proceeds in two stages at the glassy-carbon electrode and in one stage at boron-doped diamond electrodes, where, probably, the high oxidation current of the second peak is superimposed on the first one. Oxidation reactions have been found to be irreversible, diffusion-controlled, and one-electron processes, independent of pH at  $\text{pH} > 3$ .

In [16], we proposed a technique for determining methionine at an electrode modified with cyanocobalamin (vitamin B<sub>12</sub>). When choosing the technique for electrode modification, we proceeded from the following assumptions: methionine entering the human body, when interacting with enzymes, and is reduced to homocysteine [17]. Such reaction can serve as a prototype of the corresponding electrode process. We proposed the use of cyanocobalamin as an auxiliary substance. It is an electroactive substance due to the presence of cobalt(III) in the corrin ring. The process of vitamin B<sub>12</sub> chemisorption on mesoporous carbon is known [18]. By attaching vitamin B<sub>12</sub> to the surface of the electrode due to adsorption, it is possible to create conditions allowing the binding of methionine from the solution to form an electroactive compound at the electrode. The purpose of this work is to establish the mechanism of methionine oxidation at the modified electrode to optimize the conditions for the determination of methionine by stripping voltammetry.

### *Experimental*

#### *Equipment and reagents*

Methionine (Sigma, USA), multi-walled carbon nanotubes produced by “Graphen” (USA), vitamin B<sub>12</sub> (Belarus) were used in the work. All measurements were taken using standard pH solutions purchased from “Merck” (Germany). The solutions were prepared using deionized water obtained from “Sartorius” of the arium® pro brand. All the experiments were carried out at room temperature. Electrochemical measurements were performed using a TA-LAB voltammetric analyzer (NPO “Tomanalit”) in direct-current mode in a three-electrode cell. The indicator electrode was a modified carbon-containing electrode; silver-chloride electrodes in the 3 M KCl solution were used as an auxiliary electrode and a reference electrode. Multi-walled carbon nanotubes (MCNT) were applied to the surface of the carbon-containing electrode by electrolysis from a MCNT aqueous suspension by means of a universal power source UIP-2.

#### *Modification of the carbon-containing electrode*

MCNT were moistened with a small amount of ethyl alcohol; then water was added. After it MCNT were placed into the ultrasound bath for 3 hours. The ready-to-use suspension was used to apply nanotubes to the surface of the carbon-containing electrode by anodic polarization. A stainless-steel plate was used as the cathode (counter electrode). After 8 s of the electrolysis, the applied MCNT were dried and vitamin B<sub>12</sub> was deposited. Vitamin B<sub>12</sub> was deposited at the electrode modified with MCNT by cycling the potential in the range of  $-1.4 \dots +1.0$  V. The modification of the electrode is described in more detail in [18].

### *Results and Discussion*

The choice of optimal conditions for the oxidation and/ or reduction processes of the substance is the essential task in the development of a quantitative technique. Suitable conditions lead to an increase in the sensitivity of the analysis. The effect of a number of factors, such as the pH of the background electrolyte, accumulation parameters, and the potential sweep rate on the anode signal of methionine, was studied to select the optimal conditions for obtaining an analytical signal.

#### *The effect of pH*

The pH of the background electrolyte has a significant effect on the mechanism of redox processes in voltammetric analysis. Standard buffer solutions from 1.65 to 12.43 were used to establish the optimal value of the hydrogen ion concentration during methionine oxidation at the modified electrode.

Figure 1 shows the dependence of the anode peak value of methionine on the pH of the background electrolyte. With an increase in the pH from 1.65 to 4.01, the peak current of methionine oxidation increases. The decrease in the signal at  $\text{pH} < 4$  is associated with the protonation of the amino groups of methionine and cobalamin; the adsorption of methionine on the electrode is hindered as a result of electrostatic repulsion. The signal intensity decreases when the pH shifts to the neutral and alkaline regions, which is due to the lack

of protons required for methionine oxidation. The peak shift towards more negative values as the pH of the buffer solution increases. A linear dependence can be observed between the peak potential and the pH:

$$Y = -0.0492X + 0.6930. \quad (1)$$

The slope value of 49.2 mV/pH is close to the Nernst slope (59.0 mV/pH), which indicates an equal number of electrons and protons participating in the electrochemical process.

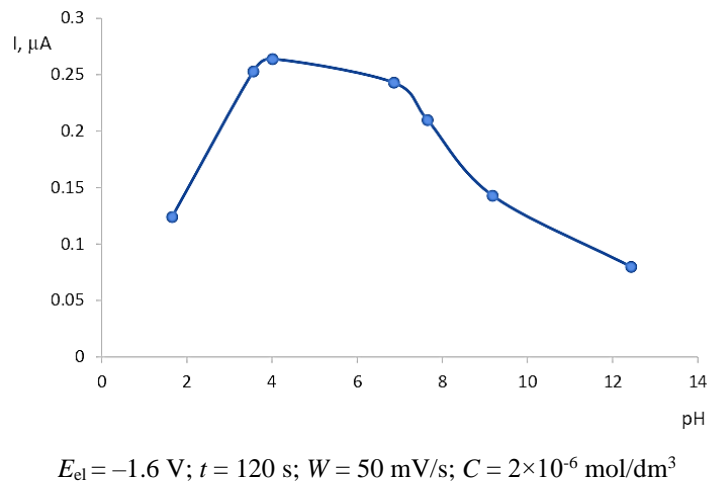


Figure 1. Dependence of the electrooxidation current of methionine at the modified electrode on the pH

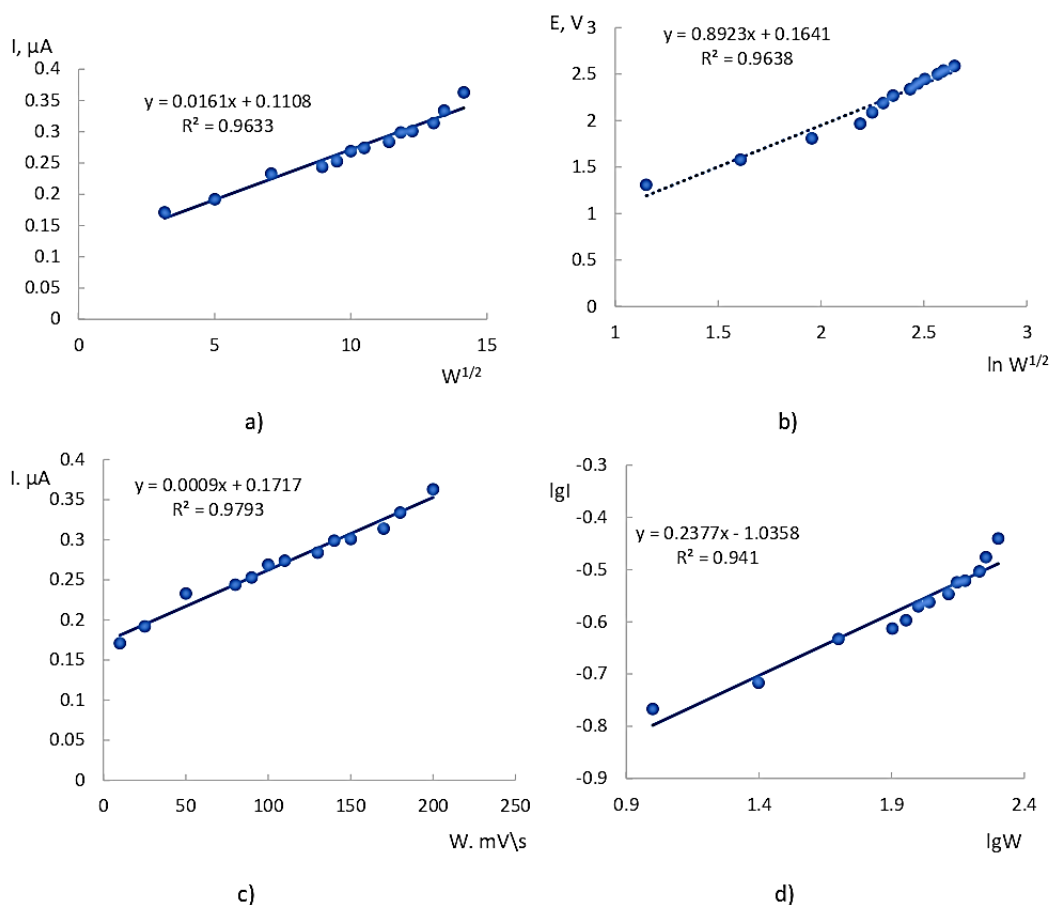


Figure 2. Dependence of the methionine oxidation current on the square root of the potential sweep rate (a), the dependence of the potential on  $\ln W^{1/2}$  (b), the dependences of the current on the potential sweep rate (c) and  $\lg I$  on  $\lg W$  (d)

*The effect of the potential sweep rate on the current and potential of the anode peak*

The dependences of the anode peak current and potential on the potential sweep rate allow us to estimate the mechanism of the electrochemical reaction. In this regard, the influence of the potential sweep rate on the anode current of methionine was studied. To establish the mechanism of methionine electrooxidation at the modified electrode, the dependences of the current on the square root of the sweep rate (Fig. 2a) and the peak potential on  $\ln(W^{1/2})$  were plotted in Figure 2b.

The linear dependence for the current (Fig. 2a) is typical of both reversible and irreversible processes while the linear dependence of the peak potential of methionine on  $\ln W^{1/2}$  evidences the irreversibility of the process (Figure 2b). Figure 2b presents the dependence of the current on the sweep rate and a similar dependence in logarithmic coordinates (Fig. 2d). The linearity of the logarithmic dependence (Fig. 2d) indicates that diffusion is not a limiting stage of the process. The Semerano criterion (the slope of the dependence of  $\lg I$  on  $\lg W$ ) was 0.24, which indicates the absence of the effect of the diffusion process during the oxidation of methionine on the electrode surface. The Semerano criterion should be 0.5 for the processes limited by diffusion [19]. A similar dependence of the current on the sweep rate demonstrates that adsorption is the limiting stage of the process.

The transfer coefficient of the irreversible process (methionine oxidation) was calculated based on the Tafel dependence. The value of the transfer coefficient was 0.44. The obtained value shows that the first electron participates in the limiting stage of the process.

The following formula was used to calculate the electrons in the case of an irreversible process:

$$\left| E_p - E_{p/2} \right| = \frac{47.7}{\alpha n}, \quad (2)$$

where  $E_p$  is the peak potential;  $E_{p/2}$  is the half-peak potential.

The value of  $n = 1.08$  indicates that one electron takes part in the oxidation reaction.

Earlier in [16] we proposed a possible reaction mechanism based on the Raman spectra of pure methionine and its oxidation products from the electrode. Homocysteine has been shown to be the oxidation product of the methionine complex with cyanocobalamin. Based on the study of the above-mentioned kinetics, it is possible to conclude that one electron and one proton participate in the oxidation process of the complex. This may be conditioned by the fact that cobalt, being in the corrin ring of vitamin B<sub>12</sub>, is oxidized to Co(III) during the anodic potential sweep. During cathodic polarization of the electrode, cobalt in cyanocobalamin is first reduced to +2, and then it is the reduced complex that interacts with methionine. The reverse process of cobalt oxidation occurs during anodic sweep: the methyl group of methionine is transferred to cobalamin and passes into the homocysteine solution (Figure 3).

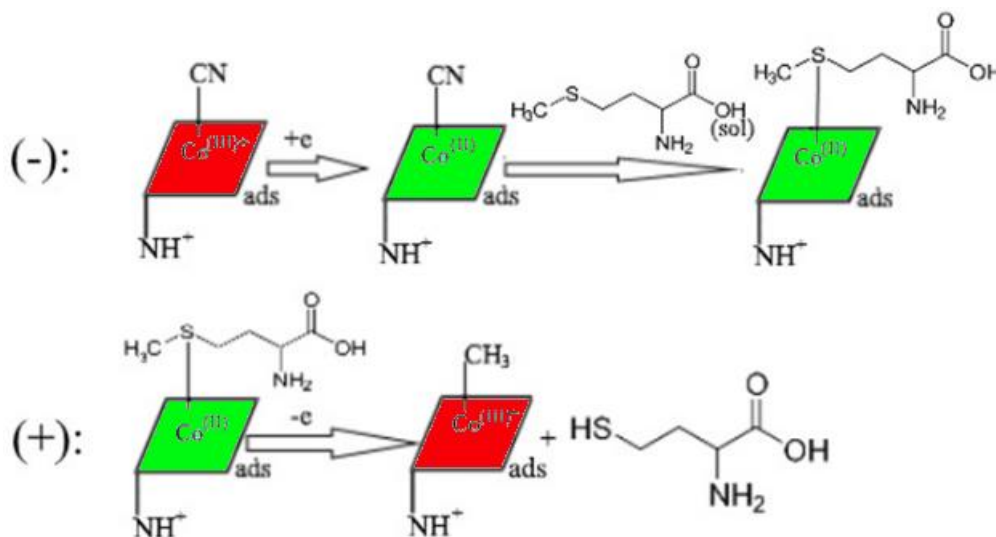


Figure 3. Blank drawing of the methionine oxidation process

*The effect of accumulation parameters on the intensity of the electrooxidation signal*

The range of values from  $-1.9$  V to  $-1.1$  V was studied when choosing the electrolysis potential (Figure 4a). The dependence of the anode peak current on the electrolysis potential passes through the maximum. The anode peaks decrease when the potential is shifted to the negative region, which is most likely due to the release of hydrogen that prevents the formation of the complex on the electrode surface. Therefore, the potential of  $-1.6$  V was chosen as optimal for concentrating methionine at the modified electrode. As can be seen from Figure 4b, after accumulation for more than 300 s, the signal intensity changes slightly, which may be conditioned by the complete filling of the electrode surface with a monolayer of the deposited methionine. Therefore, during subsequent studies, the accumulation was carried out no more than 180 s.

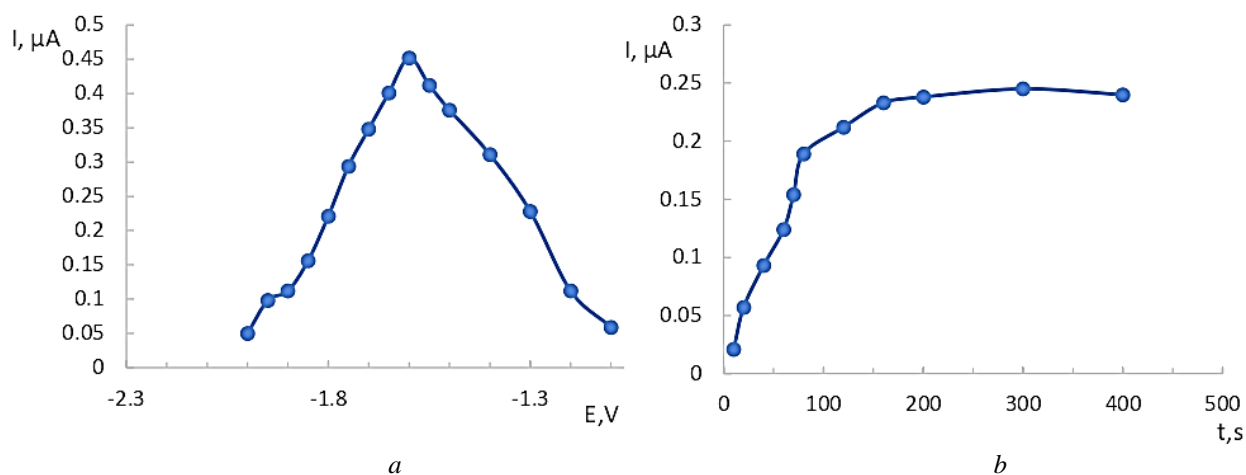


Figure 4. Dependence of the methionine electrooxidation current on the accumulation potential at the modified electrode ( $t = 120$  s,  $W = 80$  mV/s,  $C = 5 \times 10^{-6}$  mol/dm<sup>3</sup>) (a) and the dependence of the methionine electrooxidation current on the accumulation time ( $E_{el} = -1.6$  V,  $W = 80$  mV/s,  $C = 2 \times 10^{-6}$  mol/dm<sup>3</sup>) (b)

Despite the fact that the participation of adsorption during electrooxidation of methionine at the electrode has been established, it can be concluded that the mentioned factor does not prevent quantitative assessment in the specified concentration range. The dependence of current on concentration is linear in the range of  $(1-50) \times 10^{-7}$  and obeys the equation:

$$I = 0.024C + 0.003 \quad (E_{el} = -1.6 \text{ V}, t = 150 \text{ s}, W = 80 \text{ mV/s}). \quad (3)$$

The effect of other amino acids on the results of the determination of methionine was studied. The ultimate transferable concentration was defined as the maximum concentration of a hindrance substance, causing an error in the determination of amino acids of no more than 5 % [19, 20]. The 10-fold excess of ascorbic acid, tryptophan, histidine, glycine, arginine, cysteine and tyrosine does not have a noticeable distorting effect on the procedure for methionine determination.

*Some metrological characteristics of the procedure for tryptophan and 5-hydroxytryptophan determination*

According to ISR 61-2010, the indices of repeatability, intermediate precision, and accuracy were calculated (Table 1).

Table 1

**Metrological characteristics of the procedure for methionine determination ( $p = 0.95$ ,  $n = 2$ ,  $l = 15$ )**

Concentration $\times 10^{-7}$ , mol/dm <sup>3</sup>	Repeatability index, $\sigma_r^*$ , %	Intermediate precision index, $\sigma_{RI}^*$ , %	Accuracy index (relative accuracy limits at $P = 0.95$ ), $\pm \Delta$ , %
1	13.9	15.2	29.0
10	13.3	14.7	28.4
20	12.9	14.3	27.3
30	12.5	13.9	26.9
40	12.0	13.5	25.5
50	11.7	13.3	25.4

Based on the obtained metrological characteristics of the developed procedure for methionine determination, it is possible to conclude that the accuracy index does not exceed 29 %, the repeatability and intermediate precision indices do not exceed 14 % and 16 %, respectively.

The modified electrode makes it possible to obtain stable analytical signals for at least 25 cycles (blank experiment, analyzed assay, spiked sample). Further, the electrode sensitivity decreases and the electrode surface renewal is required. The electrode surface is cleansed by electrolysis for 300 s with a potential of  $-0.5$  V. Then a new film of vitamin B<sub>12</sub> is applied to the surface by cyclic potential scanning.

### Conclusions

One proton and one electron take part in the process of oxidation of methionine complex with cobalamin. During oxidation, methionine takes one proton and one electron. In the process of cathodic polarization, cobalt(III) in cobalamin is reduced to cobalt(II) to which a partially negatively-charged sulfur atom in the methionine molecule is attached due to electrostatic interactions. In case of anodic polarization, cobalt(II) in the complex is oxidized to Co(III), the methyl group is transferred from methionine to cobalamin, while homocysteine passes into solution. The process is controlled by adsorption. The following optimal conditions for methionine determination have been selected: the background electrolyte is the tartrate buffer solution with pH = 4.01; the electrolysis potential is 1.6 V; the accumulation time is up to 180 s. A number of metrological indices have been established for the procedure of methionine determination: accuracy, repeatability and intermediate precision indices. The range of detectable contents was  $(1-50) \times 10^{-7}$ ; the detection limit was  $5.0 \times 10^{-8}$  M.

### References

- 1 Martínez, Y., Li, X., Liu, G., Bin, P., Yan, W., Más, D., Valdivié, M., Hu, C.-A.A., Ren, W., & Yin, Y. (2017). The role of methionine on metabolism, oxidative stress and diseases. *Amino Acids*, 49 (12). 2091–2098. <https://doi.org/10.1007/s00726-017-2494-2>
- 2 Butterfield, D.A. & Boyd-Kimball, D. (2005). The critical role of methionine 35 in Alzheimer's amyloid  $\beta$ -peptide (1-42)-induced oxidative stress and neurotoxicity. *Biochim. Biophys. Acta. Proteins Proteomics*, 1703(2). 149–156. <https://doi.org/10.1016/j.bbapap.2004.10.014>
- 3 Jackson, R. & Hunter, T. (1970). Role of methionine in the initiation of haemoglobin synthesis. *Nature*, 227(5259), 672–676. <https://doi.org/10.1038/227672a0>
- 4 Arber, W. (1965). Host specificity of DNA produced by Escherichia coli: V. The role of methionine in the production of host specificity. *J. Mol. Biol.*, 11(2). 247–256. <https://doi.org/10.1007/BF00268883>
- 5 Reed, D.J. & Orrenius, S. (1977). The role of methionine in glutathione biosynthesis by isolated hepatocytes. *Biochem. Biophys. Res. Commun.*, 77(4). 1257–1264. [https://doi.org/10.1007/978-3-642-67132-6\\_3](https://doi.org/10.1007/978-3-642-67132-6_3)
- 6 Wilcken, D.E. & Wilcken, B. (1976). The pathogenesis of coronary artery disease. A possible role for methionine metabolism. *J. Clin. Invest.*, 57(4). 1079–1082. <http://doi.org/10.1172/JCI108350>
- 7 Man, S. (1960). Polarographie einer Sulfoniumverbindung. *Z. Anal. Chem.*, 173, 112. <https://doi.org/10.1007/BF00448739>
- 8 Lavine, T.F. (1943). An iodometric determination of methionine. *J. Biol. Chem.*, 151. [https://doi.org/10.1016/s0021-9258\(18\)72138-8](https://doi.org/10.1016/s0021-9258(18)72138-8)
- 9 Gensch, K.H. & Higuchi, T. (1967). Kinetic investigation of reversible reaction between methionine and iodine. Improved iodometric determination of methionine. *J. Pharm. Sci.*, 56, 177–184. <https://doi.org/10.1002/jps.2600560205>
- 10 Sysak, P.K., Foote, C.S. & Ching, T.-Y. (1977). Chemistry of singlet oxygen — XXV. Photooxygenation of methionine. *Photochem. Photobiol.*, 26, 19–27. <https://doi.org/10.1111/j.1751-1097.1977.tb07443.x>
- 11 Kyriacou, D. (1966). Rapid voltammetric determination of methionine with a platinum electrode. *Nature*, 211, 519–521. <https://doi.org/10.1038/211519b0>
- 12 Brabec, V. & Mornstein, V. (1980). Electrochemical behaviour of proteins at graphite electrodes. II. Electrooxidation of amino acids. *Biophys. Chem.*, 12, 159–165. [https://doi.org/10.1016/0301-4622\(80\)80048-2](https://doi.org/10.1016/0301-4622(80)80048-2)
- 13 Reynaud, J.A., Malfroy, B. & Canesson, P. (1980). Electrochemical investigations of amino acids at solid electrodes. *J. Electroanal. Chem. Interfacial Electrochem.*, 114, 195–211. [https://doi.org/10.1016/S0022-0728\(80\)80447-5](https://doi.org/10.1016/S0022-0728(80)80447-5)
- 14 Sanaullah, S. Wilson & Glass, R.S. (1994) The effect of pH and complexation of amino acid functionality on the redox chemistry of methionine and X-ray structure of [Co(en)2(L-Met)](ClO<sub>4</sub>)<sub>2</sub>·H<sub>2</sub>O. *J. Inorg. Biochem.*, 55, 87–99. [https://doi.org/10.1016/0162-0134\(94\)85031-3](https://doi.org/10.1016/0162-0134(94)85031-3)
- 15 Enache, T.A. & Oliveira-Brett, A.M. (2011). Boron doped diamond and glassy carbon electrodes comparative study of the oxidation behaviour of cysteine and methionine. *Bioelectrochemistry*, 81, 46–52. <https://doi.org/10.1016/j.bioelechem.2011.02.001>
- 16 Shelkovnikov, V.V., Altyev, A.M. & Vinogradov, M.E. (2019) Determination of Methionine in Medicines by Stripping Voltammetry. *J. Anal. Chem.*, 74(12), 1239–1244. <https://doi.org/10.1134/S1061934819120116>

17 Manta, B. & Relover, S. (2017). Regulated methionine oxidation by monooxygenases. *Free Radical Biology and Medicine*, 109, 141. <https://doi.org/10.1016/j.freeradbiomed.2017.02.010>

18 Jose, A. & Lima, Jr. (2013). Using Raman spectroscopy to understand the origin of the phase transition observed in the crystalline sulfur based amino acid l-methionine. *Vibrational Spectroscopy*, 65, 132–135. <https://doi.org/10.1016/j.vibspec.2012.12.004>

19 Keyvanfar, M., Shakeri, R., Karimi-Maleh, H. & Alizad, K. (2013). Highly selective and sensitive voltammetric sensor based on modified multiwall carbon nanotube paste electrode for simultaneous determination of ascorbic acid, acetaminophen and tryptophan. *Mater. Sci. Eng. C*, 33, 811-816. <https://doi.org/10.1016/j.msec.2012.11.005>

20 Rajabzadeh, N., Benvidi, A., Mazloum-Ardakani, M., Firozabadi, A.D. & Vafazadeh, R. (2015). A Highly Sensitive Sensor Based on Reduced Graphene Oxide. Carbon Nanotube and a Co (II) Complex Modified Carbon Paste Electrode: Simultaneous Determination of Isoprenaline. Captopril. Tryptophan. *Electroanal.*, 27, 2792–2798. <https://doi.org/10.1002/elan.201500236>

В.В. Шелковников, А.М. Алтыев, М.С. Фрянова

## В<sub>12</sub> дәрумені мен көпқабырғалы көміртекті нанотүтікшелермен модификацияланған электродта метиониннің электр тотығын зерттеу

Жұмыста В<sub>12</sub> витаминімен және көпқабырғалы көміртекті нанотүтіктермен модификацияланған электродтағы метиониннің электрохимиялық тәртібі зерттелген. Модификацияланған электродта болатын тотығу-тотықсыздану процестерінің ықтимал механизмі ұсынылған. Электродты қалыптастыру кезінде В<sub>12</sub> дәрумені адсорбция есебінен көпқабатты көміртекті нанотүтікшелермен модификацияланған көміртегі бар электродтың бетіне бекітіледі. Катодты поляризация кезінде кобаламиндегі кобальт (III) кобальт (II) дейін азаяды, оған электростатикалық өзара әрекеттесулер есебінен метионин молекуласындағы жартылай теріс зарядталған күкірт атомы қосылады. Анодты поляризация кезінде кешендегі кобальт (II) Со<sup>3+</sup> дейін тотығады, метиониннен метил тобы кобаламинге ауысады, бұл ретте гомоцистеин ерітіндіге өтеді, яғни бұл комбинациялық шашырау спектрлерімен дәлелденген. Ток пен потенциалдың жаймалау жылдамдығына тәуелділігін зерттеу негізінде тотығу процесі қайтымсыз екендігі анықталды. Шектеу сатысы адсорбция болып табылады, ал бір протон мен бір электрон электрохимиялық сатыға қатысады. Аналитикалық сигналды тіркеудің келесі оңтайлы шарттары таңдалды: фондық электролит-тарtratтық буферлік ерітінді рН = 4,01; электролиз потенциалы — 1,6 В; жинақтау уақыты — 180 с дейін. Метионинді анықтау әдісінің метрологиялық сипаттамаларына бағалау жүргізілді. Дәлдік көрсеткіші 29 %-дан аспайды. Қайталану және аралық дәлдік көрсеткіштері сәйкесінше 14% және 16% құрады. Анықталған құрамдардың диапазоны (1–50)×10<sup>-7</sup>; анықтау шегі — 5,0×10<sup>-8</sup> М. Аскорбин қышқылының, триптофанның, глициннің, цистеиннің және тирозиннің 10 есе артық болуы метионинді анықтау әдісіне айтарлықтай бұрмалаушы әсер етпейтіні көрсетілген.

*Клт сөздер:* метионин, модификацияланған электрод, В<sub>12</sub> витамині, электр тотығу, кобаламин, электрон, протон, инверсиялы вольтамперметрлеу, көпқабырғалы көміртекті нанотүтіктер.

В.В. Шелковников, А.М. Алтыев, М.С. Фрянова

## Изучение процесса электроокисления метионина на модифицированном витамином В<sub>12</sub> и многостенными углеродными нанотрубками электроде

В статье изучено электрохимическое поведение метионина на электроде, модифицированном витамином В<sub>12</sub> и многостенными углеродными нанотрубками. Предложен возможный механизм окислительно-восстановительных процессов, протекающих на модифицированном электроде. При формировании электрода витамин В<sub>12</sub> закрепляется на поверхности углеродсодержащего электрода модифицированного многостенными углеродными нанотрубками за счет адсорбции. При катодной поляризации кобальт (III) в кобаламине восстанавливается до кобальта (II), на который, за счет электростатических взаимодействий, присоединяется частично отрицательно заряженный атом серы в молекуле метионина. При анодной поляризации кобальт (II) в комплексе окисляется до Со<sup>3+</sup>, метильная группа с метионина переносится на кобаламин, при этом в раствор переходит гомоцистеин, что доказано спектрами комбинационного рассеяния. На основании изучения зависимости тока и потенциала от скорости развертки было установлено, что процесс окисления необратим. Лимитирующей стадией является адсорбция, а в электрохимической стадии участвуют один протон и один электрон. Были подобраны следующие оптимальные условия регистрации аналитического сигнала: фоновый электролит — тарtratный буферный раствор рН = 4,01; потенциал электролиза — 1,6 В; время накопления — до 180 с. Проведена оценка метрологических характеристик методики определения метионина. Показатель точности не превышал 29 %. Показатели повторяемости и промежуточной прецизионности не превы-

шали 14 и 16 % соответственно. Диапазон определяемых содержаний составил  $(1-50) \times 10^{-7}$ ; предел обнаружения —  $5,0 \times 10^{-8}$  М. Показано, что 10-кратный избыток аскорбиновой кислоты, триптофана, глицина, цистеина и тирозина не оказывает заметного искажающего влияния на методику определения метионина.

*Ключевые слова:* метионин, модифицированный электрод, витамин В<sub>12</sub>, электроокисление, кобаламин, электрон, протон, инверсионная вольтамперометрия, многостенные углеродные нанотрубки.

#### Information about authors\*

**Shelkovnikov, Vladimir Vitalievich** (*corresponding author*) — Candidate of Chemical Sciences Do-cent, Head of the Department of Analytical Chemistry, National Research Tomsk State University, Lenin avenue, 36, 634050, Tomsk, Russia, e-mail: [shvv@chem.tsu.ru](mailto:shvv@chem.tsu.ru); <https://orcid.org/0000-0002-5778-2862>

**Altiev, Alexey Muratovich** — postgraduate student of the Faculty of Chemistry, National Research Tomsk State University, Lenin avenue, 36, 634050 Tomsk, Russia, e-mail: [lexa-cors@mail.ru](mailto:lexa-cors@mail.ru); <https://orcid.org/0000-0001-8543-3451>

**Fryanova, Maria Sergeevna** — student of the Faculty of Chemistry, National Research Tomsk State University, Lenin avenue, 36, 634050 Tomsk, Russia, e-mail: [m.s.fryanova@mail.ru](mailto:m.s.fryanova@mail.ru); <https://orcid.org/0000-0002-6394-2498>

---

\*The author's name is presented in the order: *Last Name, First and Middle Names*

V.N. Fomin<sup>1</sup>, E.R. Usmanova<sup>1,2</sup>, E.F. Gyul<sup>3</sup>, N.K. Kelesbek<sup>1</sup>,  
M.A. Turovets<sup>1</sup>, O.I. Zemskiy<sup>1</sup>, D.M. Saulebekov<sup>1</sup>, S.K. Aldabergenova<sup>1\*</sup>

<sup>1</sup>Karaganda University of the name of academician E.A. Buketov, Karaganda, Kazakhstan;

<sup>2</sup>South-Uralsk State University, Chelyabinsk, Russia;

<sup>3</sup>Institute of Art Studies of the Academy of Sciences of the Republic of Uzbekistan, Tashkent, Uzbekistan

(\*Corresponding author's e-mail: [aldsau@mail.ru](mailto:aldsau@mail.ru))

## Method for Qualitative and Quantitative Analysis of Ancient Lead Enamel Using Laser Induced Breakdown Spectroscopy

The method of laser induced breakdown spectroscopy (LIBS) was used in analysis of the archaeological enamel samples from the ancient settlement of Jochi Khan (XIV century). During the qualitative analysis, it was found that the elements of the enamel matrix are Si, Pb, K, Na, Mg, Ca, Al. The glaze color is due to the presence of copper and iron. Clustering by the k-means method revealed two groups of samples similar in composition of enamel, but differing in place of origin within the settlement. For the studied samples the semi-quantitative composition of glazes was established from the spectra of LIBS using a method based on the hypothesis of local thermodynamic equilibrium (LTE) and a chemometric approach (Projection to Latent Structures, PLS). Probabilistic deterministic design of experiment was used to search for pairs of element lines that are not subject to changes when the conditions for spectra registration vary, and to determine the coefficients in the equations based on LTR. Calculations using the PLC method were carried out in the "R" programming environment. The following content of the matrix elements was obtained in terms of the most stable oxides, %: SiO<sub>2</sub> — 49–61, PbO — 23–31, MgO — 1.7–2.3, CaO — 4.6–6.9, Na<sub>2</sub>O — 4.1–5.3, K<sub>2</sub>O — 5.1–6.4, Al<sub>2</sub>O<sub>3</sub> — 0.8–1.7, CuO — 0.32–0.4, Fe<sub>2</sub>O<sub>3</sub> — 0.09–0.16. The results of both methods are generally consistent with each other. The inaccuracy between 4 parallel determinations were 15–24 % for LTE, and 9–14 % for PLS. Taking into account the data of semi-quantitative analysis, it was concluded that the division into two groups is based on a different ratio of copper and iron in enamel.

**Keywords:** LIBS, chemometrics, cluster analysis, PLS, low-melting lead enamels, probabilistic deterministic design of experiment, archeology, settlement of Jochi Khan.

### Introduction

Method of laser induced breakdown spectroscopy (LIBS) in elemental analysis of a wide variety of materials is continuously becoming more demand, despite the problems with calibration. LIBS is characterized by relatively low values of accuracy and reproducibility of the analysis that are associated with the basic impossibility of reproducing the recording conditions accurately from spectrum to spectrum. This problem can hardly be eliminated by improving the method's hardware [1]. Therefore, there is a constant search for mathematical methods for LIBS signals processing, which makes it possible to improve the analytical characteristics of this analysis method [2]. Currently, in order to achieve acceptable metrological characteristics, both theoretical approaches based on the concept of local thermodynamic equilibrium (LTE) and empirical approaches based on chemometric methods, as well as various combinations of these two approaches are being developed [3–6].

The LIBS method has a number of advantages along with limitations. First of all, the insignificance of damage to the object of analysis and the lack of sample preparation should be noted. A laser pulse carries information not only about the surface layer, but also about the bulk of the sample, since it evaporates the sample from a certain depth. This feature makes it possible to overcome the problems associated with the analysis of archaeological artifacts [7, 8], which are characterized by differences in the chemical composition of the surface material and the bulk.

The mausoleum, located in the Ulytau region of Kazakhstan, 45 km from the city of Zhezkazgan, on the left bank of the Karakengir River, is associated by Kazakh folk tradition with the name of Jochi Khan as the eldest son of Genghis Khan. The upper dome of the mausoleum, lined with glazed turquoise tiles, was built

over the lower early dome without cladding. According to radiocarbon analysis, there are two stages in the construction of the mausoleum in the XIV century [9]. In order to obtain additional historical information about the construction of the mausoleum and the settlement of Jochi Khan, it was useful to conduct a comparative study of the glaze of tile fragments from different points of the mausoleum and the settlement by the LIBS method.

Qualitative analysis by the LIBS method was carried out in the traditional way. The aim of this study was to develop methods of analysis for classification and quantification that provide satisfactory accuracy with limited possibilities for sample preparation and registration of spectra.

### Experimental

Samples of ceramic tiles containing enamel coating of various shades of blue and green were received from historians and returned to the National Historical, Cultural and Natural Reserve-Museum "Ulytau" (Ulytau village, Karaganda region, Kazakhstan) immediately after registration of the spectra (Fig. 1).



- a* — the mausoleum of Jochi Khan. A fragment of a tile. Sample 3 (Obr3.1);
- b* — the mausoleum of Jochi Khan. A fragment of a tile. Sample 4 (Obr4);
- c* — the mausoleum of Jochi Khan. Fragment of the mausoleum crown 2 (preliminary definition). Sample 5 (Obr5);
- d* — the settlement of Jochi Khan. A fragment of a tile. Sample 2 (Obr2);
- e* — the settlement of Jochi Khan. Small house. A fragment of ceramics. Sample 6 (Obr6);
- f* — the settlement of Jochi Khan. House 2. Tile fragment. Sample 1 (Obr1);
- g* — the settlement of Bytygai. Workshop. A fragment of a tile. Sample 7 (Obr2007)

Figure 1. Samples of tiles from different points of the mausoleum and the settlement

Samples were analyzed on a two-pulse spectrometer "LAES Matrix Continuum" (SJSC Spectroscopic Systems, 2016, Russia) with a double Paschen-Runge optical scheme with an optical path length of 250 mm and 125 mm, with diffraction gratings of 2400 groove/mm and 1200 groove/mm and 7 CCD detectors from Toshiba and a wavelength range of 190 up to 800 nm. The emission spectrum of all samples was recorded at the same instrument settings to facilitate subsequent comparison and interpretation of the spectra. The energy of the pump lamp was 18 Joules. The remaining settings were chosen based on previous experience [10, 11], namely: the laser frequency was 10 Hz, the delay time of the first Q-switch was 100  $\mu$ s, the second was 110  $\mu$ s, the exposure start delay was 2  $\mu$ s and the total exposure time was 5 ms. The number of pulses was limited to 15, including 2 firing pulses. Spectra were recorded at four randomly selected points without scanning by area to minimize damage and provide some smoothing of random effects. The samples were returned to storage after the spectra recording. The obtained spectra were used for qualitative analysis of samples. Both the standard spectrometer software and the NIST [12] database were used to assign lines in the spectrum.

Since each sample was examined at four points, the total number of spectra seemed sufficient for cluster analysis using the “teaching without a teacher” approach. The spectra were normalized by the intensity of the  $\text{MgI}_{280}$  line, then cluster analysis was performed in the “R” programming environment [13]. Taking into account the similarity of the qualitative composition of the samples, the reasons for the cluster separation could only be established by quantitative analysis in the absence of the possibility of re-registration of the spectra. Variants using thermodynamic [14] and chemometric [15, 16] approaches were applied to consider the possibility of quantitative analysis of samples. A set of artificially obtained samples with a qualitative composition close to the enamel on the archaeological samples was used for training in both variants. The range of variation in the ratios of elements in the composition of the furnace-charge was selected according to the data [17]. The furnace-charge, composed of oxides of silicon, lead, magnesium, iron and copper, sodium, potassium and calcium carbonates, and aluminum hydroxide, was mixed by abrasion in a mechanical mortar for 20 minutes and fused in alund crucibles for 1 hour at 1000 °C, with periodic rocking of the crucible (Table 1).

Table 1

Composition of calibration and control enamel samples

№	PbO	SiO <sub>2</sub>	Al <sub>2</sub> O <sub>3</sub>	Na <sub>2</sub> O	K <sub>2</sub> O	CaO	MgO	CuO	Fe <sub>2</sub> O <sub>3</sub>
1	0.202	0.503	0.008	0.121	0.05	0.05	0.05	0.005	0.01
2	0.287	0.43	0.019	0.076	0.076	0.067	0.029	0.008	0.008
3	0.329	0.376	0.028	0.15	0.009	0.084	0.009	0.009	0.006
4	0.371	0.325	0.037	0.046	0.112	0.009	0.084	0.011	0.005
5	0.431	0.239	0.048	0.01	0.153	0.029	0.067	0.019	0.004

The appearance of the calibration samples is shown in Figure 2.



Figure 2. Calibration samples of enamel

A number of methods for calibration of atomic emission spectrometers are based on the fact that the intensity of the analytical lines of different elements, which are low in excitation energy, almost equally depends on random factors and conditions of spectrum registration. This means that the ratio of intensities depends only on the concentration of elements. The possibility of the method of probabilistically deterministic design of the experiment (PDDoE) was used [18, 19] to search for such pairs of lines, and to identify factors on which the variable in question does not depend. PDDoE method has proven itself well for optimizing the conditions of the LIBS [20, 21] as well as for other physicochemical methods of analysis [22]. When compiling a six-factor experiment plan with five levels of variation (Table 2), the possibility of using the sample composition as a single factor was used [23]. The excitation energy of the lines was retrieved from the Atomic Spectra Database [12].

Table 2

Factors and levels of their variation in the experimental plan

№	Factor	Symb.	Level 1	Level 2	Level 3	Level 4	Level 5
1	$C_n/C_m$	$X_1$	1	2	3	4	5
2	$E_{lamp}, J$	$X_2$	12	14	16	17	18
3	$QSW_1, mks$	$X_3$	100	120	140	160	180
4	$\Delta QSW, mks$	$X_4$	1	3	5	10	20
5	Delay, mks	$X_5$	1	2	3	5	10
6	Expos, ms	$X_6$	1	2	3	4	5

The ratios of element concentrations for each sample (levels of the first factor) were calculated according to Table 1.

The spectra of the calibration samples were recorded in five repetitions, and averaged as described in [11].

*Results and Discussion*

Qualitative analysis of the samples was conducted by identification of all analytical lines of the obtained spectra. The matrix in all cases is silicon, lead, potassium, sodium, calcium, magnesium (Fig. 3). Enamel coloring is due to the presence of a small amount of iron and copper. Lines of aluminum are also present.

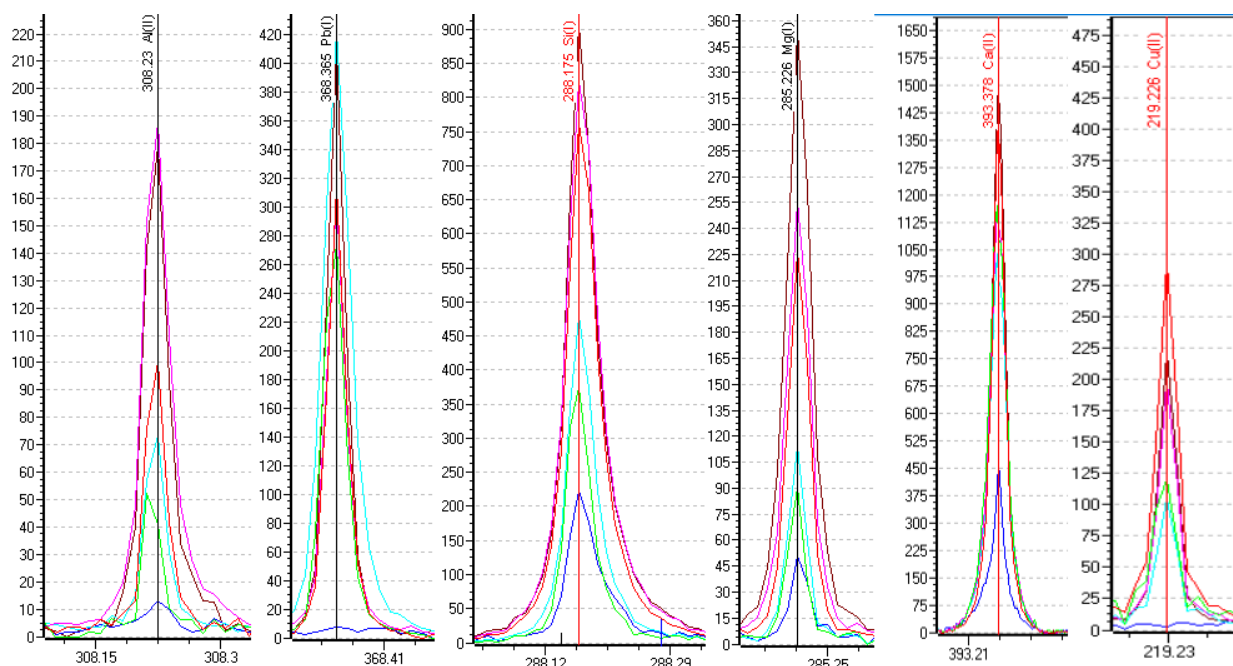


Figure 3. Some analytical lines of elements of the enamel matrix

There are analytical lines of tin in the enamel samples of modern tiles used in the restoration of the mausoleum. Tin compounds were used to reduce transparency. There is no tin in historical samples, so the restored materials were not considered in further study.

A dendrogram was obtained as a result of the classification analysis of the samples (Fig. 4). The dendrogram makes it possible to distinguish 4 groups of enamel spectra.

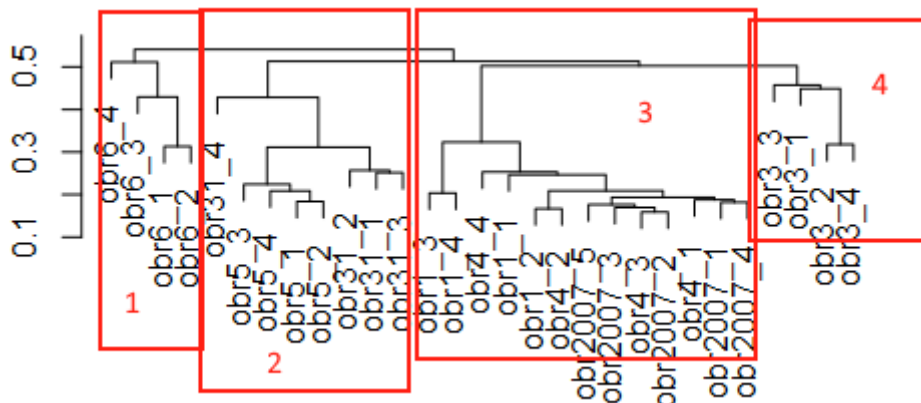


Figure 4. Cluster dendrogram of the archeological enamel samples

Samples 3, 1 and 5 have similar spectra. Samples 1, 4 and 7 can also be classified as parts of the same specimen. The spectra of samples 6 and 3 did not enter into clusters, forming separate groups. It should be noted that there is a possibility of random separation of closely related samples, while the probability of random cluster unification in the analysis by the emission spectrum is very small.

According to the results of qualitative and cluster analysis, it is possible to make conclusions of an archaeological nature that are beyond the scope of this work. At the same time, clustering can only be explained using quantitative analysis, which is difficult in this case due to limited access to the samples. In this regard, only methods of mathematical processing of obtained spectral data were used further in qualitative analysis. The first approach to quantitative analysis of samples tested in the study was based on the fact that the intensities of the analytical lines with similar excitation energies almost equally depend on the conditions of spectrum registration according to the hypothesis of local thermodynamic equilibrium (LTE). Consequently, the ratio of the intensities of such lines will depend only on the ratio of concentrations, but not on the conditions of the spectra registration and/or random factors. Figure 5 shows graphs of the dependence of the ratio of the intensities of the Mg(I)<sub>293.67</sub> and Ca(II)<sub>315.9</sub> lines on the ratio of the concentrations of elements and the energy of the laser pump lamp.

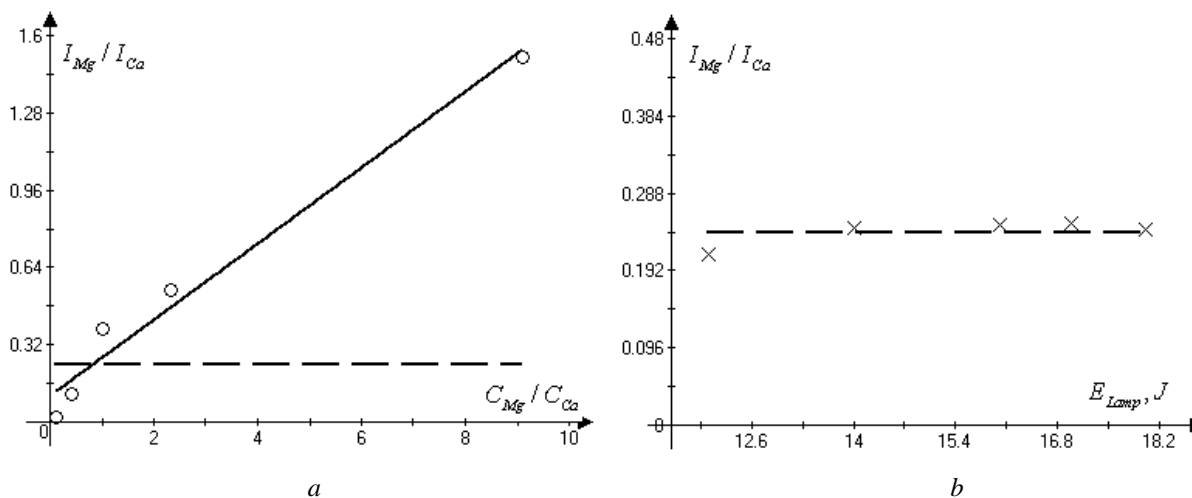


Figure 5. Dependence of the ratio of the intensities of the Mg(I)<sub>293.67</sub> and Ca(II)<sub>315.9</sub> lines on the: a) ratio of the concentrations of elements; b) the energy of the laser pump lamp

As can be seen from Figure 5, even without calculations, the pump lamp energy in the selected range has almost no effect on the ratio of the intensities of the analytical lines under consideration. The influence of other factors on this pair of lines is even less significant.

The intensity ratio of a pair of lines of different elements selected by the excitation energy and the actual presence in all 25 spectra of artificial and archaeological samples (Table 2) was used for calculation by the PDDoE method. In this case, regardless of the usual practice of the method, those lines were selected for which only the partial dependence of the intensity ratio on the concentration was significant, and the remaining partial dependencies were insignificant. Preference was given to those alternatives in which insignificant functions were most accurately described by the equation  $Y = \bar{Y}$  (Fig. 5). The relationship between the concentration and the intensity ratio was approximated by linear functions:

$$a(C_1/C_2) + b = I_1/I_2. \quad (1)$$

The coefficients  $a$  and  $b$  of these functions were used in further calculations.

Table 3

Analytical lines used for calculations

Element	$\lambda$	E
Mg I	293.67	55891
Mg II	279.08	71490
Mg I	383.23	47957
Pb I	261.42	46060
Al II	263.126	123470
Cu II	223.01	117928
Si I	252.41	39683
Si II	385.6	81251
Fe II	259.84	38858
Ca II	373.71	52166
Na I	588.96	16973
K I	769.83	12985

There are an infinite number of solutions for the equation with the formula of a function 1, as well as for systems composed of such equations. Based on this, one of the equations of the system should be normalizing, traditionally represented as the sum of the concentrations of all considered elements or elements oxides. The resulting system of equations with formula (2) was solved using the wxMaxima computer algebra system [23]:

$$\left\{ \begin{array}{l} a_1(C_1/C_2) + b_1 = I_1/I_2 \\ a_2(C_2/C_3) + b_2 = I_2/I_3 \\ a_3(C_3/C_4) + b_3 = I_3/I_4 \\ a_4(C_4/C_5) + b_4 = I_4/I_5 \\ a_5(C_5/C_6) + b_5 = I_5/I_6 \\ a_6(C_6/C_7) + b_6 = I_6/I_7 \\ a_7(C_7/C_8) + b_7 = I_7/I_8 \\ a_8(C_8/C_9) + b_8 = I_8/I_9 \\ C_1 + \dots + C_9 = 1 \end{array} \right. \quad (2)$$

For nine elements of the considered matrix, the set includes eight equations with ratios and one normalizing equation.

The solution of such equation set in the course of checking the operability of the method for enamel samples of known composition obtained in the laboratory allows us to calculate the concentrations of the matrix elements with an accuracy of  $\pm 6-8\%$ . In the case of archaeological samples, the composition was calculated for each point of spectrum registration in order to determine the uncertainty of the result. The obtained values of the concentrations of the matrix elements are presented in Table 4.

Table 4

## Composition of archaeological samples according to LTE-based data

Sample	SiO <sub>2</sub>	PbO	CaO	MgO	K <sub>2</sub> O	Na <sub>2</sub> O	Al <sub>2</sub> O <sub>3</sub>	CuO	Fe <sub>2</sub> O <sub>3</sub>
Sample 1 (Obr1)	56.43 ±6.21	28.84 ±4.04	5.89 ±1.18	1.92 ±0.33	3.84 ±0.69	6.06 ±1.21	1.18 ±0.30	0.34 ±0.05	0.10 ±0.02
Sample 3 (Obr3.1)	55.29 ±6.08	28.00 ±3.92	5.72 ±1.14	1.90 ±0.32	4.40 ±0.79	6.48 ±1.30	1.26 ±0.32	0.34 ±0.05	0.15 ±0.02
Sample 4 (Obr4)	55.29 ±6.08	27.16 ±3.80	5.78 ±1.16	1.90 ±0.32	3.76 ±0.68	6.54 ±1.31	1.43 ±0.36	0.36 ±0.06	0.10 ±0.02
Sample 5 (Obr5)	58.71 ±6.46	29.12 ±4.08	5.67 ±1.13	2.00 ±0.34	3.92 ±0.71	6.60 ±1.32	1.34 ±0.33	0.36 ±0.06	0.16 ±0.02
Sample 6 (Obr6)	55.29 ±6.08	30.80 ±4.31	6.05 ±1.21	2.00 ±0.34	4.16 ±0.75	6.42 ±1.28	1.38 ±0.34	0.29 ±0.06	0.19 ±0.02
Sample 7 (Obr2007)	60.42 ±6.65	26.88 ±3.76	5.67 ±1.13	2.06 ±0.35	3.96 ±0.71	5.94 ±1.19	1.31 ±0.33	0.37 ±0.06	0.11 ±0.02

Calculated error of the results for the mass fractions of oxides is 15–24 % that can be considered a good result for the LIBS in the absence of sample preparation. At the same time, it seemed possible to improve the accuracy of spectrum analysis using a chemometric data processing method. Based on the literature data, the projection onto latent structures (PLS) method was chosen as giving good results in most spectrometric studies [24]. The calculations were carried out in the “R” programming environment.

Table 5

## Composition of archaeological samples according to PLS data

Sample	SiO <sub>2</sub>	PbO	CaO	MgO	K <sub>2</sub> O	Na <sub>2</sub> O	Al <sub>2</sub> O <sub>3</sub>	CuO	Fe <sub>2</sub> O <sub>3</sub>
Sample 1 (Obr1)	54.72 ±5.47	26.73 ±2.94	5.62 ±0.79	2.08 ±0.27	5.70 ±0.74	4.70 ±0.66	1.44 ±0.36	0.35 ±0.03	0.01 ±0.01
Sample 3 (Obr3.1)	55.29 ±5.53	28.08 ±3.09	5.57 ±0.78	2.04 ±0.26	5.82 ±0.76	4.95 ±0.69	1.74 ±0.44	0.35 ±0.03	0.02 ±0.01
Sample 4 (Obr4)	57.57 ±5.76	27.00 ±2.97	5.25 ±0.73	2.14 ±0.28	5.94 ±0.77	5.45 ±0.76	1.66 ±0.42	0.36 ±0.03	0.01 ±0.01
Sample 5 (Obr5)	59.28 ±5.93	26.46 ±2.91	5.19 ±0.73	2.12 ±0.28	6.54 ±0.85	5.10 ±0.71	1.76 ±0.44	0.36 ±0.03	0.02 ±0.01
Sample 6 (Obr6)	59.85 ±5.99	26.19 ±2.88	5.04 ±0.70	2.21 ±0.29	6.06 ±0.79	5.15 ±0.72	1.50 ±0.38	0.35 ±0.03	0.01 ±0.01
Sample 7 (Obr2007)	56.43 ±5.64	27.54 ±3.03	5.04 ±0.70	2.04 ±0.26	5.40 ±0.70	5.10 ±0.71	1.65 ±0.41	0.37 ±0.03	0.01 ±0.01

As can be seen from Table 5, the error in the results of 4 parallel determinations was 9–14 %. It should be noted that when testing the PLS model on samples of known composition prepared artificially, the accuracy was much higher, and the error did not exceed 4 %. Therefore, the greatest contribution to the inaccuracy of the quantitative composition determination was made not by calculations, but by the lack of the possibility of sample preparation and registration of the spectrum with significant destruction of the sample.

### Conclusions

In this work, LTE thermodynamic and PLS chemometric approaches have been proposed and tested for quantitative analysis of samples using their obtained spectra. The error for each element was 15–24 % when using the LTE hypothesis approach. The chemometric approach with the use of PLS has improved the accuracy. In this case, the error for the results of 4 parallel experiments was 9–14 %. As a result of the studies carried out by the LIBS method using calculation methods based on the LTE hypothesis and the chemometric approach, the qualitative and semi-quantitative composition of the enamel of tiles from the ancient settlement of Jochi Khan was determined. It was shown that the archaeological samples are lead-silicate glass with a high potassium content, which can only be explained by its purposeful introduction into the charge. Presumably, potassium could have been introduced by using the ashes of local plants.

Classification analysis identified two groups of samples that are similar in chemical composition, therefore, made from the same raw materials. This may provide additional information on the chronology of the settlement's construction. The study also revealed that contemporary restorers used a similar enamel composition, but used tin compounds for opacification.

### Acknowledgements

We are grateful to the Sembi M.K. historian, the staff of the National Historical, Cultural and Natural Reserve-Museum “Ulytau” Shaigozina B.Sh., Baimaganbetova B.B. for the help in receiving the materials.

### References

- 1 Cremers D.A. Handbook of Laser-Induced Breakdown Spectroscopy. (2nd ed.) / D.A. Cremers, L.J. Radziemski. — Hoboken, NJ: John Wiley & Sons, 2013. — 432 p.
- 2 Basic Chemometric Techniques in Atomic Spectroscopy / Eds. J.M. Andrade-Garda. — London: RSC Publishing, 2009. — 300 p.
- 3 Zhang T.L. Progress of Chemometrics in Laser-induced Breakdown Spectroscopy / T.L. Zhang, S. Wu, H.S. Tang, K. Wang, Y.X. Duan, H. Li // Chinese Journal of Analytical Chemistry. — 2015. — Vol. 43. — P. 939–948.
- 4 Li L.N. A review of artificial neural network based chemometrics applied in laser-induced breakdown spectroscopy analysis. / Li L.N., Liu, X.-F., Yang, F., Xu, W.-M., Wang, J.-Y., Shu, R. // Spectrochim. Acta Part B: Atomic Spectroscopy. — 2021. — Vol. 180, article id. 106183. <https://doi.org/10.1016/j.sab.2021.106183>.
- 5 Zhang T.L. Chemometrics in laser-induced breakdown spectroscopy / T.L. Zhang, Tang, H. Li // Journal of Chemometrics. — 2018. — Vol. 32, Issue 11. — e2983. <https://doi.org/10.1002/H.S.cem.2983>.
- 6 Hahn D.W. Laser-Induced Breakdown Spectroscopy (LIBS), Part I: Review of Basic Diagnostics and Plasma-Particle Interactions: Still-Challenging Issues Within the Analytical Plasma Community / D.W. Hahn, N. Omenetto // Appl Spectrosc. — 2010. — Vol. 64(12). — P. 335A–366A. <https://doi.org/10.1366/000370210793561691>.
- 7 Tate J. Some problems in analysing museum material by nondestructive surface sensitive techniques / J. Tate // Nuclear Instruments and Methods in Physics Research Section B: Beam Interactions with Materials and Atoms. — 1986. — Vol. 14(1). — P. 20–23. [https://doi.org/10.1016/0168-583x\(86\)90417-9](https://doi.org/10.1016/0168-583x(86)90417-9).
- 8 Anglos D. Laser-Induced Breakdown Spectroscopy in Art and Archaeology / D. Anglos // Applied Spectroscopy. — 2001. — Vol. 55(6). — P. 186A–205A. <https://doi.org/10.1366/0003702011952398>.
- 9 Panyushkina I.P. Chronology of the Golden Horde in Kazakhstan: <sup>14</sup>C Dating of Jochi Khan Mausoleum / I.P. Panyushkina, E.R. Usmanova, K.Z. Uskenbay, M.B. Kozha, D.A. Dzhumabekov, G.A. Akhatov, A.T. Jull // Radiocarbon. — 2022. — Vol. 10, No. 24. — P. 1–9. <https://doi.org/10.1017/RDC.2022.24>.
- 10 Fomin V.N. Chemical-technological analysis of slags from the “Altynshoky” complex / V.N. Fomin, E.R. Usmanova, R.M. Zhumashev, A.V. Pokussayev, G. Motuza, Kh.B. Omarov, et al. // Bulletin of the University of Karaganda Chemistry. — 2018. — № 3 (91). — С. 64–73. <https://doi.org/10.31489/2018Ch3/64-73>
- 11 Фомин В.Н. Оптимизация параметров лазерно-искрового эмиссионного спектрометра с применением вероятностно-детерминированного планирования эксперимента / В.Н. Фомин, С.К. Алдабергенова, К.Т. Рустембеков, Х.Б. Омаров, И.Е. Рожковой, А.В. Дик, Д.М. Саулебеков // Заводская лаборатория. Диагностика материалов. — 2021. — № 87 (5). — С. 14–19. <https://doi.org/10.26896/1028-6861-2021-87-5-14-19>.
- 12 Kramida A. NIST Atomic Spectra Database (version 5.9) Retrieved from <https://physics.nist.gov/asd> [Tue Feb 22 2022]. / A. Kramida, Yu. Ralchenko, J. Reader and NIST ASD Team. — Gaithersburg, MD: National Institute of Standards and Technology, 2021. <https://doi.org/10.18434/T4W30F>.
- 13 R Core Team. R: A language and environment for statistical computing. R Foundation for Statistical Computing. — 2021. Vienna, Austria. <https://www.R-project.org/>.
- 14 Korneev V.A. Method of standardless quantitative emission spectral analysis in criminalistic, expert legal, and forensic medical practice / V.A. Korneev, V.K. Ivanov, A.M. Pcheintsev, T.F. Odinochkina, A.V. Agrafenin // Journal of Applied Spectroscopy. — 1990. — Vol. 52. — P. 4.
- 15 Wold S. PLS-regression: a basic tool of chemometrics / S. Wold, M. Sjöstöm, L. Eriksson // Chemometrics and Intelligent Laboratory Systems. — 2001. — Vol. 58, No. 2. — P.109–130, [https://doi.org/10.1016/S0169-7439\(01\)00155-1](https://doi.org/10.1016/S0169-7439(01)00155-1).
- 16 Mevik B.H. The pls package: Principal component and partial least squares regression in R / B.H. Mevik, R. Wehrens // Journal of Statistical Software. — 2007. — Vol.18, No. 2. — P. 1–24.
- 17 Абдуразаков А.А. Химические составы керамики и глазурей архитектурных памятников Узбекистана / А.А. Абдуразаков // История материальной культуры Узбекистана. — 1987. — Вып. 21. — С. 176–189.
- 18 Малышев В.П. Вероятностно-детерминированное планирование эксперимента / В.П. Малышев. — Алматы: Наука. — 1981. — 115 с.
- 19 Беляев С.В. Пути развития вероятностно-детерминированного планирования эксперимента / С.В. Беляев, В.П. Малышев // Комплексная переработка минерального сырья Казахстана. Состояние, проблемы, решения: [В 10 т]. — Т. 9. Информационные технологии в минерально-сырьевом комплексе. — Гл. 8. — Алматы, 2008. — С. 599–633.

20 Fomin V.N. Method for increasing the accuracy of quantitative determination of iron by LIBS / V.N. Fomin, S.K. Aldabergenova, K.T. Rustembekov, A.V. Dik, Yu.Yu. Kim, I.E. Rozhkovoy // Bulletin of the University of Karaganda Chemistry. — 2018. — No. 3(91). — P. 74–83. <https://doi.org/10.31489/2018Ch3/74-83>

21 Fomin V.N. Optimization of coal tar gas chromatography conditions using probabilistic-deterministic design of experiment / V.N. Fomin, A.A. Aynabaev, D.A. Kaykenov, D.T. Sadyrbekov, S.K. Aldabergenova, M.A. Turovets, N.K. Kelesbek // Bulletin of the University of Karaganda Chemistry. — 2021. — No. 4(104). — P. 39–46. <https://doi.org/10.31489/2021Ch4/39-46>.

22 Фомин В.Н. Использование многофакторных переменных в вероятностно-детерминированном планировании эксперимента / В.Н. Фомин, А.А. Ковалева, С.К. Алдабергенова // Вестн. Караганд. ун-та. Сер. Химия. — 2017. — № 3 (87). — С. 91–100.

23 Maxima, a Computer Algebra System. Version 5.46.0 (2022). <https://maxima.sourceforge.io/>.

24 Kucheryavskiy S. Mdatools — R package for chemometrics. / S. Kucheryavskiy // Chemometrics and Intelligent Laboratory Systems. — Vol. 198. — 2020. <https://doi.org/10.1016/j.chemolab.2020.103937>.

В.Н. Фомин, Э.Р. Усманова, Э.Ф. Гюль, Н.К. Келесбек,  
М.А. Туровец, О.И. Земский, Д.М. Саулебеков, С.К. Алдабергенова

### Лазерлік ұшқын эмиссиялық спектроскопия көмегімен құрамында қорғасыны бар археологиялық қорғасын эмалын сапалық және сандық талдау әдісі

Жошы хан қалашығының (XIV ғ.) эмаль археологиялық үлгілерін талдау үшін лазерлік ұшқын эмиссиялық спектроскопия (ЛҰЭС) әдісі қолданылды. Сапалық талдау барысында эмаль құрамының негізгі элементтері Si, Pb, K, Na, Mg, Ca, Al екені анықталды. Глазурьдің түсі мыс пен темірдің болуына байланысты. Орташалау әдісімен кластерлеу барысында эмальдің құрамына ұқсас, бірақ қалашық ішінде шыққан жері бойынша ерекшеленетін екі үлгі тобы анықталды. ЛҰЭС спектрлері бойынша жергілікті термодинамикалық тепе-теңдік (ЖТТ) гипотезасына негізделген әдісті және хемометриялық тәсілді (жасырын құрылымдарға проекция, ЖҚП) қолдана отырып, қарастырылған үлгілерде глазурьдің жартылай сандық құрамы айқындалды. Спектрді тіркеу шарттары өзгерген кезде өзгеріске ұшырамайтын элементтер түзуінің жұптарын іздеу және ЖТТ негізіндегі теңдеулердегі коэффициенттерді анықтау үшін эксперименттің ықтималдық-детерминирленген жоспарлауы қолданылады. ЖҚП әдісі бойынша есептеулер «R» ортасында жүргізілді. Тұрақты оксидтерге қайта есептегенде негіз элементтердің мөлшері: құрамындағы % мынадай: SiO<sub>2</sub> — 49–61, PbO — 23–31, MgO — 1.7–2.3, CaO — 4.6–6.9, Na<sub>2</sub>O — 4.1–5.3, K<sub>2</sub>O — 5.1–6.4, Al<sub>2</sub>O<sub>3</sub> — 0.8–1.7, CuO — 0.32–0.4, Fe<sub>2</sub>O<sub>3</sub> — 0.09–0.16. Екі әдістің де нәтижелері бір-біріне сәйкес келеді. ЖТТ үшін төрт параллель анықтама арасындағы айырмашылық 15–24 %, ЖҚП үшін 9–14 % құрады. Жартылай сандық талдау деректерін ескере отырып, екі топқа бөлінуінің негізінде эмальдағы мыс пен темірдің әртүрлі қатынасы жатыр деген қорытынды жасалған.

*Кілт сөздер:* ЛҰЭС, химометрика, кластерлік талдау, ЖҚП, жеңіл балқитын қорғасын эмальдары, экспериментті ықтималдық-детерминирленген жоспарлау, археология, Жошы хан қалашығы.

В.Н. Фомин, Э.Р. Усманова, Э.Ф. Гюль, Н.К. Келесбек,  
М.А. Туровец, О.И. Земский, Д.М. Саулебеков, С.К. Алдабергенова

### Метод качественного и количественного анализа свинцовой археологической эмали с использованием лазерной искровой эмиссионной спектроскопии

Метод лазерно-искровой эмиссионной спектроскопии (ЛИЭС) применен для анализа археологических образцов эмали с городища Джучи хана (XIV в.). В ходе качественного анализа показано, что элементами основы эмали являются Si, Pb, K, Na, Mg, Ca, Al. Окраска глазури обусловлена присутствием меди и железа. Кластеризацией методом *k* средних было выявлено две группы образцов, сходных по составу эмали, но отличающихся по месту происхождения внутри городища. С применением метода, основанного на гипотезе локального термодинамического равновесия (ЛТР), и хемометрического подхода (проекция на латентные структуры, ПЛС) по спектрам ЛИЭС установлен полуколичественный состав глазури на рассмотренных образцах. Для поиска пар линий элементов, не подверженных изменениям при изменении условий регистрации спектра, и определения коэффициентов в уравнениях, основанных на ЛТР, использовано вероятностно-детерминированное планирование эксперимента. Расчеты по методу ПЛС проведены в среде «R». Содержание элементов основы в пересчете на наиболее устойчивые оксиды составило, %: SiO<sub>2</sub> — 49–61, PbO — 23–31, MgO — 1.7–2.3, CaO — 4.6–

6.9, Na<sub>2</sub>O — 4.1–5.3, K<sub>2</sub>O — 5.1–6.4, Al<sub>2</sub>O<sub>3</sub> — 0.8–1.7, CuO — 0.32–0.4, Fe<sub>2</sub>O<sub>3</sub> — 0.09–0.16. Результаты обоих методов, в целом, согласуются между собой. Расхождения между 4-мя параллельными определениями для ЛТР составили 15–24 %, для ПЛС 9–14 %. С учетом данных полуколичественного анализа сделан вывод о том, что в основе разделения на две группы лежит разное соотношение меди и железа в эмали.

*Ключевые слова:* ЛИЭС, хемометрика, кластерный анализ, ПЛС, легкоплавкие свинцовые эмали, вероятностно-детерминированное планирование эксперимента, археология, городище Джучи хана.

## References

- 1 Cremers, David & Radziemski, Leon. (2013). *Handbook of Laser-Induced Breakdown Spectroscopy*: Second Edition. Hoboken, NJ: John Wiley & Sons. <https://doi.org/10.1002/9781118567371>
- 2 Andrade-Garda, J.M. (Eds.) (2009). *Basic Chemometric Techniques in Atomic Spectroscopy*. London: RSC Publishing.
- 3 Zhang, T.-L., Wu, S., Tang, H.-S., Wang, K., Duan, Y.-X., & Li, H. (2015). Progress of Chemometrics in Laser-induced Breakdown Spectroscopy. *Chinese Journal of Analytical Chemistry*, 43, 6, 939-948. [https://doi.org/10.1016/S1872-2040\(15\)60832-5](https://doi.org/10.1016/S1872-2040(15)60832-5)
- 4 Li, L.N., Liu, X.-F., Yang, F., Xu, W.-M., Wang, J.-Y., & Shu, R. (2021). A review of artificial neural network based chemometrics applied in laser-induced breakdown spectroscopy analysis. *Spectrochim, Acta Part B: Atomic Spectroscopy*, 180, article id. 106183. <https://doi.org/10.1016/j.sab.2021.106183>
- 5 Zhang, T.L., Tang, H.-S., & Li, H. (2018). Chemometrics in laser-induced breakdown spectroscopy. *Journal of Chemometrics*, 32, 11. <https://doi.org/10.1002/cem.2983>
- 6 Hahn, D.W., & Omenetto, N. (2010). Laser-Induced Breakdown Spectroscopy (LIBS), Part I: Review of Basic Diagnostics and Plasma-Particle Interactions: Still-Challenging Issues Within the Analytical Plasma Community. *Appl Spectrosc*, 64(12), 335A-366A. <https://doi.org/10.1366/000370210793561691>
- 7 Tate, J. (1986). Some problems in analysing museum material by nondestructive surface sensitive techniques. *Nuclear Instruments and Methods in Physics Research Section B: Beam Interactions with Materials and Atoms*, 14(1), 20–23. [https://doi.org/10.1016/0168-583x\(86\)90417-9](https://doi.org/10.1016/0168-583x(86)90417-9)
- 8 Anglos, D. (2001). Laser-Induced Breakdown Spectroscopy in Art and Archaeology. *Applied Spectroscopy*, 55(6), 186A-205A. <https://doi.org/10.1366/0003702011952398>
- 9 Panyushkina, I.P., Usmanova, E.R., Uskenbay, K.Z., Kozha, M.B., Dzhumabekov, D.A., Akhatov, G.A., & Jull, A.T. (2022) Chronology of the Golden Horde in Kazakhstan: <sup>14</sup>C Dating of Jochi Khan Mausoleum. *Radiocarbon*, 10, 24, 1–9. <https://doi.org/10.1017/RDC.2022.24>
- 10 Fomin, V.N., Usmanova, E.R., Zhumashev, R.M., Pokussayev, A.V., Motuza, G., & Omarov, Kh.B., et al. (2018). Chemical-technological analysis of slags from the “Altynshoky” complex. *Bulletin of the University of Karaganda Chemistry*, 3(91), 64–73. <https://doi.org/10.31489/2018Ch3/64-73>
- 11 Fomin, V.N., Aldabergenova, S.K., Rustembekov, K.T., Omarov, Kh.B., Rozhkovoy, I.E., Dik, A.V., & Saulebekov, D.M. (2021). Optimizatsiia parametrov lazerno-iskrovogo emissionnogo spektrometra s primeneniem veroiatnostno-determinirovannogo planirovaniia eksperimenta [Optimization of the parameters of a laser induced breakdown spectrometer (LIBS) using probabilistic-deterministic design of experiment]. *Zavodskaiia laboratoria. Diagnostika materialov. Industrial laboratory. Diagnostics of materials*, 87(5), 14–19. <https://doi.org/10.26896/1028-6861-2021-87-5-14-19> [in Russian].
- 12 Kramida, A., Ralchenko, Yu., & Reader, J. and NIST ASD Team (2021). NIST Atomic Spectra Database (version 5.9), Retrieved from <https://physics.nist.gov/asd> [Tue Feb 22 2022]. National Institute of Standards and Technology, Gaithersburg, MD. <https://doi.org/10.18434/T4W30F>.
- 13 R Core Team (2021). R: A language and environment for statistical computing. R Foundation for Statistical Computing, Vienna, Austria. URL <https://www.R-project.org/>
- 14 Korneev, V.A., Ivanov, V.K., Pcheintsev, A.M., Odinochkina, T.F., & Agrafenin, A.V. (1990) Method of standardless quantitative emission spectral analysis in criminalistic, expert legal, and forensic medical practice. *Journal of Applied Spectroscopy*, 52, 4.
- 15 Wold, S., Sjöström, M., & Eriksson L. (2001). PLS-regression: a basic tool of chemometrics. *Chemometrics and Intelligent Laboratory Systems*, 58, 2, 109–130, [https://doi.org/10.1016/S0169-7439\(01\)00155-1](https://doi.org/10.1016/S0169-7439(01)00155-1)
- 16 Mevik, B.H., & Wehrens, R. (2007). The pls package: Principal component and partial least squares regression in R. *Journal of Statistical Software*, 18, 2, 1–24.
- 17 Abdurazakov, A.A. (1987). Khimicheskie sostavy keramiki i glazurei arkhitekturnykh pamiatnikov Uzbekistana [Chemical compositions of ceramics and glazes of architectural monuments of Uzbekistan]. *Istoriia materialnoi kultury Uzbekistana — History of Material Culture of Uzbekistan*, 22, 176–189 [in Russian].
- 18 Malyshev, V.P. (1981). *Veroiatnostno-determinirovannoe planirovanie eksperimenta [Probabilistic-deterministic mapping]*. Almaty: Nauka [in Russian]
- 19 Beliaev, S.V., & Malyshev, V.P. (2008). Puti razvitiia veroiatnostno-determinirovannogo planirovaniia eksperimenta [Ways of stochastic-determined design of experiments development]. (Vols. 1-10; Vol. 9): *Informatsionnye tekhnologii v mineralno-syrievom komplekse — Information technologies in the mineral-raw complex*, 8, Almaty [in Russian].

- 20 Fomin, V.N., Aldabergenova, S.K., Rustembekov, K.T., Dik, A.V., Kim, Yu.Yu., & Rozhkovoy, I.E. (2018). Method for increasing the accuracy of quantitative determination of iron by LIBS. *Bulletin of the University of Karaganda Chemistry*, 3(91), 74–83. <https://doi.org/10.31489/2018Ch3/74-83>.
- 21 Fomin, V.N., Aynabaev, A.A., Kaykenov, D.A., Sadyrbekov, D.T., Aldabergenova, S.K., Turovets, M.A., & Kelesbek, N.K. (2021). Optimization of coal tar gas chromatography conditions using probabilistic-deterministic design of experiment. *Bulletin of the University of Karaganda Chemistry*, 4(104), 39–46. <https://doi.org/10.31489/2021Ch4/39-46>.
- 22 Fomin, V.N., Kovaleva, A.A., & Aldabergenova, S.K. (2017). Using multivariate variables in probabilistic-deterministic design of experiments. *Bulletin of the University of Karaganda Chemistry*, 3(87), 91–100.
- 23 *Maxima, a Computer Algebra System. Version 5.46.0* (2022). Retrieved from <https://maxima.sourceforge.io/>
- 24 Kucheryavskiy, S. (2020). *Mdatools — R package for chemometrics. Chemometrics and Intelligent Laboratory Systems*, 198, <https://doi.org/10.1016/j.chemolab.2020.103937>.

### Information about authors\*

**Fomin, Vitaly Nikolaevich** — Candidate of chemical sciences, head of LEP “PCMI” of Karagandy University of the name of academician E.A. Buketov, Universitetskaya street, 28, 100024, Karaganda, Kazakhstan; e-mail: [vitaliynikolaevich.fomin@mail.ru](mailto:vitaliynikolaevich.fomin@mail.ru); <https://orcid.org/0000-0002-2182-2885>

**Gyul, Elmira Fathlbayanovna** — Doctor of Arts, Professor, Institute of Art History of the Academy of Sciences of the Republic of Uzbekistan, Mustakillik, 2, Tashkent, Uzbekistan; e-mail: [egyul@yahoo.com](mailto:egyul@yahoo.com); <https://orcid.org/0000-0001-9445-5601>

**Usmanova, Emma Radikovna** — Leading Researcher, Karagandy University of the name of academician E.A. Buketov, Universitetskaya street, 28, 100024, Karaganda, Kazakhstan; South Ural State University, Lenina, 76, Chelyabinsk, Russia, e-mail: [emmadervish2004@mail.ru](mailto:emmadervish2004@mail.ru); <https://orcid.org/0000-0003-1625-5086>

**Kelesbek, Nabira Kydyrbekkyzy** — 3st year PhD student, Department of Inorganic and Technical Chemistry, Karagandy University of the name of academician E.A. Buketov, Universitetskaya street, 28, 100024, Karaganda, Kazakhstan; e-mail: [knk\\_93@bk.ru](mailto:knk_93@bk.ru); <https://orcid.org/0000-0002-8578-8081>

**Turovets, Milana Alexandrovna** — 1st year master student, Department of Physical and Analytical Chemistry, Karagandy University of the name of academician E.A. Buketov, Universitetskaya street, 28, 100024, Karaganda, Kazakhstan; e-mail: [turovec26.07@mail.ru](mailto:turovec26.07@mail.ru); <https://orcid.org/0000-0002-0493-6426>

**Zemskij, Oleg Igorevich** — 2st year master student, Department of Inorganic and Technical Chemistry, Karagandy University of the name of academician E.A. Buketov, Universitetskaya street, 28, 100024, Karaganda, Kazakhstan; e-mail: [Zemskiy1999@list.ru](mailto:Zemskiy1999@list.ru); <https://orcid.org/0000-0003-1429-2174>

**Saulebekov, Daniyar Mejrambekovich** — 2st year master student, Department of Inorganic and Technical Chemistry, Karagandy University of the name of academician E.A. Buketov, Universitetskaya street, 28, 100024, Karaganda, Kazakhstan; e-mail: [ironhide\\_99@bk.ru](mailto:ironhide_99@bk.ru); <https://orcid.org/0000-0001-5569-6832>

**Aldabergenova, Saule Kidirbaevna** (*corresponding author*) — Candidate of chemical sciences, Associate Professor, Karagandy University of the name of academician E.A. Buketov, Universitetskaya street, 28, 100024, Karaganda, Kazakhstan; e-mail: [aldsau@mail.ru](mailto:aldsau@mail.ru); <https://orcid.org/0000-0002-4262-911X>

\*The author's name is presented in the order: *Last Name, First and Middle Names*

## INORGANIC CHEMISTRY

Review

Received: 20 July 2022 | Revised: 03 November 2022 | Accepted: 11 November 2022 | Published online: 30 November 2022

UDC 66.097.3

<https://doi.org/10.31489/2022Ch4/4-22-17>

S.M. Zulfugarova\*, G.R. Azimova, Z.F. Aleskerova, Yu.N. Litvishkov, D.B. Tagiyev

*Institute of Catalysis and Inorganic Chemistry named after academician Murtuza Naghiyev, Baku, Azerbaijan Republic*

(\*Corresponding author's e-mail: [zsm07@mail.ru](mailto:zsm07@mail.ru))

### Synthesis of Transition Metal Ferrites (Co, Cu, Ni, Mn) by the Sol-Gel Method with Combustion and the Use of Microwave Processing

This review considers recent work on the synthesis of transition metal ferrites (Co, Cu, Ni, Mn) by sol-gel method with combustion, as well as the effect of microwave radiation. Ferrites are interesting not only for magnetic and optical properties, but also for their catalytic ones. In recent years, there has been an increasing amount of literature, which investigates the catalytic properties of transition metal ferrites in various reactions, including oxidative reactions. Given the fact that various organic components are used as complexing agents and as a fuel in the sol-gel method with combustion, the review considers the influence of the organic reagent nature, its ratio to precursors, the pH of the medium, the power and time of microwave exposure to the process of ferrite formation as factors influencing the size of formed particles and their textural characteristics, which are of great importance in the catalysis. Recently, the attention of chemists working in the field of catalysis has been attracted by studies of the effect of physical fields, to which the microwave field belongs, on various chemical processes, including the nanocatalysts synthesis. The use of microwave radiation in sol-gel synthesis of ferrite allows obtaining nanoferrites with high specific surface area. From this point of view, this paper considers the works of recent years devoted to the study of microwave sol-gel synthesis of ferrite.

**Keywords:** ferrites, sol-gel method with combustion, complexing agents, microwave technology, microwave power, dispersion, texture, specific surface area, particle size.

#### Content

List of abbreviations

Review Plan

Introduction

1. Synthesis of ferrites by the sol-gel method with combustion using citric acid as an organic reagent.

1.1. Synthesis of individual ferrites.

1.2. Synthesis of substituted ferrites.

2. Synthesis of ferrites using various organic reagents.

3. Synthesis of ferrites by the sol-gel method with combustion in “green chemistry”.

4. Textural parameters of ferrites synthesized by the sol-gel method with combustion.

5. Synthesis of ferrites by the sol-gel method with microwave combustion.

Conclusions

#### List of abbreviations

XRD — X-ray diffraction method

FESEM — Field Emission Scanning Electron Microscopy  
TEM — Transmission electron microscopy  
SEM — Scanning electron microscope  
EDS — Energy Dispersive X-Ray Spectroscopy  
FTIR — Fourier transform infrared spectroscopy  
TGA — Thermogravimetric analysis  
DTA — Differential Thermal Analysis  
BET — Brunauer-Emmett-Teller surface area analysis

#### *Review Plan*

*Inclusion and exclusion criteria:* The present review considers recent works on the synthesis of transition metal ferrites (Co, Cu, Ni, Mn), which are characterized by a wide range of applications, the sol-gel method with combustion, as well as the exposure to microwave radiation.

The review data are based on scientific publications of recent 7 years.

The review considers articles from the Scopus, Web of Science, Google Scholar databases.

The keywords used for the search are the “sol-gel method with combustion”, “copper, cobalt, nickel, manganese ferrites”, “microwave technology” and “texture”. Statistical methods were not used in the review.

#### *Introduction*

It should be noted that ferrite materials, which have special magnetic properties and combine high magnetization with the characteristics of semiconductors and dielectrics, are widely used in magnetic, electronic, and microwave devices [1–7]. In addition to their promising magnetic properties, ferrites have catalytic properties [1, 8–12]. Oxides, salts and hydroxides of appropriate metals are usually starting materials for producing ferrites. There are various ways to obtain ferrites, namely co-precipitation, thermal decomposition of salts, sol-gel method, ceramic, burning solutions in a high-temperature stream, plasma-chemical. To date, the sol-gel method has become widespread among the methods for obtaining highly dispersed materials, including nanoferrites. The main advantage of this method is the high homogenization of precursors with the production of a sol and its transformation into a gel due to hydrolysis and condensation processes, followed by aging, drying and heat treatment.

The variation of the sol-gel method is the sol-gel with self-combustion. The process of drying and heat treatment in this method takes place in one stage. The method includes an exothermic and self-sustaining redox reaction of xerogel, which is obtained from an aqueous solution containing metal salts (oxidizing agent) and an organic component (reducing agent) also known as a “fuel”. The organic component forms complexes with metal ions that prevents precipitation of metal salts and thereby improves gelation conditions. In addition to these advantages, owing to the results of the organic component combustion, a large amount of gaseous products is formed, which prevents the solid phase crystallites from sintering. The latter is obtained in the form of ash or a fine powder. The reaction proceeds quickly and at a sufficiently low temperature. The method is quite simple enough for practical implementation and economical in terms of time and energy consumption. Solutions can also be subjected to combustion, the so-called solution combustion.

In recent years, other than the thermal exposure, various types of radiation have also been used in the synthesis of compounds, in particular microwave [13–16]. Microwave technology has also found application in the synthesis of ferrites by the sol-gel method with combustion. Microwave technology is used in the synthesis of ferrites by the sol-gel method with combustion at the stage of drying and combustion. The literature data analysis shows that it is also possible to synthesize nanosized ferrites through the use of microwave radiation in the sol-gel method with combustion [17–22]. The brief review of recent works presents data on the synthesis of a number of ferrites (Co, Ni, Cu, Mn) by the sol-gel method with combustion, as well as using microwave treatment as an initiator of the combustion reaction, i.e. carrying out the combustion stage in the microwave field. The ferrites of these metals were chosen from the perspective of their use as catalysts. In recent years, more and more works have appeared in the literature in which the catalytic properties of transition metal ferrites in various reactions, including oxidative ones, are studied. For example, these are following reviews [8–10]. Previously, we carried out the microwave synthesis of these ferrites by the ceramic method from oxides [15]. The catalytic properties of copper ferrite synthesized by the ceramic and sol-gel method using microwave treatment were investigated by us in the oxidative conversion of carbon monoxide [23]. So this review focuses on the following issues:

Given the fact that various organic components are used as complexing agents and a fuel in the combustion sol-gel method, an emphasis is laid on the influence of the organic reagent nature on the formation of ferrites during combustion, as a factor affecting the size of the resulting ferrite particles and their textural indicators, which is of great importance in catalysis.

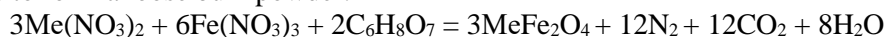
In microwave technology, the given parameters are power and time. It is important to find out how the time of microwave treatment affects the fineness of the formed ferrite particles when adjusted for the uncontrolled rise in temperature, using microwave energy in the sol-gel method with combustion.

#### *1. Synthesis of ferrites by the sol-gel combustion method using citric acid as an organic reagent*

An analysis of the literature data showed that the largest number of studies on the synthesis of both individual and mixed ferrites was carried out by the “citrate” method, i.e. using citric acid as a complexing agent and “fuel”. That is why it became necessary to summarize them in a separate section.

The process essence is the reaction of hydrolysis and condensation of precursors, which are metal nitrates and citric acid, resulting in the formation of gel, upon further drying of which it passes into xerogel, followed by its spontaneous combustion and the formation of ferrite during combustion.

The synthesis procedure is as follows: a stoichiometric amount of metal nitrates is dissolved in a small amount of deionized water with stirring and a temperature of 80–90 °C. The pH of the medium is adjusted to 7 with an ammonia solution and the solution is slowly evaporated until a viscous gel is formed which self-ignites and burns to form a loose bulk powder.



There were also considered works in which the ferrites synthesis was carried out by burning the solution.

#### *1.1. Synthesis of individual ferrites*

Although the ferrites formation at lower temperatures is one of the important advantages of the combustion sol-gel method, in many studies, the powders obtained after gel combustion are additionally annealed at higher temperatures. These are mainly works in which the magnetic properties of ferrites are investigated and where purity and high crystallinity are of great importance.

The synthesis of nanocrystalline cobalt ferrite was carried out in the works [24–26]. The powders obtained after burning the gel were additionally annealed at various temperatures from 600 °C to 900 °C for 2 h in air [24]. The particle size of the obtained ferrites strongly depends on the calcination temperature. At a temperature of 700 °C, the size of cobalt ferrite crystallites is 25–30 nm, they look like quasi-spheres. The crystallite sizes of the sample annealed at 900 °C are in the range of 40–50 nm, which is consistent with the results of X-ray diffraction (XRD) method. The authors suggest that the agglomeration increases as the annealing temperature increases, and some degree of agglomeration is unavoidable at higher annealing temperatures. The influence of the additional calcination temperature at 600, 700, and 800 °C on the structural and magnetic properties of  $\text{CoFe}_2\text{O}_4$  was also considered in [25]. The authors found that as the calcination temperature increased, clearly defined sharp peaks were observed on the X-ray pattern in line with  $\text{CoFe}_2\text{O}_4$  to indicate an increase in the ferrite crystallinity. Very pure and crystalline cobalt nanoferrite with a uniform size distribution was also obtained in [26].

Cobalt and copper ferrites obtained by the citrate method were characterized by X-ray diffraction method, Field Emission Scanning Electron Microscopy (FESEM), Transmission electron microscopy (TEM), Energy Dispersive X-Ray Spectroscopy) [6]. The average size of cobalt and copper nanoferrite crystallites was 24.7 and 37.7 nm, respectively.

The synthesis of nickel ferrite by the sol-gel method with combustion in the presence of citric acid was described in the works [27–31]. In the work [27], a mixed solution of nitrates (Ni and Fe) and citric acid was kept in an oven at 120 °C for 12 hours. The dried sample was ground and then annealed in a muffle furnace at 600 °C for 2 hours and slowly cooled to room temperature. X-ray diffraction analysis confirmed the formation of a cubic structure of nickel ferrite spinel. The average crystallite size was determined using the Debye-Scherrer formula and it was 21 and 60 nm, respectively, for the obtained samples before and after annealing. SEM analysis showed that the particles were spherical.

The authors [28] obtained nanoparticles of nickel ferrite with an average size of 23 nm calculated by the Scherrer formula.

In the work [30], the resulting powder after auto-combustion of the dried gel was also calcined at 550 °C for 4 hours for better crystallinity and purity. The average crystallite size of the prepared nickel ferrite sample was 22 nm.

In the work [29], the authors revealed that the resulting nickel ferrite particles had an approximately spherical shape and a crystal size in the range of 45–55 nm. The average grain size obtained from the TEM image of the sample was approximately 60 nm, which was in appropriate with the size determined from the X-ray diffraction patterns.

Nanosized spinel ferrites  $MFe_2O_4$  ( $M = Ni, Co$  and  $Zn$ ) were obtained in [31]. Gel ignition was observed at 623 K (350 °C). The resulting powder was sintered in two stages (at 500 °C/5 h and at 700 °C/5 h). The crystallite size (nm) for each sample was calculated from the broadening of the line of the most intense (311) diffraction peak using the Debye-Scherrer formula. It was found that sizes of crystallites depended on the nature of the  $M^{2+}$  cation. The lowest nanoscale crystallite value was found for nickel ferrite (30.6 nm), followed by zinc (34.4 nm) and cobalt (36.7 nm) ferrite.

Nickel ferrite was synthesized using various ratios of fuel (citric acid) to metal nitrate 1:1, 1:2, 1:3 and 1:4 [32]. All samples were characterized by Thermogravimetric (TG) and Differential Thermal (DT) analyzers. TG-DTA analysis confirmed the ferritization temperature, which varied slightly with the ratio of fuel to metal nitrate. All samples were sintered at an average temperature of 560 °C for 4 hours. X-ray diffraction analysis confirmed the cubic structure of the samples.

The authors [33–34] obtained copper and manganese ferrite particles with good composition uniformity and high phase purity.

### 1.2. Synthesis of substituted ferrites

When adjusted for the fact that mixed ferrites which are solid solutions, have the best magnetic characteristics, a promising method for their preparation is the sol-gel method with combustion. This is evidenced by quite a lot of works in the scientific literature dealing with the production of substituted ferrites by this method.

Consideration of these works is also important from the point of view of improving the catalytic properties of ferrites, in which atoms of other elements are introduced in a certain quantitative ratio.

A series of nanocrystalline copper-substituted cobalt-zinc ferrites  $Co_{0.6}Zn_{0.4}Cu_xFe_{2-x}O_4$  ( $x = 0.2, 0.4, 0.6, 0.8,$  and  $1.0$ ) with a cubic spinel crystal structure were synthesized by gel auto-combustion [35]. All samples after gel combustion were annealed at 400 °C, 600 °C, 800 °C and 1000 °C. X-ray diffraction analysis confirmed the formation of a cubic phase with space group  $Fd-3m$  for all nanoferrite obtained. The particles were 25 nm in size and spherical in shape. In this work, the same particle size of ferrite samples processed at different temperatures raises some doubts. High temperatures of heat treatment should undoubtedly lead to particle aggregation, which is noted in most works.

In the work [36], cobalt ferrite nanoparticles with substituted transition metals ( $CoM_xFe_{2-x}O_4$ ,  $M = Cr^{3+}, Ni^{2+}, Cu^{2+}$  and  $Zn^{2+}$ ,  $x = 0.2; 0.4; 0.6; 0.8$  and  $1.0$ ) were synthesized. The resulting ferrite powders were annealed at 400 °C, 600 °C, 800 °C and 1000 °C for 2 hours. TEM images of  $CoNi_{0.4}Fe_{1.6}O_4$  annealed at 400 °C and 1000 °C showed that ferrite particles had nano-sizes of 20 nm to 60 nm, respectively, and spherical morphology.

The authors [37] obtained nanoparticles of ferrites  $Co_{1-x}Ni_xFe_2O_4$  ( $x = 0.02, 0.04,$  and  $0.06 M$ ) with a spherical shape and a particle size in the range of 26.31–31.13 nm.

Ruthenium-doped cobalt ferrite nanoparticles ( $CoRu_xFe_{2-x}O_4$ ;  $x = 0.0, 0.02, 0.06$ ) were obtained in [38]. The average size of ferrite crystallites was 32.12 nm for  $CoFe_2O_4$ , 17.77 nm for  $CoRu_{0.02}Fe_{1.98}O_4$ , and 18.45 nm for  $CoRu_{0.06}Fe_{1.94}O_4$ .

The authors [39] synthesized polycrystalline nickel-substituted cobalt ferrites ( $Co_{1-x}Ni_xFe_2O_4$ , where  $x = 0, 0.25, 0.50, 0.75, 1$ ). From TEM images of samples after heat treatment at 700 °C for 8 h, it was found that the nanoparticles were uniform in size, which corresponded to the average size obtained from peak broadening in X-ray diffraction analysis. The effective diameter of ferrite powder particles was 20–25 nm.

Polycrystalline Ni-Zn ferrites with the chemical formula  $Ni_{0.5}Zn_{0.5}Zr_xCu_xFe_{2-2x}O_4$ , with  $x$  values from 0.0 to 0.4 and 0.08 wt.%, were prepared by the sol-gel method with auto-combustion with the addition of ethylene glycol to citric acid as an additional combustible agent (Table 1) [40].

It was determined that the size of crystals of complex ferrites  $Ni_{0.5}Co_{0.5}Nd_xFe_{2-x}O_4$ , obtained in the work was 41, 37 and 35 nm for  $x = 0.025; 0.100$  and  $0.125$ , respectively [41].

Polycrystalline ferrites with chemical formulas  $Ni_{0.5}Zn_{0.5}Fe_2O_4$ ,  $Ni_{0.5}Zn_{0.5}Er_{0.025}Fe_{1.975}O_4$ ,  $Ni_{0.5}Zn_{0.5}Er_{0.035}Fe_{1.965}O_4$ , and  $Ni_{0.5}Zn_{0.5}Er_{0.05}Fe_{1.95}O_4$  were obtained in [42]. The authors described in detail all ferrite synthesis process noting that it took less than 60 minutes from heating the sol to gelling it. And the time between the actual ignition and the end of the reaction was less than 5 seconds. An emphasis was laid

on the opportunity of using the combustion sol-gel method as a simple and affordable method for the synthesis of complex compounds.

Table 1

The sizes of the crystallite, particle and grain of Zr and Co substituted  $\text{Ni}_{0.5}\text{Zn}_{0.5}\text{Zr}_x\text{Co}_x\text{Fe}_{2-2x}\text{O}_4$ 

No.	Dopant concentration	Crystallite size, D (nm)	Particle size, (nm)	Grain size, ( $\mu\text{m}$ )
1	0.0	9.1121	15.5051	2.3137
2	0.08	10.9423	21.7809	3.043
3	0.16	10.2774	15.364	2.7436
4	0.24	10.1211	9.6893	2.6048
5	0.32	10.1474	4.1924	2.4618
6	0.4	10.3397	19.0597	2.2952

The average particle size of nickel–chromium ferrites with the general formula  $\text{NiCr}_x\text{Fe}_{2-x}\text{O}_4$  ( $x = 0.0; 0.1; 0.2; 0.3; 0.4$  and  $0.5$ ) was calculated using the Scherrer formula from the data on the broadening of diffraction peaks and amounted to 23–43 nm [43].

The authors [44] developed a method for obtaining solid solutions based on nickel-zinc ferrite of the general composition  $\text{Ni}_{0.75}\text{Zn}_{0.25}\text{Fe}_{2-x}\text{La}_x\text{O}_4$  ( $\text{Ln} = \text{Nd, Gd, Lu, Yb}$ ). Citric acid was taken in a ratio of 1:1 for trivalent elements and 3:2 for divalent ones. A solution of nitrates and citric acid was evaporated to a jelly-like state at a temperature of 700 °C for 1 hour. Then the temperature was raised to the start of a self-developing process ( $T = 100$  °C). The resulting powder was annealed at 700 °C until the remains of the organic phase were removed. The resulting reaction products were loose agglomerates consisting of nanoparticles. At an annealing temperature of samples up to 900 °C, coarsening of agglomerates and sintering of particles were observed. The average crystallite size for all synthesized compounds was 80–90 nm.

Samples of nickel-aluminum ferrites of the chemical composition  $\text{NiFe}_{2-x}\text{Al}_x\text{O}_4$  were obtained in [45]. Drying of the xerogel was carried out in air at a temperature of 120–130 °C. Upon complete drying, spontaneous combustion of the porous xerogel occurred. The average particle size found from X-ray diffraction studies was 20–60 nm.

## 2. Synthesis of ferrites using various organic reagents

In addition to citric acid, the sol-gel combustion method uses such organic compounds that are easily oxidized and do not contaminate the resulting product, namely glycine, urea, ethylene glycol, polyvinyl alcohol.

In the work [46] nanoparticles of cobalt ferrite  $\text{CoFe}_2\text{O}_4$  with a spinel structure were synthesized by the sol-gel method with auto-combustion using three different types of fuel (ethylene glycol, glycine and urea). The formation of a pure phase of cobalt ferrite with a cubic spinel structure was observed in X-ray diffraction patterns for all samples. The average crystallite size, lattice parameters and other structural parameters were calculated from XRD data. The experimental results showed that the average crystallite size of the prepared samples ranged from 15 to 22 nm. A lower average particle size of 15 nm was noted with urea as a fuel. The average grain size turned out to be in the range of 65–86 nm.

The influence of the ratio of fuel (glycine) to metal nitrates was considered in the work [47] when obtaining cobalt ferrite by the sol-gel method with combustion. The particle size of pure phase cobalt ferrite nanoparticles was found to be < 40 nm.

The authors of [48] synthesized cobalt ferrite ( $\text{CoFe}_2\text{O}_4$ ) nanoparticles using several different methods: combustion, co-precipitation and precipitation. The average particle size obtained by combustion with glycine was 69.5 nm, by co-precipitation it was 49.5 nm and by precipitation it was 34.7 nm.

Ethylene glycol as a complexing agent and fuel was used to obtain copper ferrite in the work [49].

Magnesium-cobalt spinels ( $\text{Co}_x\text{Mg}_{1-x}\text{Fe}_2\text{O}_4$ :  $x = 0.0, 0.2, 0.4, 0.6, 0.8$  and  $1.0$ ) were synthesized by the combustion sol-gel method using urea [50] as a fuel. The results showed that the final products were a cubic spinel phase with spherical nanoparticle morphology.

In our work [51], the copper ferrite was obtained using various organic reagents. It revealed that the average size of ferrite crystallites obtained using urea was in the range of 15–19 nm, with citric acid — 20–23 nm and with glycine — 29–32 nm. Dynamic light scattering (DLS) measurements of isopropyl dispersions of ferrite samples synthesized using citric acid, glycine and urea were also carried out. Before DLS

measurements, the dispersions with the studied samples were subjected to ultrasonic (US) treatment. Ultrasound treatment was carried out for 10, 20 and 60 min. The results showed that the spectral pattern significantly depended on the processing time of the dispersions. The average particle size of the synthesized samples in isopropyl alcohol dispersions subjected to ultrasonic treatment for 20 minutes ranged from 381 to 447 nm. Large values of the distribution width indicated that the dispersion contained aggregates of particles of different sizes. These values were much larger than the average crystallite size determined by X-ray diffractometry. Most likely, the studied dispersions contained aggregates that were not destroyed by ultrasonic treatment. After 60 minutes of sonication, the particle size decreased and fluctuated in the range of 123–153 nm.

The racemic mixture of the right (*d*) and left (*l*) forms of alpha-alanine was used in the work [52] for the synthesis of highly crystalline cobalt nanoferrite. The synthesized samples were annealed at two different temperatures, namely 500 °C and 800 °C for 2 hours to study the effect of temperature on crystallite size, phase purity and thermal stability. The formation of single-phase spinel nanoparticles was observed both in the initial state and in the annealed state. The size of cobalt ferrite nanoparticles after gel combustion was 37.8 nm, after sample annealing at 500 and 800 °C, 38.8 and 43.7 nm, respectively.

The effect of the ratio of glycine to oxidizing agent (metal nitrates) on the structural, morphological, and magnetic properties of  $\text{Co}_{0.8}\text{Mg}_{0.2}\text{Fe}_2\text{O}_4$  was studied in [53]. Samples were prepared with stoichiometric fuel content to nitrates ( $G/N=1.48$ ), lean fuel content ( $G/N=0.74$ ) and high fuel content ( $G/N=2.22$ ). After ignition at 180 °C and auto-combustion, the resulting powders were annealed at 600 °C for 2 hours. It was found that the crystallite size and the crystallinity of the spinel phase increased as  $G/N$  ratio increased (Table 2).

Table 2

**Effect of heat treatment and fuel-to-oxidizer ratio ( $G/N$ ) on the crystallite size nanoparticles (a) auto-combusted, (b) annealed at 600 °C**

No.	Fuel	Crystallite size, D (nm)	
1	2.22 (fuel rich)	50 (a)	62 (b)
2	1.48 (stoichiometry)	46 (a)	54 (b)
3	0.74 (fuel lean)	43 (a)	49 (b)

In the work [54] for the synthesis of  $\text{Y}_{0.2}\text{CoFe}_{1.8}\text{O}_4$ , citric acid and polyvinyl alcohol were used as a fuel. The average crystal size of the synthesized ferrite was in the range of 20–70 nm.

Ferros spinels of  $\text{CuFe}_2\text{O}_4$ ,  $\text{MgFe}_2\text{O}_4$ ,  $\text{Ni}_{0.5}\text{Co}_{0.5}\text{Fe}_2\text{O}_4$  composition were obtained using polyvinyl alcohol [55] as a fuel. Manganese ferrite was also obtained by the sol-gel method with the participation of polyvinyl alcohol [56].

As noted above, when synthesizing the compounds by the sol-gel combustion method, it is also possible to combust the solution. Therefore, works devoted to the production of ferrites by the solution combustion method are of interest [57–59].

Nanoparticles  $\text{CoFe}_2\text{O}_4$ ,  $\text{CoFe}_{1.95}\text{Bi}_{0.05}\text{O}_4$ ,  $\text{CoFe}_{1.9}\text{Bi}_{0.1}\text{O}_4$  and  $\text{Cu}_{0.5}\text{Co}_{0.5}\text{Fe}_{1.9}\text{Bi}_{0.1}\text{O}_4$  were prepared by burning a solution using glycine as a fuel [57]. Aqueous solutions of the calculated amounts of precursors and fuel, after stirring on a magnetic stirrer, were placed in an oven at 500 °C for 5 minutes.

Nanoparticles  $\text{Co}_{1-y}\text{Cu}_y\text{Fe}_{2-x}\text{Ce}_x\text{O}_4$  ( $x = 0, y = 0$ ), ( $x = 0.05, y = 0$ ), ( $x = 0, y = 0.5$ ) and ( $x = 0.05, y = 0.5$ ) were also synthesized by burning a solution of metal nitrates and glycine in a preheated furnace at 350 °C for 5–7 min, after which they were sintered at 700 and 900 °C for 2 h [58].

Especially, there is a need to note the work [59], which studied the influence of the “fuel” concentration on the composition, structure and size of crystallites in the synthesis of cobalt ferrite by solution combustion. Glycine was used as a fuel, cobalt and iron nitrates were used as precursors. The solution of precursors and glycine was placed in an electric oven (400 °C) until complete combustion (approximately 15 minutes) was formed. Three syntheses were carried out with different fuel concentrations, namely low, stoichiometric and high ones. The authors concluded that higher concentrations of glycine led to the formation of secondary phases of cobalt oxide. The sample with low fuel concentration was the only one in which a pure nanosized  $\text{CoFe}_2\text{O}_4$  phase was formed. Synthesis with an increased concentration of fuel led to rapid ignition and intense combustion during the reaction. With an excess of fuel, oxygen from the atmosphere was required to complete the reaction. This excess of oxygen could cause the formation of secondary oxide phases in addi-

tion to the primary cobalt ferrite phase. Sizes of crystallites were calculated using the Scherrer equation for various concentrations of glycine: 23.58 nm for low (smallest size among all samples), 31.14 nm for stoichiometric and 33.16 nm for high concentrations.

Thus, by varying the concentration of “fuel”, it is possible to attain both a pure ferrite phase and complex systems consisting of ferrite and oxide phases. The second variant is most interesting for the heterogeneous catalysis. During the combustion of both the sol and the gel, as a result of an exothermic reaction, various physicochemical transformations occur, namely melting, chemical reaction, diffusion, which affect the formation of the composition and structure and result in various defects. At present, the phenomenon of growth in the catalytic and adsorption activity of solids with a defective surface in comparison with the structure of a perfect crystal is considered an established fact [60]. Therefore, using various organic reagents and their concentrations in the combustion sol-gel method, it is possible to obtain not only highly crystalline ferrites, but also solid solutions of complex composition and defect structure, which are promising materials for the heterogeneous catalysis.

### 3. Synthesis of ferrites by the sol-gel method with combustion in “green chemistry”.

In recent years, works have appeared on the synthesis of ferrites by the sol-gel method with combustion, which belong to “green chemistry”. According to these works, extracts of various plants are used as an organic reagent and “fuel”. An example is the work [61], in which photocatalysts based on magnesium-doped nickel ferrite were synthesized by the sol-gel method using an extract from aloe *A.Vera* as a chelating agent, reducing agent and natural template. Stoichiometric amounts of nickel nitrate and iron nitrate were mixed with  $M^{3+}/M^{2+}$  in a molar ratio of 2:1, then a solution containing *A.Vera* extract and the calculated amount of magnesium nitrate was added dropwise. The mixture was continuously stirred for 1 hour at 80 °C until a gel formed. The resulting viscous gel was again heated to dry in an autoclave at 200 °C until auto-ignition started. Finally, the resulting  $NiFe_2O_4:Mg^{2+}$  (1 mol.%) nanoparticles were calcined at 350 °C for 1 h.

Cottage cheese was used as a fuel for the synthesis of cobalt ferrite with different contents of  $Zn^{2+}$  and the general formula  $[Zn_xCo_{1-x}Fe_2O_4]$  ( $x = 0.0, 0.2, 0.4$  and  $0.6$ ) the ZCF [62]. Solutions of metal nitrates and cottage cheese were continuously stirred for 30 min until a homogeneous mixture was obtained. The mixture was placed for 5 minutes in a muffle furnace heated to 500 °C. The resulting powder was calcined at 650 °C for about 5 hours.

A comparison of 2 methods for obtaining nickel ferrite nanoparticles, namely using citric acid and clove extract as a fuel was carried out in the work [63]. The structural properties of the resulting nickel ferrites were characterized by X-ray diffraction analysis, which revealed the cubic structure of the spinel. The average crystallite size was 24 nm and 26 nm for nanoparticles  $NiFe_2O_4$  obtained respectively through the use of clove extract and citric acid.

The use of environmentally friendly, non-toxic natural materials in the sol-gel method with combustion expands the opportunity of using it for the synthesis of complex compounds, including ferrites.

From the analysis of the literature data presented above on the synthesis of transition metal ferrites by the sol-gel method with combustion, the following conclusions can be drawn:

- Regardless of the complexing agent nature, the formation of a cubic spinel structure is observed in the X-ray diffraction patterns for all samples;
- Method makes it possible to obtain ferrite nano-powders with a crystallite size in the range of 20–60 nm. Moreover, the average crystallite size of particles increases with an increase in the calcination temperature of the nanopowders obtained after combustion.
- Use of higher (superstoichiometric) concentrations of the complexing agent makes it possible to form the secondary phases.
- Ferritization temperature varies slightly with the ratio of fuel to metal nitrate.

In most of the considered works, the structure and magnetic properties of the synthesized nanoferrites are mainly studied, which are of interest to physicists, since ferrites are used mainly as magnetic materials in radio engineering, electronics, automation and computer technology. Substances in the nanocrystalline state exhibit special magnetic and optical properties, which are not characteristic of bulk materials.

The determination only of nanosizes of ferrites can be sufficient when studying their magnetic properties; however, ferrites are also used in catalysis, where textural indicators play an important role, namely, specific surface area, pore volume, and pore radius. Therefore, the study of these parameters is extremely important in the study of the catalysts activity. This caused the need to highlight the works in which the texture characteristics of ferrites synthesized by the sol-gel method with combustion were studied, as well as

their dependence on the type of organic reagent, on the ratio of fuel to metals, since during the combustion of various types of “fuel”, different amounts of gases were released, which actually “loosen” the resulting mass of ferrite that also affected the texture of ferrites.

#### 4. Textural parameters of ferrites synthesized by the sol-gel method with combustion

In the work [64], Ni, Co, Mn, Mg, and Zn ferrites were synthesized by the gel combustion method with the participation of glycine. The sizes of the synthesized ferrite nanoparticles were determined, as well as their specific surface area (Table 3).

Table 3

**S<sub>BET</sub> — specific surface area, average crystallite size, D**

No.	Sample	S, m <sup>2</sup> /g	D, nm
1	NiFe <sub>2</sub> O <sub>4</sub>	72.0	20.5
2	CoFe <sub>2</sub> O <sub>4</sub>	15.4	20.4
3	MnFe <sub>2</sub> O <sub>4</sub>	54.4	5.8

Nickel ferrite had the largest specific surface area (72 m<sup>2</sup>/g) among Ni, Co, Mn ferrites obtained using glycine as an organic reagent, followed by manganese ferrite with a specific surface area of 54.4 m<sup>2</sup>/g and cobalt 15.4 m<sup>2</sup>/g.

Metal-substituted cobalt ferrite nanoparticles with the composition M<sub>x</sub>Co<sub>1-x</sub>Fe<sub>2</sub>O<sub>4</sub> (M = Zn, Cu, Mn; x = 0.0; 0.25; 0.5 and 0.75) were synthesized by the citrate sol-gel method in [65]. The specific surface of the samples was in the range from 37.99 to 107.05 m<sup>2</sup>/g, Zn<sub>0.5</sub>Co<sub>0.5</sub>Fe<sub>2</sub>O<sub>4</sub> nanoparticles had an average pore radius of 1.84 nm and a pore volume of 0.136 ml/g.

In the work [66], ferrites of the composition Cu<sub>0.5</sub>Ni<sub>0.5</sub>Fe<sub>2</sub>O<sub>4</sub> were prepared using various ratios between citric acid and metal ions. A number of secondary phases (Cu, Cu-Ni alloy and hematite) were found in the obtained samples. An optimal ratio of citric acid to the sum of metal ions was experimentally established, at which the resulting ferrite samples were characterized by the largest surface area. The sample synthesized at the maximum ratio of citric acid to metal ions (3:1) was characterized by the smallest size of ferrite crystallites (9.65 nm) and a larger surface area (92 m<sup>2</sup>/g).

The specific surface area of Ni-Zn-ferrite obtained by various “fuels” (citric acid, carbonylhydrazide and glycine) ranged from 12–41 m<sup>2</sup>/g [67].

Nickel ferrite powders of the composition NiFe<sub>2</sub>O<sub>4</sub> with a crystal size of 18.00 nm and a high specific surface area of 55.21 m<sup>2</sup>/g were obtained by a combustion reaction using urea as a fuel [68].

The effect of pH and metal concentration on the textural characteristics of the formed cobalt ferrite nanoparticles was considered in [69]. Xerogels obtained from solutions with different pH values (≤1, 3, 7, and 10) of precursors showed different combustion behavior. Except for pH (≤1), all xerogels quickly ignited with the formation of a large amount of gases: combustion began in the hottest zones of the crucible and spread from bottom to top, as in a volcanic eruption.

The reaction was over in 10–30 seconds with the formation of a dark gray three-dimensional structure resembling a branched tree. Table 4 lists the synthesis conditions, nanoparticle sizes and specific surface area of the cobalt ferrite synthesized.

Table 4

**Preparation parameters, BET surface area, XRD and BET average particle sizes of the sample**

No.	Sample	Preparation parameters		BET surface area (m <sup>2</sup> /g)	XRD average particle size (nm)	BET average particle size (nm)
		pH value	Metal concentration (mol L <sup>-1</sup> )			
1	A	7	0.1	38.6	24	29
2	B	7	0.2	37.9	26	30
3	C	7	0.3	31.2	28	36
4	D	<1	0.1	6.2	16	185
5	E	3	0.1	19.0	21	60
6	F	10	0.1	35.8	30	32

As can be seen from the Table 4, the specific surface area of nanoparticles formed from acidic solutions (samples D and E) was less than that of particles formed from neutral and alkaline solutions; they were also different in particle size.

Spinels  $\text{MeFe}_2\text{O}_4$ , in which the divalent cations Cu, Ni, Zn and Cd were synthesized by the sol-gel method with the participation of a 10 % solution of polyvinyl alcohol with a molecular weight of 145000 as a “fuel”, were obtained [70]. The size of the obtained nanoparticles was 33–52 nm. The texture parameters are presented in Table 5 below.

Table 5

**Powder characteristics of  $\text{MeFe}_2\text{O}_4$  ferrites**

Sample	Average agglomerat, size (nm)	Specific surface area, $S_{\text{BET}}$ ( $\text{m}^2/\text{g}$ )	Pore volume, cc/g
$\text{CuFe}_2\text{O}_4$	550	1.48	0.002
$\text{NiFe}_2\text{O}_4$	500	3.86	0.0059
$\text{CoFe}_2\text{O}_4$	350	3.26	0.0048

In the work [71] there was established the specific surface area of ferrites synthesized by the sol-gel method with auto-combustion using various organic reagents (Table 6).

Table 6

**Specific surface area of ferrites synthesized by the sol-gel method with various organic reagents**

No.	Ferrite	Specific surface area, $\text{m}^2/\text{g}$		
		citric acid	glycine	urea
1	$\text{CuFe}_2\text{O}_4$	18	4	25.5
2	$\text{CoFe}_2\text{O}_4$	12	11.7	35.3
3	$\text{NiFe}_2\text{O}_4$	6.2	7.8	34.3
4	$\text{MnFe}_2\text{O}_4$	36.5	15	32.9

As can be seen from Table 6, the ferrites obtained by the sol-gel method during the combustion with urea have the largest specific surface and the smallest — with glycine. When burning with citric acid, the final product is more voluminous and branched; the process does not last long. With glycine, the combustion occurs in the form of a flash and rapid combustion. With urea, the process takes longer with the release of a large amount of gaseous substances.

The above few works on the determination of the specific surface area of transition metal ferrites obtained by the sol-gel method with combustion involving various organic components make it possible to conclude that the nature of the organic reagent affects the specific surface area of the synthesized ferrites. It varies from a few square meters per gram to tens of square meters per gram. The different nature of combustion leads to the formation of different surface morphology and texture, which ultimately can affect the catalytic activity.

##### 5. Synthesis of ferrites by the sol-gel method with microwave combustion

During the synthesis of ferrites by the sol-gel method with combustion, microwave technology, as noted above, is used at the stage of drying and combustion. In a microwave oven, the parameters to be set are power and time. These parameters, along with the nature of the organic reagent, determine the surface morphology, texture, and fineness of the resulting ferrites.

In [72], the synthesis of cobalt ferrite doped with nickel was carried out using the method of microwave combustion of a solution using metal nitrates and urea as a reducing agent. Metal salts were dissolved in water; urea was added and homogenized on a magnetic stirrer. The combustion reaction was carried out in a domestic microwave oven at its maximum value for 5 minutes. The solution first boiled, then it dehydrated, then decomposed with the release of a large amount of gas and then spontaneous combustion occurred with the release of a large amount of heat and the formation of a free-flowing powder.

Cobalt ferrite was obtained by burning solutions of metal nitrates (precursors) and glycine and ammonium nitrate as organic promoters in a household microwave oven at a power of 900 W for 30 min [73].

Nickel ferrite nanoparticles were obtained by microwave combustion of a solution containing nickel, iron nitrates and trisodium citrate ( $\text{Na}_3\text{C}_6\text{H}_5\text{O}_7$ ) and finally, the sodium salt of citric acid [74]. The mixture

was placed in a microwave oven and irradiated for 30 minutes. The resulting mass was then ground into powder.

Nickel-magnesium ferrites were obtained with the participation of urea as a “fuel” and microwave treatment for 10 minutes at a magnetron power of 850 W [75].

Nickel ferrite was prepared by the sol-gel method from solutions of nickel and iron nitrate with the addition of citric acid and ammonia, evaporation at 100°C, followed by ignition and the formation of a free-flowing powder, which was further subjected to microwave treatment [76].

In [77], the effect of an organic reagent on the synthesis of NiFe<sub>2</sub>O<sub>4</sub> nanoparticles by combustion using microwave radiation was studied; urea, glycine, and citric acid were used as fuel reagents. The synthesized nanoparticles were characterized by X-ray diffraction, scanning electron microscopy, Brunauer-Emmett-Teller (BET) surface area. The authors found that the type of fuel affects the surface properties of nanoparticles. According to the results of X-ray diffraction analysis, the highest crystallinity was observed in nanoparticles synthesized with glycine, while nanoparticles prepared with urea had the highest surface area. The SEM micrographs showed that all nanoparticles had nanocrystalline behavior and the particles were cubic in shape. In the same work, nickel ferrite was also obtained by the “dry” method as a result of an exothermic reaction of a mixture of metal nitrates and urea. This method did not use water or any other solvent. Reagents, namely nitrates of nickel and iron, as well as urea were mixed in certain stoichiometric ratios. Owing to the crystallization water of metal nitrates, a thick mixture was formed. This mixture was placed in a laboratory type microwave oven at a maximum power of 800 W for 10 minutes. When the mixture reached the point of spontaneous combustion, it began to burn, releasing gas and heat, and the sample instantly became solid.

In [78], nickel-cobalt ferrite Ni<sub>x</sub>Co<sub>x</sub>Fe<sub>2</sub>O<sub>4</sub> was obtained by mixing solutions of nitrates and urea, heating to 100 °C, and microwave treatment for 10 minutes until combustion.

Flash synthesis of NiFe<sub>2</sub>O<sub>4</sub> nanoparticles with a particle size close to 4–5 nm and a high specific surface area (about 240 m<sup>2</sup>/g) was carried out using a RAMO autoclave microwave heater developed by the authors [79].

The microwave combustion method was used to synthesize nanocrystalline Zn<sub>x</sub>Ni<sub>1-x</sub>Fe<sub>2</sub>O<sub>4</sub> from a stoichiometric mixture of the appropriate metal nitrates and urea powders [80]. The resulting ferrite had a high-purity spinel structure with a calculated crystallite size of ~20 nm.

The paper [81] reported on the synthesis of Zn<sub>0.7</sub>Ni<sub>0.3</sub>Fe<sub>2</sub>O<sub>4</sub> nanoparticles using a microwave combustion method using urea as a fuel. X-ray diffraction and FT-IR analyzes confirmed the composition and structure of the spinel ferrite. The crystallite size was estimated using X-ray diffraction (16.4 nm). The morphological study of the products was carried out using TEM, which revealed the presence of spherical, spheroidal and polygonal crystallite shapes.

In [82], the authors synthesized a rhombohedral nanostructure of nickel ferrite by the method of rapid combustion with the help of microwave radiation using ethylenediaminetetraacetic acid as a chelating agent.

Spinel nanoparticles Zn<sub>1-x</sub>Co<sub>x</sub>Fe<sub>2</sub>O<sub>4</sub> with different particle sizes were prepared by microwave combustion with urea as a fuel [83]. Composites were prepared with the addition of cobalt in various molar ratios ( $x = 0.0-0.5$ ) to ZnFe<sub>2</sub>O<sub>4</sub>. The obtained spinel ferrites were characterized by powder X-ray diffraction (XRD) and the average grain size and morphology were determined by high resolution scanning electron microscopy (HR-SEM). The formation of a single cubic phase of spinel was confirmed by X-ray diffraction and Rietveld analysis with an average crystallite size in the range of 43–49 nm.

Nanoparticles of copper ferrite CuFe<sub>2</sub>O<sub>4</sub> were obtained by microwave combustion using an extract of the plant *Hibiscus rosa sinensis* (Chinese rose) as a fuel. X-ray diffraction and analysis by the Rietveld method confirmed the formation of a single cubic phase with a crystallite size of 25 to 62 nm due to grain growth after calcination [84].

Copper ferrite nanoparticles were prepared using starch as a fuel. The starch solution was poured into solutions of copper and iron nitrates with continuous stirring. The clear solution was placed in a household microwave oven (2.45 GHz, 950 W) for 20 minutes. After the solution reached the point of spontaneous combustion, it instantly evaporated and became solid. The obtained solids were well washed with ethanol, dried and were designated as nanostructures of CuFe<sub>2</sub>O<sub>4</sub> obtained by microwave technology [85].

Copper ferrites were synthesized by us on the basis of the ceramic method from oxides and by the sol-gel method using microwave treatment, following which the values of the specific surface area of the samples were determined (Table 7) [15, 23]. The specific surface area was also determined after additional microwave treatment of the ferrite powder obtained after burning the gel.

Values of the specific surface area of copper ferrite obtained by various methods

No.	Method for synthesis of copper ferrite $\text{CuFe}_2\text{O}_4$	Specific surface area, $\text{m}^2/\text{g}$
1	“Ceramic method” from oxides of copper and iron in microwave field	0.4
2	Sol-gel combustion method with citric acid	18
3	Sol-gel combustion method with citric acid and additional microwave treatment	1.0
4	Sol-gel combustion method with urea	25.4
5	Sol-gel combustion method with urea and additional microwave treatment	2.1

It can be seen from the Table 7, additional microwave treatment of copper ferrite powder leads to a decrease in its specific surface area. The same is true of a sample obtained by a ceramic method in a microwave field. When ferrites are obtained by solid-phase microwave synthesis from oxides, as a result of a very rapid rise in temperature and a long processing time, aggregation of the resulting ferrite particles is observed (Fig. 1)

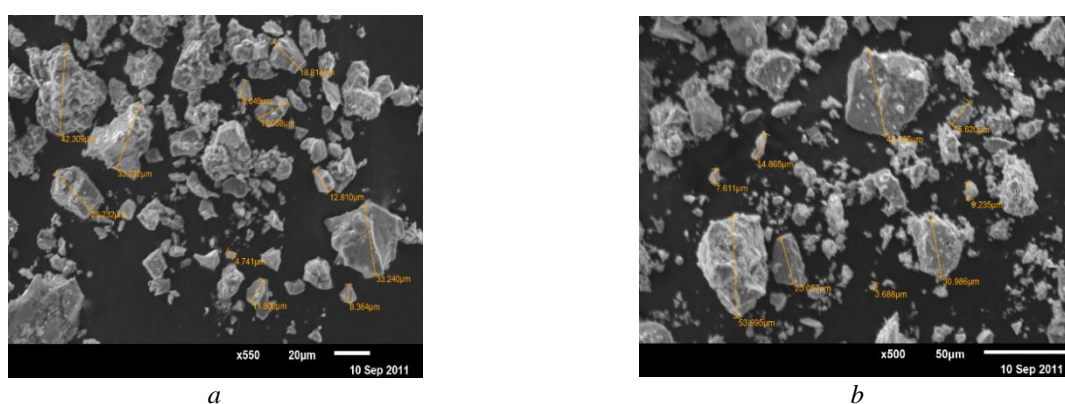


Figure 1. Micrographs of (a) nickel and (b) cobalt ferrite samples obtained by the solid-phase microwave synthesis from oxides. Reprinted from [15]

A similar picture is also observed during additional microwave heat treatment of the obtained sol-gel method with the combustion of ferrite powder. The ferrites obtained by these two microwave processing methods are characterized by low specific surface area. Based on these experimental data, we decided to use microwave energy to “ignite” the gel without further prolonged irradiation. This process took place even at low magnetron values within a few seconds. Figure 2 shows photographs of the resulting copper ferrite during the combustion of the gel in air (a) and “ignition” in a microwave oven (b). In both cases, branched, voluminous structures are observed.

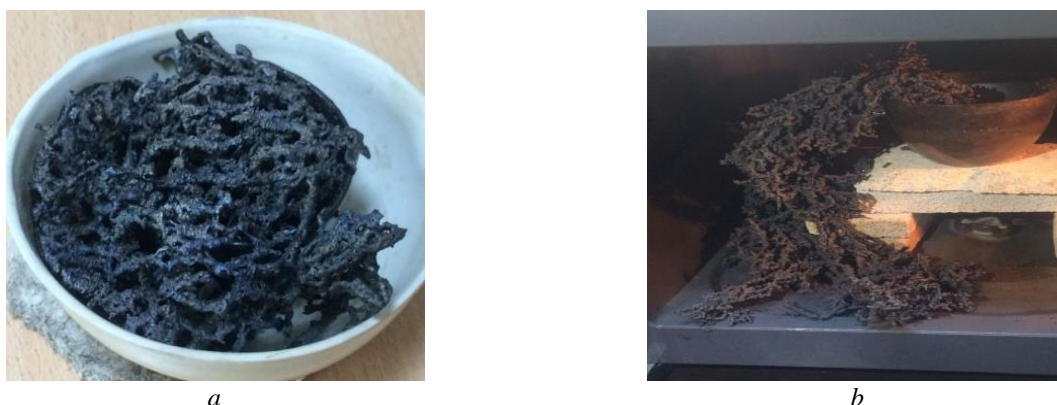


Figure 2. Samples of copper ferrite obtained by the sol-gel method with combustion (a) and gel treatment in a microwave field. The organic reagent is citric acid. Reprinted from [87]

From the diffraction patterns of ferrites obtained by the sol-gel method with conventional combustion and microwave ignition, the crystallite sizes found using the Scherrer equation are quite close (30–35 nm). The same is true of the values of their specific surface area (Table 8) [86].

Table 8

**Specific surface of ferrites synthesized by the sol-gel (s-g) method with combustion and the use of various organic reagents with conventional heating and microwave exposure (m.e)**

Sample	Citric acid		Glycine		Urea	
	s-g	s-g + m.e	s-g	s-g + m.e	s-g	s-g + m.e
Cu:Fe = 1:2	18	14.8	4	5.4	25.5	22.6
Co:Fe = 1:2	12	13.3	11.7	12	35.3	30.6
Mn:Fe = 1:2	36.5	27.2	15	13.2	32.9	27.6
Ni:Fe = 1:2	6.2	14	7.8	5.8	34.3	28

Microphotographs of Ni, Co, and Cu ferrite samples obtained by the sol-gel method and additional microwave treatment are shown in Figure 3. For comparison, a micrograph of a copper ferrite sample obtained by the conventional sol-gel method is also presented. As can be seen from the photographs, additional microwave treatment of the samples intensifies the crystallization; the photographs show an increase in the amount of ferrite nanoparticles.

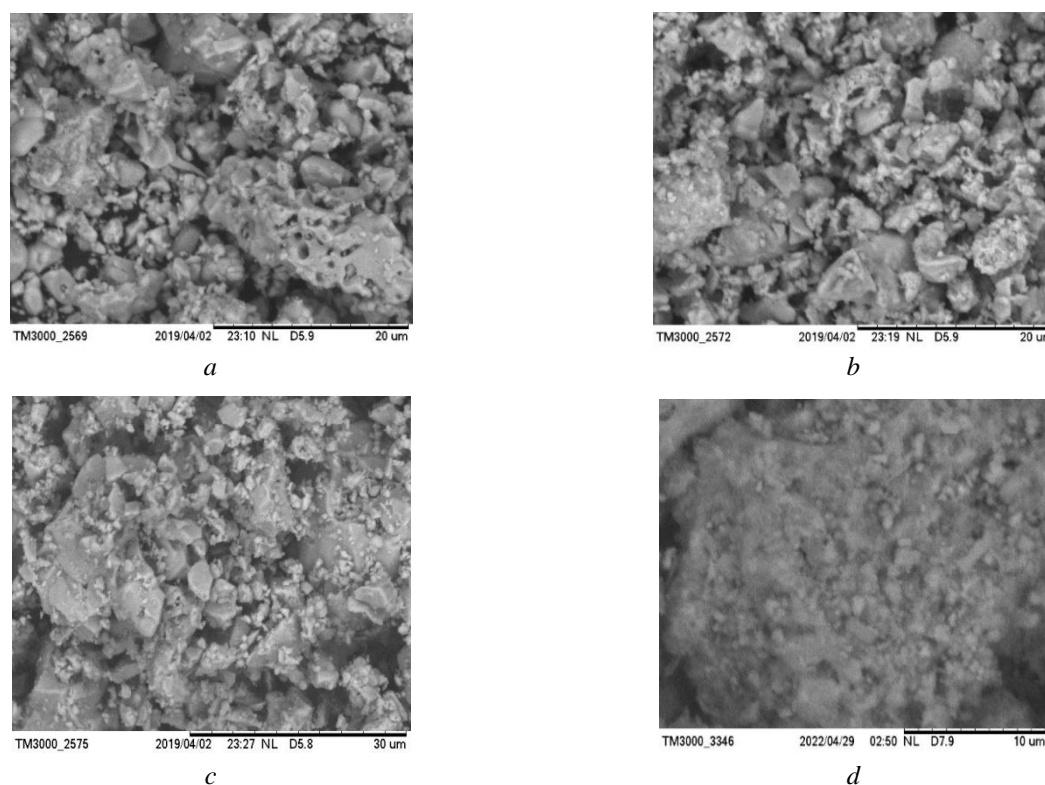


Figure 3. Micrographs of Ni, Co, Cu ferrite samples obtained by the sol-gel method with combustion and additional microwave treatment (*a, b, c*) and a copper ferrite sample without microwave treatment (*d*), an organic reagent is citric acid

The above-mentioned works on the sol-gel synthesis of ferrites using microwave radiation were indicative that in most works the synthesis of ferrites by the sol-gel method with combustion was carried out in ordinary household microwave ovens, in which only the magnetron power and exposure time could be controlled, but not the temperature. Hence, the matter was about discrepancies in both the time of microwave treatment from several minutes to half an hour and power from 120 to 700 watts.

A feature of the synthesis by the sol-gel method with combustion is that the beginning of the combustion process is initiated by an external thermal effect, in some local volume of it an exothermic reaction be-

gins. The heat released in this case is transferred to the neighboring layers, in which the reaction is occurred and so the combustion is spread throughout the system. The difference between microwave exposure and conventional thermal exposure lies in the fact that the initiation of combustion occurs simultaneously throughout the entire volume of the system, thereby reducing the duration of the combustion process. But a longer microwave exposure can lead to particle aggregation due to the high rate of temperature rise, which is especially clearly observed in the ceramic synthesis of ferrites [87]. Therefore, when using microwave radiation in the sol-gel method with combustion, along with the nature of the organic reagent, the power and time of exposure to the radiation play an important role in the formation of the surface morphology, texture of ferrites.

### Conclusions

The latest studies on the production of cobalt, nickel, copper and manganese ferrites by the sol-gel method with self-ignition and combustion in a microwave field were considered briefly. Also, the influence of various reaction parameters, namely the organic reagent nature, its ratio to precursors, pH of the medium, power and time of microwave exposure on the process of ferrite formation as factors affecting the size of the formed particles and their textural characteristics were analyzed.

### References

- 1 Ortiz-Quiñonez, J.L., Umapada Pal, U., & Villanueva, M.S. (2018). Structural, Magnetic, and Catalytic Evaluation of Spinel Co, Ni, and Co–Ni Ferrite Nanoparticles Fabricated by Low-Temperature Solution Combustion Process. *ACS Omega*, 3(11), 14986–15001. <https://doi.org/10.1021/acsomega.8b02229>.
- 2 Gul, S., Yousuf, M.A., Anwar, A., Warsi, M.F., Agboola, P.O., Shakir, I., & Shahid, M. (2020). Al-substituted zinc spinel ferrite nanoparticles: Preparation and evaluation of structural, electrical, magnetic and photocatalytic properties. *Ceram. Int.*, 46, 14195–14205. <https://doi.org/10.1016/j.ceramint.2020.02.228>.
- 3 Hakeem, A., Alshahrani, T., Muhammad, G., Alhossainy, M.H., Laref, A., Khan, A.R., Ali, I., Farid, H.M.T., Ghrib, T., Ejaz, S.R., & Khosa, R.Y. (2021). Magnetic, dielectric and structural properties of spinel ferrites synthesized by sol-gel method. *J. Mater. Res. Technol.*, 11, 158–169. <https://doi.org/10.1016/j.jmrt.2020.12.064>.
- 4 Sutka, A., & Mezinskis, G. (2012). Sol-gel auto-combustion synthesis of spinel-type ferrite nanomaterials. *Frontiers of Materials Science*, 6, 128–141.
- 5 Kefeni, K.K.; Msagati, T.A.M., & Mamba, B.B. (2017). Ferrite nanoparticles: Synthesis, characterisation and applications in electronic device. *Mater. Sci. Eng. B*, 215, 37–55. <https://doi.org/10.1016/j.mseb.2016.11.002>.
- 6 Ateia, E.E.; El-Bassuony, A.A.; Abdelatif, G., & Soliman, F.S. (2017). Novelty characterization and enhancement of magnetic properties of Co and Cu nanoferrites. *J. Mater. Sci. Mater. Electron.*, 28, 241–249. <https://doi.org/10.1007/s10854-016-5517-y>.
- 7 Narang, S.B., & Pubby, K. (2021). Nickel Spinel Ferrites: A review. *Journal of Magnetism and Magnetic Materials*, 519, 167163 <https://doi.org/10.1016/j.jmmm.2020.167163>.
- 8 Kharisov, B.I., Rasika Dias H.V., & Kharisova, O.V. (2019). Mini-review: Ferrite nanoparticles in the catalysis. *Arabian Journal of Chemistry*, 12, 7, 1234–1246 <https://doi.org/10.1016/j.arabjc.2014.10.049>.
- 9 Dutta, S.K., Akhter, M., Jamil Ahmed, Amin, Khairul Md., & Dhar, P.K. (2022). Synthesis and Catalytic Activity of Spinel Ferrites: A Brief Review. *Biointerface Research in Applied Chemistry*, 12, 4, 4399–4416. <https://doi.org/10.33263/BRIAC124.43994416>.
- 10 Kaur, M., Kaur, N. & Vibha. (2016). Ferrites: Synthesis and Applications for Environmental Remediation. In book Sharma et al.; Ferrites and Ferrates: Chemistry and Applications in Sustainable Energy and Environmental Remediation. *ACS Symposium Series*, 1238. <https://doi.org/10.1021/bk-2016-1238.ch004>.
- 11 Dabholkar, V., Kurade, S.K., & Badhe, K.S. (2016). Nickel Ferrite Heterogeneous Base Catalyst for Synthesis of Dihydropyridines. *International Journal of Latest Technology in Engineering*, 5, 8, 34-39.
- 12 Velinov, N., Koleva, K., Tsoncheva, T. et al. (2014). Copper-cobalt ferrites as catalysts for methanol decomposition. *Cent. Eur. J. Chem.*, 12(2), 250-259.
- 13 Rahmankulov, D.L., & Bikbulatov, I.H. (2003). *Mikrovolnovoe izluchenie i intensivifikatsiia khimicheskikh protsessov [Microwave radiation and intensification of chemical processes]*. Moscow: Khimiia [in Russian].
- 14 Kustov, L.M., & Sinev, I.M. (2010). SVCh-aktivatsiia katalizatorov i kataliticheskikh protsessov [Microwave activation of catalysts and catalytic processes]. *Zhurnal fizicheskoi khimii — Russian Journal of Physical Chemistry*, 84, 10, 1835–1856 [in Russian].
- 15 Litvishkov, Yu.N., Zulfugarova, S.M., Aleskerova, Z.F., Gasanguliyeva, N.M., Askerov, A.G., & Shakunova, N.V. (2018). Microwave Synthesis of Co, Ni, Cu, Zn Ferrites. *Russian Journal Of Applied Chemistry*, 91, 5, 679-687.
- 16 Zulfugarova, S.M., Aleskerova, Z.F., Huseynova, E.M., Shakunova, N.V., Gasanguliyeva, N.M., Azimova, G.R., & Litvishkov, Yu.N. (2021). Stimulirovannyi mikrovolnovym izlucheniem tverdogfaznyi sintez ferritov Ni i Co na poverkhnosti Al<sub>2</sub>O<sub>3</sub>/Al nosi-

telia. [Microwave-assisted solid-phase synthesis of Ni and Co ferrites on the surface of Al<sub>2</sub>O<sub>3</sub>/Al]. *Neftepererabotka i neftekhimiia — Oil Refining and Petrochemistry*, 3, 27–32. ISSN 0233-5727 [in Russian].

17 Feng Ji., Wang Yu., Zou L., Li B., He X., Ren Yu., Lv Ya., & Fan Z. (2015). Synthesis of magnetic ZnO/ZnFe<sub>2</sub>O<sub>4</sub> by a microwave combustion method, and its high rate of adsorption of methylene blue. *J. of Colloid and Interface Science*, 438, 318–322. <http://dx.doi.org/10.1016/j.jcis.2014.10.009>

18 Anchieta, C.G., Severo, E.C., Rigo, C., Mazutti, M.A., Kuhn, R.C., Muller, E.I., Flores, E.M.M., Moreira, R.F.P.M., Foletto, E.L. (2015). Rapid and facile preparation of zinc ferrite (ZnFe<sub>2</sub>O<sub>4</sub>) oxide by microwave-solvothermal technique and its catalytic activity in heterogeneous photo-Fenton reaction. *Mat. Chem. and Physics*, 160, 141–147. <https://doi.org/10.1016/j.matchemphys.2015.04.016>

19 Jumeri, F.A., Lim, H.N., Ariffin, S.N., Huang, N.M., Teo, P.S., Fa-tin, S.O., Chia, C.H., & Harrison, I. (2014). Microwave synthesis of magnetically separable ZnFe<sub>2</sub>O<sub>4</sub>-reduced graphene oxide for waste water treatment. *Cer. Intern.*, 40, 7057–7065.

20 Dhiwaha, A.; Sundararajan, M.; Sakthivel, P.; Dash, Ch.S.; Yuvaraj, S. (2020). Microwave-assisted combustion synthesis of pure and zinc-doped copper ferrite nanoparticles: Structural, morphological, optical, vibrational, and magnetic behavior. *Journal of Physics and Chemistry of Solids*, 138, 109257. <https://doi.org/10.1016/j.jpcs.2019.109257>

21 Sripriya, R.C.; Mahendiran, M.; Madahavan, J. and Raj, MVR. (2019). Enhanced magnetic Properties of MgFe<sub>2</sub>O<sub>4</sub> nanoparticles. *Materials Today: Proceedings*, 8, 310–314. <https://doi.org/10.1016/j.matpr.2019.02.116>

22 Ambika, S.; Gopinath, S.; Saravanan, K.; Sivakumar, K.; Sukantha, T.A.; Paramasivan P. (2019). Preparation and Characterization of Nanocopper Ferrite and Its Green Catalytic Activity in Alcohol Oxidation Reaction. *Journal of Superconductivity and Novel Magnetism*, 32, 903–910. <https://doi.org/10.1007/s10948-018-4715-7>

23 Azimova, G.R.; Zulfugarova, S.M.; Aleskerova, Z.F.; Ismailov, E.H. (2020). Catalytic activity of copper ferrite synthesized with the using of microwave treatment in the oxidation reaction of carbon monoxide. *Azerbaijan journal of chemical news*, 2(2), 29–34.

24 Lunhong, Ai.; Jing Jiang. (2010). Influence of annealing temperature on the formation, microstructure and magnetic properties of spinel nanocrystalline cobalt ferrites. *Current Applied Physics*, 10, 284–288.

25 Senthil, V.P.; Gajendiran, J.; Raj, S.G.; Shanmugavel, T.; Kumar, G.R.; Reddy, C.P. (2018). Study of structural and magnetic properties of cobalt ferrite (CoFe<sub>2</sub>O<sub>4</sub>) nanostructures. *Chemical Physics Letters*, 695, 19–23. <https://doi.org/10.1016/j.cplett.2018.01.057>

26 Jauhar, Sh.; Kaur, J.; Goyal, A.; Singhal, S. (2016). Tuning the properties of cobalt Ferrite: A road towards diverse applications. *RSC Advances* 2016, 100. <https://doi.org/10.1039/C6RA21224G>

27 Kesavamoorthi, R.; Vigneshwaran, A.N.; Sanyal, V.; Raja, C.R. (2016). Synthesis and characterization of nickel ferrite nanoparticles by sol-gel auto combustion method. *Journal of Chemical and Pharmaceutical Sciences*, 9, 1, 160–162.

28 Reddy, M.P.; Shakoor, R.A. and Mohamed, A.M.A. (2017). Auto Combustion Synthesis, Microstructural and Magnetic Characteristics of Nickel Ferrite Nanoparticles. *Indian Journal of Science and Technology*, 10(13), 1–5. <https://doi.org/10.17485/jst/2017/v10i13/88034>

29 Shanmugavel, T.; Raj, S.G.; Kumar, G.R.; Rajarajan, G.; Saravanan, D. (2015). Cost effective preparation and characterization of nanocrystalline nickel ferrites (NiFe<sub>2</sub>O<sub>4</sub>) in low temperature regime. *Journal of King Saud University–Science*, 27, 2, 176–181. <https://doi.org/10.1016/j.jksus.2014.12.006>

30 Bharati, V.A.; Patade, S.R.; Bajaj, Sh.; Parlikar, R.; Keche, A.P.; Sondur, V.V. (2020). Structural and Magnetic Properties of Nickel Ferrite Nanoparticles Prepared by Solution Combustion Method. *Journal of Physics: Conference Series*, 1644, 012005. *International Web Conference on Advanced Material Science and Nanotechnology (NANOMAT-2020)*. India. <https://doi.org/10.1088/1742-6596/1644/1/012005>

31 Samoila, P.; Cojocaru, C.; Cretescu, I.; Stan, C.D.; Nica, V.; Sacarescu, L. and Harabagiu, V. Nanosized Spinel Ferrites Synthesized by Sol-Gel Autocombustion for Optimized Removal of Azo Dye from Aqueous Solution. *Journal of Nanomaterials*, Article ID 713802, 13 pages. <http://dx.doi.org/10.1155/2015/713802>

32 Dudhal, R.D.; Patade, S.; Andhare, D.; Paralikar, R.; Chilwar, R.; More, S.D. (2020). Influence of fuel to metal nitrate ratio on the structural properties of nickel ferrite. *NANOMAT-2020. Journal of Physics: Conference Series* 1644, 012011. doi:10.1088/1742-6596/1644/1/012011

33 Tapsale, S.D.; Jadhav, K.M; Mane, D.V and Patil, S.G. (2018). Synthesis of metal spinel type of ferrite and used as a catalysts in organic reactions. *The Pharma Innovation Journal*, 7(1), 215–217.

34 Prasad, S.A.V.; Deepty, M.; Ramesh, P.N.; Prasad, G.; Srinivasarao, K.; Srinivas, Ch.; Babu, K.V.; Kumar, E.R.; Mohan, N.K.; Sastry, D.L. (2018). Synthesis of MFe<sub>2</sub>O<sub>4</sub> (M = Mg<sup>2+</sup>, Zn<sup>2+</sup>, Mn<sup>2+</sup>) spinel ferrites and their structural, elastic and electron magnetic resonance properties. *Ceramics International*, 44, 9, 10517–10524. <https://doi.org/10.1016/j.ceramint.2018.03.070>

35 Bhukal, S.; Shivali, S.S. (2014). Magnetically separable copper substituted cobalt–zinc nano-ferrite photocatalyst with enhanced photocatalytic activity. *Materials Science in Semiconductor Processing*, 26, 467–476. <https://doi.org/10.1016/j.mssp.2014.05.023>

36 Jauhar, Sh.; Singhal, S. (2014). Substituted cobalt nano-ferrites CoM<sub>x</sub>Fe<sub>2-x</sub>O<sub>4</sub> (M = Cr<sup>3+</sup>, Ni<sup>2+</sup>, Cu<sup>2+</sup>, Zn<sup>2+</sup>; 0.2 ≤ x ≤ 1.0) as heterogeneous catalysts for modified Fenton's reaction. *Ceramics International*, 40(8), 11845–11855 <https://doi.org/10.1016/j.ceramint.2014.04.019>

37 Kumar, G.S.; Raguram, T.; Rajni. K.S. (2018). Synthesis and Characterization of Nickel-Substituted Cobalt Ferrite Nanoparticles Using Sol–Gel Auto-combustion Method. *Journal of Superconductivity and Novel Magnetism*, 32(9). <https://doi.org/10.1007/s10948-018-4867-5>

- 38 Singh, S. and Singhal, S. (2019). Transition metal doped cobalt ferrite nanoparticles: Efficient photocatalyst for photodegradation of textile dye. *Materials Today: Proceedings*, 14, 453–460. <https://doi.org/10.1016/j.matpr.2019.04.168>
- 39 Hankare, P.P.; Sanadi, K.R.; Garadkar, K.M.; Patil, D.R.; Mulla, I.S. (2013). Synthesis and characterization of nickel substituted cobalt ferrite nanoparticles by sol-gel auto-combustion method. *Journal of Alloys and Compounds*, 553, 383–388. <https://doi.org/10.1016/j.jallcom.2012.11.181>
- 40 Jalaiah, K.; Babu, V.B.; Chandramouli, K.; Subba Rao, P.S.V. (2018). Effect on the structural, DC resistivity and magnetic properties of Zr and Cu co-Substituted  $\text{Ni}_{0.5}\text{Zn}_{0.5}\text{Fe}_2\text{O}_4$  using sol-gel auto-combustion method. *Physica B: Condensed Matter*, 534, 125–133. <https://doi.org/10.1016/j.physb.2018.01.02>
- 41 Kokare, M.K.; Jadhav, N.A.; Kumar, Y.; Jadhav, K.M.; Rathod, S.M. (2018). Effect of  $\text{Nd}^{3+}$  doping on structural and magnetic properties of  $\text{Ni}_{0.5}\text{Co}_{0.5}\text{Fe}_2\text{O}_4$  nanocrystalline ferrites synthesized by sol-gel auto combustion method. *Journal of Alloys and Compounds*, 748, 1053–1061. <https://doi.org/10.1016/j.jallcom.2018.03.168>
- 42 Nag, S.; Roychowdhury, A.; Das, D.; Das, S.; Mukherje, S. (2018). Structural and magnetic properties of erbium  $\text{Er}^{3+}$  doped nickel zinc ferrite prepared by sol-gel auto-combustion method. *Journal of Magnetism and Magnetic Materials*, 466, 172–179. <https://doi.org/10.1016/j.jmmm.2018.06.084>
- 43 Bushkova, V.S. (2017). Nizkotemperaturnye magnitnye svoistva ferritov  $\text{NiCr}_x\text{Fe}_{2-x}\text{O}_4$ . [Low-temperature magnetic properties of  $\text{NiCr}_x\text{Fe}_{2-x}\text{O}_4$  ferrites]. *Fizika nizkikh temperatur — Journal of low temperature physics*, 43, 12, 1724–1732 [in Russian].
- 44 Bazuev, G.V.; Gyrdasova, O.I.; Chupahina, T.I.; & Novikov, S.I. (2016). Sintez-mikrostruktura i magnitnye svoistva nikel-tsinkovogo ferrita  $\text{Ni}_{0.75}\text{Zn}_{0.25}\text{Fe}_2\text{O}_4$ , dopirovannogo redkozemelnyimi elementami [Synthesis, microstructure and magnetic properties of  $\text{Ni}_{0.75}\text{Zn}_{0.25}\text{Fe}_2\text{O}_4$  nickel-zinc ferrite doped with rare-earth elements]. *Fazovye perekhody, mezhfaznye granitsy i nanomaterialy — Phase transitions, interfaces and nanotechnology*, 1, 71–75 <http://pti-nt.ru> [in Russian].
- 45 Kopaev, A.V.; Zadnirjannyj, D.L.; & Tafijchuk, Yu. N. (2012). Struktura, svoistva i osobennosti sinteza nikel-aliuminievykh ferritov, poluchennykh metodom zol-gel s uchastiem avtogoreniia [Structure, properties and peculiarities of the synthesis of nickel-aluminum ferrites, obtained by the sol-gel method with the participation of auto-combustion]. *Наносистеми, наноматеріали, нанотехнології — Nanosystems, Nanomaterials, Nanotechnologies*, 10, 2, 289–295 [in Ukrainian].
- 46 Bhagwata, V.R.; Humbeb, A.V.; Morec, S.D.; Jadhav, K.M. (2019). Sol-gel auto combustion synthesis and characterization of cobalt ferrite nanoparticles: Different fuels approach. *Materials Science & Engineering B*, 248, 114388. <https://doi.org/10.1016/j.mseb.2019.114388>
- 47 Salunkhe, A.; Khot, V.M.; Phadatare, M.R.; Pawar, S.H. (2012). Combustion synthesis of cobalt ferrite nanoparticles — Influence of fuel to oxidizer ratio. *J. Alloys Compd.*, 514, 91–96. <https://doi.org/10.1016/j.jallcom.2011.10.094>
- 48 Houshiar, M.; Zebhi, F.; Razi, Z.J.; Ali Alidoust, Zohreh Askari. (2014). Synthesis of cobalt ferrite ( $\text{CoFe}_2\text{O}_4$ ) nanoparticles using combustion, coprecipitation, and precipitation methods: A comparison study of size, structural, and magnetic properties. *Journal of Magnetism and Magnetic Materials*, 371, 43–48.
- 49 Ye, Z.; Deng, Z.; Zhang, L.; Chen, J.; Guiwu Wang and Zhiping Wu. (2020). The structure of copper ferrite prepared by five methods and its catalytic activity on lignin oxidative degradation. *Mater. Res. Express*, 7, 035007. <https://doi.org/10.1088/2053-1591/ab778b>
- 50 Abraham, A.G.; Manikandan, A.; Manikandan, E.; Vadivel, S.; Jaganathan, S. K.; Baykal A. and Renganathan, P.S. (2018). Enhanced magneto-optical and photo-catalytic properties of transition metal cobalt ( $\text{Co}^{2+}$  ions) doped spinel  $\text{MgFe}_2\text{O}_4$  ferrite nanocomposites. *Journal of Magnetism and Magnetic Materials*, 452, 380–388. <https://doi.org/10.1016/j.jmmm.2018.01.001>
- 51 Zulfugarova, S.M.; Azimova, G.R.; Aleskerova, Z.F.; Qasimov, R.J.; Bayramov, M.A.; Ismailov, E.H.; Tagiyev, D.B. (2022). Effect of preparation method of iron-, copper- containing oxide catalysts on their activity in the reaction of oxidation of carbon monoxide to carbon dioxide. *Chemical Problems*, 20, 1, 82–94. <https://doi.org/10.32737/2221-8688-2022-1-82-94>
- 52 Prabhakaran, T.; Hemalatha, J. (2016). Combustion synthesis and characterization of cobalt ferrite nanoparticles. *Ceramics International*, 42, 12, 14113–14120. <https://doi.org/10.1016/j.ceramint.2016.06.025>
- 53 Ehi-Eromosele, C.O.; Ita I, B.I.; Iweala, E.E.J. (2015). Low-temperature combustion synthesis of cobalt magnesium ferrite magnetic nanoparticles: effects of fuel-to-oxidizer ratio and sintering temperature. *J. Sol-Gel Sci. Technol.*, 76, 298–308. <https://doi.org/10.1007/s10971-015-3777-2>
- 54 Shobana, M.K.; Kwon, H.; Choe, H. (2012). Structural studies on the yttrium-doped cobalt ferrite powders synthesized by sol-gel combustion method. *Journal of Magnetism and Magnetic Materials*, 324, 2245–2248.
- 55 Rezlescu, N.; Rezlescu, E.; Popa, P.D.; Doroftei, C.; Ignat, M.(2015). Some nano grained ferrites and perovskites for catalytic combustion of acetone at low temperature. *Ceramics international*, 41, 4430–4437.
- 56 Desai, I.; Nadagouda, M.N.; Elovitz, M.; Mills, M.; Boulanger, B. (2019). Synthesis and characterization of magnetic manganese ferrites. *Materials Science for Energy Technologies*, 2, 2, 150–160. <https://doi.org/10.1016/j.mset.2019.01.009>
- 57 Sumathi, S.; Lakshmi Priya, V. (2017). Structural, magnetic, electrical and catalytic activity of copper and bismuth co-substituted cobalt ferrite nanoparticles. *J Mater Sci: Mater Electron.*, 28, 3, 2795–2802. <https://doi.org/10.1007/s10854-016-5860-z>
- 58 Kirankumar, V.S.; Sumathi, S. (2019). Copper and cerium co-doped cobalt ferrite nanoparticles: structural, morphological, optical, magnetic, and photocatalytic properties. *Environmental Science and Pollution Research*, 26, 19189–19206. <https://doi.org/10.1007/s11356-019-05286-9>
- 59 Junior, C G.; Zampiva, R Y S; Alves, A K; Bergmann, C P; and Giorgini, L. (2019). Synthesis of cobalt ferrite ( $\text{CoFe}_2\text{O}_4$ ) by combustion with different concentrations of glycine. *IOP Conf. Ser.: Mater. Sci. Eng.* 659 012079
- 60 Brusencov, Yu. A., & Minaev, A. M. (2002). *Osnovy fiziki i tekhnologii oksidnykh poluprovodnikov [Basics of physics and technology of oxide semiconductors]*. Tambov: Izdatelstvo Tambovskogo gosudarstvennogo tehničeskogo unersitetata [in Russian].

- 61 Nadumane, A.; Shetty, K.; Anantharaju, K.S.; Nagaswarupa, H.P.; Rangappa, D.; Vidya, Y.S.; Nagabhushana, H.; Prashantha, S.C. (2019). Sunlight photocatalytic performance of Mg-doped nickel ferrite synthesized by a green sol-gel route. *Journal of Science: Advanced Materials and Devices*, 4, 1, 89–100.
- 62 Naik, M.M.; H.S. Naik, B.; Nagaraju, G.; Vinuth, M.; Vinu, K.; Viswanath, R. (2019). Green synthesis of zinc doped cobalt ferrite nanoparticles: Structural, optical, photocatalytic and antibacterial studies. *Nano-Structures & Nano-Objects*, 19, 100322. <https://doi.org/10.1016/j.nanoso.2019.100322>
- 63 Kulkarni, G.D.; Patade, S.R., Parlikar, R.R., Gopale; Chilwar, R.R.; Saraf, T.S., Jadhav, K.M. (2020). Green synthesis of NiFe<sub>2</sub>O<sub>4</sub> nanoparticles using different fuels and their structural characterization. *J. Phys.: Conf. Ser.* 1644(1): 01200. <https://doi.org/10.1088/1742-6596/1644/1/012003>
- 64 Jeong, D-W.; Jang, W-J.; Shim, J.O.; Roh, H-S.(2016). High temperature water-gas shift without prereduction over spinel ferrite catalysts synthesized by glycine assisted solgel combustion method. *International Journal of Hydrogen Energy*, 41, 6, 3870–3876. <https://doi.org/10.1016/j.ijhydene.2016.01.024>
- 65 Maksoud, M.I.A.; El-Sayyad, G. S.; Ashour, A.H.; El-Batal, A.I.; Mohamed A. Elsayed, M.A.; Gobara, M.; El-Khawaga, A.M.; Abdel-Khalek, E.K.; El-Okr. M.M. (2019). Antibacterial, antibiofilm, and photocatalytic activities of metals-substituted spinel cobalt ferrite nanoparticles. *Microbial Pathogenesis*, 127, 144–158. <https://doi.org/10.1016/j.micpath.2018.11.045>
- 66 Velinov, N.; Petrova, T.; Ivanova, R.; Tsoncheva, T.; Kovacheva, D.; Mitov, I. (2020). Synthesis and characterization of copper-nickel ferrite catalysts for ethyl acetate oxidation. *Hyperfine Interactions*, 241, 31. <https://doi.org/10.1007/s10751-019-1654-z>
- 67 Freitas, N.L.; Coutinho, J.P., Silva1, M.C.; Lira H.L., Kiminami, R. H. G. A.; Costa, A. C. F. M. (2010). Synthesis of Ni-Zn ferrite catalysts by combustion reaction using different fuels. *Materials Science Forum*, 660-661, 943–947. <https://doi.org/10.4028/www.scientific.net/MSF.660-661.943>
- 68 Ramalho, M.A.F.; Costa, A.C.F.M.; Gama, L.; Kiminami, R.H.G.A.; Hernandez, E.P.; Cornejo, D.R.; Rezende. S.M. (2006). Nanosize nickel ferrite particles synthesized by combustion reaction: evaluation of two synthesis routes. *Materials Science Forum*, 530-531, 637–642. <https://doi.org/10.4028/www.scientific.net/MSF.530-531.637>
- 69 Tong, J.; Cai, X. Wang, H.; Xi, Ch. (2013). Efficient magnetic CoFe<sub>2</sub>O<sub>4</sub> nanocrystal catalyst for aerobic oxidation of cyclohexane prepared by sol-gel auto-combustion method: effects of catalyst preparation parameters. *J. Sol-Gel Sci Technol.*, 66: 452–459. <https://doi.org/10.1007/s10971-013-3031-8>
- 70 Rezlescu, N.; Rezlescu, E.; Popa, P.D.; Popovici, E.; Doroftei, C.; Ignat M. (2013). Preparation and characterization of spinel-type MeFe<sub>2</sub>O<sub>4</sub> (Me = Cu, Cd, Ni and Zn) for catalyst applications. *Materials Chemistry and Physics*, 137, 922–927. <https://doi.org/10.1016/j.matchemphys.2012.11.005>
- 71 Azimova, G.R. (2021). Синтез ферритов Cu, Co, Ni, Mn золь-гель методом с участием различных органических реагентов и исследование их удельной поверхности [Synthesis of Cu, Co, Ni, Mn ferrites by the sol-gel method with autocombustion with the participation of various organic reagents and study of their specific surface area]. *Genj tedqiqatchi elmi-praktiki jurnal — Scientific and practical journal of the young researcher*, 1, 81–85. ISSN 2409-4838 [in Russian].
- 72 Freitas, M.R.; Gouveia, G.L.; Costab, L.J.D.C.; Oliveirab, A.J.A.; Kiminamib, R.H.G.A.(2016). Microwave Assisted Combustion Synthesis and Characterization of Nanocrystalline Nickel-doped Cobalt Ferrites. *Materials Research*, 19(1), 27–32. <http://dx.doi.org/10.1590/1980-5373-MR-2016-0077>
- 73 Ahmadi, R.; Imani, M.; Tadjarodi, A. (2021). Microwave Assisted Synthesis of CoFe<sub>2</sub>O<sub>4</sub> Nanoparticles by Utilizing Organic Promoters and Evaluation of Its Properties. *Chem. Proc.*, 3, 52. <https://doi.org/10.3390/ecsoc-24-08351>
- 74 Venkatesh, M.; Kumar, G.S.; Viji, S., Karthi, S.; Girija, E.K. (2013). Microwave assisted combustion synthesis and characterization of nickel ferrite nanoplatelets. *Modern Electronic Materials*, 2(3). <http://dx.doi.org/10.1016/j.moem.2016.10.003>
- 75 Hema, E.; Manikandan, A.; Karthika, P.; Durka, M.; Antony, S.A.; Venkatraman, B. R. (2016). Magneto-Optical Properties of Reusable Spinel Ni<sub>x</sub>Mg<sub>1-x</sub>Fe<sub>2</sub>O<sub>4</sub> (0.0 ≤ x ≤ 1.0) NanoCatalysts. *Journal of Nanoscience and Nanotechnology*, 16(7), 7325–7336.
- 76 Reddy, M.P.; Madhuri, W.; Sadhana, K.; Kim, I.G.; Hui, K.N.; Hui, K.S.; Kumar, K.V.S.; Reddy, R.R. (2014). Microwave sintering of nickel ferrite nanoparticles processed via sol-gel method. *J. Sol-Gel Sci Technol.*, 70: 400–404 <https://doi.org/10.1007/s10971-014-3295-7>
- 77 Liu, Y-Ch.; Yen-Pei Fu, Y-P. (2010). Magnetic and catalytic properties of copper ferrite nanopowders prepared by a microwave-induced combustion process. *Ceramics International*, 36(5), 1597–1601. <https://doi.org/10.1016/j.ceramint.2010.02.032>
- 78 Rodrigues, A.P.G.; Gomes, D.K.S.; Araújo, J.H.; Melo, D.M.A.; Oliveira, N.A.S.; Braga, R.M. (2015). Nanoferrites of nickel doped with cobalt: Influence of Co<sup>2+</sup> on the structural and magnetic properties. *Journal of Magnetism and Magnetic Materials*, 374, 748–754. <https://doi.org/10.1016/j.jmmm.2014.09.045>
- 79 Bousquet-Berthelin, C.; Chaumont, D.; Stuerger, D. (2008). Flash microwave synthesis of trevorite nanoparticles. *Journal of Solid State Chemistry*, 181, 3, 616–622. <https://doi.org/10.1016/j.jssc.2008.01.009>
- 80 Sertkol, M., Köseoğlu, Y.; Baykal, A.; Kavas, H.; Bozkurt, A.; Toprak, M.S. (2009). Microwave synthesis and characterization of Zn-doped nickel ferrite nanoparticles *Journal of Alloys and Compounds*, 486, 1–2, 325–329. <https://doi.org/10.1016/j.jallcom.2009.06.128>
- 81 Sertkol, M.; Köseoğlu, Y.; Baykal, A.; Kavas, H.; Toprak, M.S. (2010). Synthesis and magnetic characterization of Zn<sub>0.7</sub>Ni<sub>0.3</sub>Fe<sub>2</sub>O<sub>4</sub> nanoparticles via microwave-assisted combustion route. *J Magn Magn Mater.*, 322, 866–871.
- 82 Kumar, G.S.; Akbar J.; Govindan R.; Girija, E.K.; Kanagaraj, M. (2016). A novel rhombohedronlike nickel ferrite nanostructure: Microwave combustion synthesis, structural characterization and magnetic properties. *J Sci: Adv Mater Dev.*, 1, 3, 282–285. <https://doi.org/10.1016/j.jsamd.2016.07.003>

83 Manikandan, A.; Kennedy, L.J.; Bououdina, M.; Vijaya, J.J. (2014). Synthesis, optical and magnetic properties of pure and Co-doped ZnFe<sub>2</sub>O<sub>4</sub> nanoparticles by microwave combustion method. *J. of Magnetism and Magnetic Materials*, 349, 249–258.

84 Kombaiah, K.; Vijaya, J.J.; Kennedy, L.J.; Bououdina, M.; Al-Najar, B. (2018). Conventional and microwave combustion synthesis of optomagnetic CuFe<sub>2</sub>O<sub>4</sub> nanoparticles for hyper thermia studies. *Journal of Physics and Chemistry of Solids*, 115, 162–171. <https://doi.org/10.1016/j.jpcs.2017.12.024>

85 Ambika, S.; Gopinath, S.; Saravanan, K.; Sivakumar, K.; Sukantha, T.A.; Paramasivan, P. (2018). Preparation and Characterization of Nanocopper Ferrite and Its Green Catalytic Activity in Alcohol Oxidation Reaction. *Journal of Superconductivity and Novel Magnetism*. 32(9): 1-8. <https://doi.org/10.1007/s10948-018-4715-7>

86 Zulfugarova, S.M.; Azimova, G.R.; Aleskerova, Z.F.; Ismailov, E.H.; Litvishkov, Yu.N; Tagiyev, D.B. (2022). Microwave Sol-Gel Synthesis of Co, Ni, Cu, Mn Ferrites And The Investigation of Their Activity In The Oxidation Reaction Of Carbon Monoxide. *Current Microwave Chemistry*, 9, 1.

87 Azimova, G.R., Zulfugarova, S.M., Aleskerova, Z.F., & Ismailov, E.H. (2020). Vliyanie sposoba prigotovleniia na kataliticheskie svoistva ferrita medi v reakcii okisleniia monoooksida ugleroda [Influence of the preparation method on the catalytic properties of copper ferrite in the carbon monoxide oxidation reaction]. *Advanced technologies and materials. Vserossiiskaia nauchno-prakticheskaia konferentsiia s mezhdunarodnym uchastiem* (14–16 oktiabria 2020 goda). Sevastopol — All-Russian Scientific and Practical Conference with International Participation (pp.199–203) [in Russian].

С.М. Зулфугарова, Г.Р. Азимова, З.Ф. Алескерова, Ю.Н. Литвишков, Д.Б. Тагиев

### **Өтпелі металл ферриттерінің (Co, Cu, Ni, Mn) золь-гель әдісімен жануы және микротолқынды өңдеуді қолдану арқылы синтездеу**

Мақалада өтпелі металл ферриттерінің (Co, Cu, Ni, Mn) золь-гель әдісі арқылы жануы, сондай-ақ микротолқынды сәулеленудің әсерінен синтездеу бойынша соңғы жылдардағы жұмыстар қарастырылған. Ферриттер магниттік және оптикалық қасиеттерімен ғана емес, сонымен қатар каталитикалық қасиеттерімен де қызықты. Әдебиеттерде өтпелі металл ферриттерінің әртүрлі реакциялардағы, соның ішінде тотығу реакцияларындағы каталитикалық қасиеттері зерттелген еңбектер қатары көбейіп келеді. Золь-гель әдісінде жану кезінде комплекстүзуші және отын ретінде әртүрлі органикалық компоненттер қолданылатынын ескере отырып, мақалада органикалық реагенттің табиғаты, оның прекурсорларға қатынасы, ортаның рН-ға әсері, феррит түзілу процесі түзілген бөлшектердің мөлшеріне әсер ететін факторлар ретінде және олардың катализде маңызы зор текстуралық көрсеткіштері зерттелген. Соңғы жылдары катализ саласында жұмыс істейтін химиктердің назарын микротолқынды өріске қатысты физикалық өрістердің әртүрлі химиялық процестері, соның ішінде нанокатализаторлар синтезіне әсері туралы зерттеулер аударуда. Әдеби деректерге сәйкес, ферриттердің золь-гель синтезінде микротолқынды сәулеленуді қолдану гетерогенді катализаторлар үшін өте маңызды, яғни меншікті бетінің ауданы жоғары наноферриттерді алуға мүмкіндік береді. Осы тұрғыдан алғанда, мақалада микротолқынды золь-гель синтезін зерттеуге арналған соңғы жылдардағы жұмыстар зерттелген.

*Кілт сөздер:* ферриттер, золь-гель әдісімен жану, комплекстүзуші заттар, микротолқынды технология, ұсақтық, текстура, дисперстілік, меншікті беті, бөлшектердің мөлшері.

С.М. Зулфугарова, Г.Р. Азимова, З.Ф. Алескерова, Ю.Н. Литвишков, Д.Б. Тагиев

### **Синтез ферритов переходных металлов (Co, Cu, Ni, Mn) золь-гель методом с горением и использованием микроволновой обработки**

В обзоре рассмотрены работы последних лет по синтезу ферритов переходных металлов (Co, Cu, Ni, Mn) золь-гель методом с горением, а также воздействием микроволнового излучения. Ферриты интересны не только своими магнитными и оптическими свойствами, но и каталитическими. В литературе появляется все больше работ, в которых исследуются каталитические свойства ферритов переходных металлов в различных реакциях, в том числе и окислительных. Ввиду того, что в золь-гель методе с горением в качестве комплексообразователя и топлива используют различные органические компоненты, в настоящей работе рассмотрено влияние природы органического реагента, его соотношения к прекурсорам, рН среды на процесс образования ферритов как факторов, влияющих на размер образующихся частиц и их текстурные показатели, имеющих большое значение в катализе. В последние годы внимание химиков, работающих в области катализа, привлекают исследования по изучению влияния физических полей, к которым относится микроволновое поле, на различные химические процессы, в том числе на синтез нанокатализаторов. Согласно литературным данным, применение микроволнового излучения в золь-гель синтезе ферритов позволяет получать наноферриты с высокой

удельной поверхностью, что очень важно для гетерогенных катализаторов. С этой точки зрения авторами рассмотрены работы последних лет, посвященные изучению микроволнового золь-гель синтеза.

*Ключевые слова:* ферриты, золь-гель метод с горением, комплексообразователи, микроволновая технология, дисперсность, текстура, удельная поверхность, размер частиц.

#### Information about authors\*

**Zulfugarova, Sima Mamed** (*corresponding author*) — PhD in Chemistry, docent, head of laboratory, Institute of Catalysis and Inorganic Chemistry named after academician Murtuza Naghiyev, H. Javid ave., 113, Baku AZ 1143, Azerbaijan Republic; e-mail: [zsm07@mail.ru](mailto:zsm07@mail.ru); <http://orcid.org/0000-0001-9593-0099>;

**Azimova, Gunel Ramiz** — Researcher, Institute of Catalysis and Inorganic Chemistry named after academician Murtuza Naghiyev, H. Javid ave., 113, Baku AZ 1143, Azerbaijan Republic; e-mail: [ezimova2015@gmail.com](mailto:ezimova2015@gmail.com); <http://orcid.org/0000-0002-8501-2187>;

**Aleskerova, Zuleikha Fikret** — Researcher, Institute of Catalysis and Inorganic Chemistry named after academician Murtuza Naghiyev, H. Javid ave., 113, Baku AZ 1143, Azerbaijan Republic; e-mail: [zuleyxaalasarova@gmail.com](mailto:zuleyxaalasarova@gmail.com), <http://orcid.org/0000-0001-6144-9686>;

**Litvishkov, Yuri Nikolayevich** — Doctor of Chemical Sciences, professor, Institute of Catalysis and Inorganic Chemistry named after academician Murtuza Naghiyev, H. Javid ave., 113, Baku AZ 1143, Azerbaijan Republic; e-mail: [yuriylit@rambler.ru](mailto:yuriylit@rambler.ru), <http://orcid.org/0000-0003-0662-1257>;

**Tagiyev, Dilgam Babir** — Doctor of Chemical Sciences, professor, general director, Institute of Catalysis and Inorganic Chemistry named after academician Murtuza Naghiyev, H. Javid ave., 113, Baku AZ 1143, Azerbaijan Republic; e-mail: [dtagiyev@hotmail.com](mailto:dtagiyev@hotmail.com), <http://orcid.org/0000-0002-8312-2980>

---

\*The author's name is presented in the order: *Last Name, First and Middle Names*

B.K. Kasenov<sup>1\*</sup>, Sh.B. Kasenova<sup>1</sup>, Zh.I. Sagintaeva<sup>1</sup>, S.O. Baisanov<sup>1</sup>,  
N.Yu. Lu<sup>1</sup>, E.E. Kuanyshbekov<sup>1</sup>, M.O. Turtubaeva<sup>2</sup>, M.A. Isabaeva<sup>3</sup>

<sup>1</sup>Abishev Chemical-Metallurgical Institute, Karaganda, Kazakhstan;

<sup>2</sup>Kazakh Medical University named after S.D. Asfendiyarov, Almaty, Kazakhstan;

<sup>3</sup>Toraigyrov University, Pavlodar, Kazakhstan

(\*Corresponding author's e-mail: [kasenov1946@mail.ru](mailto:kasenov1946@mail.ru))

## Novel Titanium-Manganites of Lanthanum and Alkali Metals

The titanium-manganites of  $\text{LaMe}_2\text{TiMnO}_6$  ( $\text{Me}^I$  — Li, Na, K) were synthesized by the ceramic technology with the high-temperature reaction of oxides of  $\text{La}_2\text{O}_3$ ,  $\text{TiO}_2$ ,  $\text{Mn}_2\text{O}_3$  with carbonates of  $\text{Li}_2\text{CO}_3$ ,  $\text{Na}_2\text{CO}_3$ ,  $\text{K}_2\text{CO}_3$  within 800–1200 °C. The X-ray diffraction methods demonstrated that all of them were crystallized in the cubic syngony with the lattice parameters such as  $\text{LaLi}_2\text{TiMnO}_6$  —  $a = 13.48 \pm 0.02$  Å,  $V^o = 2449.46 \pm 0.06$  Å<sup>3</sup>,  $Z = 4$ ,  $V^o_{\text{el.cell}} = 612.87 \pm 0.02$  Å<sup>3</sup>,  $\rho_{\text{roent.}} = 3.81$ ;  $\rho_{\text{pick.}} = 3.78 \pm 0.03$  g/cm<sup>3</sup>;  $\text{LaNa}_2\text{TiMnO}_6$  —  $a = 14.06 \pm 0.02$  Å,  $V^o = 2779.43 \pm 0.06$  Å<sup>3</sup>,  $Z = 4$ ,  $V^o_{\text{el.cell}} = 694.96 \pm 0.02$  Å<sup>3</sup>,  $\rho_{\text{roent.}} = 3.67$ ;  $\rho_{\text{pick.}} = 3.65 \pm 0.01$  g/cm<sup>3</sup>;  $\text{LaK}_2\text{TiMnO}_6$  —  $a = 14.74 \pm 0.02$  Å,  $V^o = 3202.52 \pm 0.06$  Å<sup>3</sup>,  $Z = 4$ ,  $V^o_{\text{el.cell}} = 800.52 \pm 0.02$  Å<sup>3</sup>,  $\rho_{\text{roent.}} = 3.45$ ;  $\rho_{\text{pick.}} = 3.43 \pm 0.01$  g/cm<sup>3</sup>. Correctness and authenticity of the results on the indexing of X-ray photographs of titanium-manganite were confirmed with the good experimental and calculated values ( $10^4/d^2$ ), the pycnometric and X-ray densities, and also the theoretical and experimental values of cell volumes. The rising of values of the lattice parameters of the synthesized titanium-manganites was determined with increasing in the ionic radii from Li to K.

**Key words:** titanium-manganite, lanthanum, alkali metals, synthesis, X-ray diffraction, indexing, syngony, unit cell, lattice parameters.

### Introduction

To date the sustained interest in the ferroelectric materials was observed. This is caused by the ability to develop electrically controlled ultrahigh-frequency (UHF) devices on their basis. The ferroelectric materials have anomalously high nonlinearity of the dielectric properties. As a result they are very attractive to use in the ultrahigh-frequency electronics [1]. Manganites of a fixed composition are materials with the high spin polarization to research some fundamental issues and to use in the spintronic devices and in the magnetic tunnel structures. The interest in using of manganites is caused by some unique properties such as the high spin polarization reaching 100 %, high Curie temperature, chemical stability, etc. [2]. Attention is also drawn to the fact that the semiconductor titanium oxides with transition metal impurities are able to be as the advancing materials to use in the spin electronics and catalysis [3, 4]. For instance, barium titanate is a traditional electroceramic material and it has the ferro-, ferroelectric — and pyroelectric properties. It ought to be noted that the high values of dielectric permittivity in the ferroelectric materials near a transition temperature permit to use them in the miniature capacitors [5].

It should be pointed out that a field of the potential applications of materials with the colossal magnetic resistance such as  $\text{La}_{1-x}(\text{Ca}, \text{Ba})_x\text{MnO}_3$  manganites include magnetic field sensors, the reading heads for high-density magnetic recording, displacement sensors, temperature sensors, bolometers, etc. [6]. Data on the fuel cells based on perovskite-like solid solutions of  $(\text{La}_{0.5+x}\text{Sr}_{0.5-x})_{1-y}\text{Mn}_{0.5}\text{Ti}_{0.5}\text{O}_{3-\delta}$  ( $x = 0-0.25$ ,  $y = 0-0.03$ ) are described in [7, 8].

The abovementioned literature review demonstrates that compounds based on manganites and titanates of the rare-earth elements doped with oxides of s-elements are of the great scientific and practical interest. As a result, the purpose of this paper is to synthesize and study the X-ray diffraction characteristics of the novel titanium-manganites of lanthanum and alkali metals.

### Experimental

Oxides of lanthanum (III) (“puriss. spec.” 99.99 %), titanium (IV) and manganese (III), and carbonates of lithium, sodium and potassium (production Russia) (“p.a.” 99.0 %) were the initial reagents to synthesize

the titanium-manganites of  $\text{LaMe}^{\text{I}}_2\text{TiMnO}_6$  ( $\text{Me}^{\text{I}}$  — Li, Na, K). These substances were pre-annealed at 300 °C to remove the adsorption moisture. Then, the stoichiometric amounts of these substances were thoroughly mixed and ground in an agate mortar to obtain the titanium-manganites of  $\text{LaMe}^{\text{I}}_2\text{TiMnO}_6$  ( $\text{Me}^{\text{I}}$  — Li, Na, K). Further, the mixtures were placed to the alundum crucibles pre-calcined at 600 °C. Then they were annealed at 600 °C in a SNOL furnace for 5 h. Mixtures were cooled to a room temperature with the repeated processes of mixing and grinding. Then the mixtures were heat-treated at 800 °C for 5 h with processes of cooling to a room temperature, grinding and stirring. Further the analogous procedures were performed at 1000 °C for 10 h twice and at 1200 °C for 4 h. After repeating the mixing and grinding, a low-temperature annealing at 400 °C for 10 h was performed to obtain the equilibrium phases at a low temperature.

Formation of the equilibrium compositions of titanium-manganites was identified with the X-ray phase analysis on DRON-2.0 diffractometer (production Russia). The recording conditions:  $\text{CuK}\alpha$ -radiation,  $U = 30$  kV,  $J = 10$  mA, rotation speed — 1000 pps, time constant  $\tau = 5$  sec and angles  $2\theta$  from 10 to 90°. Intensity of diffraction peaks was graded on a 100-point scale.

### Results and Discussion

The indexing of X-ray photographs of titanium-manganites demonstrated that all synthesized titanium-manganites were crystallized in the cubic syngony.

The lattice parameters and X-ray densities were determined. The indexing of X-ray photographs was performed with the analytical method [9]. Table 1 below demonstrates the indexing results.

Table 1

**The indexing of X-ray photographs of  $\text{LaMe}^{\text{I}}_2\text{TiMnO}_6$  ( $\text{Me}^{\text{I}}$  — Li, Na, K) powders**

$I/I_0$	$d/\text{Å}$	$10^4/d^2_{\text{exp.}}$	$hkl$	$10^4/d^2_{\text{calc.}}$
<b><math>\text{LaLi}_2\text{TiMnO}_6</math></b>				
6	3.89	660.8	410	661.0
100	2.75	1322	433	1322
12	2.50	1600	621	1597
23	2.24	1993	7.1.1	1982
11	2.06	2356	6.5.0	2368
44	1.94	2657	8.2.0	2643
40	1.57	4057	10.2.0	4075
7	1.41	5030	10.5.2	5011
18	1.37	5328	10.6.1	5341
14	1.22	6719	13.2.0	6718
<b><math>\text{LaNa}_2\text{TiMnO}_6</math></b>				
10	3.90	657.5	320	658.0
100	2.76	1313	510	1315
11	2.40	1736	530	1720
21	2.23	2011	620	2013
38	1.93	2685	720	2685
33	1.59	3956	752	3945
13	1.37	5328	10.2.1	5311
10	1.23	6610	11.3.1	6625
<b><math>\text{LaK}_2\text{TiMnO}_6</math></b>				
7	3.94	644.2	321	644.0
100	2.82	1257	333	1242
20	2.25	1975	533	1978
30	1.97	2577	642	2577
5	1.74	3305	660	3313
27	1.59	3956	921	3957
12	1.38	5251	871	5246
5	1.23	6610	12.0.0	6626

It should be stated that the theoretical cell volumes of the synthesized titanium-manganites were determined with using the actual literature data on the cell volumes of the oxides included in their composition [10, 11] under the scheme:

$$V_{\text{el.cell}}^0 \text{LaMe}^{\text{I}}_2\text{TiMnO}_6 = 0.5 V_{\text{el.cell}}^0 \text{La}_2\text{O}_3 + V_{\text{el.cell}}^0 \text{Me}_2\text{O} + V_{\text{el.cell}}^0 \text{TiO}_2 + 0.5 V_{\text{el.cell}}^0 \text{Mn}_2\text{O}_3, \quad (1)$$

where  $\text{Me}^{\text{I}}$  — are Li, Na, K.

The X-ray density of compounds ( $\rho_{\text{roent.}}$ ) was calculated with the formula [1]:

$$\rho_{\text{roent}} = \frac{1,66 \cdot Mr \cdot Z}{V^0}, \quad (2)$$

where  $Mr$  is the molecular weight of a compound;  $Z$  is the number of formula units in the lattice;  $V^0$  is an elementary cell volume.

Four to five parallel measurements of manganite density were performed in 1-mL glass pycnometers under the procedure [12]. Toluene was used as an indifferent liquid i.e. it wetted these compounds well. It was chemically inactive towards them and its density was stable to the temperature changes.

Table 2 below demonstrates the cell parameters, X-ray and pycnometric densities of the synthesized titanium-manganites.

Table 2

**Lattice parameters of titanium-manganites of  $\text{LaLi}_2\text{TiMnO}_6$  (I),  
 $\text{LaNa}_2\text{TiMnO}_6$  (II) and  $\text{LaK}_2\text{TiMnO}_6$  (III)**

Titanium-manganite	$a, \text{Å}$	$V^{\circ}, \text{Å}^3$	$Z$	$V_{\text{el.cell}}^{\circ}, \text{Å}^3$	$\rho, \text{g/cm}^3$	
					$\rho_{\text{roent.}}$	$\rho_{\text{pick.}}$
I	$13.48 \pm 0.02$	$2449.46 \pm 0.06$	4	$612.37 \pm 0.02$	3.81	$3.78 \pm 0.03$
II	$14.06 \pm 0.02$	$2779.43 \pm 0.06$	4	$694.96 \pm 0.02$	3.67	$3.65 \pm 0.01$
III	$14.74 \pm 0.02$	$3202.52 \pm 0.06$	4	$800.63 \pm 0.02$	3.45	$3.43 \pm 0.01$

Correctness and authenticity of the results on the indexing and determination of the lattice parameters for titanium-manganites were confirmed with the good experimental and calculated values ( $10^4/d^2$ ), the X-ray and pycnometric densities, and also the theoretical and experimental data on cell volumes of  $\text{LaLi}_2\text{TiMnO}_6$  ( $V_{\text{theor.}}^{\circ} = 622.10 \text{ Å}^3$ ,  $V_{\text{exp.}}^{\circ} = 612.36 \text{ Å}^3$ ),  $\text{LaNa}_2\text{TiMnO}_6$  ( $V_{\text{theor.}}^{\circ} = 693.71 \text{ Å}^3$ ,  $V_{\text{exp.}}^{\circ} = 694.86 \text{ Å}^3$ ) and  $\text{LaK}_2\text{TiMnO}_6$  ( $V_{\text{theor.}}^{\circ} = 790.97 \text{ Å}^3$ ,  $V_{\text{exp.}}^{\circ} = 800.63 \text{ Å}^3$ ). All experimental data was processed with methods of the mathematical statistics.

Based on the described above studies, the obtained titanium-manganites can be attributed to the perovskite  $Pm\bar{3}m$  space group.

The pattern was observed in change of the lattice parameters of the synthesized titanium-manganites in transition from Li to K.

The symbate changes i.e. the rising in values of parameters “a”, the lattice volumes and the elementary cell volumes of titanium-manganites were observed with increasing in the ionic radii from Li to K.

### Conclusions

Titanium-manganites of lanthanum and alkali metals of  $\text{LaMe}^{\text{I}}_2\text{TiMnO}_6$  ( $\text{Me}^{\text{I}}$  — Li, Na, K) were first obtained with the ceramic technology, and their syngony types and lattice parameters were determined. It was found that the lattice parameters of the synthesized titanium-manganites were able to change symbatically with increasing in the ionic radii of alkali metals. The results are a basis to perform the thermodynamic and electrophysical investigations, to determine the advancing physical-chemical and physical properties of the obtained novel titanium-manganites of lanthanum and alkali metals.

### Acknowledgments

The study was performed within the program-targeted financing of the scientific and technical program “Development of novel composite materials with high exploitation properties based on the rare and rare-earth elements” of Committee for the Industrial Development of the Ministry of Industry and Infrastructure Development of the Republic of Kazakhstan.

## References

- 1 Tumarkin A.V. Structural properties of barium strontium titanate films grown under different technological conditions / A.V. Tumarkin, V.I. Al'myashev, S.V. Razumov, M.M. Gaidukov, A.G. Gagarin, A.G. Al'tynnikov, A.B. Kozyrev // *Physics of the Solid State*. — 2015. — Vol. 57, Iss. 3. — P. 553–557. <https://doi.org/10.1134/s1063783415030348>
- 2 Volkov N.B. Spintronics: manganite-based magnetic tunnel structures / N.B. Volkov // *Physics-Uspekhi*. — 2012. — Vol. 55, Iss. 3. — P. 250–269. <https://doi.org/10.3367/ufne.0182.201203b.0263>
- 3 Mesilov V.V. Soft X-ray absorption spectroscopy of titanium dioxide nanopowders with cobalt impurities / V.V. Mesilov, V.R. Galakhov, M.S. Udintseva, A.Ye. Yermakov, M.A. Uimin, G.S. Zakharova, D.A. Smirnov, A.F. Gubkin, E.A. Sherstobitova // *Journal of Experimental and Theoretical Physics*. — 2017. — Vol. 124, Iss. 6. — P. 908–913. <https://doi.org/10.1134/s106377611705003x>
- 4 Abildina A.K. Preparation and electrochemical characterization of TiO<sub>2</sub> as an anode material for magnesium-ion batteries / A.K. Abildina, K. Avchukir, R.Z. Jumanova, A.N. Beiseyeva, G.S. Rakhymbay, A.M. Argimbayeva // *Bulletin of the University of Karaganda – Chemistry*. — 2021. — № 104. — P. 104–116.
- 5 Барфут Дж. Введение в физику сегнетоэлектрических явлений / Дж. Барфут. — М.: Мир, 1970. — 359 с.
- 6 Третьяков Ю.Д. Новые поколения неорганических функциональных материалов / Ю.Д. Третьяков, О.А. Брылёв // *Журн. Рос. хим. общ-ва им. Д.И. Менделеева*. — 2000. — Т. 45. № 4. — С. 10–16.
- 7 Иванов А.И. Синтез и свойства анодов топливных элементов на основе (La<sub>0,5+x</sub>Sr<sub>0,5-x</sub>)<sub>1-y</sub>Mn<sub>0,5</sub>Ti<sub>0,5</sub>O<sub>3-δ</sub> (x = 0–0.25, y = 0–0.03) / А.И. Иванов, Д.А. Агарков, И.Н. Бурмистров, Е.А. Кудренко, С.И. Бредихин, В.В. Хартон // *Электрохимия*. — 2014. — Т. 50. № 8. — С. 814–820.
- 8 Vaimuratova Z.A., Kalmakhanova M.S., Massalimova B.K., Nurlibaeva A.A., Kulazhanova A.S., de Tuesta J.L.D., Gomes H.T. Synthesis and characterization of a new magnetic composite MnFe<sub>2</sub>O<sub>4</sub>/clay based on a natural clay obtained from Turkistan deposit // *Bulletin of the University of Karaganda – Chemistry*. — 2021. — № 104. — С. 87–94.
- 9 Ковба Л.М. Рентгенофазовый анализ / Л.М. Ковба, В.К. Трунов. — М.: Изд-во МГУ, 1976. — 2-е изд. — 256 с.
- 10 Вест А. Химия твердого топлива / А. Вест. — М.: Мир, 1988. — 588 с.
- 11 Пенкаля Т. Очерки кристаллохимии / Т. Пенкаля. — М.: Химия, 1974. — 496 с.
- 12 Кивилис С.С. Техника измерений плотности жидкостей и твердых тел / С.С. Кивилис. — М.: Стандартгиз, 1959. — 191 с.

Б.Қ. Қасенов, Ш.Б. Қасенова, Ж.И. Сағынтаева, С.О. Байсанов,  
Н.Ю. Лу, Е.Е. Қуанышбеков, М.О. Түртібаева, М.А. Исабаева

### Лантан және сілтілі металдардың жаңа титан-манганиттері

Керамикалық технология әдісімен La<sub>2</sub>O<sub>3</sub>, TiO<sub>2</sub>, Mn<sub>2</sub>O<sub>3</sub> тотықтарының Li<sub>2</sub>CO<sub>3</sub>, Na<sub>2</sub>CO<sub>3</sub>, K<sub>2</sub>CO<sub>3</sub> карбонаттарымен 800–1200 °C аралықта жоғары температуралы әрекеттесуімен LaMe<sup>1</sup><sub>2</sub>TiMnO<sub>6</sub> (Me<sup>1</sup> — Li, Na, K). құрамды титан-манганиттері синтезделді. Рентгенография әдістері олардың барлығы келесідей тор параметрлерімен кубтық сингонияда кристалданатындығын анықтады: LaLi<sub>2</sub>TiMnO<sub>6</sub> — a = 13,48±0,02 Å, V<sup>o</sup> = 2449,46±0,06 Å<sup>3</sup>, Z = 4, V<sup>o</sup><sub>эл.ұяш.</sub> = 612,87±0,02 Å<sup>3</sup>, ρ<sub>рент.</sub> = 3,81; ρ<sub>пикн.</sub> = 3,78±± 0,03 г/см<sup>3</sup>; LaNa<sub>2</sub>TiMnO<sub>6</sub> — a = 14,06±0,02 Å, V<sup>o</sup> = 2779,43±0,06 Å<sup>3</sup>, Z = 4, V<sup>o</sup><sub>эл.ұяш.</sub> = 694,96±0,02 Å<sup>3</sup>, ρ<sub>рент.</sub> = 3,67; ρ<sub>пикн.</sub> = 3,65±0,01 г/см<sup>3</sup>; LaK<sub>2</sub>TiMnO<sub>6</sub> — a = 14,74±0,02 Å, V<sup>o</sup> = 3202,52±± 0,06 Å<sup>3</sup>, Z = 4, V<sup>o</sup><sub>эл.ұяш.</sub> = 800,52±0,02 Å<sup>3</sup>, ρ<sub>рент.</sub> = 3,45; ρ<sub>пикн.</sub> = 3,43±0,01 г/см<sup>3</sup>. Титан-манганиттердің рентгенограммаларын индицирлеудің нәтижелерінің дәлділігі мен анықтылығы 10<sup>4</sup>/d<sup>2</sup> тәжірибелік пен теориялық мәндерінің, пикнометрлік және рентгендік тығыздықтарының және элементарлы ұяшықтардың теориялық және тәжірибелік көрсеткіштерінің жақсы үйлесімділігімен дәлелденді. Иондық радиустың Li-ден K-ге жоғарылауымен синтезделген титан-манганиттер тор параметрлері шамаларының артатындығы анықталды.

*Кілт сөздер:* титан-манганит, лантан, сілтілі металдар, синтез, рентгенография, индицирлеу, сингония, элементарлы ұяшық, тор көрсеткіштері.

Б.К. Касенов, Ш.Б. Касенова, Ж.И. Сагінтаева, С.О. Байсанов,  
Н.Ю. Лу, Е.Е. Куанышбеков, М.О. Туртубаева, М.А. Исабаева

### Новые титано-манганиты лантана и щелочных металлов

Методом керамической технологии с высокотемпературным взаимодействием оксидов La<sub>2</sub>O<sub>3</sub>, TiO<sub>2</sub>, Mn<sub>2</sub>O<sub>3</sub> с карбонатами Li<sub>2</sub>CO<sub>3</sub>, Na<sub>2</sub>CO<sub>3</sub>, K<sub>2</sub>CO<sub>3</sub> в интервале 800–1200 °C синтезированы титано-манганиты состава LaMe<sup>1</sup><sub>2</sub>TiMnO<sub>6</sub> (Me<sup>1</sup> — Li, Na, K). Методами рентгенографии установлено, что все

они кристаллизуются в кубической сингонии со следующими параметрами решетки:  $\text{LaLi}_2\text{TiMnO}_6$  —  $a = 13,48 \pm 0,02 \text{ \AA}$ ,  $V^0 = 2449,46 \pm 0,06 \text{ \AA}^3$ ,  $Z = 4$ ,  $V^0_{\text{эл.яч.}} = 612,87 \pm 0,02 \text{ \AA}^3$ ,  $\rho_{\text{рент.}} = 3,81$ ;  $\rho_{\text{пикн.}} = 3,78 \pm 0,03 \text{ г/см}^3$ ;  $\text{LaNa}_2\text{TiMnO}_6$  —  $a = 14,06 \pm 0,02 \text{ \AA}$ ,  $V^0 = 2779,43 \pm 0,06 \text{ \AA}^3$ ,  $Z = 4$ ,  $V^0_{\text{эл.яч.}} = 694,96 \pm 0,02 \text{ \AA}^3$ ,  $\rho_{\text{рент.}} = 3,67$ ;  $\rho_{\text{пикн.}} = 3,65 \pm 0,01 \text{ г/см}^3$ ;  $\text{LaK}_2\text{TiMnO}_6$  —  $a = 14,74 \pm 0,02 \text{ \AA}$ ,  $V^0 = 3202,52 \pm 0,06 \text{ \AA}^3$ ,  $Z = 4$ ,  $V^0_{\text{эл.яч.}} = 800,52 \pm 0,02 \text{ \AA}^3$ ,  $\rho_{\text{рент.}} = 3,45$ ;  $\rho_{\text{пикн.}} = 3,43 \pm 0,01 \text{ г/см}^3$ . Корректность и достоверность результатов индирования рентгенограмм титано-манганитов подтверждались с хорошим согласием опытных и расчетных значений  $10^4/d^2$ , пикнометрических и рентгеновских плотностей, а также теоретических и опытных значений объемов элементарных ячеек. Выявлено, что повышением ионных радиусов от Li к K увеличиваются величины параметров решеток синтезированных титано-манганитов.

**Ключевые слова:** титано-манганит, лантан, щелочные металлы, синтез, рентгенография, индирование, сингония, элементарная ячейка, параметры решеток.

## References

- 1 Tumarkin, A.V., Al'myashev, V.I., Razumov, S.V., Gaidukov, M.M., Gagarin, A.G., Al'tynnikov, A.G., & Kozyrev, A.B. (2015). Structural properties of barium strontium titanate films grown under different technological conditions. *Physics of the Solid State*, 57, 3, 553–557. <https://doi.org/10.1134/S1063783415030348>
- 2 Volkov, N.B. (2012). Spintronics: manganite-based magnetic tunnel structures. *Physics-Uspexhi*, 55, 3, 250–269. <https://doi.org/10.3367/ufne.0182.201203b.0263>
- 3 Mesilov V.V., Galakhov, V.R., Udintseva, M.S., Yermakov, A.Ye., Uimin, M.A., Zakharova, G.S., Smirnov, D.A., Gubkin, A.F., & Sherstobitova, E.A. (2017). Soft X-ray absorption spectroscopy of titanium dioxide nanopowders with cobalt impurities. *Journal of Experimental and Theoretical Physics*. 124, 6, 908–913. <https://doi.org/10.1134/S106377611705003x>
- 4 Abildina, A.K., Avchukir, K., Jumanova, R.Z., Beiseyeva, A.N., Rakhymbay, G.S., & Argimbayeva, A.M. (2021). Preparation and electrochemical characterization of  $\text{TiO}_2$  as an anode material for magnesium-ion batteries. *Bulletin of the University of Karaganda — Chemistry* (104), 104–116. <https://doi.org/10.31489/2021Ch4/104-116>
- 5 Barfut, Dzh. (1970). *Vvedenie v fiziku segnetoelektricheskikh yavlenii [Introduction to the physics of ferroelectric phenomena]*. Moscow: Mir [in Russian].
- 6 Tretyakov, Yu.D., & Brylyov, O.A. (2000). Novye pokoleniia neorganicheskikh funktsionalnykh materialov [New generations of inorganic functional materials]. *Zhurnal Rossiiskogo khimicheskogo obshchestva imeni D.I. Mendeleeva – Journal of the Russian Chemical Society named after D.I. Mendeleev*, 44, 4, 10–16 [in Russian].
- 7 Ivanov, A.I., Agarkov, D.A., Burmistrov, I.N., Kudrenko, E.A., Bredihin, S.I., & Harton, V.V. (2014). Sintez i svoystva anodov toplivnykh elementov na osnove  $(\text{La}_{0,5+x}\text{Sr}_{0,5-x})_{1-y}\text{Mn}_{0,5}\text{Ti}_{0,5}\text{O}_{3-\delta}$  ( $x = 0-0,25$ ,  $y = 0-0,03$ ) [Synthesis and properties of fuel cell anodes based on  $(\text{La}_{0,5+x}\text{Sr}_{0,5-x})_{1-y}\text{Mn}_{0,5}\text{Ti}_{0,5}\text{O}_{3-\delta}$  ( $x = 0-0,25$ ,  $y = 0-0,03$ )]. *Elektrokhimiia — Electrochemistry*, 50, 8, 814–820 [in Russian].
- 8 Baimuratova, Z. A., Kalmakhanova, M.S., Massalimova, B.K., Nurlibaeva, A.A., Kulazhanova, A.S., de Tuesta, J.L.D., & Gomes, H.T. (2021). Synthesis and characterization of a new magnetic composite  $\text{MnFe}_2\text{O}_4/\text{clay}$  based on a natural clay obtained from Turkestan deposit. *Bulletin of the University of Karaganda — Chemistry* (104), 87–94. <https://doi.org/10.31489/2021Ch4/87-94>
- 9 Kovba, L.M., & Trunov, V.K. (1976). *Rentgenofazovyy analiz [X-ray phase analysis]*. Moscow: Moskovskii gosudarstvennyi universitet [in Russian].
- 10 Vest, A. (1988). *Khimiia tverdogo tela [Chemistry of solid state]*. Moscow: Mir [in Russian].
- 11 Penkalya, T. (1974). *Ocherki kristalokhimii [Essays on crystal chemistry]*. Moscow: Khimiia [in Russian].
- 12 Kivilis, S.S. (1959). *Tehnika izmerenii plotnosti zhidkosti i tverdykh tel [Technique of measuring of the density of liquids and solids]*. Moscow: Standartgiz [in Russian].

## Information about authors\*

**Kasenov, Bulat Kunurovich** (*corresponding author*) — doctor of chemical sciences, professor, head of laboratory, laboratory of the thermochemical processes, Zh. Abishev Chemical-Metallurgical Institute, Ermekov St., 63, 100009, Karaganda, Kazakhstan; e-mail: [kasenov1946@mail.ru](mailto:kasenov1946@mail.ru), <https://orcid.org/0000-0001-9394-0592>;

**Kasenova, Shuga Bulatovna** — doctor of chemical sciences, professor, chief researcher, laboratory of the thermochemical processes, Zh. Abishev Chemical-Metallurgical Institute, Ermekov St., 63, 100009, Karaganda, Kazakhstan; e-mail: [kasenovashuga@mail.ru](mailto:kasenovashuga@mail.ru), <https://orcid.org/0000-0001-9755-7478>;

**Sagintaeva, Zhenisgul Imangaliyeva** — candidate of chemical sciences, associate professor, leading researcher, laboratory of the thermochemical processes, Zh. Abishev Chemical-Metallurgical Institute, Ermekov St., 63, 100009, Karaganda, Kazakhstan; e-mail: [kai\\_sagintaeva@mail.ru](mailto:kai_sagintaeva@mail.ru), <https://orcid.org/0000-0001-8655-356X>;

**Kuanyshbekov, Yerbolat Yermekovich** — master of technical sciences, researcher, laboratory of the thermochemical processes, Zh. Abishev Chemical-Metallurgical Institute, Ermekov St., 63, 100009, Karaganda, Kazakhstan; e-mail: [mr.ero1986@mail.ru](mailto:mr.ero1986@mail.ru), <https://orcid.org/0000-0001-9172-9566>;

**Turtubaeva, Meruert Orazgalievna** — PhD, docent, Kazakh Medical University named after S.D. Asfendiyarov, Tole Bi St., 94, 050000, Almaty, Kazakhstan; e-mail: [azat-2000@bk.ru](mailto:azat-2000@bk.ru), <https://orcid.org/0000-0001-7932-5075>;

**Baisanov, Sailaubai Omarovich** — doctor of technical sciences, professor, director of Zh. Abishev Chemical-Metallurgical Institute, Ermekov St., 63, 100009, Karaganda, Kazakhstan; e-mail: [hmi2009@mail.ru](mailto:hmi2009@mail.ru); <https://orcid.org/0000-0002-7328-2921>

**Lu, Natalya Yulievna** — candidate of technical sciences, deputy director for the scientific work, Zh. Abishev Chemical-Metallurgical Institute, Ermekov St., 63, 100009, Karaganda, Kazakhstan; e-mail: [hmi2009@mail.ru](mailto:hmi2009@mail.ru), <https://orcid.org/0000-0002-3624-0984>

**Isabaeva, Manera Amangeldievna** — candidate of Chemical Sciences, Professor of the Department of Chemistry and Chemical Technology of Toraigyrov University, Lomov St., 64, 140008, Pavlodar, Kazakhstan, e-mail: [isabaeva.manar@mail.ru](mailto:isabaeva.manar@mail.ru), <https://orcid.org/0000-0002-8119-3865>

---

\*The author's name is presented in the order: *Last Name, First and Middle Names*

A. Houbi<sup>1, 2\*</sup>, A.A. Zharmenov<sup>1, 2</sup>, Y. Atassi<sup>3</sup>,  
Z.T. Bagasharova<sup>1, 2</sup>, S. Mirzalieva<sup>1, 2</sup>, B.A. Karibayev<sup>4</sup>

<sup>1</sup>National Center on Complex Processing of Mineral Raw Materials of the Republic of Kazakhstan, Almaty, Kazakhstan;

<sup>2</sup>Department of Chemical Technology of Inorganic Substances, Al-Farabi Kazakh National University, Almaty, Kazakhstan;

<sup>3</sup>Department of Applied Physics, Higher Institute for Applied Sciences and Technology, Damascus, Syria;

<sup>4</sup>Department of Physics and Technology, Al-Farabi Kazakh National University, Almaty, Kazakhstan

(\*Corresponding author's e-mail: [Anashoubi@gmail.com](mailto:Anashoubi@gmail.com))

## Synthesis and Microwave Absorption Properties of (Ni<sub>0.5</sub>Zn<sub>0.5</sub>Fe<sub>2</sub>O<sub>4</sub>/CI/CB) Ternary Composites

In this work, ternary composites of NiZn ferrite/carbonyl iron/carbon black (Ni<sub>0.5</sub>Zn<sub>0.5</sub>Fe<sub>2</sub>O<sub>4</sub>/CI/CB) were prepared via two stages. Firstly, Ni<sub>0.5</sub>Zn<sub>0.5</sub>Fe<sub>2</sub>O<sub>4</sub> was prepared by a self-combustion method using sucrose as a fuel. After that, the operation was continued via mixing CB, CI, and Ni<sub>0.5</sub>Zn<sub>0.5</sub>Fe<sub>2</sub>O<sub>4</sub> through grinding balls. Three various weight ratios of Ni<sub>0.5</sub>Zn<sub>0.5</sub>Fe<sub>2</sub>O<sub>4</sub>/CI/CB (1:1:1, 1:1:2, and 2:1:1) with various thicknesses (2–4–6 mm) were prepared. The absorbers were prepared by dispersing (Ni<sub>0.5</sub>Zn<sub>0.5</sub>Fe<sub>2</sub>O<sub>4</sub>/CI/CB) composites with a weight ratio within a paraffin wax matrix of 40 % w/w. X-ray diffractometry and FTIR spectroscopy were used in order to characterize the samples. The morphology of the powders was investigated by SEM. The functional characterization was accomplished by measuring the microwave absorption properties in the frequency band of 8.8–12 GHz. The microwave absorption materials (MAMs) showed wide bandwidths under –10 dB in the range of 2.81–3.20 GHz and reasonable surface density in the range of 3.625–4.041 kg/m<sup>2</sup>. The absorber of 3.20 GHz bandwidth had a minimal reflection loss of –19.4 dB at the matching frequency of 9.92 GHz with a thickness of 6 mm.

**Keywords:** NiZn ferrite; Carbonyl iron, Carbon black, Reflection loss, Absorption bandwidth, Matching frequency, Paraffin wax matrix, Surface density.

### Introduction

Electromagnetic interference (EMI) would be regarded as an unwanted result of modern technology that has dangerous effects on human health, intelligent devices, and military industries. Consequently, this EMI has become a critical worldwide issue and its alleviation could be accomplished only by utilize of EMI shielding materials. Nowadays, several magnetic loss materials such as hexagonal ferrites, spinel ferrites, and carbonyl iron or dielectric loss materials such as conductive polymers and carbonaceous materials have played a significant role in high-frequency EM wave absorption. Nevertheless, the drawbacks involving elevated density, low reflection absorption, and narrow wideband have hugely limited conventional loss materials' workable benefits for EM wave absorption. In recent years, MA composites based on carbon, carbonyl iron, and ferrite, have obtained significant concern due to their excellent electrical and ferrimagnetic characteristics. Carbonaceous materials-based composites have pulled in major attention for microwave absorption lately because of the unique structure of carbon-based materials. Carbon black is usually used to fit the requirements of high-effective microwave attenuation materials because of its superior characteristics, for example, high permittivity, high specified surface region, huge interface, etc. Carbon black has a unique place in the band of elevated-frequency MAMs. Furthermore, spinel ferrites and carbonyl iron have excellent MA characteristics due to their unique magnetic characteristics. NiZn ferrites and carbonyl iron are considered suitable materials for high-frequency implementations [1, 2]. When NiZn ferrite and carbonyl iron are mixed with carbon black, the MA characteristics of the resultant composite are anticipated to enhance. According to this, BaFe<sub>12</sub>O<sub>19</sub>/CI absorbers with various powder ratio compositions in the frequency range of 2–18 GHz were successfully prepared by Feng et al. [3]. The single-layer and double-layer absorbers were prepared, and their MA characteristics were studied. The outcomes showed that the double-layer absorber was clearly more than that of the single-layer absorber. Where the reflection loss (RL) for the double-layer absorber was –13 dB in the frequency range (6–18 GHz) and less than –8 dB in the frequency range (2–18 GHz). The thicknesses of the absorbers were 3.6 and 3.7 mm, respectively. On the other hand, Yan et al. [4] prepared a

mixture of doped polyaniline (PANI) coated porous structure carbonyl iron powder (CIP) and graphene sheets. The results showed that the absorption bandwidth under  $-10$  dB ( $BW_{-10\text{ dB}}$ ) was 4.6 GHz for 2 mm thickness for the composites with 40 wt.% of PANI@ porous CIP and 5 wt.% of Graphene. The outcomes showed that graphene-PANI@ porous CIP was a promising wave absorbing composite material. Until now, to the best of our knowledge, no studies have been reported on the MA properties of composites made up of NiZn ferrite/carbonyl iron/carbon black ( $\text{Ni}_{0.5}\text{Zn}_{0.5}\text{Fe}_2\text{O}_4/\text{CI}/\text{CB}$ ). In this work, a perfect absorber was obtained by incorporating  $\text{Ni}_{0.5}\text{Zn}_{0.5}\text{Fe}_2\text{O}_4$  and CI (magnetic loss materials) and CB (dielectric loss material) within a paraffin wax matrix. Where we study the effect of different weight ratios of  $\text{Ni}_{0.5}\text{Zn}_{0.5}\text{Fe}_2\text{O}_4/\text{CI}/\text{CB}$  and its effect on the MA properties. A distinct feature of this work is that NiZn ferrite was synthesized through a self-combustion method utilizing polyvinyl alcohol (PVA) as a chelating agent. After that, the operation is continuous through mixing and grinding CB, CI, and NiZn ferrite by grinding balls.

### Experimental

**Chemicals:** polyvinyl alcohol (PVA) (hydrolyzed, MW: 72000), nickel(II) nitrate hexahydrate ( $\text{Ni}(\text{NO}_3)_2 \cdot 6\text{H}_2\text{O}$ , 98.3 % purity), zinc nitrate hexahydrate ( $\text{Zn}(\text{NO}_3)_2 \cdot 6\text{H}_2\text{O}$ , 98.7 % purity), and iron(III) nitrate nonahydrate ( $\text{Fe}(\text{NO}_3)_3 \cdot 9\text{H}_2\text{O}$ , 98.2 % purity) were purchased from TRADING COMPANY ANT, Russia. On the other hand, carbonyl iron (CI, 99.6 % purity) and carbon black (CB, 99.5 % purity) were purchased from Cabot Norit Company, Netherland.

**Instruments used:** A powder X-ray diffractometer (XRD, Rigaku Miniflex 600, Cu-Ka) was used for determining the crystal structures of the powders. Fourier Transform IR (FTIR) spectra were recorded on a Perkin Elmer spectrum 65 FTIR spectrometer in the range of  $400\text{--}4000\text{ cm}^{-1}$ . A scanning electron microscope (FEI Quanta 200 3D) was used for determining the powders morphology. The microwave absorption properties of the prepared samples were calculated by using the horn antenna connected to an oscilloscope (AKTAKOM ADS-2221M).

#### Methodology:

##### 1. Synthesis of NiZn ferrite, carbonyl iron and carbon black powders

Ferrite ( $\text{Ni}_{0.5}\text{Zn}_{0.5}\text{Fe}_2\text{O}_4$ ) nanoparticles were prepared by a self-combustion method.  $\text{Ni}_{0.5}\text{Zn}_{0.5}\text{Fe}_2\text{O}_4$  were synthesized by taking appropriate amounts of ( $\text{Ni}(\text{NO}_3)_2 \cdot 6\text{H}_2\text{O}$ ), ( $\text{Zn}(\text{NO}_3)_2 \cdot 6\text{H}_2\text{O}$ ), and ( $\text{Fe}(\text{NO}_3)_3 \cdot 9\text{H}_2\text{O}$ ). They were blended together with an aqueous solution of sucrose (2 moles per metal ion) and 1 % an aqueous solution of polyvinyl alcohol. The whole mixture was blended totally and heated at  $90\text{ }^\circ\text{C}$  for 7 h to shape a viscous liquid. The heating process was accompanied by the evolution of brown fumes of  $\text{NO}_2$  from the decomposed metal nitrate salts. Then, the mixture was transferred to the furnace for drying for 2 h at  $200\text{ }^\circ\text{C}$  to obtain a fluffy carbonaceous pyrolyzed mass. After that, the resulting mass was annealed for 4 h at  $650\text{ }^\circ\text{C}$  to obtain nanoparticles of ferrite. Typical images of a prepared ferrite by a self-combustion method are shown in Figure 1. On the other hand, CI and CB were purchased from Cabot Corporation Company. The average particle size of CI and CB powders was measured utilizing the sieve shaker and it was between  $10\text{--}25\text{ }\mu\text{m}$  and  $2\text{--}8\text{ }\mu\text{m}$ , respectively. CI and CB powders were milled for 12 h at 300 rpm via grinding balls to obtain fine powders.

##### 2. Synthesis of $\text{Ni}_{0.5}\text{Zn}_{0.5}\text{Fe}_2\text{O}_4/\text{CI}/\text{CB}$ composites

Ferrite nanoparticles were mixed and milled with CI and CB powders by grinding balls. Three various weight ratios of  $\text{Ni}_{0.5}\text{Zn}_{0.5}\text{Fe}_2\text{O}_4/\text{CI}/\text{CB}$  (1:1:1, 1:1:2, and 2:1:1) were synthesized. The  $\text{Ni}_{0.5}\text{Zn}_{0.5}\text{Fe}_2\text{O}_4/\text{CI}/\text{CB}$  composites were milled for 1 h at 300 rpm.

##### 3. Preparation of absorber samples

Paraffin wax was symmetrically blended with  $\text{Ni}_{0.5}\text{Zn}_{0.5}\text{Fe}_2\text{O}_4/\text{CI}/\text{CB}$  composites powders with a weight ratio of 40 % w/w within a paraffin wax matrix by heating and stirring for 15 min. Afterward, the single-layer samples were molded to the dimensions of  $50 \times 50\text{ mm}$  with various thicknesses ( $2\text{--}4\text{--}6\text{ mm}$ ) to measure RL in the frequency band of  $8.8\text{--}12\text{ GHz}$ .

##### 4. Experimental setup for measuring reflection loss (RL)

The metal plate is put to reflect the transmitted power of the EM waves as shown in Figure 2. As a consequence, the transmitted power of the EM waves ( $p_t$ ) is negligible in microwave absorption. Microwave absorption properties of the prepared samples are estimated with the free-space technique as shown in Figure 3. EM waves are generated by a microwave generator in the frequency band of  $8.8\text{--}12\text{ GHz}$ , where a microwave generator is connected by a WR90 waveguide instrument (IEC Standard R100, X Band). The incident EM waves ( $p_{in}$ ) are measured by the horn antenna connected to an oscilloscope (Fig. 3), then a prepared

sample is placed on the metal plate at an angle of  $45^\circ$  to measure the reflected power of the EM waves ( $P_{ref}$ ) by an oscilloscope (Fig. 4). As a result, one can calculate the RL by applying the equation (1) [5, 6]:

$$RL(dB) = 10 \log \frac{P_{in}}{P_{ref}} . \quad (1)$$



*a* — the metal salts aqueous solution in the flask; *b* — blending totally the whole mixture;  
*c* — heating the solution at  $90^\circ\text{C}$ ; *d* — formation of a viscous liquid;  
*e* — formation of a fluffy carbonaceous pyrolyzed mass; *f* — obtaining nanoparticles ferrite

Figure 1. Synthesis of NiZn ferrite nanoparticles by a self-combustion method

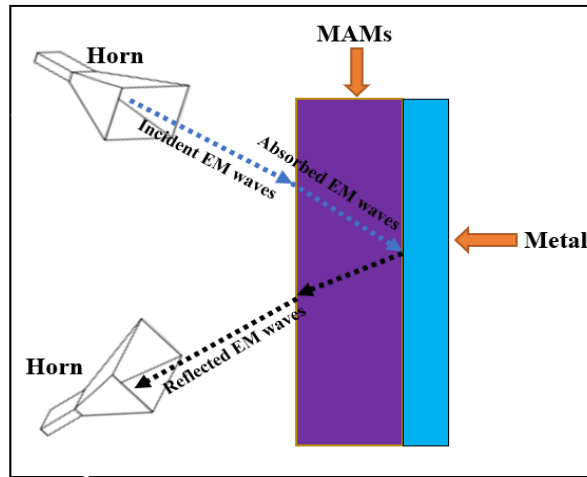
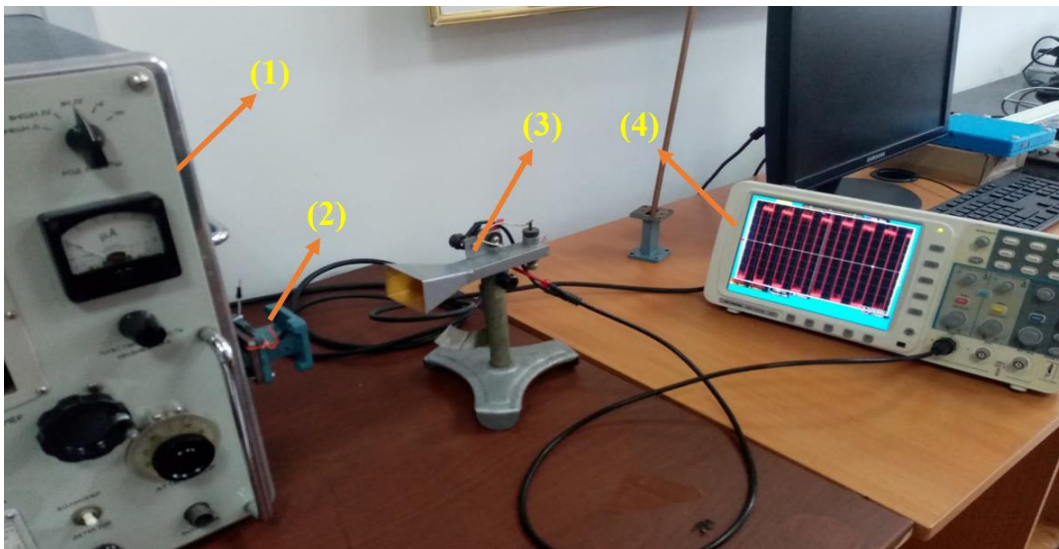


Figure 2. Sketch of the microwave absorption model used to measure reflection loss



1 — microwave generator; 2 — waveguide instrument (IEC Standard R100, X Band);  
3 — horn antenna; 4 — oscilloscope

Figure 3. Experimental setup for measuring the incident power of the EM waves by the free-space technique



Figure 4. Experimental setup for measuring the reflected power of the EM waves by the free-space technique

### 5. Statistical processing of experimental data

Four samples of  $\text{Ni}_{0.5}\text{Zn}_{0.5}\text{Fe}_2\text{O}_4/\text{CI}/\text{CB}$  composites were designed for each thickness (2–4–6 mm) to measure the microwave absorption properties. Statistical processing is used to describe the experimental data. For an estimated statistic, we can use a confidence interval. The purpose of a confidence interval is to supplement the value estimate of the sample within the formation of the uncertainty in this estimate. The method estimate  $\pm$  margin of error is used to get an interval based on each sample. The margin of error is given by the equation (2) [7]:

$$\text{Margin of error} = Z^* \cdot \frac{\text{standard deviation}}{\sqrt{n}}, \quad (2)$$

where  $Z^*$  is the confidence level which is selected at 95 %. The value of  $Z^*$  for a specific confidence level is 1.96;  $n$  is the size of the sample that is used to compute the margin of error.

The confidence interval is given by the equation (3) [7]:

$$\text{Confidence interval} = \text{Sample mean} \pm Z^* \cdot \frac{\text{standard deviation}}{\sqrt{n}}. \quad (3)$$

### Results and discussion

#### XRD patterns

The XRD patterns of  $\text{Ni}_{0.5}\text{Zn}_{0.5}\text{Fe}_2\text{O}_4$ , CI and CB powders are shown in Figure 5. For the  $\text{Ni}_{0.5}\text{Zn}_{0.5}\text{Fe}_2\text{O}_4$  pattern, nine diffraction peaks were observed, which conformed to (hkl) planes of (111), (220), (311), (222), (400), (422), (511), (440) and (533), respectively. The ideal spinel structure was observed by the peaks of NiZn ferrite [8]. All the observed peaks of  $\text{Ni}_{0.5}\text{Zn}_{0.5}\text{Fe}_2\text{O}_4$  matched with the standard XRD pattern (JCPDS, PDF no. 08–0234). On the other hand, for the carbonyl iron pattern, three characteristic peaks were observed, which conformed to (hkl) planes of (100), (200), and (211), respectively. The XRD pattern of carbonyl iron resembles crystallites in which the sample mainly contains  $\alpha$ -Fe phase [9]. All the observed peaks of CI matched with the standard XRD pattern (JCPDS, PDF no. 06-0696). Finally, for the CB pattern, two characteristic peaks were observed, which conformed to (hkl) planes of (002) and (100), respectively [10].

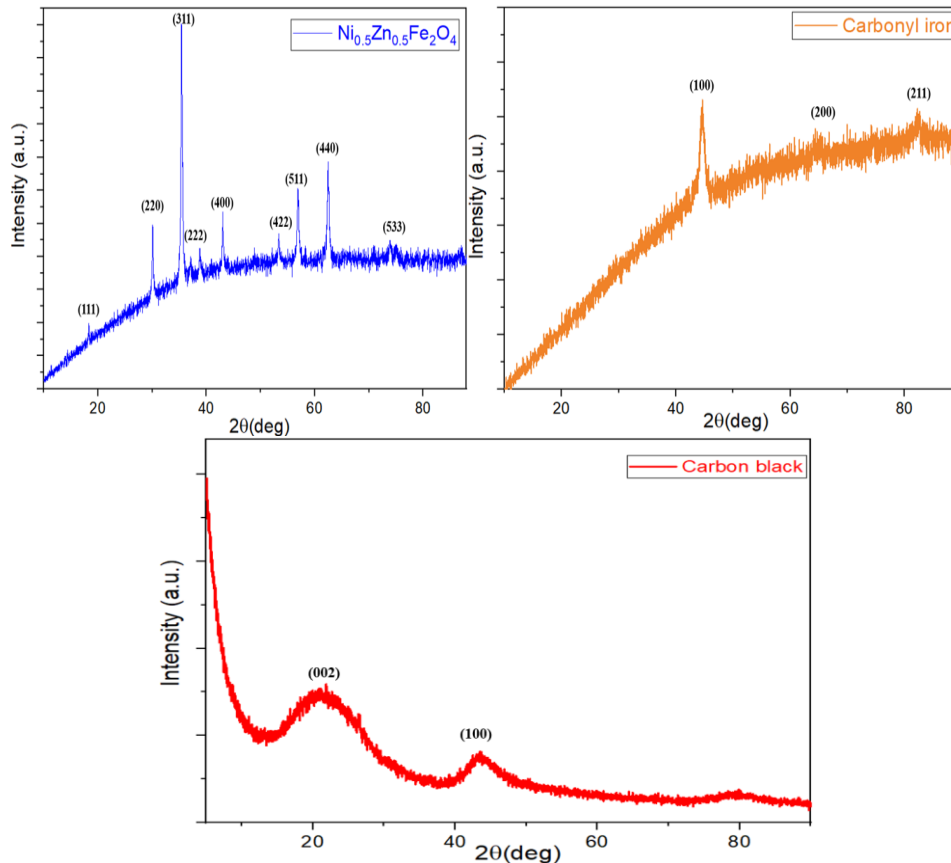


Figure 5. XRD patterns of  $\text{Ni}_{0.5}\text{Zn}_{0.5}\text{Fe}_2\text{O}_4$ , carbonyl iron and carbon black

### FTIR spectra

The FTIR spectrum of the  $\text{Ni}_{0.5}\text{Zn}_{0.5}\text{Fe}_2\text{O}_4$ , CI and CB powders is shown in Figure 6. For the  $\text{Ni}_{0.5}\text{Zn}_{0.5}\text{Fe}_2\text{O}_4$  nanoparticles, two peaks at  $565.4\text{ cm}^{-1}$  and  $432.3\text{ cm}^{-1}$  are referred to the stretching vibration of (Fe-O), which emphasizes the forming of the metal-oxygen in ferrite-based [11]. On the other hand, the peak at  $1630.4\text{ cm}^{-1}$  in  $\text{Ni}_{0.5}\text{Zn}_{0.5}\text{Fe}_2\text{O}_4$ , CI, and CB is referred to C=O stretching vibration, and the peaks at  $2348\text{ cm}^{-1}$  and  $3452\text{ cm}^{-1}$  are referred to O-H stretching vibration [12, 13].

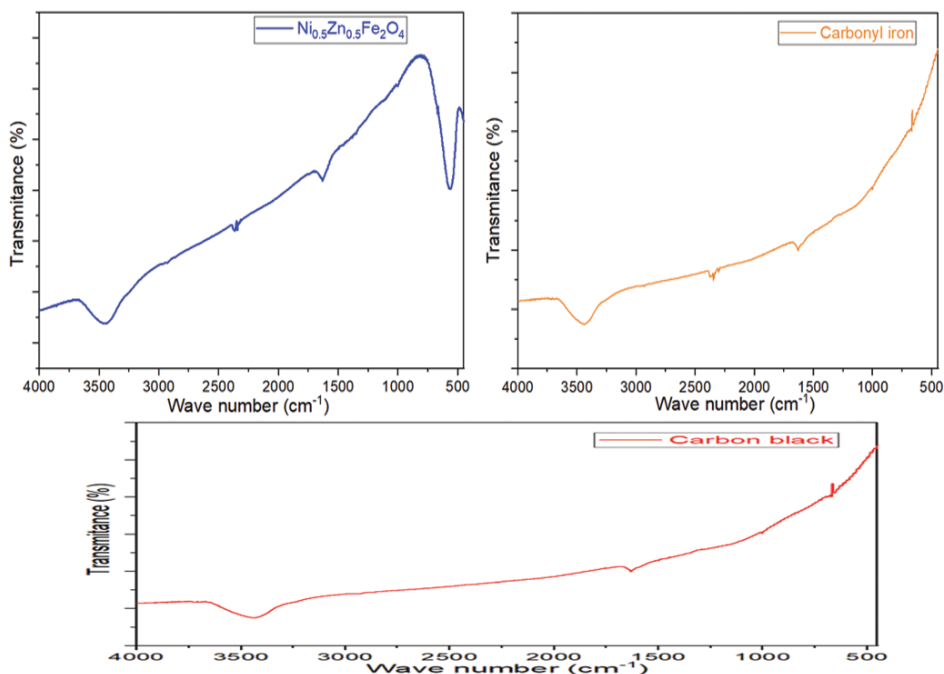
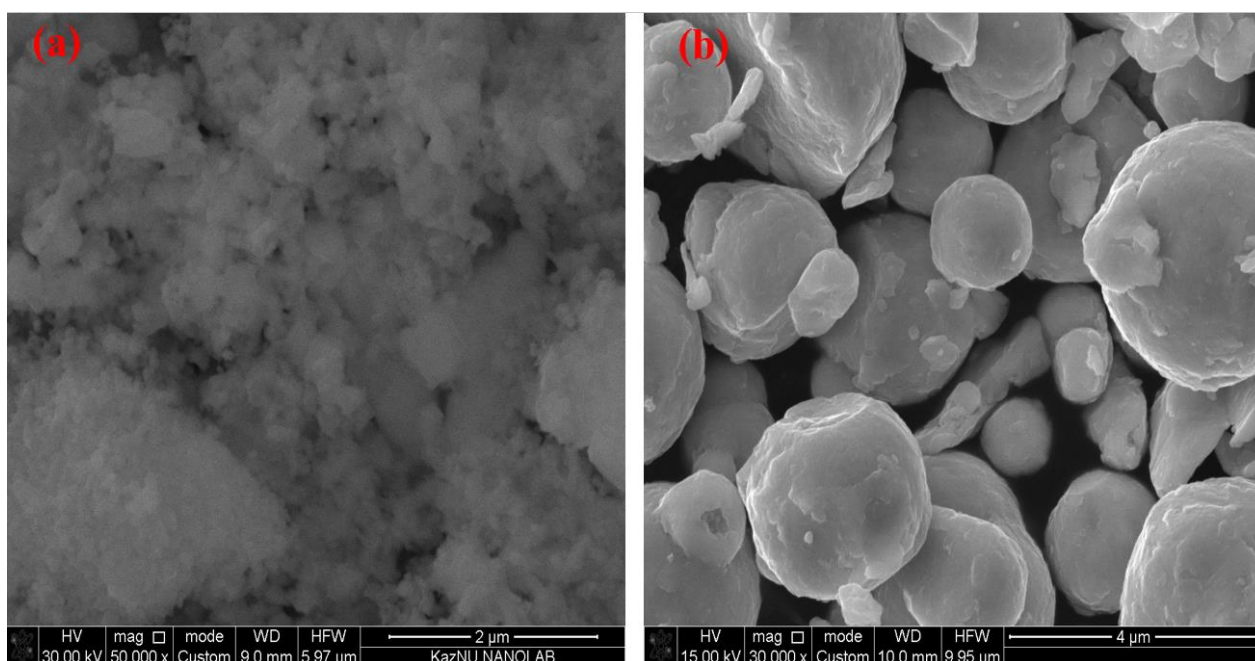


Figure 6. FTIR spectra of NiZn ferrite, carbonyl iron and carbon black

### SEM analysis

The powders morphology was investigated by SEM. The agglomerated spherical particles of NiZn ferrite and the spherical particles of carbonyl iron (Fig. 7a, b) were observed with the average diameters to be ranging between 18–52 nm and 0.2–2.4  $\mu\text{m}$ , respectively. On the other hand, the average particle size of carbon black powder (Fig. 7c) was found to be ranging between 75–481 nm.



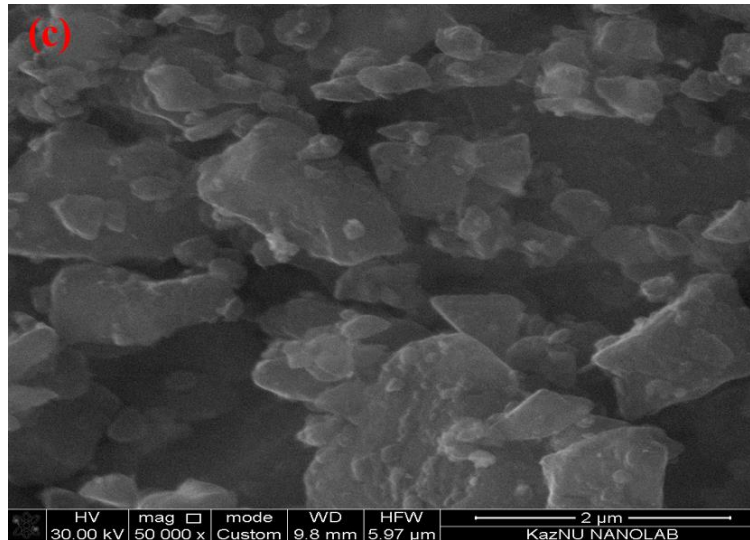


Figure 7. SEM images of (a) NiZn ferrite, (b) carbonyl iron and (c) carbon black

*Microwave absorption properties*

MA properties of the F/CI/CB composites with various thicknesses (2–4–6 mm) at the weight percentage of the absorber within a paraffin matrix (40 % w/w) were studied. The results of this investigation are exhibited in Figure 8 which illustrates the changing of the RL as a function of the EM wave frequency. The RL of the prepared samples was measured by the variation between the power of incident ( $p_{in}$ ) and reflected ( $p_{ref}$ ) EM waves as shown in Figure 3 and Figure 4. The RL curves of the samples were obtained from equation (1). The  $BW_{-10\text{ dB}}$ ,  $RL_{\text{min}}$  and  $f_m$  were deduced from RL curves. Figure 8 shows that the RL attenuation peaks of samples moved to lower frequencies with increasing sample thickness. This phenomenon may be defined by the quarter-wavelength ( $\lambda/4$ ) cancellation model, as shown in equation (4) [14–16]:

$$t_m = \frac{c}{4f_m \sqrt{|\mu_r| |\epsilon_r|}}, \tag{4}$$

where  $|\epsilon_r|$  and  $|\mu_r|$  are the modulus of the measured complex relative permittivity ( $\epsilon_r$ ) and permeability ( $\mu_r$ ) at matching frequency ( $f_m$ ), respectively;  $c$  is the velocity of light.

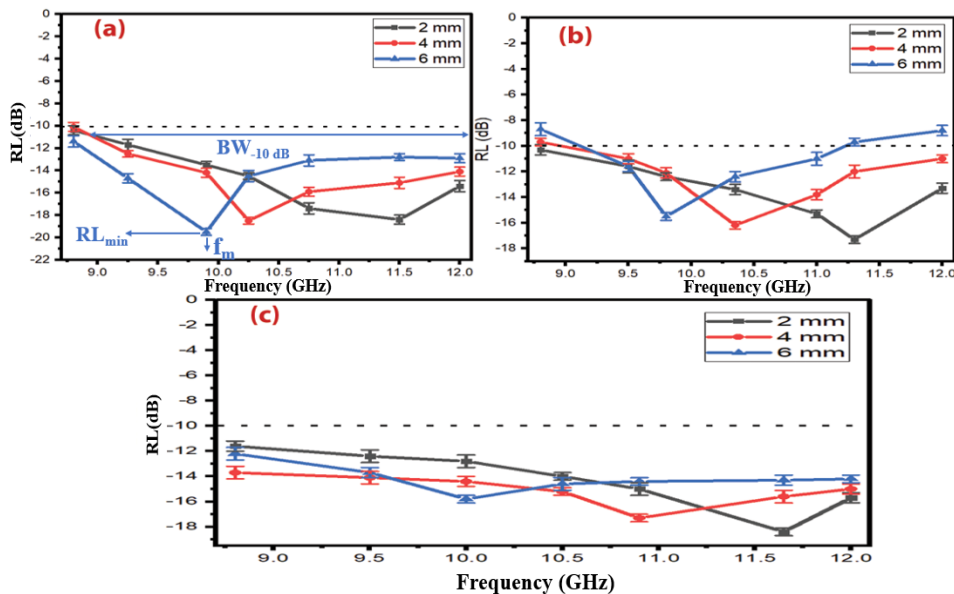


Figure 8. RL curves of (a) F/CI/CB-111 composite; (b) F/CI/CB-112 composite and (c) F/CI/CB-211 composite at various thicknesses (2–4–6 mm)

It can be noticed from equation (4) that the  $f_m$  is inversely proportionate to the thickness of an absorber. Furthermore, Table 1 shows the F/CI/CB composites have reasonable surface density, ranging from 3.625 to 4.041 kg/m<sup>2</sup>, and wide bandwidth extending from 2.81 to 3.20 GHz. The absorber of 3.20 GHz bandwidth has a minimal reflection loss of -19.42 dB at the matching frequency of 9.92 GHz with a thickness of 6 mm. One can conclude that the optimal absorption can be accomplished by modifying the absorber thickness of the absorber within a paraffin matrix. In addition to that, one can notice the impact of incorporating Ni<sub>0.5</sub>Zn<sub>0.5</sub>Fe<sub>2</sub>O<sub>4</sub> and CI (magnetic loss materials) and CB (dielectric loss material) on the MA properties of the prepared absorber. This incorporation leads to an effective and low thickness absorber with a wide bandwidth under -10 dB [17]. Statistical processing was used to describe the experimental data, as the experiments showed the effect of sample density on microwave absorption properties (Table 1), as a result, the confidence interval on the microwave absorption properties was studied.

Table 1

MA behavior of Ni<sub>0.5</sub>Zn<sub>0.5</sub>Fe<sub>2</sub>O<sub>4</sub>/CI/CB composites at various thicknesses (2–6 mm)

Composite samples	$t$ (mm)	$RL_{\min}$ (dB)	$f_m$ (GHz)	$BW_{-10\text{dB}}$ (GHz)	$SD$ (kg/m <sup>2</sup> )
F/CI/CB-111	2	-18.32±0.86	11.52±0.25	3.20±0.01	3.861±0.007
	4	-18.54±0.71	10.34±0.36	3.20±0.01	3.874±0.006
	6	-19.42±0.83	9.92±0.14	3.20±0.01	3.892±0.004
F/CI/CB-112	2	-17.36±0.62	11.34±0.37	3.20±0.01	3.625±0.005
	4	-16.33±0.86	10.41±0.16	2.92±0.05	3.643±0.005
	6	-15.58±0.73	9.82±0.23	2.81±0.03	3.652±0.008
F/CI/CB-211	2	-18.46±0.71	11.73±0.13	3.20±0.00	4.012±0.009
	4	-17.31±0.79	10.96±0.38	3.20±0.00	4.027±0.007
	6	-15.82±0.61	10.00±0.35	3.20±0.00	4.041±0.006

### Conclusion

F/CI/CB microwave absorbers were synthesized within a paraffin matrix successfully. Ni<sub>0.5</sub>Zn<sub>0.5</sub>Fe<sub>2</sub>O<sub>4</sub> and CI were used to enhance the mechanism of magnetic loss, while CB was introduced to enhance the mechanism of dielectric loss. As a result, one can notice the impact of combining Ni<sub>0.5</sub>Zn<sub>0.5</sub>Fe<sub>2</sub>O<sub>4</sub>, CI and CB on the MA properties of the absorber. This combination leads to an effective and low thickness absorber with a wide BW<sub>-10dB</sub>. The results refer that by sufficient control of the thickness of the absorption material and the weight ratio of F/CI/CB, we can design a wideband absorber based on F/CI/CB in the frequency band of 8.8–12 GHz.

### References

- 1 Ting, T.H., Yu, R.P., & Jau, Y.N. (2011). Synthesis and microwave absorption characteristics of polyaniline/NiZn ferrite composites in 2–40GHz. *Materials Chemistry and Physics*, 126(1–2), 364–368. <https://doi.org/10.1016/j.matchemphys.2010.11.011>
- 2 Houbi, A., Aldashevich, Z.A., Atassi, Y., Bagasharova Telmanovna, Z., Saule, M., & Kubanych, K. (2021). Microwave absorbing properties of ferrites and their composites: A Review. *Journal of Magnetism and Magnetic Materials*, 529, 167839. <https://doi.org/10.1016/j.jmmm.2021.167839>
- 3 Feng, W., Cao, Y., Gang, J., & Su, W. (2018). Preparation and microwave absorption property of bafe12-txixO19/carbonyl iron powder nanocomposites. *Integrated Ferroelectrics*, 190(1), 63–70. <https://doi.org/10.1080/10584587.2018.1456159>
- 4 Ren, X., Fan, H., & Cheng, Y. (2016). Microwave absorption properties of double-layer absorber based on carbonyl iron/barium hexaferrite composites. *Applied Physics A*, 122(5). <https://doi.org/10.1007/s00339-016-0041-8>
- 5 Bayat, M., Yang, H., Ko, F.K., Michelson, D., & Mei, A. (2014). Electromagnetic interference shielding effectiveness of hybrid multifunctional Fe<sub>3</sub>O<sub>4</sub>/carbon nanofiber composite. *Polymer*, 55(3), 936–943. <https://doi.org/10.1016/j.polymer.2013.12.042>
- 6 Hong, Y.K., Lee, C.Y., Jeong, C.K., Lee, D.E., Kim, K., & Joo, J. (2003). Method and apparatus to measure electromagnetic interference shielding efficiency and its shielding characteristics in broadband frequency ranges. *Review of Scientific Instruments*, 74(2), 1098–1102. <https://doi.org/10.1063/1.1532540>
- 7 Simundic, A.-M. (2008). Confidence interval. *Biochemia Medica*, 154–161. <https://doi.org/10.11613/bm.2008.015>
- 8 El Nahrawy, A.M., Salah El-Deen, H., Soliman, A.A., & Mosa, W.M.M. (2018). Crystallographic and magnetic properties of Al<sup>3+</sup>Co-doped NiZnFe<sub>2</sub>O<sub>4</sub> nano-particles prepared by sol-gel process. *Egyptian Journal of Chemistry*. <https://doi.org/10.21608/ejchem.2018.4504.1397>

- 9 Bahri-Laleh, N., Didehban, K., Yarahmadi, E., Mirmohammadi, S.A., & Wang, G. (2017). Microwave absorption properties of polyaniline/carbonyl iron composites. *Silicon*, 10(4), 1337–1343. <https://doi.org/10.1007/s12633-017-9609-y>
- 10 Hu, E., Hu, X., Liu, T., Fang, L., Dearn, K.D., & Xu, H. (2013). The role of soot particles in the tribological behavior of engine lubricating oils. *Wear*, 304(1-2), 152–161. <https://doi.org/10.1016/j.wear.2013.05.002>
- 11 Kondawar, S.B., & Nandapure, A.I. (2014). Magnetic and electrical properties of zinc-substituted nickel ferrite reinforced conducting polyaniline nanocomposites. *Journal of the Chinese Advanced Materials Society*, 2(3), 186–198. <https://doi.org/10.1080/22243682.2014.934919>
- 12 Sarker, B.K., Kang, N., & Khondaker, S.I. (2014). High performance semiconducting enriched carbon nanotube thin film transistors using metallic carbon nanotubes as electrodes. *Nanoscale*, 6(9), 4896. <https://doi.org/10.1039/c3nr06470k>
- 13 Kim, S.Y., Kwon, S.H., Liu, Y.D., Lee, J.-S., You, C.-Y., & Choi, H.J. (2013). Core-shell-structured cross-linked poly(glycidyl methacrylate)-coated carbonyl iron microspheres and their magnetorheology. *Journal of Materials Science*, 49(3), 1345–1352. <https://doi.org/10.1007/s10853-013-7818-3>
- 14 Wang, S., Jiao, Q., Shi, Q., Zhu, H., Feng, T., Lu, Q., Feng, C., Li, H., Shi, D., & Zhao, Y. (2020). Synthesis of porous nitrogen-doped graphene decorated by  $\gamma$ -Fe<sub>2</sub>O<sub>3</sub> nanorings for enhancing microwave absorbing performance. *Ceramics International*, 46(1), 1002–1010. <https://doi.org/10.1016/j.ceramint.2019.09.064>
- 15 Shu, R., Zhang, J., Guo, C., Wu, Y., Wan, Z., Shi, J., Liu, Y., & Zheng, M. (2020). Facile synthesis of nitrogen-doped reduced graphene oxide/nickel-zinc ferrite composites as high-performance microwave absorbers in the X-band. *Chemical Engineering Journal*, 384, 123266. <https://doi.org/10.1016/j.cej.2019.123266>
- 16 Jaiswal, R., Agarwal, K., Kumar, R., Kumar, R., Mukhopadhyay, K., & Prasad, N.E. (2020). EMI and microwave absorbing efficiency of polyaniline-functionalized reduced graphene oxide/ $\gamma$ -Fe<sub>2</sub>O<sub>3</sub>/epoxy nanocomposite. *Soft Matter*, 16(28), 6643–6653. <https://doi.org/10.1039/d0sm00266f>
- 17 Ali, N.N., Atassi, Y., Salloum, A., Malki, A., Jafarian, M., & Almarjeh, R.K. (2019). Lightweight broadband microwave absorbers of core-shell (polypyrrole/nickel-zinc ferrite) nanocomposites in the X-band: Insights on Interfacial Polarization. *Journal of Materials Science: Materials in Electronics*, 30(7), 6876–6887. <https://doi.org/10.1007/s10854-019-01002-y>

А. Хуби, А.А. Жарменов, И. Атасси,  
Ж.Т. Багашарова, С. Мырзалиева, Б.А. Кәрібаев

### **Үштік композиттердің синтезі және микротолқынды сіңіру қасиеттері (Ni<sub>0,5</sub>Zn<sub>0,5</sub>Fe<sub>2</sub>O<sub>4</sub>/CI/CB)**

Жұмыста феррит NiZn/темір карбонил/ қара көміртек (Ni<sub>0,5</sub>Zn<sub>0,5</sub>Fe<sub>2</sub>O<sub>4</sub>/CI/CB) үштік композиттері екі кезеңде алынды: біріншіден, Ni<sub>0,5</sub>Zn<sub>0,5</sub>Fe<sub>2</sub>O<sub>4</sub> өздігінен жану арқылы алынды. Одан кейін ұнтақтау шарлары арқылы CB, CI және Ni<sub>0,5</sub>Zn<sub>0,5</sub>Fe<sub>2</sub>O<sub>4</sub> араластыруымен операция жалғасты. Әр түрлі қалыңдықтағы (2–4–6 мм) Ni<sub>0,5</sub>Zn<sub>0,5</sub>Fe<sub>2</sub>O<sub>4</sub> (1:1:1, 1:1:2 және 2:1:1) үш түрлі салмақ қатынасы дайындалды. Абсорберлер салмағы бойынша 40 % парафинді балауыз матрицасында салмақ қатынасы бар композиттерді (Ni<sub>0,5</sub>Zn<sub>0,5</sub>Fe<sub>2</sub>O<sub>4</sub>/CI/CB) дисперсиялау арқылы жасалды. Үлгілерді сипаттау үшін рентгендік дифрактометрия және FTIR спектроскопиясы қолданылады. Ұнтақтардың морфологиясы SEM арқылы зерттелді. Функционалдық сипаттама 8,8–12 ГГц жиілік диапазонында микротолқынды сіңіру қасиеттерін өлшеу арқылы орындалды. Микротолқынды сіңіру материалдары 2,81–3,20 ГГц диапазонында –10 дБ-ден төмен кең өткізу қабілеттілігін және 3,625–4,041 кг/м<sup>2</sup> диапазонында қолайлы бет тығыздығын көрсетті. Өткізу жолағы 3,20 ГГц, қалыңдығы 6 мм болатын абсорбер 9,92 ГГц сәйкес жиілікте –19,4 дБ шағылудың минималды жоғалуына ие.

*Кілт сөздер:* NiZn ферриті, карбонилді темір, қара күйе, шағылысу жоғалтуы, сіңіру жолағы, сәйкестік жиілігі, парафинді балауыз матрицасы, беттік тығыздығы.

А. Хуби, А.А. Жарменов, И. Атасси,  
Ж.Т. Багашарова, С. Мырзалиева, Б.А. Кәрібаев

### **Синтез и микроволновые поглощающие свойства тройных композитов (Ni<sub>0,5</sub>Zn<sub>0,5</sub>Fe<sub>2</sub>O<sub>4</sub>/CI/CB)**

В настоящей работе были получены тройные композиты феррит NiZn/карбонил железа/сажа (Ni<sub>0,5</sub>Zn<sub>0,5</sub>Fe<sub>2</sub>O<sub>4</sub>/CI/CB) в два этапа. Сначала методом самовозгорания был получен Ni<sub>0,5</sub>Zn<sub>0,5</sub>Fe<sub>2</sub>O<sub>4</sub>. После этого операция продолжалась путем перемешивания CB, CI и Ni<sub>0,5</sub>Zn<sub>0,5</sub>Fe<sub>2</sub>O<sub>4</sub> через мелющие шары. Были изготовлены три различных весовых соотношения Ni<sub>0,5</sub>Zn<sub>0,5</sub>Fe<sub>2</sub>O<sub>4</sub>/CI/CB (1:1:1, 1:1:2 и 2:1:1) различной толщины (2–4–6 мм). Поглотители изготавливали путем диспергирования композитов

(Ni<sub>0,5</sub>Zn<sub>0,5</sub>Fe<sub>2</sub>O<sub>4</sub>/Cl/CB) с массовым соотношением в матрице парафинового воска 40 % по массе. Рентгеновская дифрактометрия и FTIR-спектроскопия использовались для характеристики образцов. Морфология порошков была исследована с помощью СЭМ. Функциональная характеристика получена путем измерения характеристик поглощения микроволн в диапазоне частот 8,8–12 ГГц. Материалы, поглощающие микроволновое излучение (ПМИ), показывали широкую полосу пропускания ниже –10 дБ в диапазоне 2,81–3,20 ГГц и приемлемую поверхностную плотность в пределе 3,625–4,041 кг/м<sup>2</sup>. Поглотитель с полосой пропускания 3,20 ГГц имеет минимальные потери на отражение — 19,4 дБ на частоте согласования 9,92 ГГц при толщине 6 мм.

*Ключевые слова:* феррит NiZn, карбонильное железо, сажа, потери на отражение, ширина полосы поглощения, частота согласования, парафиновая матрица, поверхностная плотность.

#### Information about authors\*

**Houbi, Anas** (*corresponding author*) — 3rd year PhD student, Department of Chemical Technology of Inorganic Substances, Al-Farabi Kazakh National University, Al-Farabi street, 71, 050040, Almaty, Kazakhstan; e-mail: [anashoubi@gmail.com](mailto:anashoubi@gmail.com); <https://orcid.org/0000-0001-9282-774X>;

**Zharmenov, Abdurassul Aldashevich** — General Director of the RSE “National Center on Complex Processing of Mineral Raw Materials of the Republic of Kazakhstan”, Dr. Sci. (Eng.), Prof., academician of the NAS of RK, State Premium Double Laureate, Jandossov street, 67, 050036, Almaty, Kazakhstan; e-mail: [nc@cmrp.kz](mailto:nc@cmrp.kz); <https://orcid.org/0000-0001-5651-5343>;

**Atassi, Yomen** — Professor of Chemistry of Materials, Director of Materials Science Laboratory, Higher Institute for Applied Science and Technology (HIASST), Barzeh street, Damascus, Syria; e-mail: [yomen.atassi@gmail.com](mailto:yomen.atassi@gmail.com); <https://orcid.org/0000-0002-1338-4993>;

**Bagasharova, Zhenisgul Telmanovna** — Candidate of Technical Sciences, RSE “National center for complex processing of mineral raw materials of the Republic of Kazakhstan”, senior lecturer at Al-Farabi Kazakh National University, Al-Farabi street, 71, 050040, Almaty, Kazakhstan; e-mail: [zh.t\\_bagasharova@mail.ru](mailto:zh.t_bagasharova@mail.ru); <https://orcid.org/0000-0001-8996-8656>;

**Mirzalieva, Saule** — Doctor of chemical Sciences, Professor, Head of the Department for training of scientific personnel national center for complex processing of mineral raw materials of the Republic of Kazakhstan, professor at Al-Farabi Kazakh National University, Al-Farabi street, 71, 050040, Almaty, Kazakhstan; e-mail: [saulekerchaiz@mail.ru](mailto:saulekerchaiz@mail.ru); <https://orcid.org/0000-0003-2997-0716>;

**Karibayev, Beibit Abdirbekovich** — Acting assistant professor of Physics and Technology, Al-Farabi Kazakh National University, Al-Farabi street, 71, 050040, Almaty, Kazakhstan; e-mail: [beibitkaribaev7@gmail.com](mailto:beibitkaribaev7@gmail.com); <https://orcid.org/0000-0003-1057-0296>

\*The author's name is presented in the order: *Last Name, First and Middle Names*

A. Bayeshov<sup>1</sup>, A.S. Kadirbayeva<sup>1</sup>, A.K. Bayeshova<sup>2\*</sup>, A.A. Zharmenov<sup>1</sup>

<sup>1</sup>National Center on Complex Processing of Mineral Raw Materials of the Republic of Kazakhstan, Almaty, Kazakhstan;

<sup>2</sup>Al-Farabi Kazakh National University, Almaty, Kazakhstan

(\*Corresponding author's e-mail: [azhar\\_b@bk.ru](mailto:azhar_b@bk.ru))

## Electrochemical Method for Producing a TiO<sub>2</sub> Film with Photocatalytic Properties

The purpose of this work is to study the production process of titanium dioxide during anode polarization in sulfuric acid and hydrochloric acid solutions. The studies were carried out by recording cyclic voltammogram and by measuring the titanium oxidation current with a change in the voltage between the electrodes. It has been established that with a change in the concentration of sulfuric acid in the range of 50–250 g/l and the voltage between the electrodes in the range of 0–25 V, the magnitude of the titanium oxidation current increases and reaches 29.4 mA. With an increase in the concentration of hydrochloric acid from 35 to 100 g/l and a change in the voltage between the electrodes, the titanium oxidation rate increases evenly, but in the voltage range of 10–12 V, a sharp increase in the current magnitude up to 360 mA is observed. A change in the oxidation current indicates an increase in the rate of titanium dissolution. With an increase in the duration of electrolysis, the magnitude of the anode current generally decreases. In all probability, at a voltage of 14 V and higher, a breakdown of the oxide semiconductor film of titanium dioxide is observed in the hydrochloric acid solution. In this regard, a noticeable dissolution of titanium occurs and, subsequently, an oxide film is not produced, but titanium ions are produced. Visual observations have shown that titanium passes into solution in the form of titanium (IV).

**Keywords:** titanium dioxide, coating, electrode, electrolyzer, polarization, voltage, sulfuric acid, hydrochloric acid.

### Introduction

Titanium and its compounds have unique physical, chemical and technical characteristics, and therefore have many applications. Of particular interest is titanium dioxide in the form of powders, as well as in the form of a film produced on its surface. For example, nanocrystalline titanium dioxide (TiO<sub>2</sub>) films have photocatalytic properties, and therefore are used in solar cells as an N-type conductivity material and a hole-blocking layer. The thickness of the TiO<sub>2</sub> film and its structure have a significant effect on the characteristics of the solar cell [1].

Titanium dioxide has semiconductor properties and is used in heterogeneous catalysis processes. The photocatalytic activity of titanium dioxide is determined by its physicochemical properties, which depend on the conditions of production [2–6]. Due to its photocatalytic activity, TiO<sub>2</sub> contributes to improving the efficiency of water and air purification processes from toxic organic impurities, to synthesize hydrogen as a result of water photocatalysis, to reduce CO<sub>2</sub> to CH<sub>4</sub> and its homologues [7–10].

Titanium dioxide is increasingly being used as a photocatalyst due to its high chemical resistance, lack of toxicity and low cost [11].

The authors [12] A.K. Abildina, K. Avchukir, R.Z. Dzhumanova, et al. present the results of a study of the morphological characteristics of an anode based on titanium dioxide powder using ellipsometry, scanning electron microscopy (SEM) coupled with energy-dispersive X-ray spectroscopy (EDS) and X-ray diffraction (XRD), as well as electrochemical properties by cyclic voltammetry. The main stages of anode production were: dispersing, mixing the initial reagents for obtaining homogenized paste and its coating to a substrate, drying and cutting the electrodes. The results of ellipsometry, SEM and EDS showed a uniformly distributed layer of about 200 μm thickness with porous structure, particle diameter in the range of 50–80 nm and titanium dioxide content (45.7 %). The XRD data confirm the formation of an active anode matrix with a monoclinic crystal lattice corresponding to the modification of titanium dioxide (B) with small inclusions of anatase. The electrochemical behavior of the resulting electrode was examined in an Mg(TFSI)<sub>2</sub> solution

based on acetonitrile. In [13], a self-organized nanotubular titanium dioxide (TiO<sub>2</sub>) array was obtained by anodizing pure titanium in a mixture of glycerol, distilled water (8 % vol.), and ammonium fluoride using a system with two electrodes. The size and distribution of nanopores were controlled in the DC voltage range from 30 V to 60 V. It was shown that the diameter of TiO<sub>2</sub> nanopores depends on the anodizing voltage. There are research works [14], which show that electrodes for a supercapacitor were prepared by doping titanium dioxide with gold. It has been established that electrodes with a low gold concentration have the best electrochemical characteristics.

A one-step electrochemical method for the deposition of nanocrystalline titanium dioxide films on various carbon substrates is presented by authors [15]. By optimizing the synthesis conditions, the electrodeposition of layers of nanocrystalline and porous titanium dioxide was achieved in only a few minutes. The phase composition of TiO<sub>2</sub> was controlled by varying the composition of the solution. The photoelectrochemical performance of the electrodeposited titanium dioxide films was better or at least comparable to the benchmark P25 titanium dioxide films.

Ali, H.M. in the review [16] presented detailed information about the properties and applications of titanium dioxide. He emphasizes the distinctive characteristics of titanium dioxide, such as high refractive index, extremely high melting and boiling point, high toughness and hardness, photocatalytic nature, ability to absorb or reflect UV rays, DeNox catalyst, nontoxicity, inertness, etc., have led to massive use of TiO<sub>2</sub> in various traditional as well as advanced engineering applications.

The purpose of this work is to study the production process of titanium dioxide during anode polarization in sulfuric acid and hydrochloric acid solutions. The studies were carried out by recording cyclic voltammogram and by measuring the titanium oxidation current with a change in the voltage between the electrodes.

The novelty of the work is due to the fact that for the first time the investigation results of the TiO<sub>2</sub> oxide films formation process on the surface of a titanium electrode by measuring the value of the oxidation current depending on the voltage between the electrodes are presented.

### Experimental

The mechanism of titanium dioxide production on the titanium surface was studied by recording anode-cathode cyclic voltammograms and by electrolysis under potentiostatic conditions. Voltammograms recorded with a Cortest CS120 single-channel potentiostat (potential range/resolution:  $\pm 10$  V/10 mV, current measurement range  $\pm 2$  A) (Corrtest Instruments Company, China). The voltammograms are recorded using the NOVA 1710 program installed on a personal computer. The main voltammograms were recorded at a potential scan rate of 100 mV/s. Polarograms were recorded in a three-electrode cell. The surface edge of a titanium wire with a diameter of 1.5 mm was used as the working electrode, and a platinum wire was used as the second additional electrode. A silver chloride electrode immersed in a saturated solution of KCl was used as a reference electrode ( $E=+203$  mV).

Titanium was used for the experiments, the purity of which corresponds to the elemental analysis data given in Table 1 (all results in mass.%):

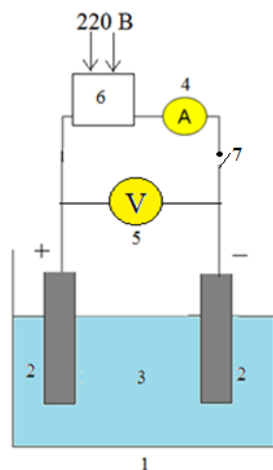
Table 1

Elemental composition of metallic titanium

Spectrum	Ti	Si	Al	O	Total
Spectrum 1	97.56	0.30	0.48	1.67	100
Spectrum 2	98.16	0.30	0.51	1.03	100
Spectrum 3	97.24	0.44	0.44	1.88	100
Average	97.65	0.34	0.48	1.52	100

Further, to clarify the mechanism of production of the titanium oxide film, electrolysis was carried out under potentiostatic conditions, i.e. at certain voltages between the electrodes. The schematic diagram of the installation for obtaining a titanium dioxide film on the titanium surface is shown in Figure 1.

The anodic behavior of the titanium electrode was studied in sulfuric acid (0–250 g/l) and hydrochloric acid (0–100 g/l) solutions. The experiments were carried out in an electrolyzer with a volume of 100 ml, a titanium plate was used as a cathode. The electrolysis was carried out under stationary conditions, i.e. in the absence of electrolyte mixing. The electrodes were polarized using a GPS-1830 D current rectifier.



1 — electrolyzer; 2 — titanium electrodes; 3 — electrolyte (different medium);  
4 — ammeter; 5 — voltmeter; 6 — rectifier; 7 — key

Figure 1. Schematic diagram of the installation for obtaining a TiO<sub>2</sub> film on the surface of a titanium electrode

We carried out preliminary studies, which showed that during the anode polarization of the titanium electrode, a very small current flows through the circuit. The electrode surface is instantly covered with an oxide film, and passivation occurs. In this regard, we studied the effect of the voltage between the electrodes on the current value to study the conditions for the production of titanium dioxide films on the surface of the titanium anode.

The structure of the titanium dioxide film obtained as a result of electrolysis was investigated by methods of physico-chemical analysis. Micrographs of the surface of the synthesized electrode and its elemental composition were obtained using a JSM-6610 LV Scanning Electron Microscope (JEOL company (Japan)). Images of the obtained films were taken using a Canon EOS 2000D EF-S 18-55 SLR camera (Canon company (Japan)).

### Results and Discussion

On the anode-cathode voltammograms, obtained in a solution of sulfuric acid with a concentration of 100 g/l, a weakly noticeable maximum is observed at a potential of 0.01 V (Fig. 2). When the potential is shifted further, in the anode direction, the height of the current maximum does not increase. At the same time, it is visually seen that the titanium surface darkens, in all likelihood, titanium oxide films are produced. We believe that, at these potentials, titanium is oxidized through the stage of production of Ti<sub>x</sub>O<sub>y</sub> oxide films. With a further shift of the anode potential to “plus” 2.6 V, oxygen release on the surface of the titanium electrode is not observed. When the potential is shifted in the cathode direction, at potentials close to “minus” 1.2 V, the hydrogen ion reduction current is observed on the voltammogram.

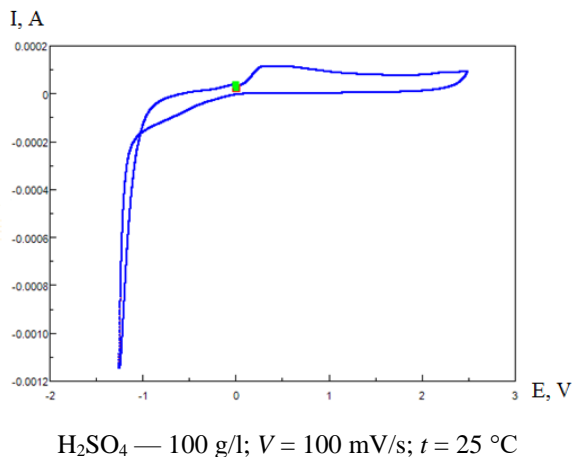
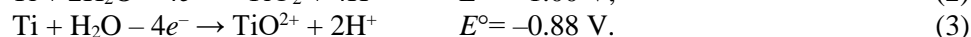
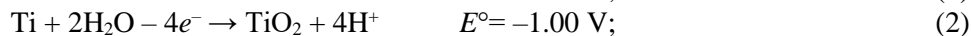
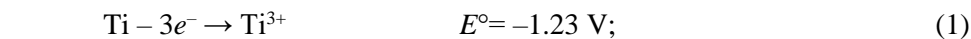


Figure 2. Cyclic anode-cathode voltammograms of titanium electrode in sulfuric acid solution

Then the anode-cathode cyclic voltammograms were recorded in hydrochloric acid solution. The voltammograms have a similar character, but the value of the anode trans-passivation current has a higher value. The voltammograms are analogous, but the value of the anode transpassivation current is higher. This indicates a more active anodic oxidation of titanium with the production of titanium oxide films.

Based on the analysis of the anode-cathode cyclic voltammograms, it can be assumed in acidic solutions during anode polarization, an oxide film is produced on the titanium surface and, possibly, the electrode is partially dissolved at a very low rate. In this case, the following reactions can occur on the titanium anode:



The main objective of this article is to obtain titanium dioxide on the surface of titanium metal in the form of a thin film. Preliminary studies have shown that during anode polarization of a titanium electrode in aqueous solutions, titanium dioxide (Ti<sub>x</sub>O<sub>y</sub>) is produced on its surface depending on the experimental conditions (i.e., on the voltage between the electrodes, current density, solution composition, electrolyte temperature, etc.). It is established that, depending on the polarization conditions, various colors of titanium dioxide is produced on the titanium surface.

With anodic polarization of the titanium electrode, apparently it is completely passivated immediately. However the detected currents on the voltammograms and the change in the color of the electrode surface show that titanium is not completely passivated, and its dissolution continues through a layer of oxide films. We have studied the processes occurring under various conditions of electrolysis. The results of the study showed that first a thin layer of titanium oxide with high electrical resistance is formed. Then there is a further increase in the thickness of the titanium oxide films at a very low rate. The oxidation of titanium and the formation of the next layer occur according to a very complex mechanism. The production of new TiO<sub>2</sub> oxide film layers can occur as a result of titanium ionization reactions through micropores of the obtained oxide films. These processes, depending on the conditions of electrolysis (the composition of the electrolyte, the voltage between the electrodes, etc.), the reaction rate of oxide films production proceed differently.

We have studied the rate of titanium oxidation and the production of TiO<sub>2</sub> on its surface depending on various parameters. The influence of the voltage between the electrodes on the current power of titanium oxide production at various concentrations of sulfuric acid is established. The results are presented in Table.2. It is shown that with the concentration growth of sulfuric acid and the voltage between the electrodes, the initial current value for obtaining titanium oxide films by reaction (2) increases (Table 2). For example, at a voltage between the electrodes of 15.0 V, the titanium oxidation current at concentrations of 50, 150, 250 g/l, respectively, is 11.7; 15.5; 18.9 mA. At a concentration of sulfuric acid of 150 g/l and at a voltage between the electrodes of 5.0 V, the oxidation current is 10.0 mpa, and at 25.0 V is 26.1 mA.

Table 2

**Influence of voltage between the electrodes on the value of the anode current at various concentrations of sulfuric acid (the current value was measured 3 minutes after the voltage was applied)**

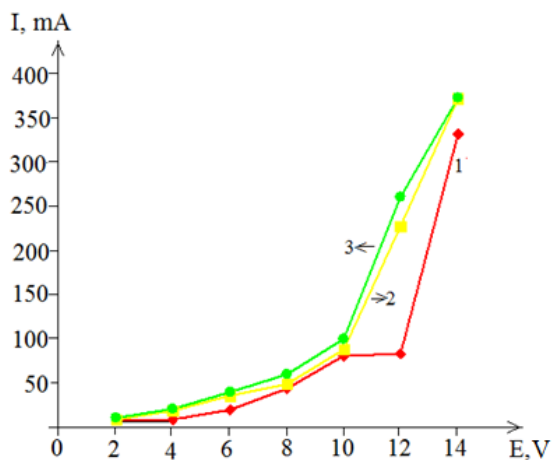
H <sub>2</sub> SO <sub>4</sub> , g/l	The value of the anode current, mA					
	E, V					
	0	5.0	10.0	15.0	20.0	25.0
50	0	1.1	5.0	11.7	16.0	23.4
150	0	10.0	12.4	15.5	19.3	26.1
250	0	12.2	13.3	18.9	20.8	29.4

The experimental results showed that, in all cases, the value of the anode oxidation current decreases over time (Table 3). At the beginning of the polarization process, the oxidation current has a large value, but after a while its decrease is observed. Within 60 minutes, the anode current decreases and its value reaches 0. This indicates that in a sulfuric acid solution, the anode current flowing through the titanium electrode is mainly consumed for the production of titanium dioxide on its surface.

**Influence of the duration of electrolysis on the value of the anode current at different voltages between the electrodes in a solution of sulfuric acid: H<sub>2</sub>SO<sub>4</sub> — 150 g/l, t = 25 °C**

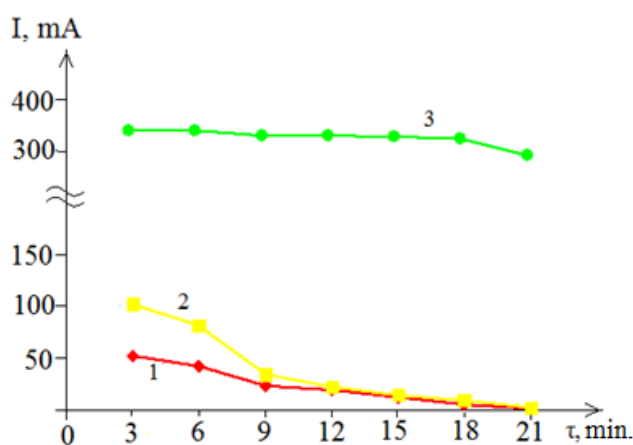
E, V	The value of the anode current, mA								
	τ, min								
	0	3	6	9	12	15	18	21	24
5.0	121.1	10.0	0.64	0.38	0.28	0.25	0.19	0.15	0.12
10.0	152.2	12.4	11.5	11.3	8.6	7.7	6.3	5.9	5.1
15.0	154.4	15.5	12.3	11.6	10.4	9.5	8.4	8.0	7.5

The process of production of an oxide film on titanium in hydrochloric acid solutions was studied. It was established that the oxidation of titanium in a hydrochloric acid solution proceeds more intensively compared to the process occurring in a sulfuric acid solution. There are dependences on the Figures 3 and 4 showing that with an increase in the concentration of hydrochloric acid and the voltage between the electrodes, the rate of titanium oxidation grows evenly. However, at a voltage of 10–12 V, a sharp increase in the dissolution rate of titanium is observed (judging by the magnitude of the oxidation current). At hydrochloric acid concentrations of 35, 70, 100 g/l, the anode current value is 325, 365, 366 mA, respectively (the current value was measured 3 minutes after the voltage was applied) (Fig. 3). With an increase in the duration of electrolysis, the value of the anode current decreases. However, at a voltage of 14 V, the anode current increases sharply within 30 minutes and slightly decreases from 360 to 320 mA (Fig. 4). We believe that a breakdown of the oxide film of titanium dioxide is observed in a hydrochloric acid solution at a voltage of 14 V and above. In this regard, titanium dissolves, further oxide production does not occur, but titanium ions are produced. It is visually observed the solution remains colorless, which indicates the production of tetravalent titanium ions. The production of trivalent ions is excluded, since they have a purple color.



Concentrations of hydrochloric acid, g/l:  
1 — 35; 2 — 70; 3 — 100

Figure 3. Influence of the voltage between the electrodes on the value of the anode oxidation current on titanium at different concentrations of hydrochloric acid



HCl — 70 g/l, t = 25 °C;  
1 — 8.0 V; 2 — 10.0 V; 3 — 14.0 V

Figure 4. Influence of the duration of electrolysis on the value of the anode oxidation current of titanium at different voltages between the electrodes

Thus, we have established that in a hydrochloric acid solution with anode polarization, the production of titanium dioxide occurs only at low voltages between the electrodes, not exceeding 10 V, and in a sulfuric acid solution, inclusive, 25 V.

Identification of the TiO<sub>2</sub> film produced as a result of electrolysis of sulfuric acid solutions at a voltage not higher than 10 V was carried out using physical and chemical methods. As the results of the physical and chemical analysis showed, in all cases, titanium oxide of the composition TiO<sub>2</sub> is produced on the surface of titanium (Table 4).

Table 4

The composition of the oxide film produced on the surface of the electrode in a solution of sulfuric acid:  
H<sub>2</sub>SO<sub>4</sub> — 50 g/l, E=20 V, τ=1 hour, t=25 °C

Spectrum	O	Ti	Si	Al	Fe	Zn	Total
Spectrum 1	37.09	62.42	0.09	0.07	0.26	0.09	100
Spectrum 2	39.55	59.79	0.10	0.05	0.37	0.14	100
Spectrum 3	40.28	58.90	0.09	0.09	0.37	0.28	100
Average	<b>38.97</b>	<b>60.37</b>	<b>0.09</b>	<b>0.07</b>	<b>0.33</b>	<b>0.17</b>	<b>100</b>

Micrographs of films on a titanium electrode are shown in Figure 5. The micrograph in Figure 5a was obtained by a magnification of 3000 times, in Figure 5b — by a magnification of 1000 times. In both cases, the grain size of the particles is visible.

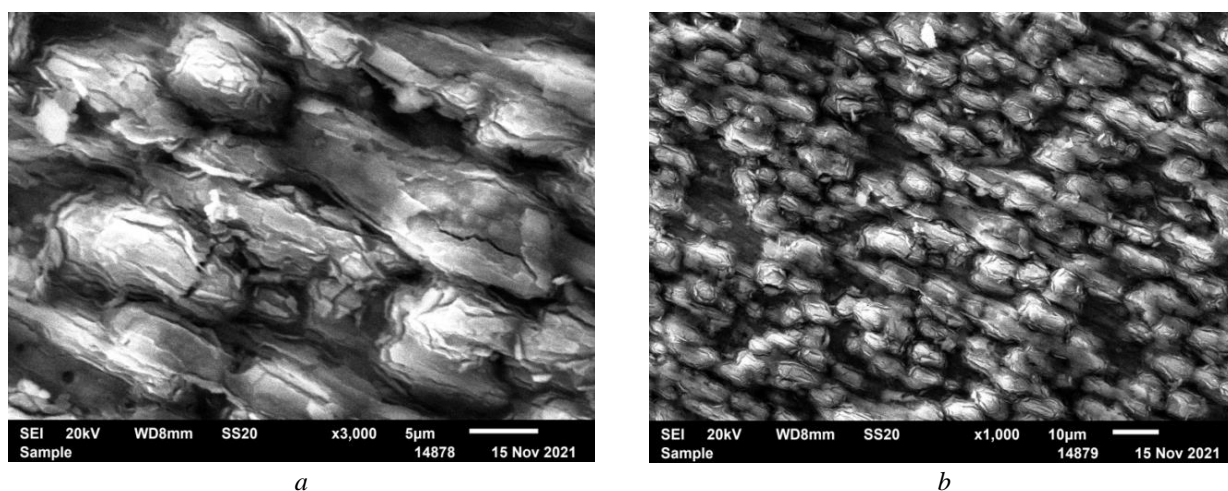
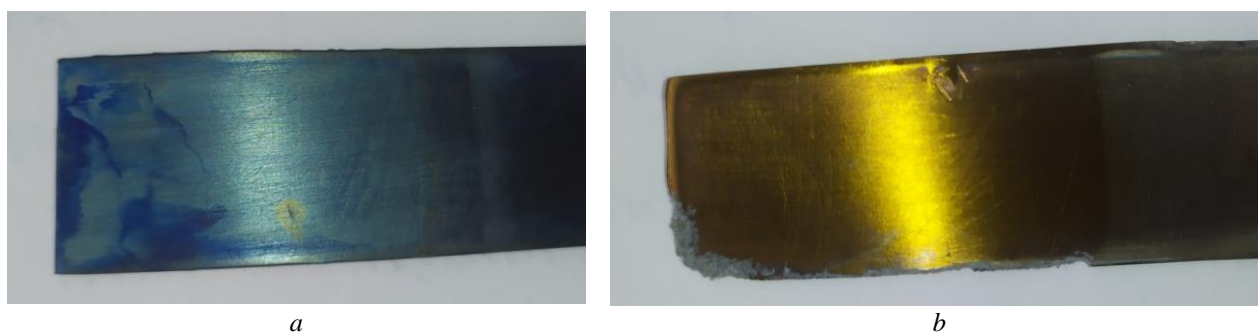


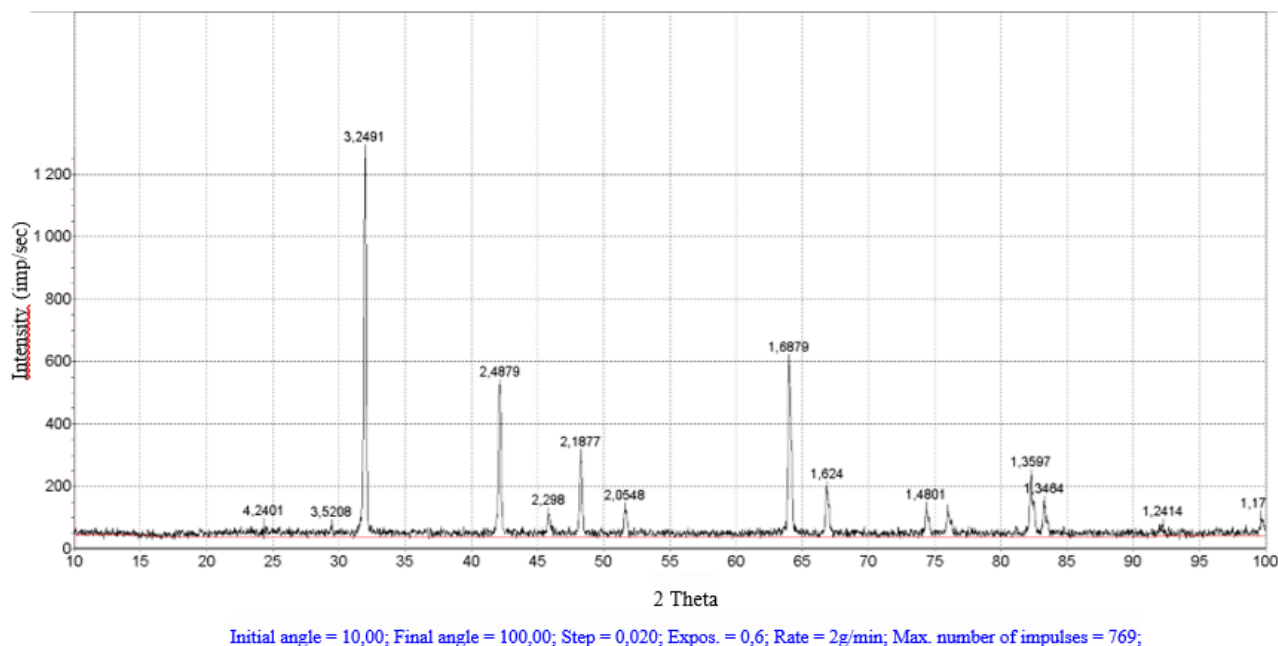
Figure 5. Micrographs of titanium dioxide films produced on the surface of a titanium anode in a sulfuric acid solution with an increase: a) 3000 times; b) 1000 times



*a* — H<sub>2</sub>SO<sub>4</sub> — 150 g/l; E = 10 V; τ = 1 hour; *b* — HCl — 70 g/l, E = 10 V; τ = 1 hour

Figure 6. Photographs of the titanium surface after electrolysis of the coated oxide film

Researchers Kuz'mina M.Yu., Belik O.D. [17] argue that films often produced on the surface of metals have non-uniform thickness. Using X-ray diffraction analysis, they studied the composition of oxide layers on titanium during its anodization in aqueous solutions of acids and alkalis in galvanostatic and potentiostatic conditions. It is shown that the composition of the films obtained in aqueous electrolytes, along with the basic oxide TiO<sub>2</sub> (anatase), also includes a number of lower oxides (Ti<sub>4</sub>O<sub>7</sub>, Ti<sub>3</sub>O<sub>5</sub>, Ti<sub>2</sub>O<sub>3</sub>, TiO). It is known from the literature [18] that, during the electrochemical oxidation of titanium, oxide films with an interference color are formed. In our experiments, light blue films were obtained in a solution of sulfuric acid and golden yellow in a solution of hydrochloric acid (Fig. 6). The composition of the film was identified by X-ray phase analysis (Fig. 7) as titanium dioxide in the form of anatase (all reflections refer to TiO<sub>2</sub>).



Reflexes: 3.24; 2.48; 2.29; 2.18; 2.05; 1.68; 1.62; 1.48; 1.35; 1.34; 1.24; 1.17 Å — TiO<sub>2</sub> (ASTM 73-2224)

Figure 7. X-ray of titanium dioxide

### Conclusions

Titanium is an unusual metal with special properties. It does not dissolve under normal conditions in aqueous solutions of acids and during anodic polarization, i.e. it undergoes passivation, since an oxide film forms on its surface. It is believed that after the formation of an oxide film, the dissolution of titanium stops completely. However, the results of our studies have shown, titanium continues to oxidize even with further polarization. This can be judged by the increase current value of the titanium oxidation with a change in the voltage between the electrodes as a function of time. It has been established that transpassive dissolution occurs in the sulfuric acid medium, while the value of the oxidation current reaches 29.4 mA at a voltage of 25 V, and in the hydrochloric acid medium, the oxidation current reaches 360 mA at a voltage of 14 V. These data show that titanium continues transpassive oxidation in electrolyte solutions, and in a hydrochloric acid medium, the dissolution rate increases significantly.

### Acknowledgments

The work was carried out in accordance with the program BR09458955 “Creation of new composite materials with high performance properties based on rare and rare earth elements”, funded by the Committee of Industrial Development of the Ministry of Industry and Infrastructure Development of the Republic of Kazakhstan, and also in accordance with section 1.1 of the project AP08856929, funded by the Ministry of Education and Science of the Republic of Kazakhstan.

### References

- 1 Малюков С.П. Исследование влияния толщины пленки TiO<sub>2</sub> на фотоэлектрические характеристики перовскитовых солнечных элементов / С.П. Малюков, А.В. Саенко, Д.А. Бондарчук // Инженер. вестн. Дона. — 2016. — № 4. — С. 63.
- 2 Shvets P.V. Suppression of the metal-insulator transition in magnetron sputtered Ti<sub>2</sub>O<sub>3</sub> films / P.V. Shvets, D. Caffrey, K. Fleischer, I. Shvets, K. O'Neill, G.S. Duesberg, A.N. Vinichenko, Yu.K. Maksimova, & Yu.A. Goikhman // Thin Solid Films. — 2020. — 694, 137642. <https://doi.org/10.1016/j.tsf.2019.137642>
- 3 Бессель В.В. Изучение солнечных фотоэлектрических элементов: учеб.-метод. пос. / В.В. Бессель, В.Г. Кучеров, Р.Д. Мингалеева — М.: Изд. центр РГУ нефти и газа (НИУ) им. И.М. Губкина, 2016. — 90 с.
- 4 Wang X., Fang Y., He L., Wang Q., Wu T. Influence of compact TiO<sub>2</sub> layer on the photovoltaic characteristics of the organometal halide perovskite-based solar cells // Materials Science in Semiconductor Processing. — 2014. — Vol. 27. — P. 569–576. <https://doi.org/10.1016/j.mssp.2014.07.039>

- 5 Jung H.S., Park N.-G. Perovskite solar cells: From materials to devices // *Small*. — 2014. — Vol. 11, No. 1. — P. 10–25. <https://doi.org/10.1002/sml.201402767>
- 6 Minemoto T., Murata M. Device modeling of perovskite solar cells based on structural similarity with thin film inorganic semiconductor solar cells // *Journal of Applied Physics*. — 2014. — Vol. 116, No. 5. — P. 054505. <https://doi.org/10.1063/1.4891982>
- 7 Рыков А.Н. Фотокатализаторы на основе диоксида титана: получение и применение / А.Н. Рыков, В.А. Белоусова // *Инженеры будущего: Открытая городская науч.-практ. конф.* — 2020. — С. 367–370.
- 8 Сидак И.Л. Фотокаталитические устройства и способы очистки воды / И.Л. Сидак, В.Ф. Раков, В.М. Погибко // *Инновационные перспективы Донбасса*. — 2020. — С. 30–34.
- 9 Бубнов В.В. Разработка плазмодинамического метода синтеза ультрадисперсного диоксида титана TiO<sub>2</sub>, обладающего фотокаталитическими свойствами получения водорода: магистер. дис. / В.В. Бубнов; Национальный исследовательский Томский политехнический университет; Инженерная школа энергетики; Отделение электроэнергетики и электротехники; науч. рук. А.А. Сивков. — Томск, 2019.
- 10 Деревщиков В.С. Способ получения метана из атмосферного диоксида углерода / В.С. Деревщиков, А.Г. Окунев, А.И. Лысиков, Ж.В. Веселовская. Патент № 2533710 С1 Российская Федерация, МПК C07C 9/04, C07C 1/12, B01J 23/60. № 2013143033/04: заявл. 23.09.2013; опубл. 20.11.2014; заявитель Федеральное государственное бюджетное учреждение науки Институт катализа им. Г.К. Борескова Сиб. отд. РАН.
- 11 Zhou Y., Gray-Weale A. A numerical model for charge transport and energy conversion of perovskite solar cells // *Physical Chemistry Chemical Physics*. — 2016. — Vol. 18, No. 6. — P. 4476–4486. <https://doi.org/10.1039/c5cp05371d>
- 12 Abildina A.K., Avchukir K., Dzhumanova, R.Z., Beiseyeva A.N., Rakhymbay G.S., Argimbayeva A.M. Preparation and electrochemical characterization of TiO<sub>2</sub> as an anode material for magnesium-ion batteries // *Bulletin of the University of Karaganda Chemistry*. — 2021. — Vol. 104(4). — P. 104–116. <https://doi.org/10.31489/2021ch4/104-116>
- 13 Zakir O., Idouhli R., Elyaagoubi M., Khadiri M., Aityoub A., Koumya Y., Rafqah S., Abouelfida A., Outzourhit A. Fabrication of TiO<sub>2</sub> nanotube by Electrochemical Anodization: Toward photocatalytic application // *Journal of Nanomaterials*. — 2020. — Vol. 1. — P. 11. <https://doi.org/10.1155/2020/4745726>
- 14 Shaalan N.M., Ahmed F., Rashad M., Kumar S., Saber O., Al-Naim A.F., Kotb H.M., Ezzeldien M., Mahmoud A.Z. Ceramic Ti/TiO<sub>2</sub>/AuNP Film with 1-D Nanostructures for Selfstanding Supercapacitor Electrodes // *Crystals*. — 2022. — Vol. 12. — P. 791. <https://doi.org/10.3390/cryst12060791>
- 15 Endrődi B., Kecsenovity E., Rajeshwar K., Janáky C. One-step electrodeposition of nanocrystalline TiO<sub>2</sub> films with enhanced photoelectrochemical performance and Charge Storage // *ACS Applied Energy Materials*. — 2018. — Vol. 1, No. 2. — P. 851–858. <https://doi.org/10.1021/acsaem.7b00289>
- 16 Ali H.M. Titanium Dioxide-Advances and Applications. — London: IntechOpen, 2022. — 244 p. <https://doi.org/10.5772/intechopen.94670>
- 17 Кузьмина М.Ю. Изучение коррозионной стойкости оксидных плёнок на титане / М.Ю. Кузьмина, О.Д. Белик // *Машины, агрегаты и процессы. Проектирование, создание и модернизация*. — 2018. — С. 179–181.
- 18 Кузьмина М.Ю. Коэффициент контраста титанового электрохромного электрода / М.Ю. Кузьмина, М.П. Кузьмин // *Вестн. ИрГТУ*. — 2011. — № 8 (55). — С. 139–143.

А. Баешов, А.С. Кадирбаева, А.Қ. Баешова, А.А. Жарменов

### Фотокаталитикалық қасиетке ие TiO<sub>2</sub> жабынын алудың электрохимиялық әдісі

Жұмыстың мақсаты күкіртқышқылды және тұз қышқылды ерітінділерде анодтық поляризация кезінде титан диоксидінің түзілу процесін зерттеу. Зерттеулер циклді потенциодинамикалық вольтамперлік қисықты түсіру және электродтар арасындағы кернеудің өзгеруіне байланысты титанның тотығу тогының шамасын өлшеу арқылы жүргізілді. Күкірт қышқылының концентрациясын 50–250 г/л аралығында және электродтар арасындағы кернеуді 0–25 В аралығында өзгерткенде, титанның тотығу тогының шамасы өсетіні және бұл шама 29,4 мА-ге жететіні анықталды. Тұз қышқылының концентрациясын 35-тен 100 г/л-ге дейін өзгерткенде және электродтар арасындағы кернеуді 0–14 В аралығында өзгерткенде, титанның еру жылдамдығы бір қалыпты өсетіні, бірақ кернеудің мәні 10–12 В арасында болғанда титанның тотығу тогы күрт өсіп, 360 мА-ге жететіні көрсетілді. Тотығу тогының өзгеруі титанның еру жылдамдығының артатынын дәлелдеді. Электролиз ұзақтығын арттыру кезінде анодтық токтың шамасы негізінен азаяды. Шамасы, кернеу 14 В және одан да жоғары болған кезде тұз қышқылды ерітіндіде жарғылай өткізгіштік қасиетке ие титан диоксидінің пленкасының тесілуі орын алады. Осыған байланысты титанның айтарлықтай мөлшерде еруі байқалады және одан ары қарай оксидтік пленка түзілмейді де, титан иондары түзіледі. Көрнекі бақылаулар титанның титан (IV) түріндегі ерітіндіге ауысатынын көрсетті.

*Кілт сөздер:* титан, титан диоксиді, пленка, электрод, тотығу тогы, поляризация, кернеу, күкірт қышқылы, тұз қышқылы.

А. Баешов, А.С. Кадирбаева, А.К. Башова, А.А. Жарменов

## Электрoхимический способ получения пленки TiO<sub>2</sub>, обладающей фотокаталитическими свойствами

Целью работы является изучение процесса формирования диоксида титана при анодной поляризации в серноокислых и солянокислых растворах. Исследования проводили методом снятия потенциодинамической циклической вольтамперной кривой и методом измерения величины тока окисления титана при изменении напряжения между электродами. Установлено, что с изменением концентрации серной кислоты в интервале 50–250 г/л и напряжения между электродами в пределах 0–25 В величина тока окисления титана возрастает и достигает 29,4 мА. При увеличении концентрации соляной кислоты от 35 до 100 г/л и изменении напряжения между электродами величина скорости окисления титана растет равномерно, но в интервале значений напряжения 10–12 В наблюдается резкое повышение величины тока до 360 мА. Изменение тока окисления свидетельствует об увеличении скорости растворения титана. С увеличением продолжительности электролиза величина анодного тока в основном уменьшается. По всей вероятности при напряжении, равном 14 В и выше, в солянокислом растворе наблюдается пробой оксидной полупроводниковой пленки диоксида титана. В этой связи происходит заметное растворение титана и в дальнейшем оксидная пленка не образуется, а образуются ионы титана. Визуальные наблюдения показали, что титан переходит в раствор в виде титана (IV).

*Ключевые слова:* титан, диоксид титана, пленка, электрод, ток окисления, поляризация, напряжение, серная кислота, соляная кислота.

### References

- 1 Maliukov, S.P., Saenko, A.V., & Bondarchuk, D.A. (2016). Issledovanie vliianiia tolshchiny plenki TiO<sub>2</sub> na fotoelektricheskie kharakteristiki perovskitovykh solnechnykh elementov [Investigation of the effect of TiO<sub>2</sub> film thickness on the photovoltaic characteristics of perovskite solar cells]. *Inzhenernyi vestnik Dona — Engineering Bulletin of the Don* [in Russian].
- 2 Shvets, P.V., Caffrey, D., Fleischer, K., Shvets, I., O'Neill, K., Duesberg, G.S., Vinichenko, A.N., Maksimova, Yu.K., & Goikhman, Yu.A. (2020). Suppression of the metal-insulator transition in magnetron sputtered Ti<sub>2</sub>O<sub>3</sub> films. *Thin Solid Films*, 694, 137642. <https://doi.org/10.1016/j.tsf.2019.137642>
- 3 Bessel, V.V., Kucherov, V.G., & Mingaleeva, R.D. (2016). *Izuchenie solnechnykh fotoelektricheskikh elementov [Study of solar photovoltaic cells]*. Moscow: Izdatelskii tsentr RGU nefti i gaza (NIU) imeni I.M. Gubkina [in Russian].
- 4 Wang, X., Fang, Y., He, L., Wang, Q., & Wu, T. (2014). Influence of compact TiO<sub>2</sub> layer on the photovoltaic characteristics of the organometal halide perovskite-based solar cells. *Materials Science in Semiconductor Processing*, 27, 569–576. <https://doi.org/10.1016/j.mssp.2014.07.039>
- 5 Jung, H.S., & Park, N.-G. (2014). Perovskite solar cells: From materials to devices. *Small*, 11(1), 10–25. <https://doi.org/10.1002/sml.201402767>
- 6 Minemoto, T., & Murata, M. (2014). Device modeling of perovskite solar cells based on structural similarity with thin film inorganic semiconductor solar cells. *Journal of Applied Physics*, 116(5), 054505. <https://doi.org/10.1063/1.4891982>
- 7 Rykov, A.N., & Belousova, V.A. (2020). Fotokatalizatory na osnove dioksida titana: poluchenie i primeneniye [Photocatalysts based on titanium dioxide: production and application]. *Otkrytaia gorodskaiia nauchno-prakticheskaiia konferentsiia «Inzheneriy budushchego»*, 367–370 [in Russian].
- 8 Sidak, I.L., Rakov, V.F., & Pogibko, V.M. (2020). Fotokataliticheskie ustroistva i sposoby ochistki vody [Photocatalytic devices and water treatment methods]. *Innovatsionnye perspektivy Donbassa*, 30–34 [in Russian].
- 9 Bubnov, V.V. (2019). Razrabotka plazmodinamicheskogo metoda sinteza ultradispersnogo dioksida titana TiO<sub>2</sub>, obladaushchego fotokataliticheskimi svoystvami polucheniia vodoroda [Development of a plasmodynamic method for the synthesis of ultrafine titanium dioxide TiO<sub>2</sub>, which has photocatalytic properties for hydrogen production]. *Master's dissertation — masterskaia dissertatsiia*. Tomsk: Natsionalnyi issledovatel'skii Tomskii politekhnicheskii universitet [in Russian].
- 10 Derevshchikov, V.S., Okunev, A.G., Lysikov, A.I., & Veselovskaia, J.V. (2014). Sposob polucheniia metana iz atmosfernogo dioksida ugleroda [Method for producing methane from atmospheric carbon dioxide]. *Patent № 2533710 CI Rossiiskaia Federatsiia* [in Russian].
- 11 Zhou, Y., & Gray-Weale, A. (2016). A numerical model for charge transport and energy conversion of perovskite solar cells. *Physical Chemistry Chemical Physics*, 18(6), 4476–4486. <https://doi.org/10.1039/c5cp05371d>
- 12 Abildina, A.K., Avchukir, K., Dzhumanova, R.Z., Beiseyeva, A.N., Rakhymbay, G.S., & Argimbayeva, A.M. (2021). Preparation and electrochemical characterization of TiO<sub>2</sub> as an anode material for magnesium-ion batteries. *Bulletin of the Karaganda University. "Chemistry" Series*, 104(4), 104–116. <https://doi.org/10.31489/2021ch4/104-116>
- 13 Zakir, O., Idouhli, R., Elyaaoubi, M., Khadiri, M., Aityoub, A., Koumya, Y., Rafqah, S., Abouelfida, A., & Outzourhit, A. (2020). Fabrication of TiO<sub>2</sub> nanotube by Electrochemical Anodization: Toward photocatalytic application. *Journal of Nanomaterials*, 2020, 1–11. <https://doi.org/10.1155/2020/4745726>

- 14 Shaalan, N.M., Ahmed, F., Rashad, M., Kumar, S., Saber, O., Al-Naim, A.F., & Mahmoud, A.Z. (2022). Ceramic Ti/TiO<sub>2</sub>/AuNP Film with 1-D Nanostructures for Selfstanding Supercapacitor Electrodes. *Crystals*, 12(6), 791. <https://doi.org/10.3390/cryst12060791>
- 15 Endrődi, B., Kecsenovity, E., Rajeshwar, K., & Janáky, C. (2018). One-step electrodeposition of nanocrystalline TiO<sub>2</sub> films with enhanced photoelectrochemical performance and Charge Storage. *ACS Applied Energy Materials*, 1(2), 851–858. <https://doi.org/10.1021/acs.aem.7b00289>
- 16 Ali, H.M. (2022). Titanium Dioxide-Advances and Applications. <https://doi.org/10.5772/intechopen.94670>
- 17 Kuzmina, M.Yu., & Belik, O.D. (2018). Izuchenie korrozionnoi stoikosti oksidnykh plenok na titane. *Mashiny, agregaty i protsessy. Proektirovanie, sozdanie i modernizatsiia*, 179–181 [in Russian].
- 18 Kuzmina, M.Yu., & Kuzmin, M.P. (2011). Koeffitsient kontrasta titanovogo elektrokromnogo elektroda. *Vestnik IrGTU*, 8(55), 139–143 [in Russian].

#### Information about authors\*

**Bayeshov, Abduali** — Doctor of Chemical Science, Professor, Academician of the National Academy of Sciences of the Republic of Kazakhstan, Republican State Enterprise “National Center on Complex Processing of Mineral Raw Materials of the Republic of Kazakhstan”, Karasay batyr street, 111–113, 050012, Almaty, Kazakhstan, e-mail: [bayeshov@mail.ru](mailto:bayeshov@mail.ru); <https://orcid.org/0000-0003-0745-039X>

**Kadirbayeva, Altynay** — PhD, Senior researcher, Republican State Enterprise “National Center on Complex Processing of Mineral Raw Materials of the Republic of Kazakhstan”, MTF-2 street, 44/1, 040998, Almaty, Kazakhstan, e-mail: [altinay\\_aidyn2789@mail.ru](mailto:altinay_aidyn2789@mail.ru); <https://orcid.org/0000-0003-0702-1114>

**Bayeshova, Azhar** (*corresponding author*) — Doctor of Technical Sciences, Professor, Al-Farabi Kazakh National University, 050012, Almaty, Kazakhstan, e-mail: [azhar\\_b@bk.ru](mailto:azhar_b@bk.ru); <https://orcid.org/0000-0002-9076-8130>

**Zharmenov, Abdurassul** — Doctor of Technical Sciences, Professor, Academician of the National Academy of Sciences of the Republic of Kazakhstan, Republican State Enterprise “National Center on Complex Processing of Mineral Raw Materials of the Republic of Kazakhstan”, Zhandosov street, 67, 050036, Almaty, Kazakhstan, e-mail: [nc@cmrp.kz](mailto:nc@cmrp.kz); <https://orcid.org/0000-0001-5651-5343>

\*The author's name is presented in the order: *Last Name, First and Middle Names*

## CHEMICAL TECHNOLOGY

Article Received: 28 January 2022 | Revised: 02 July 2022 | Accepted: 31 October 2022 | Published online: 16 November 2022

UDC 665.662.661.183

<https://doi.org/10.31489/2022Ch4/4-22-1>

E.A. Guseinova\*

*Azerbaijan State Oil and Industry University (ASOIU), Baku, Azerbaijan  
(\*Corresponding authors e-mail: [elvira\\_huseynova@mail.ru](mailto:elvira_huseynova@mail.ru))*

### Adsorption Purification of Used Industrial Oil Using Natural Aluminosilicates

The results of adsorption purification of used industrial oil in the presence of natural aluminosilicates, bentonite and mordenite, are discussed. It was found that the maximum degree of purification was achieved in the presence of mordenite and reached 61.68 % at an oil, adsorbent ratio of 2.3 at a temperature of 70 °C. The data of the structural-group analysis of the oil showed that the main share of the hydrocarbon components removed during purification is accounted for by highly condensed aromatic ones. The supposed reasons for the different adsorption activity of bentonite and mordenite samples were judged from the data of chemical, mineralogical, textural, and IR spectroscopic analysis. Based on the results of the IR spectra of mordenite samples, it was concluded that energetically active hydroxyl groups can be responsible for their increased adsorption activity. The used oil before purification is characterized by a high cyclicality of the hydrocarbons which included in the composition (aromatic hydrocarbons account for 38 % of the total), while the oil subjected to adsorption purification with mordenite (M-50) mainly becomes free of aromatic rings (the proportion of aromatic hydrocarbons decreases up to 19.6 %). This is a consequence of the high polarizability of aromatic hydrocarbons, in which, compared with other oil components, a dipole moment is easily induced under the influence of the electrostatic field of the adsorbent.

*Keywords:* adsorption purification, waste industrial oil, bentonite, mordenite, degree of purification, IR-spectrum, structural group composition.

#### Introduction

Adsorption purification methods are some of the most common purification techniques, with a wide range of applications in the chemical, oil refining, food industries, in medicine, radio engineering, printing, etc. The most common adsorbents are activated carbons, silica gels, aluminum gels, artificial and natural zeolites, etc. The practical application of adsorption technologies in the processes of cleaning the earth, air, water from oil pollution [1], the extraction of lead, copper [2], fluorine [3] ions and many others, is the subject of a number of interesting review papers. At the same time, both synthetic sorbents and natural mineral resources are successfully used. Indicators which affect adsorption activity are the size of the adsorption surface and its availability, polarity, chemical composition, and the nature of intermolecular interaction with adsorbate [4–7]. When specifying a specific choice of the type of adsorbent, all its characteristics are taken into account, since in the end their use is economically justified only if a high degree of purification and the possibility of reusable regeneration are ensured, and if they are available, cheap, non-toxic, etc.

The issues of cost are a matter of history if the indicators of the adsorption activity of the sorbent are directly related to its physicochemical properties. Along with the fact that synthetic sorbents produced by the industry are characterized by high cost, the use of effective natural adsorbents, in particular, aluminosilicates, can become one of the links in the “green” technology, since, on the one hand, this will help to reduce the volume of consumed production resources, while on the other hand, it will reduce the negative effect on the environment, for example, to the purification of used lubricating oils.

More than 30 types of natural zeolites are known, and the most common of them are chabazite, philipsite, lomontite, bentonite, mordenite, clinoptilolite, analcime, stilbite and erionite. Of these minerals, clinoptilolite and mordenite are of the greatest practical importance. They in the form of powders and filter materials are also used to purify water from synthetic surfactants, aromatic and carcinogenic organic compounds, dyes of various classes.

On the territory of Azerbaijan there are large industrial deposits of clinoptilolite, mordenite, kaolinite and bentonite (Aydag, Chananab, Dash-Salakhli deposits, etc.). Systematic studies conducted at the M.F. Nagiyev Institute made it possible to study the influence of nature, the charge of exchange cations, as well as the pH of the medium, thermal stability, porosity on the physicochemical characteristics of natural aluminosilicates of Azerbaijan [5–10]. The data obtained by the authors made it enable to develop scientifically based recommendations on the use of clinoptilolite, mordenite, kaolinite and bentonite for wastewater treatment from organic pollutants of various origins [9, 13].

Natural aluminosilicates of Azerbaijan also attracted close attention of catalytic chemists. The fundamental researches carried out [11–13], made it available to develop new zeolite catalysts for the production of alicyclic dienes, acetylene, and oxygen-containing compounds. It is shown that by varying the structure and composition of the zeolite, it is possible to implement different directions of hydrocarbon conversion to obtain the target products.

The given data testifies to the undoubted prospects of use of Azerbaijan's natural zeolites in the field of chemical technology. However, along with the listed advantages, they also have certain disadvantages, for which it should be noted that natural zeolites are complex and variable in composition multicomponent systems, the physicochemical properties of natural sedimentary zeolites significantly depend on the content of zeolite phases in the rock, type of cation-exchange form and nature of impurities, etc. Thus, even with the same content of the zeolite phase, depending on the selected deposit, there may be a discrepancy in the adsorption properties of individual samples.

A comparative study of the efficiency indicators of adsorption purification of used industrial oil (OIM) using natural aluminosilicates based on bentonite and mordenite, establishing the nature of their molecular sieve action, is the purpose of this study.

### Experimental

Industrial oil BP ENERGOL GR XP 320 was taken as used oil (duration of operation 4500 hours at a temperature of 30–40 °C). The causes of aging, the possibility of its acid and solvent regeneration, as well as the energy and environmental efficiency of its combustion were considered in [14–16].

Two samples of natural zeolites of Nakhchivan (the main mineral is mordenite, the samples differ in depth, 30 and 50 cm, **M-30** and **M-50**, respectively) and the Dash-Salakhli deposit (the main mineral is bentonite, **B**) of Azerbaijan were taken for the study. Samples of all studied samples of aluminosilicates were taken directly at the deposits. Air-dried pieces of minerals were freed from impurities and inclusions visible to the naked eye. Further, the purification of bentonite and mordenite minerals, which dominate in one or another clay deposit, was carried out by soaking. At the same time, an approximately 10 % aqueous suspension of clays was prepared, thoroughly mixed with a mechanical stirrer until the lumps disappeared, left alone for two hours, and the most highly dispersed fraction was decanted with a siphon.

Bulk, apparent, and true density, porosity, layer void ratio, absolute water content and water absorption of adsorbents, specific surface area and pore volume were determined by known methods...

The method of single-stage static sorption was used in the work. Sorption was carried out by adding a sample of aluminosilicate rocks crushed to grains of 0.5–2.0 mm in size to the studied UIO samples. Then the mass was stirred with a magnetic stirrer for 15 minutes and then centrifuged. After that, oil samples were taken and the degree of purification was determined.

The degree of purification  $\beta_{pur}$  was calculated based on the results of the optical density of oil samples according to the formula:

$$\beta_{pur} = 100 - \frac{n_{init} - n_{eq}}{n_{init}} \cdot 100 \%,$$

where  $n_{init}$  — is the optical density of initial UIO;  $n_{eq}$  — is the optical density of UIO in the equilibrium state.

Adsorbents mineralogical and chemical composition analysis was studied using the XRD “MiniFlex 600” and the “S8 TIGER Series 2 WDXRF” spectrometer.

The refractive index ( $n_D$ ) of oil samples was determined on an IRF-54V refractometer with an accuracy of 0.0001. The structural group composition of oil samples was determined by the  $n$ - $d$ - $M$  method.

To check the reproducibility of the results, each single experiment was repeated 3 times. Statistical processing of experimental data showed their satisfactory reproducibility. The experimental error did not exceed 5 %.

### Results and Discussion

Comparative characteristics of the chemical and mineralogical composition of the studied adsorbents are presented in Tables 1 and 2. As can be seen from the presented data, the qualitative chemical composition of both types of adsorbents is characteristic of these types of zeolites. The main distinction between their chemical composition lies in the different mass ratio of  $\text{SiO}_2$ : $\text{Al}_2\text{O}_3$ : it made up 4:1 for bentonite and 5.4:1 for mordenite samples, as well as the content of calcium oxide (for bentonite, it is almost 4 times higher).

The main mineralogical components of the sample B are montmorillonite (more than 70 %) and feldspars, while M-30 and M-50 are characterized by the presence of a significant amount of quartz, illite, calcite, and hematite.

Table 1

#### Chemical composition of the adsorbents

Adsorbent	Na <sub>2</sub> O	MgO	Al <sub>2</sub> O <sub>3</sub>	SiO <sub>2</sub>	SO <sub>3</sub>	K <sub>2</sub> O	CaO	TiO <sub>2</sub>	Fe <sub>2</sub> O <sub>3</sub>	HTC*
B	2.17	4.62	12.23	48.75	0.93	1.89	6.32	0.64	10.18	9.73
M-30	1.34	2.16	13.25	71.64	–	2.05	1.42	0.68	0.04	7.42
M-50	1.35	2.3	13.04	70.21	–	2.09	1.83	0.7	0.21	8.27

\*HTC — is the amount of components evaporating at 950 °C.

Table 2

#### Mineralogical composition of the adsorbents

Adsorbent	SiO <sub>2</sub> ( $\alpha$ -quartz)	Feldspar	Illite	CaCO <sub>3</sub> (calcite)	Montmo- rillonite	Fe <sub>2</sub> O <sub>3</sub> (hematit)	Volcan. ash	Etc. impurities
B	2.3	12.5	0.4	3.1	72.2	0.6	7.1	1.5
M-30	10.2	19.1	10.6	11.8	32	8.3	5.8	2.1
M-50	10.4	19	10.5	12.6	31.1	8	5.7	2.6

During the research, it was found that mordenite samples have a significantly lower bulk density (9 times less) and, on the contrary, large specific surface values (Table 3), which is explained by differences in the porous structure (given that a specific adsorbent fraction was used in the course of the experiments, it is possible the effect of particle size was not considered). In accordance with the type of zeolite and the noted structural features, differences are also observed in the water absorption of the samples. Mordenite samples are characterized by lower water absorption (2 times less relative to bentonite). The observed differences are due to their crystal structure.

Table 3

#### Physical properties of the adsorbents

Adsorbent	$S_{sa}$ , m <sup>2</sup> /g	Density, q/sm <sup>3</sup>			$V_{sp.pr.ar}$	$\alpha$	$\epsilon$	W	WA
		$\rho_{bulk}$	$\rho_{app}$	$\rho_{tr}$					
B	172	0.930	0.810	0.752	13.36	54.62	0.005	14.1	127.6
M-30	425	0.102	0.942	0.860	20.18	65.50	0.11	7.53	52.1
M-50	480	0.115	0.905	0.811	29.47	69.73	0.15	6.28	59.8

Note.  $\alpha$  — porosity;  $\epsilon$  — void ratio; W — absolute water content; WA — water absorption.

The analysis of the obtained IR spectra confirmed that the studied zeolite samples belong to their structural types (Table 4): the spectra contain absorption bands specific to zeolites in 2 regions: vibrational regions inside tetrahedra (internal asymmetric valence bands 1250–950 cm<sup>-1</sup>, symmetrical valence stretch 720–

650  $\text{cm}^{-1}$  and deformations in the T-O tetrahedron 500–420  $\text{cm}^{-1}$ ); vibrations by external bonds of zeolite tetrahedra (double ring vibrations 650–500  $\text{cm}^{-1}$ , pore opening vibrations 300–420  $\text{cm}^{-1}$ , symmetric valence stretch 750–820  $\text{cm}^{-1}$  and asymmetrical stretch 1050–1150  $\text{cm}^{-1}$ ). Separate characteristic fluctuations were also identified. Thus, absorption bands in the region of 401–440  $\text{cm}^{-1}$ , which correspond to the vibrations of cations in the zeolite (interionic vibrations), were found only in mordenite samples. In addition, their spectra contain a band at about 780  $\text{cm}^{-1}$ , which is characteristic of the Al–O bond inside aluminum-oxygen tetrahedra. Moreover, it has a greater intensity in M-50. This indicates a relatively higher aluminum content in it. The band at 665  $\text{cm}^{-1}$  noted for bentonite indicates vibrations of Al–O–Si in the mixed silicon-aluminum-oxygen framework.

Table 4

## Characteristic bandwidths (bw) in the IR-spectra of zeolites

B		M-30		M-50		Frequency of the assignment
A.b., $\text{sm}^{-1}$	Int., %	A.b., $\text{sm}^{-1}$	Int., %	A.b., $\text{sm}^{-1}$	Int., %	
				401.44	7.001	$\delta$ (T-O <sub>4</sub> )
		409.53	0.512	407.53	5.305	$\delta$ (T-O <sub>4</sub> )
		418.37	0.419	414.11	2.490	$\delta$ (T-O <sub>4</sub> )
				423.15	2.276	$\delta$ (T-O <sub>4</sub> )
		433.63	0.682	434.10	4.256	$\delta$ (T-O <sub>4</sub> )
440.49	0.264	441.12	3.257	441.06	4.385	$\delta$ (T-O <sub>4</sub> )
		456.31	0.754	449.84	2.568	$\delta$ (T-O <sub>4</sub> )
				473.72	4.593	$\delta$ (T-O <sub>4</sub> )
				502.97	5.818	K.c.K.
		514.29	1.110	509.30	5.385	K.c.K.
				523.69	5.580	K.c.K.
665.81	10.634					K.c.K.
		713.32	2.255			$\nu_s$
721.76	9.785	721.86	2.328	721.94	9.796	$\nu_s$
		776.10	3.482	772.58	14.704	$\nu_{as}$ (Si–O)
794.61	10.995					$\nu_{as}$ (Al–O)
		872.22	1.117	873.05	9.831	$\nu_s$
		972.56	0.745			$\nu_{as}$
				1022.95	3.210	$\nu_{as}$
1038.29	5.714					$\nu_{as}$
1644.47	9.539	1633.29	5.535	1643.73	17.568	$\delta$ (H <sub>2</sub> O)
		3390.06	2.310	3396.17	8.194	$\nu_{as}$ H <sub>2</sub> O
3417.95	7.026					B.c.OH
3626.65	6.257	3626.57	3.178	3626.35	9.574	B.c.OH
		3742.21	18.990	3742.21	23.045	$\nu_{as}$ H <sub>2</sub> O
		3748.01	19.284	3748.96	24.637	$\nu_{as}$ H <sub>2</sub> O
		3756.20	19.411	3756.10	24.551	$\nu_{as}$ H <sub>2</sub> O
		3793.96	19.432	3794.02	23.939	$\nu_{as}$ H <sub>2</sub> O
		3813.59	19.266	3813.58	27.022	$\nu_{as}$ H <sub>2</sub> O
		3835.19	19.220	3829.92	27.259	$\nu_{as}$ H <sub>2</sub> O
3851.04	20.800	3850.73	18.932	3850.71	27.200	$\nu_{as}$ H <sub>2</sub> O
3861.00	26.185	3867.94	18.841			$\nu_{as}$ H <sub>2</sub> O
		3897.37	18.439			$\nu_{as}$ H <sub>2</sub> O

\*h.b. — hydrogen bond; v.d.r. — vibrations of double rings.

However, the main differences in the IR spectra of bentonite and mordenite samples were associated with the absorption bands of water molecules. In the absorption spectrum of bentonite, a band of deformation vibrations of water at 1644  $\text{cm}^{-1}$  (typical for adsorbed water) and stretching symmetric and asymmetric vibrations of OH groups at 3417.95 and 3626.65  $\text{cm}^{-1}$ , respectively, was noted. In contrast to bentonite, in the spectrum of mordenite samples, the bands of deformation vibrations and stretching vibrations of OH groups

are shifted to the high-frequency region, and bands related to stretching asymmetric vibrations of hydroxyl groups in the range of  $3742\text{--}3850\text{ cm}^{-1}$  were also found.

It is known that absorption bands in the region of stretching vibrations of OH groups can be caused by both structural hydroxyl groups and physically adsorbed water. Taking into account the data obtained, it can be concluded that both cases take place: the presence of adsorbed water on the surface of aluminosilicate samples is indicated by bands at  $1633$ ,  $1644$  and  $2146$ ,  $2329$  and  $3417\text{ cm}^{-1}$ ; structural hydroxyl groups in bentonite, but located only in large cavities — at  $3626\text{ cm}^{-1}$ , while in mordenite — by bands both in large ( $3626\text{ cm}^{-1}$ ) and small (medium-intensive bands at  $3742$ ,  $3748$ ,  $3756$ ,  $3796$ ,  $3813$ ,  $3835\text{ cm}^{-1}$ ) cavities [17]. In this position, the structural hydroxyl groups of mordenite are bonded to the silicon atom. The latter is now the generally accepted view. Also, when comparing the IR spectra of mordenite samples, attention was drawn to the increase in the intensity of structural hydroxyl groups at  $3626\text{ cm}^{-1}$  relative to bentonite, as well as the average intensity of the bands at  $3742\text{--}3835\text{ cm}^{-1}$ . Since the surfaces of clay minerals can act as centers for adsorption of coordinatively unsaturated ions of silicon, aluminum, magnesium, oxygen, and uncharged, as well as energetically active hydroxyl groups [18], for the latter the noted distinctive features in the IR spectra of the studied samples may indicate with a greater degree of probability their different adsorption activity.

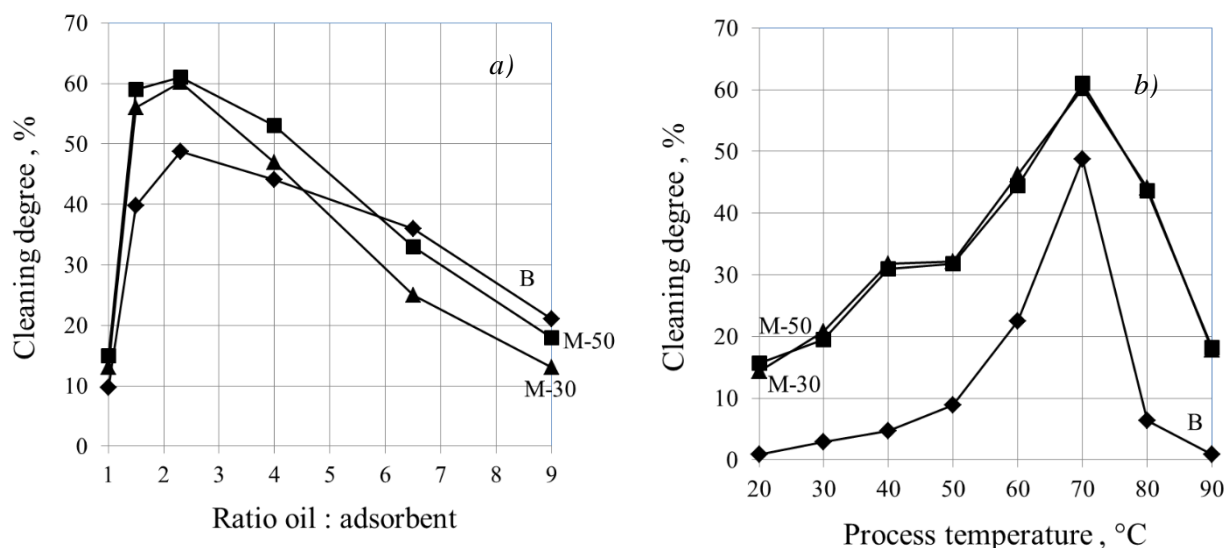


Figure. Dependence of the degree of oil purification on the ratio of oil: adsorbent (a) and process temperature (b)

The adsorption activity of zeolites was assessed by the degree of purification of UIO. The adsorption activity of zeolites was assessed by the degree of purification of UIO. The results obtained in the study of the effect of the oil to adsorbent ratio on the degree of oil purification made it possible to establish that mordenite samples had much greater sorption capacity with respect to aging products (Fig. a)). The degree of oil purification in the presence of bentonite and mordenite differed by almost 13 % and amounted to 48.7 % and 61.86 % (for M-30), respectively. This is probably due to the manifestation by zeolites of the so-called “sieve effect” — selective throughput sorption of pores. According to the data available in the literature, the probable pore size of bentonite is  $4\text{ \AA}$  versus  $8\text{ \AA}$  for mordenite. The presence of this difference is apparently one of the reasons responsible for the differences in the sorption properties exhibited relative to the components of the used oil. And here a reservation should be made: the maximum values of this indicator for both adsorbents were noted at oil: adsorbent ratio in the range of  $1.5\div 2.3$ . The similarity of this parameter for all three considered adsorbents indicates that the dimension of the inlet pores is of secondary importance, while the chemical structure of zeolites is of primary importance. It is understood as the presence of uncompensated surface force fields formed by complexes of silicon, aluminum and surface hydroxyl groups. Physical sorption on the surface of zeolites is carried out due to the excess negative charge of tetrahedrally forming metals, on the faces of crystals, as well as surface hydroxyl groups of an acidic and basic character.

According to now classical concepts, they are responsible for the orientational and inductive interaction of polar adsorbents with oil components. The low degree of purification at low oil: adsorbent ratio is identical for both types of zeolites and, according to the literature data [15], is associated with the aggregation of

adsorbent particles, which leads to a decrease in the total specific surface area and an increase in the diffusion path during adsorption.

The influence of the temperature of adsorption purification is shown in Figure b). When comparing the effect of the process temperature on the degree of purification of UIO, it can be noted that the best results were obtained at 70 °C, which is in good agreement with the parameters recommended in the literature [19].

Used oil before purification is characterized by a high cyclicality of the constituent hydrocarbons (Table 5). Special attention should be paid to the distribution of the number of rings in the molecule of the original used oil — aromatic hydrocarbons account for 38 % of the total number, which indicates their high condensation and the corresponding carbon content (18.08 %). Whereas the oil subjected to adsorption purification with mordenite (M-50) gets rid mainly of aromatic rings. This is indicated by a decrease in the proportion of aromatic hydrocarbons to 19.6 % of the total, and an increase in the mass fraction of carbon in cycloalkane and alkyl substituents against the background of a 2-fold decrease in arene rings. This is a consequence of the high polarizability of aromatic hydrocarbons, in which, compared with other oil components, a dipole moment is easily induced under the influence of the electrostatic field of the adsorbent [19, 20].

Table 5

Structural-group composition of oil samples according to the *n-d-M* method

Sample of oil	$d_{20}^4$	$n_d^{20}$	$M$	Carbon distribution, %				Average number of rings per molecule		
				$C_{ap}$	$C_H$	$C_{коп}$	$C_{II}$	$K_{ap}$	$K_H$	$K_o$
Initial	0.898	1.4996	311.82	18.08	29.54	47.61	52.38	0.67	1.10	1.77
after M-50 cleaning	0.878	1.4834	263.91	9.90	41.88	51.79	48.21	0.32	1.31	1.63

### Conclusions

Thus, comparative studies of the sorption activity of natural aluminosilicates — bentonite and mordenite in the process of purification of used industrial oil made it possible to establish that the maximum degree of purification was achieved in the presence of mordenite and reached 61.68 % at oil: adsorbent ratio of 2.3 at a temperature of 70 °C. The data of the structural-group composition of the purified oil indicated that the main components removed during adsorption purification are highly condensed aromatic hydrocarbons. The induction of a dipole moment in aromatic hydrocarbons is more likely due to the excess charge of surface hydroxyl groups, which, according to the results of IR-spectroscopic analysis, are localized in bentonite mainly in large cavities, while in mordenite, both in large and small ones. Thus, among the reasons for the different sorption activity of bentonite and mordenite, the dimension of the inlet pores is of secondary importance, while the chemical structure of zeolites is of primary importance.

### References

- 1 Bandura L. Application of Mineral Sorbents for Removal of Petroleum Substances: A Review / L. Bandura, A. Wozuk, D. Kołodyńska, W. Franus // Minerals. — 2017. — Vol. 7, No. 3. — P. 37. <https://doi.org/10.3390/min7030037>
- 2 Kozera-Sucharda B. The Comparison of the Efficacy of Natural and Synthetic Aluminosilicates, Including Zeolites, in Concurrent Elimination of Lead and Copper from Multi-Component Aqueous Solutions / B. Kozera-Sucharda, B. Gworek, I. Kondzielski, J. Chojnicki // Processes. — 2021. — Vol. 9, No. 5. — P. 812. <https://doi.org/10.3390/pr9050812>
- 3 Kumari S. Adsorptive mitigation of fluoride ions using aluminosilicate adsorbents: A state-of-the-art review / S. Kumari, V. Anjitha, S. Sengupta // Environmental Challenges. — Vol. 5, December 2021. — P. 100329. <https://doi.org/10.1016/j.envc.2021.100329>
- 4 Nyankson E. Synthesis and characterisation of zeolite-A and Zn-exchanged zeolite-A based on natural aluminosilicates and their potential applications / E. Nyankson, J.K. Efavi, A. Yaya, G. Manu, K. Asare, J. Daafuor & R.Y. Abrokwah // Cogent Engineering. 2018. — Vol. 5, No. 1. — P. 1440480. DOI:10.1080/23311916.2018.1440480
- 5 Коссовская А.Г. Природные цеолиты / А.Г. Коссовская. — М.: Наука, 1980. — 232 с.
- 6 Брек Д.В. Цеолитовые молекулярные сита / Д.В. Брек (пер. с англ.). — М.: Мир, 1976. — 781 с.
- 7 Абдуллаев А.А. Природные сорбенты цеолитовой структуры / А.А. Абдуллаев, А.А. Агзамходжаев, Э.А. Арипов, К.С. Ахмедов, М.З. Закиров, А.А. Колдаев, М.М. Мирсаидов, А.М. Мирсалимов, С.З. Муминов. — Ташкент, 1974. — 108 с.

- 8 Аннагиев М.Х. Сорбенты на основе природных цеолитов / М.Х. Аннагиев, Н.А. Иманова, С.Г. Алиева. — Баку: Элм, 2007. — 108 с.
- 9 Исмаилова В.Э. Закономерности равновесия сорбции ионов свинца ( $Pb^{2+}$ ) и марганца ( $Mn^{2+}$ ) из растворов на природных и синтетических сорбентах / В.Э. Исмаилова, А.И. Ягубов, Ф.Т. Махмудов, Н.М. Мурадова // Прикладная химия. — 2016. — Т. 89. Вып. 1. — С. 56–60 <https://doi.org/10.1134/s1070427216010080>
- 10 Ильясова Х.Н. Кинетика сорбции ионов кобальта ( $Co^{2+}$ ) и кадмия ( $Cd^{2+}$ ) из растворов на природных и синтетических сорбентах / Х.Н. Ильясова, А.Н. Нуриев, Ф.Т. Махмудов, А.И. Ягубов, Н.М. Мурадова // Азербайджан. хим. журн. — 2018. — № 1. — С. 88–95. <https://doi.org/10.32737/0005-2531-2018-1-88-95>
- 11 Тагиев Д.Б. Каталитические свойства цеолитов в реакции окисления / Д.Б. Тагиев, Х.М. Миначев // Успехи химии. — 1981. — Т. 50. Вып. 11. — С. 1929–1959. <https://doi.org/10.1070/RC1981v050n11ABEH002718>
- 12 Алиев А.М. Окислительное дегидрирование циклогексана на модифицированных цеолитах / А.М. Алиев, З.А. Шабанова, У. Наджаф-Кулиев, С.М. Меджидова // Нефтехимия. — 2016. — № 4. — С. 407–414. <https://doi.org/10.7868/S002824211604002X>
- 13 Алиев А.М. Кинетика и механизм реакции окислительного превращения n-амилового спирта в валериановую кислоту на модифицированном цеолитном катализаторе / А.М. Алиев, М.Ф. Бахманов, Ф.А. Агаев, В.Ш. Агаев, З.А. Шабанова, А.Р. Сафаров // Журн. физ. хим. — 2018. — Т. 92. — С. 362–366. <https://doi.org/10.7868/S0044453718040064>
- 14 Гусейнова Э.А. Энерго-экологическая эффективность горения отработанного индустриального масла / Э.А. Гусейнова // Заметки ученого. — 2021. — № 5. — С. 271–277.
- 15 Guseinova E.A. Influence of the structure of  $C_6$  hydrocarbons on the indicators of solvent cleaning waste industrial oil / E.A. Guseinova, K.Y. Ajamov // Herald of the Azerbaijan Engineering Academy. — 2020. — Vol. 12, № 2. — P. 58–64.
- 16 Способ очистки отработанных смазочных масел. Евразийский патент № 039347.
- 17 Ягубов А.И. Научные основы регулирования поверхностных свойств сорбентов на основе природных алюмосиликатов и их использование: дис. ... д-ра хим. наук: 02.00.04 — «Физическая химия» / Ягубов Али Ибрагим оглы; НАН Азербайджана; Ин-т хим. проблем им. акад. М.Ф. Нагиева. — Баку, 2012. — 284 с.
- 18 Bhattacharyya K.G. Pb (II) uptake by kaolinite and montmorillonite in aqueous medium: influence of acid activation of the clays / K.G. Bhattacharyya, S.G. Susmita // Colloids and Surfaces. — 2006. — Vol. 277. — P. 191–200. <https://doi.org/10.1016/j.colsurfa.2005.11.060>
- 19 Казакова Л.П. Физико-химические основы производства нефтяных масел / Л.П. Казакова, С.Э. Крейн. — М.: Химия, 1978. — 320 с.
- 20 Novikova L. Adsorption of Industrial Pollutants by Natural and Modified Aluminosilicates / L. Novikova, L. Belchinskaya // Clays, Clay Minerals and Ceramic Materials Based on Clay Minerals, Gustavo Morari do Nascimento (March 9th 2016). IntechOpen. <https://doi.org/10.5772/61678>

Э.А. Гусейнова

## Табиғи алюмосиликаттар көмегімен өндірістік мұнай қалдықтарын адсорбциялық тазарту

Мақалада табиғи алюмосиликаттар — бентонит пен мордениттің қатысуымен пайдаланылған өнеркәсіптік мұнайды адсорбциялық тазарту нәтижелері талқыланды. Тазартудың максималды дәрежесіне мордениттің қатысуымен қол жеткізілетіні және мұнайдың арақатынасы: яғни 70 °С температурада адсорбент 2,3-ке тең болған жағдайда 61,68%-ға жеткені дәлелденді. Бентонит пен морденит үлгілерінің әртүрлі адсорбциялық белсенділігінің болжамды себептері химиялық, минералогиялық, текстуралық және ИҚ-спектроскопиялық талдау деректері бойынша анықталды. Морденит үлгілерінің ИҚ-спектрлерінің нәтижелері бойынша олардың адсорбциялық белсенділігінің жоғарылауына энергетикалық белсенді гидроксил топтары жауапты болуы мүмкін деген қорытынды жасалған. Мұнайдың құрылымдық-топтық талдауының мәліметтері тазарту кезінде жойылатын көмірсутекті компоненттердің негізгі үлесін жоғары конденсацияланған ароматтылар құрайтынын көрсетті. Тазартуға дейінгі мұнай қалдықтары құрамына кіретін көмірсутектердің жоғары циклділігімен сипатталады (ароматты көмірсутектер жалпы көлемнің 38 %-ын құрайды), ал морденитпен (М-50) адсорбциялық тазартуға ұшыраған мұнай негізінен ароматты сақиналардан арылады (ароматты көмірсутектердің үлесі 19,6 %-ға дейін төмендейді. Бұл басқа мұнай компоненттерімен салыстырғанда адсорбенттің электростатикалық өрісінің әсерінен дипольдік момент оңай индукцияланатын ароматты көмірсутектердің жоғары поляризациялануының салдары.

*Кілт сөздер:* адсорбциялық тазалау, өнеркәсіптік мұнай қалдықтары, бентонит, морденит, тазарту дәрежесі, ИҚ-спектрі, құрылымдық топ құрамы.

Э.А. Гусейнова

## Адсорбционная очистка отработанного индустриального масла с применением природных алюмосиликатов

Обсуждены результаты адсорбционной очистки отработанного индустриального масла в присутствии природных алюмосиликатов — бентонита и морденита. Установлено, что максимальная степень очистки достигалась в присутствии морденита и равнялась 61,68 % при соотношении «масло: адсорбент», равном 2,3, при температуре 70 °С. О предполагаемых причинах проявляемой различной адсорбционной активности образцов бентонита и морденита судили по данным химического, минералогического, текстурного и ИК-спектроскопического анализов. На основе результатов ИК-спектров морденитных образцов сделан вывод о том, что за их повышенную адсорбционную активность могут быть ответственны энергетически активные гидроксильные группы. Данные структурно-группового анализа масла показали, что основная доля удаляемых в ходе очистки углеводородных компонентов приходится на высококонденсированные ароматические. Отработанное масло до очистки характеризуется высокой цикличностью входящих в состав углеводородов (на долю ароматических углеводородов приходится 38 % от общего числа), тогда как масло, подвергнутое адсорбционной очистке морденитом (М-50), избавляется в основном именно от ароматических колец (доли ароматических углеводородов уменьшается до 19,6 %). Это является следствием высокой поляризуемости ароматических углеводородов, в которых по сравнению с прочими компонентами масла под влиянием электростатического поля адсорбента легко индуцируется дипольный момент.

*Ключевые слова:* адсорбционная очистка, отработанное индустриальное масло, бентонит, морденит, степень очистки, ИК-спектр, структурно-групповой состав.

### References

- 1 Bandura, L., Wozuk, A., Kołodźńska, D., Franus, W. (2017). Application of Mineral Sorbents for Removal of Petroleum Substances: A Review. *Minerals*, 7, 37. <https://doi.org/10.3390/min7030037>
- 2 Kozera-Sucharda, B., Gworek, B., Kondzielski, I., Chojnicki, J. (2021). The Comparison of the Efficacy of Natural and Synthetic Aluminosilicates, Including Zeolites, in Concurrent Elimination of Lead and Copper from Multi-Component Aqueous Solutions. *Processes*, 9, 812. <https://doi.org/10.3390/pr9050812>
- 3 Kumari, S., Anjitha V., Sengupta, S. (2021). Adsorptive mitigation of fluoride ions using aluminosilicate adsorbents: A state-of-the-art review. *Environmental Challenges*, Volume 5, December, 100329 <https://doi.org/10.1016/j.envc.2021.100329>
- 4 Nyankson, E., Efavi, J.K., Yaya, A., Manu, G., Asare, K., Daafuor, J. & Abrokwah, R.Y. (2018). Synthesis and characterisation of zeolite-A and Zn-exchanged zeolite-A based on natural aluminosilicates and their potential applications, *Cogent Engineering*, 5:1, 1440480. <https://doi.org/10.1080/23311916.2018.1440480>
- 5 Kossovskaya, A.G. (1980). *Prirodnye tseolity [Natural zeolites]*. Moscow: Nauka [in Russian].
- 6 Brek, D.V. (1976). *Tseolitovye molekuliarnye sita [Zeolite Molecular Sieves]*. Moscow: Mir [in Russian].
- 7 Abdullaev, A.A., Agzamhodzhaev, A.A., Aripov, E.A., Ahmedov, K.S., Zakirov, M.Z., & Koldaev, A.A., et al. (1974). *Prirodnye sorbenty tseolitovoi struktury [Natural sorbents of zeolite structure]*. Tashkent [in Russian].
- 8 Annagiev, M.H., Imanova, N.A., & Alieva, S.G. (2007). *Sorbenty na osnove prirodnikh tseolitov [Sorbents based on natural zeolites]*. Baku: Elm [in Russian].
- 9 Ismailova, V.E., Yagubov, A.I., Mahmudov, F.T., & Muradova, N.M. (2016). Zakonomernosti ravnovesiia sorbtzii ionov svintsa (Pb<sup>2+</sup>) i margantsa (Mn<sup>2+</sup>) iz rastvorov na prirodnikh i sinteticheskikh sorbentakh [Equilibrium patterns of sorption of lead (Pb<sup>2+</sup>) and manganese (Mn<sup>2+</sup>) ions from solutions on natural and synthetic sorbents]. *Prikladnaia khimiia — Applied Chemistry*, 89, 1, 56–60 [in Russian]. <https://doi.org/10.1134/s1070427216010080>
- 10 Il'yasova, H.N., Nuriev, A.N., Mahmudov, F.T., Yagubov, A.I., & Muradova, N.M. (2018). Kinetika sorbtzii ionov kobalta (Co<sup>2+</sup>) i kadmiia (Cd<sup>2+</sup>) iz rastvorov na prirodnikh i sinteticheskikh sorbentakh [Sorption Kinetics of Cobalt (Co<sup>2+</sup>) and Cadmium (Cd<sup>2+</sup>) Ions from Solutions on Natural and Synthetic Sorbents]. *Azerbaidzhanskii khimicheskii zhurnal — Azerbaijan Chemical Journal*, 1, 88–95 [in Russian]. <https://doi.org/10.32737/0005-2531-2018-1-88-95>
- 11 Tagiev, D.B., & Minachev, X.M. (1981). Kataliticheskie svoystva tseolitov v reaktzii okisleniia [Catalytic Properties of Zeolites Towards Oxidation Reactions]. *Uspekhi khimii — Advances in Chemistry*, 50(11), 1929–1959 [in Russian]. <https://doi.org/10.1070/RC1981v050n11ABEH002718>
- 12 Aliev, A.M., Shabanova, Z.A., Nadzhaf-Kuliev, U., & Medzhidova, S.M. (2016). Okislitelnoe degidrirovaniie tsiklogeksana na modifitsirovannykh tseolitakh [Oxidative dehydrogenation of cyclohexane on modified zeolites]. *Neftekhimiia — Petrochemistry*, 4, 407–414 [in Russian]. <https://doi.org/10.7868/S002824211604002X>
- 13 Aliev, A.M., Bahmanov, M.F., Agaev, F.A., Agaev, V.Sh., Shabanova, Z.A., & Safarov, A.R. (2018). Kinetika i mekhanizm reaktzii okislitel'nogo prevrashcheniia n-amilovogo spirta v valerianovuiu kislotu na modifitsirovannom tseolitnom katalizatore [Kinetics and Mechanism of the Oxidative Conversion of n-Amyl Alcohol to Valeric Acid on a Modified Zeolite Catalyst]. *Zhurnal fizicheskoi khimii — Journal of Physical Chemistry*, 92, 362–366 [in Russian]. <https://doi.org/10.7868/S0044453718040064>

- 14 Guseinova, E.A. (2021). Energo-ekologicheskaia effektivnost gorenii otrabotannogo industrialnogo masla [Energy and environmental efficiency of waste industrial oil combustion]. *Zametki uchenogo — Notes of a scientist*, 5, 271–277 [in Russian].
- 15 Guseinova, E.A., & Ajamov, K.Y. (2020). Influence of the structure of C<sub>6</sub> hydrocarbons on the indicators of solvent cleaning waste industrial oil. *Herald of the Azerbaijan Engineering Academy*, 12, 2, 58–64.
- 16 Eurasian patent № 039347 (2022). Sposob ochistki otrabotannykh smazochnykh masel [Method for cleaning used lubricating oils] [in Russian].
- 17 Yagubov, A.I. (2012). Nauchnye osnovy regulirovaniia poverkhnostnykh svoystv sorbentov na osnove prirodnykh alyumosilikatov i ikh ispolzovanie [Scientific basis for regulating the surface properties of sorbents based on natural aluminosilicates and their use]. *Doctor's thesis*. Azerbaidzhan [in Russian].
- 18 Bhattacharyya, K.G., & Susmita, S.G. (2006). Pb (II) uptake by kaolinite and montmorillonite in aqueous medium: influence of acid activation of the clays. *Colloids and Surfaces*, 277, 191–200. <https://doi.org/10.1016/j.colsurfa.2005.11.060>
- 19 Kazakova, L.P., & Crane, S.E. (1978). *Fiziko-khimicheskie osnovy proizvodstva neftiannykh masel [Physico-chemical bases for the production of petroleum oils]*. Moscow: Khimiia [in Russian].
- 20 Novikova L., Belchinskaya, L. (2016). Adsorption of Industrial Pollutants by Natural and Modified Aluminosilicates. *Clays, Clay Minerals and Ceramic Materials Based on Clay Minerals, Gustavo Morari do Nascimento, IntechOpen*. <https://doi.org/10.5772/61678>

#### Information about author\*

**Guseinova, Elvira Anverovna** — PhD, docent, Department of Petrochemical Technology and Industrial Ecology, Head of laboratory “Protective coatings and lubricating oils”, Azerbaijan State Oil and Industry University, Azadliq av. 16/21, AZ1010, Baku, Azerbaijan, e-mail: [elvira\\_huseynova@mail.ru](mailto:elvira_huseynova@mail.ru); <https://orcid.org/0000-0003-0297-1516>

---

\*The author's name is presented in the order: *Last Name, First and Middle Names*

L.G. Chekanova<sup>1\*</sup>, V.N. Vaulina<sup>1</sup>, Yu.B. Elchischeva<sup>2</sup>,  
E.S. Bardina<sup>1</sup>, P.T. Pavlov<sup>2</sup>

<sup>1</sup>*Institute of Technical Chemistry, Ural Branch of Russian Academy of Sciences,  
Perm Branch of Perm Federal Research Center, Ural Branch of RAS, Perm, Russia;*

<sup>2</sup>*Perm State National Research University, Perm, Russia*

(\*Corresponding author's e-mail: [larchek.07@mail.ru](mailto:larchek.07@mail.ru))

## The Selection of Reagents for Ionic Flotation of Non-Ferrous Metals in the Series of N-Acyl-N'-Mezylhydrazines

A series of new ligands — N-acyl-N'-mesylhydrazines (MSH) — of the general formula  $RC(O)NHNHSO_2CH_3$  has been obtained and considered as reagents for ionic flotation (IF) of non-ferrous metals (M(II)). Reagents with a radical length of  $C_6H_{13}$  and above form hardly soluble complexes with M(II) so it is possible to implement a kind of the ionic flotation techniques — “precipitate flotation”. The ranges of pH values of the most complete precipitation of cations from solutions have been determined. Precipitates of the metal complexes were isolated; their composition was confirmed by IR spectroscopy and elemental analysis. The conditional values of the solubility product (SP) of the complexes  $[M(HL)_2]$  were calculated. The dependence  $-\lg SP = 11.8 + 0.61N$  is fulfilled for the MSH series and Cu(II) ions. The surface-active properties of compounds with  $R > C_6H_{13}$  were established. The reagents with optimal radical length for ionic flotation were selected. The ionic flotation of non-ferrous metals with N-nonanoyl-N'-mesylhydrazine was carried out. The up to 95–99 % recovery of metal ions, separation of copper and associated metal ions in diapason of pH 5–6.5 was shown to be possible.

**Keywords:** ionic flotation, precipitate flotation, sulfonylhydrazines, non-ferrous metals, physico-chemical properties, surface-active substances.

### Introduction

Ion flotation (IF) is a simple and effective method for concentrating and separating metals from solutions containing fewer 500 mg/l of metal ions. Versatility, high performance and efficiency of this technique [1; 9] are of interest for purifying and deep post-treating waste waters and recycled waters, as well as for recovering valuable metals in industrial productions and in hydrometallurgy [2–5]. Improving the efficiency of IF is largely related to the efficiency of the reagents used [6]. At present, alkyl carboxylates [7], alkyl sulfonates, alkyl sulfates, alkylamines, quaternary ammonium salts [8–12], and xanthates [13] have been practically employed. As for the development of ion flotation, it would seem as appropriate to develop and improve a methodology for selecting an optimal collector. The traditional way of selecting a flotation reagent-collector is using compounds with a functional group capable of forming a chemical bond to a metal cation. Today the calculation of quantum-chemical characteristics of potential collectors (nucleophilic hardness, molecular electric moments, energy of complexation, etc.) has widely been used. It greatly facilitates the search for reagents, narrowing the range of ligands suitable for further studies [14]. However, as a rule, these calculations do not take into account the influence of solvents, salt composition, and competing complexation reactions in polycationic systems. In addition, the most important factor of the synthesis direction at developing potential collectors is the presence of a set of properties in the reagent that meet the basic requirements for flotation reagents [6]. One approach in the development of collectors for nonferrous metal ions is the directed synthesis method based on the choice of a suitable functionally active atom group (FAG) capable of forming compounds with metal ions and the organic radical (R). The optimal composition and structure of the radical are selected on the basis of “composition-property” dependences derived by semi-empirical methods as a result of a comprehensive study of the physico-chemical properties of a homologous series of ligands. Polydentate compounds, which form sparingly soluble metal complexes, are known to be of interest for the IF [6]. From this viewpoint, noteworthy are acylsulfonylhydrazines containing in their composition a hydrazide group capable of forming chelate complexes with non-ferrous metal ions [15; 34–50], and sulfonyl, which enhances acidic properties of the compounds. Previously, the physico-chemical properties of

some N-acyl-N'-(aryl-, naphthyl)sulfonylhydrazines were studied, with a fundamental possibility of using them in flotation processes shown [16, 17].

This work is devoted to the study of the physic-chemical properties and patterns of recovery of Cu(II), Co(II), Ni(II), Zn(II), Cd(II) ions in the series of N-acyl-N'-mesylhydrazines in order to determine the possibility of their application as collectors in ion flotation and to select a reagent with optimal properties.

### Experimental

N-acyl-N'-mesylhydrazines (MSH) of the general formula  $RC(O)NHNHSO_2R^1$  (1), where  $R = C_4H_9$  (I),  $C_6H_{13}$ (II),  $C_8H_{17}$ (III),  $C_4H_9CH(C_2H_5)$ (IV),  $C_{10}H_{21}$ (V),  $C_{12}H_{25}$ (VI),  $C_{14}H_{29}$ (VII);  $R^1=CH_3$ , was obtained by the interaction of equimolar amounts of hydrazides of the corresponding acids with methanesulfonylchloride at  $t = 0 \div 5$  °C in a dry pyridine medium [18; 128]. The compounds obtained are white crystalline substances. The individuality and purity of the reagents were confirmed by IR and  $^1H$  NMR spectroscopy and elemental analysis. IR spectra in the range  $400-4000\text{ cm}^{-1}$  were recorded on a Fourier spectrometer Vertex 80V (Bruker) (suspension in vaseline oil);  $^1H$  NMR spectra were recorded on a Bruker Avance Neo spectrometer (400 MHz; in  $CDCl_3$ , internal standard hexamethyldisilazane (0.055 ppm)). Elemental analysis was performed on a Vario EL cube CHNS analyzer (Elementar); thermal analysis of complex compounds — on a TGA/DSC1 thermogravimetric analyzer (Mettler Toledo).

The solubility of the reagents was determined by gravimetric (in EtOH) and spectrophotometric (in 0.1 mol/L KOH) methods. The spectrophotometric method was used to explore protolytic equilibria [19; 144–161]. UV-spectra were recorded on spectrophotometer SF-2000; pH values were measured on ionometer I-160M equipped glass and silver chloride electrodes. The surface tension at the interface between an AMH solution and the air was determined by the Dew Nui ring method [20] on a processor tensiometer K100 (KRÜSS). The measurements were performed at 25 °C in a 0.1 mol/L solution of KOH, as the reagents under study are insoluble in water, but moderately soluble in alkaline solutions. The choice of the concentration range was related to the solubility limitations of the reagents. The surface activity ( $G$ ,  $mN \cdot m^2/mol$ ) was calculated as the value of the slope tangent of the straight line tangent to the isotherm of the surface tension of reagent solutions in the range of low concentrations according to the formula:

$$G = \lim \left( -\frac{d\sigma}{dc} \right) = \frac{\Delta\sigma}{C_{\Delta\sigma}}, \quad (1)$$

where  $C$  is the concentration of the reagent solution (mol/L);  $\sigma$  is the surface tension of the solution (mN/m);  $C_{\Delta\sigma}$  is the concentration of the reagent, causing a decrease in surface tension by the value  $\Delta\sigma$ .

The values of critical micelle formation concentrations (CMC) were determined graphically at the inflection point of the curve mirroring the dependence of surface tension on solution concentrations (surface tension isotherm) when it reaches an area parallel to the abscissa axis [20; 152].

The complexation of metal ions with MSH was studied by the precipitation technique. To this end, a reagent solution was added to an aqueous solution of the metal salt, therewith adjusting the ratio of  $[M(II)]:[AMH] = 1:2$ . Ammonia solutions were used to regulate the pH values. 10–30 Minutes later, with the equilibrium time determined experimentally for each metal, the formed precipitate was filtered off. The ionic flotation experiments were carried out on a laboratory pneumatic flotation cell according to the procedure described in [21]. The residual concentration of metals in the filtrate was determined on an atomic-absorption spectrometer with flame atomization iCE 3500 (Thermo Scientific). The degree of precipitation (flotation) ( $S(E)$ , %) was calculated using the formula:

$$S(E) = \frac{(C_0 - C_i)}{C_0} \cdot 100\%, \quad (2)$$

where  $C_0$  is the initial metal concentration in the aqueous phase, mg/l;  $C_i$  is the metal concentration in the aqueous phase after precipitation (flotation), mg/l.

The conditional solubility product (SP) of the complexes was calculated by the method described in [15; 114–118], without taking into account the ionic states of the metals in solution, according to the formula:

$$SP_{[M(HL)_2]} = \left( \frac{K_{a_1} \cdot (C_{H_2L} - 2C_{M(II)}) \cdot \frac{S_i}{100}}{[H^+]} \right)^2 \cdot [M(II)]_{equil}, \quad (3)$$

where  $K_{a1}$  is the ionization constant of ligands ( $H_2L$ ) at I stage;  $M(II)$  and  $C_{H_2L}$  are the initial concentrations of  $M(II)$  and ligand, respectively, mol/L;  $S_i$  is the degree of  $M(II)$  deposition, %;  $[H^+]$  is the equilibrium concentration of  $H^+$ , mol/L;  $[M^{2+}]_{equil}$  is the equilibrium concentration of  $M(II)$  in the solution after precipitation, determined experimentally, mol/L.

The following reagents were used in the work:  $CuSO_4 \cdot 5H_2O$  (pure, 98.5 %),  $NiSO_4 \cdot 7H_2O$  (chemically pure, 99.0 %),  $ZnSO_4 \cdot 7H_2O$  (pure, 98.0 %),  $3CdSO_4 \cdot 8H_2O$  (chemically pure, 99.5 %),  $CoSO_4 \cdot 7H_2O$  (pure, 99.0 %);  $NH_3$  (aqueous), (analytical grade, 25 %),  $HCl$  (chemically pure, 35 %),  $HNO_3$  (chemically pure, 65 %),  $H_2SO_4$  (chemically pure, 93.5–95.6 %).

### Results and Discussion

The main requirements for IF collectors are as follows: sufficient solubility in aqueous solutions, availability of surface activity and foam-forming properties, ability to form insoluble compounds with metal ions, selectivity. The studied reagents were found as being moderately soluble in aqueous solutions of alkalis and EtOH; they exhibited themselves as weak dibasic acids ( $H_2L$ ) [16]. The diagrams demonstrating distribution of the protolytic equilibrium forms of the reagents as a function of the pH were constructed (Fig. 1, an example for reagent III). They make it possible to predict the ranges of pH values for the formation of compounds of reagents with metal ions. The reagents' solubility was determined as being decreasing with lengthening the hydrocarbon radical chain; at this point, acid properties weaken (Table 1).

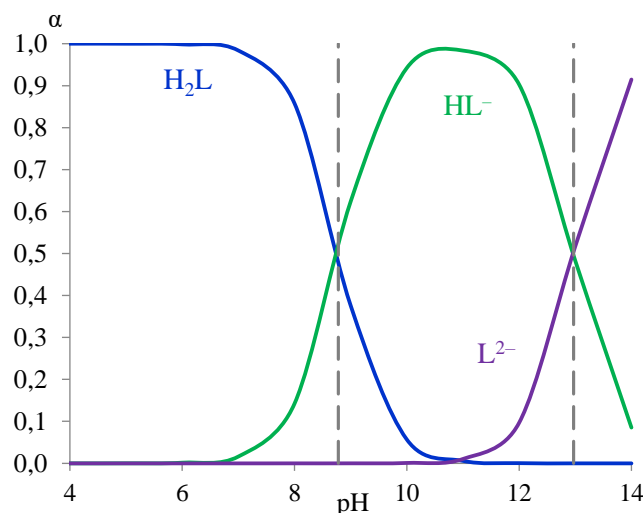


Figure 1. Distribution diagram of molecular ionic forms of reagents ( $H_2L$ ) for N-nonanoyl-N'-mesylhydrazine (III) as a function of solution pH

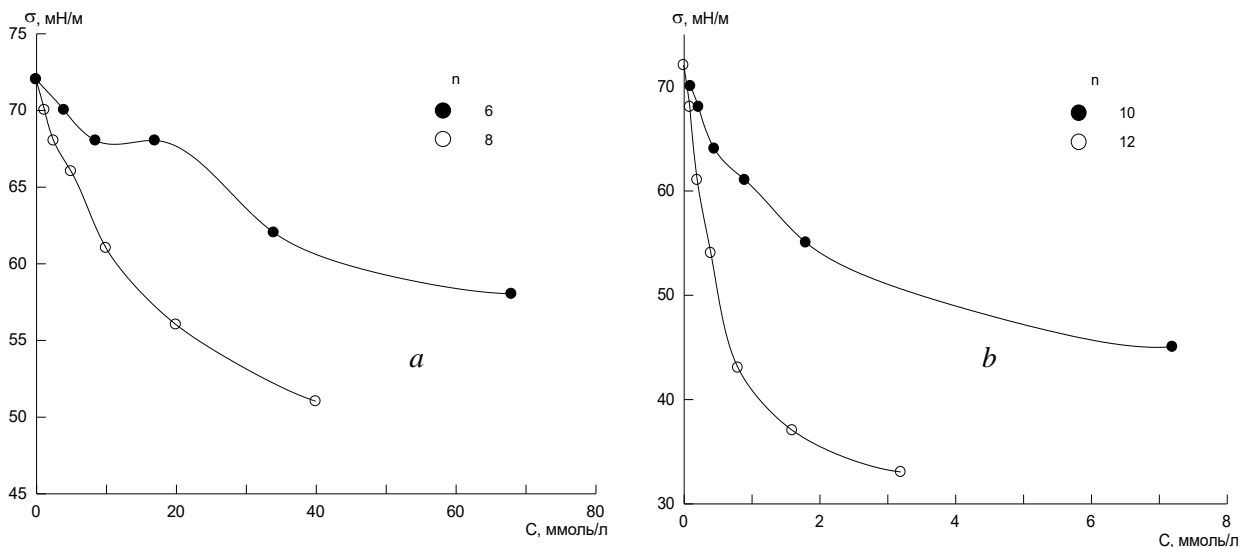
Surface-active substances are commonly used as collectors for ionic flotation. The surface tension isotherms of MSH compounds are shown in Figure 2, the results of their processing are summarized in Table 2. As follows from the data obtained, all the reagents of the series with  $R = C_6H_{13}$  exhibit surfactant properties, while those with  $R = C_{10}H_{21}$  and  $C_{12}H_{25}$  are strong surfactants decreasing surface tension at solvent-air interface in 1.5–2 times as compared to pure solvent (0.1 mol/l KOH). A decrease in CMC in the homologous series with increasing the number of carbon atoms in a radical, indicates an enhancing micelle-forming ability. The increment of the adsorption potential ( $\Delta W$ ) as a contribution to the adsorption work of the methylene unit of the alkyl chain at the phase boundary was calculated. For this, a graph of dependence “ $\ln C-N$ ” (with  $C$  is a substance concentration causing a decrease in the surface tension by a value  $\Delta\sigma$ , and  $N$  is the number of methylene groups) was plotted. The graph is constructed as a line with the slope angle tangent (where  $W$  — increment of adsorption potential). For the MSH series, the equation of linear dependence looks as follows:  $-\ln C = 0.75N - 5.87$  ( $R^2 = 0.9633$ );  $W = 1.86$  kJ/mol.

Physico-chemical properties of the compounds  $\text{RC(O)NHNHSO}_2(\text{CH}_3)$ 

R	$T_m, ^\circ\text{C}$	Solubility, mol/l (g/l)		$\text{pK}_{a1}^{**}$ $\text{pK}_{a2}$	$R_f^*$
		EtOH	0.1 mol/l KOH		
$\text{C}_5\text{H}_{11}$ (I)	81–82	$7.8 \cdot 10^{-1}$ (162,2)	$9.2 \cdot 10^{-2}$ (19.14)	$8.5 \pm 0.06$ –	–
$\text{C}_6\text{H}_{13}$ (II)	82–84	$7.3 \cdot 10^{-1}$ (161.0)	$8.0 \cdot 10^{-2}$ (17.7)	$8.68 \pm 0.05$ –	0.74
$\text{C}_8\text{H}_{17}$ (III)	89–91	$3.2 \cdot 10^{-1}$ (79.8)	$4.5 \cdot 10^{-2}$ (11.3)	$8.84 \pm 0.09$ $12.71 \pm 0.02$	0.70
$\text{C}_4\text{H}_9\text{CH}(\text{C}_2\text{H}_5)$ (IV)	91–93	1.2 (282.6)	$1.18 \cdot 10^{-2}$ (2.8)	$8.78 \pm 0.08$	0.77
$\text{C}_{10}\text{H}_{21}$ (V)	95–96	$9.4 \cdot 10^{-2}$ (26.0)	$7.5 \cdot 10^{-3}$ (2.1)	$9.19 \pm 0.04$ –	0.72
$\text{C}_{12}\text{H}_{23}$ (VI)	96–98	$1.0 \cdot 10^{-2}$ (3.1)	$3.6 \cdot 10^{-3}$ (1.1)	$9.27 \pm 0.20$ $12.91 \pm 0.12$	–
$\text{C}_{14}\text{H}_{29}$ (VII)	102–103	$2.3 \cdot 10^{-3}$ (0.74)	$2.5 \cdot 10^{-3}$ (0.84)	$9.67 \pm 0.19$ –	0.32

Note. \*Thin-layer chromatography was carried out for compounds II–V in the solvent system benzene : ethyl acetate, 1:1; for VII — benzene : ether — 3:2.

\*\*  $\text{pK}_{a1}$  and  $\text{pK}_{a2}$  are constants characterizing the process of ionization of reagents. The process of ionization of compounds at the first stage is attributed to detaching a proton of the  $\text{NHSO}_2$  fragment due to a greater acceptor action of the sulfonyl group as compared with the carbonyl group [22].



R: (a) 6 —  $\text{C}_6\text{H}_{13}$ , 8 —  $\text{C}_8\text{H}_{17}$ ; (b) 10 —  $\text{C}_{10}\text{H}_{21}$ , 12 —  $\text{C}_{12}\text{H}_{25}$

Figure 2. Surface tension isotherms of  $\text{RC(O)NHNHSO}_2\text{CH}_3$  at  $t = 25^\circ\text{C}$  in 0.1 mol/L KOH

The dependence of the degree of recovery of non-ferrous metals(II) with N-pentadecanoyl-N'-mesyl-hydrazine on  $\text{pH}_{\text{equil}}$  is shown in Figure 3. Equilibrium in the formation process of copper, nickel, and cobalt complexes is attained for 10 min, with this time for zinc and cadmium equaling 30 min. The most complete precipitation of cations was ascertained in the following pH ranges: Cu(II) — 5.5–10.0; Zn — 7.5–10.5; Co — 8.0–9.5; Ni — 8.0–10.0; Cd — 7.8–11.0. At this point, maximal degree of recovery (%) and residual metal concentration in the solution after precipitation (mg/l) equaled, respectively: Cu(II) — 99.9 (0.06); Co(II) — 97.7 (1.31); Ni(II) — 99.5 (0.37); Zn(II) — 99.8 (0.14); Cd(II) — 99.4 (0.29).



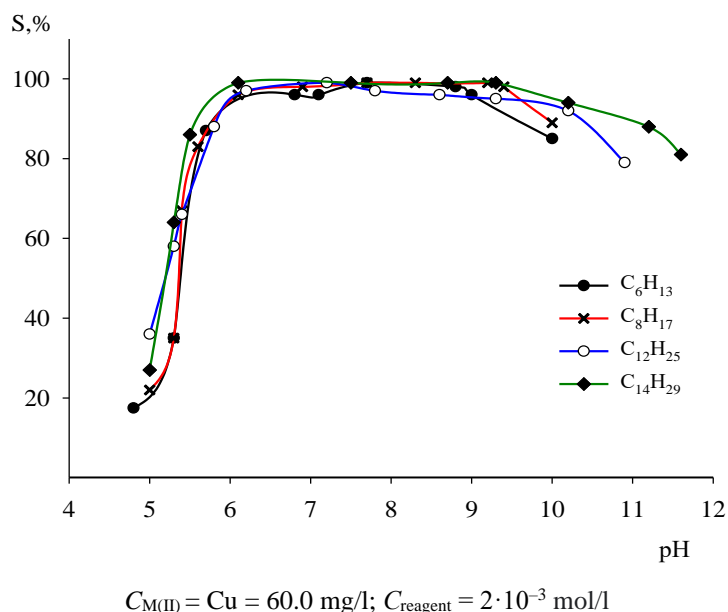


Figure 4. Dependence degree of copper (II) recovery (S, %) with N-acyl-N-mesylhydrazines by precipitation method on  $pH_{\text{equil}}$

Table 3

#### Characteristics of M(II) Complex with N-pentadecanoyl-N-mesylhydrazine

Complex*	Element composition					Stretching vibrations frequencies (v, $\text{cm}^{-1}$ )	
	Theoretical./Prakt., %					Reagent	Complex
	C	H	N	S	M		
[Cu(HL) <sub>2</sub> ] green M.M. = 729.5	<u>52.64</u> 51.74	<u>9.05</u> 8.38	<u>7.68</u> 7.28	<u>8.77</u> 8.21	<u>8.70</u> 7.78	$\text{R}-\overset{\text{H}}{\underset{\text{O}}{\parallel}}\text{C}-\text{N}-\overset{\text{H}}{\text{N}}-\overset{\text{O}}{\parallel}\text{S}-\text{CH}_3$ 3326 (NHCO), 3247 (NH <sub>2</sub> SO <sub>2</sub> ); 1687, 1675 (C=O); 1322, 1157 (SO <sub>2</sub> )	3319 (NHCO); 1543 (C=O); 1324, 1167 (SO <sub>2</sub> ); 721–741 (Cu–L)
[Ni(HL) <sub>2</sub> ]·2H <sub>2</sub> O** dark blue M.M. = 760.7	<u>50.48</u> 50.25	<u>9.20</u> 8.75	<u>7.36</u> 7.21	<u>8.41</u> 7.98	<u>7.72</u> 6.98		3305 (NHCO); 1604 (C=O); 1281, 1131 (SO <sub>2</sub> ); 3419 (H <sub>2</sub> O)
[Co(HL) <sub>2</sub> ]·2H <sub>2</sub> O dark pink M.M. = 760.9	<u>50.47</u> 51.89	<u>9.20</u> 9.73	<u>7.36</u> 7.39	<u>8.41</u> 8.05	<u>7.74</u> 7.05		3299 (NHCO); 1582 (C=O); 1281, 1123 (SO <sub>2</sub> ); 3395 (H <sub>2</sub> O)
[Cd(HL) <sub>2</sub> ] white M.M. = 778.4	<u>49.33</u> 49.37	<u>8.48</u> 9.34	<u>7.19</u> 6.92	<u>8.22</u> 7.88	<u>14.44</u> 13.65		3287 (NHCO); 1599 (C=O); 1304, 1125 (SO <sub>2</sub> ); 668 (Cd–L)
[Zn(HL) <sub>2</sub> ]·2H <sub>2</sub> O white M.M. = 767.4	<u>50.03</u> 48.97	<u>9.12</u> 8.45	<u>7.30</u> 6.78	<u>8.34</u> 7.79	<u>8.52</u> 7.89		3320(NHCO); 1608 (C=O); 1321, 1145 (SO <sub>2</sub> ); 3434 (H <sub>2</sub> O)

Note. \*HL- — ionized form of the reagent by I stage; \*\* Presence of crystallization water in Ni, Co, and Zn complexes was confirmed by thermal analysis.

The calculated SP values (Table 4) confirm the complex compounds of all the metals under study as being sparingly soluble substances; therefore, implementation of one variant of ionic flotation — “precipitate flotation” — appears to be possible [24]. The data of Table 4 evince copper and zinc complexes to have the lowest solubility, with cobalt having the highest.

I.A. Kakovsky showed that the PR values of compounds formed by the extracted ion in the homologous series of ionogenic collectors are related to the number of carbon atoms ( $N$ ) in the radical:  $-\lg\text{PP} = \alpha + \beta N$ . The calculated coefficients of the equation for the series of xanthates, dithiophosphates, etc. correlate well with the experimental data and enable the optimal  $N$  values in the series of the compounds under study to be determined [1; 55–62]. The conditional SP values of the reagent complexes with Cu(II) ions were calculated (Table 5).

Table 4

Data for calculations and  $-\lg SP$  values of N-pentadecanoyl-N'-mesylhydrazine (H<sub>2</sub>L) complexes

Complex	pH <sub>equil.</sub>	S <sub>i</sub>	[M(II)] <sub>equil.</sub> , mol/l × 10 <sup>-6</sup>	[HL <sup>-</sup> ], mol/l	-lgSP
[Cu(HL) <sub>2</sub> ]	7.0	99.9	0.90	1.03 · 10 <sup>-7</sup>	19.99
[Ni(HL) <sub>2</sub> ]	8.3	99.5	6.30	2.27 · 10 <sup>-7</sup>	17.94
[Co(HL) <sub>2</sub> ]	8.5	97.7	22.2	7.61 · 10 <sup>-6</sup>	14.89
[Cd(HL) <sub>2</sub> ]	7.8	99.4	2.58	1.56 · 10 <sup>-5</sup>	15.20
[Zn(HL) <sub>2</sub> ]	8.5	99.8	2.14	2.70 · 10 <sup>-7</sup>	18.81

Note. PS is the conditional PS of complexes; S<sub>i</sub> is the degree of M(II) precipitation, %; [M(II)]<sub>equil</sub> is the equilibrium concentration of M(II) in the solution after precipitation; [HL<sup>-</sup>] is the equilibrium concentration of HL<sup>-</sup> ions

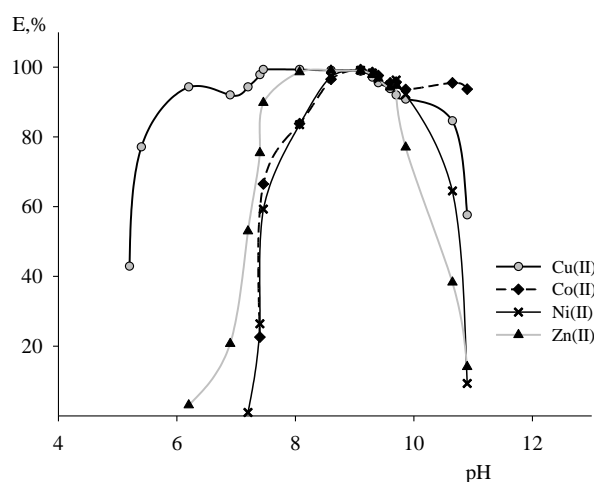
Table 5

Data for calculations,  $-\lg SP$  values of [Cu(HL)<sub>2</sub>] complexes for RC(O)NHNHSO<sub>2</sub>(CH<sub>3</sub>) ligands

Reagent	R	pH <sub>equil.</sub>	S <sub>i</sub>	[M(II)] <sub>equil.</sub> , mol/l × 10 <sup>-6</sup>	[HL <sup>-</sup> ], mol/l × 10 <sup>-6</sup>	-lgSP
<b>II</b>	C <sub>6</sub> H <sub>13</sub>	7.7	98.2	17.6	8.29	14.92
<b>III</b>	C <sub>8</sub> H <sub>17</sub>	7.7	99.2	7.12	1.57	16.75
<b>IV</b>	C <sub>4</sub> H <sub>9</sub> CH(C <sub>2</sub> H <sub>5</sub> )	6.8	99.2	7.34	0.34	18.07
<b>V</b>	C <sub>10</sub> H <sub>21</sub>	7.0	99.4	5.87	0.33	18.20
<b>VI</b>	C <sub>12</sub> H <sub>23</sub>	6.9	99.7	2.91	0.19	18.99
<b>VII</b>	C <sub>14</sub> H <sub>29</sub>	7.0	99.9	0.90	0.10	19.99

When calculating, the composition of the complexes for all the reagents was assumed to be the same and analogous to that established for N-tridecanoyl-N'-mesylhydrazine [Cu(HL)<sub>2</sub>]. It is determined that the dependence:  $-\log SP = 11.8 + 0.61N$  ( $R^2 = 0.9601$ ) is fulfilled in the series MSH with linear radicals. As follows from the equation obtained, in the series of ligands, minimal residual concentration of copper from solution during precipitation is possible when reagent VII is used. However, with lengthening the alkyl radical chain, the solubility of the reagents in aqueous and alcoholic solutions sharply decreases (Table 1), therewith hindering their practical use. The reagents III and IV appear to be the most promising ligands of the series.

The experiments on individual and collective flotation of M(II) ions with N-nonanoyl-N'-mesylhydrazine (III) were carried out (Fig. 5). Recovering metal ions up to 95-99 % in their conjoint presence (residual concentrations, mg/l: Cu — 0.21 (pH 7.0–7.5); Co — 1.4 (pH 8.5–8.8); Ni — 0.89 (pH 8.5–9.0); Zn — 1.1 (pH 8.5–8.9)), as well as separation of copper and associated metal ions at pH 5–6.5 was shown to be possible.



C<sub>M(II)</sub>, mg/l: Cu = 29.9; Co = 24.7; Ni = 24.0; Zn(II) — 21.0; [Cu(II)]:[Reagent] = 1:1; τ = 5 min

Figure 5. Dependence of the recovery degree of metals by ionic flotation on pH<sub>equil.</sub>

### Conclusions

The exploratory research of physic-chemical properties of N-acyl-N'-mesylhydrazines gave rise to ligands characterized by optimal length of hydrocarbon radical chain and suitable for ionic flotation processes: N-nonanoyl- and 2-ethylhexanoyl-N'-mesylhydrazines. The reagents, being moderately soluble in aqueous alkali solutions, are medium-strong surfactants and form hardly soluble complexes with non-ferrous metals. This trait enables using them as collectors for "precipitate flotation". The experiments aimed at exploring individual and collective flotation processes of M(II) ions with N-nonanoyl-N'-mesylhydrazine had evinced the possibility of recovering metal ions up to 95–99 %, separating copper and associated metal ions in the range of pH 5–6.5.

### Acknowledgments

The work was financially supported by the Russian Science Foundation (grant 20-69-46066) using the equipment of the Center for Collective Use "Investigations of Materials and Substances" of the Perm Federal Research Center of the Ural Branch of the RAS.

### References

- 1 Гольман А.И. Ионная флотация / А.И. Гольман. — М.: Недра, 1982. — 144 с.
- 2 Медяник Н.Л. Удаление тяжелых металлов из растворов методом ионной флотации / Н.Л. Медяник, Н.К. Тусупбаев, И.А. Варламова, Х.Я. Гиревая, Н.Л. Калугина // Вестн. Магнитогор. гос. техн. ун-та им. Г.И. Носова. — 2016. — № 1. — С. 18–26.
- 3 Абрютин Д.В. Перспективы применения процесса ионной флотации / Д.В. Абрютин, К.А. Стрельцов // Изв. вузов. Цветная металлургия. — 2013. — № 3. — С. 3–6.
- 4 Hoseinian F.S. Kinetic study of Ni(II) removal using ion flotation: Effect of chemical interactions / F.S. Hoseinian, B. Rezai, E. Kowsari, M. Safari // Minerals Engineering. — 2018. — Vol. 119. — P. 212–221.
- 5 Yenial Ü. Examination of flotation behavior of metal ions for process water remediation / Ü. Yenial, G. Bulut // Journal of Molecular Liquids. — 2017. — Vol. 241 — P. 130–135.
- 6 Радусhev А.В. Реагенты для ионной флотации цветных металлов (обзор) / А.В. Радусhev, Л.Г. Чеканова, Г.В. Чернова // Цветные металлы. — 2005. — № 7. — С. 34–39.
- 7 Stoica L. Cu(II) Recovery from Aqueous Systems by Flotation / L. Stoica, G.C. Oproiu // Separation Science and Technology. — 2005. — Vol. 39, № 4. — P. 893–909.
- 8 Peleka E.N. A perspective on flotation: a review / E.N. Peleka, G.P. Gallios, K.A. Matis // Journal of Chemical Technology & Biotechnology. — 2017. — Vol. 93, № 3. — P. 615–623.
- 9 Hoseinian F.S. Ion flotation for removal of Ni(II) and Zn(II) ions from wastewaters / F.S. Hoseinian, M. Irannajad, A.J. Nooshabadi // International Journal of Mineral Processing. — 2015. — Vol. 143. — P. 131–137.
- 10 Mohammed A.A. Flotation and Sorptive-Flotation Methods for Removal of Lead Ions from Wastewater Using SDS as Surfactant and Barley Husk as Biosorbent / A.A. Mohammed, S.E. Ebrahim, A.I. Alwared // Journal of Chemistry. — 2013. — Vol. 6. — P. 1–6.
- 11 Zakeri Khatir M. Selective separation of neodymium from synthetic wastewater by ion flotation / M. Zakeri Khatir, M. Abdollahy, M.R. Khalesi, B. Rezai // Separation Science and Technology. — 2021. — Vol. 56, № 10. — P. 1802–1810.
- 12 Taseidifar M. Ion flotation removal of a range of contaminant ions from drinking water / M. Taseidifar, M. Ziaee, R.M. Pashley, B.W. Ninham // Journal of Environmental Chemical Engineering. — 2019. — Vol. 7, № 4. — P. 103263.
- 13 Otero-Calvis A. Selectivity in the flotation of copper with xanthate over other ions present in wastewater: An experimental and computational study / A. Otero-Calvis, B. Ramirez-Serrano, A. Coello-Velazquez // Journal of Molecular Graphics and Modeling. — 2020. — Vol. 98. — P. 107587.
- 14 Медяник Н.Л. Количественная оценка активности собирателей для флотационного извлечения катионов цветных металлов из техногенных рудничных вод / Н.Л. Медяник // Горн. информ.-аналит. бюл. — 2009. — Т. 14, № 12. — С. 210–214.
- 15 Радусhev А.В. Гидразиды и 1,2-диацилгидразины. Получение, свойства, применение в процессах концентрирования металлов / А.В. Радусhev, Л.Г. Чеканова, В.Ю. Гусев. — Екатеринбург: Уральский центр академического обслуживания, 2010. — 146 с.
- 16 Чеканова Л.Г. Извлечение ионов цветных металлов из аммиачных растворов с N-ацил-N'-(п-толуолсульфонил)гидразинами / Л.Г. Чеканова, А.В. Радусhev, О.А. Воронкова, Е.В. Байгачева, Ю.В. Алехина // Химическая технология. — 2011. — № 12. — С. 754–759.
- 17 Ельчищева Ю.Б. Физико-химические и поверхностно-активные свойства N-тридеcanoил-N'-(2-нафтилсульфонил)гидразина / Ю.Б. Ельчищева, П.А. Шалагинова, П.Т. Павлов, А.С. Максимов // Журн. Вода: химия и экология. — 2019. — № 7–9. — С. 116–122.

- 18 Овербергер Ч.Дж. Органические соединения со связями азот–азот / Ч.Дж. Овербергер, Ж.–П. Ансели, Дж.Г. Ломбардино. — Л.: Химия, 1970.
- 19 Бернштейн И.Я. Спектрофотометрический анализ в органической химии / И.Я. Бернштейн, Ю.Л. Каминский. — Л.: Химия, 1986. — 116 с.
- 20 Ланге К.Р. Поверхностно-активные вещества. Синтез, свойства, анализ, применение / К.Р. Ланге; пер. с англ. — СПб.: Профессия, 2004. — 239 с.
- 21 Yuan X.Z. Evaluation of tea-derived biosurfactant on removing heavy metal ions from dilute wastewater by ion flotation / X.Z. Yuan, Y.T. Meng, G.M. Zeng, Y.Y. Fang, J.G. Shi // *Colloids and Surfaces A: Physicochem. Eng. Aspects.* — 2008. — V. 317. — P. 256–261.
- 22 Черных В.П. Реакционная способность замещенных амидов и гидразидов ароматических сульфокислот / В.П. Черных, В.И. Макурина // *Реакционная способность органических соединений.* — 1977. — Т. XIV. № I (49). — С. 106–115.
- 23 Чеканова Л.Г. Производные неопентановой кислоты как реагенты для флотационного извлечения цветных металлов / Л.Г. Чеканова, Ю.Б. Ельчищева, А.В. Харитоновна, П.Т. Павлов, С.А. Заболотных, Г.В. Чернова // *Журн. прикл. хим.* — 2021. — Т. 94. № 4. — С. 41–51.
- 24 Deliyanni E.A. Various flotation techniques for metal ions removal / E.A. Deliyanni, G.Z. Kyzas, K.A. Matis // *Journal of Molecular Liquids.* — 2017. — Vol. 225. — P. 260–264.

Л.Г. Чеканова, В.Н. Ваулина, Ю.Б. Ельчищева, Е.С. Бардина, П.Т. Павлов

### **N-ацил-N'-мезилгидразиндер қатарындағы түсті металдардың иондық флотациясына арналған реагенттерді таңдау**

Бірқатар жаңа лигандтар,  $RC(O)NHNHSO_2CH_3$  жалпы формуласының N-ацил-N'-мезилгидразиндері (МСГ) алынды және түсті металдардың (ТМ) иондық флотациясының (ИФ) реагенттері ретінде қарастырылды. Радикалды ұзындығы  $C_6H_{13}$  және одан жоғары МСГ ТМ иондарымен аз еритін комплекстер түзетіні анықталды, сондықтан иондық флотацияның нұсқаларының бірі — преципиациялық флотацияны жүзеге асыруға болады. Ерітінділерден катиондардың ең толық тұнбаға түсуі болатын рН мәндерінің диапазондары нақтыланды. ТМ кешендерінің шөгінділері айқындалды; олардың құрамы ИҚ-спектроскопия және элементтік талдау арқылы расталды. Кешендердің ПР шартты мәндері  $[M(HL)_2]$ .  $Cu(II)$  иондарын мысал ретінде қолданып, МСГ қатарында тәуелділік орындалатыны көрсетілді:  $-\log PP = 11,8 + 0,61N$ , оны қолдану лигандтардың жиынтық қасиеттерін олар түзетін қосылыстардың ерігіштігі бойынша болжауға мүмкіндік береді.  $R > C_6H_{13}$  бар қосылыстарда беттік-белсенді қасиеттердің болуы анықталды, бұл қосымша көбік түзетін агенттерді қолданбай-ақ МСГ-ді ИФ пайдалануға мүмкіндік жасайды. МСГ физика-химиялық қасиеттерін зерттеу нәтижелері бойынша оптималды радикал ұзындығы бар ИФ үшін реагенттер таңдалды:  $BuCH(Et)$ ,  $C_8H_{17}$ . N-нонаноил-N'-мезилгидразинмен ТМ(II) иондарын жеке және ұжымдық флотациялау үшін эксперименттер жүргізілді. Металл иондарын 95–99 %-ға дейін бөліп алуға, рН 5–6,5 диапазонында мыс пен онымен бірге жүретін ТМ иондарын бөлуге болатыны көрсетілген.

*Кілт сөздер:* иондық флотация, шөгінді флотациясы, ацилсульфонилгидразиндер, түсті металдар, тұндыру, физика-химиялық қасиеттері, беттік белсенді заттар.

Л.Г. Чеканова, В.Н. Ваулина, Ю.Б. Ельчищева, Е.С. Бардина, П.Т. Павлов

### **Выбор реагентов для ионной флотации цветных металлов в ряду N-ацил-N'-мезилгидразинов**

Получен и рассмотрен в качестве реагентов для ионной флотации (ИФ) цветных металлов (ЦМ) ряд новых лигандов — N-ацил-N'-мезилгидразинов (МСГ) общей формулы  $RC(O)NHNHSO_2CH_3$ . Установлено, что МСГ с длиной радикала  $C_6H_{13}$  и выше образуют труднорастворимые комплексы с ионами ЦМ, поэтому возможна реализация одного из вариантов ионной флотации — флотация осадков. Определены области значений рН, при которых происходит наиболее полное осаждение катионов из растворов. Выделены осадки комплексов ЦМ; их состав подтвержден данными ИК-спектроскопии и элементного анализа. Рассчитаны условные значения ПР комплексов  $[M(HL)_2]$ . На примере ионов  $Cu(II)$  показано, что в ряду МСГ выполняется зависимость:  $-\lg PP = 11,8 + 0,61N$ , использование которой позволяет прогнозировать собирательные свойства лигандов по растворимости образуемых ими соединений. Установлено наличие поверхностно-активных свойств у соединений с  $R > C_6H_{13}$ , что позволяет использовать МСГ в ИФ без применения дополнительных пенообразователей. На основе результатов исследования физико-химических свойств МСГ выбраны реагенты для ИФ с оптимальной длиной радикала:  $BuCH(Et)$ ,  $C_8H_{17}$ . Проведены опыты индивидуальной и коллективной флотации

ионов ЦМ(II) с N-нонаноил-N'-мезилгидразином. Показано, что возможно извлечение ионов металлов до 95–99 %, отделение меди и сопутствующих ионов ЦМ в области pH 5–6,5.

*Ключевые слова:* ионная флотация, флотация осадков, ацилсульфонилгидразины, цветные металлы, осаждение, физико-химические свойства, поверхностно-активные вещества.

## References

- 1 Golman, A.I. (1982). *Ionnaia flotatsiia [Ion flotation]*. Moscow: Nedra [in Russian].
- 2 Medyanik, N.L., Tusupbaev, N.K., Varlamova, I.A., Girevaya, H.Y., & Kalugina, N.L. (2016). Udalenie tiazhelykh metallov iz rastvorov metodom ionnoi flotatsii [Removing of heavy metals from solutions by the ion flotation method]. *Vestnik Magnitorskogo gosudarstvennogo tekhnicheskogo universiteta imeni G.I. Nosova — Bulletin of Magnitogorsk State Technical University named after G.I. Nosov*, 1, 18–26 [in Russian]. <https://doi.org/10.18503/1995-2732-2016-14-1-18-26>.
- 3 Abryutin, D.V., & Strelcov, K.A. (2013). Perspektivy primeneniia protsessa ionnoi flotatsii [Prospects for the application of the ion flotation process]. *Izvestiia vuzov. Tsvetnaia metallurgii — Russian Journal of Non-Ferrous Metals*, 3, 3–6 [in Russian]. <https://doi.org/10.17073/0021-3438-2013-3-3-6>.
- 4 Hoseinian, F.S., Rezai, B., Kowsari, E. & Safari, M. (2018). Kinetic study of Ni(II) removal using ion flotation: Effect of chemical interactions. *Minerals Engineering*, 119, 212–221. <https://doi.org/10.1016/j.mineng.2018.01.028>.
- 5 Yenial, Ü., & Bulut, G. (2017). Examination of flotation behavior of metal ions for process water remediation. *Journal of Molecular Liquids*, 241, 130–135. <https://doi.org/10.1016/j.molliq.2017.06.011>.
- 6 Radushev, A.V., Chekanova, L.G., & Chernova, G.V. (2005). Reagenty dlia ionnoi flotatsii tsvetnykh metallov [Reagents for ion flotation of non-ferrous metals]. *Tsvetnye metally — Non-Ferrous Metals*, 7, 34–39 [in Russian].
- 7 Stoica, L., & Oproiu, G.C. (2005). Cu(II) Recovery from Aqueous Systems by Flotation. *Separation Science and Technology*, 39(4), 893–909. <https://doi.org/10.1081/ss-120028452>.
- 8 Peleka, E.N., Gallios, G.P., & Matis, K.A. (2017). A perspective on flotation: a review. *Journal of Chemical Technology & Biotechnology*, 93(3), 615–623. <https://doi.org/10.1002/jctb.5486>.
- 9 Hoseinian, F.S., Irannajad, M., & Nooshabadi, A.J. (2015). Ion flotation for removal of Ni(II) and Zn(II) ions from wastewaters. *International Journal of Mineral Processing*, 143, 131–137. <https://doi.org/10.1016/j.minpro.2015.07.006>.
- 10 Mohammed, A.A., Ebrahim, S.E., & Alwared, A.I. (2013). Flotation and Sorptive-Flotation Methods for Removal of Lead Ions from Wastewater Using SDS as Surfactant and Barley Husk as Biosorbent. *Journal of Chemistry*, 6, 1–6. <https://doi.org/10.1155/2013/413948>.
- 11 Zakeri Khatir, M., Abdollahy, M., Khalesi, M.R., & Rezai, B. (2021). Selective separation of neodymium from synthetic wastewater by ion flotation. *Separation Science and Technology*, 56(10), 1802–1810. <https://doi.org/10.1080/01496395.2020.1793779>
- 12 Taseidifar, M., Ziaee, M., Pashley, R.M., & Ninham, B.W. (2019). Ion flotation removal of a range of contaminant ions from drinking water. *Journal of Environmental Chemical Engineering*, 7(4), 103263. <https://doi.org/10.1016/j.jece.2019.103263>.
- 13 Otero-Calvis, A., Ramírez-Serrano, B., & Coello-Velazquez, A. (2020). Selectivity in the flotation of copper with xanthate over other ions present in wastewater: An experimental and computational study. *Journal of Molecular Graphics and Modelling*, 98, 107587. <https://doi.org/10.1016/j.jmgm.2020.107587>.
- 14 Medyanik, N.L. (2009). Kolichestvennaia otsenka aktivnosti sobiratelei dlia flotatsionnogo izvlecheniia kationov tsvetnykh metallov iz tekhnogennykh rudnichnykh vod [Quantitative assessment of the activity of collectors for flotation of non-ferrous metal cations from technogenic mine waters]. *Gornyi informatsionno-analiticheskii biulleten — Mining information and analytical Bulletin* 14(12), 210–214 [in Russian].
- 15 Radushev, A.V., Chekanova, L.G., & Gusev, V.Yu. (2010). *Gidrazidy i 1,2-diatsilgidraziny. Poluchenie, svoistva, primenie v protsessakh kontsentrirvaniia metallov [Hydrazides and 1,2-Diacylhydrazines. Preparation, properties, application in metal concentration processes]*. Ekaterinburg: Uralskii tsentr akademicheskogo obsluzhivaniia [in Russian].
- 16 Chekanova, L.G., Radushev, A.V., Voronkova, O.A., Bajgacheva, E.V., & Alekhina, Yu.V. (2011). Izvlechenie ionov tsvetnykh metallov iz ammiachnykh rastvorov s N-acil-N'-(p-toluolsul'fonil)gidrazinami [Recovery of non-ferrous metal ions from ammonia solutions with N-acyl-N'-(p-toluenesulfonyl)hydrazines] *Khimicheskaiia tekhnologiiia — Russian Journal of Chemical Technology*, 12, 754–759 [in Russian].
- 17 Elchishcheva, Yu.B., Shalaginova, P.A., Pavlov, P.T., & Maksimov, A.S. (2019). Fiziko-khimicheskie i poverkhnostno-aktivnye svoistva N-tridekanoil-N'-(2-naftilsul'fonil)gidrazina [Physico-chemical and surface-active properties of N-tridecanoyl-N'-(2-naphthylsulfonyl)hydrazine]. *Zhurnal Voda: Khimiiia i ekologiiia — Water: Chemistry and Ecology*, 7–9, 116–122 [in Russian].
- 18 Overberger, Ch.Dzh., Anseli, Zh.–P., & Lombardino, Dzh.G. (1970). *Organicheskie soedineniia so sviaziami azot–azot [Organic compounds with nitrogen-nitrogen bonds]*. Leningrad: Khimiiia [in Russian].
- 19 Bernshtein, I.Ya., & Kaminskii, Yu.L. (1986). *Spektrofotometricheskii analiz v organicheskoi khimii [Spectrophotometric analysis in organic chemistry]*. Leningrad: Khimiiia [in Russian].
- 20 Lanhe, K.R. (2004). *Poverkhnostnoaktivnye veshchestva: sintez, svoistva, analiz, primenie [Surface-active substances: synthesis, properties, analysis, application]*. Saint Petersburg: Professiiia [in Russian].

21 Yuan, X.Z., Meng, Y.T., Zeng, G.M., Fang, Y.Y., & Shi, J.G. (2008). Evaluation of tea-derived biosurfactant on removing heavy metal ions from dilute wastewater by ion flotation. *Colloids and Surfaces A: Physicochem. Eng. Aspects*, 317, 256–261. <https://doi.org/10.1016/j.colsurfa.2007.10.024>.

22 Chernyh, V.P., & Makurina, V.I. (1977). Reaktsionnaia sposobnost zameshchennykh amidov i gidrazidov aromaticheskikh sulfokislot [Reactivity of substituted amides and hydrazides of aromatic sulfonic acids]. *Reaktsionnaia sposobnost organicheskikh soedinenii — Reactivity of organic compounds, XIV*, 1(49), 106–115 [in Russian].

23 Chekanova, L.G., Elchishcheva, Yu.B., Kharitonova, A.V., Pavlov, P.T., Zabolotnykh, S.A., & Chernova, G.V. (2021). Proizvodnye neopentanovoi kisloty kak reagenty dlia flotatsionnogo izvlecheniia tsvetnykh metallov [Derivatives of Neopentanoic Acid Hydrazide as Reagents for Flotation Recovery of Non-Ferrous Metals]. *Russian Journal of Applied Chemistry*, 94 (4), 461–471. <https://doi.org/10.1134/s1070427221040054>.

24 Deliyanni, E.A., Kyzas, G.Z., & Matis, K.A. (2017). Various flotation techniques for metal ions removal. *J. Mol. Liq.*, 225, 260–264. <https://doi.org/10.1016/j.molliq.2016.11.069>.

#### Information about authors\*

**Chekanova, Larisa Gennad'evna** (*corresponding author*) — PhD in Chemistry, Associate Professor, Head of Laboratory of Organic Complexing Reagents, Institute of Technical Chemistry, Ural Branch of Russian Academy of Sciences, Perm Branch of Perm Federal Research Center, Ural Branch of RAS; Korolev St. 3, 614013, Perm, Russia, e-mail: [larchek.07@mail.ru](mailto:larchek.07@mail.ru); <https://orcid.org/0000-0003-1792-6945>.

**Vaulina, Vera Nikolaevna** — PhD in Chemistry, Researcher of the Laboratory of Organic Complexing Reagent, Institute of Technical Chemistry, Ural Branch of Russian Academy of Sciences, Perm Branch of Perm Federal Research Center, Ural Branch of RAS; Korolev St. 3, 614013, Perm, Russia, e-mail: [tveran79@mail.ru](mailto:tveran79@mail.ru); <https://orcid.org/0000-0002-4993-3528>

**Elchischeva, Yulia Borisovna** — PhD in Chemistry, Associate Professor, Department of Analytical Chemistry and Expertise, Perm State University, 15, Bukirev st., 614990, Perm, Russia, e-mail: [anali-tik1973@mail.ru](mailto:anali-tik1973@mail.ru); <https://orcid.org/0000-0001-9182-9508>

**Bardina, Ekaterina Sergeevna** — engineer Researcher of the Laboratory of Organic Complexing Reagent, Institute of Technical Chemistry, Ural Branch of Russian Academy of Sciences, Perm Branch of Perm Federal Research Center, Ural Branch of RAS; Korolev St. 3, 614013, Perm, Russia, e-mail: [ekaterina\\_yurovskikh@mail.ru](mailto:ekaterina_yurovskikh@mail.ru); <https://orcid.org/0000-0002-6441-6887>

**Pavlov, Petr Timofeevich** — PhD in Chemistry, Associate Professor, Department of Organic Chemistry, Perm State University, 15, Bukirev st., 614990, Perm, Russia, e-mail: [pavlovpt@mail.ru](mailto:pavlovpt@mail.ru); <https://orcid.org/0000-0002-1029-8790>

---

\*The author's name is presented in the order: *Last Name, First and Middle Names*

Z.M. Muldakhmetov, A.M. Gazaliev, A.Kh. Zhakina, Ye.P. Vassilets\*, O.V. Arnt

LLP "Institute of Organic Synthesis and Coal Chemistry of the Republic of Kazakhstan", Karaganda, Kazakhstan

(\*Corresponding author's e-mail: [vassilets88@mail.ru](mailto:vassilets88@mail.ru))

## Synthesis of a Composite Based on Humic Acid Tuned to Sorbed Copper Ion

We obtained modified humic acid-based cross-linked composite pre-tuned to the sorbed copper ion. The composite synthesis had three stages. At first, we obtained prepolymerization complex using humic acids isolated from Shubarkol deposit oxidized coals and multi-walled carbon nanotubes (MWCNTs) with template (CuSO<sub>4</sub>). We used ultrasonic activation for uniform dispersion of multi-walled carbon nanotubes. Second stage comprised copolymerization in the presence of amine and cross-linker; here the prepolymerization composite complex with the template was fixed in certain nodes of polymer network. At the third stage, acid hydrolysis destroyed the bonds of the template with the composite macromolecules, the template was removed, and imprints complementary to the template in shape, size, and functionality were formed and retained "molecular memory". Such tuning forms adsorption centers in the polymer network of the composite, which can repeatedly and highly specifically interact with the template, and highly selectively extract target molecules from solution, leading to significant increase in sorbent capacity. The reaction was controlled by direct and back titration, and added amine, which was determined using Elementar Unicube elemental analyzer. The crosslinked composite can be used as a selective sorbent tuned to a specific metal ion.

**Keywords:** natural polymer, multi-walled carbon nanotubes, composite, template, tuning, sorption, functionalization, ultrasound.

### Introduction

Currently, natural polymer sorbents with molecular imprints due to their recognition ability to selectively sorb ions from mixtures have become one of the topical topics for researchers. Natural polymeric sorbents with high selectivity, which recognize target molecules or ions, attract special attention [1–3]. However, due to their inherent significant drawback, namely a slow sorption rate, such polymer sorbents have not yet received wide practical application, although their scope of application is extremely wide [4–7].

In the literature, a relatively small number of studies have been devoted to the methods of obtaining, mechanism and kinetics of ion sorption by natural polymer sorbents with molecular imprints [8–16].

It should be noted that humic acids (HA) are increasingly being used as sorbents for purification man-made environments from heavy metals. The presence of a variety of oxygen-containing functional groups in combination with aromatic, heterocyclic and other structural fragments enables humic acids for almost any kind of interactions, namely ionic, redox, donor-acceptor and sorption ones. Numerous studies have proved that HA can bind almost all types of ecotoxicants, including transition metal ions [17–21].

Previously, we [22] investigated methods for obtaining aminohumic sorbents pre-tuned to an ion using the Molecular Imprinting method. The proposed method gives opportunity to obtain products for selective binding of target metals. However, the use of the obtained products in technological processes is hampered by changes in the molecular structure of sorbents under the influence of chemical factors. In this regard, it is of interest to increase the chemical stability and mechanical strength of HA by modifying them with other reagents.

The aim of this work is the synthesis of modified polymer sorbents based on humic acids, with the introduction of multi-walled carbon nanotubes (MWCNTs) pre-tuned to copper ion and investigation of their properties.

### Experimental

Used materials were humic acids isolated from oxidized coals of the Shubarkol deposit with the following characteristics, %: humidity (W<sup>a</sup>) — 12.1±0.3, ash content (A<sup>a</sup>) — 22.0±0.2, carbon (C<sup>g</sup>) — 36.30±0.2, hydrogen (H<sup>g</sup>) — 3.73±0.1, nitrogen (N<sup>g</sup>) — 0.70±0.1, sulfur (S<sup>g</sup>) — 1.02±0.1, oxygen (O<sup>g</sup>) — 58.30±0.5, (Σ(COOH+OH)) — 5.0 mg·eq·g<sup>-1</sup>; multi-walled carbon nanotubes (MWCNTs, "Taunit" series); hexameth-

ylenetetramine was used as an amine; formaldehyde was used as a crosslinking agent;  $\text{CuSO}_4$  was used as a template.

The object of the study was a cross-linked composite based on humic acid with incorporated MWCNTs and amine tuned to the copper ions sorption.

Synthesis of composite (HA: MWCNTs: M: Amine) was carried out in three stages in an aqueous-alkaline medium at a ratio of HA: MWCNTs: Amine = 2:0.1:1, pH=8 according to the method developed by us earlier [22]. The content of copper ions introduced during tuning was 4 mg-eq per gram of composite.

Ultrasonic dispersion of MWCNTs was carried out on an IL-100-6/2 ultrasonic disperser with a vertical cylindrical waveguide, with a radiation frequency of 22 kHz.

The stability investigation of the "tuned" sorbents to acid hydrolysis was carried out as follows: the metal-containing composite was filled with 1 N HCl solution, heated to 50 °C and kept for 30 minutes. Then the mixture of "tuned" sorbents was filtered, repeatedly washed with distilled water to a neutral medium and the absence of Cl<sup>-</sup> ions in the washing waters, and dried to a constant mass.

The structure of the obtained composites was also confirmed by IR spectroscopy data taken on the device IR Fourier spectrometer FSM-1201 in KBr tablets. The range of wave numbers was 4000–400 cm<sup>-1</sup>, the error in determining the wave numbers did not exceed 2 cm<sup>-1</sup>. Mathematical processing was carried out using the program for curve fitting and data analysis Fityk 1.3.1.

Experiments on static adsorption of copper ions were carried out to study the sorption capacity of cross-linked composites after "tuning". The binding capacity of the "tuned" cross-linked composites was estimated by the value of the static exchange capacity (SEC, mg-eq·g<sup>-1</sup>). For comparative analysis, cross-linked composites were prepared simultaneously under identical conditions, but without "tuning".

The content of oxygen-containing groups in the composite was determined by direct and reverse conductometric titration using laboratory conductometer Anion 4100 (Russia). The measurements were carried out sequentially on three samples of the composite; the average value of three experiments was taken as the final value. The measurement error was ±0.2 %.

Elemental analysis for the content of carbon, hydrogen, nitrogen, sulfur and oxygen was carried out on the Elementar Unicube elemental analyzer.

The stability of the composites was studied by differential thermal analysis (DTA) using a Perkin Elmer STA 6000 synchronous thermogravimetric differential analyzer in the measurement range: T<sub>m</sub> up to 800 °C in nitrogen atmosphere, v=10°/min.

### *Results and Discussion*

At the first stage, a pre-polymerization complex based on humic acid was obtained, with the introduction of a nanofiller (MWCNTs) and a molecular template (M). At the same time, a stable pre-polymerization complex (HA:MWCNTs:M) between humic acid, MWCNTs and template molecules was formed. Due to the formation of such a pre-polymerization complex, polymer molecules are arranged and fixed in a certain way around the template molecule.

The difference between MWCNTs and other nanofillers is their smooth surface, which leads to the stretching of the macromolecules of the matrix polymer on this surface and the formation of a densely packed polymer matrix-MWCNTs interfacial layer. However, it should be noted that carbon nanomolecules are packed in tight bundles and tend to form conglomerates that prevent their uniform distribution in the matrix and thus do not allow achieving the desired efficiency when modifying the polymer.

An effective way to overcome this problem is ultrasonic treatment (UST). Ultrasound is the most accessible and powerful factor influencing the properties, structure, velocity and direction of reactions. Under the influence of ultrasound, the processes of oxidation and reduction are enhanced, heterogeneous reactions on the surface of MWCNTs are significantly accelerated, which is due to an increase in their porosity and surface activity.

The introduction of the filler into the HA was carried out using ultrasound. In the course of the study, the influence of the duration of UST and temperature on the process of functionalization of MWCNTs was studied. The results of the study are shown in Table 1.

Table 1

**Functionalization of MWCNTs under the influence of ultrasound**

Sample	Time period for ultrasonic treatment, min	Temperature, °C	Yield, %	$\Sigma(\text{COOH})$ , mg-eq·g <sup>-1</sup>
MWCNTs (original)	–	–	–	1.4
MWCNTs	15	25	84	1.8
		50	68	1.6
		70	84	1.8
	30	25	88	1.4
		50	72	1.6
		70	80	1.2
	60	25	80	1.6
		50	72	1.8
		70	80	1.2
	120	25	84	1.6
		50	76	1.8
		70	80	1.0

The data in Table 1 show that minimal exposure to UST and room temperature is sufficient to increase the number of reaction centers of MWCNTs. Prolonged exposure to UST leads to a decrease in the amount of oxygen-containing groups. For further research, we used MWCNTs, ultrasound-activated at a temperature of 25 °C for 15 minutes.

At the second stage, the synthesis of a crosslinked composite preconfigured for sorption by a local arrangement of macromolecule sites was carried out by copolymerization of the pre-polymerization complex (HA:MWCNTs:M) with an amine and a crosslinking agent.

The essence of two stages consists in the interaction of the modified polymer and the sorbed ion under conditions when the links of macromolecules still have sufficient mobility, with subsequent fixation of the resulting conformations optimal for sorption, which in turn should lead to a significant improvement in the sorption characteristics of the composite.

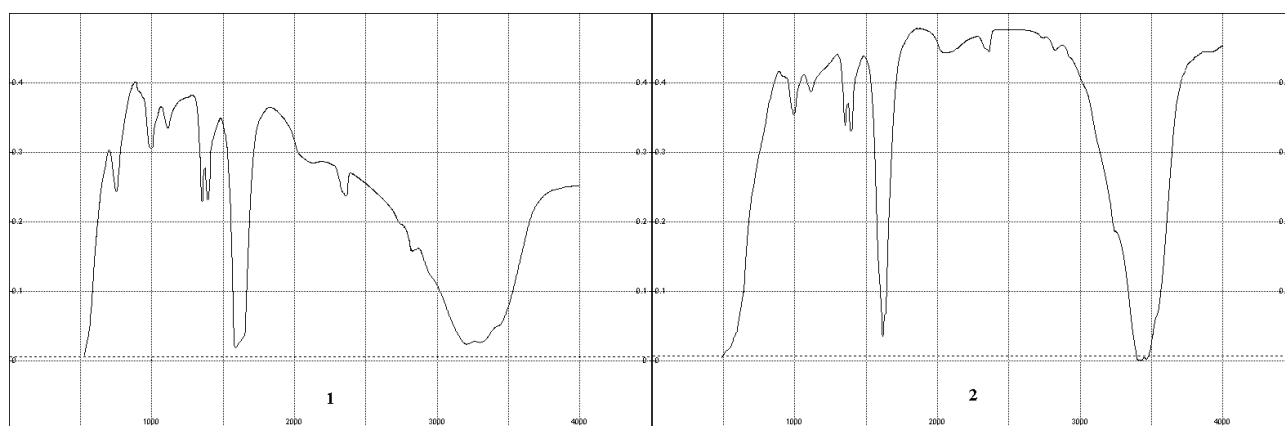
At the third stage, a molecular template was removed from the polymer mesh. The stability of the “tuned” sorbents to acid hydrolysis was studied by treating the composite with a hydrochloric acid solution with further filtration, repeated washing and drying. The reaction in the composite was controlled by the attached amine, which was determined using the Elementar Unicube elemental analyzer, as well as by direct and reverse conductometric titration. The composition of the obtained composites was confirmed by the data of X-ray phase analysis. The results of the study are presented in Table 2.

Table 2

**Characteristics of synthesized composites**

Composite	C <sup>g</sup> , %	H <sup>g</sup> , %	N <sup>g</sup> , %	S <sup>g</sup> , %	O <sup>g</sup> , %	Yield, %	$\Sigma(\text{COOH}+\text{OH})$ mg-eq·g <sup>-1</sup>
before hydrolysis							
HA	36.30±0.2	3.73±0.1	0.70±0.1	1.02±0.1	58.30±0.5	75.01	5.0
HA:MWCNTs:M:A	44.50±0.2	3.90±0.1	1.08±0.1	0.91±0.1	49.61±0.5	79.40	4.5
after hydrolysis							
HA:MWCNTs:A	44.61±0.2	3.99±0.1	1.13±0.1	0.97±0.1	49.30±0.5	75.40	5.8

The increase in the sum of oxygen-containing groups in the samples subjected to acid hydrolysis (Table 2) confirmed our assumption about the possible breaking of the coordination bonds of copper ions with the functional groups of the composite. This assumption was also confirmed by the data of IR spectroscopy (Fig. 1).



1 — HA:MWCNTs:M:A (before hydrolysis); 2 — HA:MWCNTs:A (after hydrolysis)

Figure 1. IR spectra of synthesized composites

In Figure 1, we can observe the appearance of a peak at  $741\text{ cm}^{-1}$  for the HA:MWCNTs:M:A composite (before hydrolysis), which refers to the stretching vibrations of the Cu–O bond. The absence of similar absorption bands in the composite after hydrolysis indicates a change in the structure of chemical bonds and the removal of copper from the crosslinked composite during hydrolysis. The appearance of a pronounced band at  $3400\text{ cm}^{-1}$  in the HA:MWCNTs:A composite (after hydrolysis), which can be attributed to vibrations of OH-groups bound by intermolecular hydrogen bonds, also indicates the destruction of oxygen bonds with copper and the formation of hydroxyl groups in their place.

The interaction strength of the obtained composites was studied by differential thermal analysis (DTA). The thermogravimetric curve of the composites before and after hydrolysis showed a low-temperature weight loss. The main weight loss began in the temperature range of  $448\text{--}564\text{ }^{\circ}\text{C}$ . Thus, the main mass loss for the composite before hydrolysis (15 wt.%) began in the temperature range of  $456\text{--}564\text{ }^{\circ}\text{C}$ , and after hydrolysis (19.10 wt.%) at  $448\text{--}556\text{ }^{\circ}\text{C}$ . The total weight loss of the samples was estimated at about 32 wt.%.

The sorption properties of cross-linked composites obtained with and without “tuning” to the copper ion were studied. A study of the sorption properties of a composite pre-tuned to copper ions showed that after acid hydrolysis its capacity sharply increased compared to a similar composite cross-linked without “tuning”. The effect of improving the sorption properties for  $\text{Cu}^{2+}$  for the HA: MWCNTs: A composite was equal to  $4.1\text{ mg-eq g}^{-1}$ , and for the composite cross-linked without “tuning” it was equal to  $2.2\text{ mg-eq g}^{-1}$ . This once again confirmed the assumption about the efficiency of the cross-linked composite selectively tuned to the adsorbed ion.

### Conclusions

Thus, the synthesis of a cross-linked composite based on humic acid with the introduction of MWCNTs and a molecular template was carried out using the Molecular Imprinting method under ultrasonic dispersion conditions, followed by copolycondensation with amine and formaldehyde tuned to the sorbed copper ion. One of the important properties of MWCNTs, which determines the possibility of their use in new technologies, is associated with their high sorption characteristics and chemical stability. Since MWCNTs are a surface structure, their entire mass is enclosed in the layers surface; therefore, they have an anomalously high specific surface area, which, in turn, determines the features of their sorption characteristics and high strength. The introduction of nitrogen atoms into the composition of humic acids, which are more prone to the formation of donor-acceptor bonds with metal ions compared to oxygen atoms, will increase both the complexing properties of HA and at the same time impart polyampholyte properties to HA. Ultrasound contributes to the increase and regulation of their porous structure, changing the chemical nature of the surface. The structure of the resulting composites was proven by modern physicochemical methods. The reaction was monitored by the added amine, using an elemental analyzer, and by the content of oxygen-containing groups determined by conductometric titration. With the introduction of a tuned cross-linked composite of MWCNTs and amine, the content of carbon increased by 8.20 % and nitrogen by 0.38 %, and the sum of oxygen-containing groups was equal to  $4.5\text{ mg-eq g}^{-1}$ . The study of the sorption properties of the preliminarily “tuned” crosslinked composite to copper ions suggested the formation of cavities (imprints) in the “tuned” crosslinked composite, which were capable of interacting with target template molecules and increasing the

capacity of the sorbent by a factor of two compared to the same composite stitched without tuning. The static exchange capacity for the “tuned” composite was  $4.1 \text{ mg-eq g}^{-1}$ , which made it possible to double the capacity of the sorbent compared to the same composite cross-linked without “tuning”.

### Acknowledgments

This research is funded by the Science Committee of the Ministry of Education and Science of the Republic of Kazakhstan (Grant No. BR10965230 “Development of “green” technologies for obtaining multi-functional materials based on deep processing of organomineral raw materials of Kazakhstan”).

### References

- 1 Popov S.A. Synthesis and study of a sorbent based on silica gel modified with hyperbranched poly(dichloromethylsilylpropyl)carbosilane with molecular imprints of 2,4-dichlorophenoxyacetic acid / S.A. Popov, V.V. Irkha, S.G. Dmitrienko, Yu.A. Zolotov, E.V. Getmanova, A.M. Muzafarov // *Moscow University Chemistry Bulletin*. — 2008. — Vol. 63. — P. 36–42. <https://doi.org/10.1007/s11967-008-1008-y>
- 2 Gentsheva G. Analytical characterization of a silica gel sorbent with thioetheric sites / G. Gentsheva, P. Tzvetkova, P. Vassileva, L. Lakov, O. Peshev, E. Ivanova // *Microchimica Acta*. — 2006. — Vol. 156. — P. 303–306. <https://doi.org/10.1007/s00604-006-0644-4>
- 3 Khimchenko S.V. New effective sorbents for purification of aqueous media from technogenic contaminants / S.V. Khimchenko, T.A. Blank, K.N. Belikov, K.Yu. Bryleva, I.B.-Kh. Shcherbakov, V.A. Chebanov, et.al. // *Functional Materials*. — 2017. — Vol. 24, Iss. 4. — P. 706–714. <https://doi.org/10.15407/fm24.04.706>
- 4 Zougagh M. Chelating sorbents based on silica gel and their application in atomic spectrometry / M. Zougagh, J.M. Cano Pavón, A. Garcia de Torres // *Analytical and Bioanalytical Chemistry*. — 2005. — Vol. 381. — P. 1103–1113. <https://doi.org/10.1007/s00216-004-3022-2>
- 5 Olalekan A.P. Review: Silica Aerogel as a Viable Absorbent for Oil Spill Remediation / A.P. Olalekan, A.O. Dada, O.A. Adesina // *Journal of Encapsulation and Adsorption Sciences*. — 2014. — Vol. 4, No. 4. — P. 122–131. <https://doi.org/10.4236/jeas.2014.44013>
- 6 Bondareva L. Direct and Indirect Detoxification Effects of Humic Substances / L. Bondareva, N. Kudryasheva // *Agronomy*. — 2021. — Vol. 11 (2). — P. 198. <https://doi.org/10.3390/agronomy11020198>
- 7 Interiano López M.L. Removal of hydrocarbons from drill cuttings using humic acids in washing processes / M.L. Interiano López, V.A. Ramírez Coutiño, E. Zamudio Pérez, L.A. Godínez, F.J. Rodríguez-Valadez // *Rev. Int. Contam. Ambie*. — 2019. — Vol. 35(3) — P. 705–712. <https://doi.org/10.20937/RICA.2019.35.03.15>
- 8 Vetrova O.V. Application of Humic Sorbents for  $\text{Pb}^{2+}$ ,  $\text{Cu}^{2+}$  and  $\text{Hg}^{2+}$  Ions Preconcentration from Aqueous Solutions / O.V. Vetrova, K.B. Konovalov, M.A. Gavrilenko // *Procedia Chemistry*. — 2014. — Vol. 10. — P. 120–126. <https://doi.org/10.1016/j.proche.2014.10.022>
- 9 Erny G.L. Immobilized humic substances and immobilized aggregates of humic substances as sorbent for solid phase extraction / G.L. Erny, B.M. Gonçalves, V.I. Esteves // *Journal of Chromatography A*. — 2013. — Vol. 1306. — P. 104–108. <https://doi.org/10.1016/j.chroma.2013.07.057>
- 10 Ćwieląg-Piasecka I. Humic acid and biochar as specific sorbents of pesticides / I. Ćwieląg-Piasecka, A. Medyńska-Juraszek, M. Jerzykiewicz, M. Dębicka, J. Bekier, E. Jamroz, et.al. // *Journal of Soils and Sediments*. — 2018. — Vol. 18. — P. 2692–2702. <https://doi.org/10.1007/s11368-018-1976-5>
- 11 Fresco-Cala B. Molecularly Imprinted Polymer Micro- and Nano-Particles: A Review / B. Fresco-Cala, A.D. Batista, S. Cárdenas // *Molecules*. — 2020. — Vol. 25, Iss. 20. — P. 4740. <https://doi.org/10.3390/molecules25204740>
- 12 Zarejousheghani M. Molecularly Imprinted Polymer Materials as Selective Recognition Sorbents for Explosives: A Review / M. Zarejousheghani, W. Lorenz, P. Vanninen, T. Alizadeh, M. Cämmerer, H. Borsdorf // *Polymers*. — 2019. — Vol. 11, Iss. 5. — P. 888. <https://doi.org/10.3390/polym11050888>
- 13 Zarejousheghani M. Molecularly Imprinted Polymer-Based Sensors for Priority Pollutants / M. Zarejousheghani, P. Rahimi, H. Borsdorf, S. Zimmermann, Y. Joseph // *Sensors*. — 2021. — Vol. 21, Iss. 7. — P. 2406. <https://doi.org/10.3390/s21072406>
- 14 Beyazit S. Molecularly imprinted polymer nanomaterials and nanocomposites by controlled/living radical polymerization / S. Beyazit, B.T.S. Bui, K. Haupt, C. Gonzato // *Progress in Polymer Science*. — 2016. — Vol. 62. — P. 1–21. <https://doi.org/10.1016/j.progpolymsci.2016.04.001>
- 15 Pichon V. Sample Preparation Using Molecularly Imprinted Polymers / V. Pichon, N. Delaunay, A. Combeš. // *Analytical chemistry*. — 2020. — Vol. 92, Iss. 1. — P. 16–33. <https://doi.org/10.1021/acs.analchem.9b04816>
- 16 Haupt K. Molecularly Imprinted Polymers: Antibody Mimics for Bioimaging and Therapy / K. Haupt, P.X. Medina Rangel, B.T.S. Bui // *Chemical Reviews*. — 2020. — Vol. 120, Iss. 17. — P. 9554–9582. <https://doi.org/10.1021/acs.chemrev.0c00428>
- 17 Klučáková M. Lignitic Humic Acids as Environmentally-Friendly Adsorbent for Heavy Metals / M. Klučáková, M. Pavlíková // *Journal of Chemistry*. — 2017. — Vol. 2017. — Article ID 7169019 — 5 p. <https://doi.org/10.1155/2017/7169019>
- 18 Shaker M.A. Dynamics and thermodynamics of toxic metals adsorption onto soil-extracted humic acid / M.A. Shaker, H.M. Albishri // *Chemosphere*. — 2014. — Vol. 111. — P. 587–595. <https://doi.org/10.1016/j.chemosphere.2014.04.088>

19 Town R.M. Intraparticulate speciation analysis of soft nanoparticulate metal complexes. The impact of electric condensation on the binding of  $\text{Cd}^{2+}/\text{Pb}^{2+}/\text{Cu}^{2+}$  by humic acids / R.M. Town, H.P. van Leeuwen // Physical Chemistry Chemical Physics. — 2016. — Vol. 18. — P. 10049–10058. <https://doi.org/10.1039/C6CP01229A>

20 Kloster N. Aggregation kinetics of humic acids in the presence of calcium ions / N. Kloster, M. Brigante, G. Zanini, M. Avena // Colloids and Surfaces A: Physicochemical and Engineering Aspects. — 2013. — Vol. 427. — P. 76–82. <https://doi.org/10.1016/j.colsurfa.2013.03.030>

21 Zhakina A.Kh. Synthesis of a composite material based on coal mining waste using wave chemistry methods / A.Kh. Zhakina, Ye.P. Vassilets, O.V. Arnt, A.N. Akzholtay, A.M. Gazaliyev, Z.M. Muldakhmetov, S.O. Kenzhetayeva // Bulletin of Karaganda University. Chemistry series. — 2019. — № 3 (95). — P. 14–20. <https://doi.org/10.31489/2019Ch3/14-20>

22 Жакина А.Х. Темплатный амино-гуминовый сорбент на основе отходов угледобычи [Электронный ресурс] / А.Х. Жакина, Е.П. Василец, О.В. Арнт, Е.В. Кудрявцева, А. Альжанкызы // Universum: химия и биология: электрон. науч. журн. — 2021. — № 11 (89). — Режим доступа: <https://universum.com/ru/nature/archive/item/12512>. <https://doi.org/10.32743/UniChem.2021.89.11.12512>

З.М. Молдахметов, А.М. Ғазалиев, А.Х. Жакина, Е.П. Василец, О.В. Арнт

### **Сорбцияланған мыс ионына бапталған, гумин қышқылы негізіндегі композиттің синтезделуі**

Модификацияланған гумин қышқылының негізінде алдын ала сорбцияланатын мыс ионына реттелген тігілген композит алынды. Композит синтезі үш кезеңде жүзеге асырылды. Бірінші кезеңде, Шұбаркөл кен орнының тотыққан көмірінен бөлінген гумин қышқылдары мен шаблону ( $\text{CuSO}_4$ ) бар көпқабырғалы көміртекті нанотүтікшелер (ККНТ) арасындағы өзара әрекеттесуі арқылы полимеризация алдындағы кешені алынды. ККНТ біркелкі диспергирлеу үшін ультрадыбыстық белсендіру жүргізілді. Екінші кезеңде, амин және тігу агентінің қатысуымен сополимеризация жүзеге асырылды, онда шаблону бар композиттің полимеризацияға дейінгі кешені полимер торының белгілі бір позицияларына бекітілді. Үшінші кезеңде, қышқылдық гидролиз процесінде шаблонның композиттік макромолекулаларымен байланыстары бұзылады, шаблон жойылып, пішіні, өлшемі және функционалдығы бойынша шаблонға қосымша болып табылатын іздер түзіледі және олардың «молекулалық жадысын» сақтайды. Осындай баптау нәтижесінде композиттің полимерлік торында шаблонмен қайталанатын жоғары спецификалық өзара әрекеттесуге және ерітіндіден мақсатты молекулаларды жоғары селективті алынуына қабілетті адсорбциялық орталықтар түзіледі, бұл сорбенттің сыйымдылығының айтарлықтай артуына әкеледі. Реакция тікелей және кері титрлеу арқылы, сондай-ақ қосылған амин бойынша бақыланды, ол Elementar Unicube анализаторының көмегімен анықталды. Рентгендік фазалық талдаудың көмегімен алынған композиттердің құрамы дәлелденді. Тігілген композитті белгілі бір мыс ионына реттелген селективті сорбент ретінде пайдалануға болады.

*Кілт сөздер:* табиғи полимер, ККНТ, композит, шаблон, реттелген, сорбция, функционализация, ультрадыбыс.

З.М. Мулдахметов, А.М. Газалиев, А.Х. Жакина, Е.П. Василец, О.В. Арнт

### **Синтез композита на основе природного полимера, настроенного на сорбируемый ион меди**

На основе модифицированной гуминовой кислоты получен сшитый композит, предварительно настроенный на сорбируемый ион меди. Синтез композита осуществлен в три этапа. На первом этапе получен предполимеризационный комплекс взаимодействием между гуминовыми кислотами, выделенными из окисленных углей Шубаркольского месторождения, и многостенными углеродными нанотрубками с шаблоном ( $\text{CuSO}_4$ ). Для равномерного диспергирования многостенных углеродных нанотрубок проведена ультразвуковая активация. На втором этапе в присутствии амина и сшивающего агента осуществлена сополимеризация, при которой предполимеризационный комплекс композита с шаблоном фиксируется в определенных позициях полимерной сетки. На третьем этапе в процессе кислотного гидролиза происходит разрушение связей шаблона с макромолекулами композита, удаление шаблона и образование отпечатков, комплементарных шаблонным по форме, размеру и функциональности и сохраняющие «молекулярную память» о них. В результате такой настройки в полимерной сетке композита формируются адсорбционные центры, способные к повторному высокоспецифичному взаимодействию с шаблоном и к высокоселективному извлечению молекул-мишеней из раствора, что приводит к значительному увеличению емкости сорбента. Контроль реакции осуществляли методом прямого и обратного титрования, а также по присоединенному амину, который определяли с

использованием элементного анализатора Elementar Unicube. С помощью рентгенофазового анализа доказан состав полученных композитов. Шитый композит может найти применение в качестве селективного сорбента, настроенного на определенный ион металла.

*Ключевые слова:* природный полимер, МУНТ, композит, шаблон, настройка, сорбция, функционализация, ультразвук.

## References

- 1 Popov, S.A., Irkha, V.V., Dmitrienko, S.G., Zolotov, Yu.A., Getmanova, E.V., & Muzafarov, A.M. (2008). Synthesis and study of a sorbent based on silica gel modified with hyperbranched poly(dichloromethylsilylpropyl)carbosilane with molecular imprints of 2,4-dichlorophenoxyacetic acid. *Moscow Univ. Chem. Bull.*, 63, 36–42. <https://doi.org/10.1007/s11967-008-1008-y>.
- 2 Gentsheva, G., Tzvetkova, P., Vassileva, P., Lakov, L., Peshev, O., & Ivanova, E. (2006). Analytical characterization of a silica gel sorbent with thioetheric sites. *Microchimica Acta*, 156, 303–306. <https://doi.org/10.1007/s00604-006-0644-4>.
- 3 Khimchenko, S.V., Blank, T.A., Belikov, K.N., Bryleva, K.Yu., Shcherbakov, I.B.-Kh., Chebanov, V.A., Muravyova, E.A., Saraev, V.E., Zviagin, I.M., Komykhov, S.A., Ostras, K.S., & Chernenko, V.N. (2017). New effective sorbents for purification of aqueous media from technogenic contaminants. *Functional Materials*, 24(4), 706–714. <https://doi.org/10.15407/fm24.04.706>
- 4 Zougagh, M., Cano Pavón, J.M., & Garcia de Torres, A. (2005). Chelating sorbents based on silica gel and their application in atomic spectrometry. *Anal. Bioanal. Chem.*, 381, 1103–1113. <https://doi.org/10.1007/s00216-004-3022-2>
- 5 Olalekan, A.P., Dada, A.O., & Adesina, O.A. (2014). Review: Silica Aerogel as a Viable Absorbent for Oil Spill Remediation. *Journal of Encapsulation and Adsorption Sciences*, 4(4), 122–131. <https://doi.org/10.4236/jeas.2014.44013>
- 6 Bondareva, L., & Kudryasheva, N. (2021). Direct and Indirect Detoxification Effects of Humic Substances. *Agronomy*, 11(2), 198. <https://doi.org/10.3390/agronomy11020198>
- 7 Interiano López, M.L., Ramírez Coutiño, V.A., Zamudio Pérez, E., Godínez, L.A., & Rodríguez-Valadez, F.J. (2019). Removal of hydrocarbons from drill cuttings using humic acids in washing processes. *Rev. Int. Contam. Ambie.*, 35(3), 705–712. <https://doi.org/10.20937/RICA.2019.35.03.15>
- 8 Vetrova, O.V., Konovalov, K.B., & Gavrilenko, M.A. (2014). Application of Humic Sorbents for Pb<sup>2+</sup>, Cu<sup>2+</sup> and Hg<sup>2+</sup> Ions Preconcentration from Aqueous Solutions. *Procedia Chemistry*, 10, 120–126. <https://doi.org/10.1016/j.proche.2014.10.022>
- 9 Erny, G.L., Gonçalves, B.M., & Esteves, V.I. (2013). Immobilized humic substances and immobilized aggregates of humic substances as sorbent for solid phase extraction. *Journal of Chromatography A*, 1306, 104–108. <https://doi.org/10.1016/j.chroma.2013.07.057>.
- 10 Ćwieląg-Piasecka, I., Medyńska-Juraszek, A., Jerzykiewicz, M., Dębicka, M., Bekier, J., Jamroz, E., & Kawałko, D. (2018). Humic acid and biochar as specific sorbents of pesticides. *J. Soils Sediments*, 18, 2692–2702. <https://doi.org/10.1007/s11368-018-1976-5>
- 11 Fresco-Cala, B., Batista, A.D., & Cárdenas, S. (2020). Molecularly Imprinted Polymer Micro- and Nano-Particles: A Review. *Molecules*, 25(20), 4740. <https://doi.org/10.3390/molecules25204740>.
- 12 Zarejousheghani, M., Lorenz, W., Vanninen, P., Alizadeh T., Cämmerer M., & Borsdorf H. (2019). Molecularly Imprinted Polymer Materials as Selective Recognition Sorbents for Explosives: A Review. *Polymers*, 11(5), 888. <https://doi.org/10.3390/polym11050888>
- 13 Zarejousheghani M., Rahimi P., Borsdorf H., Zimmermann S., & Joseph Y. (2021). Molecularly Imprinted Polymer-Based Sensors for Priority Pollutants. *Sensors*, 21(7), 2406. <https://doi.org/10.3390/s21072406>
- 14 Beyazit, S., Bui, B.T.S., Haupt, K., & Gonzato, C. (2016). Molecularly imprinted polymer nanomaterials and nanocomposites by controlled/living radical polymerization. *Progress in Polymer Science*, 62, 1–21. <https://doi.org/10.1016/j.progpolymsci.2016.04.001>.
- 15 Pichon, V., Delaunay, N., & Combeš, A. (2020). Sample Preparation Using Molecularly Imprinted Polymers. *Analytical chemistry*, 92(1), 16–33. <https://doi.org/10.1021/acs.analchem.9b04816>
- 16 Haupt, K., Medina Rangel, P.X., Bui, B.T.S. (2020). Molecularly Imprinted Polymers: Antibody Mimics for Bioimaging and Therapy. *Chemical Reviews*, 120(17), 9554–9582. <https://doi.org/10.1021/acs.chemrev.0c00428>
- 17 Klučáková, M., & Pavlíková, M. (2017). Lignitic Humic Acids as Environmentally-Friendly Adsorbent for Heavy Metals. *J. of Chem.*, 2017, 5 p. <https://doi.org/10.1155/2017/7169019>
- 18 Shaker, M.A., & Albishri, H.M. (2014). Dynamics and thermodynamics of toxic metals adsorption onto soil-extracted humic acid. *Chemosphere*, 111, 587–595. <https://doi.org/10.1016/j.chemosphere.2014.04.088>
- 19 Town, R.M., & van Leeuwen, H.P. (2016). Intraparticulate speciation analysis of soft nanoparticulate metal complexes. The impact of electric condensation on the binding of Cd<sup>2+</sup>/Pb<sup>2+</sup>/Cu<sup>2+</sup> by humic acids. *Phys. Chem. Chem. Phys.*, 18, 10049–10058. <https://doi.org/10.1039/C6CP01229A>
- 20 Kloster, N., Brigante, M., Zanini, G., & Avena, M. (2013). Aggregation kinetics of humic acids in the presence of calcium ions. *Colloids and Surfaces A: Physicochemical and Engineering Aspects*, 427, 76–82. <https://doi.org/10.1016/j.colsurfa.2013.03.030>
- 21 Zhakina, A.Kh., Vassilets, Ye.P., Arnt, O.V., Akzholtay, A.N., Gazaliyev, A.M., Muldakhmetov, Z.M., & Kenzhetayeva S.O. (2019). Synthesis of a composite material based on coal mining waste using wave chemistry methods. *Bulletin of Karaganda University. Chemistry series*, 3(95), 14–20. <https://doi.org/10.31489/2019Ch3/14-20>

22 Zhakina, A.Kh., Vassilets, Ye.P., Arnt, O.V., Kudryavtseva, Ye.V., & Alzhankyzy, A. (2021). Templatnyi amino-guminovyi sorbent na osnove otkhodov ugledobychi [Template amino-humic sorbent based on coal mining waste]. *Universum: khimia i biologia: elektronnyi nauchnyi zhurnal — Universum: Chemistry and Biology: Electron. Scientific. J.*, 11(89). Retrieved from <https://7universum.com/ru/nature/archive/item/12512> [in Russian] <https://doi.org/10.32743/UniChem.2021.89.11.12512>

#### Information about authors\*

**Muldakhmetov, Zeinolla Muldakhmetovich** — Academician of the National Academy of Sciences of the Republic of Kazakhstan, Doctor of Chemical Sciences, director of LLP “Institute of Organic Synthesis and Coal Chemistry of the Republic of Kazakhstan”, Alikhanov str. 1, 100012, Karaganda, Kazakhstan; e-mail: [iosu@mail.ru](mailto:iosu@mail.ru); <https://orcid.org/0000-0001-9497-2545>

**Gazaliev, Arstan Maulenovich** — Academician of the National Academy of Sciences of the Republic of Kazakhstan, Doctor of Chemical Sciences, Deputy Director for Research of LLP “Institute of Organic Synthesis and Coal Chemistry of the Republic of Kazakhstan”, Alikhanov str. 1, 100012, Karaganda, Kazakhstan; e-mail: [iosu@mail.ru](mailto:iosu@mail.ru); <https://orcid.org/0000-0003-2161-0329>

**Zhakina, Alma Khasenovna** — Candidate of Chemical Sciences, Assoc. Professor, Head of the Laboratory of Polymer Chemistry of LLP “Institute of Organic Synthesis and Coal Chemistry of the Republic of Kazakhstan”, Alikhanov str. 1, 100012, Karaganda, Kazakhstan; e-mail: [alzhakina@mail.ru](mailto:alzhakina@mail.ru); <https://orcid.org/0000-0001-5724-2279>

**Vassilets, Yevgeniy Petrovich** (*corresponding author*) — Master of Pedagogical Sciences, Researcher at the Laboratory of Polymer Chemistry of LLP “Institute of Organic Synthesis and Coal Chemistry of the Republic of Kazakhstan”, Alikhanov str. 1, 100012, Karaganda, Kazakhstan; e-mail: [vassilets88@mail.ru](mailto:vassilets88@mail.ru); <https://orcid.org/0000-0003-2242-486X>

**Arnt, Oxana Vasilievna** — Master of Technical Sciences, Researcher at the Laboratory of Polymer Chemistry of LLP “Institute of Organic Synthesis and Coal Chemistry of the Republic of Kazakhstan”, Alikhanov str. 1, 100012, Karaganda, Kazakhstan; e-mail: [oxana230590@mail.ru](mailto:oxana230590@mail.ru); <https://orcid.org/0000-0002-8996-4572>

\*The author's name is presented in the order: *Last Name, First and Middle Names*

**Index of articles published in  
«Bulletin of the Karaganda University. Chemistry Series»  
in 2022**

№ p.

**PREFACE**

Karagandy University of the name of academician E.A. Buketov is pleased to announce that “Bulletin of the Karaganda university. Chemistry series” scientific journal has been accepted for indexing in the Scopus abstract database.....	1	4
<i>Kudaibergenov S.E., Nuraje N.</i> Foreword by the Editors of the Special Issue .....	3	5

**ORGANIC CHEMISTRY**

<i>Ayazbayeva A.Ye., Shakhvorostov A.V., Kudaibergenov S.E.</i> Temperature and Salt Responsivity of Anionic, Cationic and Amphoteric Nanogels Based on N-Isopropylacrylamide, 2-Acrylamido-2-Methyl-1-Propanesulfonic Acid Sodium Salt and (3-Acrylamidopropyl) Trimethylammonium Chloride .....	4	14
<i>Bhole R.P., Karche P.M., Shinde Y., Kute P.R., Gurav S.S., Wavhale R.D.</i> Design and Synthesis of Vitamin Drug Conjugate for its Probable Potential Against SARS-COV-2 Infections.....	4	46
<i>Bhole R.P., Swamy M.R., Wavhale R., Bonde C.G., Chikhale R.</i> Design of potential vitamin-drug conjugate for enhanced anticancer activity.....	1	6
<i>Burkeyev M.Zh., Zhunissova M.S., Plocek J., Kazhmuratova A.T., Zhumagalieva T.S.</i> Properties of cross-linked copolymers of polypropylene glycol maleate with acrylic acid obtained at various concentrations of the RAFT agent .....	1	15
<i>Burkeyeva G.K., Tazhbayev Ye.M., Muslimova D.M., Nurseit G.D., Zhaparova L.Zh.</i> “Cold Curing” of Polyethylene Glycol Maleate with Acrylic Acid and Some Physicochemical Properties of Their Solutions .....	2	23
<i>Kassanova A.Zh., Yestayeva M.T., Turtubayeva M.O.</i> Arenediazonium sulfonates: synthesis, comparison of structural and physicochemical properties.....	1	25
<i>Kudaibergen G.K., Zhunussova M.S.</i> Study of the Effect of Temperature on the Properties of Gelatin-Chitosan Cryogels.....	2	4
<i>Mendigaliev S.S., Birimzhanova D.A., Irgibaeva I.S., Barashkov N.N., Sakhno Y.E.</i> Aggregation-induced emission of 5-(benzylidene) pyrimidine-2,4,6-triones.....	1	39
<i>Normurodov N.F., Berdinazarov Q.N., Abdurazakov M., Ashurov N.R.</i> Mechanical and Thermal Properties of Biodegradable Composites Based on graft copolymer LLDPE-g-MA/Gelatin .....	4	35
<i>Nurmaganbetov Zh.S., Fazylov S.D., Turdybekov K.M., Nurkenov O.A., Turdybekov D.M., Mukusheva G.K., Minayeva Ye.V., Khabdolda G.</i> Synthesis and Structure of 4-Substituted (1 <i>S</i> ,9 <i>aR</i> )-1-[(1,2,3-triazol-1-yl)methyl]octahydro-1 <i>H</i> -quinolines of Lupinine .....	2	12
<i>Panshina S.Yu., Bakibaev A.A., Guslyakov A.N., Malkov V.S.</i> Synthesis of Cucurbit[6]uril Using 1-Hydroxyethylidene-1,1-Diphosphonic Acid as a “Green Catalyst” .....	5	5
<i>Turgunaliyeva D.M., Dilbaryan D.S., Vasilchenko A.S., Nurkenov O.A., Fazylov S.D., Karipova G.Zh., Seilkhanov T.M., Kulakov I.V.</i> Synthesis and Antibacterial Activity of Hydrazones of Isonicotinic and Salicylic Acids Based on Acetyl Derivatives of Coumarin and Benzo[g][1,3,5]Oxadiazocine.....	4	25

**PHYSICAL AND ANALYTICAL CHEMISTRY**

<i>Annarapu T., Kamepalli S., Kondala S.K., Kotra V., Challa S.R., Rudrapal M., Bendale A.R.</i> Anti-inflammatory and antioxidant activities of 4-allylpyrocatechol and its derivatives with molecular docking and ADMET investigations .....	1	50
<i>Asgaonkar K.D., Patil S.M., Chitre T.S., Wani S.D., Singh M.T.</i> QSAR tool for optimization of nitrobenzamide pharmacophore for antitubercular activity .....	1	60
<i>Bhimanwar R., Thomas A., Kothapalli L., Godase A., Gandhi S., Chandani S., More G., Jadhav G., Choudhary S.</i> Prospective Hybrid Molecules with Dual Anti-Viral and Anti-Thrombotic Activity Against the SARS-CoV-2 Infection and Its Associated Complications Employing <i>in Silico</i> Studies..	4	76

<i>Chitlange S.S., Chandani S.R., Gandhi S.P., Thorat P.A., Lad H.B.</i> Development and Validation of HPTLC Method for Simultaneous Estimation of Berberine, Gallic Acid and Ursolic Acid in a Polyherbal Blend .....	2	33
<i>Fomin V.N., Usmanova E.R., Gyul E.F., Kelesbek N.K., Turovets M.A., Zemskiy O.I., Saulebekov D.M., Aldabergenova S.K.</i> Method for Qualitative and Quantitative Analysis of Ancient Lead Enamel Using Laser Inducted Breakdown Spectroscopy .....	4	107
<i>Galiyeva A.R., Tazhbayev Ye.M., Zhumagaliyeva T.S., Sadyrbekov D.T., Kaikenov D.A., Karimova B.N., Shokenova S.S.</i> Polylactide-co-glycolide nanoparticles immobilized with isoniazid: optimization using the experimental Taguchi method.....	1	69
<i>Gandhi S.P., Gawhane A.R., Kapse S.D., Nagore D., Chitlange S.S.</i> Validated High Performance Thin Layer Chromatography Method for Simultaneous Estimation for Gallic Acid and Quercetin in Polyherbal Blend and Their Quantitative Estimation .....	4	54
<i>Jalmakhanbetova R.I., Suleimen Ye.M., Abe N., Oyama M., Metwaly A.M., Eissa I.H., Ishmuratova M.Yu., Ibatayev Zh.A.</i> Isolation and in silico SARS-CoV-2 main protease inhibition potential of chrysoeriol from <i>Chondrilla brevirostris</i> Fisch. & Mey C.A. ....	1	78
<i>Kurmanova A.F., Abilkanova F.Zh., Rakhimzhanova A.S., Pustolaikina I.A.</i> DFT Study of Complexation Reactions Involving Dicarboxylic Acids: Hydrogen Bonds, Influence of Solvent Nature .....	2	43
<i>Makasheva A.M., Malyshev V.P., Bekbayeva L.A.</i> Direct Correlation between Fluid Cluster Structure and Its Viscosity .....	4	65
<i>Nurdillayeva R.N., Zhylysbayeva A.N., Askarov A.K., Bayeshov A.</i> Electrochemical Method of Lead (II) Ions Removal from Wastewater Using Granular Graphite Electrodes .....	2	61
<i>Ryabykh A.V., Maslova O.A., Beznosyuk S.A., Masalimov A.S.</i> The Role of Zinc Ion in the Active Site of Copper-Zinc Superoxide Dismutase.....	2	77
<i>Sarsenbekova A.Zh., Bolatbay A.N., Morgun V.V., Havlicek D., Davrenbekov S.Zh., Nasikhatuly E.</i> Study of thermal stability and determination of effective activation energy values during degradation of unsaturated polyester copolymers in the air atmosphere .....	1	86
<i>Shelkovnikov V.V., Altyev A.M., Fryanova M.S.</i> Study of the Methionine Electrooxidation at an Electrode Modified with Vitamin B <sub>12</sub> and Multi-Walled Carbon Nanotubes .....	4	99
<i>Stadnik I.L., Abilkanova F.Zh., Kudryavtseva Ye.V., Nikolskiy S.N., Masalimov A.S.</i> ESR-Study of the Proton Exchange with Aliphatic Amino Acids in Toluene.....	2	69
<i>Turdybekov K.M., Ivasenko S.A., Turdybekov D.M., Makhmutova A.S., Gatilov Yu.V., Adekenov S.M.</i> Isolation and Structure of the New Sesquiterpene Lactone 3-oxo-10 $\beta$ -hydroxy-5,7 $\alpha$ (H),4,6 $\beta$ (H)-guai-1,11(13)-diene-6,12-olide .....	2	52
<i>Tyanakh S., Baikenov M.I., Gulmaliev A.M., Ma Feng-Yun, Musina G., Khamitova T.O., Bolatbay A.N.</i> Kinetics of Thermolysis of a Low-Temperature Tar in the Presence of a Catalyzer Agent with Deposited Metals .....	4	89

### INORGANIC CHEMISTRY

<i>Aliyev F.R., Orujlu E.N., Babanly D.M.</i> Synthesis and study of a new mixed-layered compound GeBi <sub>3</sub> Te <sub>4</sub> belonging to the $n\text{Bi}_2-m\text{GeBi}_2\text{Te}_4$ homologous series.....	1	92
<i>Bayeshov A., Kadirbayeva A.S., Bayeshova A.K., Zharmenov A.A.</i> Electrochemical Method for Producing a TiO <sub>2</sub> Film with Photocatalytic Properties .....	4	152
<i>Houbi A., Zharmenov A.A., Atassi Y., Bagasharova Z.T., Mirzalieva S., Karibayev B.A.</i> Synthesis and Microwave Absorption Properties of (Ni <sub>0.5</sub> Zn <sub>0.5</sub> Fe <sub>2</sub> O <sub>4</sub> /Cl/CB) Ternary Composites .....	4	142
<i>Kasenov B.K., Kasenova Sh.B., Sagintaeva Zh.I., Baisanov S.O., Lu N.Yu., Kuanyshbekov E.E., Turtubaeva M.O., Isabaeva M.A.</i> Novel Titanium-Manganites of Lanthanum and Alkali Metals.....	4	136
<i>Korolkov I.V., Zibert A.V., Lisovskaya L.I., Ludzik K., Anisovich M.V., Vasilyeva M.M., Shumskaya A.E., Usseinov A., Yeszhanov A.B., Zdorovets M.V.</i> Simultaneous Immobilization of Gadolinium Ions and Di( <i>o</i> -carborano-1,2-dimethyl)borate on Fe <sub>3</sub> O <sub>4</sub> Nanoparticles .....	2	87
<i>Medvedeva N.A., Mironova A.A., Skryabina N.E., Plotnikova M.D., Fruchart D., Shcherban' M.G.</i> The Effect of Aging on the Microstructure of Alloys (TiCr <sub>1.8</sub> ) <sub>100-x</sub> V <sub>x</sub> after Electrolytic Hydrogen Charging .....	2	95
<i>Vissurkhanova Ya.A., Ivanova N.M., Soboleva E.A., Mukhamedzhanova A.K.</i> Mono- and Bimetallic Silver-Containing Nitrogen-Doped Carbon Composites and Their Electrocatalytic Activity .....	2	103

<i>Zulfugarova S.M., Azimova G.R., Aleskerova Z.F., Litvishkov Yu.N., Tagiyev D.B.</i> Synthesis of Transition Metal Ferrites (Co, Cu, Ni, Mn) by the Sol-Gel Method with Combustion and the Use of Microwave Processing.....	4	118
-------------------------------------------------------------------------------------------------------------------------------------------------------------------------------------------------------------------------------	---	-----

### CHEMICAL TECHNOLOGY

<i>Chekanova L.G., Vaulina V.N., Elchischeva Yu.B., Bardina E.S., Pavlov P.T.</i> The Selection of Reagents for Ionic Flotation of Non-Ferrous Metals in the Series of N-Acyl-N'-Mezylhydrazines .....	4	171
<i>Guseinova E.A.</i> Adsorption Purification of Used Industrial Oil Using Natural Aluminosilicates.....	4	162
<i>Kim S.V., Baikenov M.I., Ibishev K.S., Meiramov M.G., Ma Fengyun, Khamitova T.O.</i> Effect of Nickel Nanopowder on the Thermal Degradation of Coal Tar Distillate .....	2	134
<i>Muldakhmetov Z.M., Gazaliev A.M., Zhakina A.Kh., Vassilets Ye.P., Arnt O.V.</i> Synthesis of a Composite Based on Humic Acid Tuned to Sorbed Copper Ion .....	4	182
<i>Muldakhmetov Z.M., Ordabaeva A.T., Meiramov M.G., Gazaliev A.M., Shaikenova Zh.S., Mukusheva G.K., Zhivotova T.S.</i> Obtaining Carbon Sorbent from "Euromet" LLP Coke Breeze.....	2	115
<i>Sagyndikov M.S., Salimgarayev I.I., Ogay E.K., Seright R.S., Kudaibergenov S.E.</i> Assessing polyacrylamide solution chemical stability during a polymer flood in the Kalamkas field, Western Kazakhstan.	1	99
<i>Shlyapov R.M., Amerkhanova Sh.K., Uali A.S., Omarbekov T.B., Belgibayeva D.S.</i> Thermodynamics of chalcocite dissolving in solutions of flotation reagents .....	1	122
<i>Skachkov V.M., Pasechnik L.A., Medyankina I.S., Bibanaeva S.A., Sabirzyanov N.A.</i> Improvement of Extraction Technology and Electrotechnological Equipment for Obtaining Gallium from Alumina Production Solutions.....	2	125
<i>Yuminova A.A., Giniyatullina E.A., Kariyeva L.M., Chekanova L.G.</i> Physical-chemical properties of FM-1 reagent as a potential collector for ion flotation of lanthanoids .....	1	113

### MEMORABLE DATES

<i>Kudaibergenov S.E.</i> The Contribution of Professor Esen Bekturov to Physical Chemistry of Polymers.....	3	9
--------------------------------------------------------------------------------------------------------------	---	---

### SPECIALTY POLYMERS IN OIL INDUSTRY, BIO-, NANOTECHNOLOGY AND MEDICINE

<i>Avazova O.B., Milusheva R.Yu., Nurgaliev I.N., Rashidova S.Sh.</i> Polymolecular Complexes of Chitosan with the <i>Bombyx Mori</i> Protein.....	3	87
<i>Ayazbayeva A.Ye., Nauryzova S.Z., Aseyev V.O., Shakhvorostov A.V.</i> Immobilization of Methyl Orange and Methylene Blue within the Matrix of Charge-Imbalanced Amphoteric Nanogels and Study of Dye Release Kinetics as a Function of Temperature and Ionic Strength.....	3	127
<i>Bekturov E.A., Moustafine R.I., Kudaibergenov S.E., Khutoryanskiy V.V.</i> Interpolymer Complexes of Synthetic, Natural and Semi-Natural Polyampholytes: A Review .....	3	14
<i>Berdinazarov Q.N., Khakberdiev E.O., Normurodov N.F., Ashurov N.R.</i> Mechanical and Thermal Degradation Properties of Isotactic Polypropylene Composites with Cloisite15A and Cloisite20A .....	3	283
<b>Burkeyev M.Zh.</b> , <i>Shibayeva S.R., Khamitova T.O., Plocek Jiri, Nurmaganbetova M.T., Kazhmuratova A.T., Zhumagaliyeva T.S.</i> Synthesis and Investigation of the Properties of Polymer-immobilized Silver- and Gold Nanoparticles.....	3	198
<i>Deberdeev T.R., Akhmetshina A.I., Karimova L.K., Grishin S.V., Kochemasova D.V.</i> Thermal Behavior of Novel Aromatic Oligoesters and Oligoesteramides .....	3	180
<i>Du Juan, Xu Shimei.</i> Solvents Triggered Coil-to-Globule-to-Coil Transition of Dual Nanocomposite Hydrogels with Inorganic Hybrid Crosslinking.....	3	115
<i>Galiyeva A.R., Tazhbayev Ye.M., Zhumagaliyeva T.S., Daribay A.T.</i> Encapsulation of Isoniazid in Polylactide-Co-Glycolide Nanoparticles by Nanoprecipitation .....	3	208
<i>Houbi A., Zharmenov A.A., Atassi Y., Bagasharova Z.T., Mirzaliyeva S., Karibayev B.A.</i> Synthesis and Microwave Absorption Properties of Ni <sub>0.5</sub> Zn <sub>0.5</sub> Fe <sub>2</sub> O <sub>4</sub> /CI Composite Coated with Polyaniline within Paraffin Wax Matrix .....	3	254
<i>Kanabekova P., Martin A., Kemelbekova A., Kulsharova G.</i> Applications of Nanofier Membranes in Microphysiological Systems .....	3	56

<i>Kazhmuratova A.T., Zhunissova M.S., Plocek Jiri, Fomin V.N., Sarsenbekova A.Zh., Khamitova T.O.</i> Influence of the RAFT Agent on the Reaction Direction of the Copolymerization of Polypropylene Glycol Maleate with Acrylic Acid .....	3	189
<i>Mamytbekov G.K., Beksultanov Zh.I., Bannykh V.I., Dan'ko I.V.</i> Synthesis, Structure and Properties of Hybrid Composite Bentonite-Based Materials .....	3	267
<i>Mashentseva A.A., Aimanova N.A., Parmanbek N., Altynbaeva L.Sh., Nurpeisova D.T.</i> Application of the Cu@PET Composite Track-Etched Membranes for Catalytic Removal of Cr(VI) Ions .....	3	227
<i>Michurov D.A., Kolosova O.Yu., Lozinsky V.I.</i> Cryostructuring of Polymeric Systems. 61. Physicochemical Properties of Poly(vinyl alcohol) Cryogels Prepared on the Basis of Urea-Containing DMSO-Solutions of the Polymer and Evaluation of the Resultant Gel Materials as Potential Drug Carriers ...	3	75
<i>Mukhametgazy N., Gussenov I.Sh., Shakhvorostov A.V., Tenhu Heikki.</i> Oil Recovery at High Brine Salinity Conditions Using Amphoteric Terpolymer .....	3	141
<i>Nurgaliev I.N.</i> DFT Study of Chitosan Ascorbate Nanoparticles Structure .....	3	218
<i>Sagyndikov M.S., Kushekov R.M., Seright R.S.</i> Review of Important Aspects and Performances of Polymer Flooding versus ASP Flooding .....	3	35
<i>Shinohara H., Nishide H.</i> Polymer Complexes for Electrocatalytic Oxygen Evolution.....	3	67
<i>Toktarbaiuly O., Kurbanova A., Ualibek O., Seralin A., Zhunussova T., Sugurbekova G., Nuraje N.</i> Fabrication of Superhydrophobic Self-Cleaning Coatings by Facile Method: Stable after Exposure to Low Temperatures and UV Light .....	3	158
<i>Wu C.Y., Ling W.Q., Yao Y.C., Guo M., Nuraje N.</i> Three-Dimensional Fingerprint Spectroscopy Study on the Biopolymer System of Polyphenol Oxidase Binding with Cumalic Acid .....	3	168
<i>Zhinzhilo V.A., Litvinova A.Yu., Lyamina V.M., Dzhardimalieva G.I., Uflyand I.E.</i> Coordinating Polymers Based on Nickel(II) and Cobalt(II) Trimesinates as Promising Adsorbents of Organic Dyes.....	3	239
<i>Zhubanov A.A., Bondaletov V.G., Kozhabekov S.S., Galymzhan A.Z.</i> Amidation of Polyethylene-Acrylic Acid Copolymer as Pour Point Depressants for Waxy Crude Oils.....	3	150
<i>Mussabayeva B.Kh., Kassymova Zh.S., Orazzhanova L.K., Klivenko A.N., Sabitova A.N., Bayakhmetova B.B.</i> Interpolyelectrolyte Complex Chitosan – Alginate for Soil Structuring .....	3	102